NTNU
Norwegian University of Science and Technology
Department of Marine Technology

M.Sc.THESIS

Title:	**Delivered:**
An investigation of wave conditions and wave induced loads for design of wind turbine foundations at 15 – 40m depth.	14.06.2011
	Availability: Open
Student: Erik Svangstu	**Number of pages:** 105+Appendices

Abstract:

The motivation for this thesis is to investigate how storm sea states in deep water transforms as the waves propagate towards shallow water. This is connection with the design of bottom fixed wind turbines in finite water depths. In order to investigate how the sea state is transformed, there have been performed a model test where the generated waves are measured as they propagate over a sloping beach.

Theory behind different shallow water effects and how these will transform the sea state, is presented. The results obtained from the present model test have also been compared to similar model tests, and the comparison generally shows the same behavior.

The results show that the surface process of the waves transforms into a nonlinear process, and the deviations from a Gaussian process shows this clearly in terms of values for skewness and kurtosis. It is seen that wave breaking will be an dissipation important in the wave spectra, significant wave height and the distributions of wave and crest heights in the sea state. Where wave breaking is seen to reduce the energy content in the wave spectrum, and contributes to make the proposed conventional distribution functions for both wave and crest height distributions conservative. The significant wave height is also seen to be transformed by effects from shoaling.

For the largest individual waves it is seen that the waves in the measured time series are asymmetrical with respect to the front and back of the wave. This effect along with the calculated Ursell number for these waves indicates that there is a need for sophisticated wave model in order to model the surface elevation of the waves with corresponding wave kinematics.

Keyword:

Shallow water
Model test
Bottom fixed wind turbines

Advisor:

Dr. ing. Carl Trygve Stansberg

Proff. II Sverre Haver

Address:
NTNU
Department of Marine Technology
N-7491 Trondheim

Location
Marinteknisk Senter
O. Nielsens vei 10

Tel. +47 73 595501
Fax +47 73 595697

NTNU
Norwegian University of Science and Technology
Department of Marine Technology

M.Sc.THESIS

NTNU Trondheim
Norwegian University of Science and Technology
Faculty of Engineering Science and Technology
Department of MarineTechnology

M.Sc. thesis 2011

for

Stud.techn.

Erik Svangstu

An investigation of wave conditions and wave induced loads for design of wind turbine foundations at 15 – 40m depth.

(Undersøkelse av bølgeforhold og bølgelaster for å dimensjonere vindturbinfundamenter på 15 – 40m dyp.)

The background for Statoil interest in waves in intermediate water depths is that the company is in the process of installing wind turbines off the east coast of England. Furthermore, there are plans for major wind turbine parks in the southern North Sea. The wind turbines that are in the process of being installed and this work will be a part of the work done in order to verify the design loads. More important is to ensure that Statoil with respect to future design of wind turbines have a solid scientific and engineering foundation for what is done.

It is assumed that a sufficient knowledge regarding surface wave elevation process for water depths from 70-80m and deeper. In connection with this project, 70-80m is considered to represent deep water although this depth formally speaking is not deep water for storm waves. The wind turbines are installed in water depths from 15-35m. We will refer to this as shallow water, but formally this depth is more likely to represent intermediate depth.

The steps involved in predicting design loads on the wind turbine foundation are as follows. The start is to establish a set of design storms in deep water (80m). These storm events are considered as the boundary condition for the wave analyses transforming the deep water wave conditions to more shallow water. In such an analysis are effects wind, wave refraction, and dissipative mechanisms like bottom friction and wave breaking accounted for. Interactions between the various wave components are also included. The wave models are spectral models, i.e. the calculate the changes of energy content of the various wave components, but the phasing between the components are not monitored. As a consequence spectral models can not produce wave histories for the surface elevation. Thus the models do not give any information regarding the shapes of extreme waves, in particular not if non-linearities become important.

It is assumed that in a near future, adequate estimates for the wave spectra for design sea states in shallow water will become available. The challenge is to establish reliable estimates for the surface elevation process being a result of this energy distribution. Even more challenging may be the shape of the largest or most dangerous wave episodes regarding hydrodynamic loads on bottom fixed wind turbines. This will be the major focus of this thesis. The background for the thesis work is the literature study performed during the project work. During the master thesis, an important part will be to perform a model test experiment with waves on a sloping bottom. The MSc candidate is expected to play a major role both with respect to define the model test program and the execution of the model

test. An important part of the work will thereafter be to analyse model test results and identify information that will be of importance regarding design of bottom fixed wind turbines.

In closing the work, the load for idealized wind turbine foundation shall be considered. The relative importance of the various terms of the formula for the hydrodynamic load (generalized Morrisons equation).

A possible approach for assessing the problem could include the following steps:

1. Review the problem of estimating the design load on a wind turbine foundation. This should be a part of the basis when deciding the content of the model test program. In the model test, focus is to be given to the modelling of surface waves

2. Contribute in defining a scope of work for the model test – this includes also plans for possible video recordings. The work is to be done in cooperation with Marintek and Statoil. Sub-task should be concluded with a test plan for the model test.

3. Execute model test. It is recommended that preliminary analyses are performed during the test period to ensure that the test program includes necessary tests in view of the of the master thesis.

4. Analyses of model test results in view of scope of work. Subjects that should be assessed are:

   * Measure of deviation from the Gaussian assumption as function of wave steepness (s) and Ursell number (U).

   * Distribution of wave crest and wave height for various combinations of s and U. A comparison with available probabilistic models shall be done.

   * The shape of the most extreme individual wave events for various s and U. Is there a relation between horizontal asymmetry and the parameters s and U?

   * Frequency of wave breaking? What type of breaking is observed?

   The analyses do not need to be limited to these few points. The candidate may also focus on other subjects that may be of concern for the problem under consideration.

5. The load on a pile shall be determined. Thereafter one shall investigate the importance of the various terms of generalized Morrisons equation with respect to quasi-static and dynamic response of wind turbine. Whether an available computer code (Nirwana) should be used or one should make a small program in Matlab is left for the candidate to consider. The surface elevation to be used is the surface elevation measured in the model test. A simplified kinematic model is to be used.

6. The work shall be clearly presented. Conclusions shall be drawn and possible future work shall be established.

The work may show to be more extensive than anticipated. Some topics may therefore be left out after discussion with the supervisor without any negative influence on the grading.

The candidate should in his report give a personal contribution to the solution of the problem formulated in this text. All assumptions and conclusions must be supported by mathematical models and/or references to physical effects in a logical manner. The candidate should apply all available sources to find relevant literature and information on the actual problem.

The report should be well organised and give a clear presentation of the work and all conclusions. It is important that the text is well written and that tables and figures are used to support the verbal presentation. The report should be complete, but still as short as possible.

The final report must contain this text, an acknowledgement, summary, main body, conclusions, suggestions for further work, symbol list, references and appendices. All figures, tables and equations must be identified by numbers. References should be given by author and year in the text, and presented alphabetically in the reference list. The report must be submitted in two copies unless otherwise has been agreed with the supervisor.

The supervisor may require that the candidate should give a written plan that describes the progress of the work after having received this text. The plan may contain a table of content for the report and also assumed use of computer resources.

From the report it should be possible to identify the work carried out by the candidate and what has been found in the available literature. It is important to give references to the original source for theories and experimental results.

The report must be signed by the candidate, include this text, appear as a paperback, and - if needed - have a separate enclosure (binder, diskette or CD-ROM) with additional material.

Supervisor: Dr. Carl Trygve Stansberg, Marintek
Prof. II Sverre Haver, Statoil ASA.

Preface

This M.Sc. thesis is written as part of a Master of Science degree at NTNU Trondheim, institute of Marine Technology. The workload of the thesis accounts for the entire final semester.

The background for this thesis is to investigate how the surface process of water waves transforms from deep to shallow water, with respect to wave induced loads on wind turbines fixed to the sea bottom on water depths in the region of 15-40 meters.

As the waves were seen to be influenced by nonlinear effects such that it was impossible to describe the waves with corresponding kinematics without a sophisticated wave model, the attempt to estimate loads on the wind turbines were left out of the problem description after discussion with my supervisors.

I would like to use the opportunity to thank my supervisors Dr. ing. Carl Trygve Stansberg (Marintek) and Proff. II Sverre Haver (Statoil ASA & NTNU), which have been a great inspiration throughout both the model test and the present work with this thesis.

Finally Marintek and Statoil ASA are acknowledged for their contributions with both funding and efforts made in order to perform the model test in connection with this thesis.

Trondheim, 14. June, 2011

_____

Erik Svangstu

Summary

In this thesis it is investigated how the wave conditions transforms as storm condition sea states propagate from deep to shallow water, by means of a model test with a sloping beach.

There is given a short overview of important effects in shallow water and how these effects transform the wave spectra. Theoretical models for wave spectra in finite water depths, wave and crest height distributions are also presented.

The present model test is presented with a description of observations, setup, test programs and uncertainties.

The data from the present model test have been analyzed, and it is seen that the skewness and kurtosis increase with decreasing water depth. The growth of the skewness is fund to be proportional to the Ursell number, similar relations for the kurtosis are not fund. It is seen as the skewness grows larger than zero and the kurtosis grows larger than 3, that the process grows into a non Gaussian process. The significant wave height is seen to be dependent on wave shoaling and wave breaking.

The wave spectrum remains fairly constant throughout the propagation from deep to shallow water, but significant dissipation due to wave breaking is seen in a region corresponding to a full scale water depth of 15-20 meters. In general dissipation from bottom friction should cause a significant decrease of the energy in the wave spectra, but this is not seen in the present model test.

There have been performed a comparison with the spectral estimates and the TMA spectra for finite water depths. It is seen that the TMA spectrum over predicts the energy dissipation of the spectra compared to what is seen in the spectral estimates for the present model test.

Wave and crest height distributions have been compared to data by performing a zero up crossing analysis, and from the present model test it is seen that the largest waves from the largest sea states seem to be significantly affected by wave breaking. This causes the conventional distribution functions to be conservative.

There are also presented plots of the largest waves from the measured time series in space. And from the largest sea states the waves are clearly asymmetrical with respect to the front and back of the wave.

Table of Contents

List of figures

List of tables

Nomenclature

γ_1	Skewness
γ_2	Kurtosis
c	Crest height
CFD	Computational fluid dynamics
d	Water depth
FFT	Fast Fourier Transform
h	Water depth, and for wave height distributions; Wave height
H	Wave height
h/λ_P	Relative water depth
H_{m0}	Significant wave height estimated from spectra
H_s	Significant wave height mean of 1/3 largest waves
JONSWAP	Joint North Sea Wave Project
k	Wave number
S_1	Wave steepness based on peak period (T_P)
S_k	Wave steepness (radians)
S_P	Wave steepness based on mean wave period (T_1)
S_λ	Wave steepness
T_1	Mean wave period
T_P	Peak period
Ur	Ursell number
WP	Wave probe
η	Surface elevation
λ	Wave length
λ_P	Wave length corresponding to the peak period
σ	Standard deviation
ω	Angular frequency
ω_P	Angular peak frequency

1 Introduction

The background for this thesis is related to bottom fixed wind turbines in a water depth of 15-40 meters. These structures are already being built, thus the work in the present thesis will be related to verification and to give a theoretical basis for future builds.

The focus of this thesis will be related to how the wave conditions transform from deep to shallow water. Effects like bottom friction, wave breaking, shoaling and other nonlinear effects will be considered. In connection with these effects the following will be discussed:

- Will the process deviate from a Gaussian process? And can any of these deviations be quantified by nonlinearity parameters such as wave steepness or the Ursell number?
- How does the wave spectrum change? Are there analytical models that can describe this transformation?
- How do the distributions for wave crests and wave heights change? Can existing analytical models predict this?
- How do the largest waves in a time series look like with respect to asymmetry?
- Wave breaking are likely to be important, what type of wave breaking can be seen in such a case? And what contribution will wave breaking have for the surface process in a water depth of 15-40 meters?

In order to investigate how the waves transform from deep to shallow water, there have been performed a model test in cooperation with Marintek and Statoil ASA. Where the surface elevation is measured as the generated waves propagated over a constantly sloping beach, most of the wave probes are positioned corresponding to full scale water depths of 15-40 meters. The time series from these measurements are the basis for the calculations made in this thesis.

In chapter 2 there will be presented background theory, established analytical models and there are also found publications in which similar model tests are analyzed.

In chapter 3 the present model test is described in detail, with specifications, observations and uncertainties.

In chapter 4 the results from the model test are presented, discussed and compared with results from previous model tests.

As the results from the model test have given a lot of data, all of them cannot be presented in the discussion of the results. Therefore tests from the most interesting cases have been selected, along with smaller sea states for comparison. Representative examples of these tests have been presented in the discussion. Complete sets of data from these examples can be found in the respective appendices. Furthermore complete sets of results from all the selected tests can be found in the digital appendix attached to this thesis.

2 Theory and previous work

2.1 Wave transformation in finite water depth

The wave transformation as the waves propagate from deep to shallow water is a process where many factors contribute. There will be made no attempt to calculate these effects in this thesis, but they are mentioned here in order to give the reader some insight in the terminology that will be used throughout this thesis. Some practical examples and more detailed physical description can be found in Svangstu (2010), if specific references are made to other authors the reader should use these for a more detailed description of the phenomenon in question.

Waves entering intermediate water depth will no longer have a constant relation between wave period and wave length (dispersion relation), and as the wave propagates towards shallower water the wave length will decrease. This will cause the wave height to length ratio (steepness) to increase.

As the wave steepness increases nonlinear effects will contribute to the surface process of the waves, which causes them to grow in the crest to through asymmetry. In other words the peaks of the wave will be steeper and higher, and the through of the wave will be flatter and smaller.

As a wave propagates from deep to shallow water a great deal of the energy flux will be conserved, and some of the energy will be lost due to dissipation effects. The theory behind so called linear shoaling describes the effect this will induce on the wave height, neglecting effects from dissipation. Since the wave height is proportional to the total energy in the wave, the linear shoaling theory shows that the wave height will increase as the wave propagates from deep to shallow water.

In real live sceneries it is observed that waves hits the shore line normally, and it is found that turning of the waves can be described by so called refraction theory. As waves turns towards a beach the energy will be spread out over a larger area, causing a lower energy concentration and thus reducing the wave height. However in this thesis we only consider long crested waves (2D), and thus this is only mentioned as a part of the bigger picture.

Dissipation mechanisms are of great importance in such a case and the two most important dissipation mechanisms in such a process is bottom friction and wave breaking.

Bottom friction is caused by the viscous interaction between the sea bottom and the boundary layer in the water. This only causes dissipation when the wave “feels” the bottom, when the water depth is less than half the wavelength, i.e. the effect starts being noticeable in intermediate water depth. With the expression that the wave “feels” the bottom, we mean that wave kinematics is large enough to cause any significant interaction with the bottom. As frictional energy in general, dissipation due to bottom friction is dependent on how long the wave have traveled. Thus the energy dissipation from bottom friction will be larger on a beach with a small slope than a beach with a large slope. Since the distance traveled when the wave “feels” the bottom will be longer on a beach with a small slope. A more detailed description of bottom friction can be found in Dean et. al. (1991).

In deep water the wave breaking criteria is when the height to length ratio (steepness) of the wave is larger than 1/7. It is observed that waves in intermediate and shallow water have a stricter breaking

criterion. Wave breaking in deep water is only dependent on the wave steepness, the waves in shallow and intermediate water depths are additionally dependent on the wave height to depth ratio. Due to the fact that waves grow steeper and higher in shallow waters, we can then say that wave breaking will occur more frequently, and thus that the energy dissipation due to wave breaking in shallower water will of great importance. A detailed description of breaking waves can be found in Svendsen (2007).

2.2 Wave models

There will not be a large focus on wave models in this thesis, but this chapter is included in order to give the reader an overview of what kind of theoretical models in which such a problem can be solved with. There will be presented some examples in increasing complexity and precision.

2.2.1 Linear wave theory

Linear wave theory is what is most commonly used in marine applications, and are based on a simple harmonic shape of the wave. What limits the linear theory is that it is assumed that the wave steepness is small in order to solve the kinematic boundary condition. As a result of this the linear theory will have a limitation with respect to the wave steepness, according to Svangstu (2010) this limitation is kA=0.05-0.1

2.2.2 Second order theory

Second order theory is based on the perturbation principle proposed by Stoke, detailed information of this principle can be found in Dean et.al. (1991). From Svangstu (2010) the applicability of stoke 2nd order theory is investigated, and it is found that typical storm waves can only be described until water depths of approximately 50 meters. This is also seen in Stansberg (2011), where the applicability of the second order random wave theory is investigated. And it is also here found that the irregular second order formulation could be used until a water depth of 40 meters for the test cases, or a more general limitation with respect to the Ursell number; Ur=0.33.

2.2.3 Stokes 5th order theory

Stokes 5th order theory is described in Fenton (1985), and are basically a continuation of the work in which Gabriel Stokes performed up to 3rd order. This theory was also investigated in Svangstu (2010), and it was found that Stokes 5th order theory for storm size waves were applicable until a water depth of approximately 40 meters. This is slightly better than that of the second order theory, but the theory is still not applicable in shallow enough water in order to solve the problem in this thesis.

2.2.4 Wave models based on the Boussinesq equations

Wave models based on the enhanced Boussinesq equations proposed by Nwogu (1993) show great promises for the future, as the theory accounts for effects such as shoaling, bottom friction and wave breaking. Thus the model is capable of describing the propagation of waves on a beach. The limitations of wave models based on the Boussinesq equations have for a long time been that they only are applicable in shallow water, but the work done by Nwogu (1993) have made the theory applicable well into intermediate water depths, and further work based on the work from Nwogu have made the theory applicable in even deeper waters. The problem is however that at the present state these theories are somewhat complicated to use without a large effort, as the numerical solution scheme is based on solving a large number of high order partial differential equations. Thus

there have been made no effort in this thesis to use any wave models based on the Boussinesq equations.

2.2.5 Computational fluid dynamics (CFD)

Computational fluid dynamics is based on solving the Navier Stokes equation numerically, and this approach is considered the most exact to the present date. However this approach is very time consuming for marine applications, as the free surface makes the computational process more difficult. Simulations of waves with durations of a minute can take as long as half a day to calculate, and that is on a high end computer. Thus this kind of simulations basically needs a supercomputer in order to get adequate results in a reasonable amount of time.

2.3 Ursell number and wave steepness

In order to keep track of the different definitions that is used throughout this thesis, this chapter introduces some important wave characteristics; wave steepness and Ursell number.

2.3.1 Wave steepness

The classical definition of the wave steepness is related to the maximum angle in a linear harmonic wave, defined as:

$$S_\lambda = \frac{H}{\lambda} \qquad (1)$$

The steepness presented in terms of radians is expressed as:

$$S_k = kA \qquad (2)$$

Where the difference between the equations is pi, thus that equation 1 times pi are equal to equation 2.

For a nonlinear wave who has a clear crest to trough asymmetry these expressions will not give the maximum angle of the wave, as for linear waves. But it is a commonly accepted measure of wave steepness, even for nonlinear waves. These formulas are however related to individual or harmonic waves. As we often utilize irregular wave histories it is time consuming calculating the individual wave steepness for all the waves in the time series. A common measure of steepness in irregular waves is based on the parameters defining the sea state. Using the significant wave height (Hs), peak period (Tp) or mean period (T1), sea state steepness is given by, DNV(2007):

$$S_p = \frac{2\pi}{g}\frac{H_s}{T_p^2} \qquad (3)$$

$$S_1 = \frac{2\pi}{g}\frac{H_s}{T_1^2} \qquad (4)$$

The expression including the mean wave period (equation 4) is what has been used in this thesis. However when considering individual events, the two previous formulations have been used. In figures in this thesis a version of equation 2 is also used frequently, where the wave number

corresponding to the peak period following the linear dispersion relation have been used. As a representative amplitude of the sea state the half of the measured significant wave height in the relevant position have been used. The expression can be seen in equation 5.

$$S_k = k_p \frac{1}{2} H_{m0} \tag{5}$$

2.3.2 Ursell number

The Ursell number is a recognized measure of nonlinearity. The expression for the Ursell parameter is given from DNV(2007):

$$U_r = \frac{H\lambda^2}{d^3} \tag{6}$$

Equation 6 gives the Ursell number for individual waves, where d is the water depth and lambda is the wave length. When we have given an irregular sea state this does not help us much when trying to quantify the nonlinearity of the sea state. From DNV(2007) there are given a formula based on the significant wave height, and the wave number corresponding the mean wave period (k1):

$$U_r = \frac{H_s}{k_1^2 d^3} \tag{7}$$

And it is equation 7 that has been used to quantify the nonlinearity in the sea states in this thesis. However for the individual events that have been analyzed, there have been calculated the Ursell number of individual waves based on equation 6.

2.4 Transformation of the wave spectrum in finite water depth

2.4.1 Shape of the spectrum tail

In Holthuijsen (2007) it is argued that the high frequency tail of the wave spectrum in finite water depths grows flatter, from an f^{-5} to an f^{-3} tail. Where the f^{-5} tail is seen in the high frequency range in deep water.

The last part of the high frequency tail corresponds to that in deep water. There is no general agreement whether an f^{-5} or f^{-4} tail is correct. The f^{-5} tail is the most commonly used in engineering practice, and is implemented in known models such as the JONSWAP and Pierson Moskowitz spectrums. However according to Holthuijsen (2007) the f^{-4} tail fits better to data from deep water.

2.4.2 Bottom friction

The bottom friction as explained earlier is the friction between the boundary layer in the water and the bottom itself, induced by the particle motion from the waves. In Holthuijsen (2007) there are presented a couple of spectral bottom friction models, and it is seen that these are highly dependent on the roughness of the bottom surface. For further description of the models, see Holthuijsen (2007).

As the bottom friction is a dissipation effect it will reduce the total energy in the wave spectrum, this is predominant for the low and mid range frequencies, and the high frequency part of the wave spectrum is only affected in a small degree by bottom friction. An example of this is illustrated in Figure 1.

In general for energy dissipation due to friction, it is highly dependent on the distance traveled.

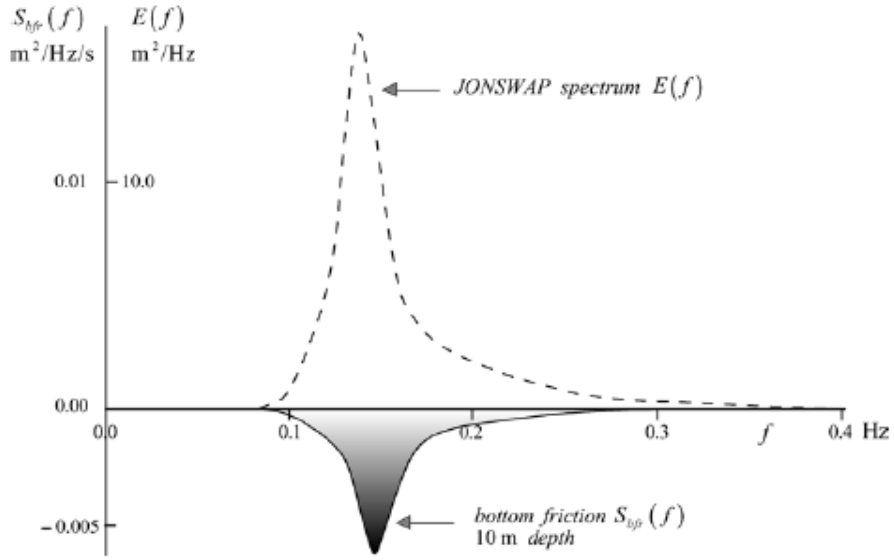

Figure 1: Illustration of bottom friction, taken from Holthuijsen (2007)

2.4.3 Shoaling

As the waves shoal the wave height will increase and thus the significant wave height will increase. The effect from shoaling can then be seen in the wave spectrum with an increase of the area in the wave spectrum concentrated around the peak frequency. As the low frequency waves in the

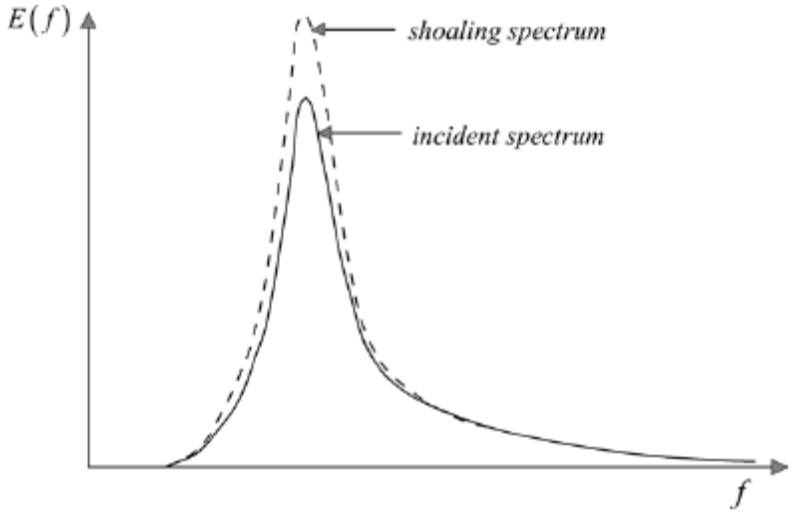

Figure 2: Illustration of shoaling, taken from Holthuijsen (2007).

spectrum will be at lower relative water depth, the effect from shoaling will be more dominant for

the low frequency part of the wave spectrum. This will result in a slight downshift of the dominant frequency in the wave spectrum, Holthuijsen (2007). This is illustrated in Figure 2.

Although the effect from shoaling causes the peak frequency to shift towards the lower frequencies, the magnitude of this change is often not of great significance. Thus the peak frequency can in most cases be assumed as constant, Holthuijsen (2007).

2.4.4 Wave breaking

First of all the wave breaking can be divided into two main categories, the first on is often referred to as white capping or deep water breaking. Where the wave breaking only is dependent on the wave steepness, and the waves will break as the wave steepness exceeds 0.14 ($H/\lambda=1/7$). This is the only reason why waves break in deep water, but it is also a very frequent phenomenon in intermediate water depths. The reason for this is that the wave shoaling will contribute to increased wave steepness, and thus triggering the deep water breaking criteria. The second category is what is called depth induced wave breaking or surf breaking, which occurs in shallow water as a result of depth induced effects.

Wave breaking is a dissipation mechanism and will reduce the total energy in the wave spectrum. According to Holthuijsen (2007) this reduction is distributed with the shape of the wave spectrum, thus the dissipation is largest around the peak frequency, and the resulting wave spectrum after the effect of wave breaking are considered will be of the same shape as the incident wave spectrum, only smaller. Additionally the wave breaking will disturb the smooth high frequency tail of the wave spectrum, this effect is however reversed by so called quadruple wave-wave interactions, which is described below.

2.4.5 Quadruple wave-wave interactions

Quadruple wave-wave interactions are resonant behavior of four wave components. For a thorough description of the phenomena the reader is referred to Holthuijsen (2007).

Quadruple wave-wave interactions will shift the energy from the high frequencies (from ω_P till $2\omega_P$) to the mid range frequencies. These interactions will contribute to “stabilize” the wave spectrum as the waves break, thus shifting the energy from the chaotic behavior in the high frequency tail into the mid range frequencies. The behavior is then seen to preserve the smooth high frequency tail of the wave spectrum, Holthuijsen (2007).

According to Holthuijsen (2007) the energy will be shifted to mid range frequencies lower than the peak frequency, resulting in a downshift of the peak frequency. It is also observed that the quadruple wave-wave interactions appear both in deep and shallow water, but they are stronger in shallow water, Holthuijsen (2007). An example of the contribution from quadruple wave-wave interaction in both deep and shallow water can be seen in Figure 3.

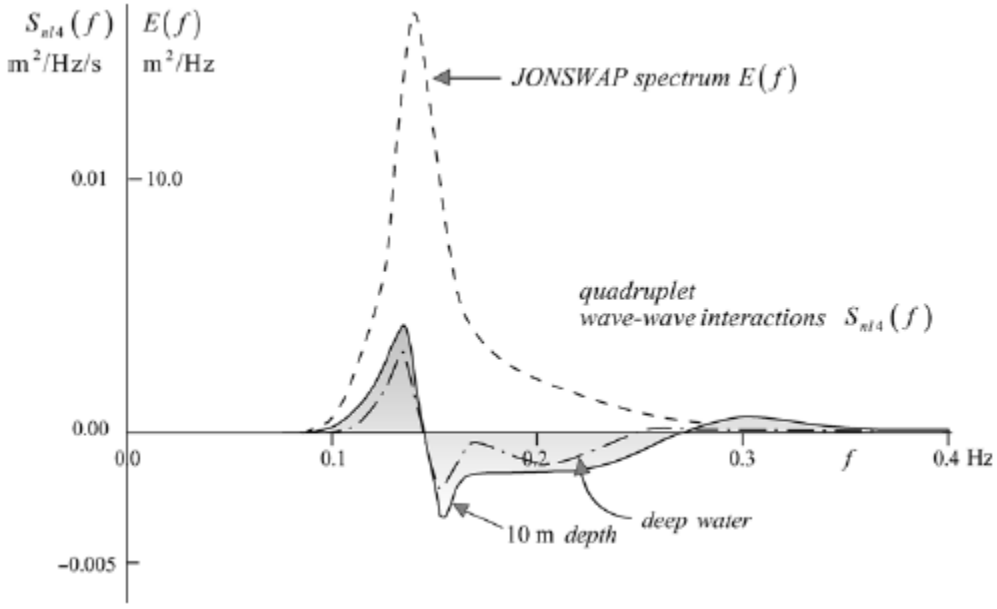

Figure 3: Illustration of quadruplet wave-wave interactions, taken from Holthuijsen (2007).

2.4.6 Triad wave-wave interactions

Triad wave-wave interactions are resonant behavior from three wave components, and only appear in shallow water since the resonance conditions cannot be satisfied with the linear dispersion relation in deep water, Holthuijsen (2007). The phenomenon is seen to appear in very shallow water, in the shallow water region ($h/\lambda_P<0.05$). But near resonant behavior may occur in slightly deeper

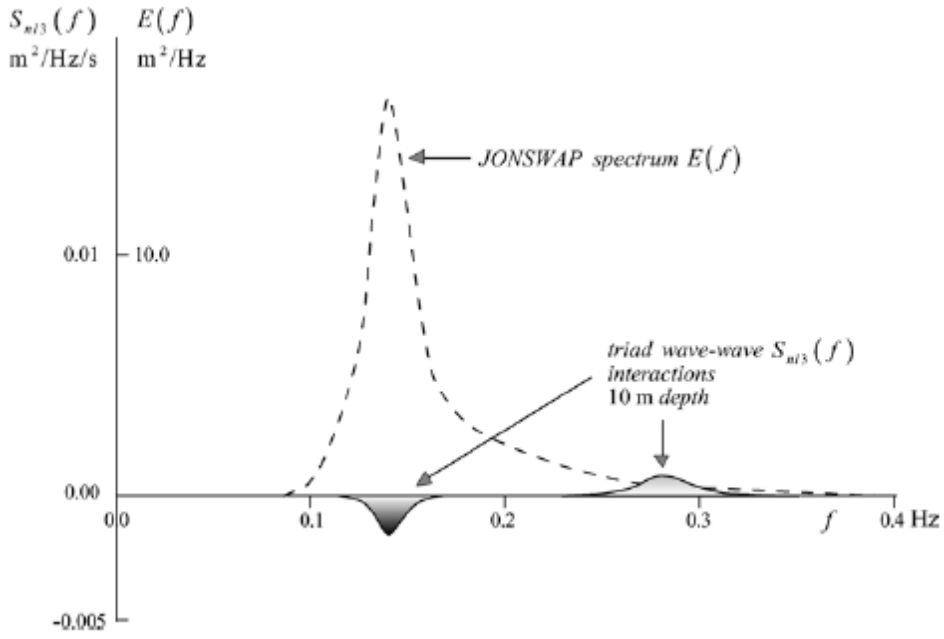

Figure 4: Illustration of triad wave-wave interactions, taken from Holthuijsen (2007).

water. For a more thorough description of the phenomena the reader is referred to Holthuijsen (2007).

Triad wave-wave interactions often cause a secondary peak at two times the peak frequency in the wave spectrum in shallow water. Where the energy will be shifted or transferred from the peak frequency to a secondary peak at two times the peak frequency, this is illustrated in Figure 4.

These secondary peaks are seen to persist only for a couple of wavelengths, before the effect is reversed from the same effect. Triad wave-wave interactions may also transfer energy to the lower frequencies, and thus generate a sub harmonic peak in the low frequency part of the wave spectrum. This peak represents the effect that is most commonly referred to as surf beats, Holthuijsen (2007). This can be considered as slow variations in the water depth.

2.5 Wave statistics and analytical wave spectra

2.5.1 Analytical wave spectrum in finite water depths

The TMA spectrum is described in Bows et.al. (1985). It is an analytical wave spectrum based on an scaling procedure in order to account for the depth induced changes in the wave spectrum as the waves propagate from deep to shallow water. The basis of the shape of TMA is the JONSWAP spectrum, and thus in deep water the TMA spectrum is identical to the JONSWAP spectrum. TMA takes into account effects of variable water depth and bottom friction, but does not take into account the dissipation effect of wave breaking DNV (2007). It is also worth mentioning that TMA makes no attempt to account for secondary peaks in the high frequency tail of the spectrum. The approach is based on a constant or gently sloping bottom. Further information regarding this spectrum can be found in Bows et.al. (1985) and Holthuijsen (2007).

2.5.2 Generating spectral estimates

The spectra estimated from measured time series by means of FFT are called raw spectra. The spectra will give a very noisy spectrum estimate and may be difficult to interpret. In order to get spectral estimates that are easy to compare and interpret we need to perform a so called smoothing of the raw spectra. What has been used in this thesis is something called a Welch averaged periodogram with overlapping batches. In short this approach is based on dividing the time series into many smaller “windows”, and then averaging the spectral densities from these windows into a spectral estimate. The standard approach is that a new window starts where the previous window ends, in such a way that the time series is divided into a finite number of equally sized windows where one window starts where the other ends, and so on. For the approach with overlapping batches the next window starts inside the previous window. In this thesis the WAFO (2000) function “dat2spec” have been used in Matlab. The only parameters that have been changed from the default values in this program are the smoothing method and the length of the windows.

Before the spectral estimates are generated the mean water level are set to zero, and after the spectral estimates are generated they are scaled in order to fit the variance of the time series. This is performed after general tips regarding generation of spectral estimates from Goda (2010).

The method chosen is as previously mentioned a Welch averaged periodogram with overlapping batches, i.e. with overlapping windows. The parameters determining the length of the windows is significant with respect to the magnitude of smoothing that are preformed. The default value of the parameter is 400 points, which with a sampling frequency of 100Hz corresponds to a window length of 4 seconds. This was seen to smooth the spectrum too much, and by that we mean that the smoothing is preformed to such a degree that it removes important trends in the spectrum. After some trial and error there where found that a parameter of 1500 gave a good balance between smoothing enough to see the trends clearly, and not removing to much in order actually see these trends. A smoothing parameter of 1500 corresponds to a smoothing window of 15 seconds for a sampling frequency of 100Hz. In Figure 5 it is presented a comparison were the spectral estimates are smoothed a small (L=400), medium (L=1500) and large (L=10 000) smoothing parameter.

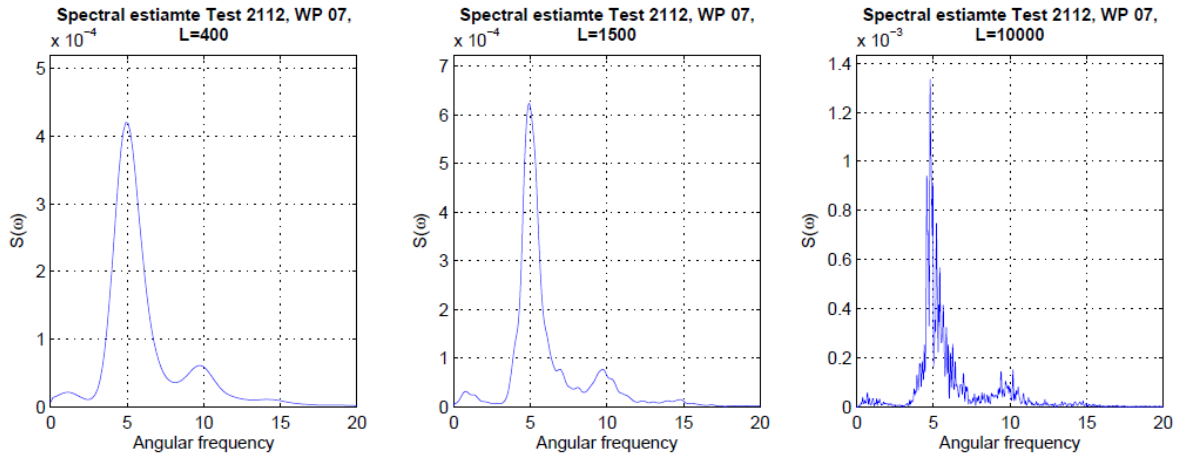

Figure 5: Example of spectral estimates with different smoothing parameters (L)

2.5.3 Spectral and statistical properties

Significant wave height

H_{m0} is the symbol for the significant wave height estimated from the wave spectrum, with the relation:

$$H_{m0} = 4\sqrt{m_0} \tag{8}$$

Where m_0 is the variance, and given by:

$$m_n = \int_{-\infty}^{\infty} \omega^n S(\omega) d\omega \tag{9}$$

i.e. m_0 is equal to the area of the wave spectrum. Since $Var[x] = \sigma_x^2$, the expression for the significant wave height (equation 8) can be presented as function of the standard deviation of the surface elevation (σ):

$$H_{m0} = 4\sigma \qquad (10)$$

From equation 10 the significant wave height can be estimated directly from the standard deviation of the time series of surface elevation.

It is important to be aware that H_S, also called the significant wave height, is not necessarily the same as H_{m0}. H_s is calculated as the mean of the 1/3 largest waves in a sea state, whereas H_{m0} are estimated directly from the wave spectrum. In deep water they are approximately the same, but in shallow water they may differ significantly.

Examples of measured H_{m0} can be found in both Nilsen (1997) and Wei et. al. (1999). The papers show that the significant wave height decreases slowly in the first part of the propagation from deep to shallow waters, until it drops significantly in shallow water.

Skewness

The skewness coefficient gives information about the asymmetry in the distribution. For a Gaussian process the skewness will be equal to zero, and the distribution will be symmetrical. This distribution is often referred to as the normal distribution, an example of this can be seen in Figure 6(b). Distributions with skewness values that differ from zero, will indicate that the process is not Gaussian. Examples of distributions with negative and positive values of skewness can be seen in Figure 6(a) and Figure 6(b) respectively.

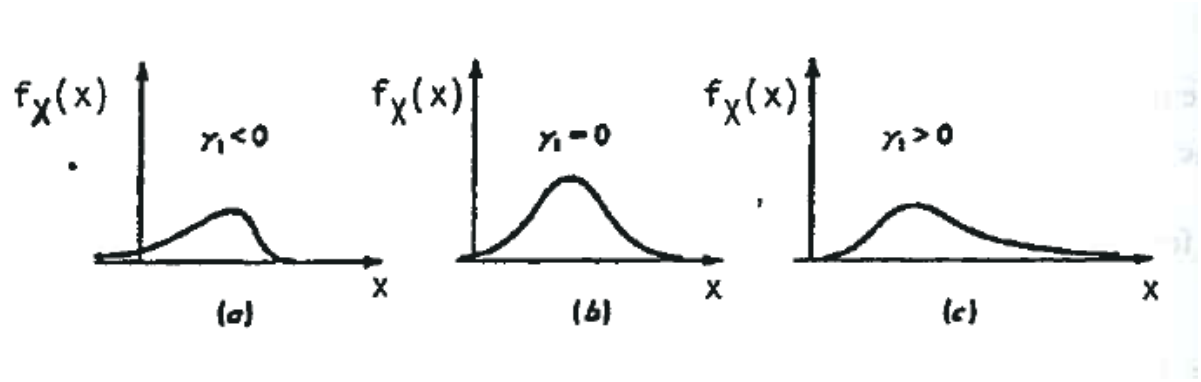

Figure 6: Illustration of skewness, taken from Leira (2010)

The physical meaning of the skewness coefficient can be explained as an indication of crest to trough asymmetry of the waves from the respective time series, where for example a skewness larger than zero means that the waves in the time series has larger and sharper peaks and smaller and flatter troughs.

From Leira(2010), the expression for the skewness coefficient is given in terms of central moments:

$$\gamma_1 = \frac{\bar{\mu}_x^{(3)}}{(\bar{\mu}_x^{(2)})^{\frac{3}{2}}} \qquad (11)$$

Where $\bar{\mu}_x^{(n)}$ is given by:

$$\bar{\mu}_x^{(n)} = \int_{-\infty}^{\infty} (x - \mu_x)^n f_x(x) dx \quad (12)$$

Where $f_x(x)$ is the probability density function and μ_x is the mean of x. The variance is given as:

$$Var[x] = \sigma_x^2 = \int_{-\infty}^{\infty} (x - \mu_x)^2 f_x(x) dx \quad (13)$$

Thus in terms of central moments the variance can be expressed as:

$$\sigma_x^2 = \bar{\mu}_x^{(2)} \quad (14)$$

Then the skewness coefficient can be written as:

$$\gamma_1 = \frac{\bar{\mu}_x^{(3)}}{\sigma_x^3} \quad (15)$$

From sample data we can estimate the skewness by:

$$\gamma_1 = \frac{\bar{\mu}_x^{(3)}}{(\bar{\mu}_x^{(2)})^{\frac{3}{2}}} = \frac{\frac{1}{n}\sum_{i=1}^{n}(x_i - \mu_x)^3}{(\frac{1}{n}\sum_{i=1}^{n}(x_i - \mu_x)^2)^{\frac{3}{2}}} \quad (16)$$

The skewness coefficient is also given by definition as:

$$\gamma_1 = E\left[\left(\frac{x - \mu_x}{\sigma_x}\right)^3\right] \quad (17)$$

Since equation 17 easily can be implemented into matlab, it is this formula that has been used in order to calculate an estimate of the skewness coefficient in this thesis.

In Nilsen (1997) there are calculated skewness coefficients for a lot of different 2D model tests. And it is seen that the skewness increases as the wave propagates from deep to shallow water. And since the skewness values are larger than zero, the transformation of the waves results in a process which is not Gaussian. The same is also seen in Nwogu (1993) and Wei et. al. (1999), however only with a single example in each paper. From Goda(2010) the same is also seen, where the skewness is compared to an analytical solution. In Goda (2010) it is proposed that the skewness is proportional to the wave steepness in deep water.

Kurtosis

The kurtosis coefficient gives information about the peakdness of the distribution. A Gaussian process will have a kurtosis coefficient equal to 3. Kurtosis values that are larger than 3 will give a distribution that have a sharper peak and longer tail compared to that of a Gaussian process. Kurtosis values smaller than 3 will give the complete opposite, i.e. a distribution with a flat peak and shorter tails. These cases are illustrated in Figure 7, where the distribution of a Gaussian process is presented with dashed lines.

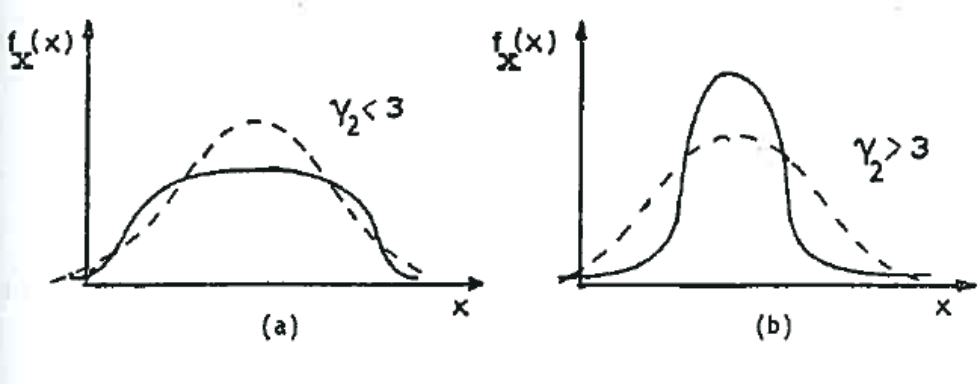

Figure 7: Illustration of kurtosis, taken from Leira (2010).

From Leira(2010) the kurtosis coefficient is given as:

$$\gamma_2 = \frac{\bar{\mu}_x^{(4)}}{(\bar{\mu}_x^{(2)})^2} \quad (18)$$

Following the same procedure as for the skewness, the kurtosis can be presented as:

$$\gamma_2 = \frac{\bar{\mu}_x^{(4)}}{\sigma_x^4} \quad (19)$$

Which gives:

$$\gamma_2 = E\left[\left(\frac{x-\mu_x}{\sigma_x}\right)^4\right] \quad (20)$$

Equation 20 can easily be implemented into matlab, and it is this formula that has been used to calculate the kurtosis coefficient in this thesis.

In Nilsen (1997) there are estimated kurtosis coefficients. The trend is that the kurtosis is slightly less influenced by the water depth than that of the skewness, and remains fairly constant with a slight increase until it increases significantly in shallow waters. The same trend is also seen in Goda (2010).

2.5.4 Crest height distributions

Rayleigh

The Rayleigh distribution for crest heights is given in Forristall (2000) as:

$$F_C(c) = 1 - \exp\left\{-8\left(\frac{c}{H_{m0}}\right)^2\right\} \qquad (21)$$

With a time series available the standard deviation and thus the estimated significant wave height ($H_{m0} = 4\sigma$) can be estimated fairly quickly with for example matlab, and thus the parameters in the Rayleigh distribution can easily be found directly from the time series.

The Rayleigh distribution is mainly used for the distribution of maxima for narrow banded stationary processes which follows the normal distribution with a mean value equal to zero. In a realistic situation the surface process of water waves are often broad banded, and deviates from the Gaussian process, however the deviation is not always of great significance. According to Myrhaug(2005), the Rayleigh distribution gives an upper limit for the distribution of maxima. And due to this the Rayleigh distribution is often used as a conservative estimate to the probability of exceedance above a certain level. This is illustrated in Figure 8, where it in the upper tail of the distributions can be seen that the Rayleigh distribution predicts a higher probability of exceedance than the Ritz distribution throughout the entire tail. Where the Ritz distribution is acknowledged as a more realistic distribution, thus the Rayleigh crest height distribution can be considered conservative for a Gaussian process.

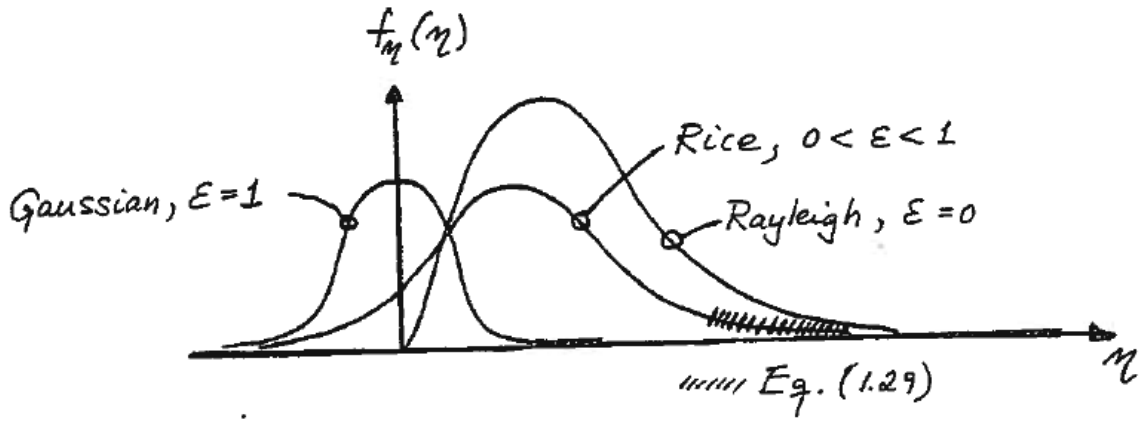

Figure 8: Rayleigh vs. Rice distribution, taken from Myrhaug (2005)

The Rayleigh distribution assumes linear waves, and thus designed for wave conditions where linear theory is applicable. The wave conditions in our model tests are fairly steep, and often beyond applicability of linear theory even in deep waters. As the waves propagate from deep to shallow water, they will grow even steeper, and non-linear effects will be more predominant. One non-linear effect of great importance here is the crest to trough asymmetry. Assuming a Gaussian process may give an initial error in the crest height of 10-15%, effects from wave shoaling may make this error

even larger. And thus it seems reasonable to suggest that the Rayleigh crest height distribution should be used with care in shallow water, and is likely to be none conservative. The Rayleigh crest height distribution should therefore be used with care even in deep water.

Forristall

The crest height distribution proposed by Forristall (2000), has gained a lot of recognition, and is used extensively. The distribution is based on a second order surface profile, and includes parameters as wave steepness and water depth. The exceedance probability is given by Forristall (2000):

$$P(\eta_c > \eta) = \exp\left\{-\left(\frac{\eta}{\alpha H_s}\right)^{\beta}\right\} \tag{22}$$

This then gives the cumulative distribution function:

$$F_C(c) = 1 - \exp\left\{-\left(\frac{c}{\alpha H_s}\right)^{\beta}\right\} \tag{23}$$

This is a Weibull type distribution function. For a 2-dimentional (long crested) simulation the alpha and beta parameters is given by:

$$\alpha_2 = 0.3536 + 0.2892S_1 + 0.1060U_r \tag{24}$$

$$\beta_2 = 2 - 2.1597S_1 + 0.0968U_r \tag{25}$$

The steepness parameter (S_1) and Ursell parameter (U_r) is given by:

$$S_1 = \frac{2\pi}{g}\frac{H_s}{T_1^2} \tag{26}$$

$$U_r = \frac{H_s}{k_1^2 d^3} \tag{27}$$

From Forristall (2000) the significant wave height taken as an input parameter in the distribution should be estimated from the wave spectrum, hence the significant wave height to be used in this distribution is H_{m0}. Further T_1 is the mean wave period in the wave spectra, more commonly referred to as T_{m01}.

$$T_{m01} = 2\pi\frac{m_0}{m_1} \tag{28}$$

Where the spectral moments m_0 and m_1 were found using the WAFO (2000) function “spec2mom” from the pre generated spectrums. And k_1 is the wave number corresponding to the mean wave period. When the relation between wave period and angular frequency is known:

$$\omega = \frac{2\pi}{T} \tag{29}$$

And k_1 was then found from ω_1 using the linear dispersion relation by the WAFO (2000) function "w2k", and finally d is the water depth.

2.5.5 Wave height distributions

Rayleigh

From equation 21 the expression for the Rayleigh crest height distribution is given, considering that the wave height is equal to two times the crest height, according to linear theory.

$$c = \frac{1}{2}H \tag{30}$$

Inserting equation 30 into equation 21 gives:

$$F_H(h) = 1 - \exp\left\{-8\left(\frac{0.5h}{H_{m0}}\right)^2\right\} = 1 - \exp\left\{-2\left(\frac{h}{H_{m0}}\right)^2\right\} \tag{31}$$

In accordance to second order theory the wave height will only increase slightly, the crest to trough asymmetry will however increase significantly. Since the Rayleigh crest height distribution gives conservative crest heights for linear waves, this will also be a conservative wave height distribution for linear waves. Thus as long as the second order contributions are dominating, the Rayleigh wave height distribution will be conservative. This will for most practical purposes be the case in deep water, therefore the Rayleigh distribution is considered to be conservative in deep water.

Battjes & Groenendijk

The wave height distribution proposed by Battjes et. al. (2000) is a so called composite Weibull distribution, i.e. consisting of two Weibull distributions. The first one should fit the smallest waves, and is the Rayleigh distribution. While the second one takes into account the reduced wave heights from depth induced wave breaking, and should fit the largest waves in the time series.

The wave height distribution is based on several model tests performed at WL/Delft hydraulics, where the model tank is 50 meters long, 1 meter wide and 1.2 meters deep. The model tests that this distribution has been fitted to is preformed with different bottom slopes (1:20-1:250), and thus the authors have been able to make an empirical fit of the so called transition wave height, as a function of the bottom slope. Where the transition wave height (H_{tr}) is the wave height where the distribution changes from a Rayleigh to a Weibull distribution. The transition wave height is given by:

$H_{tr} = \gamma_{tr}(\alpha)d$; Where d is the water depth, and $\gamma_{tr}(\alpha)$ is given by:

$\gamma_{tr}(\alpha) = c_1 + c_2 \tan(\alpha)$; Where alpha is the angle of the bottom slope, c_1=0.35 and c_2=5.8 are found empirically from data by the authors. From Battjes et. al. (2000) the distribution is given by:

$$F_H(h) = \begin{cases} F_1(h) = 1 - exp\left\{-\left(\frac{h}{H_1}\right)^{k_1}\right\} \; for \; h \leq H_{tr} \\ F_2(h) = 1 - exp\left\{-\left(\frac{h}{H_2}\right)^{k_2}\right\} \; for \; h \geq H_{tr} \end{cases} \quad (32)$$

Where k_1 and k_2 are the shape parameters, and H_1 and H_2 are the scale parameters of the distribution. Since $F_1(h)$ is the Rayleigh distribution, k_1=2 and H_1=H_{rms}. In Battjes (2000) k_2 is found empirically to be 3.6, and given the relation:

$$\left(\frac{H_{tr}}{H_1}\right)^{k_1} = \left(\frac{H_{tr}}{H_2}\right)^{k_2} \quad (33)$$

Which gives:

$$H_2^{k_2} = H_{tr}^{k_2-k_1} H_1^{k_1} \quad (34)$$

Using that;

$$H_1^2 = H_{rms}^2 = \left(\sqrt{8m_0}\right)^2 = 8m_0 = \frac{16}{2}m_0 = \frac{1}{2}(4m_0)^2 = \frac{1}{2}H_{m0}^2 \quad (35)$$

The distribution can be expressed as:

$$F_H(h) = \begin{cases} F_1(h) = 1 - exp\left\{-2\frac{h^2}{H_{m0}^2}\right\} \; for \; h \leq H_{tr} \\ F_2(h) = 1 - exp\left\{-2\frac{h^2}{H_{tr}^{k_2-2}H_{m0}^2}\right\} \; for \; h \geq H_{tr} \end{cases} \quad (36)$$

Mai et. al. (2010) has compared the model with long term in-situ wave measurements in the southern part of the north-sea (Germany). The waves are measured at locations with water depths in the region of 8-29 meters. They concluded that the model fits well to the field data, after changing the parameters c_1 to 0.23 and k_2 to 2.31. It is shown that the distribution from Battjes et. al. (2000) both under and over predicts the wave heights for large cumulative exceedance probability.

Næss

The Rayleigh distribution is as mentioned earlier considered to be conservative, the distribution proposed by Næss (DNV(2007)) is a bandwidth corrected Rayleigh distribution. The principle is to correct for the conservative Rayleigh distribution, and thus we have a wave height distribution that fits more realistically to data. The distribution from Næss is given in DNV(2007) as:

$$F_H(h) = 1 - exp\left\{-\left(\frac{h}{\alpha_H H_S}\right)^2\right\} \quad (37)$$

Where α_H is given as:

$$\alpha_H = \frac{1}{2}\sqrt{1-\rho} \tag{38}$$

The parameter ρ contains information about bandwidth effects, and is typically in the range of -0.6 to -0.75. For JONSWAP spectrum with a gamma equal to 3.3 the rho is equal to -0.73, and it is this value that has been used for calculations in this thesis.

Forristall

The wave height distribution proposed by Forristall (1978) is a Weibull distribution, and is based on buoy data from the Gulf of Mexico. From DNV(2007) the distribution is given as:

$$F_H(h) = 1 - exp\left\{-\left(\frac{h}{\alpha_H H_S}\right)^{\beta_H}\right\} \tag{39}$$

The parameter values are given from Forristall (1978):

$$\alpha_H = 0.681 \; and \; \beta_H = 2.126 \tag{40}$$

2.6 Similar model tests

In order to verify the results obtained from our model test, it is of great interest to compare the results with those obtained from similar model tests. To accomplish this, a literature search where preformed.

Nilsen (1997) presents a model test in a facility with similar dimensions as “lilletanken”, with a beach with the exact same slope (1:20) and a water depth in the same order of magnitude. Memos (2002) have also presented results from this model test.

Nwogu (1993) preformed a model test in order to compare results with his attempt to expand the validity of the Boussinesq equations. The model test performed in this paper is performed in a tank smaller than “lilletanken”, and a slightly smaller slope (1:25).

Wei et.al. (1999) have also performed a model test to verify calculations with the Boussinesq equations. The facilities are similar to that of Nwogu (1993), but the tank is longer and the slope is slightly smaller (1:20).

3. Description of present model test

3.1 Background

The transformation of waves from deep to shallow water is a complicated process, where different nonlinear interactions will be of importance. In order to study the phenomena in detail a model test can be a very helpful tool. With respect to the scope of this thesis the results from such a model test will be used in order to investigate how statistical parameters, wave spectrums and distributions are affected by the transformation of the surface process. In our case there will be interesting to compare the results obtained with similar model tests, and see if we get similar results. It will also be used to see if the transformation can be dependent on nonlinearity parameters such as the wave steepness and Ursell number. Furthermore such a model test gives the opportunity to verify previously suggested theories for various subjects. As the scope of this thesis is the transformation of the waves itself, the present model test will only be related to the waves. Thus the model in this model test will be the beach, and the only quantity that will be measured is the surface elevation of the waves at different water depths.

3.2 Facilities

The model test was performed at “lilletanken”, NTNU. Which are 25 meters long, 2.8 meters wide and 1 meter deep. Inside the tank a channel was built, 1.2 meters wide 17.02 meters long and 0.83 meters deep. Furthermore this channel has the capability of being raised in order to achieve a constant sloping beach. The slope used in the present model test is 1:20, which corresponds to an angle of 2.8 degrees. The channel is illustrated in Figure 9, here in an inclined position.

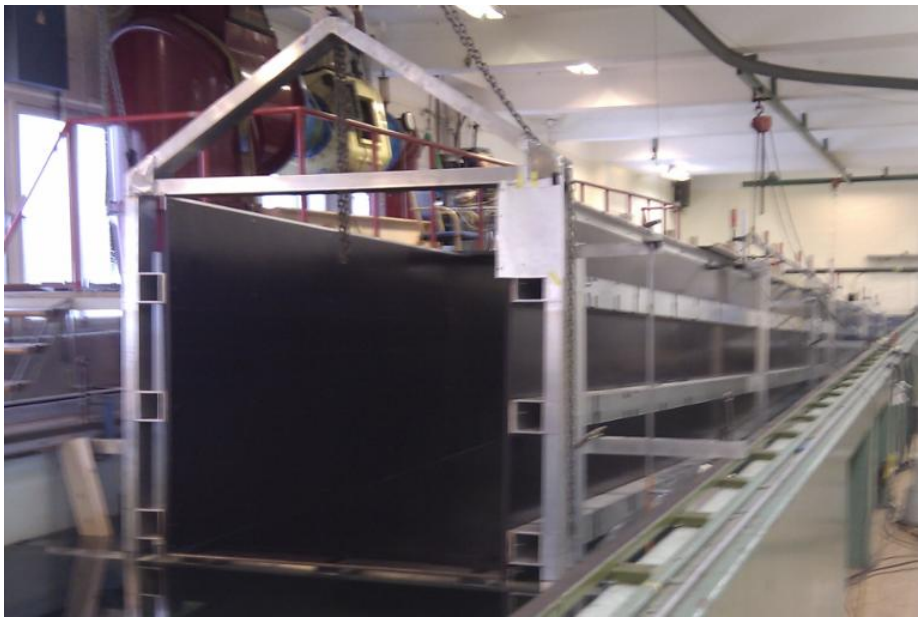

Figure 9: The channel in “lilletanken”

The model tank is equipped with a wave maker which can produce regular and irregular waves form a JONSWAP specter with the built in software. The software allows the use of pre generated time series from a binary file, as input to the wave maker.

A towing wagon is also available in the tank, but this was not used in our model test.

3.2.1 Wave probes

In this model test we have 16 wave probes at our disposal, where two of them are placed on the flap of the wave maker measuring the surface elevation along the flap as the waves are generated. The first one of these is taped like wave probe, where a metal strip is glued along the surface of the flap on the wave maker. This wave probe is however seen to produce some strange results, and these will not be considered in this thesis. The other wave probe positioned on the flap of the wave maker, is a conventional type of wave maker, and is similar to the rest of the wave probes used in this model test. An example of such a wave maker can be seen in Figure 10. Furthermore the position of the flap on the wave maker was also measured by a displacement sensor. The sampling frequency for the wave probes and the sensor where set to 100 Hz.

In general these wave probes work by measuring the voltage trough two metal bars, and by calibrating the probes by forcing a given displacement and then measuring the output voltage. There can then be found a relationship between displacement and voltage output from the wave probe. The signals measured from the wave probe is then sent to an amplifier before it is directed to a computer, in which the software converts the measurements from voltage to meters of surface elevation. The setup of the equipment and calibration have been performed by experienced lab technicians from Marintek and will not be discussed in further detail in this thesis, the interested reader is referred to Steen et.al. (2010) or Dean et.al (1991) for further details regarding wave probes and a detailed description of how these work.

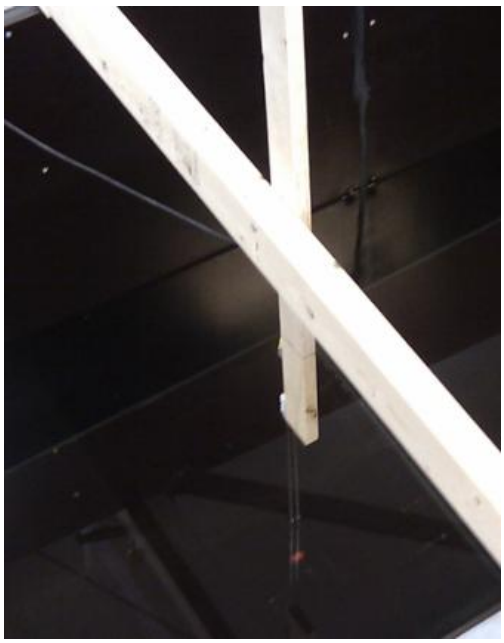

Figure 10: Wave probe

The setup of the wave makers have been changed a couple of times during the model tests, initially the tests were performed on a flat bottom and then the wave probes were equally spaced

throughout the channel (WP setup 1). For the tests performed in the inclined position, the wave probes were positioned according to water depths of interest corresponding to full scale water

depths in the region 40-15 meters (WP setup 2). Finally the wave probes were concentrated around an area corresponding to a full scale water depth of 25 meters (WP setup 3).

The numbering of the different tests is related to which set up of the wave probes that has been used for that particular test, a description of this is given in Table 1. For sketches of the different case setups, the reader is referred to Appendix A where these can be found.

Series	Description
1100	Flat bottom, WP setup 1
2100	Sloping bottom, WP setup 2
2200	Sloping bottom, WP setup 3
2300	Slping bottom, no wave probes

Table 1: Series description of irregular waves.

3.3 Test program

As mentioned earlier in this chapter the focus in this thesis will be on irregular waves on a sloping bottom, however also irregular waves on a flat bottom are useful for comparison. In addition, tests with regular waves and wave packets Clauss et.al. (1986) on both flat and sloping bottoms have been performed. In Table 2 there are listed the numbering of the different tests with irregular waves that have been performed. Similar tables for regular waves can be found in Appendix B.

As there is no physical model in this model test we have more freedom regarding the scale of the tests. The only thing depending on the choice of scale (accept for the waves itself of course) is the water depth. For practical reasons regarding the water depth the model scale was set to 1:81.

The most interesting sea states for our purpose will be sea states that correspond to ULS and ALS conditions in deep water. ULS conditions in deep water correspond to the specifications for xx11 and xx15 in Table 2. Similarly the ALS conditions in deep water correspond to xx12 and xx16 in

	Hs [m]		Tp [s]	
Test nr.	Model s.	Full s.	Model s.	Full s.
xx01	0,015	1,22	0,8	7,2
xx02	0,030	2,43		
xx03	0,045	3,65		
xx04	0,060	4,86		
xx05	0,025	2,03	1	9
xx06	0,050	4,05		
xx07	0,075	6,08		
xx08	0,100	8,10		
xx09	0,035	2,84	1,25	11,25
xx10	0,070	5,67		
xx11	0,105	8,51		
xx12	0,140	11,34		
xx13	0,035	2,84	1,5	13,5
xx14	0,070	5,67		
xx15	0,105	8,51		
xx16	0,140	11,34		
xx17	0,035	2,84	1,75	15,75
xx18	0,105	8,51		
xx19	0,140	11,34		

Table 2: List of test sea states

Table 2.

As for repetitions of sea states the ULS and ALS sea states have been the main focus, and most of the repetitions have been performed for these sea states. But for comparison reasons there have also been included test cases for smaller sea states. For similar reasons there have also been included some tests with longer peak periods, as these are expected to show clearer signs of depth induced effects, as the relative water depth will be lower.

3.4 Observations during the test

At first we started performing tests with a flat bottom. The reason for this is to have some references with respect to the surface process for the sloping bottom, since both spectra and probabilistic distributions may change along the channel even for a flat bottom. The position of the wave probes was in this case positioned as presented in Appendix A (WP setup 1). At this stage we also encountered some problems with the wave maker, where there was observed some strange “shut downs” of the wave maker. This was seen in the time series measuring the position of the wave maker. What we see is random shutdowns in some areas. However when the error was identified as outdated software in connection with transfer of control signals from the wave maker computer, the problem was solved fairly quickly. And we have not observed this behavior in any later stages of the model test.

What was observed when running tests with a flat bottom, a chaotic behavior at the end of the channel. This was especially noticeable for the tests with the longest periods, and the explanation is simply the limitations of the beach designed to damp reflexes from incoming waves. Thus the beach does not work properly for waves with long periods. And due to this chaotic behavior we can say with a reasonable degree of certainty that the results obtained from the two wave probes closest to the end of the channel, are clearly influenced by reflected waves. This is most noticeable for the regular waves, but it is likely that reflected waves also influence the results for irregular waves. However for irregular waves it is more difficult to see this visually. As a consequence of the presence of these reflexes, the data from the tests performed with a flat bottom should be used with care. For a case with a sloping beach there are obviously reflexes that will interfere with the results, but these reflexes will be present in a natural situation where a wave propagates towards a beach, and we can then say that the behavior for the tests performed with a sloping beach will give a realistic “image” of the situation.

During the start of the tests we experienced some resonant like behavior of the channel, this was especially noticeable for regular waves with a period of 1.5 s. This was corrected by stiffening the channel with diagonal braces.

When we raised the channel to the inclined position, the wave probes where moved to the positions described in Appendix A (WP setup 2). This was done in order to get measurements from water depths related to the most interesting in our case, which is in the area of 40-15 meters in full scale. During this process it was also decided to increase the model scale from 1:144 to 1:81, since the scale we initially intended to use would give model scale water depths that are difficult to get good results from. The results were only analyzed roughly during the tests, but both the time series and statistical properties seem good at this stage. Where the waves clearly becomes more asymmetrical

(crest/trough) as they propagates, and this was also the case for the statistical values of skewness and kurtosis, which will be described further in chapter 4.1.

Then the wave probes where moved closer together around the full scale water depth of 25 meters, and we tried to capture a breaking wave with the use of a wave packet Clauss et.al. (1986). The setup of the wave probes can be seen in Appendix A (WP setup 3). The idée behind this approach is to generate waves with different periods and amplitudes, initially waves with a small celerity followed by waves with a larger celerity. And they will then coincide in a focus point and become a large wave. This approach is however made for deep water waves, and have not accounted for any transformation of the waves as they propagate towards shallower water, which will happen in our case. And due to this we experienced some problems when we tried to focus a large wave in the region where the wave probes had been placed. Examples of this were too steep waves due to shoaling, which would break before they reached the intended position. Due to the differences in celerity in shallow water for the different frequency components, this caused the wave packet to miss the focus point entirely. The largest problem by far was the effect from shoaling, and we had to increase the peak period significantly in order to get a wave packet that did not break before the focus point. But after some trial and error we managed to achieve a quite large breaking wave within the area of the wave probes.

At the end of the model test we did some runs without wave probes, where we repositioned the video camera in order to capture the behavior of the waves in a larger area of the channel.

3.5 Uncertainties

For the runs preformed with the flat bottom, there were as mentioned earlier observed some chaotic behavior at the end of the channel. We can say from visual observations from tests with regular waves that reflections from this behavior clearly will influence the measurements for the two closest wave probes (WP 06 and WP 07), but we cannot rule out that the reflexes also interfere with wave probes further from the end of the channel, but this was not observed visually. This is also the case for the runs with irregular waves, where this could not be seen visually, but most likely still is present for the wave probes close to the end of the channel. So the results from these runs should be handled with care.

It has been observed that the wave maker is not perfectly calibrated, this is especially clear for the regular waves where the input wave height deviates from the measured wave height the wave maker produces. However this is not a very serious error, we only have to be aware that input into the wave maker does not correspond to the exact size of the measured waves, and then use the measurements before the wave transformation as the reference. The wave periods are unaffected by this, thus the measured periods are equal to those specified as input to the wave maker.

For runs with irregular waves the input to the wave maker is a JONSWAP spectrum with a peakdnesskoefficient of 3.3, and it is seen from the resulting spectral estimates that this is not what the wave maker generates. However this is not a major concern, since we have wave probes close to the wave maker which will measure the generated waves before the wave transformation occurs. Thus we will have a reliable reference at these wave probes, and since it is the transformation that is of interest and not that the wave makers ability to generate the exact waves we have specified, this

should not be any critical error. But it is important to be aware of that it is the measurements close to the wave maker that has to be used as a reference and not the specific input to the wave maker.

There was observed diffraction from the structure at the start of the channel, as the waves entered. And there was created some small disturbances, however they do not seem to be of any great significance for the results. Visually the waves propagating through the channel seem to be almost perfectly in 2D, but after a while the surface is disturbed by some small waves which may seem like short crested sea. But the magnitude of this disturbance is not of much significance for the final results, since the size of these waves are in the order of magnitude of a couple millimeters.

The water level in the towing tank was not constant for the entire duration of the model tests, however the variation was small. The largest problem associated with this was that the wave probes where positioned in order to capture the surface process at water depths corresponding to water depths of interest in full scale (in the region of 40-15 meters). And small errors here corresponds to large errors in the full scale water depth, but the water depths of the wave probes have been checked and they were within a reasonable margin of error. There was a deviance of approximately 3-5 mm in the worst cases.

Since the maximum water depth in the tank is 1 meter, the longest deep water waves that can be run are waves with a period of 1.13 seconds. And thus a lot of our tests which initially should have started in deep water, really starts of on an intermediate water depth. The transformation of waves from these tests will then only be from intermediate to shallow water, and not from deep water. Not really a major concern, but important to be aware of when post processing.

The effect from breaking waves in model scale will not be the same as in full scale, since the capillary effects will be much more dominating in model scale. And it is not certain that the energy dissipation in model scale wave breaking will be comparable with that of a full scale event, since the behavior of the dissipation due to wave breaking cannot be Froude scaled.

4 Data analysis and discussion

As the amount of data from the present model test is large, the tests that are analyzed in this chapter are limited to ULS (test2111 and test2115) and ALS (test2112 and test2116) conditions. But for comparison reasons there have also been included more moderate sea states (test2109 and test2117). As a longer peak period will give a lower relative water depth at the position of the wave probes, thus more noticeable shallow water effects, there have also been included results for large sea states with a longer peak period (test2118 and test211).

4.1 Statistical properties and statistical parameters

4.1.1 Estimated significant wave height (Hm0)

From the model test results the significant wave height has been calculated at each wave probe from the measured time series. But as mentioned earlier the input significant wave height deviates from the measured one, this is however not a big problem as it is the change that is of interest and not the wave makers ability to reproduce the specified input. This is however noted, and could have been avoided if the wave maker where calibrated before the model tests started. The specified peak period however remains the same as the one measured. In Table 3 the mean of the estimated significant wave height at wave probe 2 is presented for the different tests along with the input parameters.

	Input		Measured
Test nr.	Hs	Tp	Hm0
2109	0,035	1,25	0,047
2111	0,105		0,130
2112	0,140		0,162
2115	0,105	1,5	0,114
2116	0,140		0,147
2117	0,035	1,75	0,032
2118	0,105		0,097
2119	0,140		0,127

Table 3: Input and measured significant wave height

Effects from shoaling are expected to influence the results for the significant wave heights, and important dissipation effects such as wave breaking and bottom friction will also be considered. The effect from shoaling will be dependent on the relative water depth (h/λ) and the increase in the wave height will not be of great significance before it enters shallow water ($h/\lambda >= 0.05$), and thus be most noticeable for the tests with the longest wave periods. The general effect from shoaling will however contribute to the waves from the deep water limit, and will until a relative water depth of approximately 0.2 contribute to decrease the individual wave heights with almost 10% according to the theory of linear shoaling, according to Svangstu (2010). This is also the case for bottom friction, where it is considered as an effect that will be of importance in shallow water. Also remembering that bottom friction only should give noticeable contributions over longer distances.

As the waves propagate towards shallow water shoaling will contribute to increase the wave height, this will cause the steepness to increase. But also the decreasing wavelength in shallow water as a result of dispersion will contribute to increased steepness. From the time series it can also be seen that the wave profile grows asymmetrical with respect to the crest and trough of the wave, as a result of nonlinear effects. The presence of such asymmetry in the wave profile will cause the maximum angle of the wave profile (steepness) to be larger than that of the analytical expression (kA or H/λ) gives for linear waves, thus the wave steepness will be larger as the wave profile grows asymmetrical with respect to the crest and through of the wave. Eventually the increase in the wave steepness will cause the waves to waves to break, thus causing the dissipation and a decrease in the significant wave height.

The figures presented in this chapter are significant wave height plotted against the relative water depth, and thus the waves travel from right to left.

The comparisons between different model tests have been done by first comparing tests with the same peak period.

Tp=1.25 seconds

The lowest peak period from the tests of the most interest is 1.25 seconds. The Figure 11 shows test 2109, which has a significant wave height of 0.047 meters. This is a model test with a low steepness and wave breaking was observed to appear far beyond the wave probe closest to the beach, i.e. no wave breaking appeared before the waves had passed the last wave probe. Thus the behavior of the significant wave height in this test is only affected by bottom friction and shoaling. From Figure 11 it is seen that the wave height initially drops and then the curve flattens out, the most probable cause for this effect is a result of shoaling of the waves. As this effect is seen to reduce the wave height in intermediate water depths, before it starts to contribute to an increased wave height at a relative water depth of approximately 0.2. The presence of bottom friction cannot be neglected on the basis of this figure, but as the waves have not traveled over a large distance it seems unlikely to the author that there are any significant contributions from bottom friction.

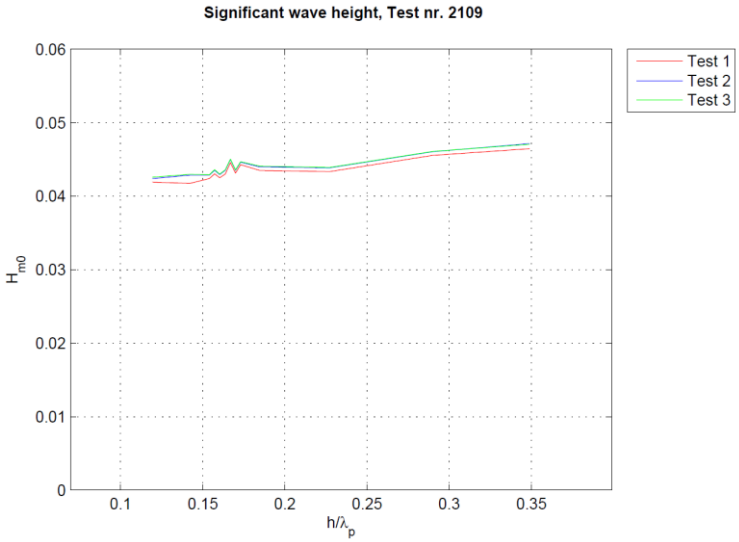

Figure 11: Measured significant wave height for test2109

In Figure 12 tests with the same period as in Figure 11 can be seen. The measured significant wave height at the entrance of the channel (WP 02) is 0.13 meters. This is a fairly steep sea state and it was observed that the largest waves break as they came out of the wave maker, in the area around the first wave probe. This was also the case for the largest test with the same period, which can be seen fin Figure 13, thus some care should be taken concluding that the significant drop in the wave height in the start of the channel only is a contribution from shoaling. As there probably are significant energy dissipation contributions from wave breaking at the two wave probes at the start of the channel. But further down the channel much of the same behavior as for test2109 can be seen. Where the wave height decreases, flattens out and then starts to increase. And it seems reasonable that this is a result of shoaling.

At the end of the channel it is observed that the significant wave height decreases, this is most likely due to depth induced wave breaking, as this was observed visually in this area during the model tests.

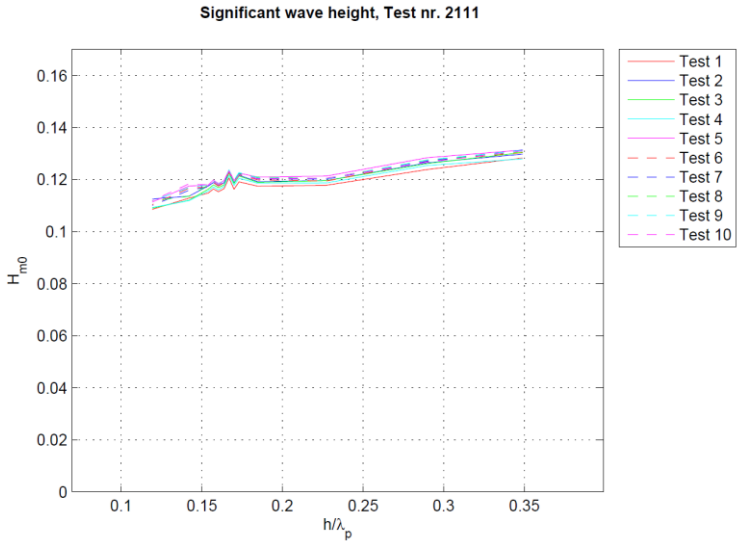

Figure 12: Measured significant wave height for test2111

In Figure 13 the significant wave height is 0.162 meters. Much of the same trend as in Figure 12 can be seen, however the wave breaking seems to appear earlier in the channel, which coincides with the visual observations from these tests. With steeper and higher waves this seems realistic, and

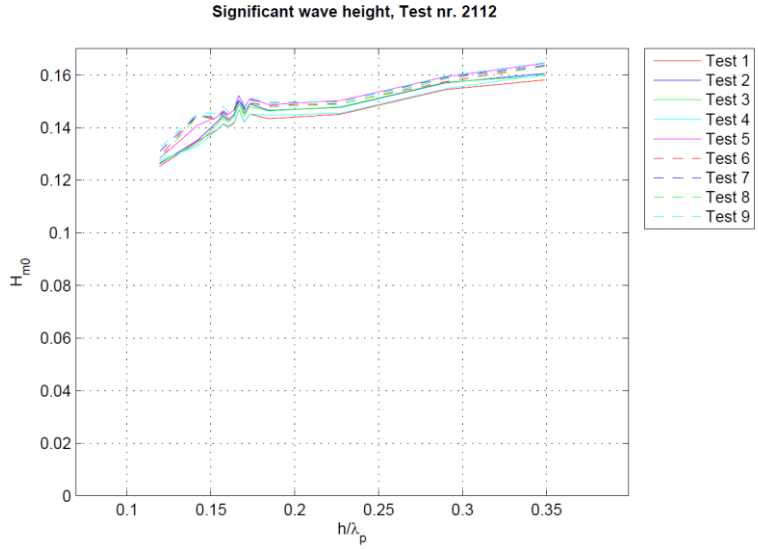

Figure 13: Measured significant wave height for test2112

since they break earlier the drop in the significant wave height can be seen more clearly in the figure. Further at the start of the channel it may seem that the decrease in the wave height is slightly larger than that of Figure 13, which can be explained as this sea state have larger waves then test2111 and thus depth induced wave breaking will appear in deeper water making the effect more visible for this case.

Tp=1.5 seconds

From the tests with a peak period of 1.5 seconds one should expect that the effects from both shoaling and bottom friction should be of more significance. The longer period means a larger wave length and thus that the wave has more contact with the bottom with respect to particle kinematics, i.e. larger particle velocities at the sea bottom resulting in a larger contribution from the bottom friction. As the wavelength is longer the relative water depth will be smaller at the positions of the wave probes, and thus the effect from shoaling will be more visible. In general the wave breaking should also be more frequent at larger water depths, but in shallow waters the wave breaking is not only dependent steepness but also the relation between the wave height and water depth. However the only noticeable effect of a larger wavelength is that the effect from shoaling becomes more visible. But as an increased wavelength will also contribute to smaller initial wave steepness, that may explain the smaller drop in the wave height close to beach in the tests with a peak period of 1.5 seconds. An example can be seen in the Figure 14, where the significant wave height is presented for test 2116 which has a measured significant wave height of 0.147 meters at the first wave probe.

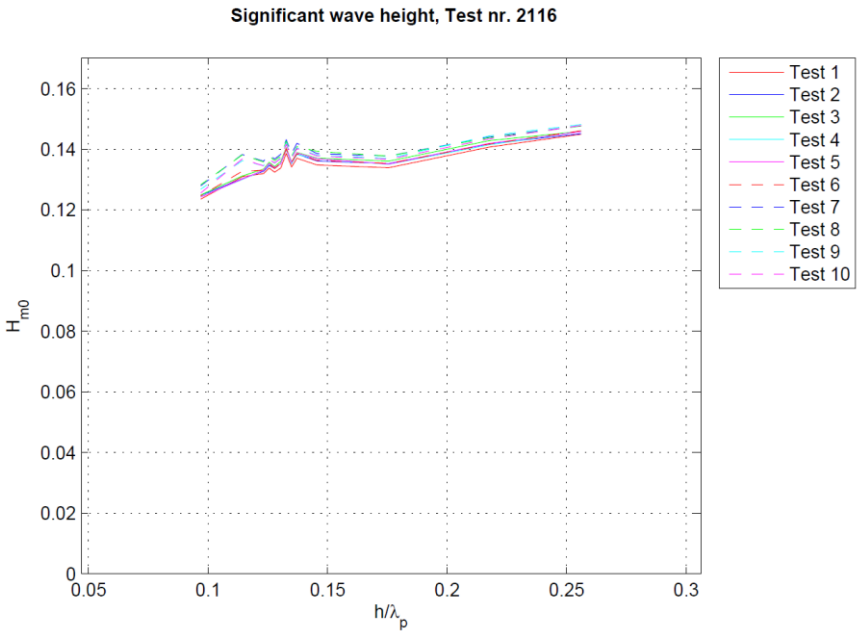

Figure 14: Measured significant wave height for test2116

Tp=1.75 seconds

The tests performed with a peak period of 1.75 seconds have not been repeated as many times as the previous tests, but there have been included some tests for comparison. What we see in these tests are a much clearer increase in the significant wave heights which is caused by contributions from shoaling, further a smaller initial wave steepness seem to reduce the amount of dissipation from wave breaking. An example of this can be seen in Figure 15, where the measured significant wave heights for test2119 with corresponding repetitions are presented.

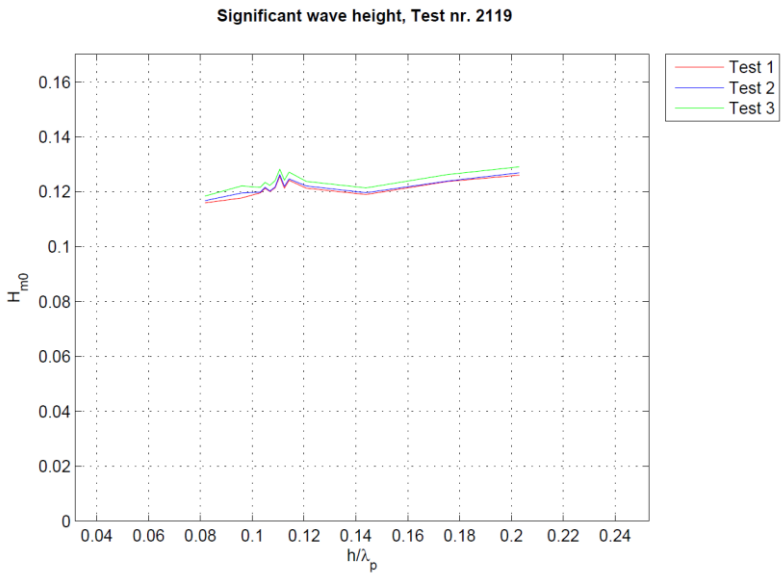

Figure 15: Measured significant wave height for test2119

Summary of observations

To summarize the different tests, the mean of the significant wave height for the different have been plotted, and can be seen in Figure 16.

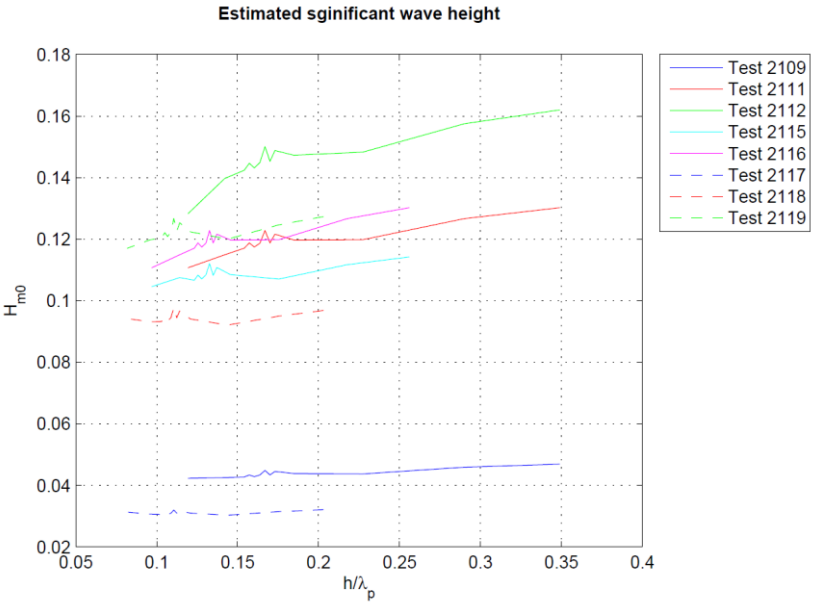

Figure 16: Summary of measured significant wave height

For the tests with large initial wave steepness it is seen that there will be a significant drop in the significant wave height due to wave breaking in the first part of the channel. It is also seen that shoaling seems to reduce the wave heights for the first part of the channel, before it is increased by the same effect when the waves approaches shallow water.

As bottom friction is an effect that is of importance in shallow water over longer distances it seems unlikely that the effect makes a significant contribution to energy dissipation in this model test. As the area where bottom friction will contribute only will be over a couple of wave lengths at most.

Comparison with previous work

From the model test which is presented in Nilsen (1997), the measured values of the significant wave height remains fairly constant. And it is augmented that the shoaling effect is canceled out by the effect from bottom friction for the wave probes closest to the beach. When comparing between our model tests it is worth mentioning that the sea states used in our model test often is quite steeper than those presented in Nilsen (1997). The cases who are fairly close to our test cases are the ones used for comparison. The setup of the wave probes is different, where the wave probes in the present model test are s positioned at shallower water depths. The shallowest water depth measured in Nilsen (1997) is 31 cm, and our shallowest water depth is at 18.5 cm (model scale). The result of this is that there are no measured significant wave height measured in Nilsen (1997) below a relative water depth of 0.14, and it is in this area that the wave breaking is indicated in our results, thus the results can only be compared with effects from shoaling and bottom friction. A clear deviation between the two model tests can however be observed, and the clear deviation is that our model tests has a clear drop in the significant wave height at the start of the slope, whereas the tests in Nilsen (1997) show a more or less constant value at this point. The most reasonable explanation for this is the difference in the steepness of the different tests. Where our tests as mentioned earlier are observed to break frequently at the start of the channel, which should cause a significant drop in the wave height. The observations from Nilsen (1997) comments that wave breaking only is observed sporadically. When comparing test 2109 as a test with low steepness we get the same trend in Nilsen (1997), as the wave height decreases slightly and almost linearly as the depth decreases.

The model test performed in Wei et. al. (1999) has wave probes in even shallower water than in our model test, and there is included a figure in the paper where the standard deviation is plotted versus the water depth. Remembering that the significant wave height is equal to 4 times the standard deviation, the shape of the curve should give a good comparison. The peak period from this model test is 1 second, thus a shorter period than the cases analyzed in our model tests. But the general shape of the curve should still be comparable. What can be seen is that the standard deviation decreases slightly before there is a significant drop and the wave height goes towards zero. The start of this significant drop is seen to appear at a relative water depth of approximately 0.14-0.11. Since the depth induced wave breaking is dependent on the wave length we cannot compare our results directly against this model test, but it shows that the trend appears to be in the same order of magnitude. The comparison can be seen in Figure 17.

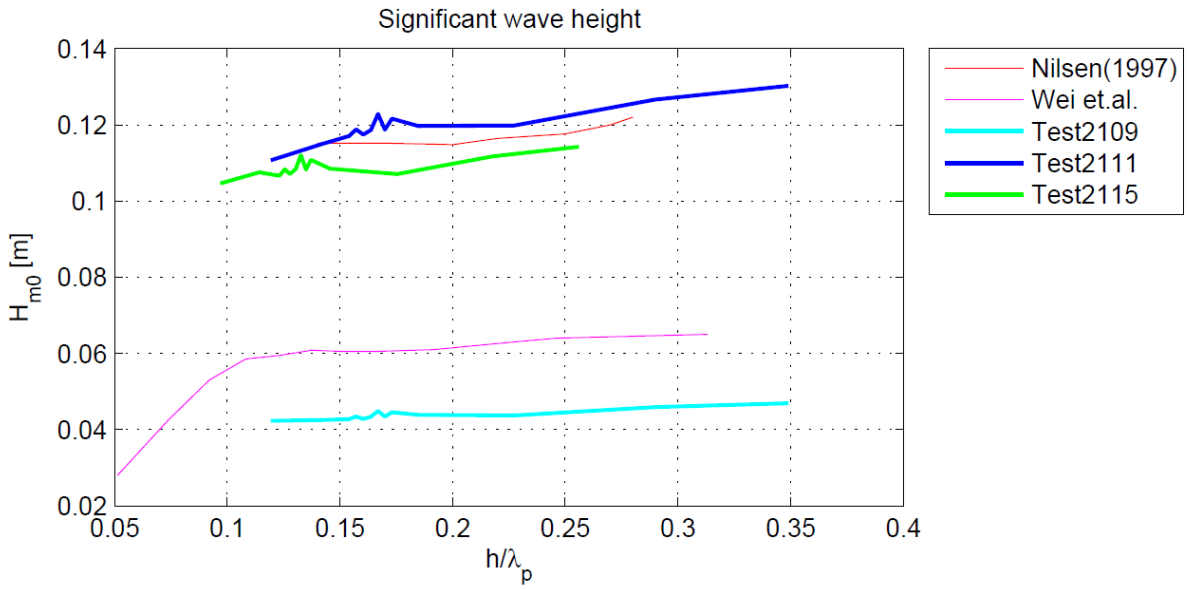

Figure 17: Comparison with measured significant wave height for similar model tests

4.1.2 Skewness

The skewness has been estimated from each of the time series measured from the wave probes for each test. And the general trend is that the skewness increases as the water depth decreases. The results are presented in terms of relative water depth and nonlinearity parameters as the wave steepness and Ursell number.

From all the tests we see that the skewness grows as the water depth decreases. Figure 18 shows the mean of repetitions for the tests in question, for relative water depths. The relative water depth is based on the assumption that a representative wavelength of the time series is the wavelength corresponding to the peak period, it is also assumed that the waves follow the linear dispersion relation.

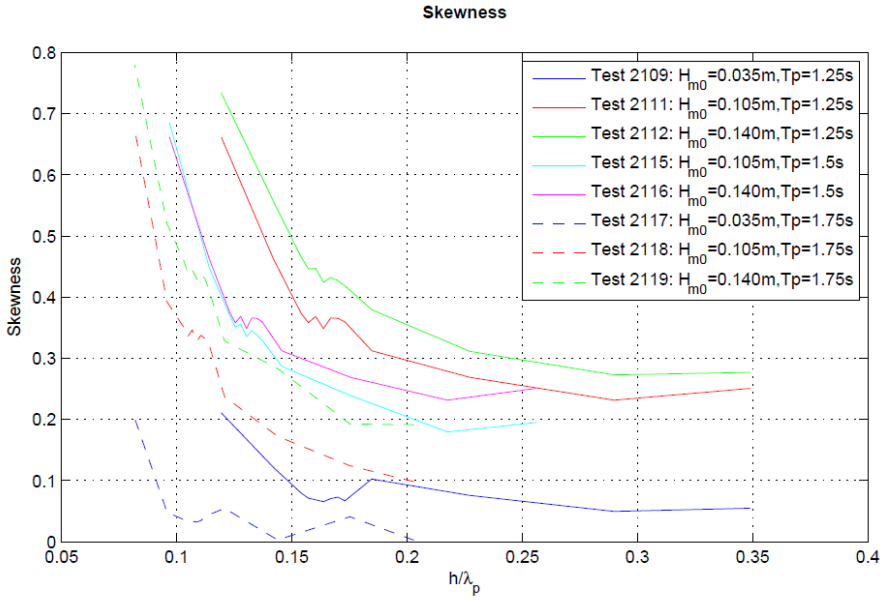

Figure 18: Skewness against relative water depth

The trend is that the skewness grows slowly at the start of the channel, before it grows exponentially when it comes close to the shallow water limit. In general we can say that the skewness is seen to increase with decreasing water depth, and that the increase is exponentially when the waves approach the shallow water limit (h/λ_P =0.05).

Goda (2010) proposes that the change in the skewness coefficients for waves in deep water is proportional to the wave steepness. In order to investigate how this change as the waves propagates towards shallow water, the skewness has been plotted against wave steepness for the tests in question. Another interesting parameter in this respect is the Ursell parameter, which is a general measure of nonlinearity in shallow water.

As mentioned earlier the skewness gives an indication of the crest to trough asymmetry from the measured time series, where a skewness larger than zero will indicate that the waves in the time series have larger crests and smaller through. As this asymmetry is caused by nonlinear interactions,

we can say that the deviation from a Gaussian process in terms of a skewness coefficient larger than zero will appear when nonlinear contributions are present in the surface elevation.

As a matter of form the different tests will be presented with those of corresponding peak periods.

Tp=1.25 seconds

The smallest test in this period band is test2109, which has a significant wave height of 0.047 meters. Figure 19 shows the skewness as a function of the wave steepness, and seems that a linear growth of the skewness is not far off the truth if we accept some degree of scatter.

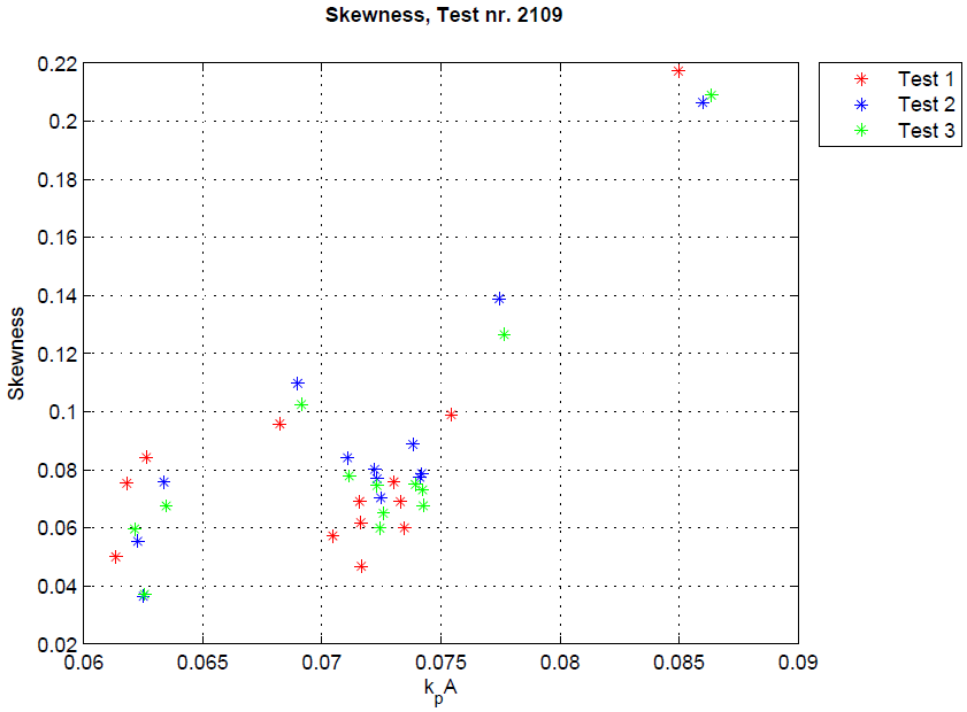

Figure 19: Skewness vs. wave steepness, test2109

In Figure 20 the skewness is shown vary linearly (approximately) with the Ursell number, here also if we accept some degree of scatter. For the low Ursell numbers in these curves it is noticed some significant scatter around a proposed linear fitted curve, the explanation for this might be that this are waves with small nonlinearity. According to Svangstu (2010) the limitation of linear theory can be applied for waves with a steepness up to 0.05-0.1 (kA). It seen from Figure 19 these waves can be described by linear theory, and thus that the waves are linear. And it is then not surprising that an attempt to quantify the skewness of linear waves with a nonlinearity parameter gives somewhat strange results. For higher Ursell numbers in Figure 20 it may seem that we have an linear relation between the skewness and the Ursell number, but before drawing that conclusion the reader should notice that Ursell number jumps significantly between the second to last and the last wave probe. And in order to say anything certain about the behavior in this region we should have had wave probes measuring the skewness between these two wave probes. However it seems from these measurements that as the waves propagate towards shallow water, they grow in nonlinearity and that a significant change can be seen in a region where the wave steepness is roughly 0.075. And that

the skewness for the purposed nonlinear waves seems to grow proportionally with the Ursell number, while increase in skewness for the linear waves is not well described by the Ursell parameter.

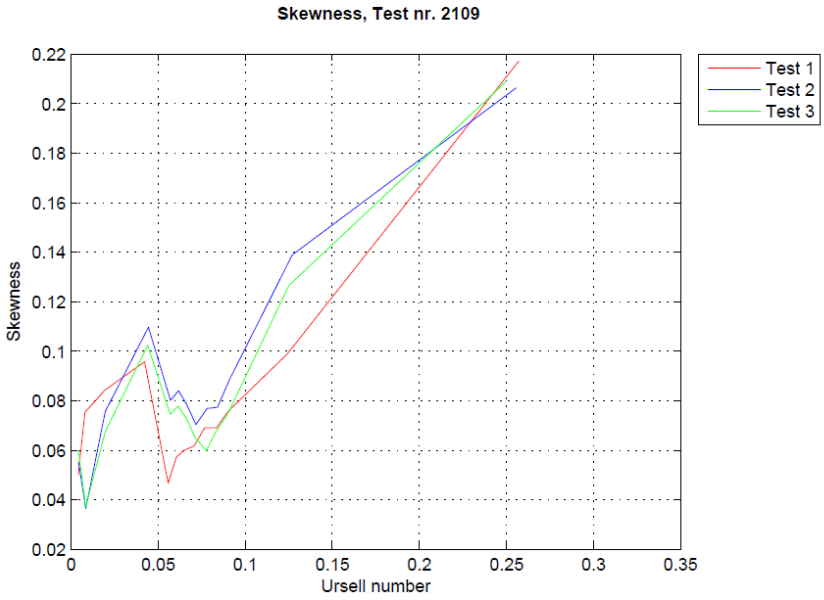

Figure 20: Skewness vs. Ursell number, test2109

From Figure 21 the skewness for test2111 can be seen, this test has a significant wave height of 0.13 meters. It can be seen that the skewness the wave steepness with a nonlinear relation. It is worth mentioning that the skewness coefficients for a steepness smaller than 0.21, is proportional to the wave steepness. Further the steepness indicates that the waves are far beyond the reach of linear wave theory, and thus are nonlinear.

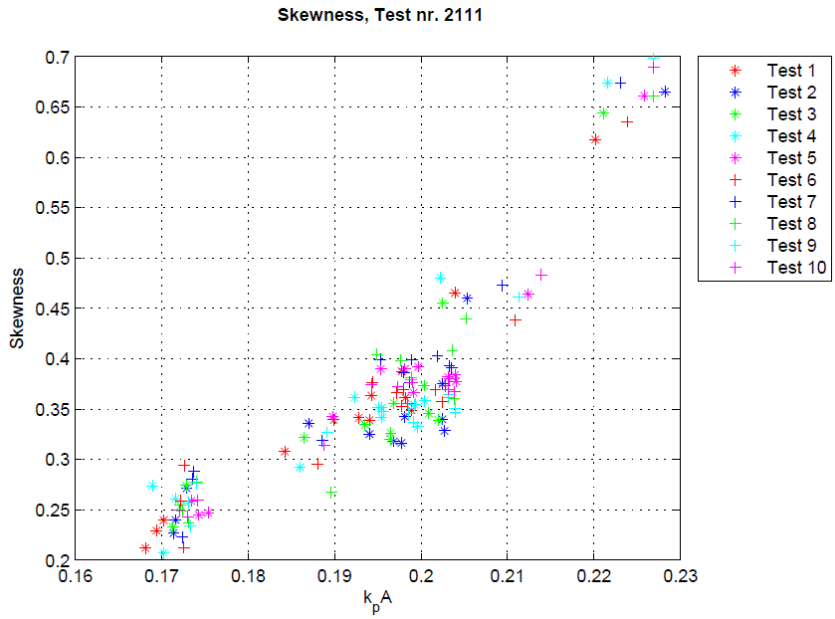

Figure 21: Skewness vs. wave steepness, test2111

In Figure 22 the skewness is plotted against the Ursell number, in this case it can be seen that the skewness follows the Ursell number with a linear relation. This seems reasonable since this sea state is clearly a nonlinear process even in deep water, and thus is the nonlinearity shown in the skewness is proportional to the nonlinearity parameter given as the Ursell number. For the two last points in this figure (at Ur=0.4 and Ur=0.7) we have the same uncertainty as previously mentioned for test2109, where we do not have any verification of the behavior between these points. However since there have been performed so many repetitions for this test and since they coincide as well as they do, it seems like a reasonable explanation.

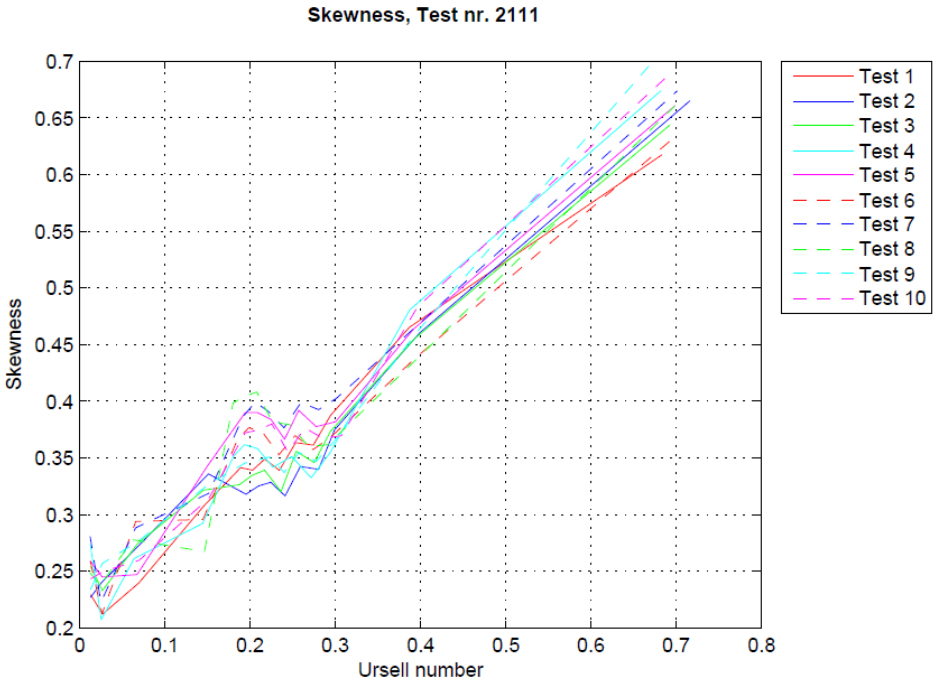

Figure 22: Skewness vs. Ursell number, test2111

Figure 23 shows how the skewness varies with the wave steepness for test2112. We can see that it also here seem to be a linear dependence up to a steepness of 0.25, but since this is higher than for test2111 there cannot be found a clear linear relation.

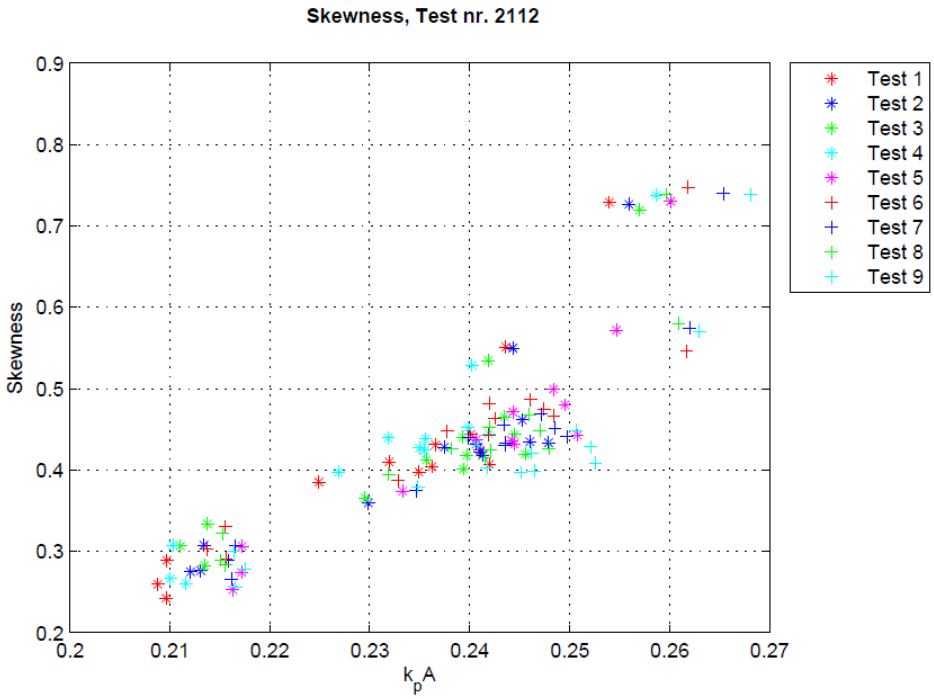

Figure 23: Skewness vs. wave steepness, test2112

This is a fairly steep sea state, and this is also confirmed from Figure 23, and it is seen in Figure 24 that this may to influence the dependence on the Ursell parameter. As there can be seen an almost perfect linear relationship between the skewness and the Ursell number.

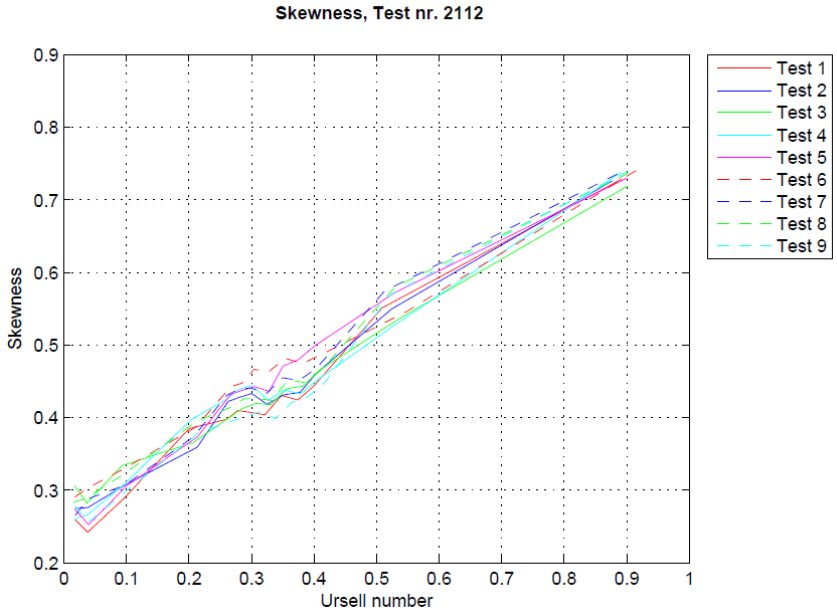

Figure 24: Skewness vs. Ursell number, test2112

Tp=1.5 seconds

In Figure 25 test2115 the skewness is presented as a function of the wave steepness, the significant wave height is 0.114 meters. Here we can observe that the trend is very similar to that of test2111 (seen in Figure 21), but the steepness values are lower in this case.

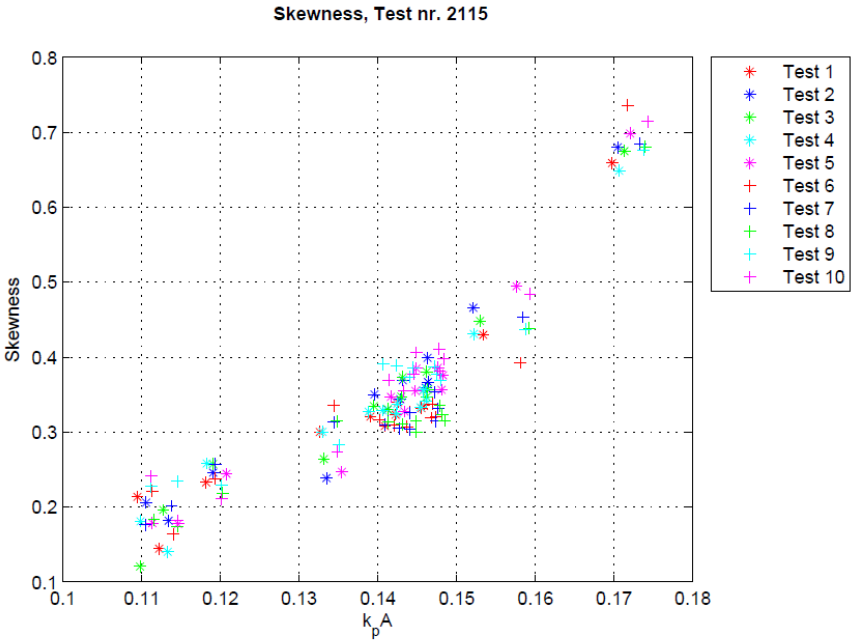

Figure 25: Skewness vs. wave steepness, test2115

This seems reasonable since the longer peak period corresponds to a longer wave length, and thus a lower initial steepness. Another interesting thing is that the wave maker seems to be able to reproduce a wave height close to the given input for this period band. This is not of great significance but it is mentioned as the wave maker seems to give a smaller significant wave height, for larger peak periods.

Figure 26 presents the skewness in terms of the Ursell number. The trend here is similar to that of the tests presented earlier in this chapter, that the skewness is proportional to the Ursell number.

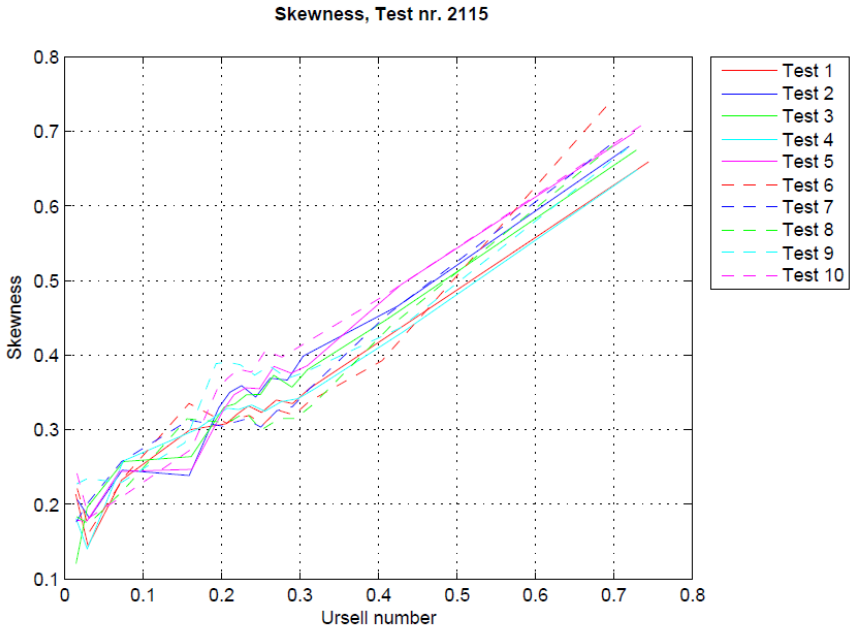

Figure 26: Skewness vs. Ursell number, test2115

In Figure 27 the skewness for test2116 is plotted against the wave steepness, the significant wave height for this test is 0.147 meters. The same is seen here as for the previous tests, where the skewness seem to be proportional to the wave steepness for the measured skewness corresponding to the lowest steepness. In order to fit all the data we can say that the skewness varies nonlinearly with the wave steepness.

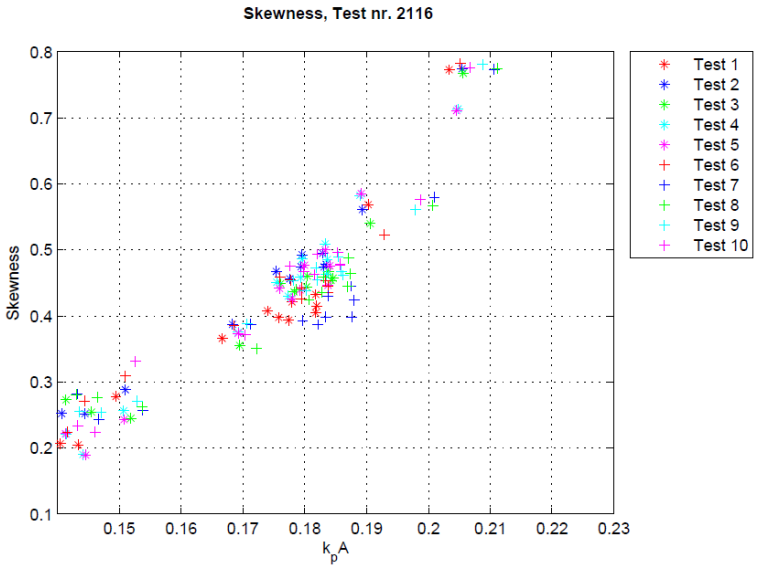

Figure 27: Skewness vs. wave steepness, test2116

Figure 28 shows how the skewness as a function of the Ursell number, and again it is seen to be a linear relation between the two. It is however that repetition number 5 (Test 5 in the figure) deviates

from the rest at the last point of the curve, however the magnitude of the deviation does not cause any great concern. A reasonable amount of scatter has to be accepted.

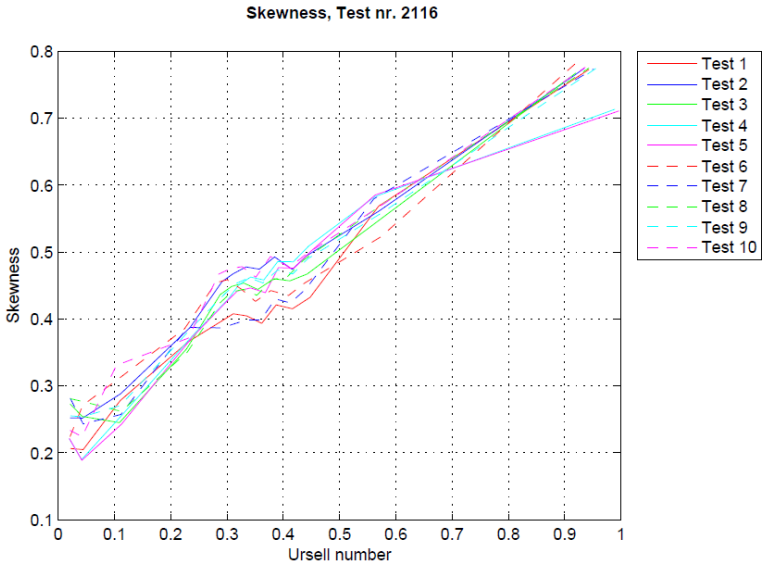

Figure 28: Skewness vs. Ursell number, test2116

Tp=1.75 seconds

In Figure 29 the skewness from test2117 is presented in terms of the wave steepness, the significant wave height for this test is 0.032 meters. The trend is that the skewness depends on the square of the wave steepness.

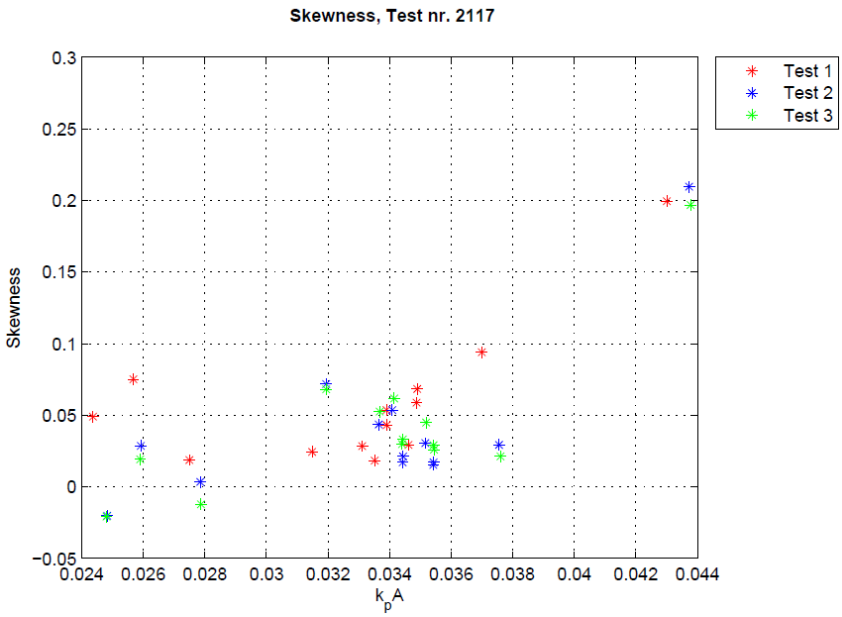

Figure 29: Skewness vs. wave steepness, test2117

Figure 30 shows that there is not a linear relation between the measured skewness and the Ursell number. This is probably due to the same reason as for test2109, where the wave steepness is within the limitation of linear theory. Thus the waves can be considered linear, and it does not come as a surprise that an attempt to quantify the growth of the skewness in terms of a nonlinearity parameter don't give linear relationship.

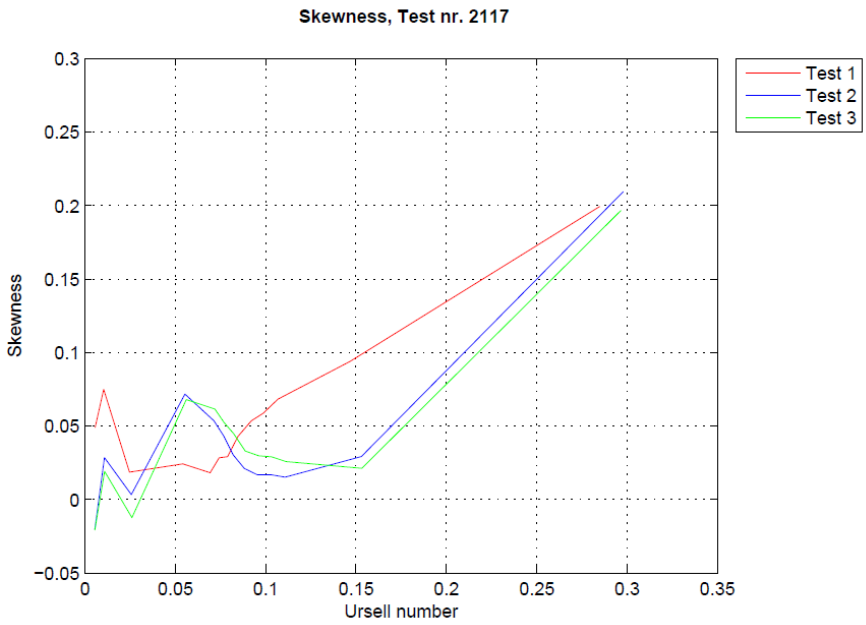

Figure 30: Skewness vs. Ursell number, test2117

In Figure 31 the skewness as a function of the wave steepness for test2118, where the significant wave height is 0.097 meters. The skewness is seen to proportional to the square of the wave steepness, and once again the skewness for the lowest steepness seems to be proportional to the steepness.

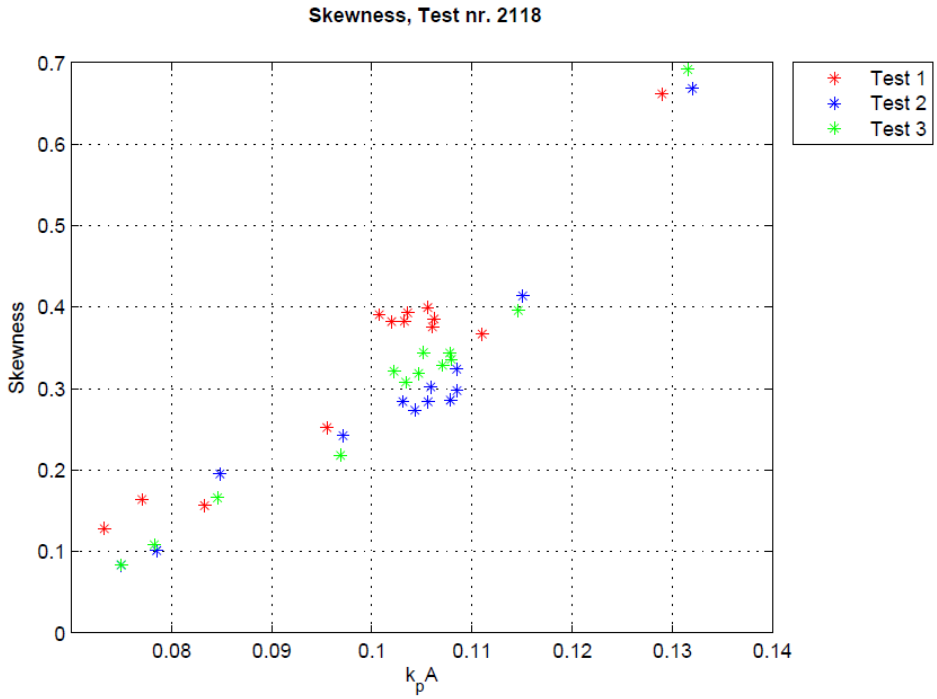

Figure 31: Skewness vs. wave steepness, test2118

Figure 32 shows that the skewness is proportional to the Ursell number.

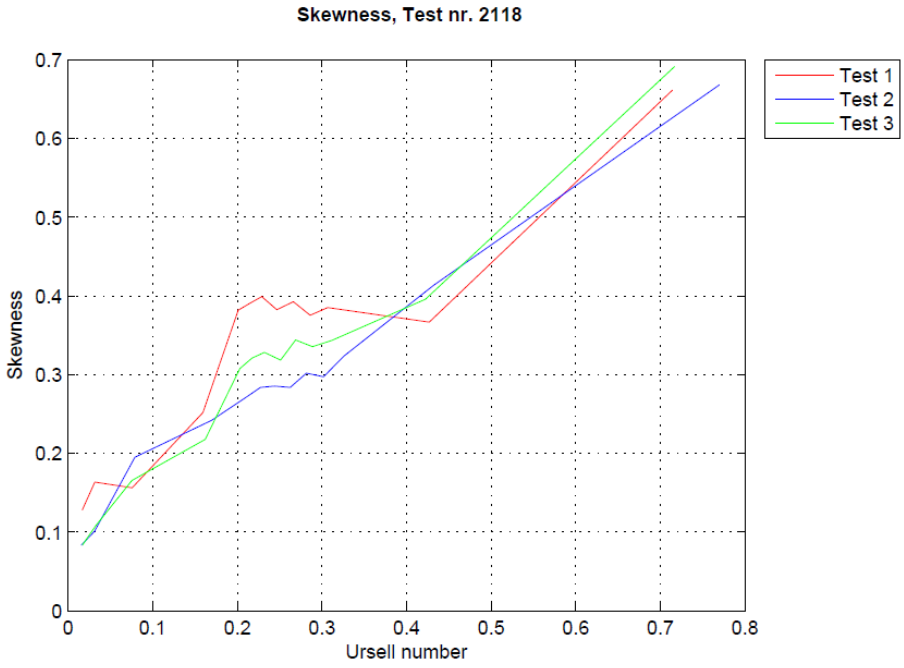

Figure 32: Skewness vs. Ursell number, test2118

In Figure 33 the skewness for test2119 is plotted against the wave steepness, this test has an significant wave height of 0.127 meters. Once again the skewness is seen to follow the steepness in a

linear relation for the lowest values of the steepness, but we need a nonlinear expression to the describe the behavior throughout the channel.

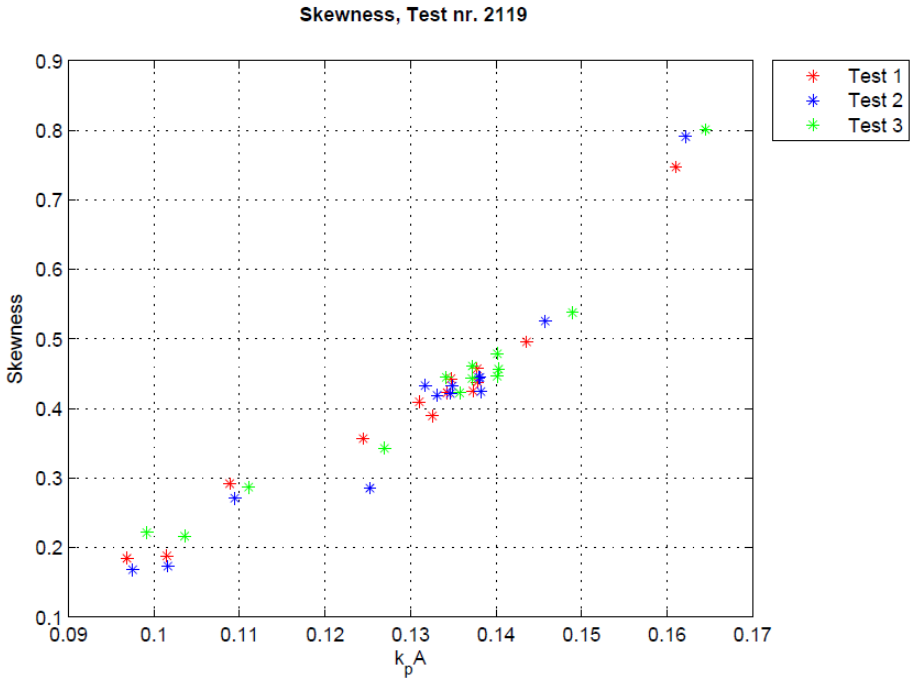

Figure 33: Skewness vs. wave steepness, test2119

Figure 34 shows that the skewness varies linearly with the Ursell number.

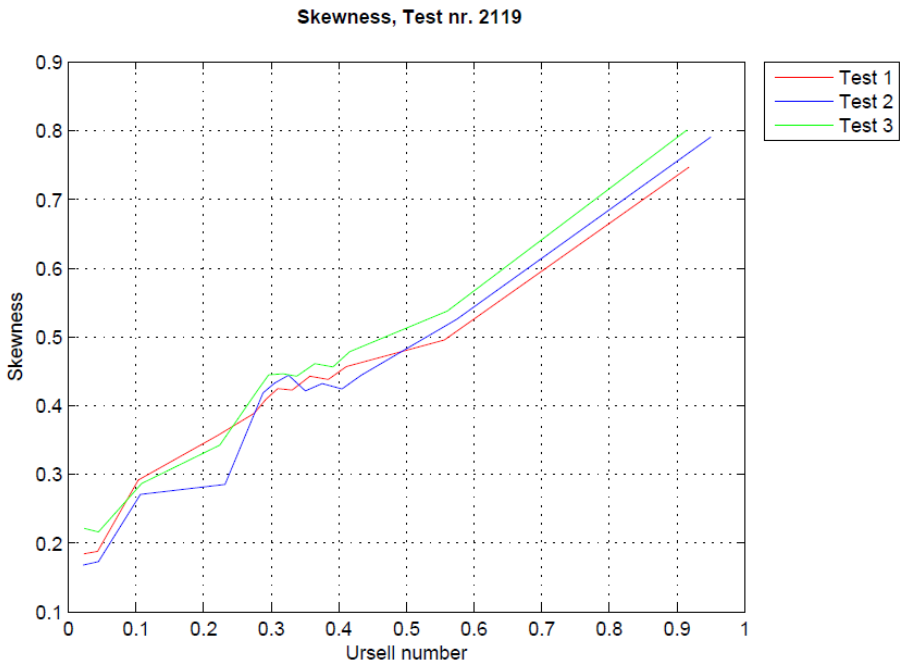

Figure 34: Skewness vs. Ursell number, test2119

Summary of observations

For the different tests the dependence on the wave steepness seems evident, for a large region in intermediate water depth. However as the water depth decreases further the relationship with the wave steepness is no longer linear. The explanation for this may be wave breaking, as this deviation from a linear relation is more evident for the tests where wave breaking was observed most frequently and in deeper areas of the channel. The wave breaking will decrease the wave steepness, and thus a fitted curve will have a larger gradient. But it cannot really be concluded that this is the single factor that this causes the skewness to grow "steeper", since this is also seen in the less steep sea states, but then in a smaller degree. However it seems reasonable to the author that this is an effect that may contribute.

The dependence on the Ursell number seems very good, where all the steep and nonlinear sea states have a skewness that is proportional to the Ursell number. The less steep sea states however does not seem to follow the same relation. Further it is worth mentioning that the distance between the last two points in all these figures is quite large, and we do not have any measurements in between these wave probes to confirm this behavior. But since this is the trend for all the relevant tests, it seems plausible that this is the case, i.e. that the skewness is proportional to the Ursell number.

Comparison with previous work

From the literature it is found three different publications which consider the change of the skewness coefficient on a sloping beach. Nilsen (1997), Wei et. al. (1999) and Nwogu (1993) all show the same, which is that the skewness increases as the water depth decreases, but they have not investigated the behavior any further. The same trend is clearly seen in our model test as well, this can be seen in Figure 18 at the beginning of this chapter.

In Goda (2010), as mentioned earlier, it is said that the skewness in deep water is proportional to the wave steepness. Our model tests are never in deep water, so we do not have the opportunity to verify this. But there seems like a clear trend that the skewness grows proportional to the wave steepness for the first part of the slope, in intermediate water depth. Thus that the behavior described in Goda (2010) seems to be valid even in intermediate water depth, but not for the entire range of intermediate water depths.

In Memos et. al. (2002) there is proposed an empirical formula to the skewness as a function of a non-dimensional water depth. This have been tested with the data from our model test, and it is found that except for the results from the wave probe on the shallowest water depth the skewness follows a straight line. However the only case where it follows the empiric formula is for test2111, for the larger sea states the formula under predicts the skewness. For the tests with low steepness (test2109 and test2117), the formula over predicts the skewness.

From the tables of data presented in Nilsen (1997) there are one test that compare fairly well to our model test with respect to the input data, that is test "Kj31" with Hs=0.12 meters, Tp=1.4 seconds and a peakedness parameter equal to 3.3. Furthermore the results from Nwogu (1993) and Wei et. al. (1999) have been extracted from the graphs in the respective papers. The model test from Nwogu (1993) was preformed with a sea state with Hs=0.09 meters and Tp=1.5 seconds, in Wei et. al. (1999) the sea state where Hs=0.065 meters and Tp=1 second. The data from these model tests have been

plotted with results from representative sea states in our model test (test2111 and test2115), against the relative water depth and is shown in Figure 35.

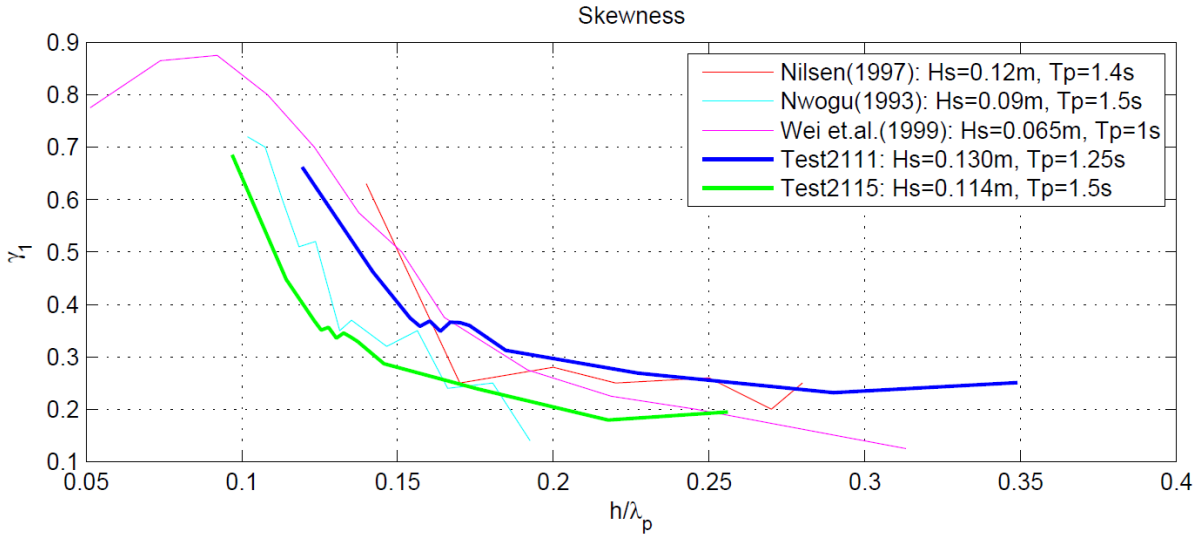

Figure 35: Comparison for skewness with previous model tests

What we see from Figure 35 is that the results we have obtained from our model test are in the same order of magnitude as the tests from Nilsen (1997), Wei et.al. (1999) and Nwogu (1993).

4.1.3 Kurtosis

The kurtosis coefficient is a far less stable parameter than the skewness. The results will be presented in a similar way as for the skewness, thus in terms of relative water depth, wave steepness and Ursell number.

In Figure 36 the mean of the kurtosis coefficient for the different tests are presented in terms of the relative water depth, the behavior is somewhat chaotic but the trend is clear, the kurtosis increases with decreasing water depth. The gradient is increasing with decreasing water depth, thus the increase of kurtosis is significant when approaching the shallow water limit. There cannot be established a clear relation between the steepness of the different sea states, as for the skewness. This is probably due to the more random nature of the kurtosis. The kurtosis will also have variations in a Gaussian process, the magnitude of these variations can be determined by performing simulations of Gaussian processes resulting in an interval of variations that can be expected in a Gaussian process. Thus we would have a clearer indication of whether or not the process in question deviates from a Gaussian process, this has however not been done in this thesis due to lack of time.

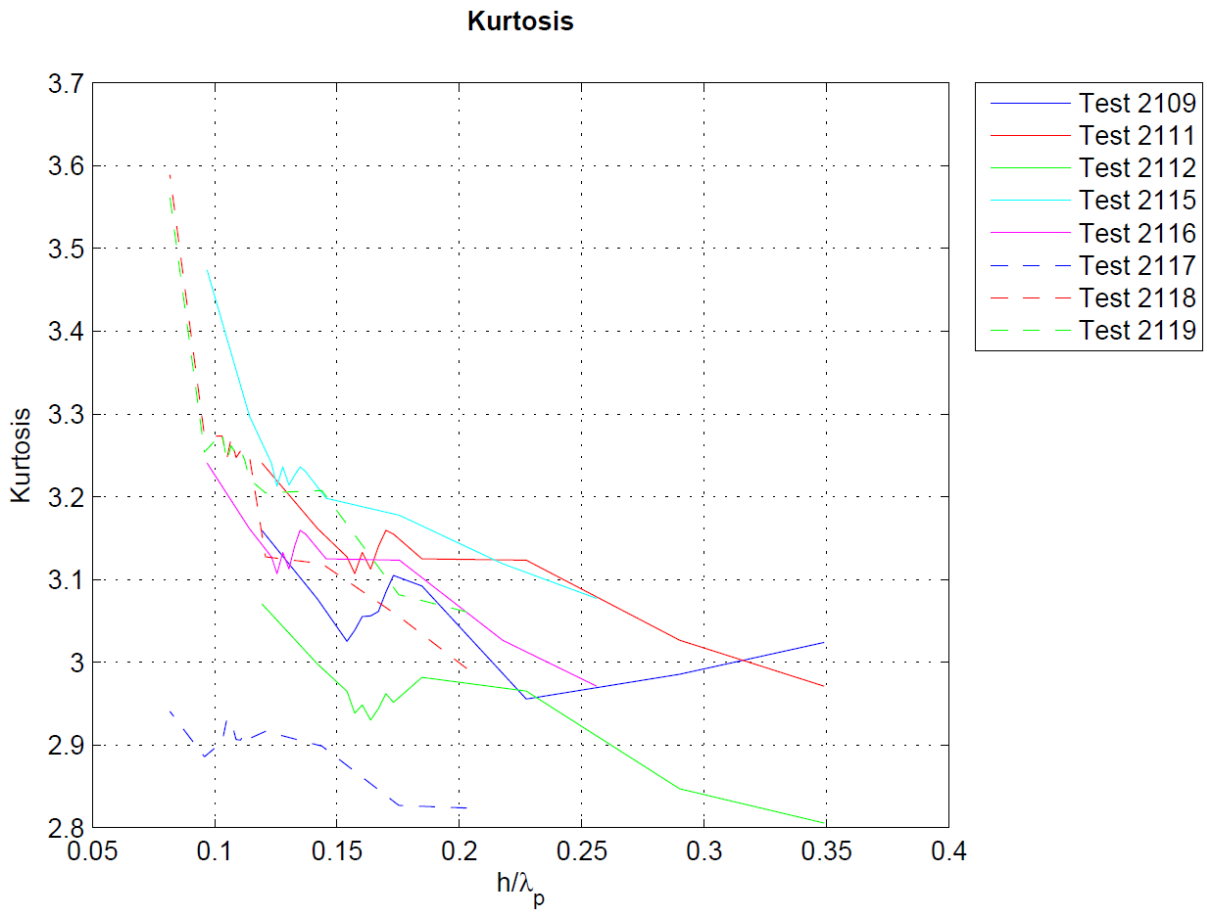

Figure 36: Kurtosis for relative water depths

The results from the repetitions of these tests will be presented as earlier with those of corresponding peak periods.

Tp=1.25 seconds

Figure 37 shows the kurtosis for test2109 as a function of the wave steepness, the input significant wave height for this test is 0.047 meters. It is seen that the kurtosis appears to grow linearly with the steepness, but there are some degree of scatter.

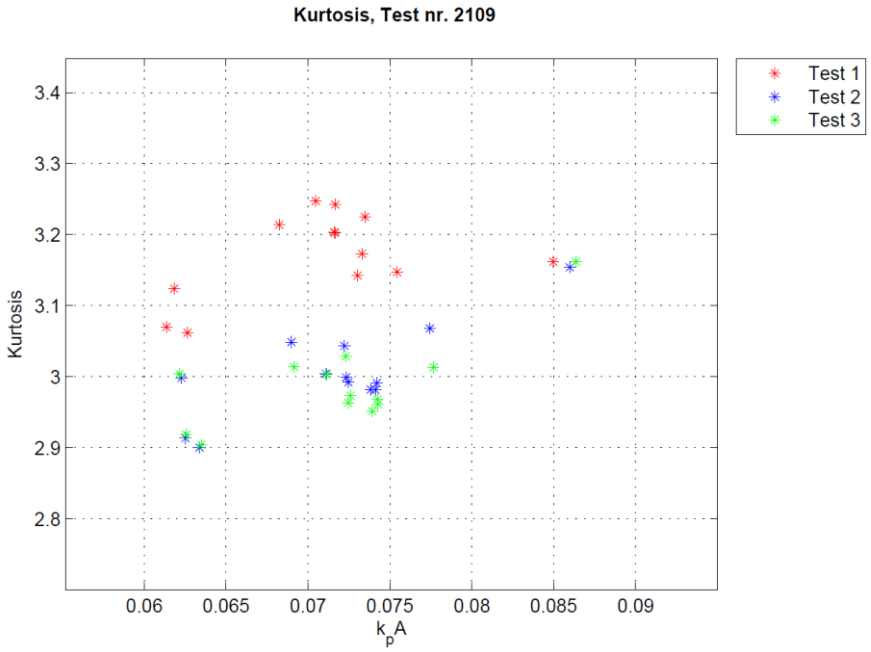

Figure 37: Kurtosis vs. wave steepness, test2109

From Figure 38 the skewness has been plotted against the Ursell number. What we see from this figure is that there does not seem to be any relation between the Ursell number and the kurtosis, at least for the lowest values of the Ursell number, however for higher Ursell numbers the kurtosis seem to grow proportional to the Ursell number. But the distance between the data points for “high” Ursell numbers is large, and thus the uncertainty of the behavior in-between is also large.

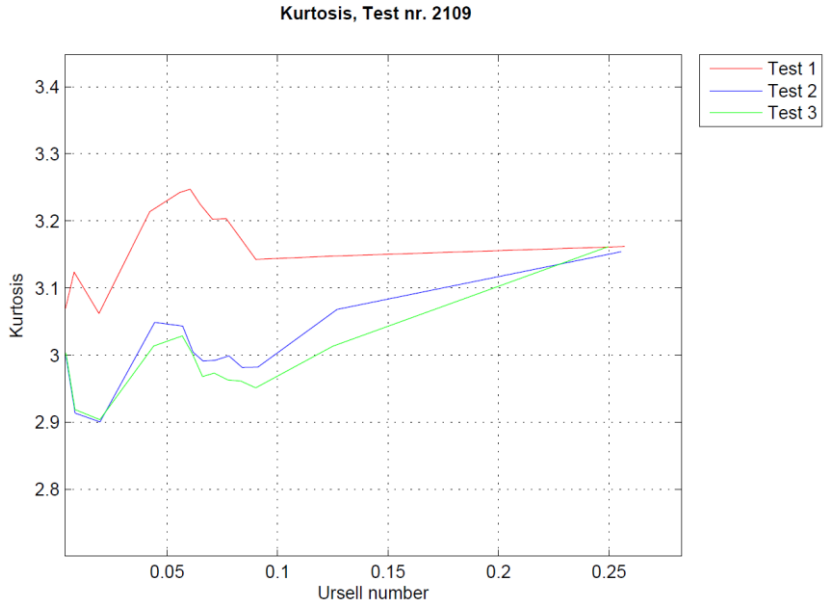

Figure 38: Kurtosis vs. Ursell number, test2109

In Figure 39 the kurtosis for test2111 is presented in terms of the wave steepness. The different repetitions seem to follow the steepness in a relation that can be approximately linearly, but the magnitude of the different tests is different. It is difficult to make out any trend from this figure, due to the scatter.

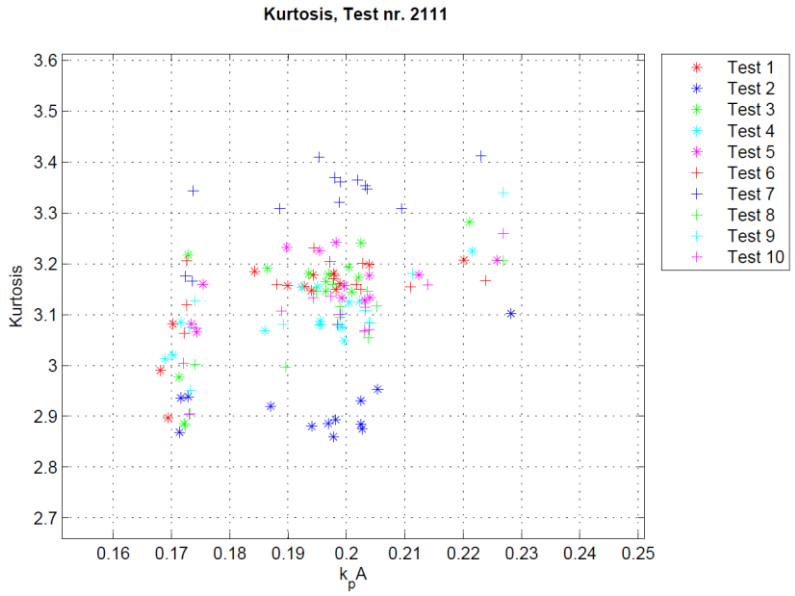

Figure 39: Kurtosis vs. wave steepness, test2111

From Figure 40 the kurtosis is plotted against the Ursell number, and it is seen that the kurtosis from the tests follow the Ursell number linearly for the highest values of the Ursell number. But the increase of kurtosis for the lowest Ursell number differs quite significantly, and thus is it difficult to conclude with any clear trend.

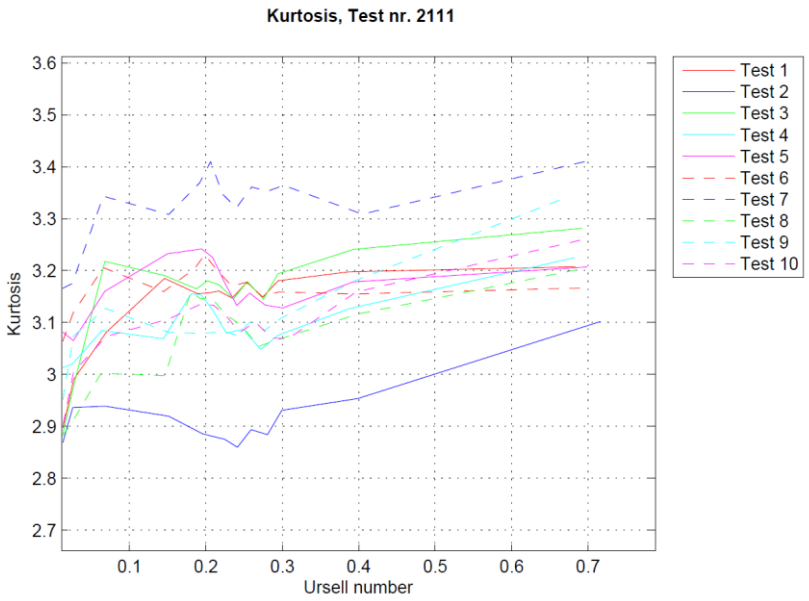

Figure 40: Kurtosis vs. Ursell number, test2111

The kurtosis from test2112 is shown in terms of the wave steepness in Figure 41. The figure shows that the kurtosis is slightly less scattered than the previous tests, but the initial values from the tests are strangely low. Remembering that the kurtosis in a Gaussian process is equal to 3, this figure shows that the distribution of the time series is flatter or less peaked than that of a Gaussian process. The reason for this may be that a wave maker that is not properly calibrated will give waves with a distribution that is wider than the input, i.e. a distribution which is flatter than the Gaussian input, and thus a kurtosis value that are smaller than 3.

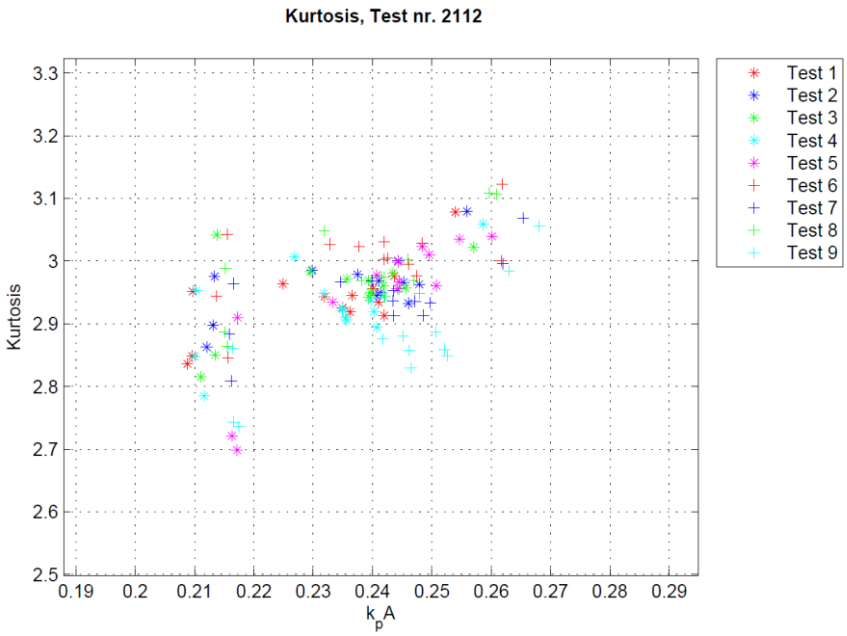

Figure 41: Kurtosis vs. wave steepness, test2112

In Figure 42 the kurtosis is plotted against the Ursell parameter. We can see a jump or a high gradient between the first and second wave probe, before the growth in the kurtosis seem to be proportional to the Ursell number. The scatter in the kurtosis values also seem less scattered in this case, as indicated previously.

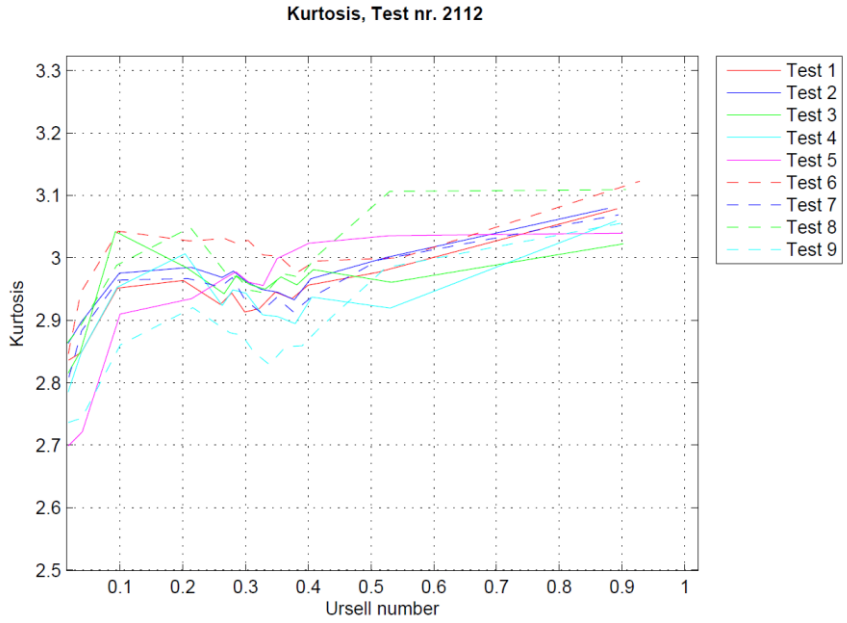

Figure 42: Kurtosis vs. Ursell number, test2112

There can also be seen a "jump" in the kurtosis coefficient early in the channel which probably is a result of an un-calibrated wave maker giving a broad distribution of the time series, another explanation may be that this occurs and additionally unphysical waves due to this effect breaks. By a broad distribution it is mean that the tails of the distribution are steeper, and the peak of the spectrum is wide and flat. This is similar to the behavior of a distribution with a kurtosis lower than 3, and thus it seems like a reasonable explanation that the effects from an un-calibrated wave maker results in low kurtosis.

Tp=1.5 seconds

In Figure 43 the kurtosis for test2115 is presented in terms of the wave steepness. We can see that the trend can be approximated with a linear relation between the kurtosis and the wave steepness.

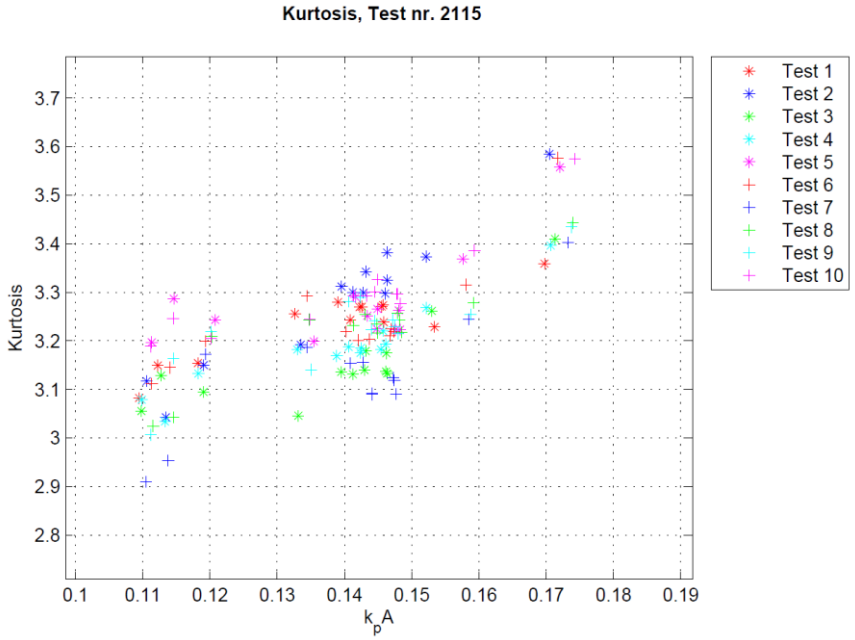

Figure 43: Kurtosis vs. wave steepness, test2115

From Figure 44 the kurtosis is plotted against the Ursell number. We can see a kurtosis which is proportional to the Ursell number.

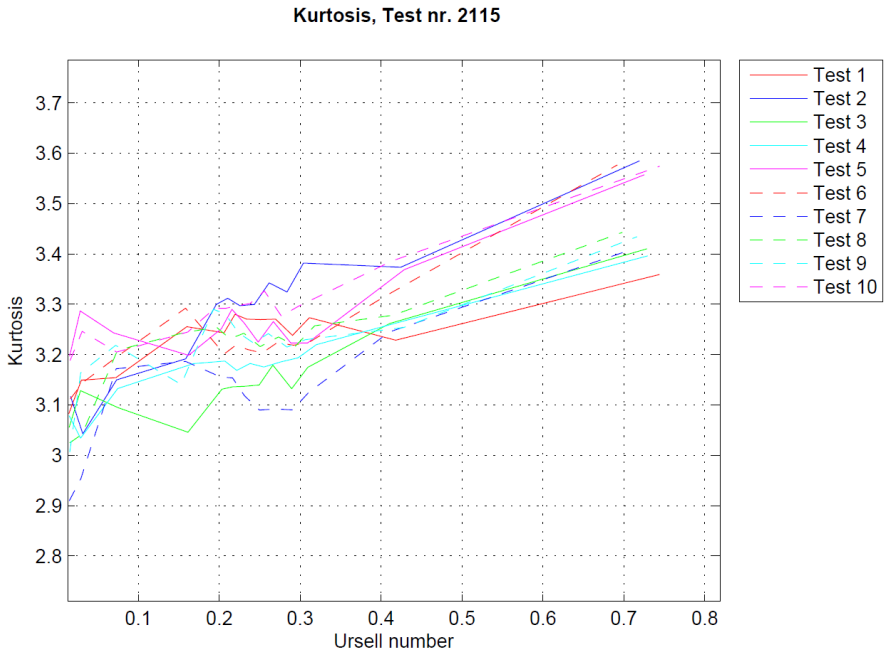

Figure 44: Kurtosis vs. Ursell number, test2115

In Figure 45 the kurtosis for test2116 is plotted against the wave steepness. From the figure we can see that the kurtosis follows the wave steepness with a linear relation, although with more scatter than that of test2115.

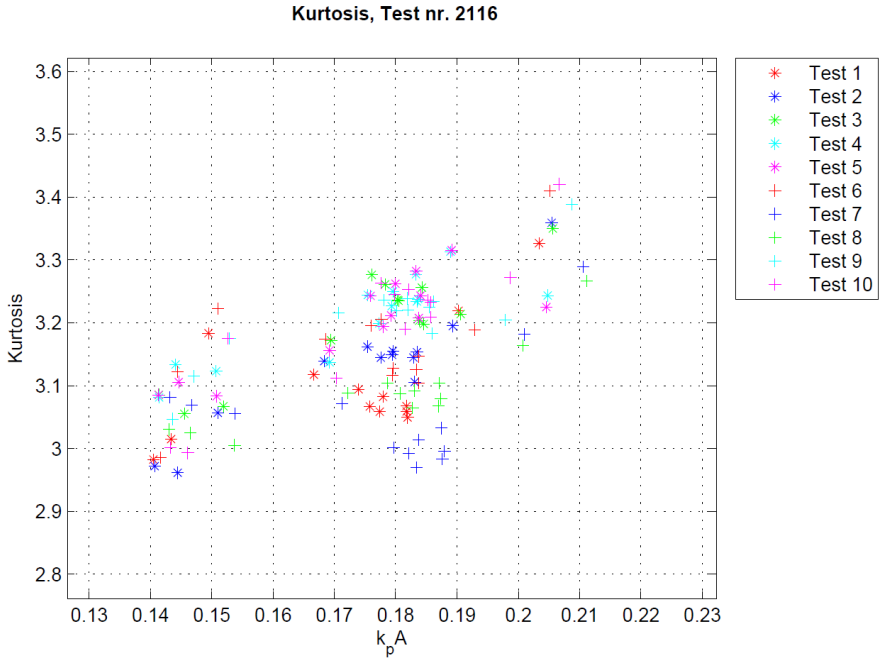

Figure 45: Kurtosis vs. wave steepness, test2116

From Figure 46 the kurtosis is presented in terms of the Ursell number. We can see that the kurtosis follows the Ursell number with a linear relation, but the scatter is of a significant magnitude.

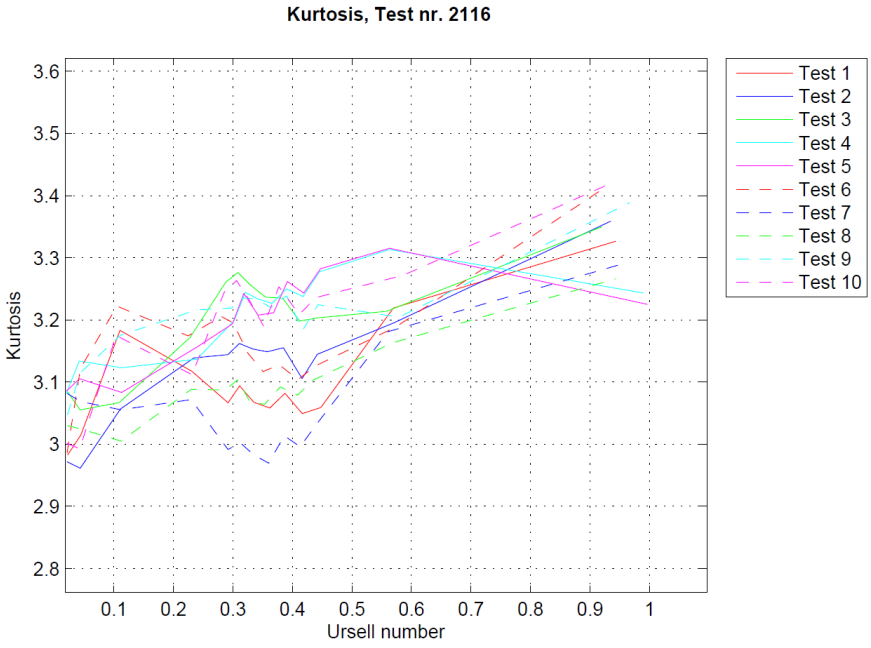

Figure 46: Kurtosis vs. Ursell number, test2116

Tp=1.75 seconds

From Figure 47 the kurtosis for test2117 is presented in terms of the wave steepness. The results are somewhat strange, since the kurtosis remains below 3 through the entire channel. And thus the kurtosis is below that of a Gaussian process, where the expected behavior should be that the kurtosis starts out as a Gaussian process and then grows to a distribution steeper than that of a Gaussian process.

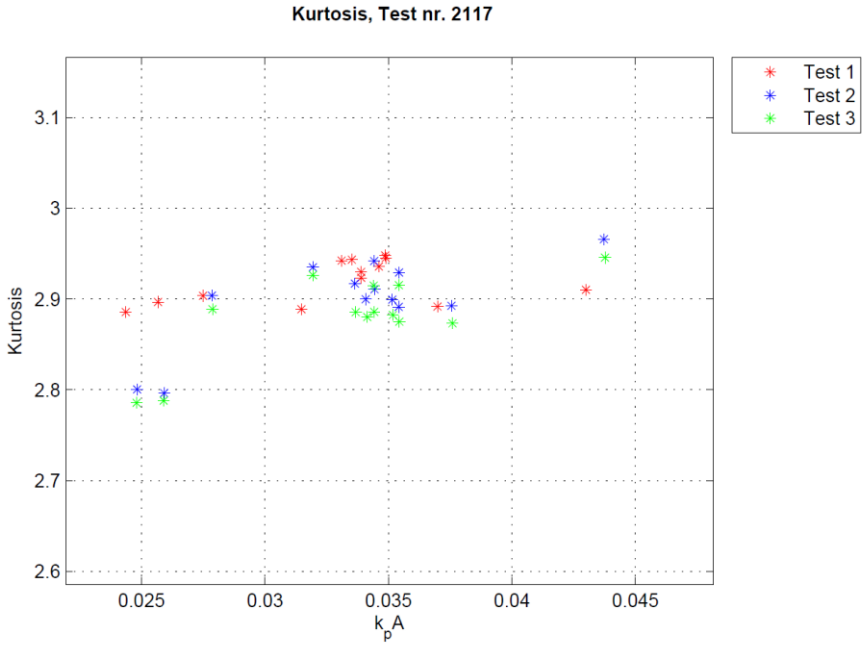

Figure 47: Kurtosis vs. wave steepness, test2117

An explanation may be that as argumented previously the waves generated by the wave maker have a too wide distribution, giving a too flat distribution, thus a kurtosis below 3. This is something that has been seen predominately for the steepest sea states, but it is also seen clearly in this case. We see that the kurtosis increases with the steepness and the relative water depth (Figure 36), but as this is a fairly moderate sea state it seems likely that it should not follow as steep a gradient as for the steeper sea states, at least before entering shallow water.

In Figure 48 the kurtosis has been plotted against the Ursell number. It is difficult to make out any trend in this case, it may be assumed to vary linearly with the Ursell number.

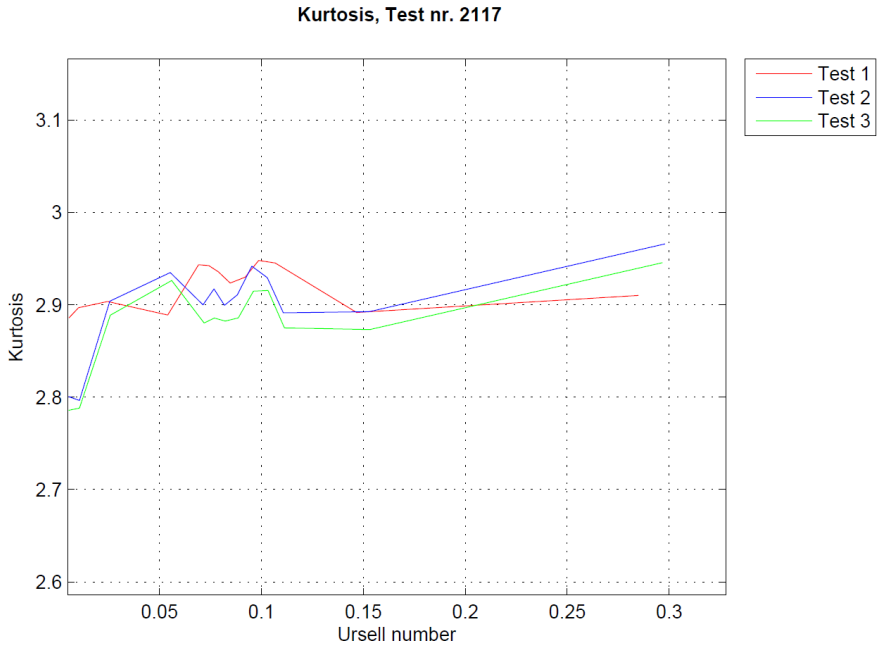

Figure 48: Kurtosis vs. Ursell number, test2117

From Figure 49 the kurtosis for test2118 has been plotted against the wave steepness. It seems that the kurtosis here has a linear relation with the wave steepness.

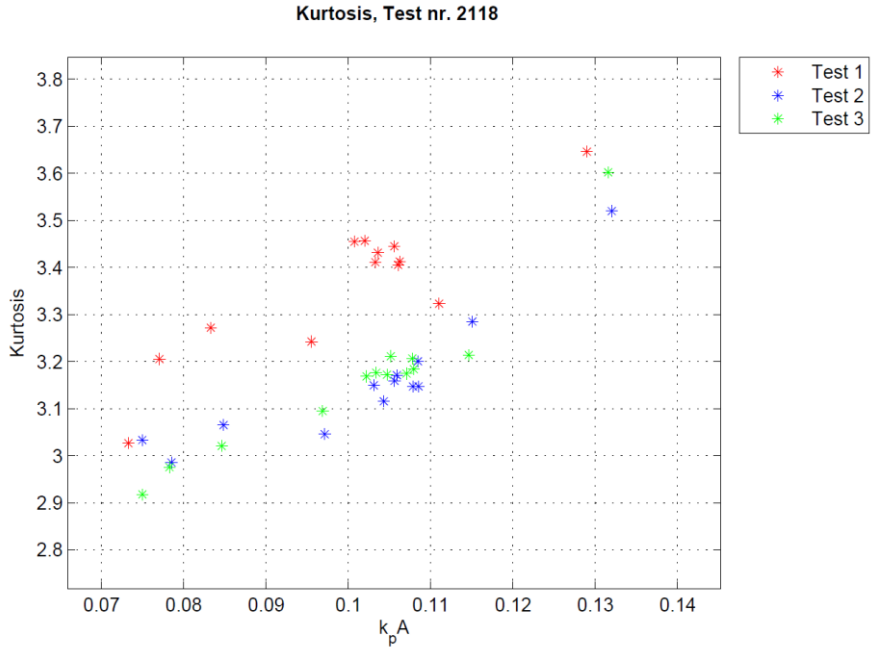

Figure 49: Kurtosis vs. wave steepness, test2118

In Figure 50 the kurtosis is presented in terms of the Ursell number. It is seen that some of the repetitions follows the Ursell number linearly, but it cannot be concluded to be very reliable.

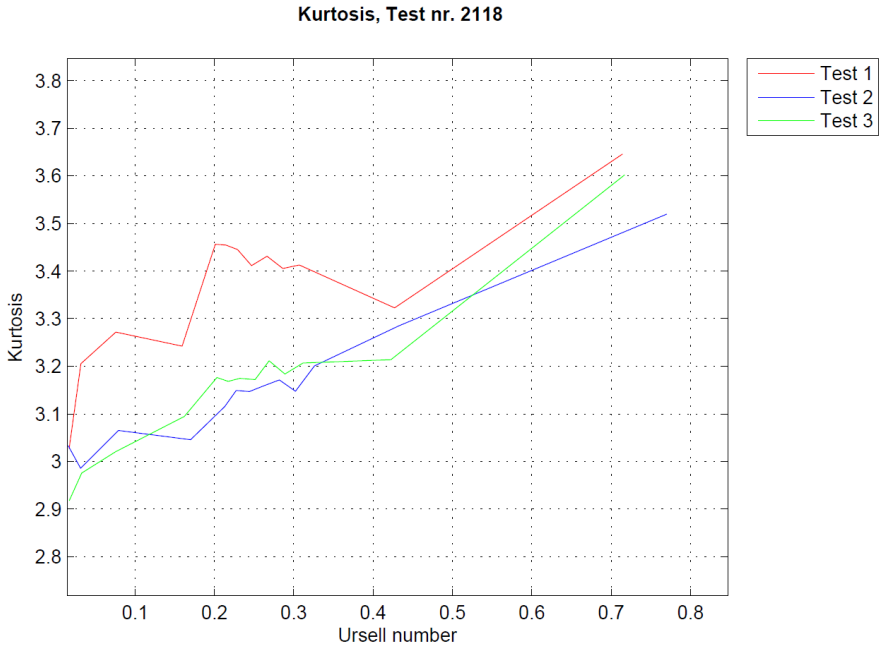

Figure 50: Kurtosis vs. Ursell number, test2118

In Figure 51 the kurtosis for test2119 is presented in terms of the wave steepness. It is clear that the data do not fit a straight line, and thus the kurtosis is not proportional to the wave steepness in this test.

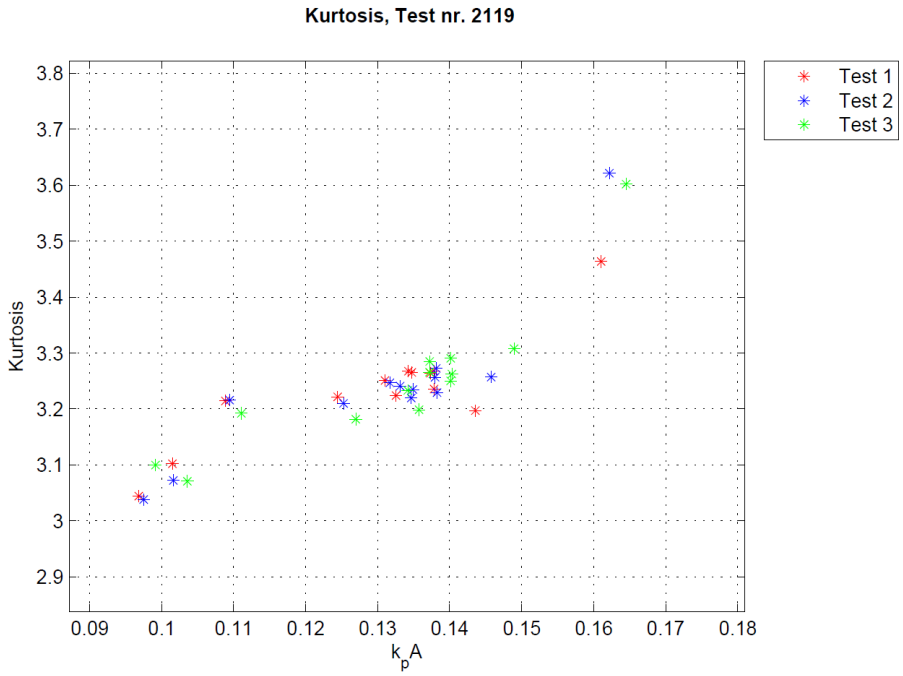

Figure 51: Kurtosis vs. wave steepness, test2119

From Figure 52 the kurtosis has been plotted against the Ursell number, but there are no clear linear relation between the kurtosis and the Ursell number.

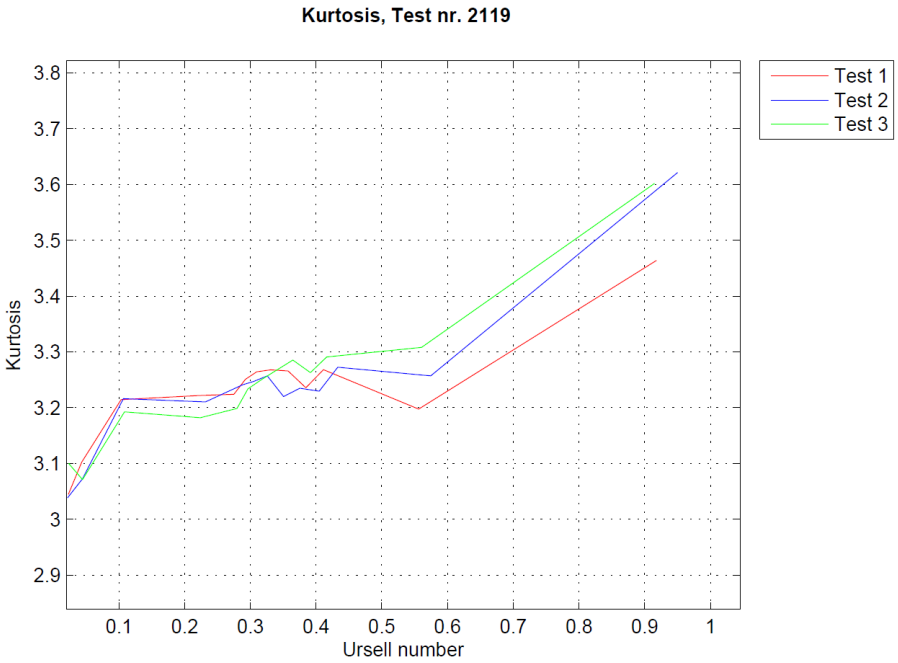

Figure 52: Kurtosis vs. Ursell number, test2119

Summary of observations

The figures presented in this chapter show that the change of the kurtosis as the waves transform from deep to shallow water fits a linear relation with the Ursell number and sometimes don't. Thus it cannot be established any clear connection between the kurtosis coefficient and the parameters wave steepness and Ursell number from these model tests. The kurtosis values are largest for the largest periods, and small for the smallest periods. This makes sense since the longest periods should be most affected by the effect from wave shoaling, and thus gets larger waves which results in a more peaked distribution of the time series.

It is observed that the kurtosis for the first wave probe often gives values that are below 3, and thus a distribution of the time series less peaked and with steeper tails than that of a Gaussian process. A possible explanation for this is that the wave maker is not properly calibrated, which may cause the distribution of the generated waves to be broader than the initial input. Another explanation may be that this is just variations of the kurtosis which is in the typical range of a Gaussian process, but as this tendency is the same for many repetitions this seem unlikely. This effect stabilizes itself as the waves propagate to the second wave probe, this is seen as a "jump" or a large gradient between the first and the second point in the figures.

Comparison with previous work

From previous work there are found two publications that presents the measured kurtosis coefficient from a model test, which can be found in Nilsen (1997) and Memos (2002). Further Goda (2010) also compares the kurtosis with full scale measurements, with respect to a nonlinearity parameter. This nonlinearity parameter converges towards the wave steepness in deep water, and towards the Ursell number in shallow water. It seen that the kurtosis increases with increasing nonlinearity, and thus decreasing water depth. This is the same trend seen in our model test, but there are no successful

attempt to get a connection between the kurtosis and other parameters. In Memos (2002) there have been established an empirical relation between the kurtosis and a normalized water depth from data of a model test with the same slope as ours, given as:

$$\gamma_2 = 0.1095\left(-1+\frac{d_0}{d}\right)+3 \tag{41}$$

Where d0 is the water depth associated with the deep water limit for the peak period of the input wave spectrum, and d is the water depth at the location of the different measurements. This empiric formula overpredicts the kurtosis for all of the tests performed in our model test, with the exception of test2111, which fits fairly well. The empirical formula from Memos (2002) does not fit our data. But it is only the gradient of the line that do not fit our data, the kurtosis from our data follows the normalized water depth proposed by Memos approximately by a straight line. Thus the kurtosis appears to be proportional to the normalized water depth proposed by Memos (2002). An example of this can be seen in Figure 53 where the kurtosis for test2116 has been plotted against a normalized water depth, the empirical formula by Memos (2002) is the solid blue line whereas the data from our model tests can be seen as black single data points.

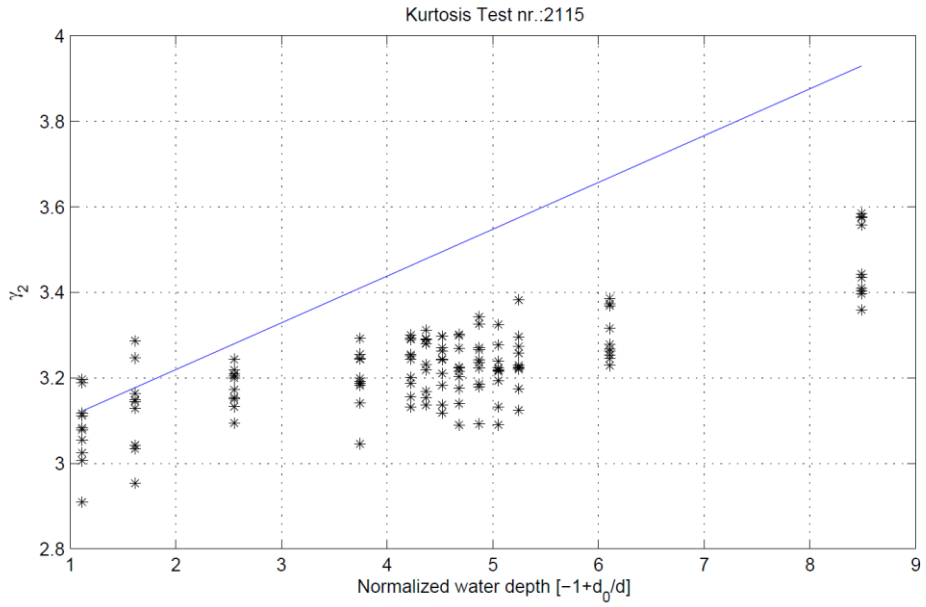

Figure 53: Kurtosis compared to equation 39 from Memos (2002), for normalized water depths

The model test which is analyzed in Nilsen (1997) is the same as the one analyzed in Memos (2002), thus we should expect the same trend when comparing against the data from this model test. The model test from Nilsen (1997) that compare the best with respect to input parameters from our model test is a test with Hs=0.12 meters and Tp=1.4 seconds. This test has been compared with test2111 (Hm0=0.13m, Tp=1.25s) and test2115 (Hs=0.114m, Tp=1.5s), and is plotted against the relative water depth. And the same trend as in Memos (2002) can be seen in Figure 54, where the gradient of the kurtosis are larger. For the larger water depths we get the same results, but the

kurtosis from Nilsen (1997) increases in deeper water and with a larger gradient compared to the results from our model test, the results are however not that far off, and we can say that we at least are in the same order of magnitude as the test performed by Nilsen (1997).

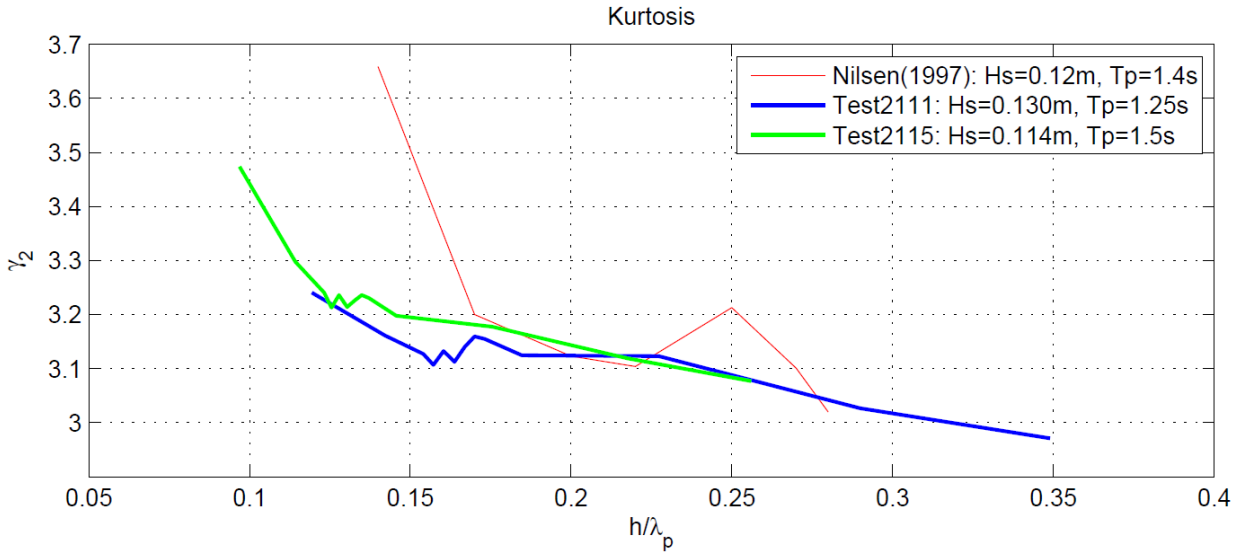

Figure 54: Comparison with kurtosis from Nilsen (1997)

4.2 Spectral estimates

The spectral estimates in this model test have been generated using the WAFO (2000) function "dat2spec", using and approach called Welch averaged periodogram, which is described in chapter 2.5.2. There have been generated spectral estimates for the recorded time series at each wave probe for all the relevant model tests, which obviously gives a lot of figures. In this chapter there will be presented examples where interesting behavior is observed. The reader is referred to appendices for a complete set of figures for the tests in question. The rest of the figures can be found in the digital appendix attached to this thesis. The results will be presented in the order that the wave propagates, i.e. there will be presented results from the start of the channel in the beginning of this chapter, and it will finish with the results from the last wave probe. In order to cut down on the amount of data to present, we will present the results from a large sea state (test2116), a medium sea state (test2111) and one low sea state (test2117) with respect to the significant wave height. The complete set of spectral estimates for these tests can be found in Appendix C, spectral estimates for the rest of the tests can be found in the digital appendix.

4.2.1 Test 2116

Beginning at the first wave probe, which is located in the entrance to the channel. From the steeper sea states it was observed a significant amount of wave breaking in this area, as the waves coming out of the wave maker where higher and thus steeper than specified as input. In connection with these observations it seems reasonable that there should be a large wave spectrum in this position, and possibly some deviations in the high frequency tail as a result of broken waves. In Figure 55 the wave spectrum for test2116 is presented for all the repetitions.

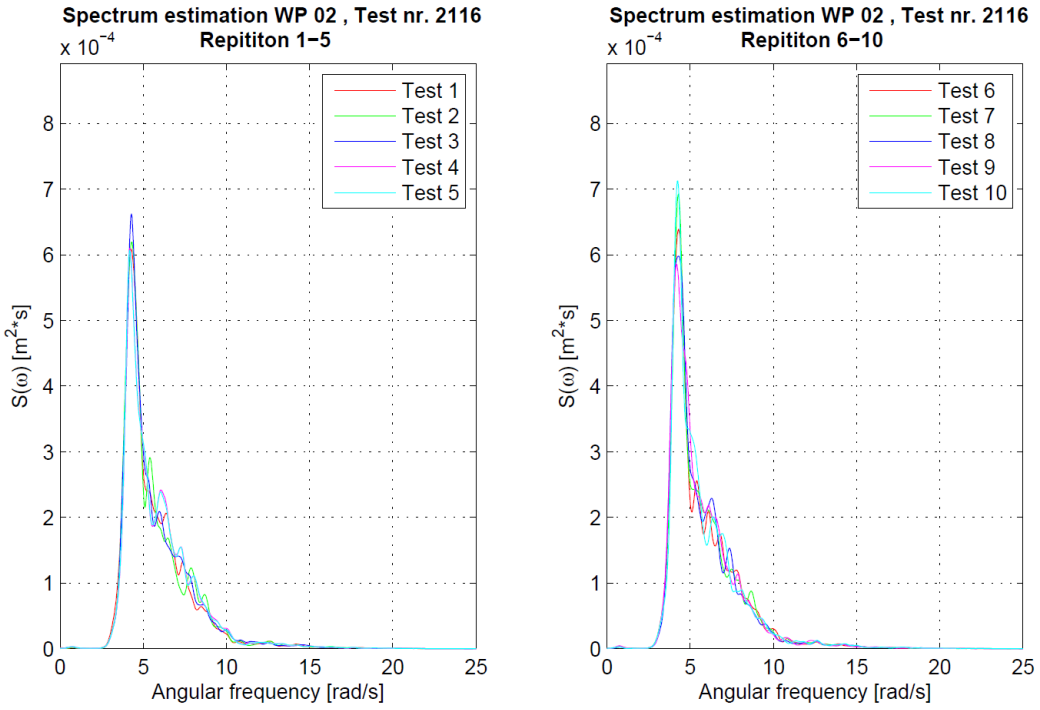

Figure 55: Spectral estimates at wave probe 2, for test2116

It seen that there are some considerable disturbances in the high frequency tail of the spectra (5<ω<10), it cannot be said with an absolute degree of certainty that this is due to wave breaking since some of the disturbances certainly is a result process of generating the spectrum. If trends should be visible in the spectrum, then you have to allow some "noise" in the spectrum. However compared to Figure 56 which is the spectral estimates from the next wave probe, it seems clear that a portion of the disturbances are due to wave breaking. As the tails in this figure is smoother it seems evident that some portion of the energy has been transferred from the high frequency tail to the lower frequencies in the spectrum by means of quadruple wave-wave interactions. Further it seems like the height of the peak for most of the tests remained unchanged for most of the repetitions, indicating that the observed wave breaking is predominant before the first wave probe. Repetition number seven and ten (Test 7 and Test 10 in the figures) have however a significant drop in the area of the spectrum, and thus in the energy of the spectrum. This is an indication that there has occurred a significant amount of wave breaking between the first and second wave probe.

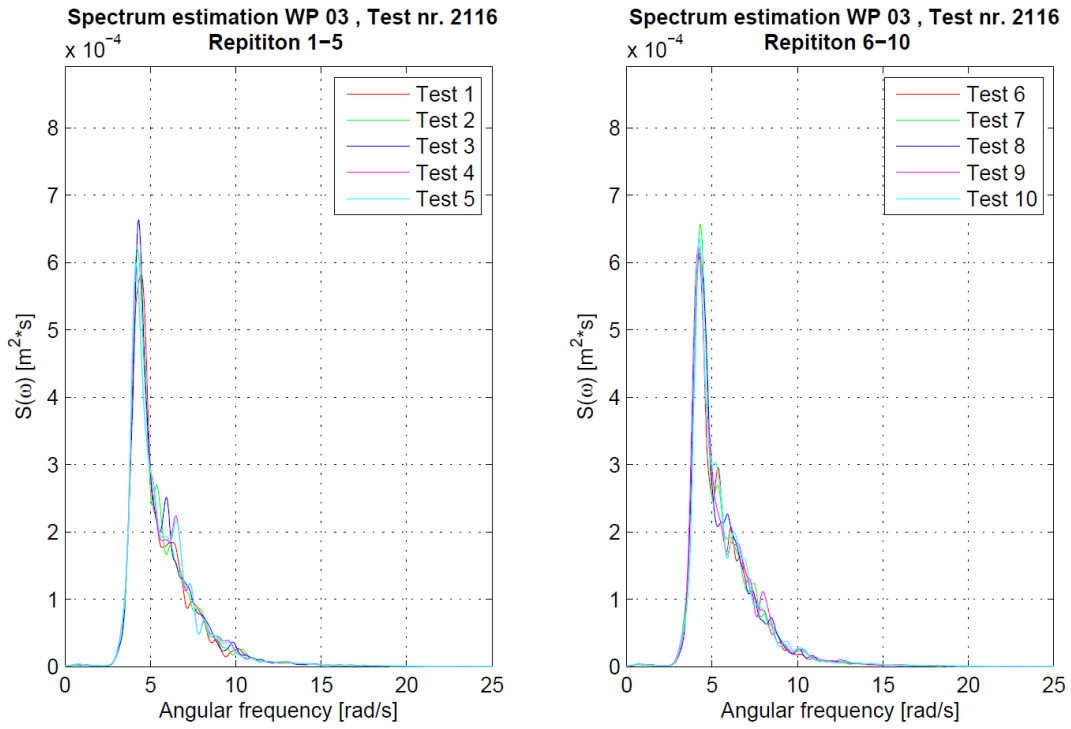

Figure 56: Spectral estimates at wave probe 3, for test2116

It is observed that the waves seem to shoal, as the peak of the spectrum increases. This is illustrated in Figure 57 where the estimated spectrum for wave probe 11 is shown. This is in the area of interest for this model test, the estimated spectrums in the area close till this wave probe shows approximately the same behavior. But it also noticed that the effect from shoaling is not very significant for all the repetitions. The spectrums then decrease slightly before a clear abrupt change can be seen in the region of wave probe 6 and 7.

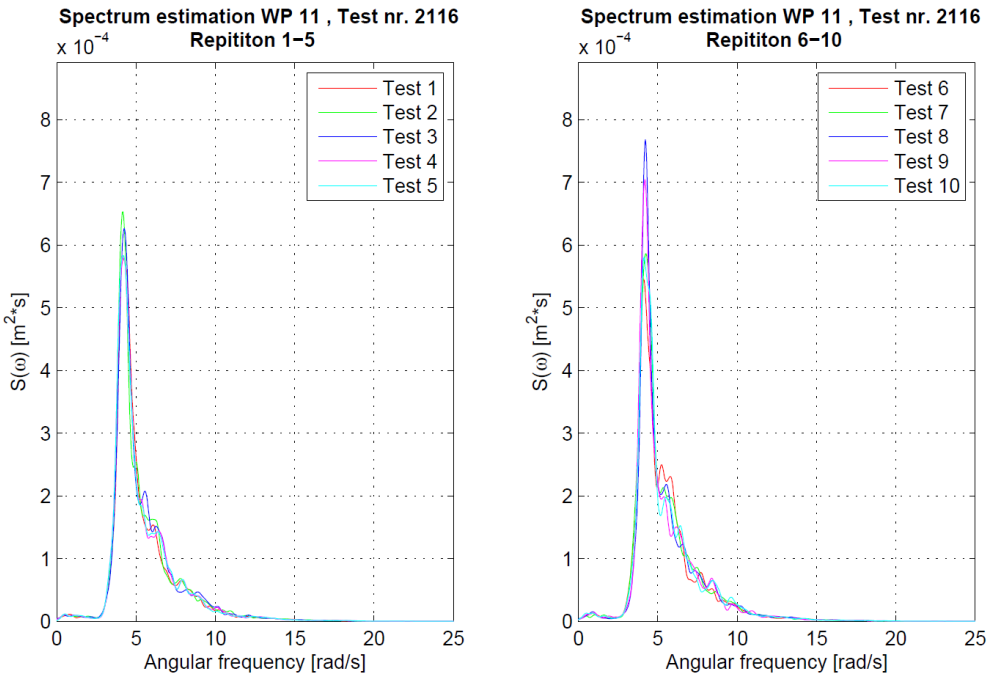

Figure 57: Spectral estimates at wave probe 11, for test2116

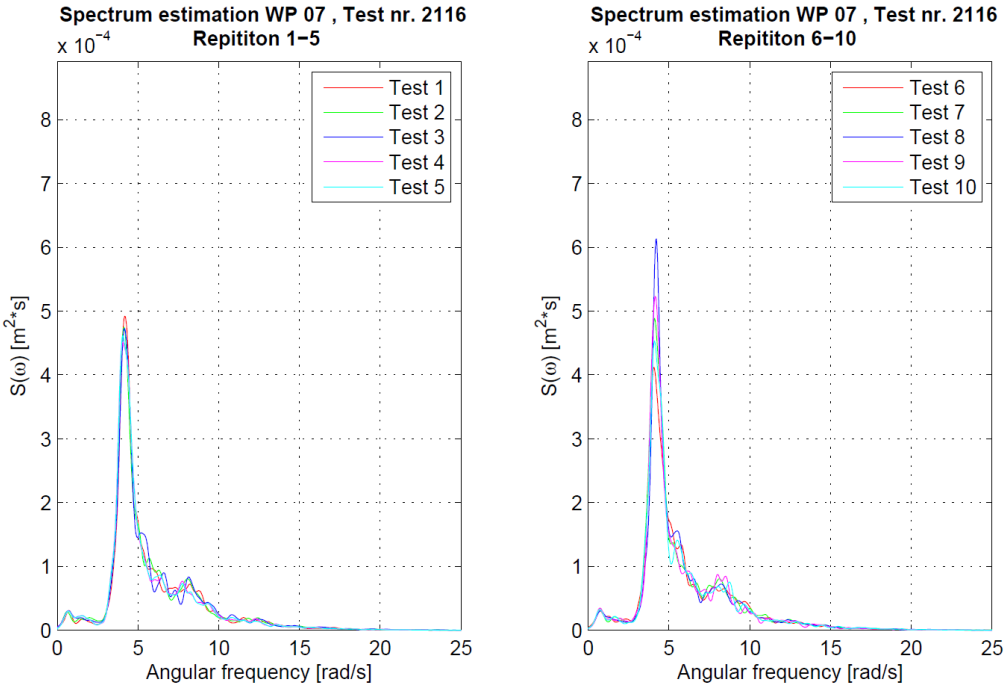

Figure 58: Spectral estimates at wave probe 7, for test2116

As the waves move closer to the shore the largest waves start to break, this is seen clearly in the spectrums from wave probe 7 which is shown in Figure 58. The spectrums are seen to decrease significantly, and as it was observed a significant amount of wave breaking in this region during the

model test it seems reasonable that the reduction is caused by dissipation effects from wave breaking. However there cannot rule out that there are effects from bottom friction that contributes to the dissipation, this will however be discussed further for the low steepness case in this chapter. In test2117 wave breaking where observed to appear in shallower water than the last wave probe, and will thus give a clearer indication of whether or not the bottom friction has contributed with significant dissipation in this model test.

From Figure 58 it is also seen sub- and super-harmonic peaks in the spectrum, these peaks are a result of triad wave-wave interactions. As triad wave-wave interactions are a nonlinear phenomenon that occurs in relatively shallow water, the presence of these interactions indicate that the surface process from these model tests are nonlinear.

4.2.2 Test 2111

In this test there were observed some wave breaking in the vicinity of the first wave probe. This test has a lower significant wave height than test2116, but is actually steeper. Thus one could expect to see much of the same behavior between the first and second wave probe as in the previous chapter, thus traces of breaking waves. The estimated spectrum for the first wave probe is seen in Figure 59, and it is seen the tail of these spectrums are somewhat scattered and deviate from a smooth shape. Which may be an indication that wave breaking have occurred prior to the first wave probe.

In Figure 59 the wave spectra for the second wave probe are presented, here it can be seen that the tail although scattered has a tail that is smoother and more like the shape we should expect. This indicates that quadruple wave-wave interactions are present, and have contributed to shifting energy from the high frequency tail towards the mid frequencies in the wave spectrum, thus

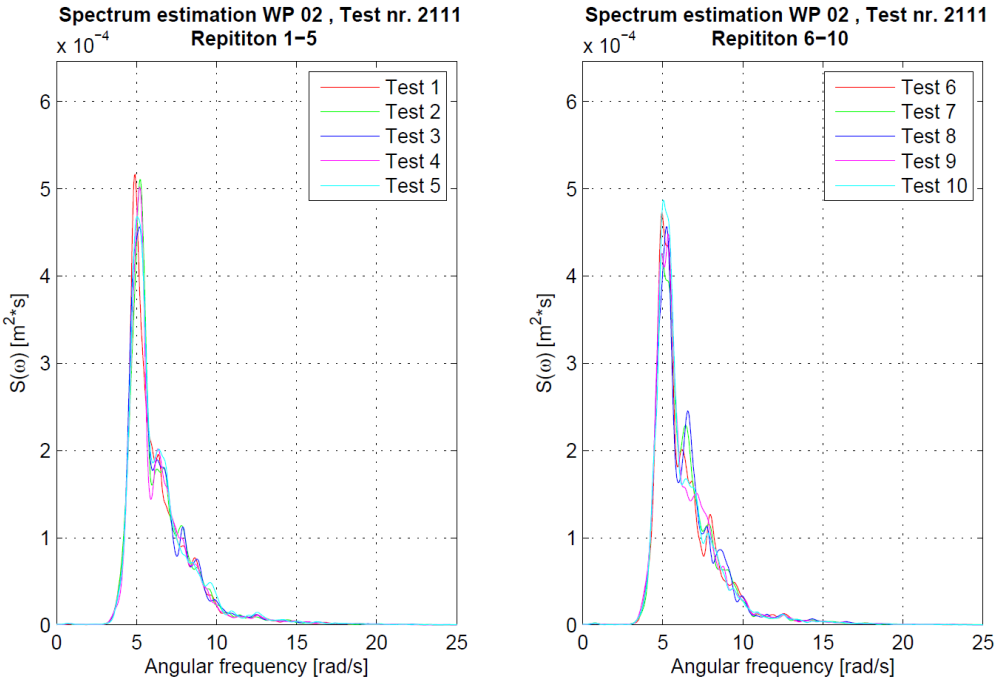

Figure 59: Spectral estimates at wave probe 2, for test2111

preserving the shape of the tail. Further it is observed that some of the spectrum energy has dissipated between the first and second wave probe, this indicating that there have occurred wave breaking between the two wave probes. This fits the visual observations, as there was observed breaking waves in the area before, at and after the first wave probe.

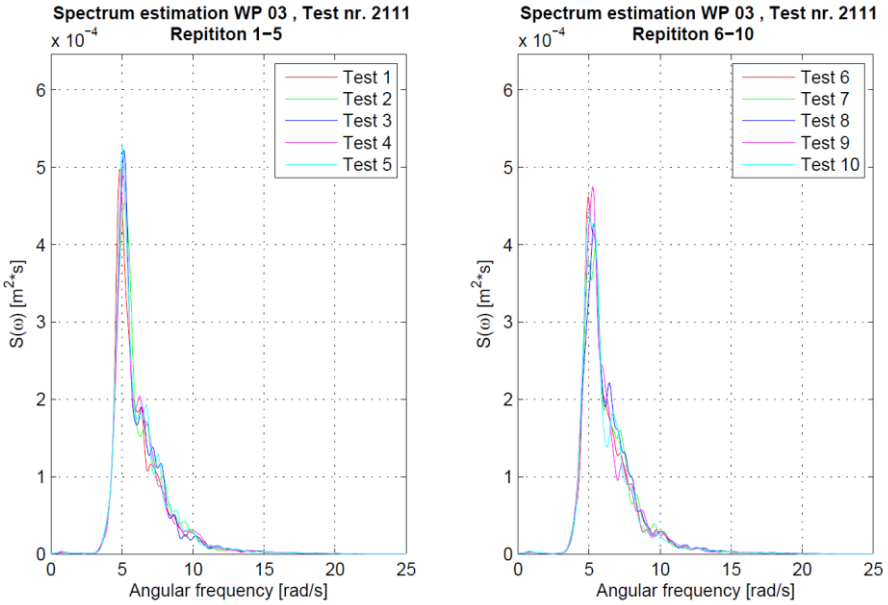

Figure 60: Spectral estimates at wave probe 3, for test2111

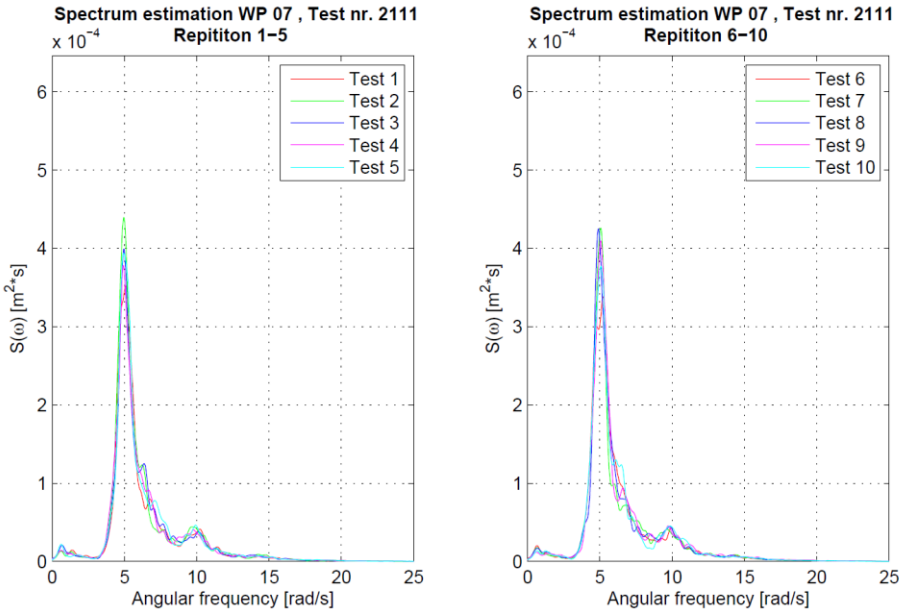

Figure 61: Spectral estimates at wave probe 7, for test2111

Further down the channel the spectral estimates remain fairly unchanged, with some local variations. For the wave probes closest to the beach we see a small increase in the spectra, before dissipation effects from wave breaking become noticeable. The spectral estimates from the last wave probe can be seen in Figure 61, and we see that there have been dissipated a significant amount of energy in

the spectrums, it seems evident to the author that this primarily is due to dissipation effects from wave breaking. But as previously mentioned this is primarily based on visual observations, and the presence of dissipation due to bottom friction cannot be ruled out. This can however be indicated by the spectrums from test2117 where wave breaking was not observed before the waves passed the last wave probe, and thus the only dissipation effect should then be bottom friction. From Figure 61, sub- and super-harmonic peaks are seen, which are caused by triad wave-wave interactions. The triad wave-wave interactions are nonlinear phenomena, and the presence of these interactions indicates that there are predominant nonlinear effects in the surface process. The sub harmonic peak in the low frequency part of the spectrum represents surf beat, which can be explained as slow variations in the mean water level, according to Holthuijsen (2007) this sub harmonic peak has a period of a couple of minutes, which compares fairly well as it in this case corresponds to a period of approximately 95 seconds. The Super harmonic peak can be seen to appear at two times the peak frequency, this is in accordance to theory.

4.2.3 Test 2117

For the smallest test in this comparison there where only observed no wave breaking within the vicinity of the wave probes, i.e. the wave breaking occurred on shallower water than that of the wave probe closes to the beach. The spectral estimates for the first wave probe for this test can be seen in Figure 62, and it is seen that the high frequency tail of the spectrum does not behave as expected. The tail is simply too wide and not as smooth as could be expected. The explanation for this may be that an un-calibrated wave maker produces a wave spectrum tail that are too broad, and that this is the cause if the behavior seen in the figure.

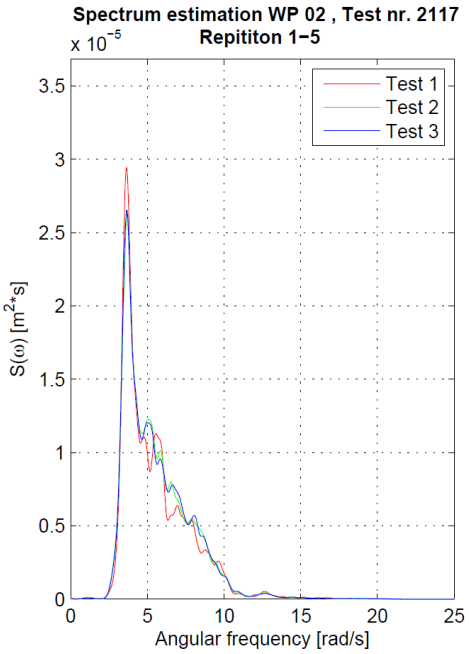

Figure 62: Spectral estimates at wave probe 2, for test2117

From Figure 63a) it seems however that the shape of the tail has been transformed into something that is more like expected, the spectrum seems narrower and the tail seems smoother. This is possibly due to effects from quadruple wave-wave interactions, which according to the theory should shift the energy from the high frequency tail towards the mid range frequencies in the spectrum.

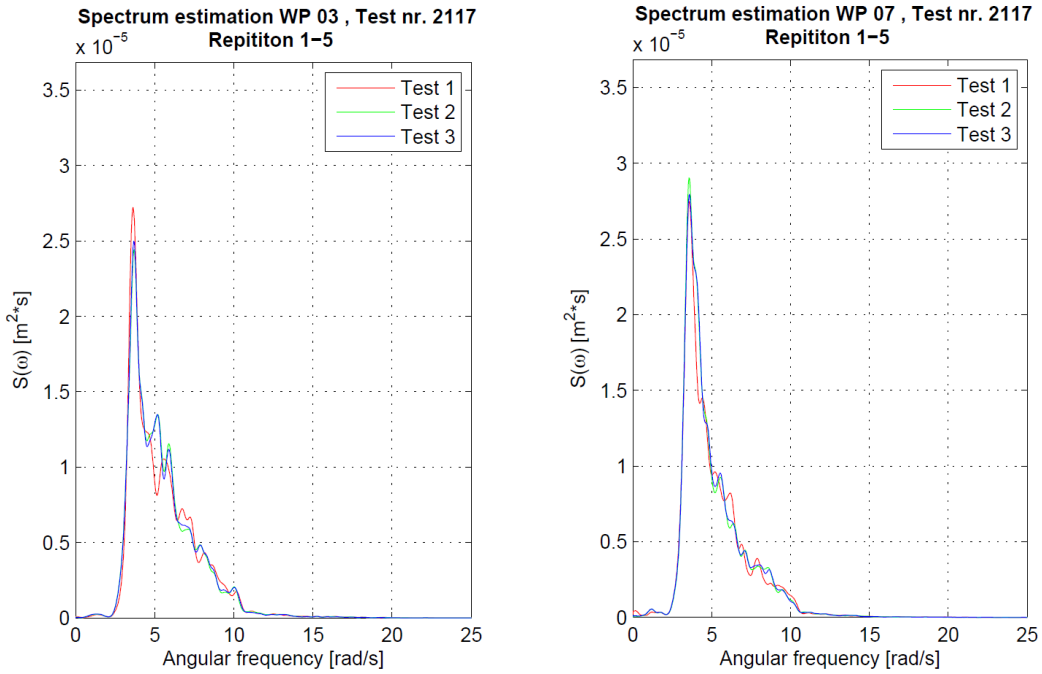

Figure 63: a) Spectral estimates at wave probe 03, for test2117. b) Spectral estimates at wave probe 07

It is also noted that peak of the spectrum decreases slightly compared to Figure 62, what causes the peak to decrease is not certain but when compared to the rest of the spectrums this seems to be in the order of magnitude of typical random variations.

Further down the channel the spectrums remain fairly unchanged with only small variations and a small decrease in the peak of the spectrum, but at the last wave probe (closest to the beach) the peak of the spectrum increases again. This is illustrated in Figure 63b). From this figure it can also be seen that the sub- and super-harmonic peaks found in the two other test cannot be seen in this spectrum, it seems evident that as the triad wave-wave interactions generating these peaks are nonlinear phenomenon, then the surface process for this test at the last wave probe are not nonlinear to that magnitude as seen for the steeper tests presented earlier.

4.2.4 Summary of observations

"Deep water" breaking

For the largest tests (test2111 and test2116) we can see clear traces of wave breaking in the spectral estimates at the first wave probe, as "noise" in the high frequency tail. Further we see unnaturally broad spectra at this position for all the tests, this is as argued in previous chapters most likely caused by an un-calibrated wave maker. As the wave propagates to the next wave probe, most of this behavior seems to have disappeared. Or to be more specific the energy does not disappear as it is shifted to the mid frequencies in the spectrum due to so called quadruple wave-wave interactions,

preserving the smooth tail of the spectra. For the largest sea states in question it is also seen that the peak of the spectrum decreases from the first to the second wave probe, this is due to energy dissipation caused by wave breaking.

Shoaling

From the test analyzed in this chapter the presence of shoaling in the spectral estimates can only be seen in one test (test2117). The reason for this may be that the effect from shoaling will be stronger for lower relative water depths, i.e. for the tests with the largest peak period. The fact that we do not see this before the last wave probe on the tests with the longest periods suggests that the effect should not be visible at all before we enter shallower water.

Bottom friction

As the spectral estimates from the tests above are compared, there cannot be seen any clear evidence of effects from bottom friction in the spectrums.

As the spectral estimates from the tests above are compared, there cannot be seen any clear evidence of effects from bottom friction in the spectra. As mentioned previously the bottom friction should be an important dissipation mechanism in shallow water. But as the only significant dissipation occurs where waves are observed to break, and as the spectral estimates for test2117 in which the waves do not break within the vicinity of the wave probes, observe no visible contribution from bottom friction. The contribution can be assumed to be small and thus negligible for our tests. Also remembering that test2117 have a longer dominant period than the other tests, it should be expected that bottom friction will be more significant here than for other tests, this enhance the hypothesis.

From the authors point of view there are three possible explanations to the absence of bottom friction. The first being that as this is a phenomenon that is said to make a significant contribution in shallow water, and thus a possible explanation may be that our wave probes are not in shallow enough water to capture the dissipation effects from bottom friction is such a degree that it is visible. However considering an example from Holthuijsen (2007) which can be seen in Figure 1, where the bottom friction is estimated for a sea state with Hs=3.5 meters and Tp=7 seconds on 10 meters water depth. But by calculating the relative water depth in test2117 it is seen that this test actually is on a lower relative water depth than the example given in Holthuijsen (2007), thus we can say that we are on shallow enough water for the effect from bottom friction to be present.

Secondly if we consider frictional forces in general, the energy dissipation is highly dependent on the distance traveled. Thus considering that our model test setup gives the wave 17 meters to contribute to energy dissipation, whereas say two or three wavelengths of this distance are in an area where bottom friction will contribute, it does not seem unlikely that this energy dissipation will be small. This in accordance with observations from Holthuijsen (2007), where he states that the contribution from bottom friction only will be of significance as the waves travel over long distances.

Thirdly the surface roughness is a very important parameter when considering bottom friction. Where a smooth surface (such as in our model test) will give a lot less friction than a typical sea bottom which may be covered with for example sand or rocks.

The reader should be aware that although there cannot be seen any significant contributions from bottom friction in the present model test, the effect are expected to make a significant contribution in a full scale event. Where there will not be idealized conditions such as the present model test.

Depth induced wave breaking

For the two wave probes closest to the beach we see clear effects of dissipation in the spectral estimations for the largest sea states. From visual observations the waves was seen to break in this area, also for the largest sea states. Thus it seems reasonable that this decrease in the energy of the spectrums is caused by energy dissipation due to wave breaking. This area corresponds to full scale water depths from 15-20 meters. For the largest sea states there were observed wave breaking as deep as a full scale water depth of 25 meters, but this was more sporadically and there are not seen any significant dissipation effects in the spectral estimates at this position.

Since these waves break so close to the shore it seems evident that these are influenced by depth induced effects. Depth induced wave breaking are caused by nonlinear interactions in which causes the waves to grow asymmetrical (front/back of the wave) with decreasing water depth. As a result of this asymmetry the waves will eventually break. There were seen a significant difference between the shape of the waves in this position compared to those at the start of the channel, and it can then be said with a reasonable degree of certainty that these waves break as a result of depth induced effects. Thus the decreases of the energy in the spectral estimates are caused by depth induced breaking.

Sub- and super-harmonic peaks

In the two largest tests analyzed here it was noticed both sub- and super-harmonic peaks in the spectral estimates, this caused by triad wave-wave interactions which shifts energy from the mid range frequencies in the spectrum to a sub-harmonic peak in the low frequency range and to a super-harmonic peak at two times the peak frequency. The presence of such nonlinear interactions indicates that the surface has transformed into a process where nonlinear contributions are important.

4.2.5 Behavior of the high frequency tail of the spectral estimates

An interesting aspect of the waves spectrums in finite water depths, are that the tail deviates from the tail observed in deep water. What is proposed in the TMA spectrum is that the first part of the high frequency tail will follow f^{-3} and the last part of the tail will follow f^{-5}. In order to investigate this proposed behavior the wave spectrums have been multiplied with both f^3 and f^5 (separately), if the tail follows let's say f^{-3} it should appear as a straight line when multiplied with f^3 and likewise for a tail following f^{-5}. One behavior that will not be accounted for in a spectral model such as the TMA spectrum is the sub- and super-harmonic peaks that are observe in our spectral estimates. As the TMA spectrum has been proposed as a possible spectral model, the behavior of this spectrum tail is also compared to that of our spectral estimates. As the TMA spectrum don't estimate the same dissipation of energy as we have measured in our model test (this will be documented in chapter 4.2.6), the spectrum tail has been scaled for a better visual comparison.

When comparing the behavior of the tail in the spectral estimates, the root mean square (RMS) of the spectrums has been used. But there have also been included a figure with several spectrum tails, then the reason for the RMS seems evident, since they follow approximately the same trend but with such overlapping curves that it is difficult to compare results from multiple wave probes in the same figure. The RMS values of the spectrum tails have been plotted for wave probe 2, 5 and 7 in order to get a measure of how the tail transforms from deep to shallow water. In this chapter there will be focused on test2111 and test2116, the high frequency tail from the rest of the tests can be found in Appendix D.

Omega to the power of -3

From Figure 64 the spectral estimates times f^3 are presented for test2111, and it is seen that the first part of the high frequency tail is not straight for any of the wave probes. They are however that far off. The tail of the TMA spectrum should in theory transform from a f^{-3} to a f^{-5} shape from "low" to high frequencies in the wave spectrum, this is not seen to occur for more than very small frequency band in the early stage of the high frequency tail. But it is important to have in mind that this tail has been scaled in order to compare the shape with our spectral estimates, and the spectrum have been

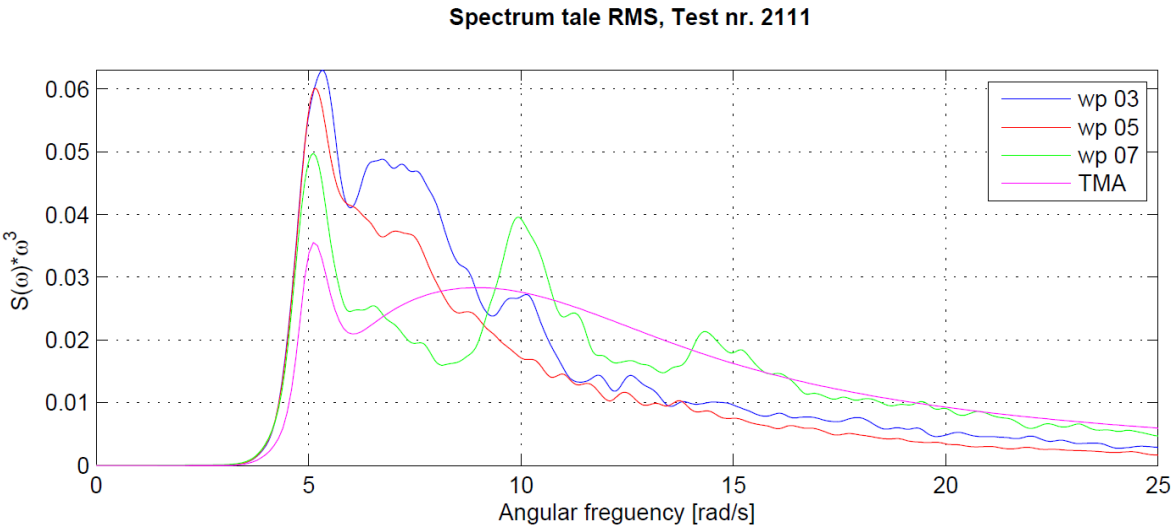

Figure 64: RMS of spectrum tail times omega^3, test2111

scaled up from something that have been significantly dissipated by bottom friction. Nevertheless the shape of the tail is not that far off. There are also observed a super-harmonic peak at three times the peak frequency that not are visible directly from the spectral estimates.

In Figure 65 the RMS of the spectral estimates times f^{-3} are presented for test2116, and it is seen that the first part of the tail from wave probe 7 are constant (just before the 2*omega_p peak). This shows that the tail follows $omega^{-3}$ for the first part of the high frequency tail. It is also noticed that the scaled tail of the TMA spectrum follows the behavior of the spectral estimates at wave probe 7 fairly well. Also here a super-harmonic peak at three times the peak frequency can be noticed.

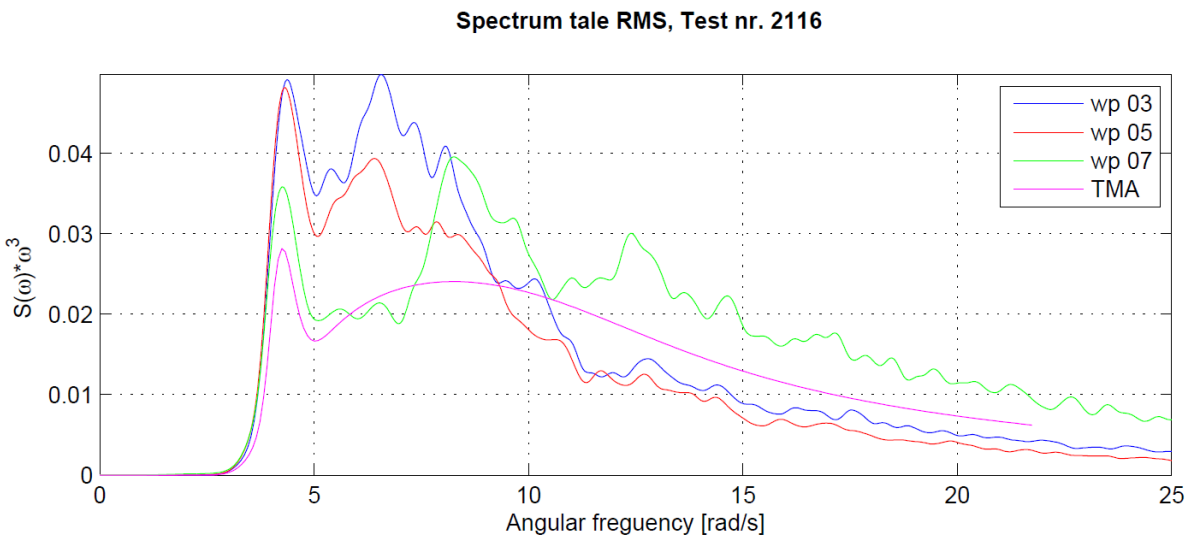

Figure 65: RMS of spectrum tail times omega^3, test2116

For the wave probes closer to the wave maker there cannot be found a relation for the high frequency tail with omega^-3.

Omega to the power of -5

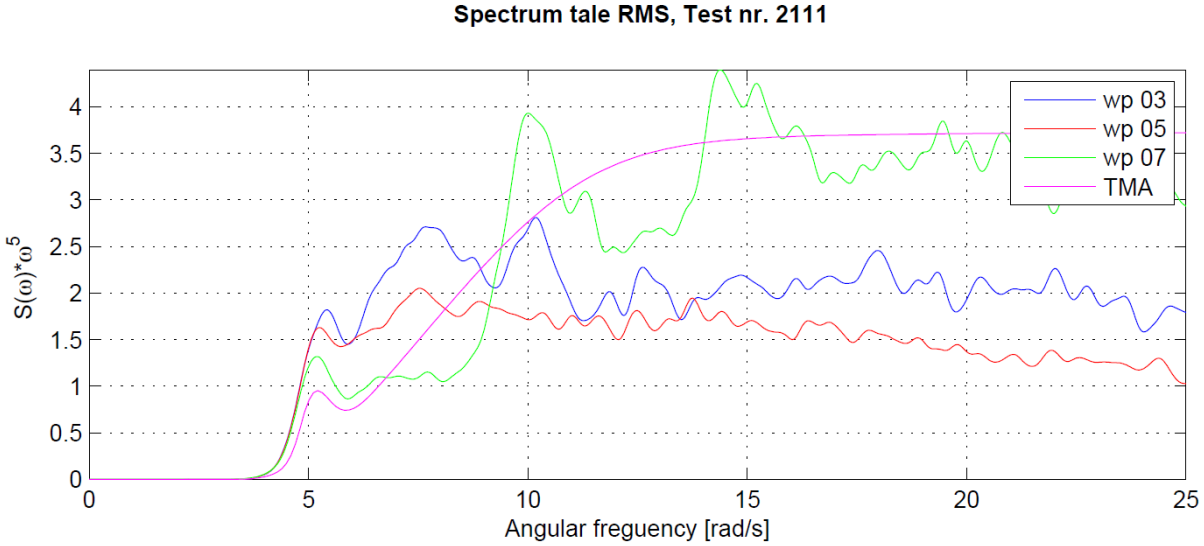

Figure 66: RMS of spectrum tail times omega^5, test2111

From Figure 66 the RMS of the spectrum tail for test2111 is presented, and the tail from wave probe 3 can be seen to follow approximately a straight line, thus the shape of the tail are approximately omega^{-5}. The tail at wave probe 5 is seen to decrease slightly, but it could also be said that it approximately follows omega to the power of -5. For wave probe 7 it seems that the tail follows omega to the power of -5 for all the places in the tail accept for the super-harmonic peaks at two and three times the peak frequency. Further it is seen that the TMA tail follows the behavior of the tail at wave probe 7 fairly well, however with the exception of the super-harmonic peaks.

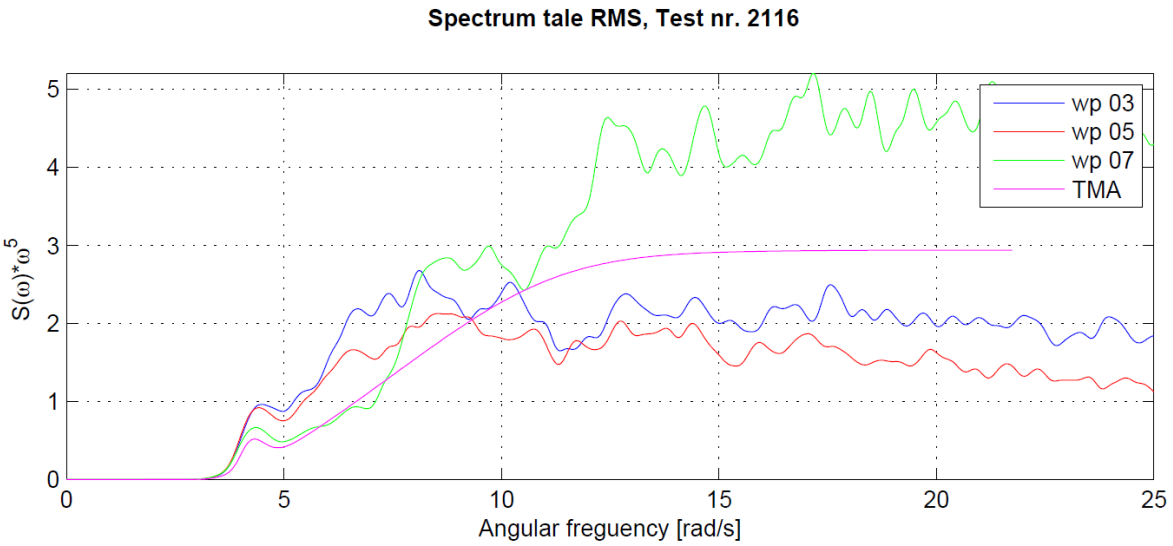

Figure 67: RMS of spectrum tail times omega^5, test2116

In Figure 67 the RMS values of the spectral estimates times omega to the power of 5 is presented for test2116, it is seen that wave probe 5 and 7 follows the behavior seen in Figure 66. Whereas the tail from wave probe 7 does not follow omega^-5 before it enters the last part of the high frequency tail.

Summary of observations

The behavior of the high frequency tail seems to follow omega to the power of -5 for the wave probes in deepest water.

The tail in shallow water should be dependent on ω^{-3} which is transformed into ω^{-5} in the high frequency part of the high frequency tail. This is seen to be the case for test2116, but for test2111 the proposed ω^{-3} behavior in the first part of the high frequency tail. And it seems like the tail of test2111 follows ω^{-5} between the super-harmonic peaks. But although the behavior of the tail between the super-harmonic peaks follow ω^{-5}, the presence of these peaks seem to increase the "thickness" of the high frequency tail, which is a behavior that cannot be described by pure ω^{-5} high frequency tail tail.

The TMA tail illustrated in these figures are as mentioned earlier scaled to fit the first part of the high frequency tail from the spectral estimates at wave probe 7, and should only be considered as an estimate of how a fitted TMA spectrum might behave. Considering this the tail of the TMA spectrum behaves fairly well, it does not predict the behavior exactly but it gives a good indication of how the tail transforms in finite water depths. It is also noted that the TMA tail grossly underestimates the magnitude of the high frequency part of the tail for test2116 (Figure 67), but it seems to accurately predict the place (frequencies) where the tail is transformed from ω^{-3} to ω^{-5}.

4.2.6 Comparison with analytical spectral models (TMA)

The TMA spectrum is described in chapter 2.5.1, and is basically a JONSWAP spectrum scaled to finite water depths. The TMA spectrum have been fitted to our spectral estimates by using the measured

significant wave height and the given water depth from each wave probe, further the spectrum have been fitted to match the peak of the spectral estimate by adjusting the peakdness coefficient (gamma) in the TMA spectrum. The TMA spectrum have been fitted to match the second wave probe in the propagation direction of the waves (wave probe 2), and the parameters remain the same throughout the channel in order for us to be able to compare the transformation of the spectral estimates with the TMA spectrum. The trend seen when comparing TMA with our spectral estimates is the same, thus there have only been included one example in this chapter. The comparison will be illustrated by examples from different wave probe, a complete set of plots where the spectral estimates are compared with the TMA spectrum can be found in Appendix E. Comparisons with the TMA spectrum and spectral estimates from other tests can be found in Digital appendix 2.

The first repetition of test2116 will be used as an example in this chapter. From the Figure 68 the spectrum estimation from test2116 can be seen in a solid red line, whereas the TMA is shown in a dotted blue line. It is seen that it is not a perfect fit, but that is of small significance. They are in the same order of magnitude, and it is the change further down the channel that is of interest.

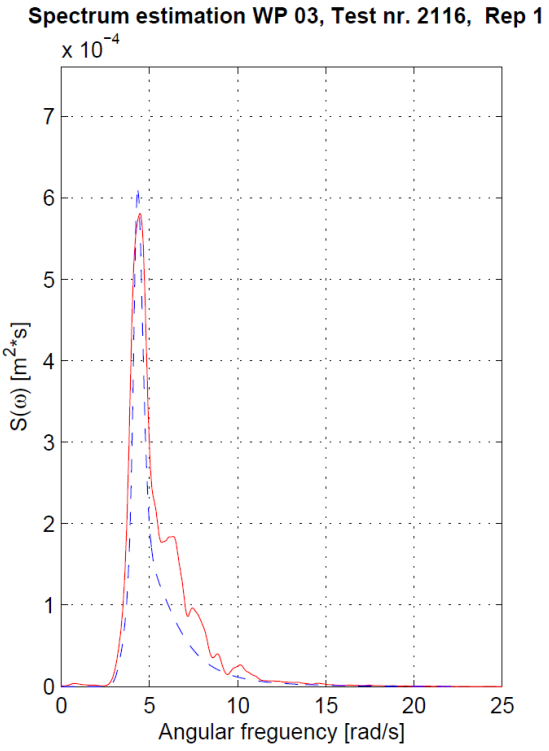

Figure 68: Comparison with spectral estimate and TMA at wave probe 3, test2116

In the most interesting area for a full scale water depth in the region of 25 meters, this corresponds to the water depth where wave probe 11 is placed (h=0.309m). The comparison for wave probe 11 can be seen in Figure 70, and it is seen that the TMA spectrum grossly underestimates the energy in the wave spectrum, compared to that of the generated spectral estimate in the same position.

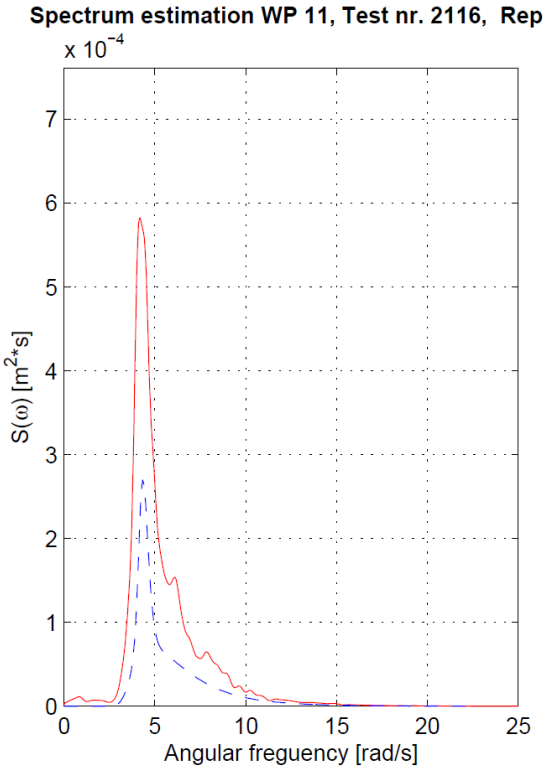

Figure 70: Comparison with spectral estimate and TMA at wave probe 11, test2116

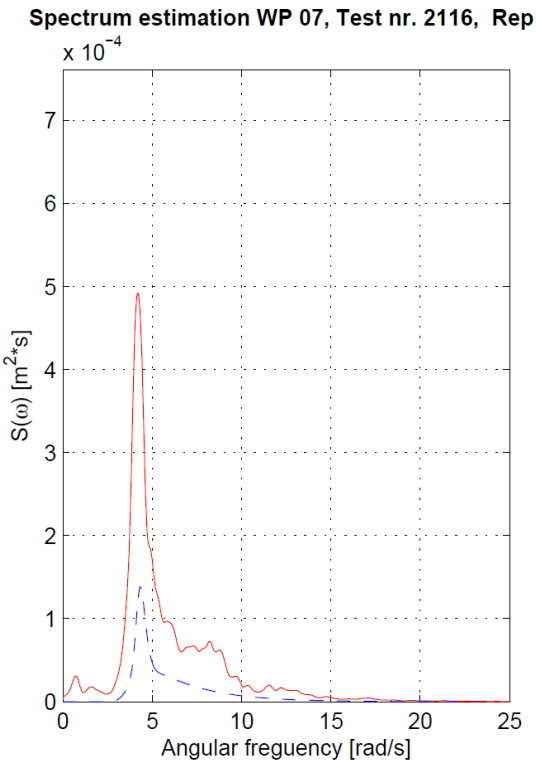

Figure 69: Comparison with spectral estimate and TMA at wave probe 7, test2116

It is obvious that the TMA spectrum has taken into account a significant amount of dissipation, the only place we have noticed a significant amount of dissipation in the spectral estimates are for the wave probe close to the beach. Then TMA is also compared to the spectral estimates for the last wave probe (wave probe 7), this can be seen in Figure 69.

It then seems clear to the author that the TMA spectrum overestimates the energy dissipation in the wave spectrums in the results from our model test. The explanation for this may be that the TMA spectrum only considers dissipation from bottom friction, whereas there in our model test are no noticeable effects from bottom friction.

It is worth reminding the reader that TMA does not account for dissipation due to wave breaking at all, but from Figure 69 it is seen that the estimated dissipation from bottom friction in the TMA spectrum are larger than the measured dissipation from wave breaking in our model test.

Using the TMA may have been a bit optimistic in the first place, as it is an spectral model that assumes that the sea bottom is gently sloping, which it is not in our case. An as argued in the previous chapter the slope, and thus propagation distance of the waves seems like an obvious explanation of the absence of bottom friction in our results.

As can be seen from chapter 4.2.5 the tail of the TMA spectrum seems to predict the behavior in the high frequency range of the spectrum fairly well.

4.2.7 Comparison with previous work

In Nilsen (1997) there have also been estimated spectral estimates, and there have been found one test that corresponds fairly well to some of the tests performed in our model test. The test used for comparison has a Hm0=0.1151 meters, Tp=1.417 seconds and a peakedness parameter of 3.3 the water depth is 0.31 meters. We do not have any exact matches of this test, but test2116 corresponds fairly well, and will be used for comparison. Furthermore the position of wave probe 12 corresponds to approximately the same water depth as from Nilsen (1997). The data from Nilsen (1997) are found by eye from figures presented in the thesis, and should only be taken as a rough trend. But the values for the peak frequency are fairly close to exact values, and this should be enough for us to determine whether or not the spectral estimates from our model test are in the same order of magnitude as those from Nilsen (1997). But as the spectral estimates in Nilsen are presented in terms of Hz instead of angular frequency, the spectral estimates have to be converted to a frequency (Hz) domain. This can be done fairly simple by specifying that you want the spectral estimates in terms Hz in the WAFO (2000) function "dat2spec" in matlab. Similar smoothing and scaling procedure as previously has also been performed.

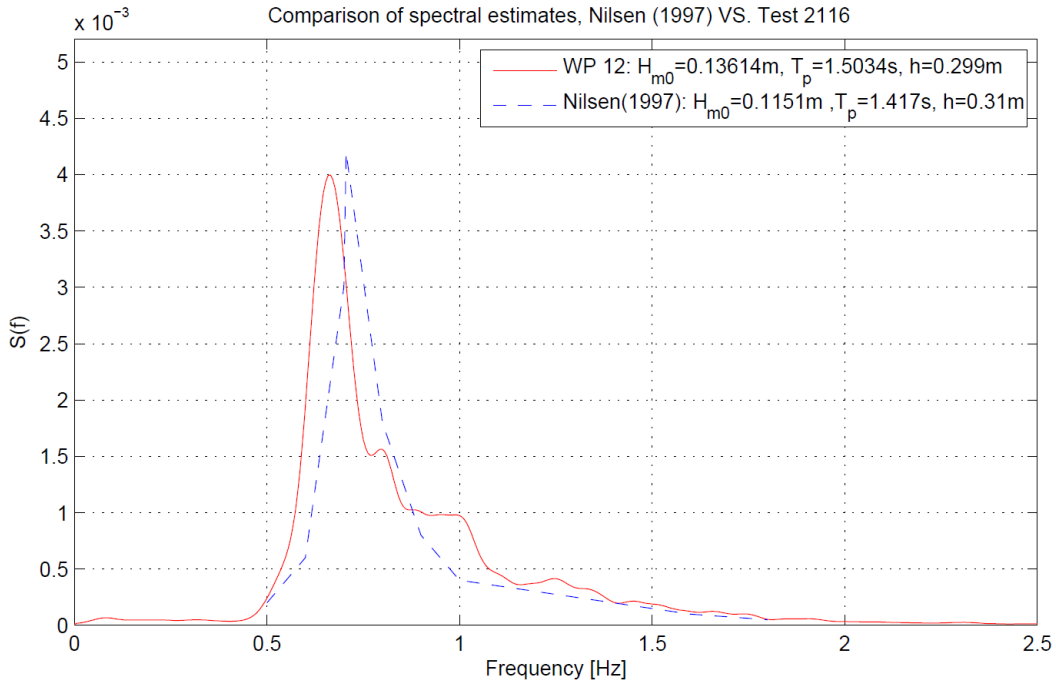

Figure 71: Comparison with spectral estimates from present model test and Nilsen (1997)

From Figure 71 the comparison are presented, and it is seen that the results compare fairly well. Test2116 has a larger significant wave height than that of Nilsen (1997), but this is mostly due to a broader wave spectrum. And it seems reasonable to say that the results compare fairly well.

4.3 Wave and crest height distributions

In order to identify the wave and crest heights from a time series of surface elevation, there have to be performed either a zero up crossing or a zero down crossing analysis. For a Gaussian process the two approaches should yield statistically the same wave heights. In finite water depth where the process might not be Gaussian we do not know with certainty that this will be the case. Then in order to check that a zero up crossing analysis can be used, there have been performed analysis with both approaches along with a Rayleigh reference all the selected tests in this thesis. These figures can be found in the Digital appendix 3 attached to this thesis. An example of this is however presented in Figure 72, and it is seen that the resulting wave heights from zero up- and down crossing analysis gives resulting wave heights in the same order of magnitude. The crest heights will be exactly the same for both zero up- and down crossing analysis.

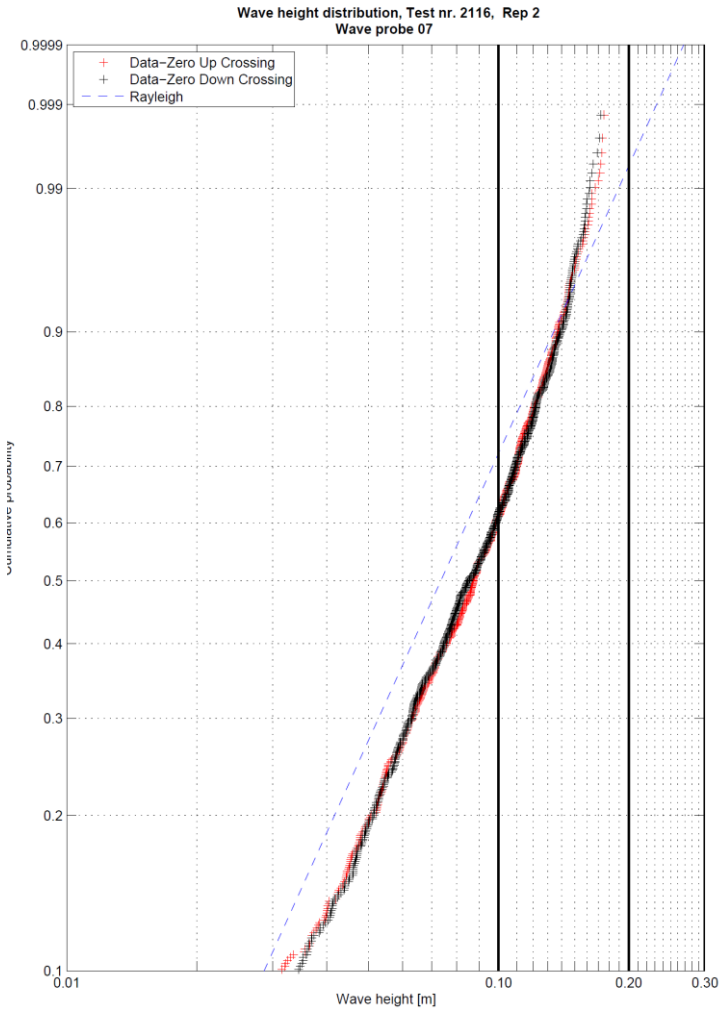

Figure 72: Comparison with data from zero up and down crossing analysis, and Rayleigh

This trend is also seen for the rest of the tests only with some exceptions, which is within a reasonable degree of error. It can then be said that the wave heights can be approximated as independent of the type analysis used to obtain them.

Goda (2010) states that a zero up crossing analysis will yield slightly larger individual wave periods than a zero down crossing analysis when the waves are asymmetrical with respect to the front and back of the wave. But the characteristic wave heights will be statistically the same for both approaches.

Since wave periods not will be of importance here, a zero up crossing analysis are performed in order to find the wave and crest heights in the time series.

The data from the model test will then be compared with analytical models, the description of these models can be found in chapter 2.5.4 and 2.5.5 for wave crest and wave height distributions respectively. The distributions have been generated at each wave probe for all the relevant tests with corresponding repetitions that are of interest in this thesis. As a result of this there have been generated a large number of figures, thus in this chapter only representative examples will be presented. The complete set of figures from the presented tests can be found in Appendix 4 and Appendix 5 for wave height and crest height distributions respectively. For the rest of the tests and corresponding repetitions the reader is referred to the digital appendix attached to this thesis, where figures from all the tests can be found.

There will be presented results for a large, medium and small sea state. The tests that are chosen are test2117, test2111 and test2116. Further the results will be presented in the propagation direction of the wave, thus starting with the measured results from the wave probes closest to the wave maker, and finishing with results from the wave probes closest to the beach.

4.3.1 Wave height distributions

Test2116

In Figure 73 the wave height distributions are compared with data from test2116, at the start of the channel (wave probe 2). In this figure the distribution proposed by Battjes et.al. (2000) are following the Rayleigh distribution, as the threshold wave height is larger than the largest waves in the time series. The data is seen to approximately follow the Rayleigh distribution for the lower probabilities, but for the higher probabilities the distributions proposed by Forristall (1978) and Næss (DNV(2007)) are seen to fit the data better. This seems reasonable as the Rayleigh distribution is considered as a conservative distribution. There are also noticed that there are a wave height exceeding that predicted of Forristall and Næss, however this does not exceed the wave height predicted of the Rayleigh distribution.

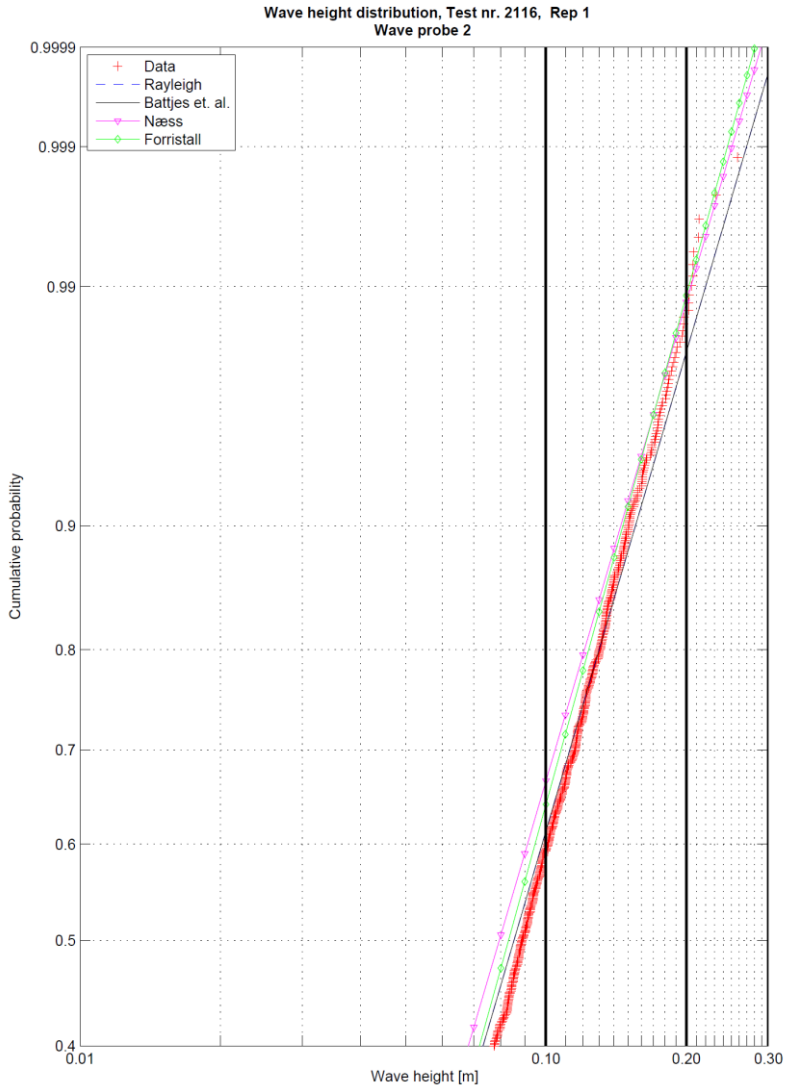

Figure 73: Wave height distributions at wave probe 2, test2116

From Figure 74 the wave height distributions are compared with data at wave probe 11, and it is seen that the data seem curve upwards as the data no longer follows a straight line in the Weibull

paper. This behavior seems to be reasonable well captured by the distribution proposed by Battjes et.al. (2000). The Rayleigh distribution is as expected conservative, but both the Forristall and Næss distribution predicts the wave heights fairly well for the higher probabilities.

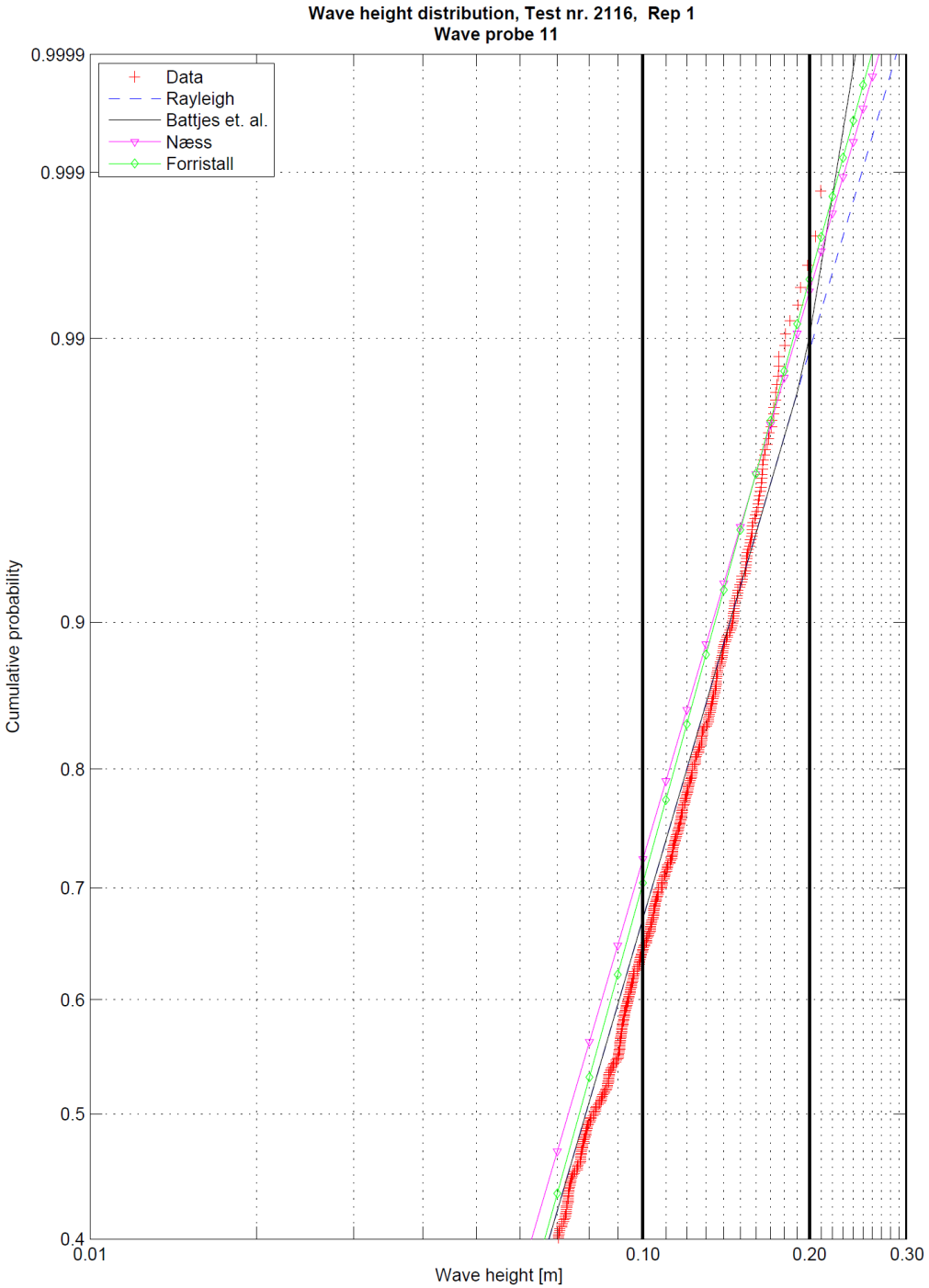

Figure 74: Wave height distributions at wave probe 11, test2116

In Figure 75 the wave height distributions for the wave probe closest to the beach are shown, and it is seen that the Battjes distribution under predicts the wave heights for the higher probabilities. The

gradient of the break in the curve seem to fit the data, but the threshold wave height is obviously too low. Once again the Forristall and Næss distribution predicts the wave heights for the higher probabilities fairly well, and the Rayleigh distribution gives conservative wave heights at high probabilities.

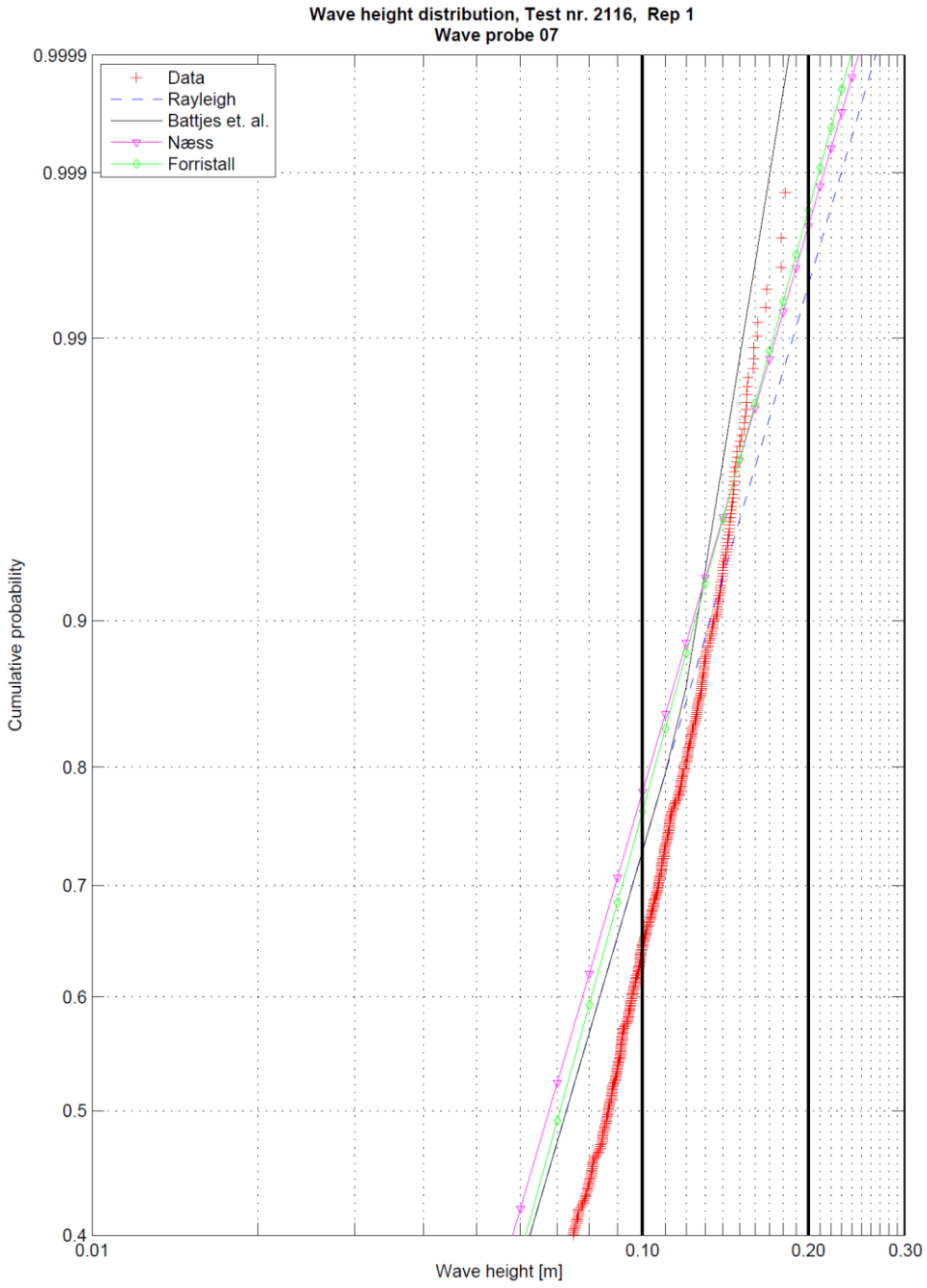

Figure 75: Wave height distributions at wave probe 7, test2116

Test 2111

In Figure 76 the wave height distributions are compared with data from test2111, at the start of the channel (wave probe 2). The data is seen to follow the Forristall and Næss distribution for the higher

probabilities, and as observed previously the Rayleigh distribution is conservative for the higher probabilities.

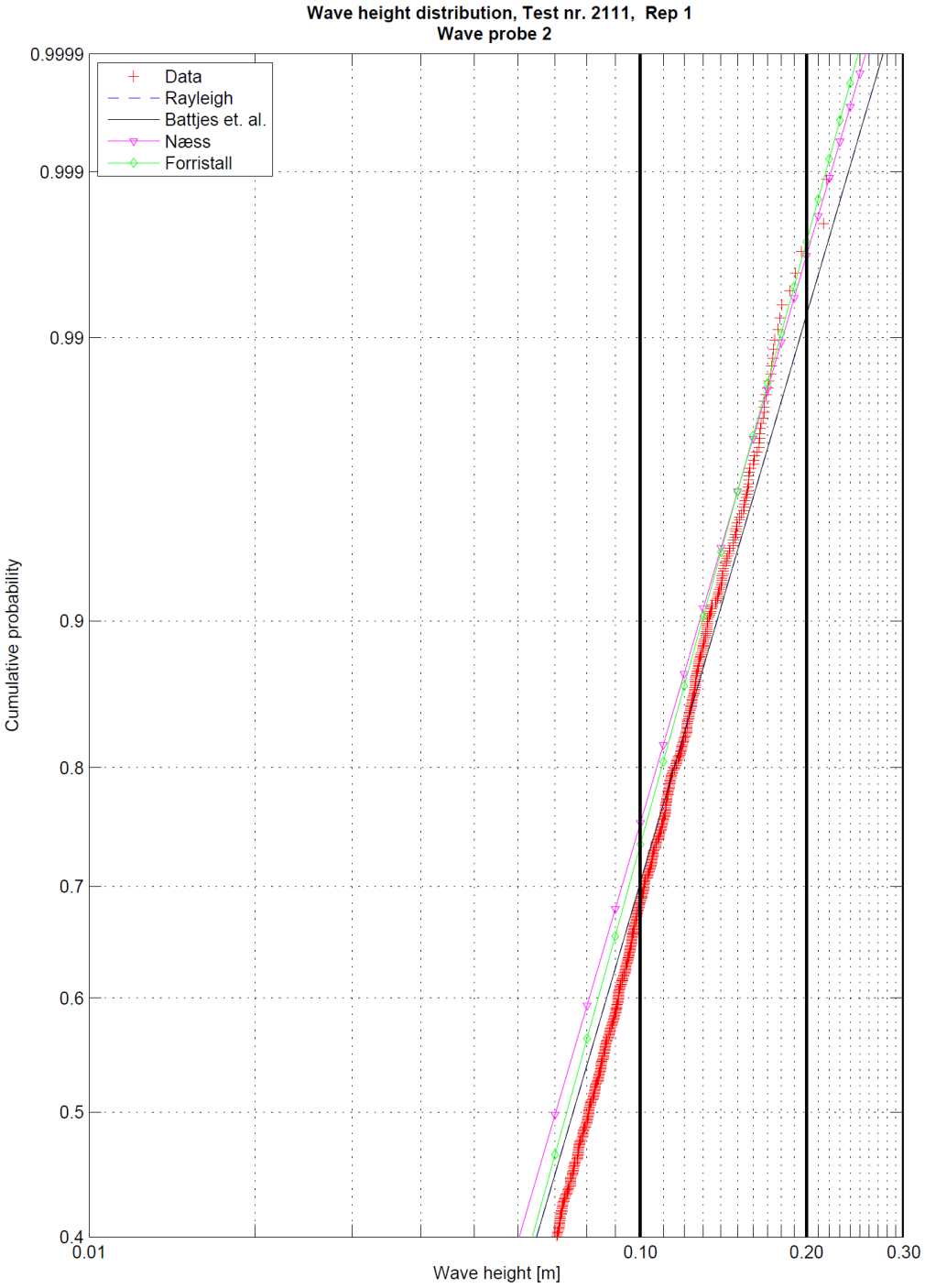

Figure 76: Wave height distributions at wave probe 2, test2111

From Figure 77 the wave height distributions at wave probe 11 is presented and it is seen that the data follows the Rayleigh distribution for the lower probabilities, and it seems to shift towards the

Forristall and Næss distribution for the higher probabilities. Thus the Rayleigh distribution is once again seen to be conservative for the higher probabilities.

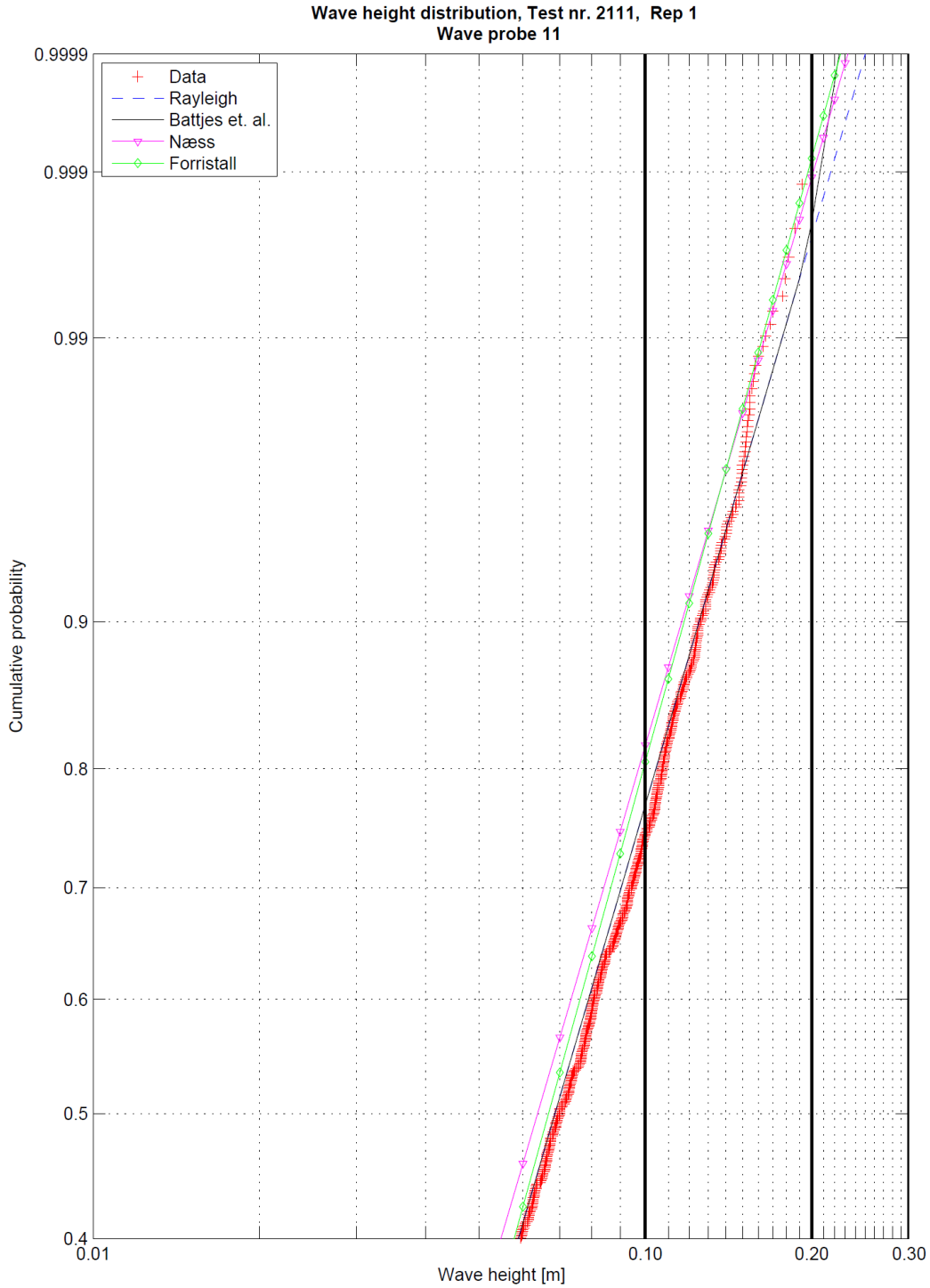

Figure 77: Wave height distributions at wave probe 11, test2111

In Figure 78 the wave height distributions are compared to the data at wave probe 7, and it is seen that the Battjes distribution fits the data well at high probabilities. And thus the Forristall, Næss and Rayleigh distribution will all be conservative in this case. When comparing the distributions from the

rest of the repetitions at this position, it is seen similar behavior for most of the cases. But for some repetitions the data is located between the Battjes distribution and Forristall&Næss distributions.

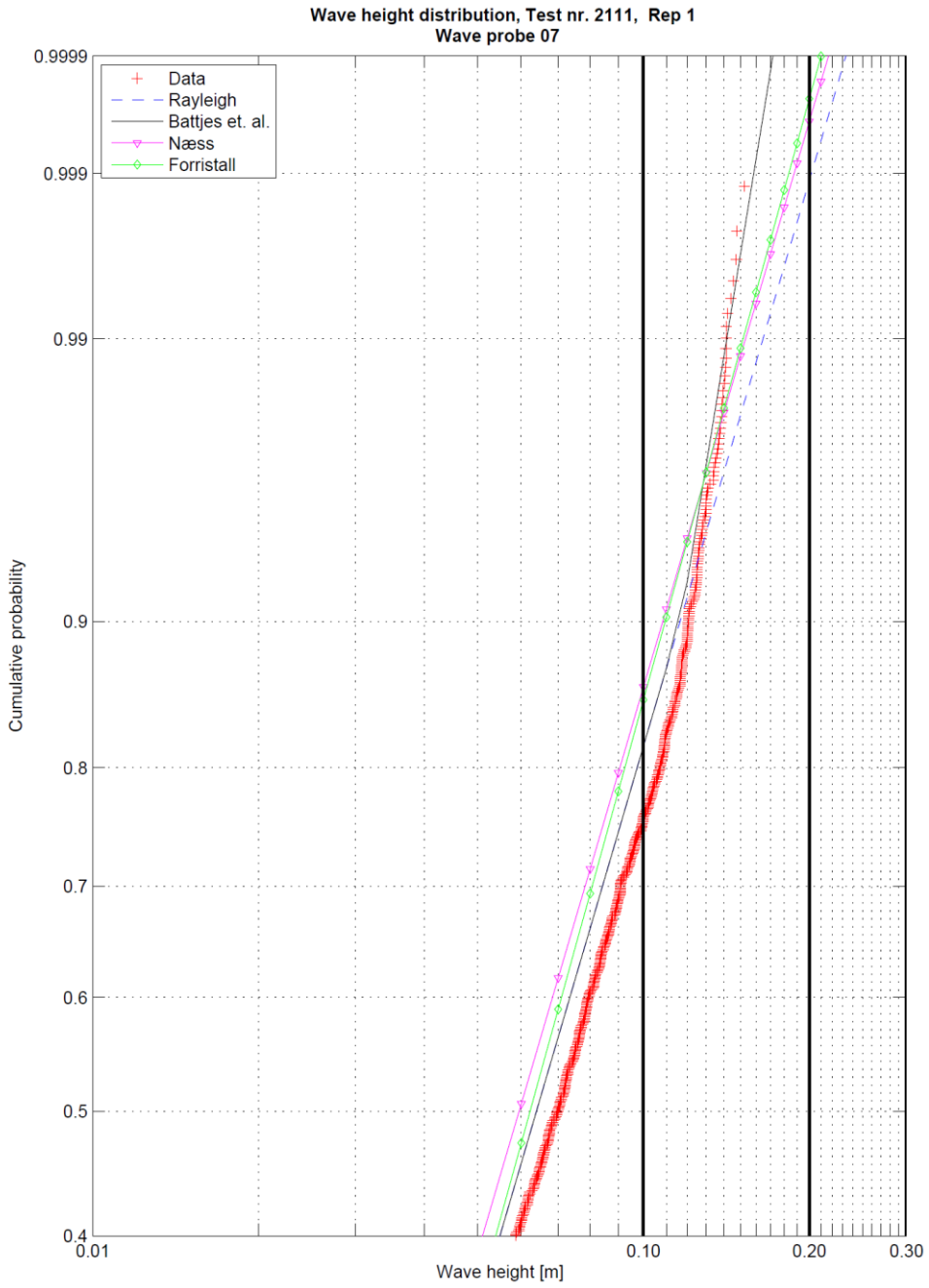

Figure 78: Wave height distributions at wave probe 7, test2111

Test 2117

In Figure 79 the wave height distributions for test2117 is shown for wave probe 2, and it is seen that the data follows the Forristall distribution both for high and low probabilities. For the high probabilities the Næss distribution also gives a reasonable estimate of the wave heights, once again the Rayleigh distribution are conservative for high probabilities.

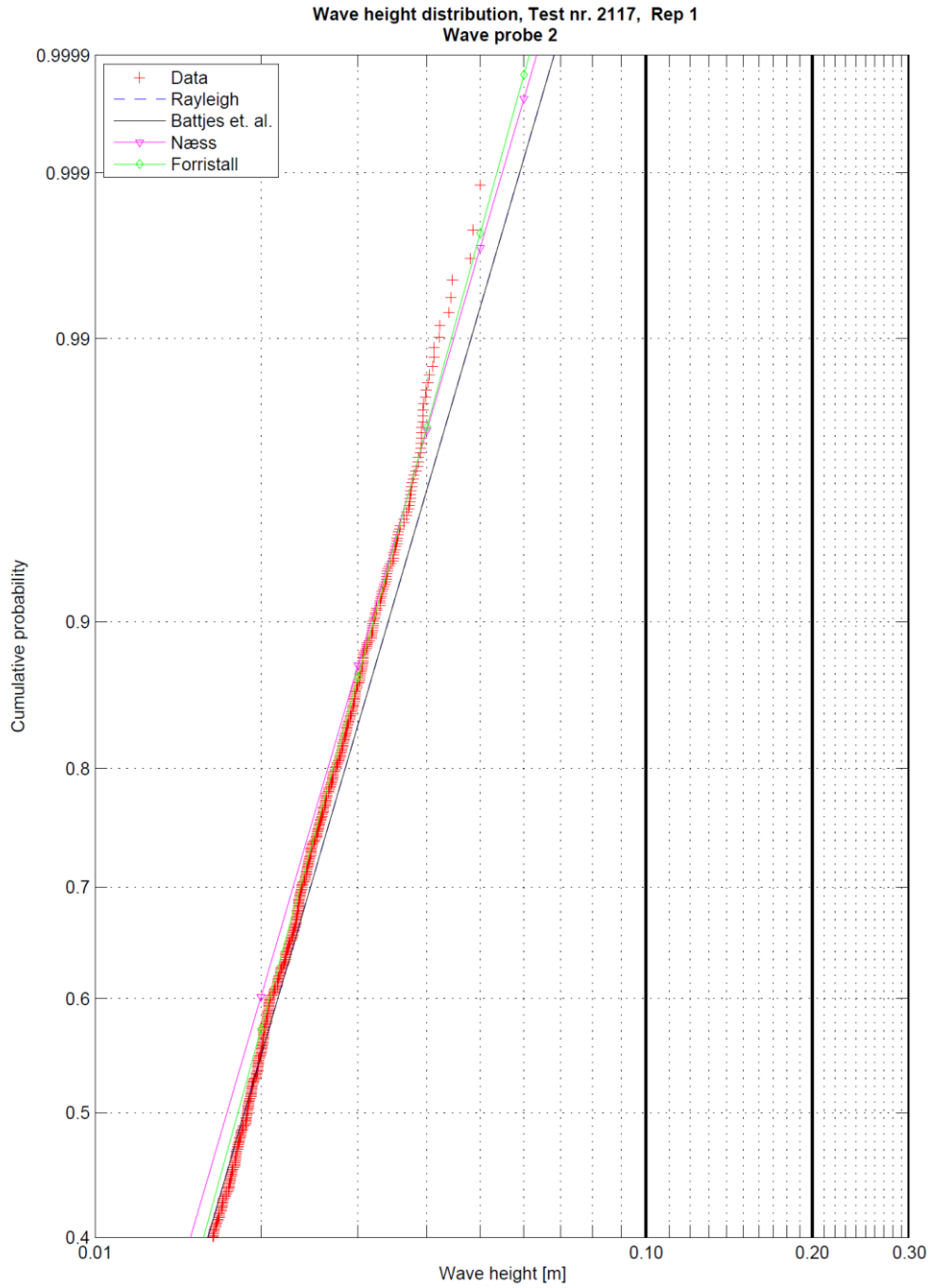

Figure 79: Wave height distributions at wave probe 2, test2117

In Figure 80 the wave height distributions are shown at wave probe 11, and it is seen that the data follows the Forristall distribution. For high probabilities the Næss distribution also gives a good fit, as this distribution is very similar to the Forristall distribution for high probabilities. It is also seen that the Rayleigh distribution is conservative for high probabilities.

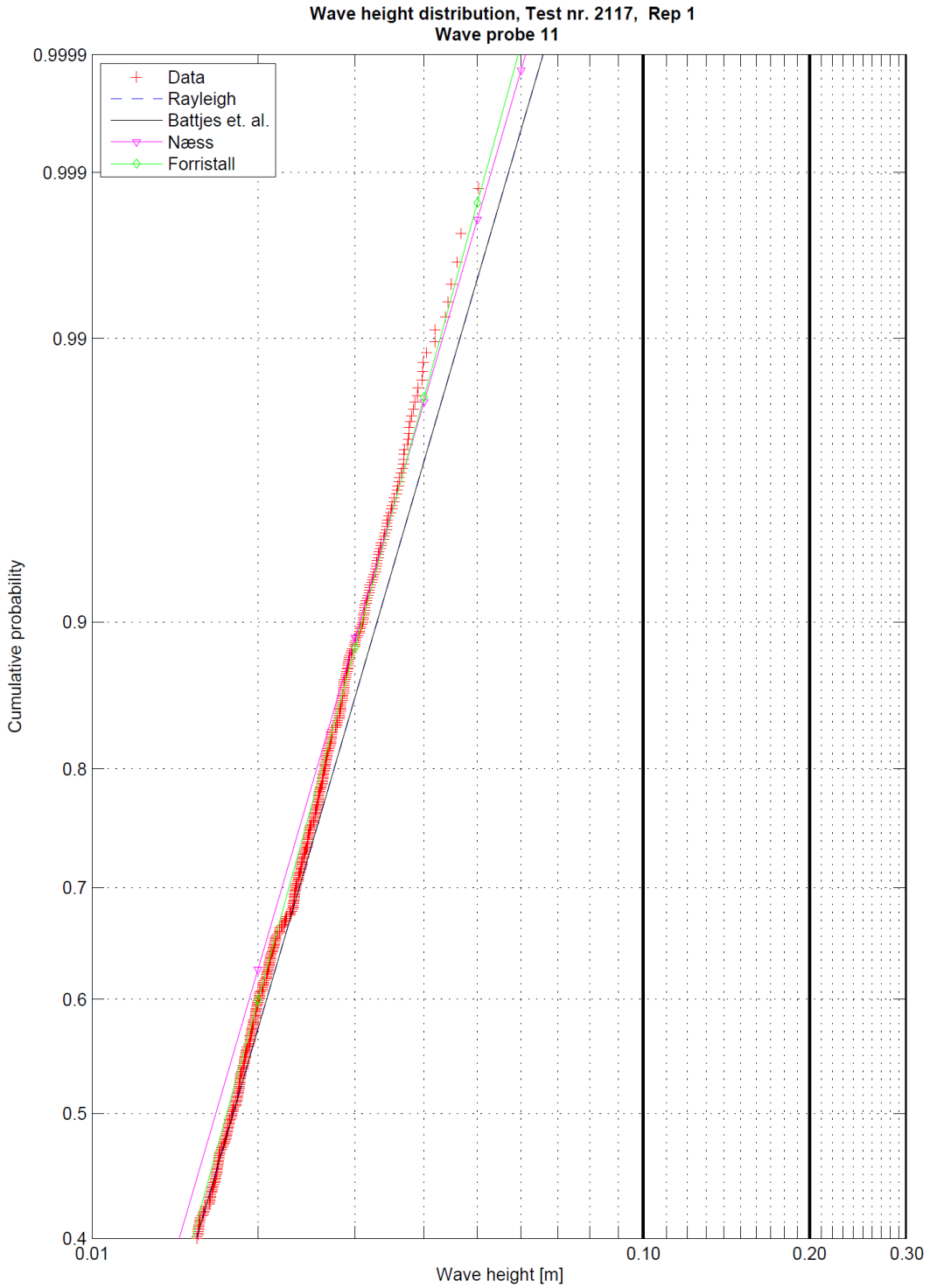

Figure 80: Wave height distributions at wave probe 11, test2117

From Figure 81 the wave height distribution at wave probe 7 are shown, and much of the same behavior as for the other wave probes are seen here as well, where the data fits the Forristall distribution for both high and low probabilities. Thus the Næss distribution also fits the data well for high probabilities. And as seen before the Rayleigh distribution remains conservative.

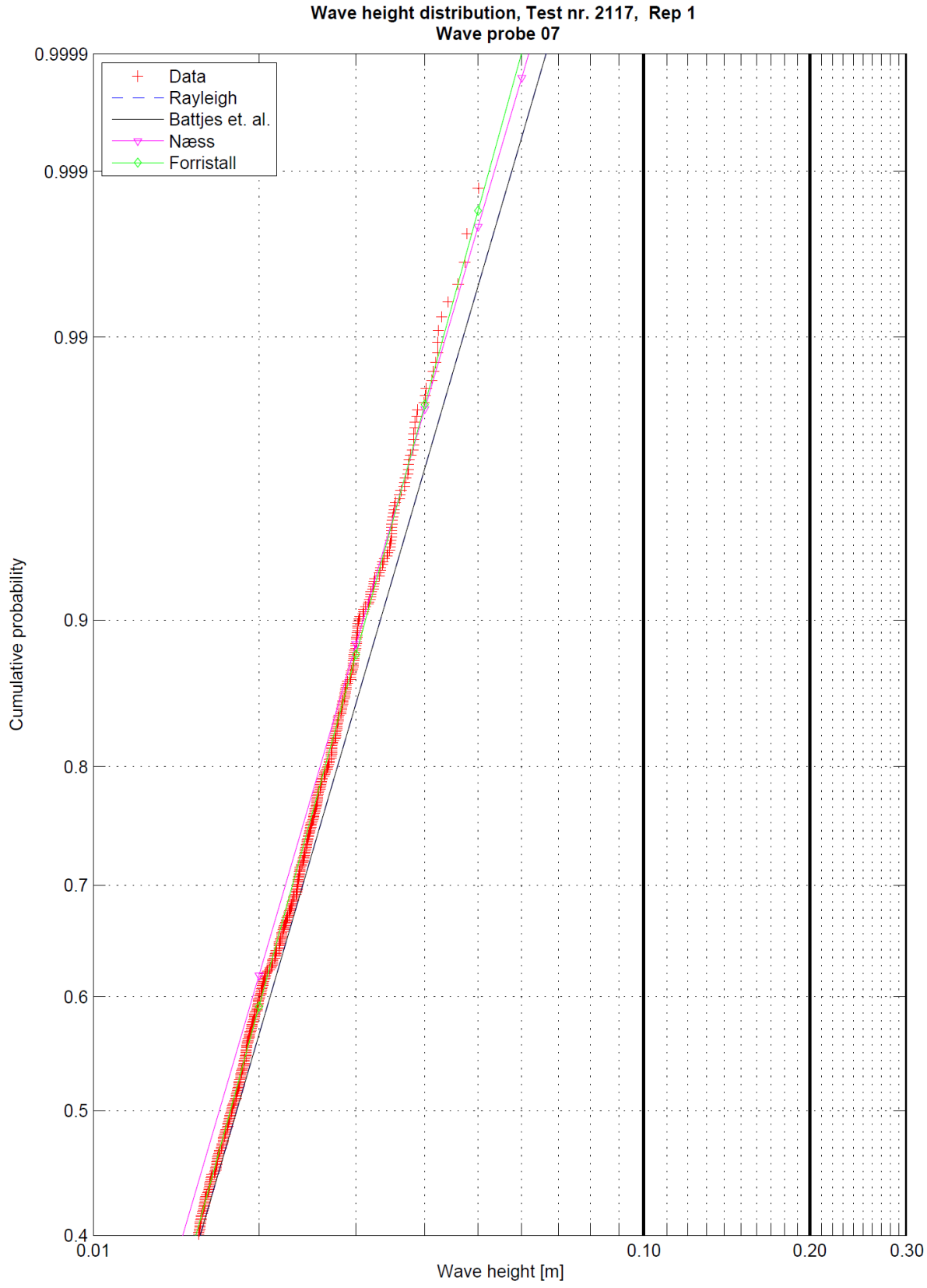

Figure 81: Wave height distributions at wave probe 7, test2117

Summary of observations

For the larger sea states it is observed that the data appear to follow a line with a larger gradient for the higher probabilities, this is something that are more clearly seen in shallow water and is most probably a result of depth induced wave breaking. This phenomena is reasonable well described by the distribution proposed by Battjes et.al. (2000), but for some repetitions of both test2111 and 2116 this distribution underestimates the wave heights. The data in these cases seem to follow a shape similar to the Battjes distribution, but the threshold wave height (which is the wave height of the discontinuity in this distribution) seem to be to small in these cases.

On deeper water the data seem to fit the distributions proposed by Forristall (1978) and Næss (DNV(2007)) for high values of cumulative probability.

The smaller sea states are seen to follow the Forristall distribution, but the Næss distribution also gives an accurate prediction of the wave heights for high probabilities (cumulative). This applies for measurements throughout the channel.

It is however seen a different behavior for test2109 , which not have been analyzed in this chapter. Here the data at high probabilities turns in the opposite direction as seen for the depth induced wave breaking in the larger sea states, and thus the proposed distributions underestimates the wave heights. This phenomenon is observed at the wave probe closest to the beach (wave probe 7), at wave probe 6 this phenomena is present but the magnitude is not that large and the data is seen to follow the Rayleigh distribution. It is speculated that the cause of this may be from effects of shoaling on the wave heights, but the author does not have any evidence that this is the case. But this explanation makes sense, as it is seen for the larger sea states that the wave heights with lower cumulative probability seem to have the same tendency, before effects from wave breaking seem to be predominant.

4.3.2 Crest height distributions

Test 2116

In Figure 82 the crest height distributions are compared with data for test2116 at wave probe 2, and it is seen that the crest heights for low probabilities are underestimated by the distribution proposed by Forristall (2000). For the higher probabilities the Forristall distribution are in good agreement with data. The Rayleigh distribution for crest heights underestimates the crest heights as previously predicted.

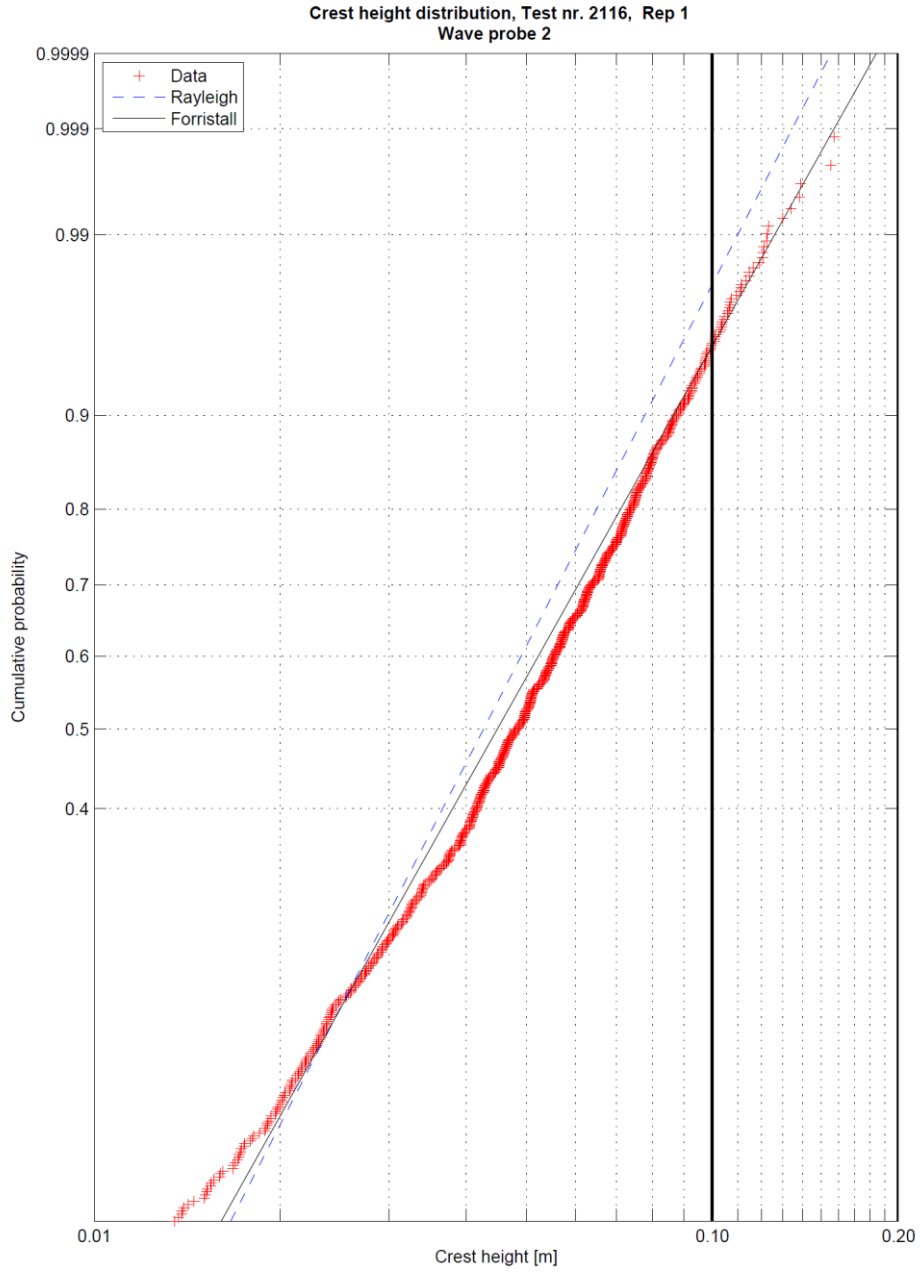

Figure 82: Wave crest height distributions at wave probe 2, test2116

From Figure 83 the crest height distributions are compared with data from wave probe 11, and it is seen that the Forristall distribution predicts the crest heights fairly well. As previously seen the Rayleigh distribution under predicts the crest heights.

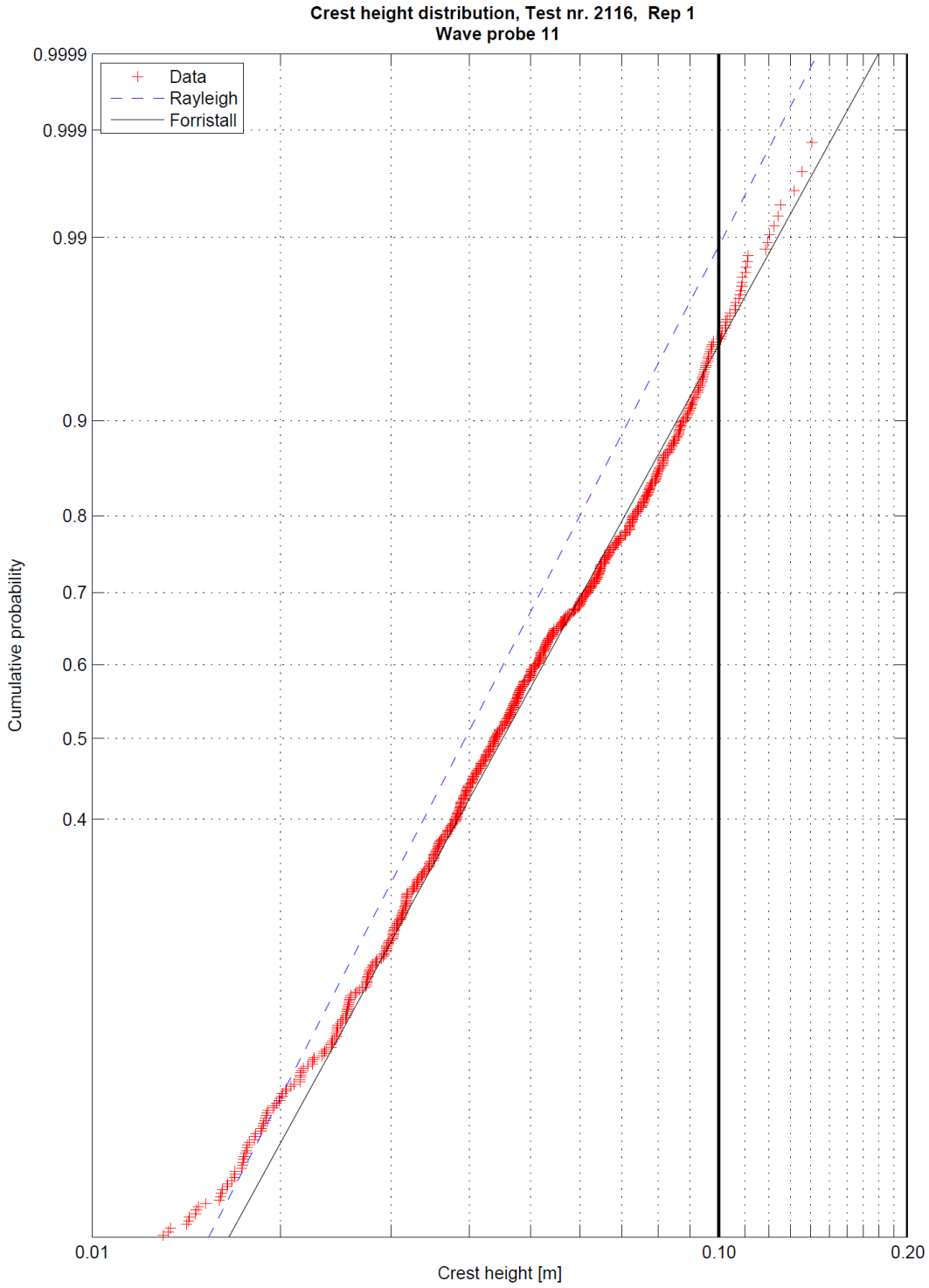

Figure 83: Wave crest height distributions at wave probe 11, test2116

In Figure 84 the crest height distributions at wave probe 7 are compared to data, and it is seen that the crest heights are affected be wave breaking as they seem to increase with a steeper gradient. As a result of this the Forristall distribution will be conservative for the higher probabilities, for lower probabilities the distribution are slightly un-conservative.

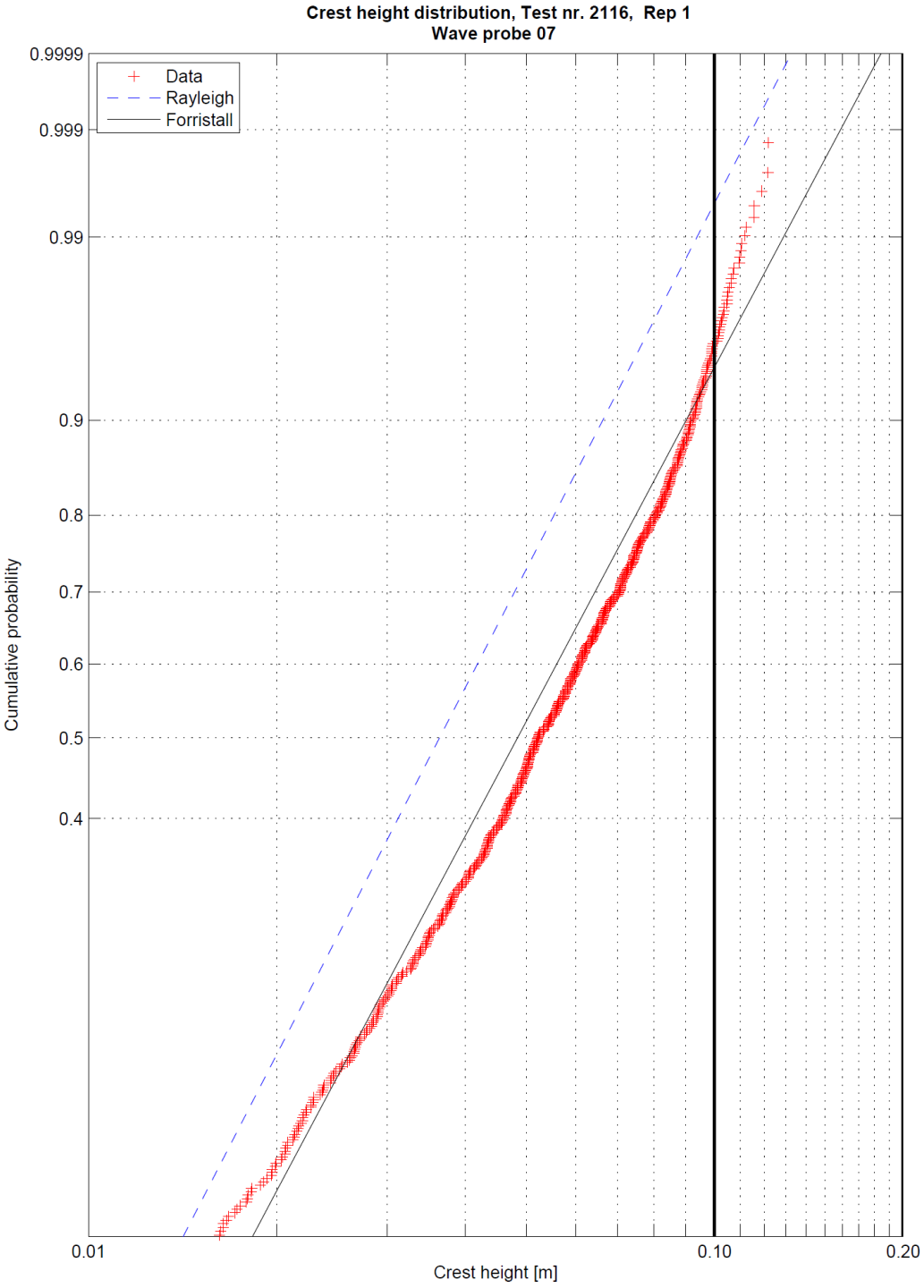

Figure 84: Wave crest height distributions at wave probe 7, test2116

Test 2111

From Figure 85 the crest height distributions from test2111 can be seen at wave probe 2, and it is seen that the Forristall distribution follows the data fairly well. And once again the Rayleigh distribution underestimates the crest heights.

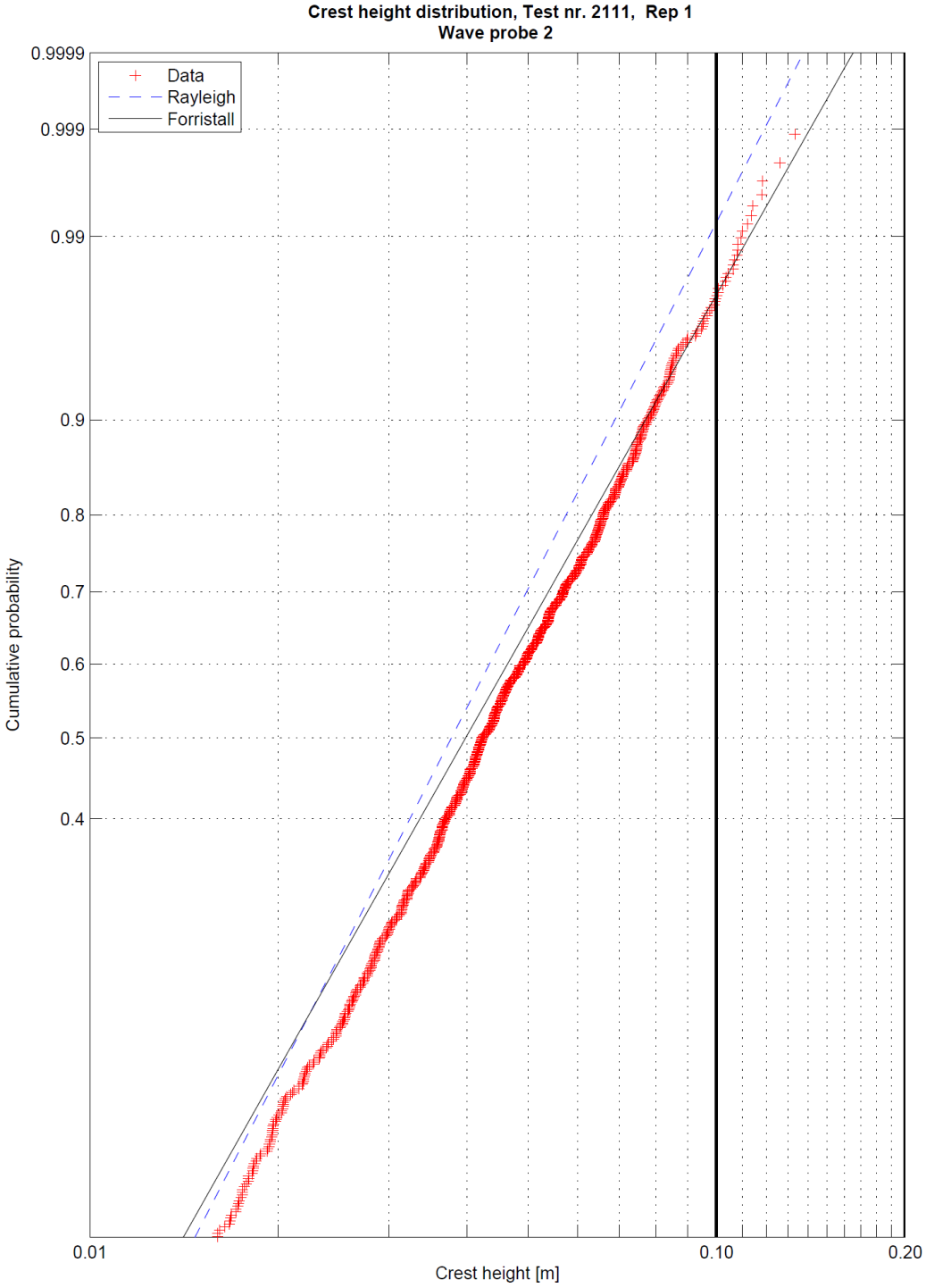

Figure 85: Wave crest height distributions at wave probe 2, test2111

In Figure 86 the crest height distributions are compared with data at wave probe 11, and it is seen that the crest heights are fairly equal to those predicted by the Forristall distribution. Once again the Rayleigh distribution is un-conservative.

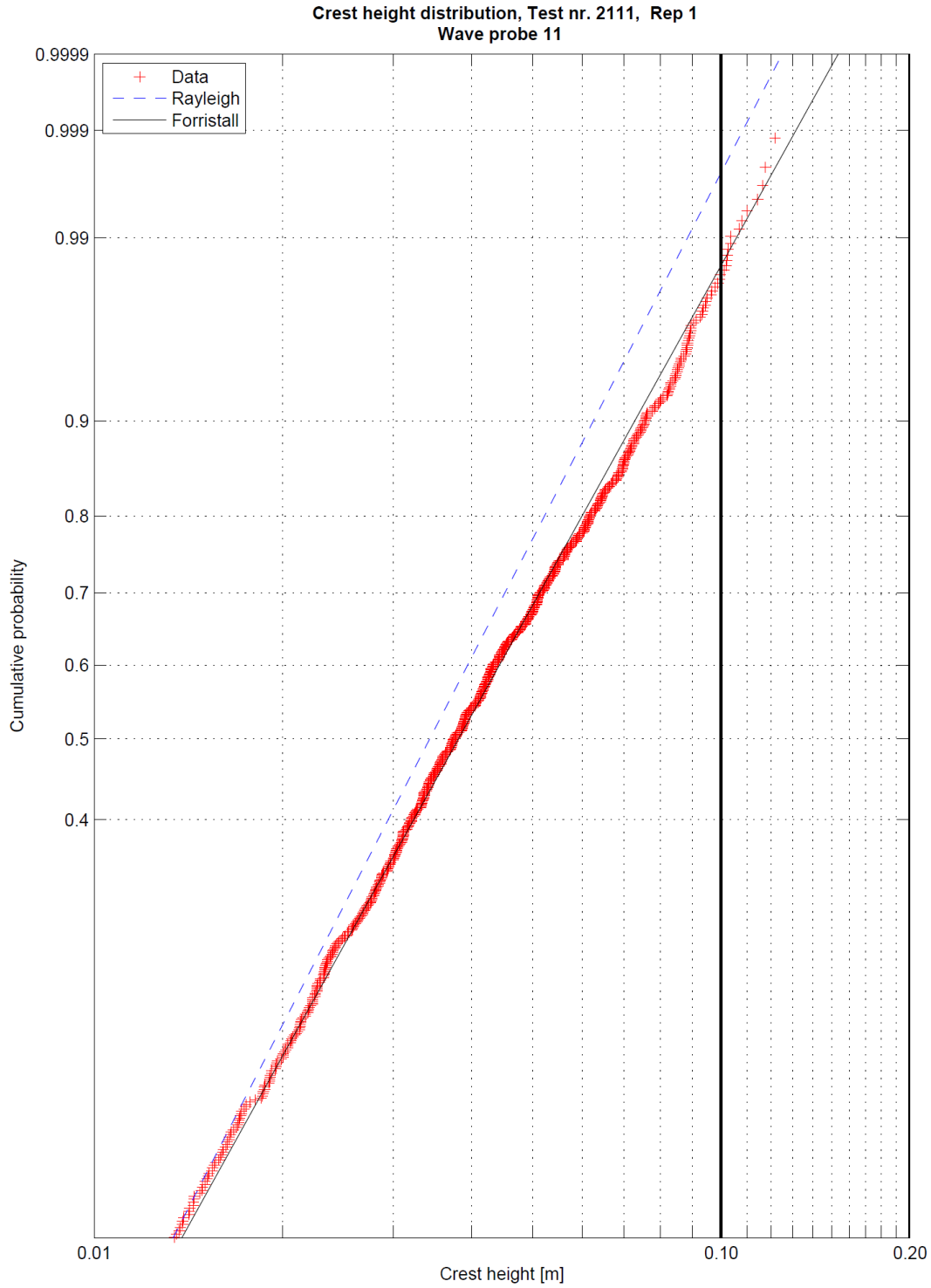

Figure 86: Wave crest height distributions at wave probe 11, test2111

From Figure 87 the crest height distributions at wave probe 7 is presented, and it is seen that the crest heights from data increases with a larger gradient which most likely is caused by depth induced wave breaking. And thus the Forristall distribution will be conservative for the higher probabilities, the Rayleigh distribution will still be non-conservative. Although the largest wave in the time series almost can be predicted by the Rayleigh distribution, it will give a significant under estimation of the crest heights for the rest of the data from the time series.

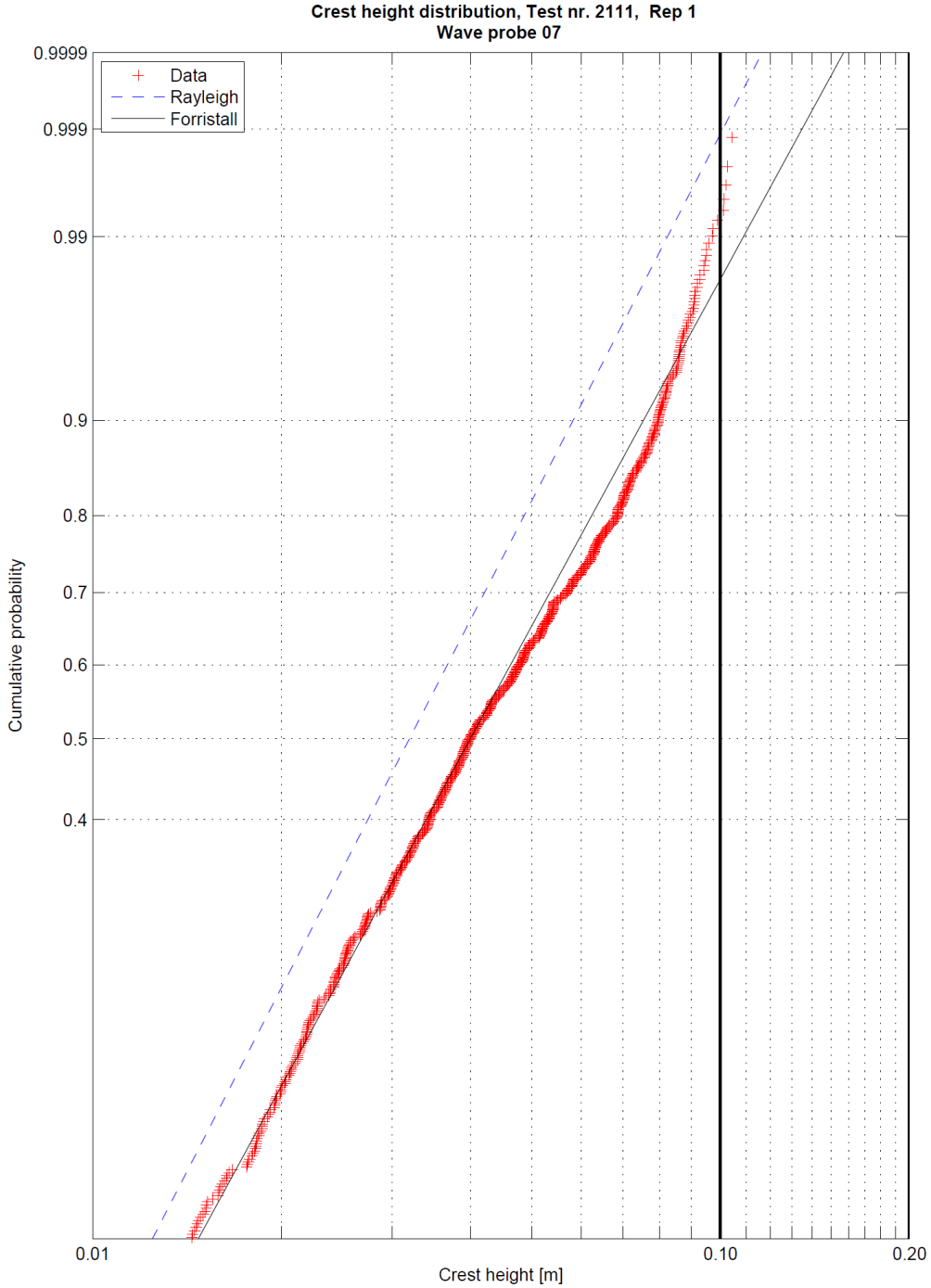

Figure 87: Wave crest height distributions at wave probe 7, test2111

Test 2117

In Figure 88 the crest height distributions are compared with data from test 2117 at wave probe 2, and it is seen that both the Forristall and Rayleigh distribution follows the data fairly well. However for the highest probabilities the crest heights are slightly under estimated.

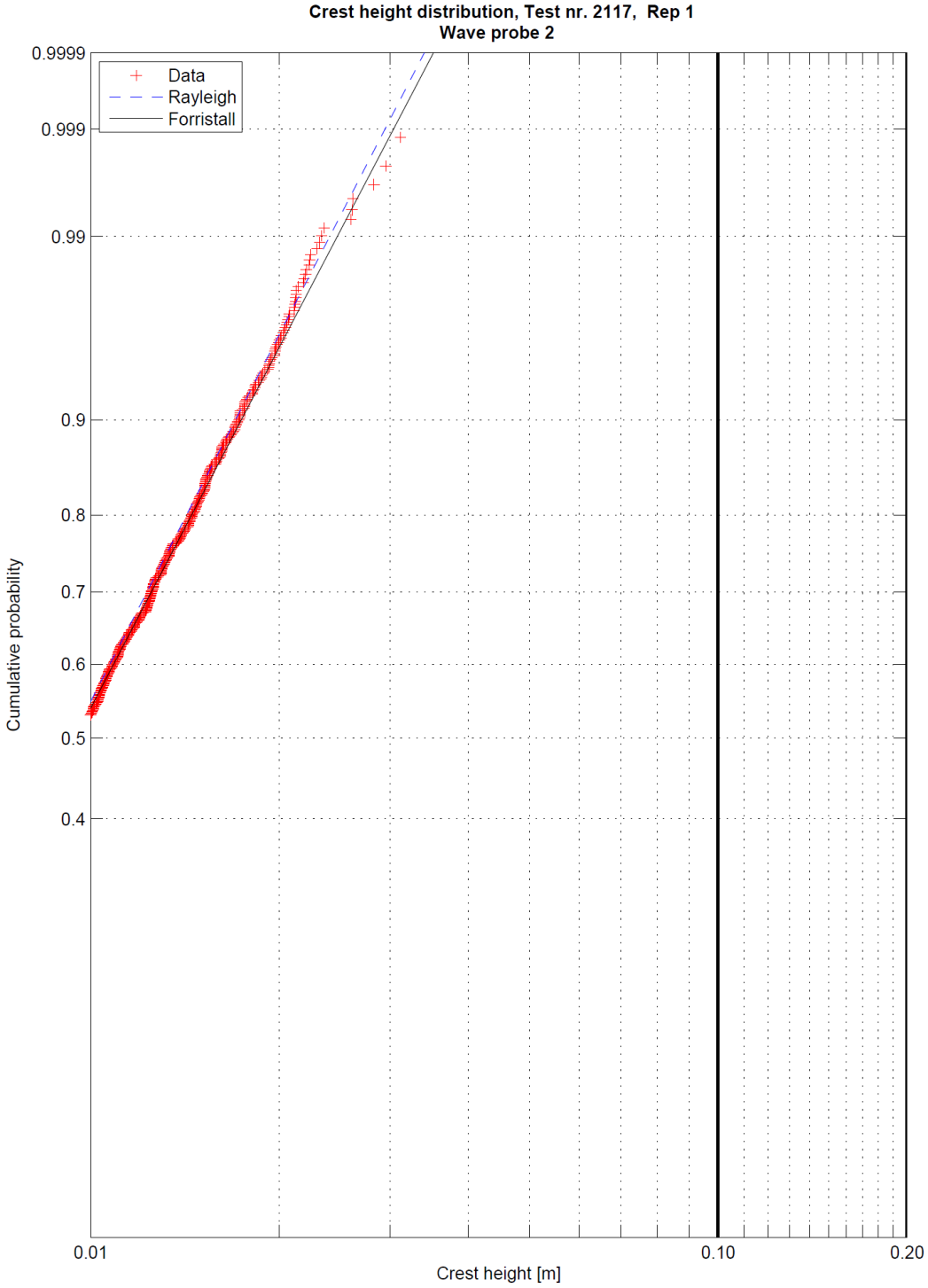

Figure 88: Wave crest height distributions at wave probe 2, test2117

From Figure 89 the crest height distributions are compared to data at wave probe 11, and it is seen that the data compares fairly well to both the Forristall and Rayleigh distribution. However the crest heights are slightly underestimated for the highest probabilities.

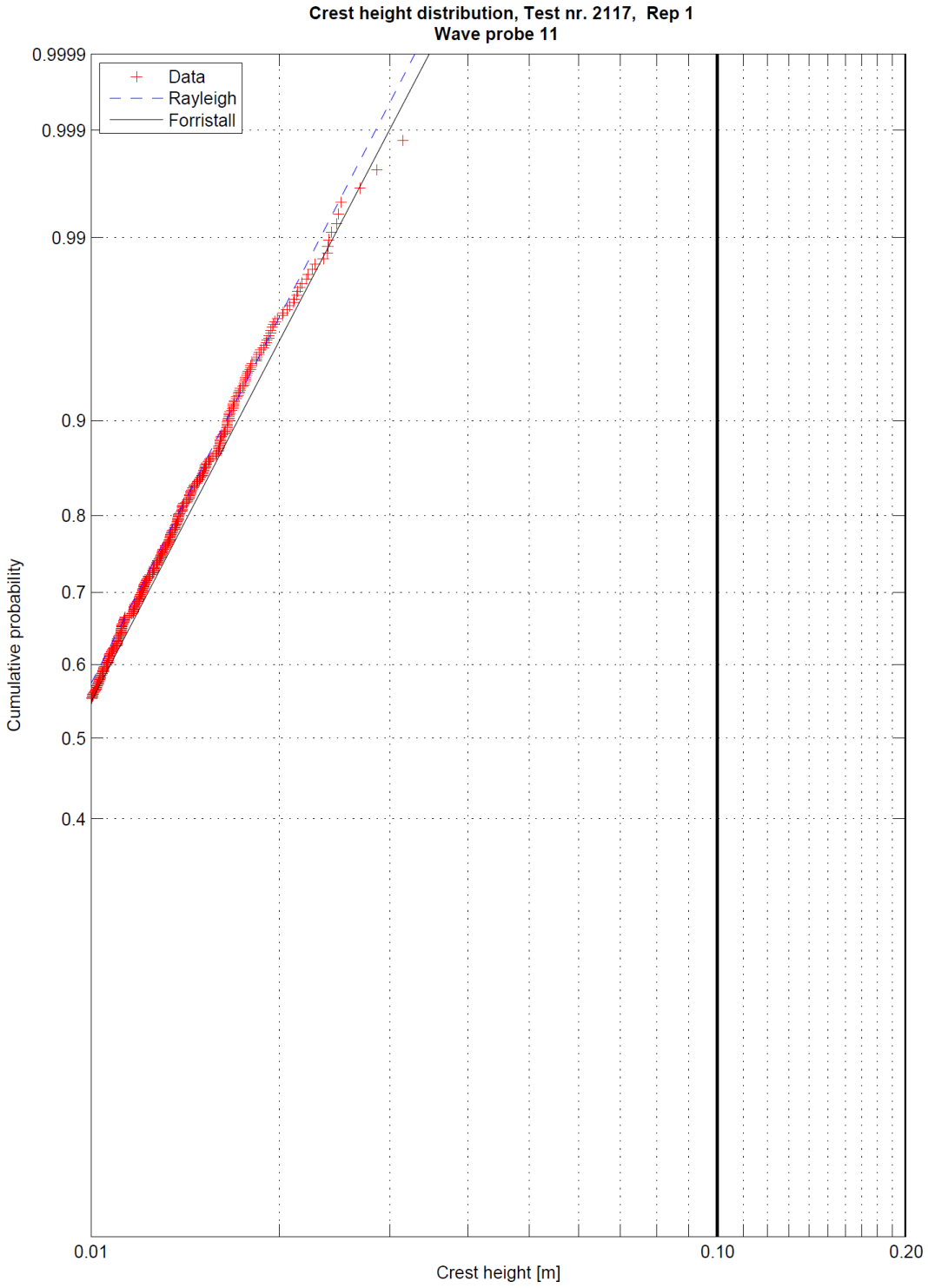

Figure 89: Wave crest height distributions at wave probe 11, test2117

In Figure 90 the crest height distributions is shown along with the data from the time series at wave probe 7, and it is seen that the data compares fairly well to the Forristall distribution. The Rayleigh distribution is non conservative in this case as well. It is also seen that the crest heights from data deviates from the Forristall distribution at high probabilities, thus making the Forristall conservative for high probabilities in this case. The reason for this behavior is not certain.

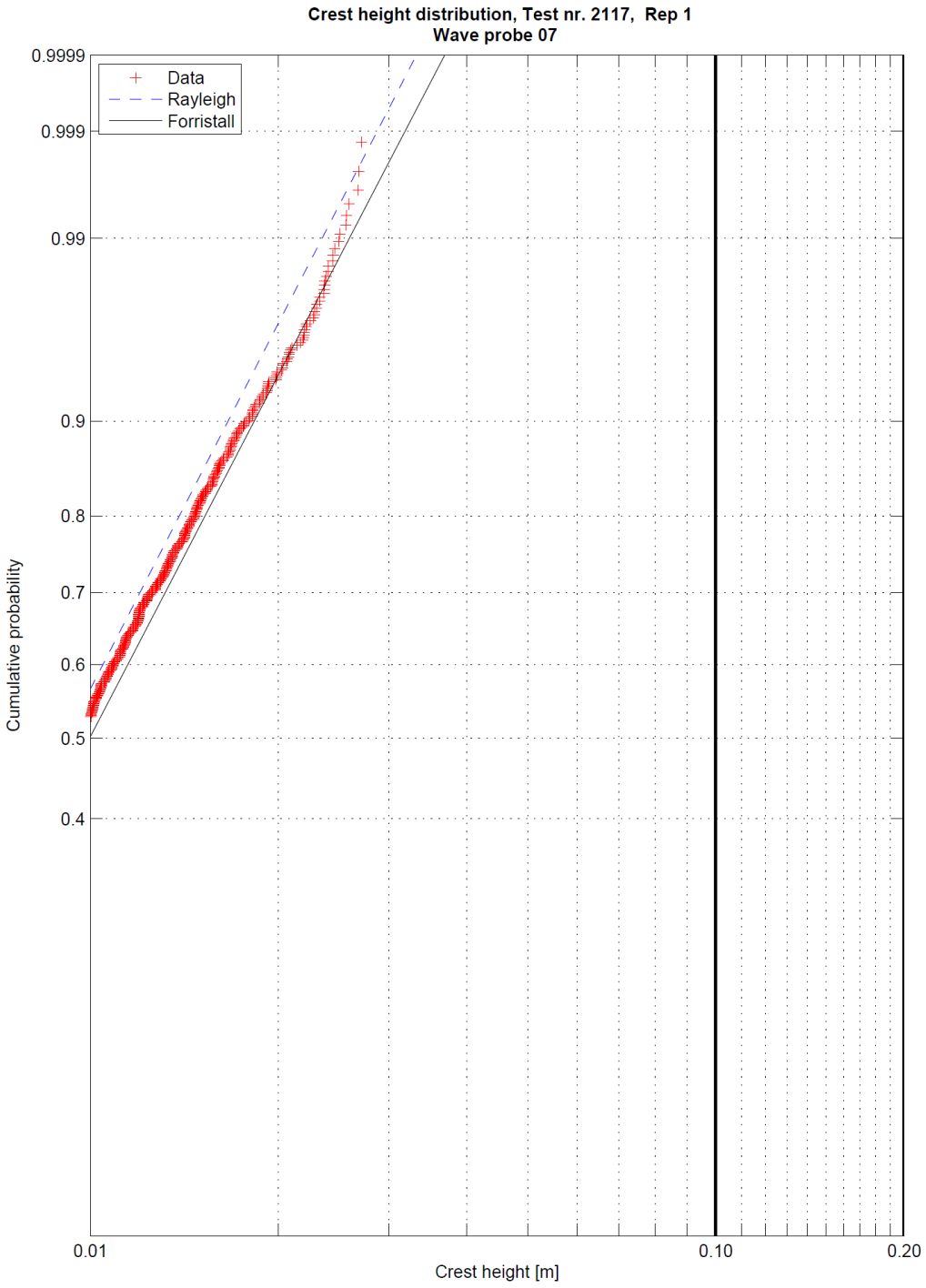

Figure 90: Wave crest height distributions at wave probe 7, test2117

Summary of observations

The distribution proposed by Forristall (2000) fits the crest height data from this model test fairly well. But in some cases in shallow water the Forristall distribution over estimates the crest heights as depth induced wave breaking limits the largest crest heights in the time series. Thus the Forristall distribution can be considered to be conservative for the high probability crest heights in shallow water. In some cases it is seen that some individual cases deviates from the usual pattern and in these cases some conservatism is nice to have, as these waves still do not exceed the crest heights predicted by the Forristall distribution.

The Rayleigh distribution is as predicted un-conservative for the largest sea states, for the smaller sea states the Rayleigh distribution is fairly similar to the Forristall distribution. But also here the Forristall distribution is seen to fit better to the data, however with a much smaller margin for these cases.

4.4 Individual events

In order to investigate how the largest waves in the time series behave, the largest, second largest and third largest waves in the time series have been plotted in space for the selected tests and the corresponding repetitions. This is performed by means of the times series from the wave probes in the array. Where the largest waves are found from the time series at the wave probe in the center of the array (wave probe 11), then the wave probes have been plotted in space with the indexes corresponding to that of the peaks at wave probe 11.

There have also been calculated individual wave steepness and Ursell numbers for these waves, these calculations are based on the time series from wave probe 11. In order to calculate the wavelengths (which is an parameter for both steepness and Ursell numbers) the linear dispersion relation have been assumed, and the wavelengths have been calculated by the WAFO (2000) function "w2k" which solves the linear dispersion relation with the wave number as output. But as the wave periods from the time series are determined by means of a zero crossing analysis, the reader should be aware that this may cause slightly larger wave periods as the front/back asymmetry of the waves become large.

In this chapter there will be presented one example for the largest waves from test2116 with corresponding repetitions, the rest of the tests with corresponding steepness and Ursell numbers can be found in Appendix H.

From Figure 91 the largest waves from test2116 are presented, and it is seen that the waves are clearly asymmetrical with respect to the front and back of the wave.

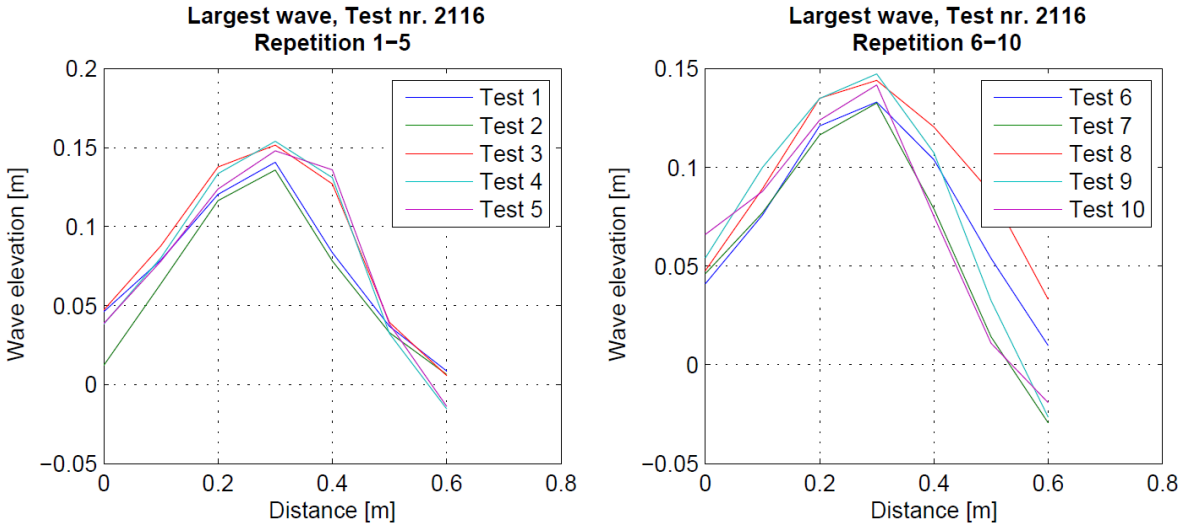

Figure 91: Largest waves for test2116

In Figure 92 the second largest waves from test2116 with corresponding repetitions are presented, and it is seen that the waves also here are clearly asymmetrical.

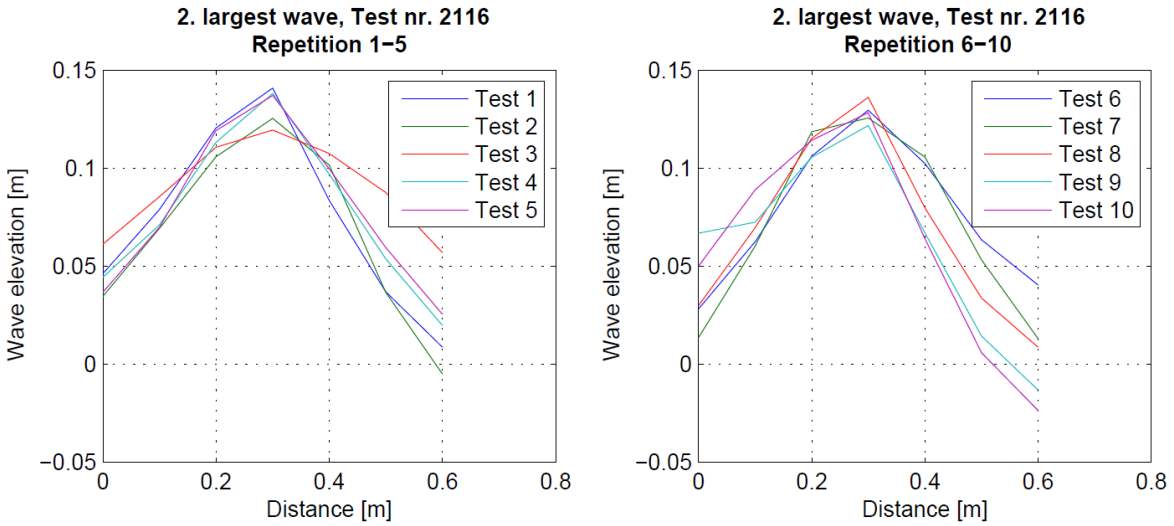

Figure 92: Second largest waves for test2116

From Figure 93 the third largest wave from test2116 is presented, and it is seen that also here the waves are asymmetrical.

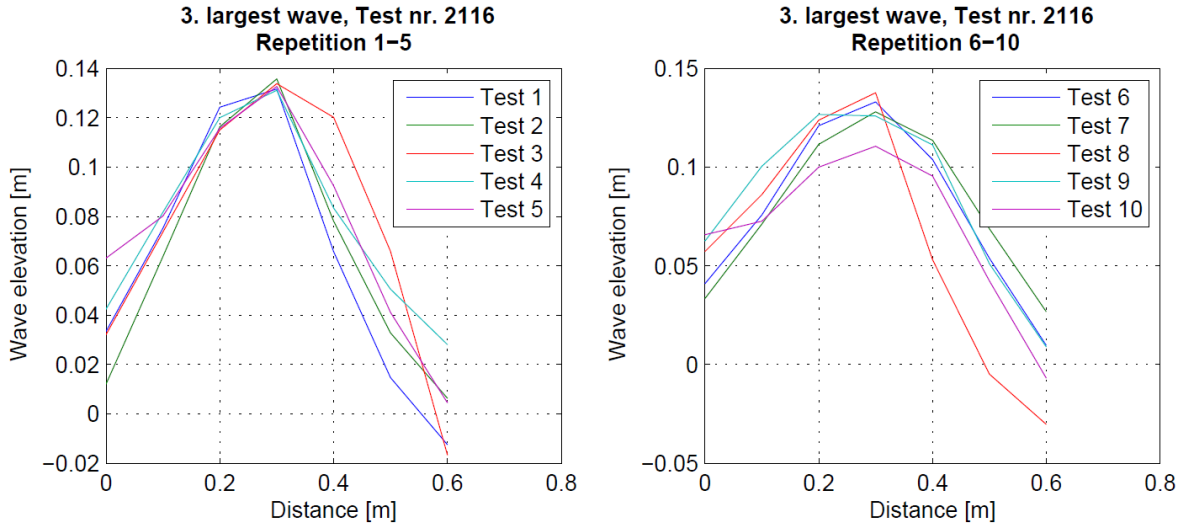

Figure 93: Third largest waves for test2116

As seen in this chapter the largest waves in the time series for test2116 are asymmetrical with respect to the front and back of the wave, i.e. the wave are tilting forwards. This behavior seen for test2116 is similar to that of the other large sea states. Usually as the wave grows asymmetrical in this direction, it grows unstable and wave breaking are likely to occur.

This effect also makes it difficult to model the surface elevation with corresponding wave kinematics by an analytical wave model, as this type of asymmetry are not described by classical higher order wave theory like stokes theories and Stream function wave theories. Thus in order to describe the wave kinematics in these kind of water depths for such sea states a much more advanced solution

method needs to be applied. Like for example wave models based on the Boussinesq equations or computational fluid dynamics.

5 Conclusion and propositions for further work

5.1 Conclusion

The present master thesis has investigated the wave conditions for bottom fixed wind turbines in shallow water. By means of a model test with a sloping beach, the transformation of the surface process from deep to shallow water is measured. The results are compared to analytical models and similar model tests.

The parameters that have been investigated show clear signs of shallow water effects. Effects from shoaling are noticeable in the measured significant wave height. The parameters skewness and kurtosis for the distribution of single points in the time series increase with decreasing depth, thus as the waves propagate from deep to shallow water the surface process will gradually deviate from a Gaussian process. The attempt to quantify the growth of skewness in terms of nonlinearity parameters have been successful, as the skewness are found to increase linearly with the Ursell number. Similar relations are not fund for the kurtosis.

In the wave spectra there can be seen clear signs of nonlinear interactions as the waves propagate towards shallow water. At the wave probe closest to the beach it is seen both sub- and super-harmonic peaks in the wave spectra. This is a result of triad wave-wave interactions. The predominant dissipation mechanism in the present model test is depth induced wave breaking, which is visible as a smaller wave spectrum. In general the wave spectrum remains fairly constant before the dissipation due to depth induced wave breaking reduces the size of the wave spectrum significantly, in regions corresponding to full scale water depths of 15-20 meters. Wave breaking does also appear in positions corresponding to a full scale water depth of 25 meters for the larger sea states, but this is more sporadically and does not seem to affect the energy content in the wave spectra significantly.

The TMA spectrum does not predict the transformation of the wave spectra, as the energy dissipation in the spectra is grossly overestimated. The reason for this is that the TMA spectrum takes into account dissipation from bottom friction, which is negligible in the present model test. Furthermore the TMA does not take into account the dissipation effect of breaking waves, which is seen to be the predominant dissipation mechanism in the present model test. The predicted dissipation due to bottom friction in TMA are however larger than what is seen for depth induced wave breaking in the spectral estimates. The tail of the TMA spectra captures the behavior from the spectral estimates fairly well.

The wave height distribution proposed by Battjes et.al. (2000) is seen to predict the measured wave heights in the present model test fairly well, for some sea states it is however seen that the distribution is un-conservative. But in general the distribution fits the measured results fairly well. The crest height distribution proposed by Forristall (2000) follows the measured data of crest heights fairly well. The estimated crest heights from the distribution gives conservative results compared with the results closest to the beach, as these crest heights are significantly reduced due to wave breaking for the steepest sea states. But in general the distribution by Forristall (2000) follows the measured crest heights from the present model test.

The largest individual waves in the time series have been analyzed at a position corresponding to a full scale water depth of 25 meters, and it is seen that these waves have a clear asymmetry with respect to the front and back of the wave. As a consequence of this there have to be used a sophisticated wave model in order to describe the surface process and corresponding of the waves.

From what is seen from this model test, it can be said that a bottom fixed structure in water depths of 25 meters and shallower, are in a region where wave breaking will occur for the ULS and ALS sea states. And if several wind turbines are to be built in this area there are likely that some of them will be hit by large breaking waves.

5.2 Proposition for further work

First of all the further work on this subject could be related to the parts of this thesis that there has not been enough time to finish. Firstly related to the uncertainty of the kurtosis, this is seen to vary significantly. In order to determine whether or not these variations are due to the transformation of waves from deep to shallow water, or just typical variations of a Gaussian process, there can be established an interval of typical variations of the kurtosis by performing simulations of a Gaussian process.

The next step in the process would be to estimate the loads on a bottom fixed cylinder in shallow water, this can be done by considering the load as the drag term from Morrisons equation and consider the loads of breaking waves as a slamming load, as proposed by Nestegård et.al (2004). But in order to estimate the loads, there have to be calculated wave kinematics. This could be done by implementing a wave model based on the enhanced Boussinesq equations, which are capable of describing the transformation of the waves.

References

Battjes, J.A., Groenendijk, H.W., (2000), " *Wave Height Distributions on Shallow Foreshores*", Elsevier, Coastal Engineering, Vol. 40 , p. 161-182.

Bouws, E., Günther, H., Rosenthal, W., Vincent, C.L., (1985), "*Similarity of the Wind Wave Spectrum in Finite Depth Water 1. Spectral Form*", Journal of Geophysical Research, Vol. 90, p. 975-986

Clauss, G.F., Bergmann, J., (1986), " *Gaussian wave packets – a new approach to seakeeping tests of offshore structures*", Applied Ocean Research, Vol. 8, No. 4, p. 190-206

Dean, R.G., Darlymple, R.A., (1991), "*Water Wave Mechanics for Engineers and Scientists*", World Scientific, Singapore.

DNV, (2007), "*Recommended practice DNV-RP-C205; Environmental Conditions and Environmental Loads*", Det Norske Veritas.

Fenton, J.D., (1985), "*A Fifth-Order Stokes Theory for Steady Waves*", "Journal of Waterway, Port, Coastal and Ocean Engineering", Vol. 111, No. 2, p. 216-234.

Forristall, G.Z., (1978), "*On the Statistical Distribution of Wave Heights in a Storm*", Journal of Geophysical Research, Vol. 83.

Forristall, G.Z., (2000), " *Wave Crest Distributions: Observations and Second-Order Theory*", Journal of Physical Oceanogrofy, Vol. 30.

Goda,Y., (2010), "*Random Seas and Design of Maritime Structures*", World Scientific, Singapore.

Holthuijsen, L.H, (2007), " *Waves in Oceanic and Coastal Waters*", Cambridge University Press, Cambridge, United Kingdom.

Leira, B.J., (2010), " *Probabilistic Moddeling and Estimation*", Compendium, NTNU, Trondheim, Norway.

Nwogu, O., (1993), " *Alternative Form of Boussinesq Equations for Nearshore Wave Propagation*", "Journal of Waterway, Port, Coastal and Ocean Engineering", Vol. 119, No. 6, p. 618-638.

Mai, S., Wilhelmi, J., Barjenbruch, U., (2010), " *Wave Height Distributions in Shallow Water*", Coastal Engineering 2010.

Memos, C., Tzanis, K., Zographou, K., (2002), " *Stochastic description of sea waves*", Journal of Hydraulic research, Vol. 40, No. 3, p. 265-274

Myrhaug, D., (2005), "*Statistics of Narrow Band Processes and Equivalent Linearization* ", compendium, Institute for Marine Technology, NTNU, Trondheim, Norway.

Myrhaug, D., (2007), "*Kompendium i MARIN DYNAMIKK; Uregelmessig sjø*", compendium, Institute for Marine Technology, NTNU, Trondheim, Norway.

Nestegård, A., Kalleklev, J.A, Hagatun, K., Wu, Y.L., Haver, S., Lehn, E., (2004), "*Resonant Vibrations of Riser Guide Tubes due to Wave Impact*", Proceednigs of OMAE'04, ASME, Vancouver, Canada.

Nilsen, B., (1997), "*Egenskaper ved uregelmessige bølger på grunt vann*", M.Sc. thesis, NTNU, Trondheim, Norway.

Stansberg, C.T., (2011), " *Characteristics of Steep Second-order Random Waves in Finite and Shallow Water - Draft*", OMAE2011-50219, Marintek, Trondheim, Norway.

Steen, S., Aarsnes, J.V., (2010), " *Experimental Methods in Marine Hydrodynamics*", Compendium, NTNU, Trondheim, Norway.

Svangstu, E., (2010), "*Bølger fra dypt til grunt vann: Hva skjer med bølgenes asymmetri og kinematikk?*", pre project, NTNU, Trondheim, Norway.

Svendsen, Ib.A., (2006), "*Introduction to Nearshore Hydrodynamics"*, World Scientific, Singapore.

WAFO, (2000), "*WAFO – A Matlab Toolbox for Analysis of Random Waves and Loads – A Tutorial*", Matlab Toolbox, Lund, Sweden.

Wei, G., Kirby, J.T., Shina, A., (1999), " *Generation of waves in Boussinesq models using a source function method*", Costal Engineering, Vol. 36, p. 271-299.

Appendix

Appendix A - Sketches of different wave probe set ups

Appendix B – Overview of tests for regular waves

Appendix C – Spectral estimates

Appendix D – High frequency tail of the spectra

Appendix E – TMA spectrum

Appendix F – Wave height distributions

Appendix G – Crest height distributions

Appendix H – Individual events

Digital Appendices

Digital 1 – Spectral estimates

Digital 2 – TMA spectrums

Digital 3 – Zero up crossing vs. zero down crossing

Digital 4 – Wave height distributions

Digital 5 – Crest height distributions

Digital 6 – Matlab scripts

Appendix A

Sketches of different wave probe set ups

WP setup 1

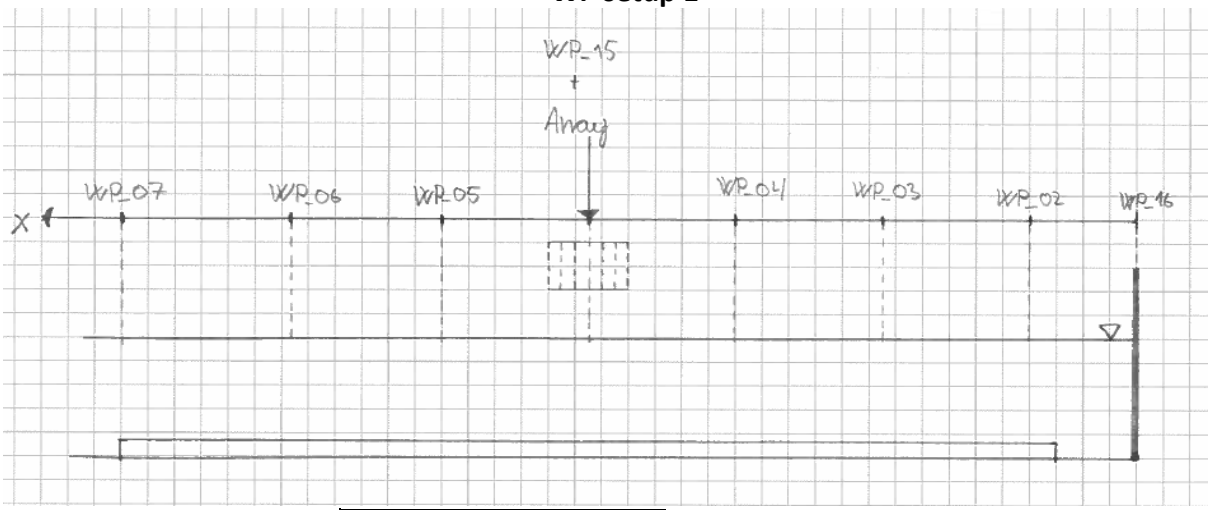

	Water depth		Position
	Model sc.	Full sc.	x
WP_16	1,00	81,00	0,00
WP_02	0,83	67,23	2,00
WP_03	0,83	67,23	4,76
WP_04	0,83	67,23	7,51
WP_08	0,83	67,23	9,97
WP_09	0,83	67,23	10,07
WP_10	0,83	67,23	10,17
WP_11	0,83	67,23	10,27
WP_12	0,83	67,23	10,37
WP_13	0,83	67,23	10,47
WP_14	0,83	67,23	10,57
WP_05	0,83	67,23	13,02
WP_06	0,83	67,23	15,78
WP_07	0,83	67,23	18,20

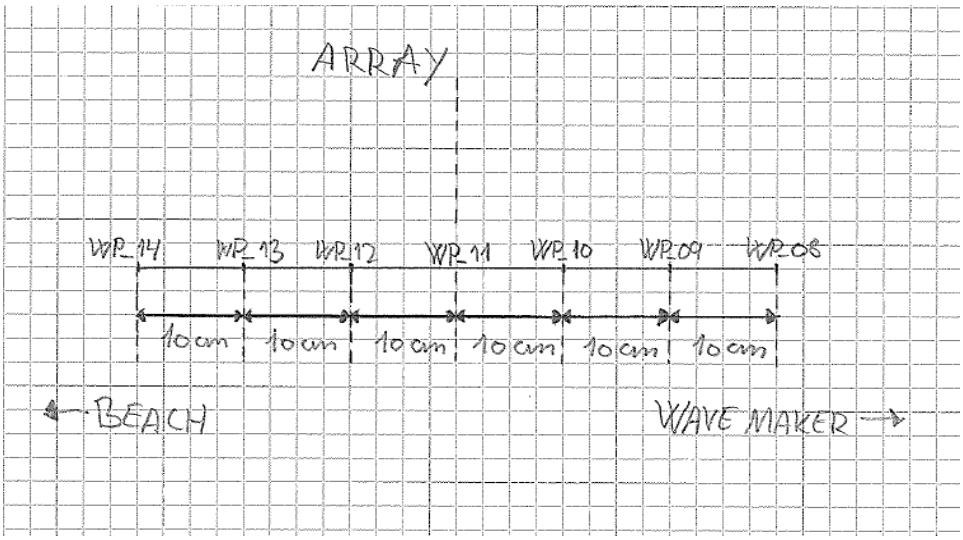

WP setup 2

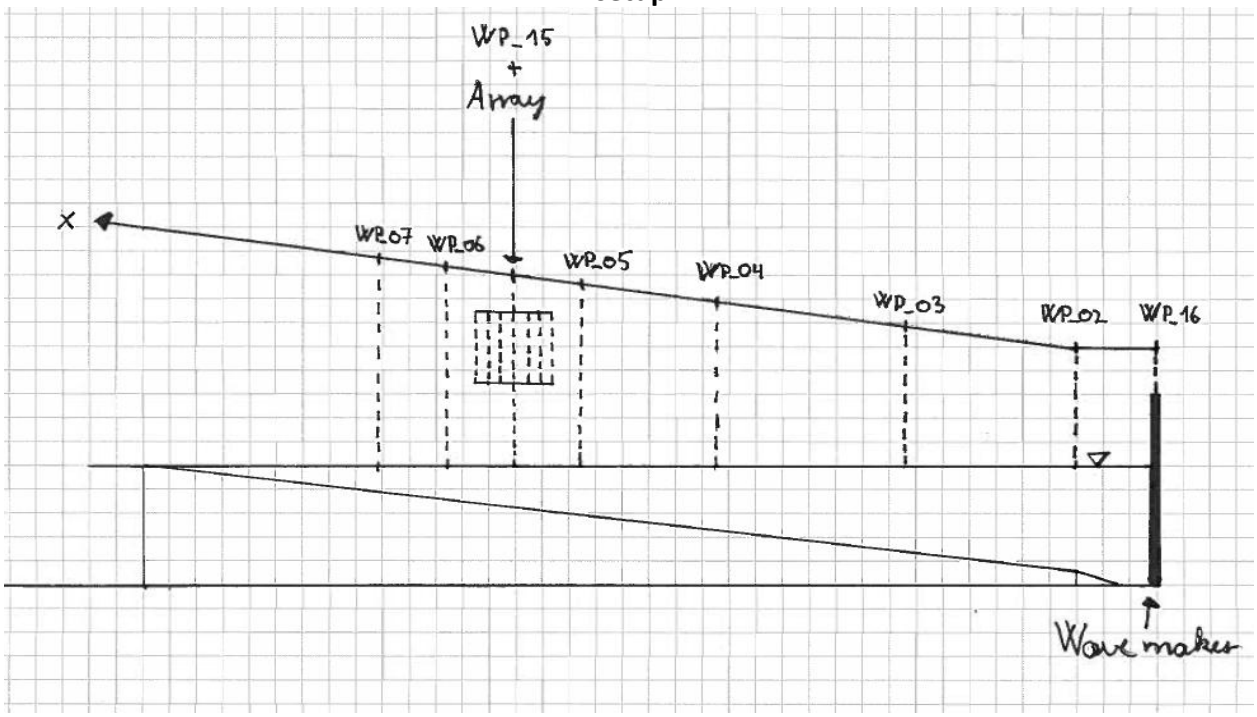

	Water depth		Position
	Model sc.	Full sc.	x
WP_16	1,000	81,00	0,000
WP_02	0,830	67,23	1,530
WP_03	0,671	54,35	4,755
WP_04	0,494	40,00	8,400
WP_05	0,370	30,00	10,935
WP_08	0,336	27,22	11,905
WP_09	0,327	26,49	12,005
WP_10	0,318	25,76	12,105
WP_11	0,309	25,00	12,205
WP_12	0,299	24,22	12,305
WP_13	0,290	23,49	12,405
WP_14	0,281	22,76	12,505
WP_06	0,247	20,00	13,470
WP_07	0,185	15,00	17,740

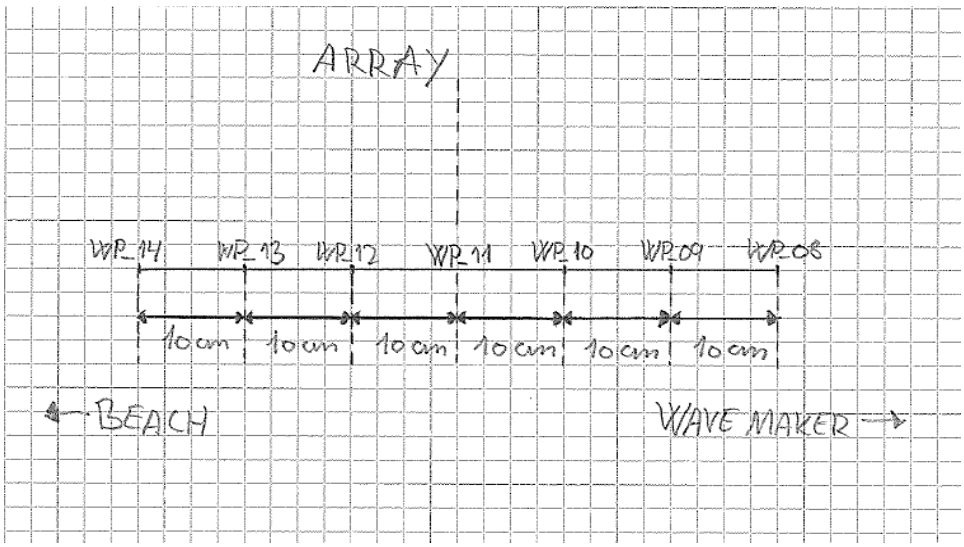

WP setup 3

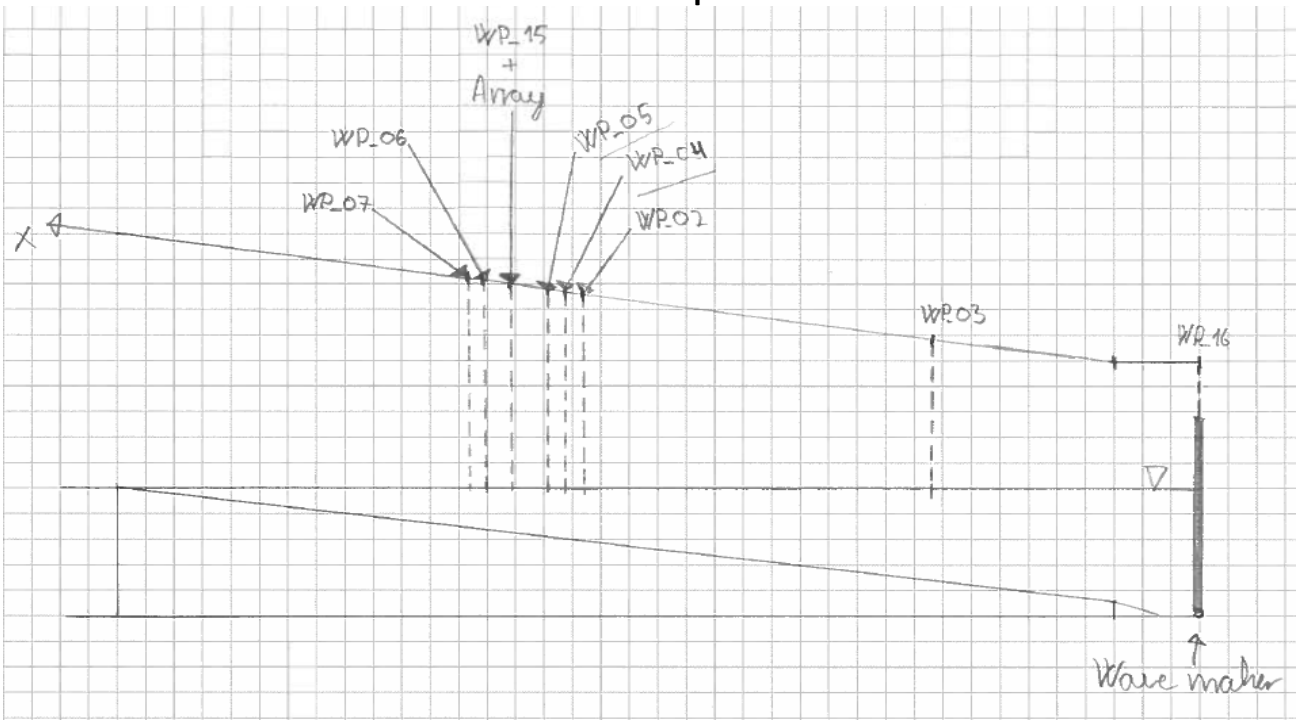

	Water depth		Position
	Model sc.	Full sc.	x
WP_16	1,000	81,00	0,000
WP_03	0,671	54,35	4,755
WP_02	0,355	28,73	11,265
WP_04	0,345	27,94	11,465
WP_05	0,335	27,15	11,665
WP_08	0,323	26,20	11,905
WP_09	0,319	25,80	12,005
WP_10	0,314	25,41	12,105
WP_11	0,309	25,01	12,205
WP_12	0,304	24,62	12,305
WP_13	0,299	24,22	12,405
WP_14	0,294	23,83	12,505
WP_06	0,282	22,88	12,745
WP_07	0,273	22,09	12,945

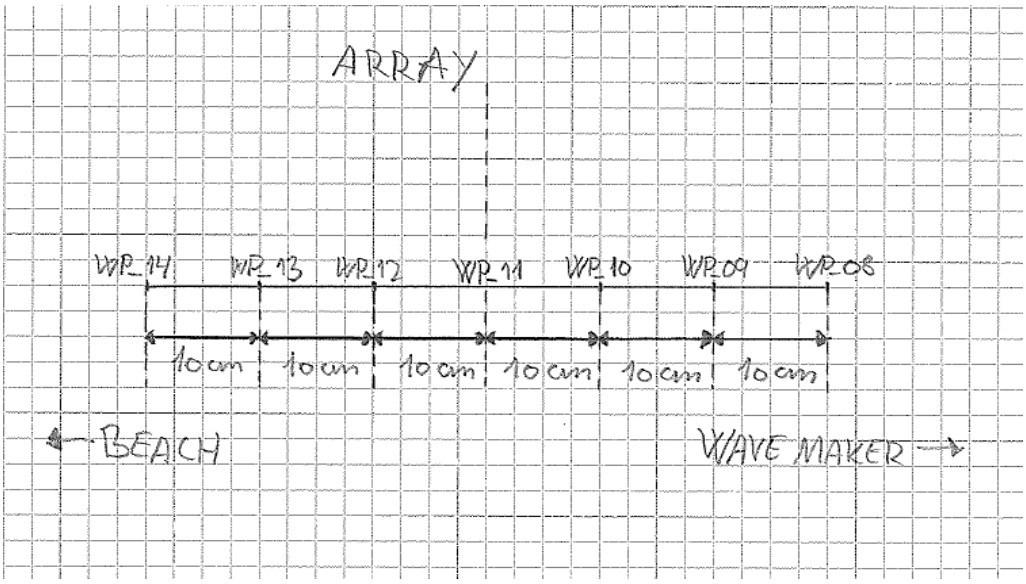

Appendix B

Overview of tests for regular waves

Test nr.	H [m]		T [s]	
	Model s.	Full s.	Model s.	Full s.
0x01	0,030	2,43	0,8	7,2
0x02	0,060	4,86		
0x03	0,090	7,29		
0x04	0,120	9,72		
0x05	0,050	4,05	1	9
0x06	0,100	8,10		
0x07	0,150	12,15		
0x08	0,200	16,20		
0x09	0,070	5,67	1,25	11,25
0x10	0,140	11,34		
0x11	0,210	17,01		
0x12	0,070	5,67	1,5	13,5
0x13	0,140	11,34		
0x14	0,210	17,01		
0x15	0,240	19,44		
0x16	0,210	17,01	1,75	15,75
0x17	0,240	19,44		

Series	Description
0100	Flat bottom, WP setup 1
0200	Sloping bottom, WP setup 2

Appendix C

Spectral estimates

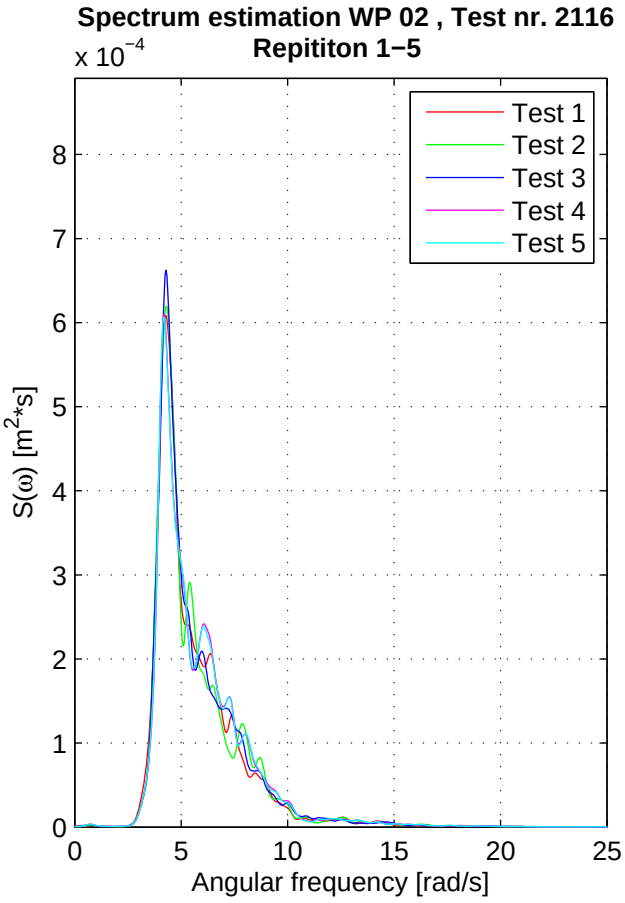
Spectrum estimation WP 02 , Test nr. 2116
Repititon 1−5
x 10^−4
Test 1
Test 2
Test 3
Test 4
Test 5
S(ω) [m^2*s]
Angular frequency [rad/s]

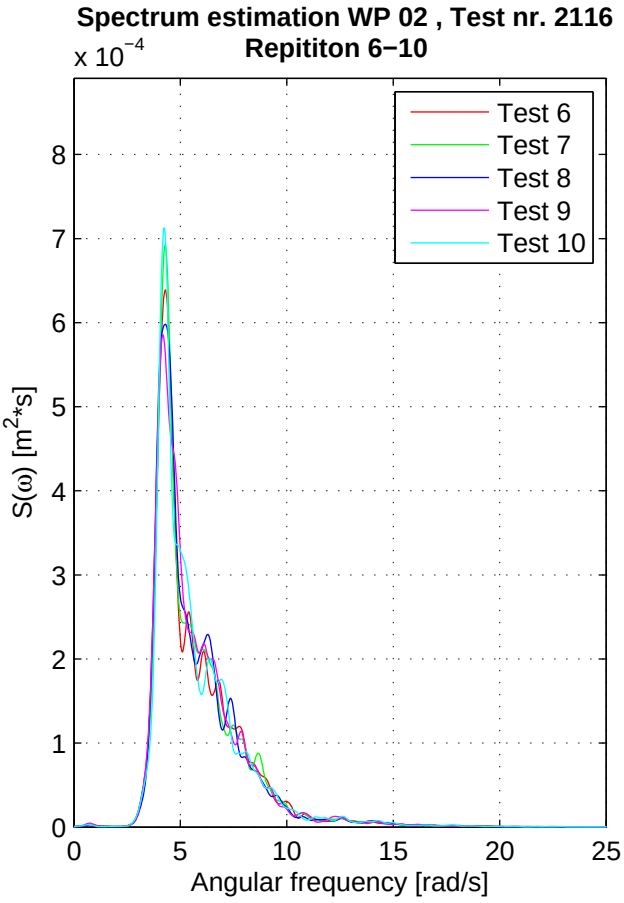
Spectrum estimation WP 02 , Test nr. 2116
Repititon 6−10
x 10^−4
Test 6
Test 7
Test 8
Test 9
Test 10
S(ω) [m^2*s]
Angular frequency [rad/s]

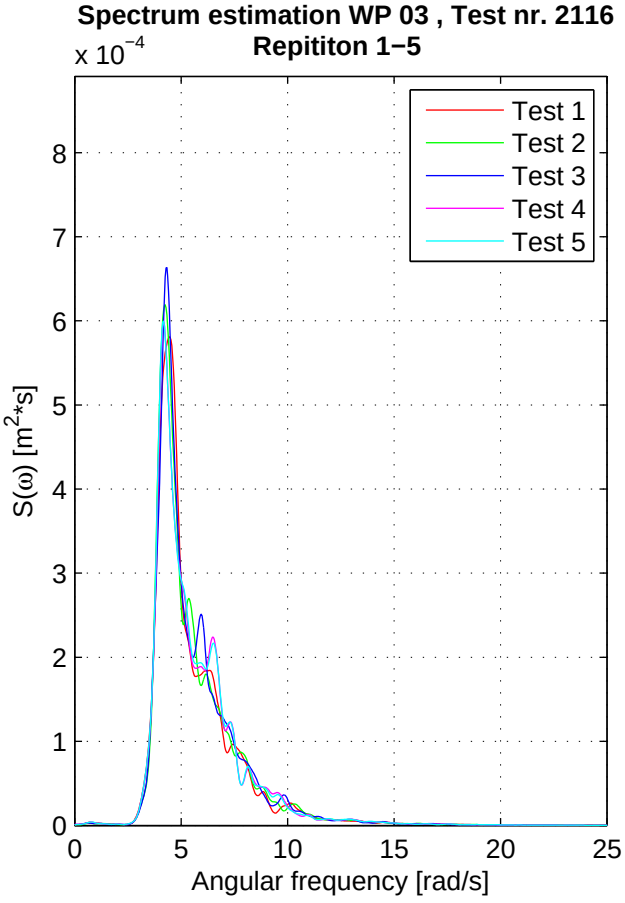
Spectrum estimation WP 03 , Test nr. 2116
Repititon 1−5
x 10^−4
Test 1
Test 2
Test 3
Test 4
Test 5
S(ω) [m^2*s]
Angular frequency [rad/s]

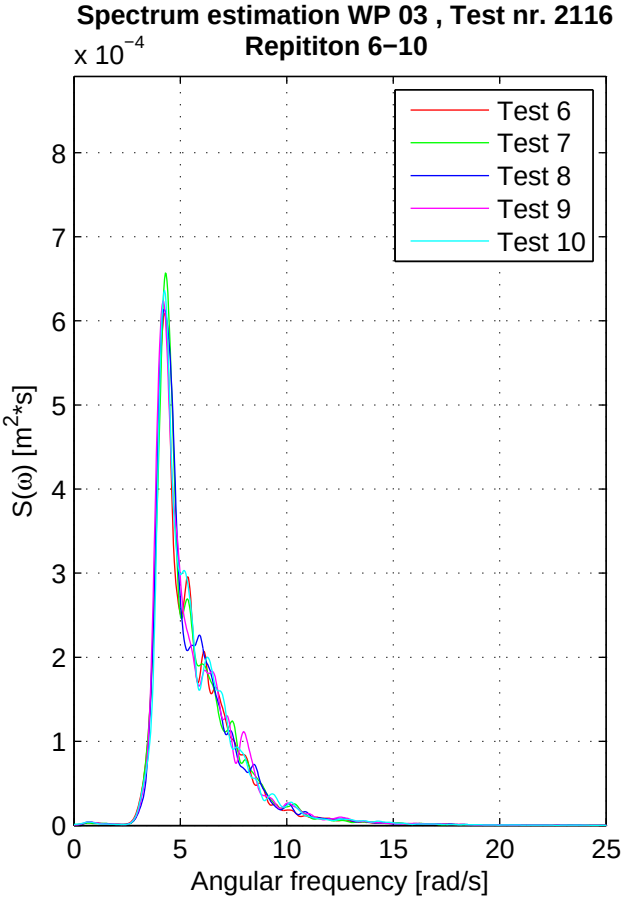
Spectrum estimation WP 03 , Test nr. 2116
Repititon 6−10
x 10^−4
Test 6
Test 7
Test 8
Test 9
Test 10
S(ω) [m^2*s]
Angular frequency [rad/s]

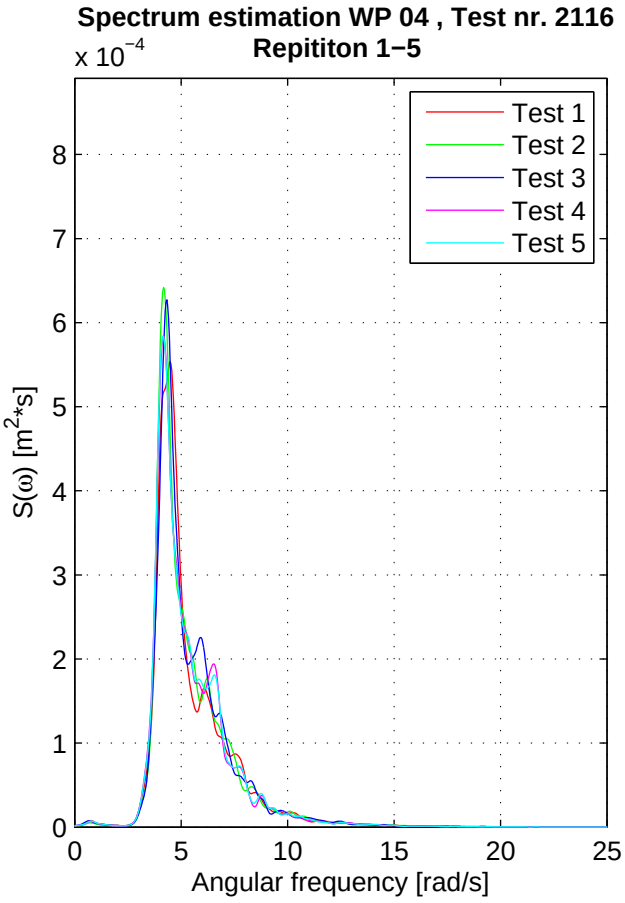
Spectrum estimation WP 04 , Test nr. 2116
Repititon 1−5
x 10^−4
Test 1
Test 2
Test 3
Test 4
Test 5
S(ω) [m^2*s]
Angular frequency [rad/s]

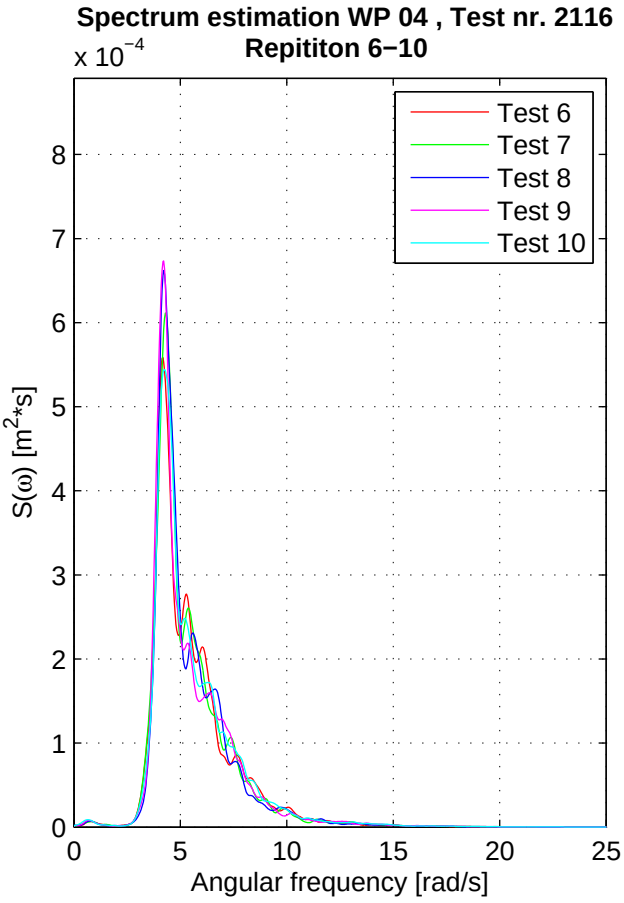
Spectrum estimation WP 04 , Test nr. 2116
Repititon 6−10
x 10^−4
Test 6
Test 7
Test 8
Test 9
Test 10
S(ω) [m^2*s]
Angular frequency [rad/s]

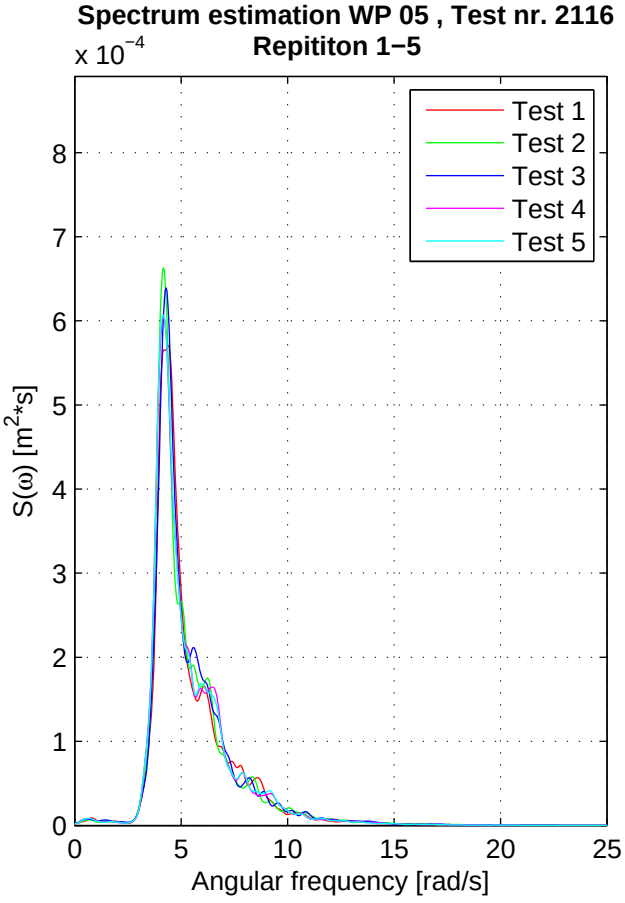
Spectrum estimation WP 05 , Test nr. 2116
Repititon 1−5
x 10^−4
Test 1
Test 2
Test 3
Test 4
Test 5
S(ω) [m^2*s]
Angular frequency [rad/s]

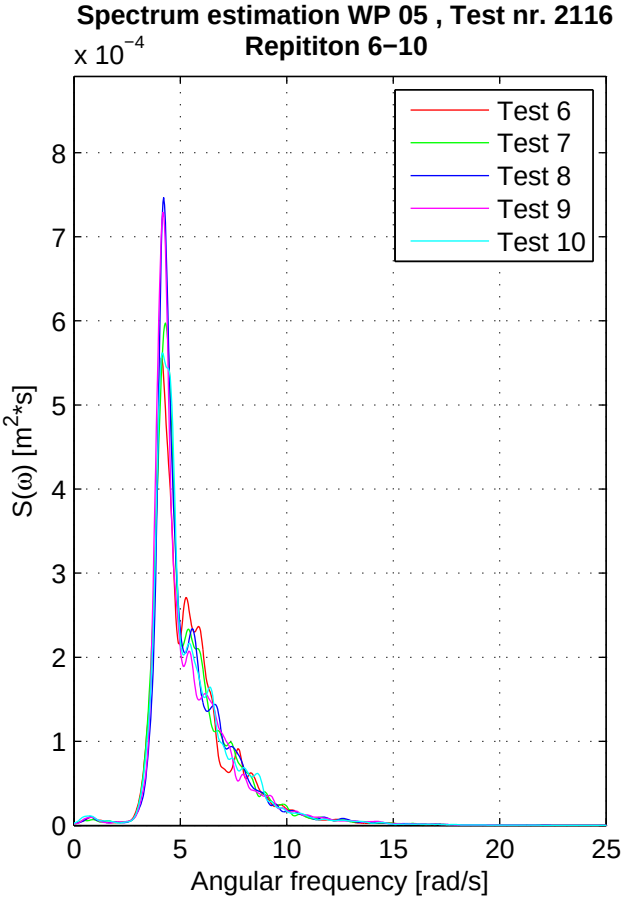
Spectrum estimation WP 05 , Test nr. 2116
Repititon 6−10
x 10^−4
Test 6
Test 7
Test 8
Test 9
Test 10
S(ω) [m^2*s]
Angular frequency [rad/s]

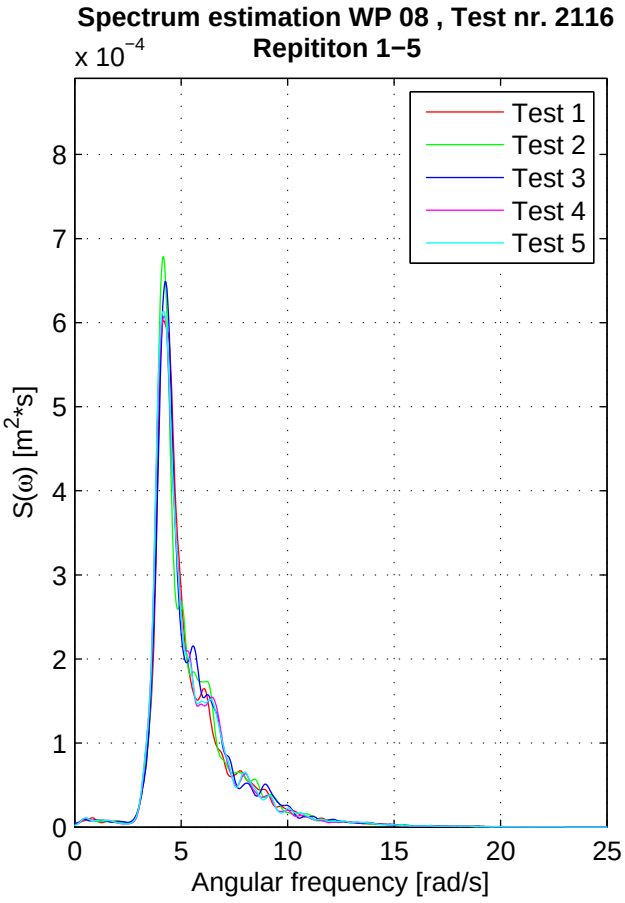
Spectrum estimation WP 08 , Test nr. 2116
Repititon 1−5
x 10^−4
Test 1
Test 2
Test 3
Test 4
Test 5
S(ω) [m^2*s]
Angular frequency [rad/s]

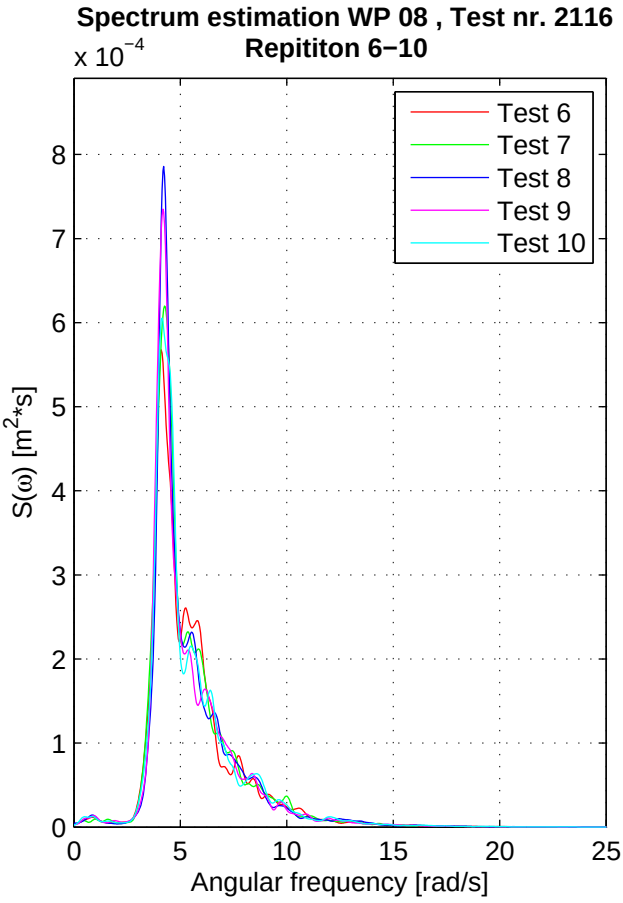
Spectrum estimation WP 08 , Test nr. 2116
Repititon 6−10
x 10^−4
Test 6
Test 7
Test 8
Test 9
Test 10
S(ω) [m^2*s]
Angular frequency [rad/s]

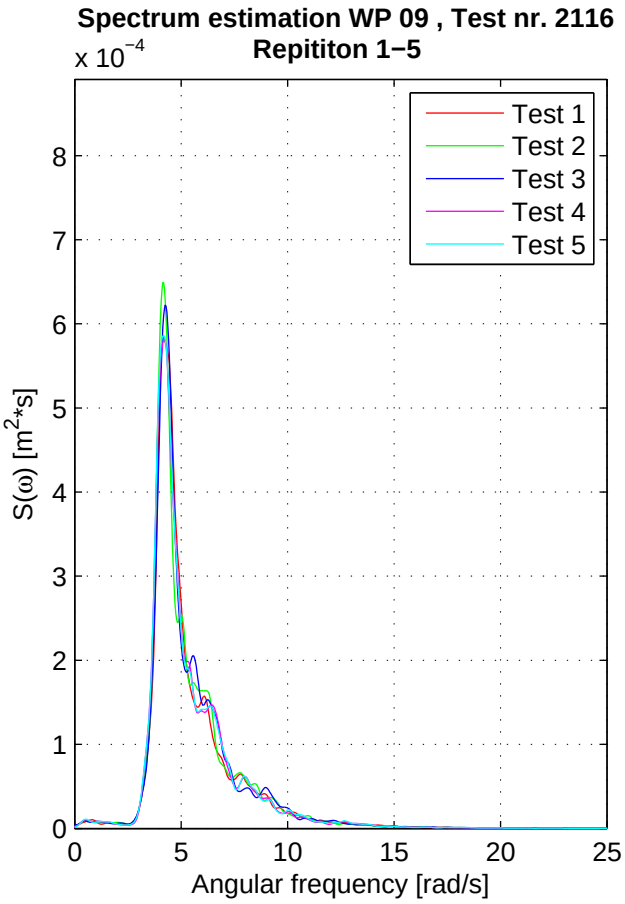
Spectrum estimation WP 09 , Test nr. 2116
Repititon 1−5
x 10^−4
Test 1
Test 2
Test 3
Test 4
Test 5
S(ω) [m^2*s]
Angular frequency [rad/s]

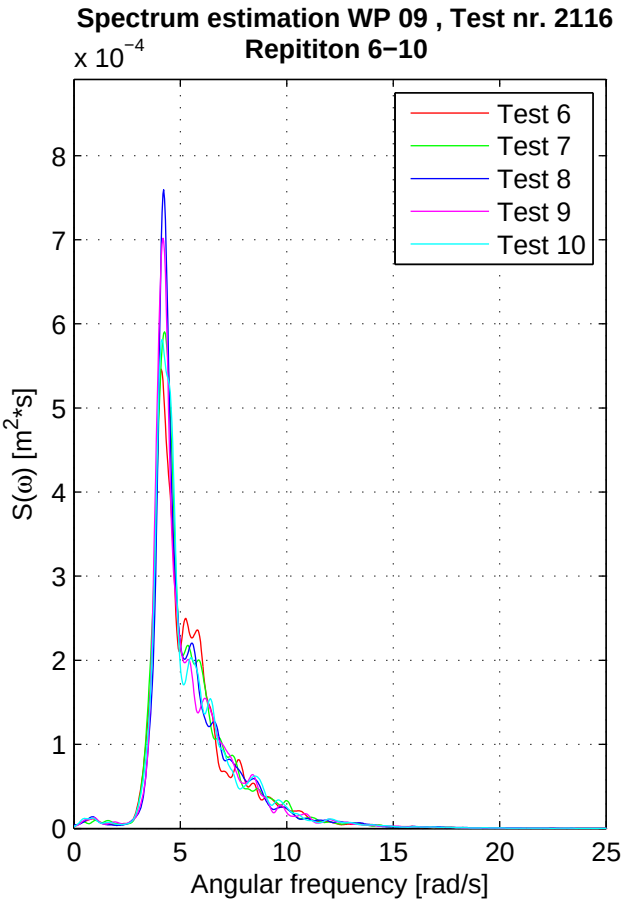
Spectrum estimation WP 09 , Test nr. 2116
Repititon 6−10
x 10^−4
Test 6
Test 7
Test 8
Test 9
Test 10
S(ω) [m^2*s]
Angular frequency [rad/s]

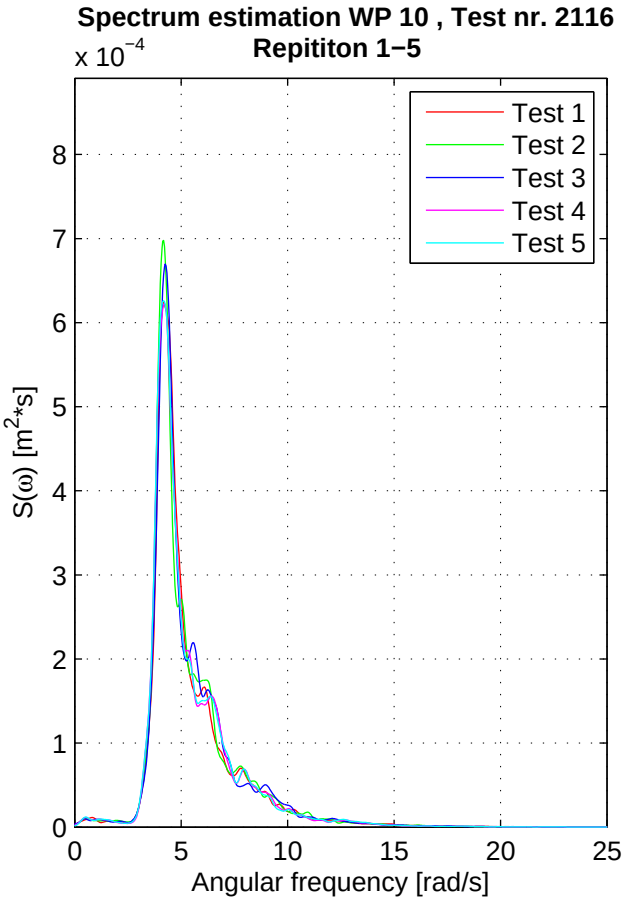
Spectrum estimation WP 10 , Test nr. 2116
Repititon 1−5
x 10^−4
Test 1
Test 2
Test 3
Test 4
Test 5
S(ω) [m^2*s]
Angular frequency [rad/s]

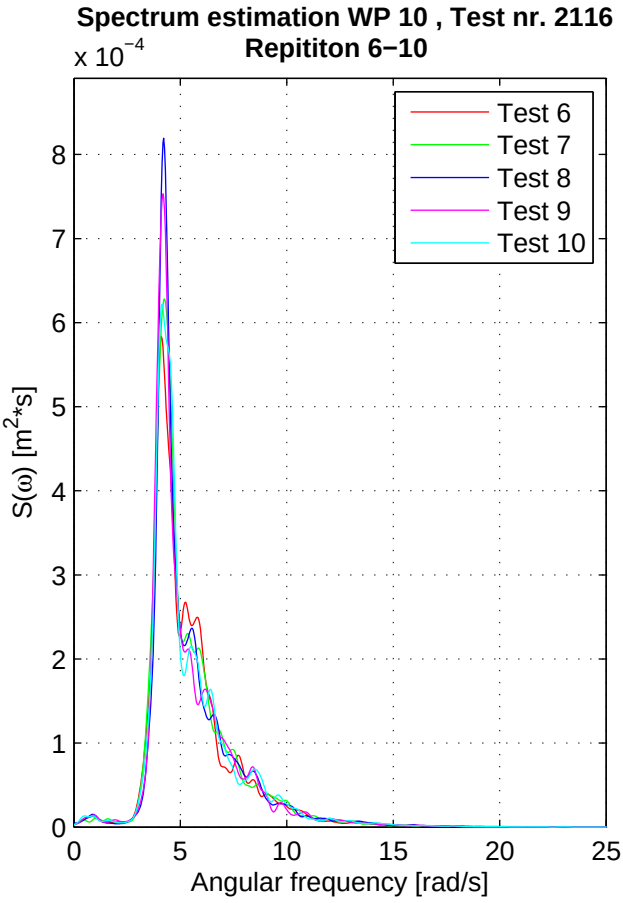
Spectrum estimation WP 10 , Test nr. 2116
Repititon 6−10
x 10^−4
Test 6
Test 7
Test 8
Test 9
Test 10
S(ω) [m^2*s]
Angular frequency [rad/s]

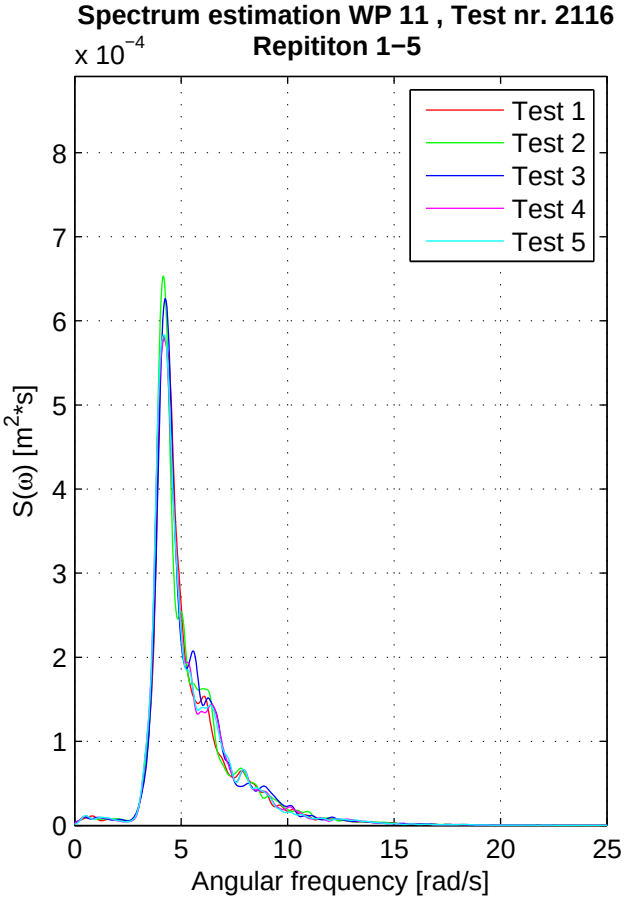
Spectrum estimation WP 11 , Test nr. 2116
Repititon 1−5
x 10^−4
Test 1
Test 2
Test 3
Test 4
Test 5
S(ω) [m^2*s]
Angular frequency [rad/s]

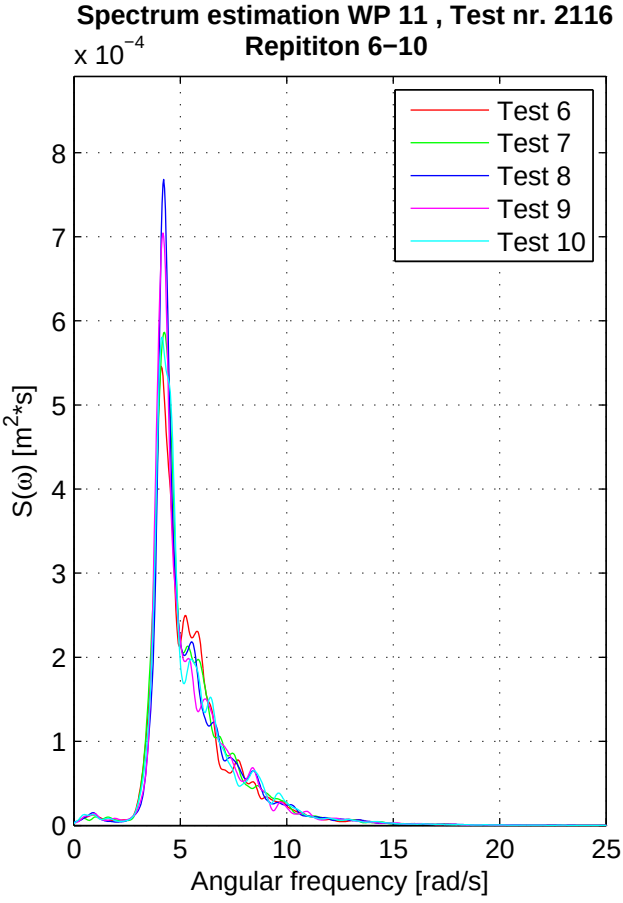
Spectrum estimation WP 11 , Test nr. 2116
Repititon 6−10
x 10^−4
Test 6
Test 7
Test 8
Test 9
Test 10
S(ω) [m^2*s]
Angular frequency [rad/s]

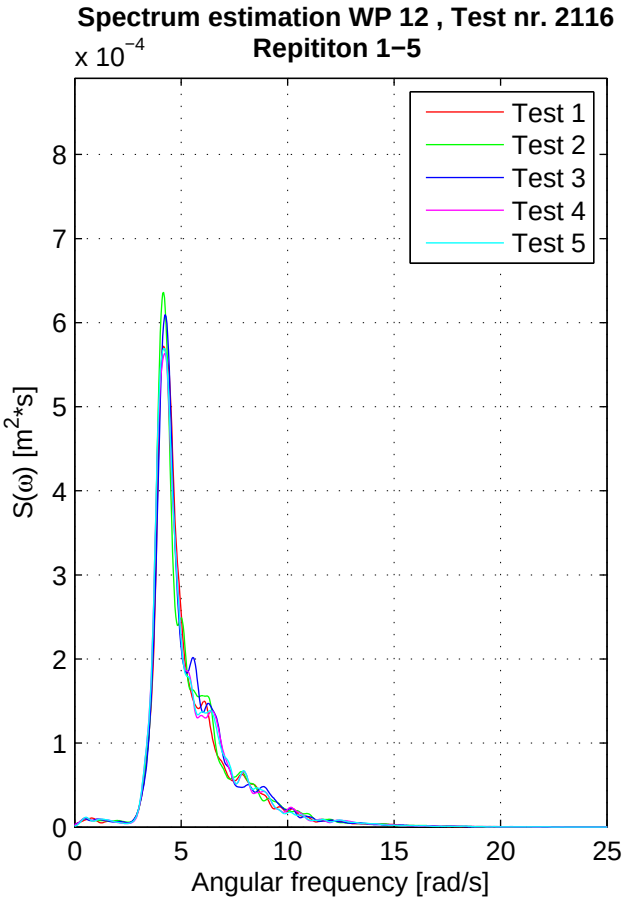
Spectrum estimation WP 12 , Test nr. 2116
Repititon 1−5
x 10^−4
Test 1
Test 2
Test 3
Test 4
Test 5
S(ω) [m^2*s]
Angular frequency [rad/s]

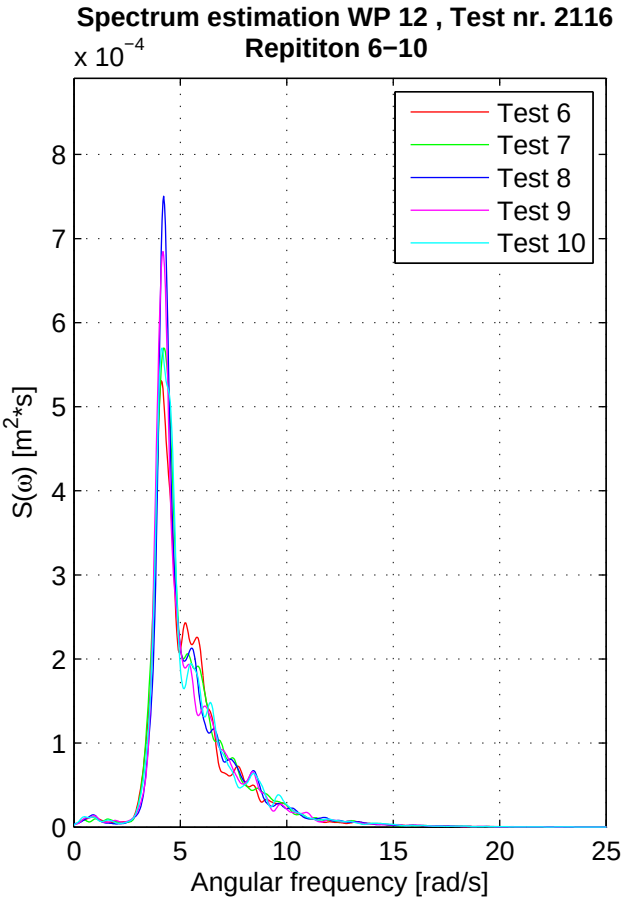
Spectrum estimation WP 12 , Test nr. 2116
Repititon 6−10
x 10^−4
Test 6
Test 7
Test 8
Test 9
Test 10
S(ω) [m^2*s]
Angular frequency [rad/s]

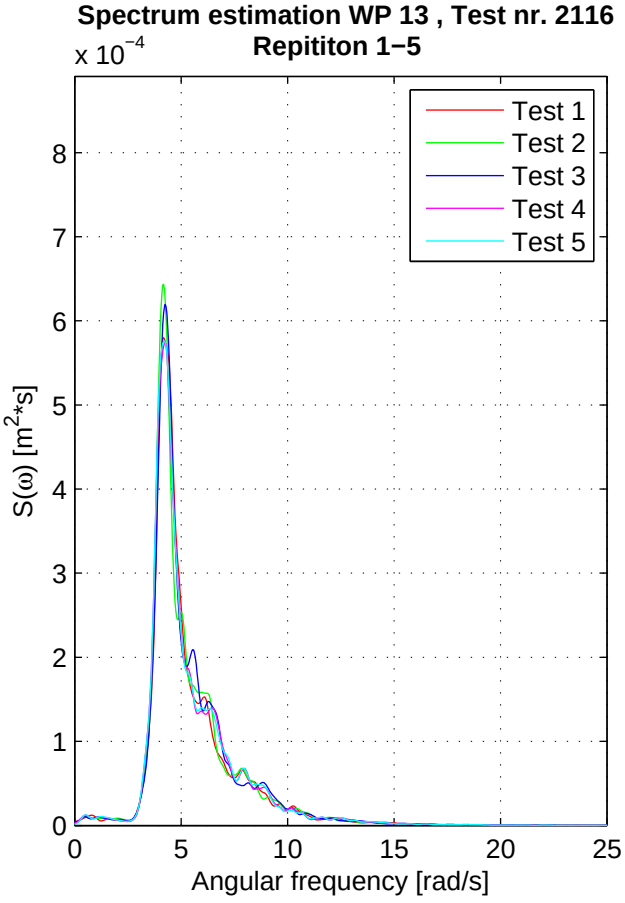
Spectrum estimation WP 13 , Test nr. 2116
Repititon 1−5
x 10^−4
Test 1
Test 2
Test 3
Test 4
Test 5
S(ω) [m^2*s]
Angular frequency [rad/s]

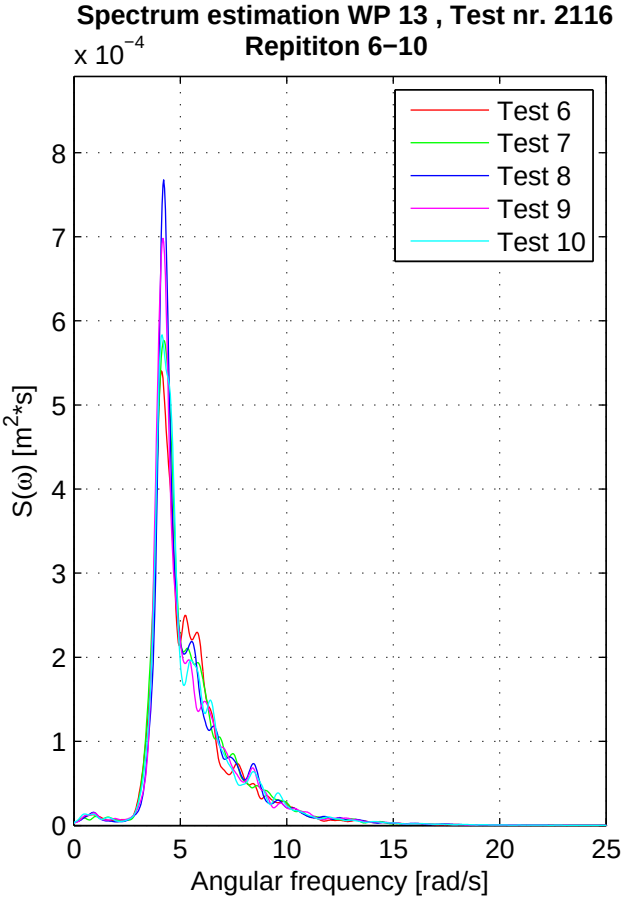
Spectrum estimation WP 13 , Test nr. 2116
Repititon 6−10
x 10^−4
Test 6
Test 7
Test 8
Test 9
Test 10
S(ω) [m^2*s]
Angular frequency [rad/s]

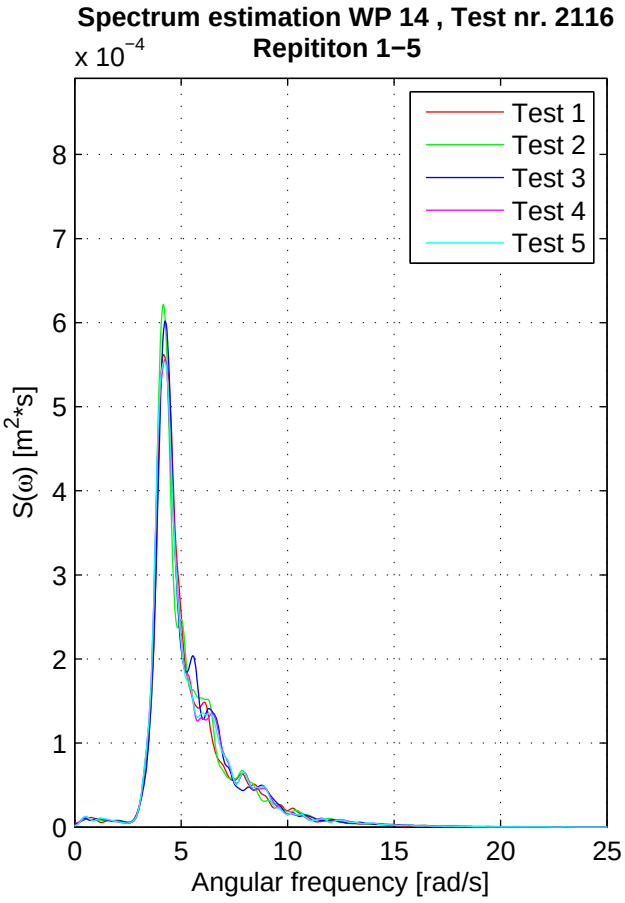
Spectrum estimation WP 14 , Test nr. 2116
Repititon 1−5
x 10^−4
Test 1
Test 2
Test 3
Test 4
Test 5
S(ω) [m^2*s]
Angular frequency [rad/s]

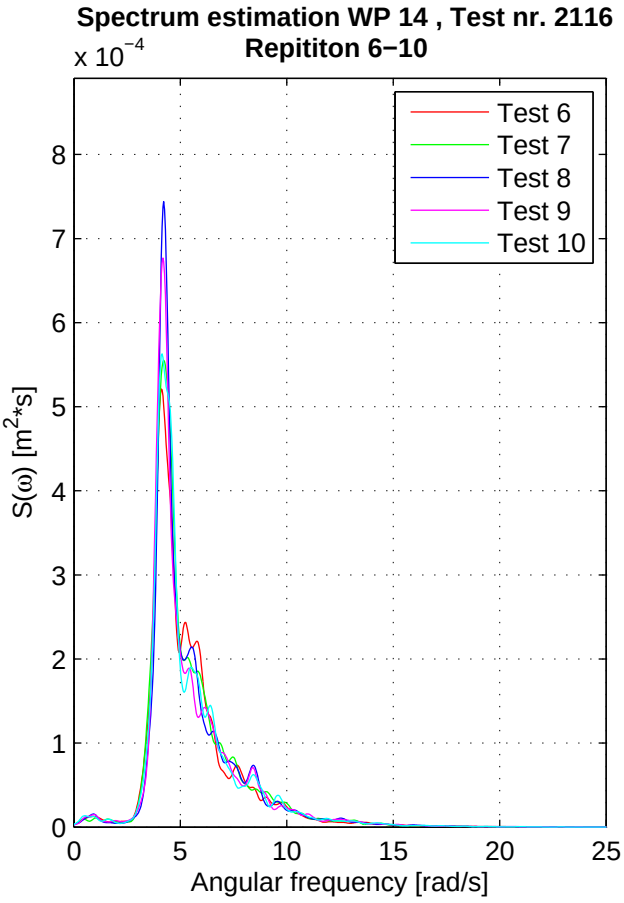
Spectrum estimation WP 14 , Test nr. 2116
Repititon 6−10
x 10^−4
Test 6
Test 7
Test 8
Test 9
Test 10
S(ω) [m^2*s]
Angular frequency [rad/s]

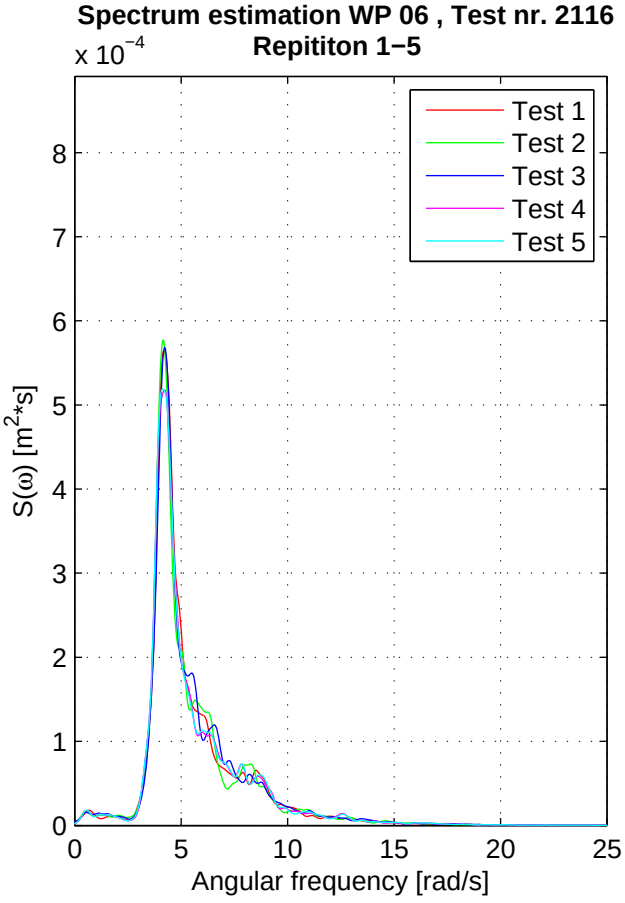
Spectrum estimation WP 06 , Test nr. 2116
Repititon 1−5
x 10^−4
Test 1
Test 2
Test 3
Test 4
Test 5
S(ω) [m^2*s]
Angular frequency [rad/s]

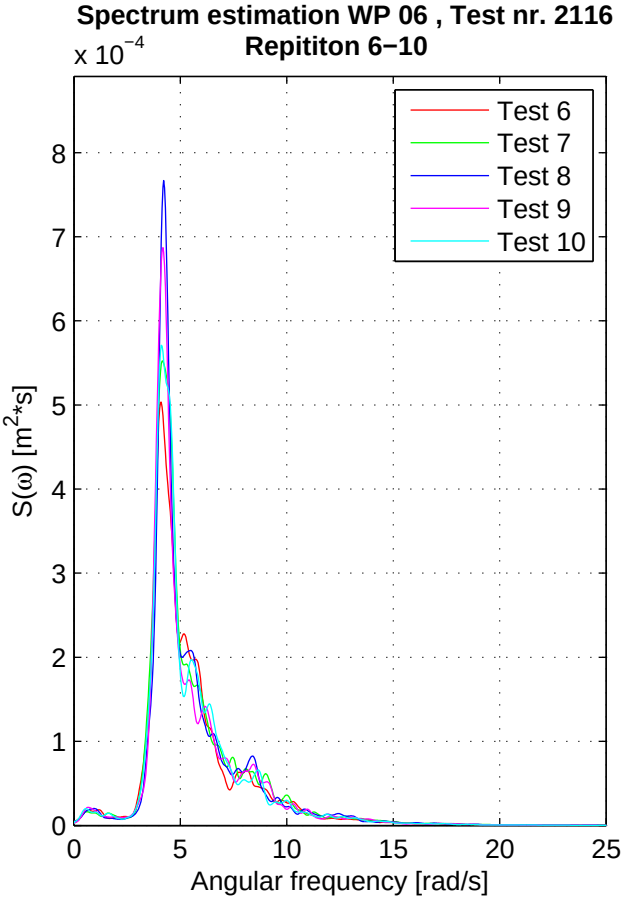
Spectrum estimation WP 06 , Test nr. 2116
Repititon 6−10
x 10^−4
Test 6
Test 7
Test 8
Test 9
Test 10
S(ω) [m^2*s]
Angular frequency [rad/s]

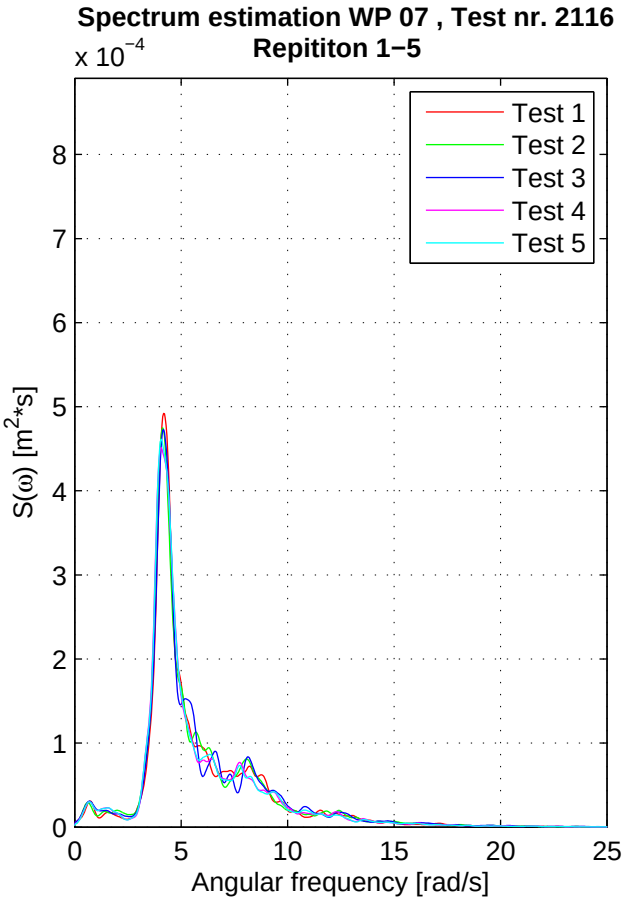
Spectrum estimation WP 07 , Test nr. 2116
Repititon 1−5
x 10^−4
Test 1
Test 2
Test 3
Test 4
Test 5
S(ω) [m^2*s]
Angular frequency [rad/s]
0
1
2
3
4
5
6
7
8
0
5
10
15
20
25

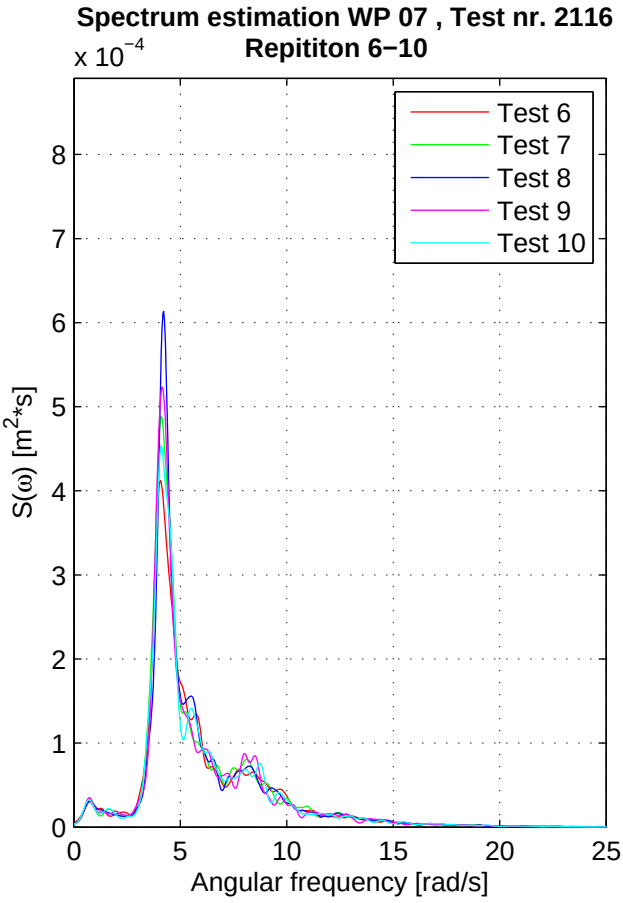
Spectrum estimation WP 07 , Test nr. 2116
Repititon 6−10
x 10^−4
Test 6
Test 7
Test 8
Test 9
Test 10
S(ω) [m^2*s]
Angular frequency [rad/s]
0
1
2
3
4
5
6
7
8
0
5
10
15
20
25

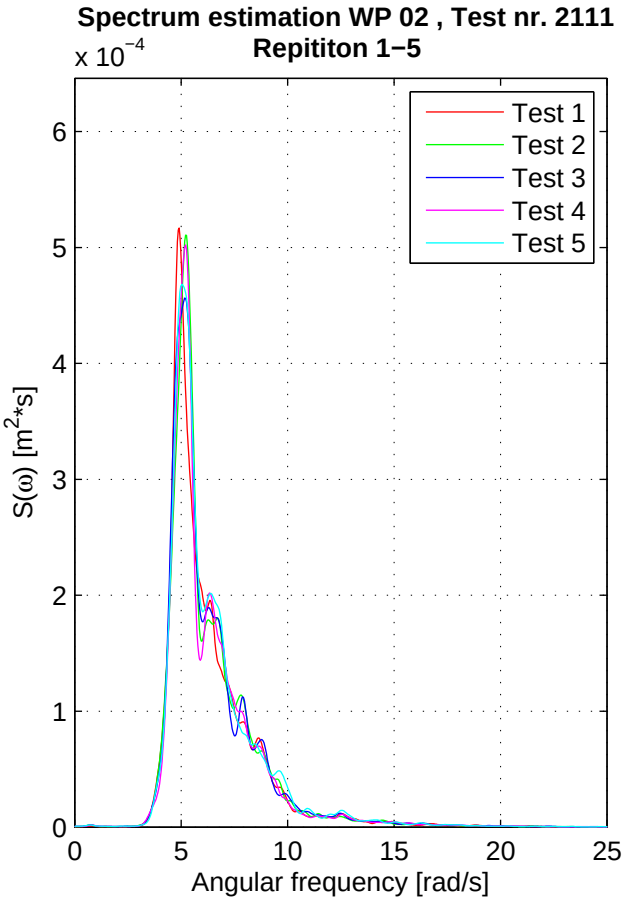
Spectrum estimation WP 02 , Test nr. 2111
Repititon 1−5
x 10^−4
Test 1
Test 2
Test 3
Test 4
Test 5
S(ω) [m^2*s]
Angular frequency [rad/s]

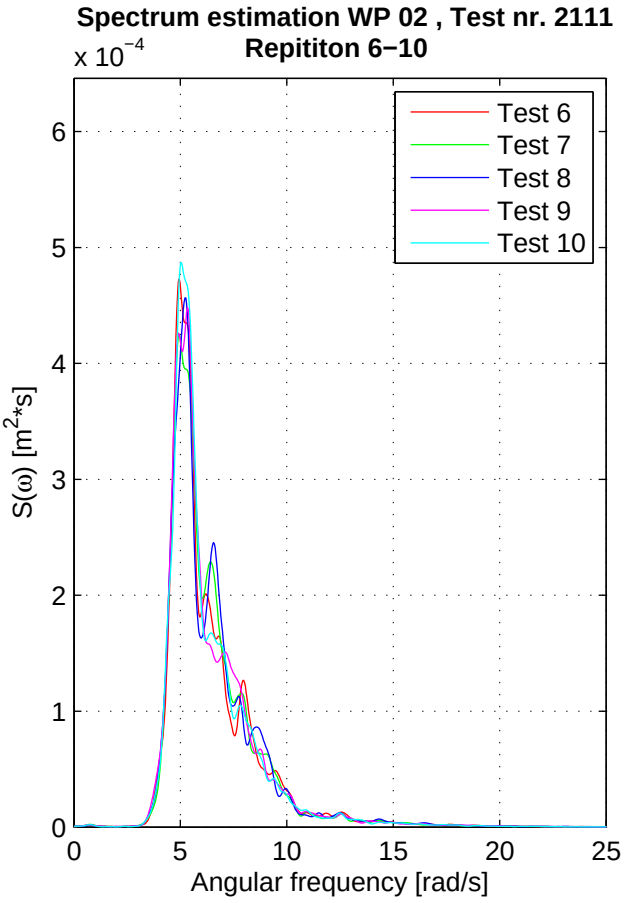
Spectrum estimation WP 02 , Test nr. 2111
Repititon 6−10
x 10^−4
Test 6
Test 7
Test 8
Test 9
Test 10
S(ω) [m^2*s]
Angular frequency [rad/s]

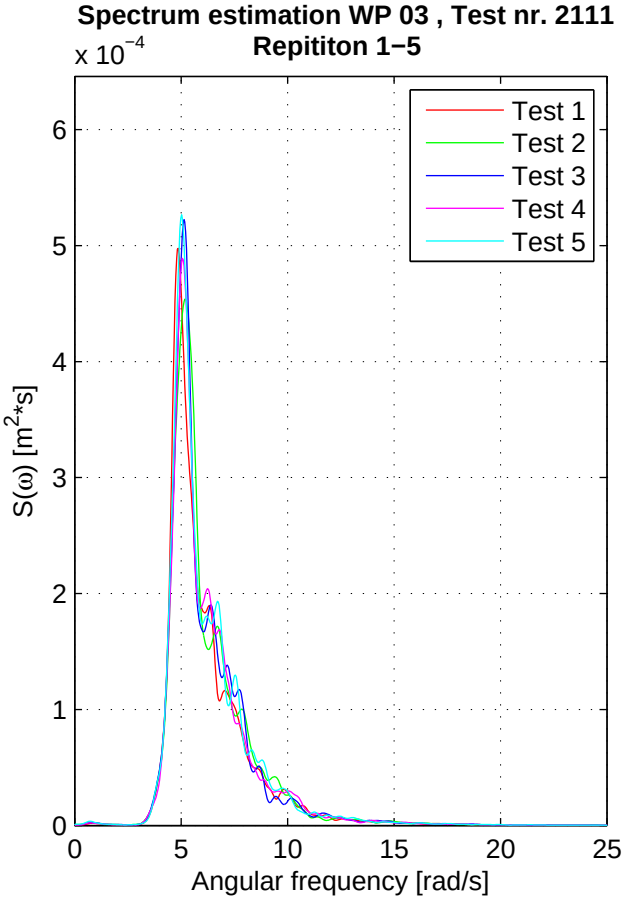
Spectrum estimation WP 03 , Test nr. 2111
Repititon 1−5
x 10^−4
Test 1
Test 2
Test 3
Test 4
Test 5
S(ω) [m^2*s]
Angular frequency [rad/s]

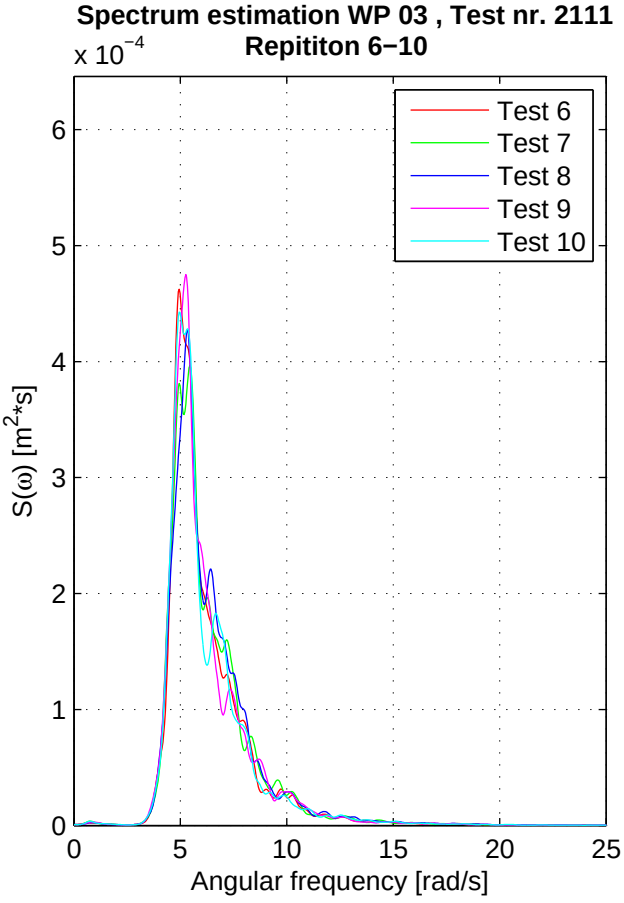
Spectrum estimation WP 03 , Test nr. 2111
Repititon 6−10
x 10^−4
Test 6
Test 7
Test 8
Test 9
Test 10
S(ω) [m^2*s]
Angular frequency [rad/s]

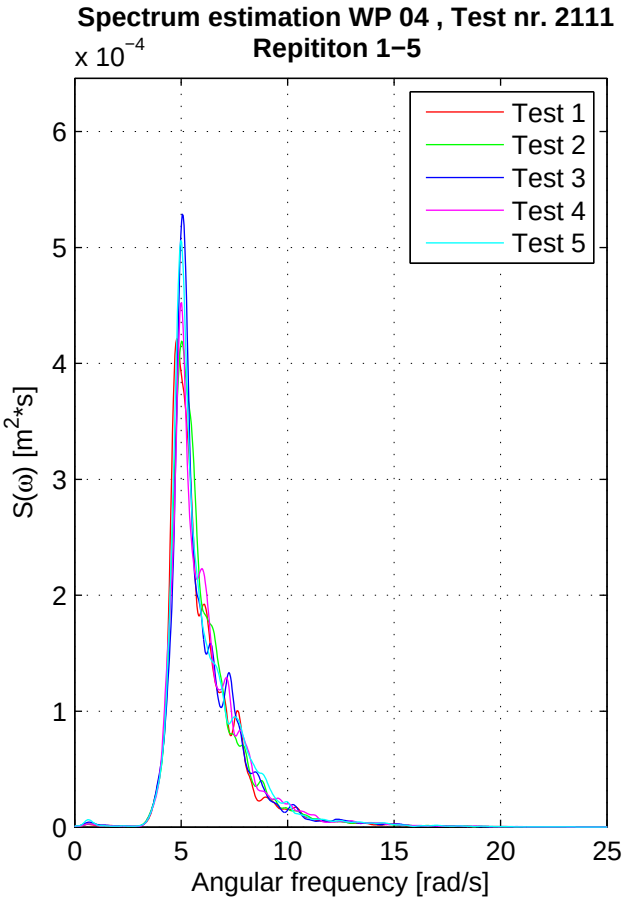
Spectrum estimation WP 04 , Test nr. 2111
Repititon 1−5
x 10^−4
Test 1
Test 2
Test 3
Test 4
Test 5
S(ω) [m^2*s]
Angular frequency [rad/s]

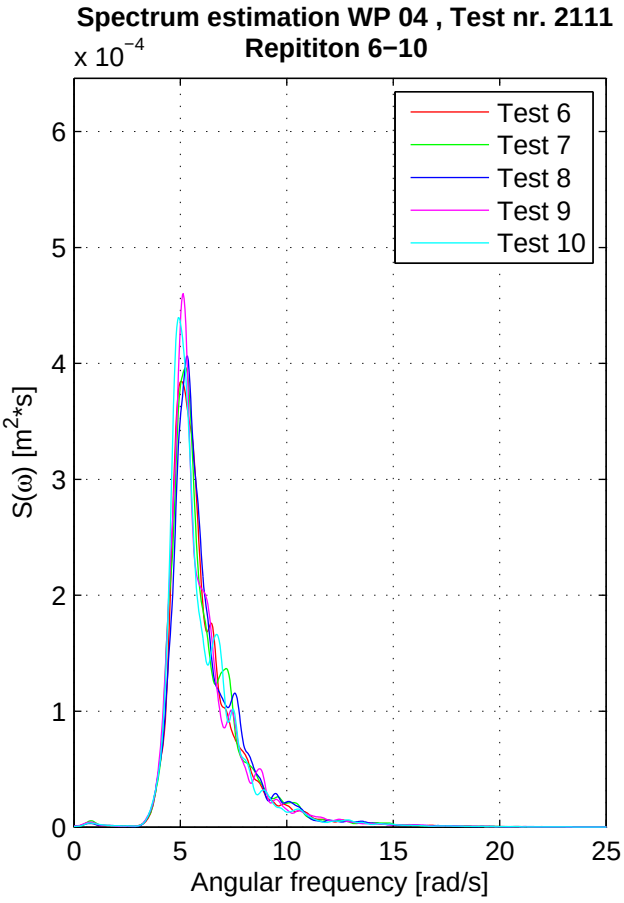
Spectrum estimation WP 04 , Test nr. 2111
Repititon 6−10
x 10^−4
Test 6
Test 7
Test 8
Test 9
Test 10
S(ω) [m^2*s]
Angular frequency [rad/s]

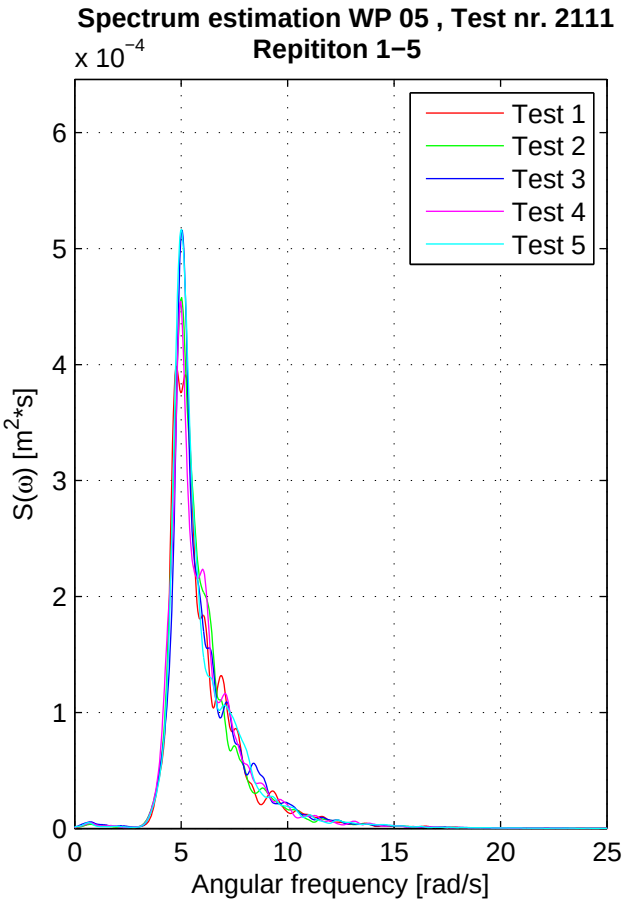
Spectrum estimation WP 05 , Test nr. 2111
Repititon 1−5
x 10^−4
Test 1
Test 2
Test 3
Test 4
Test 5
S(ω) [m^2*s]
Angular frequency [rad/s]

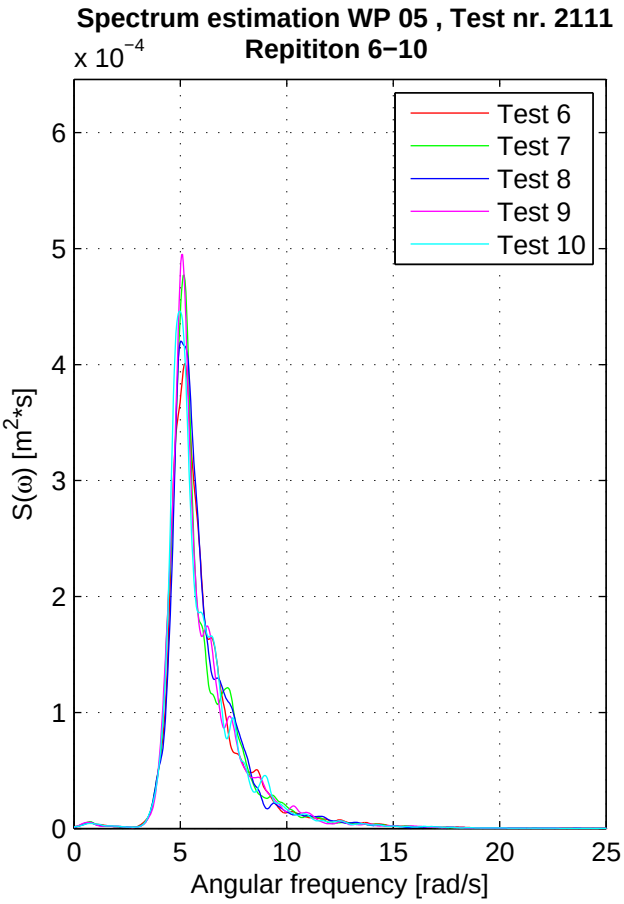
Spectrum estimation WP 05 , Test nr. 2111
Repititon 6−10
x 10^−4
Test 6
Test 7
Test 8
Test 9
Test 10
S(ω) [m^2*s]
Angular frequency [rad/s]

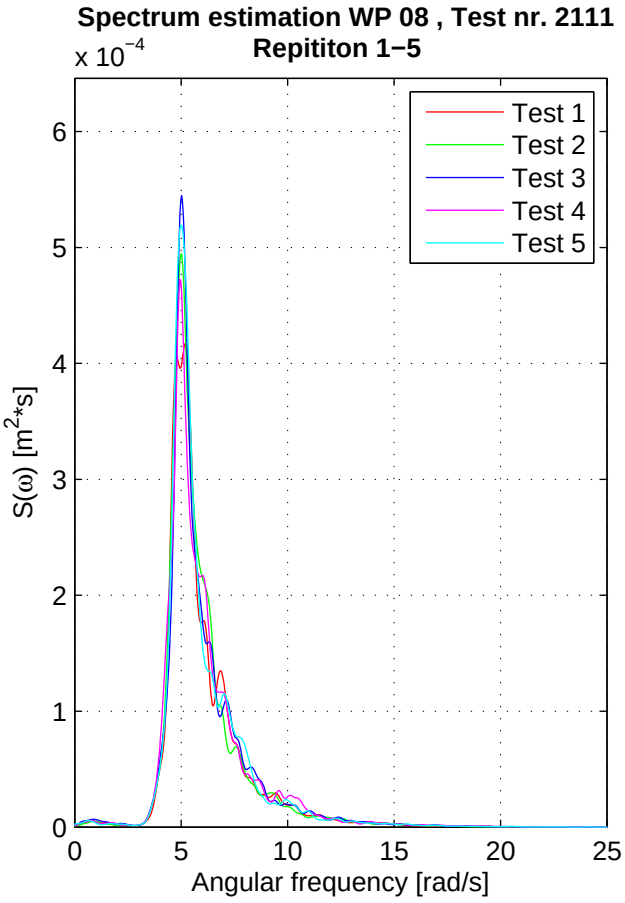
Spectrum estimation WP 08 , Test nr. 2111
Repititon 1−5
x 10^−4
Test 1
Test 2
Test 3
Test 4
Test 5
S(ω) [m^2*s]
Angular frequency [rad/s]

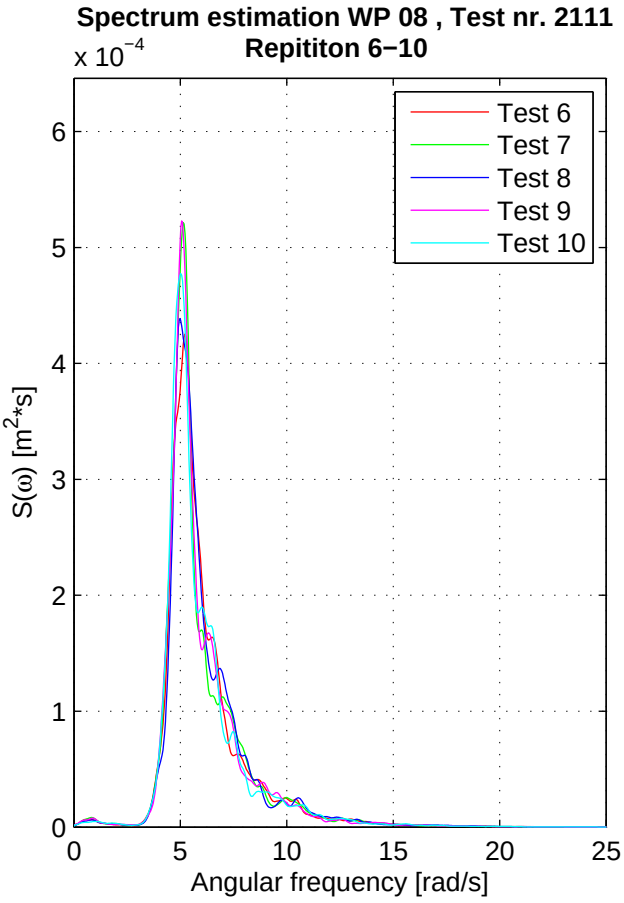
Spectrum estimation WP 08 , Test nr. 2111
Repititon 6−10
x 10^−4
Test 6
Test 7
Test 8
Test 9
Test 10
S(ω) [m^2*s]
Angular frequency [rad/s]

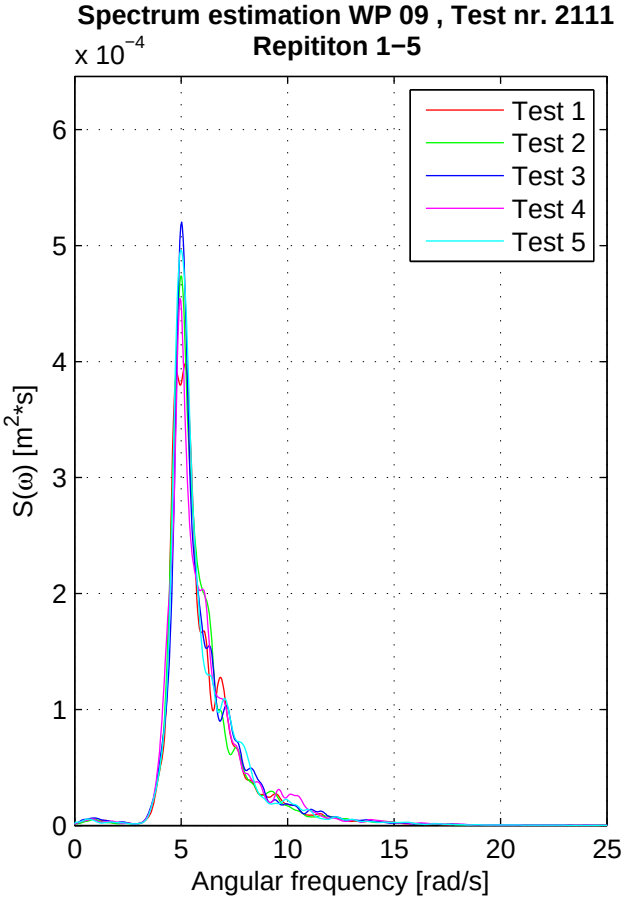
Spectrum estimation WP 09 , Test nr. 2111
Repititon 1−5
x 10^−4
Test 1
Test 2
Test 3
Test 4
Test 5
S(ω) [m^2*s]
Angular frequency [rad/s]

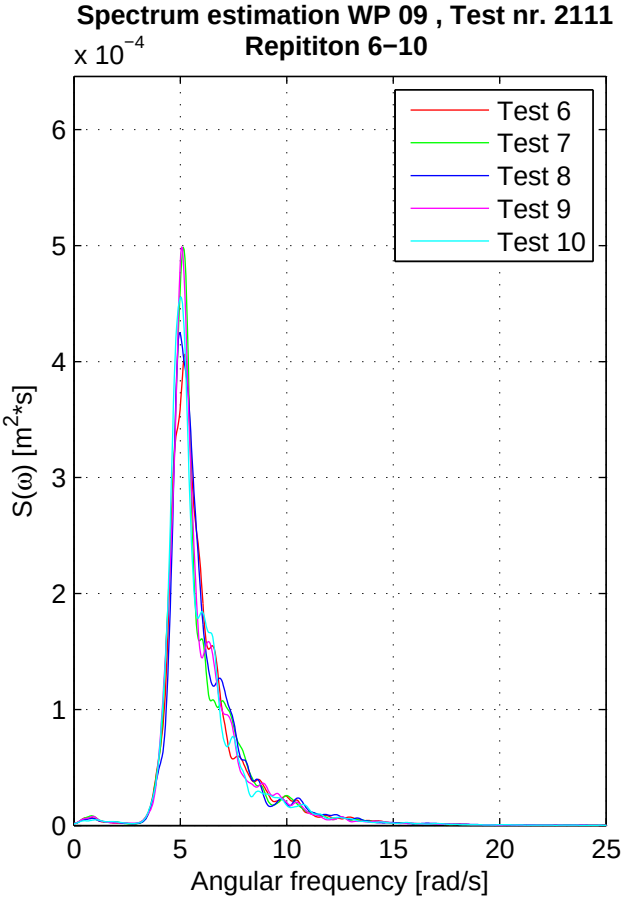
Spectrum estimation WP 09 , Test nr. 2111
Repititon 6−10
x 10^−4
Test 6
Test 7
Test 8
Test 9
Test 10
S(ω) [m^2*s]
Angular frequency [rad/s]

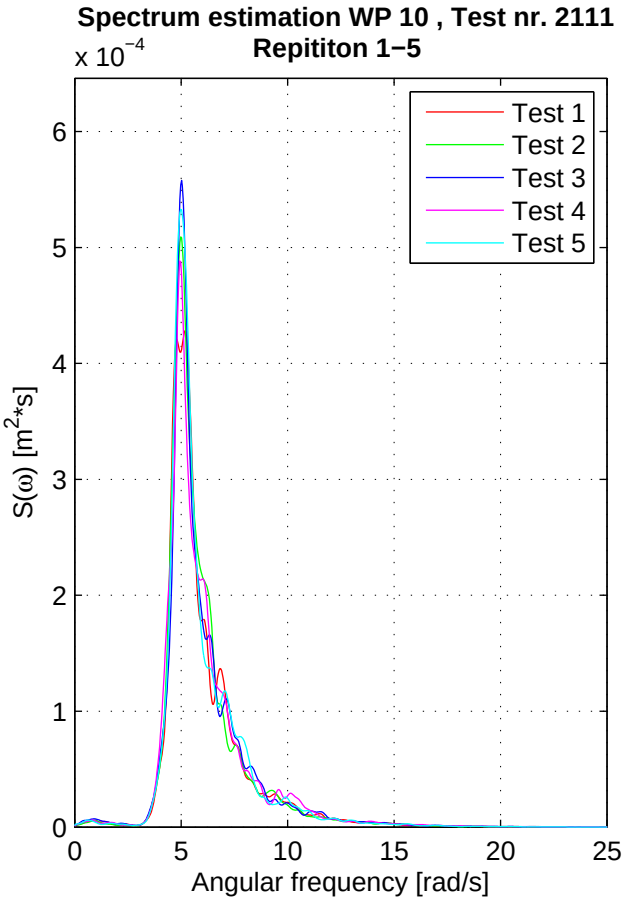
Spectrum estimation WP 10 , Test nr. 2111
Repititon 1−5
x 10^−4
Test 1
Test 2
Test 3
Test 4
Test 5
S(ω) [m^2*s]
Angular frequency [rad/s]

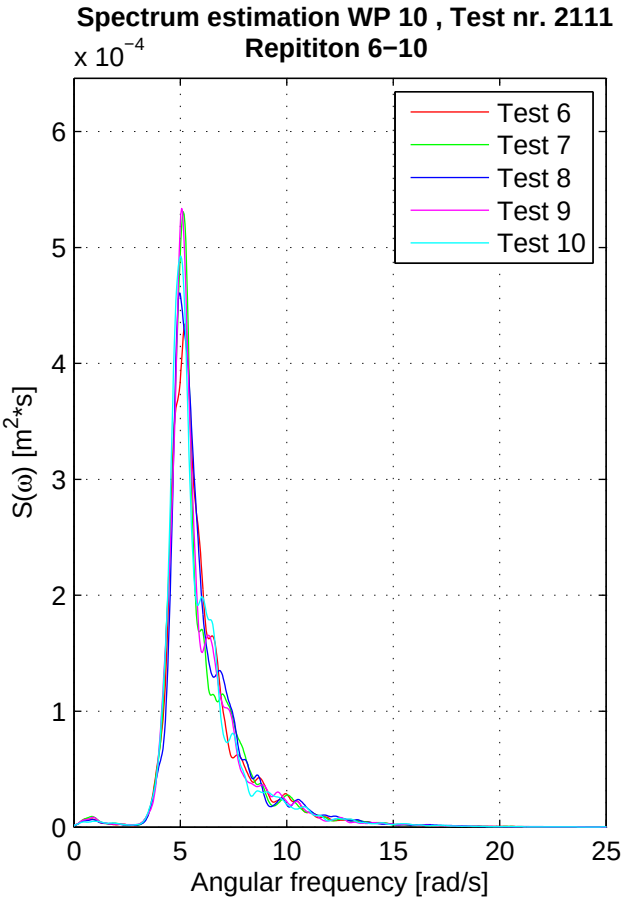
Spectrum estimation WP 10 , Test nr. 2111
Repititon 6−10
x 10^−4
Test 6
Test 7
Test 8
Test 9
Test 10
S(ω) [m^2*s]
Angular frequency [rad/s]

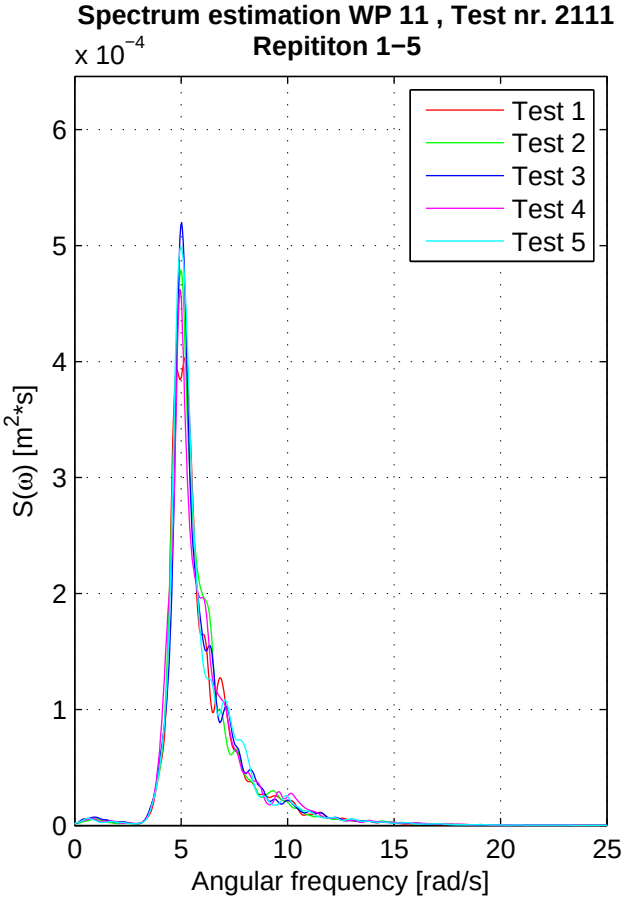
Spectrum estimation WP 11 , Test nr. 2111
Repititon 1−5
x 10^−4
Test 1
Test 2
Test 3
Test 4
Test 5
S(ω) [m^2*s]
Angular frequency [rad/s]

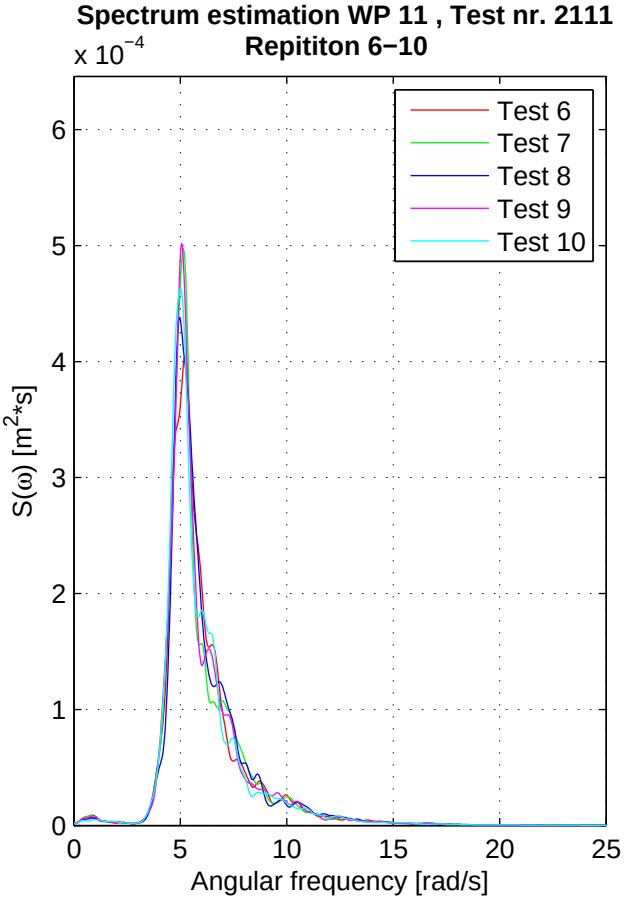
Spectrum estimation WP 11 , Test nr. 2111
Repititon 6−10
x 10^−4
Test 6
Test 7
Test 8
Test 9
Test 10
S(ω) [m^2*s]
Angular frequency [rad/s]

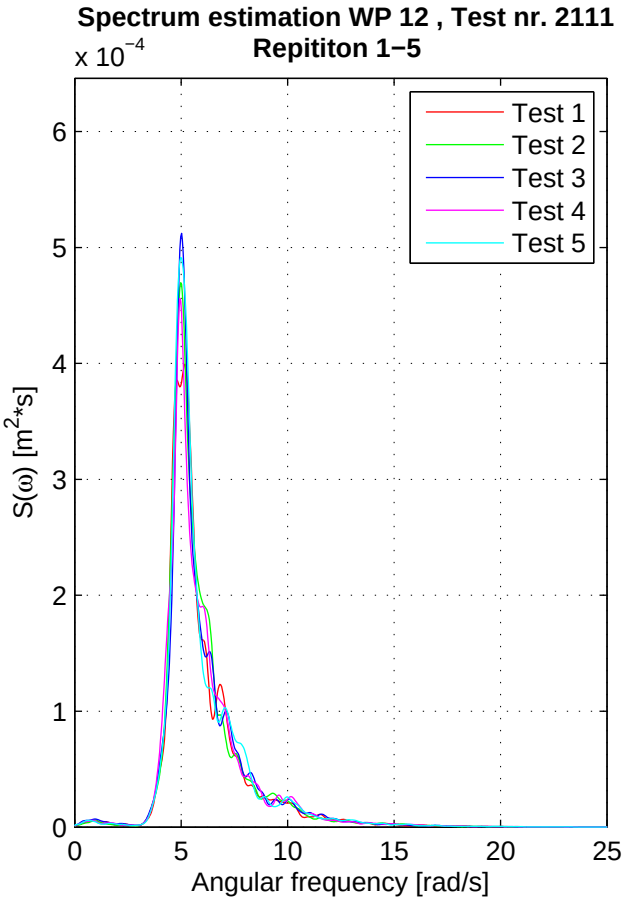
Spectrum estimation WP 12 , Test nr. 2111
Repititon 1−5
x 10^−4
Test 1
Test 2
Test 3
Test 4
Test 5
S(ω) [m^2*s]
Angular frequency [rad/s]

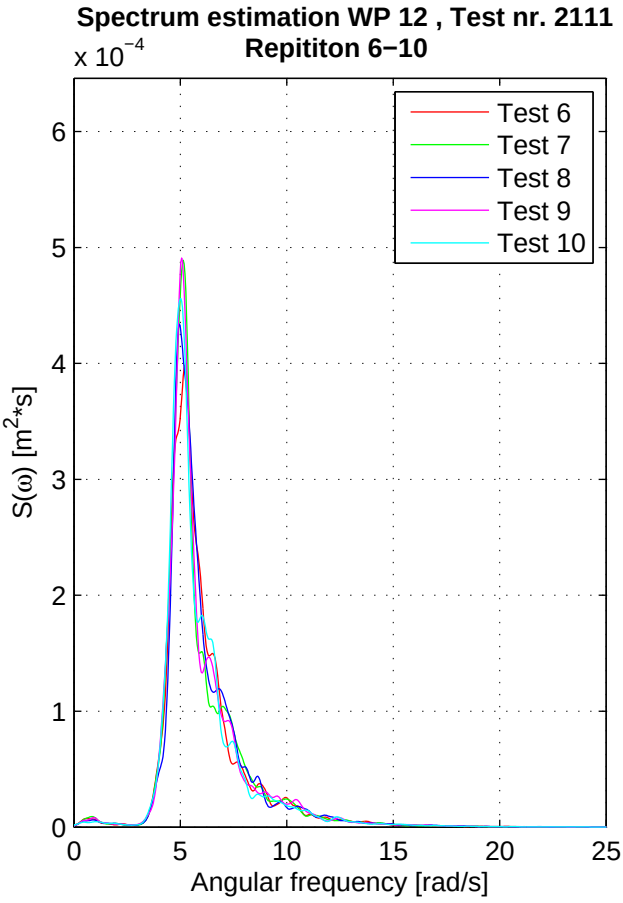
Spectrum estimation WP 12 , Test nr. 2111
Repititon 6−10
x 10^−4
Test 6
Test 7
Test 8
Test 9
Test 10
S(ω) [m^2*s]
Angular frequency [rad/s]

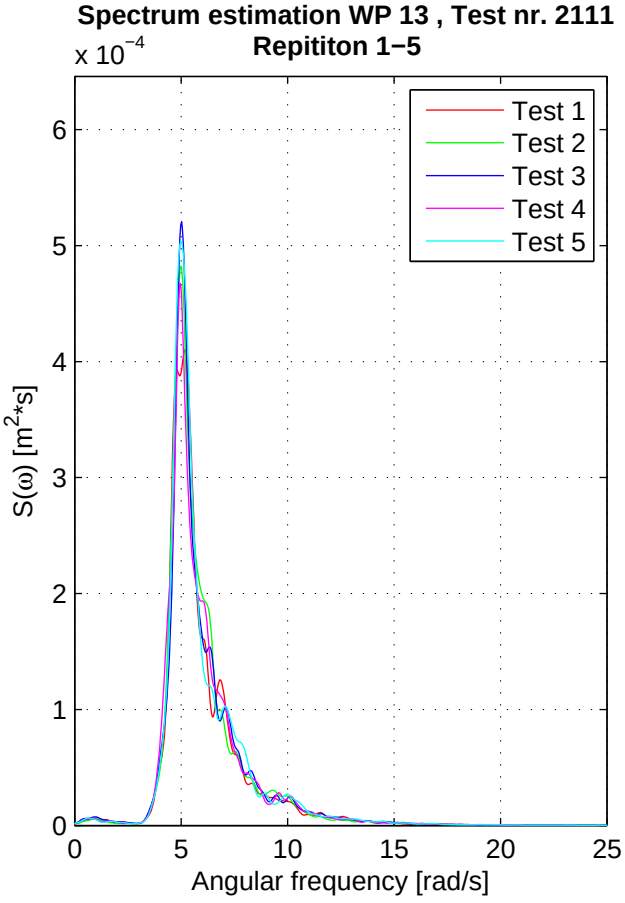
Spectrum estimation WP 13 , Test nr. 2111
Repititon 1−5
x 10^−4
Test 1
Test 2
Test 3
Test 4
Test 5
S(ω) [m^2*s]
Angular frequency [rad/s]

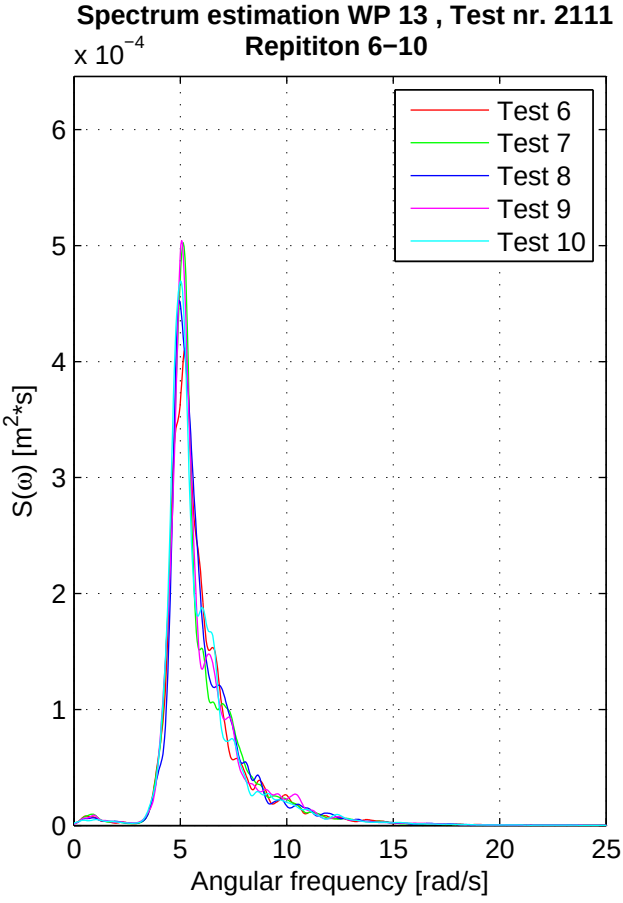
Spectrum estimation WP 13 , Test nr. 2111
Repititon 6−10
x 10^−4
Test 6
Test 7
Test 8
Test 9
Test 10
S(ω) [m^2*s]
Angular frequency [rad/s]

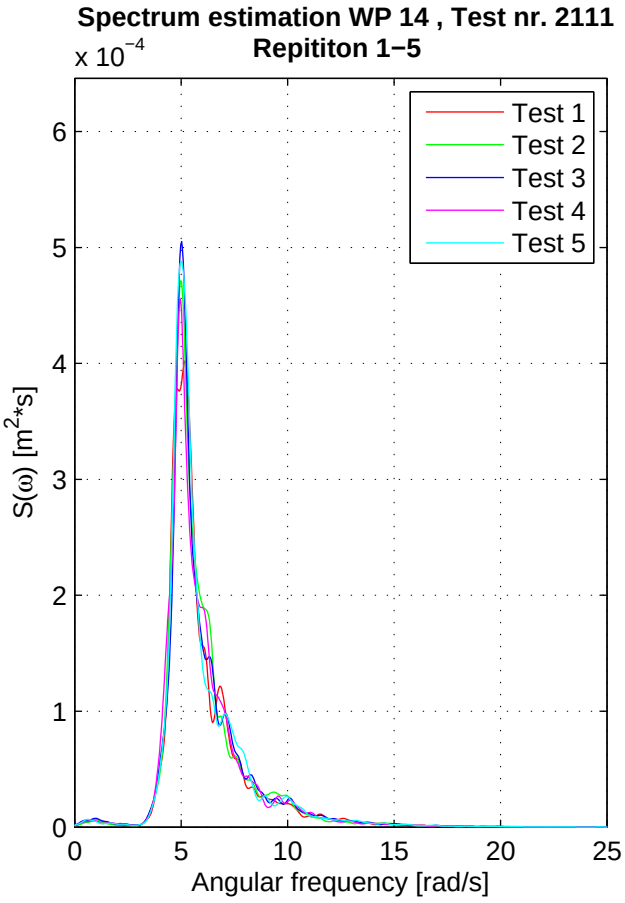
Spectrum estimation WP 14 , Test nr. 2111
Repititon 1−5
x 10^−4
Test 1
Test 2
Test 3
Test 4
Test 5
S(ω) [m^2*s]
Angular frequency [rad/s]

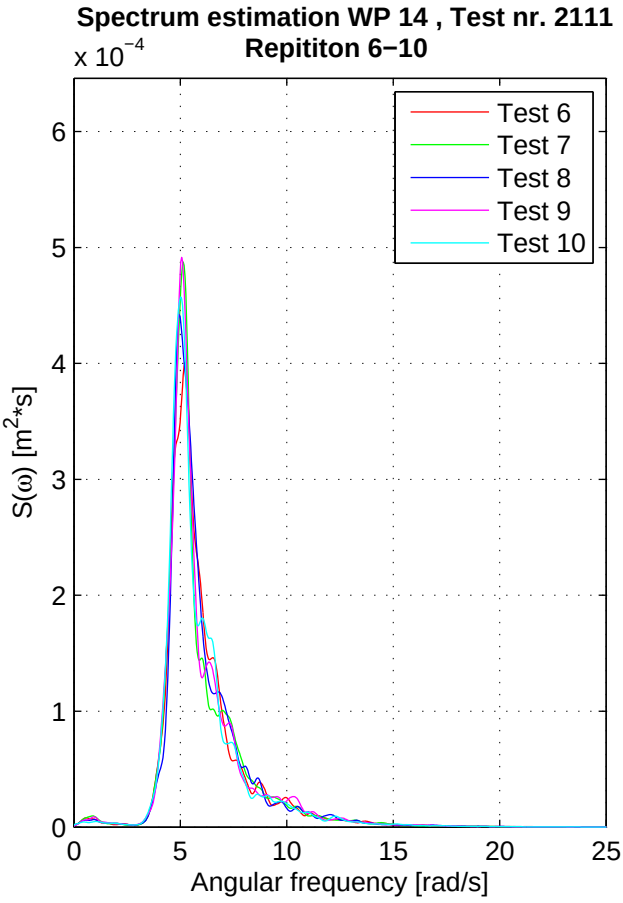
Spectrum estimation WP 14 , Test nr. 2111
Repititon 6−10
x 10^−4
Test 6
Test 7
Test 8
Test 9
Test 10
S(ω) [m^2*s]
Angular frequency [rad/s]

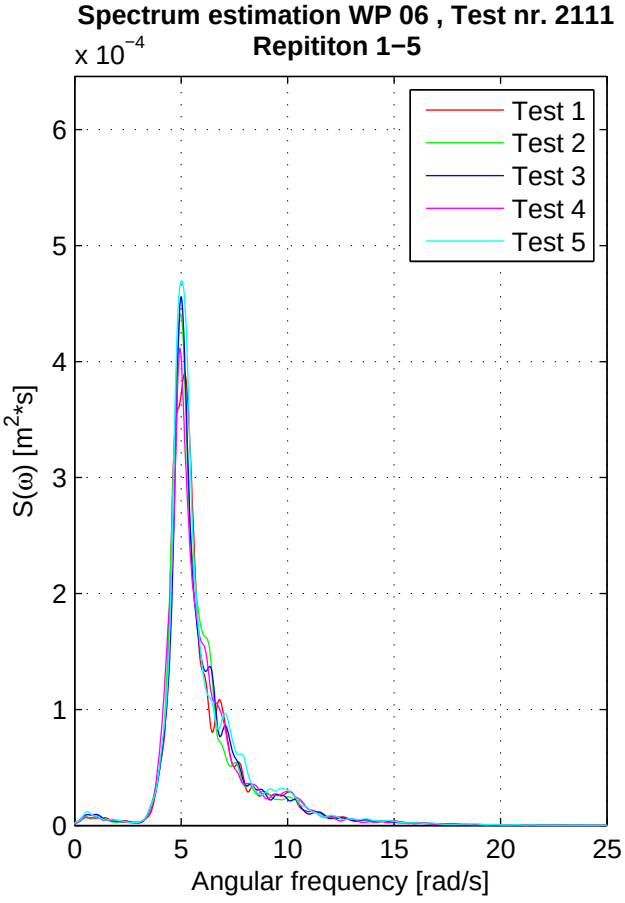
Spectrum estimation WP 06 , Test nr. 2111
Repititon 1−5
x 10^−4
Test 1
Test 2
Test 3
Test 4
Test 5
S(ω) [m^2*s]
Angular frequency [rad/s]

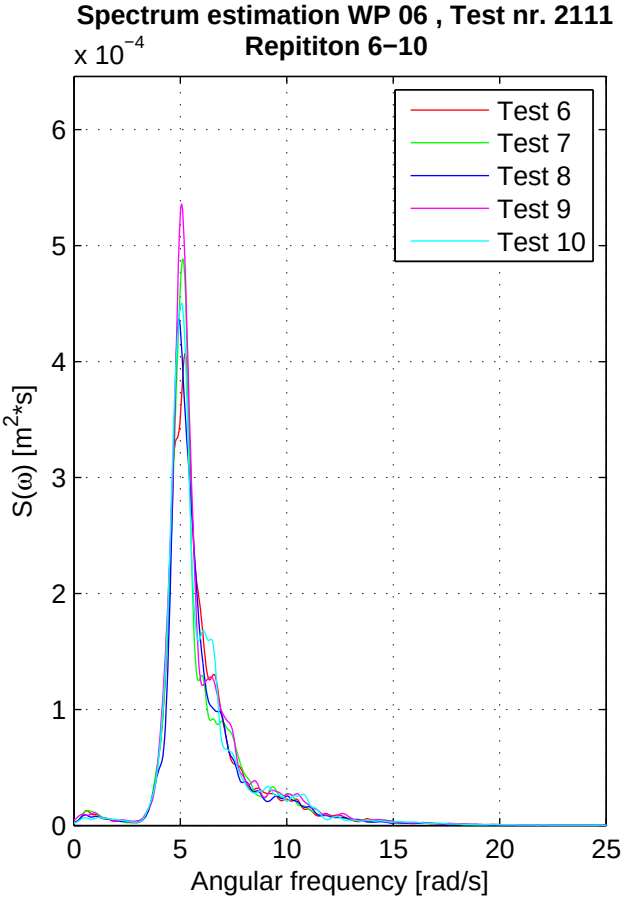
Spectrum estimation WP 06 , Test nr. 2111
Repititon 6−10
x 10^−4
Test 6
Test 7
Test 8
Test 9
Test 10
S(ω) [m^2*s]
Angular frequency [rad/s]

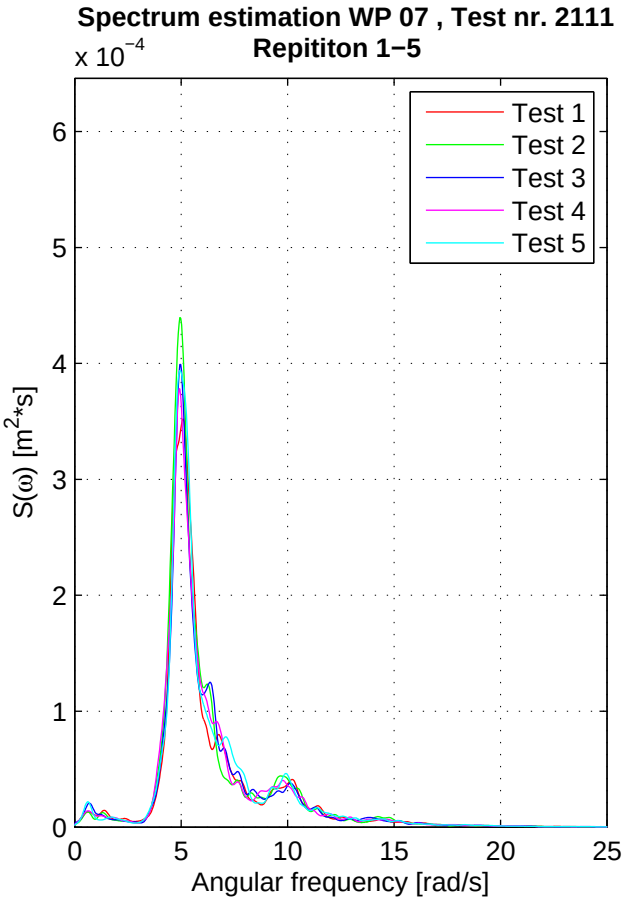
Spectrum estimation WP 07 , Test nr. 2111
Repititon 1−5
x 10^−4
Test 1
Test 2
Test 3
Test 4
Test 5
S(ω) [m^2*s]
Angular frequency [rad/s]
0
1
2
3
4
5
6
0
5
10
15
20
25

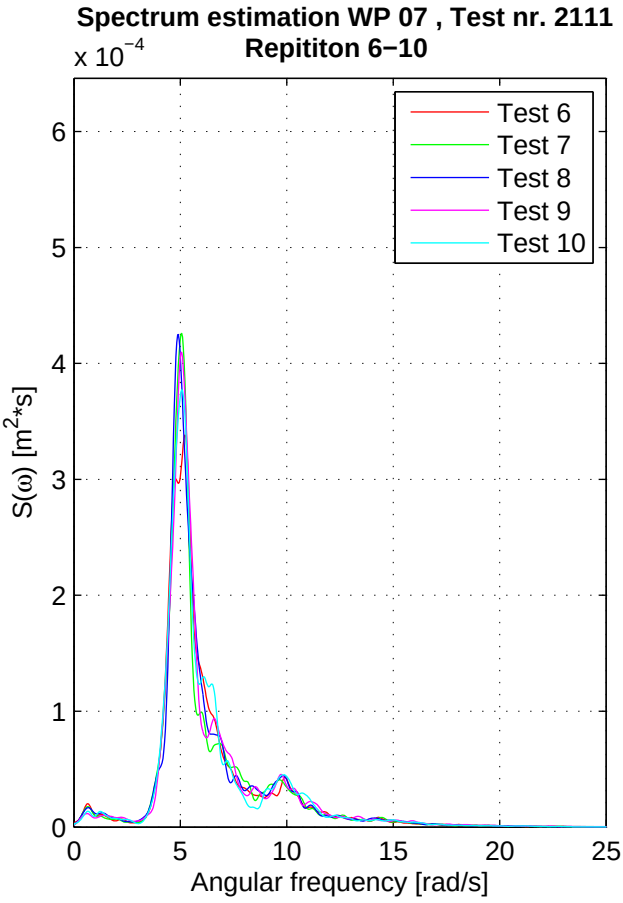
Spectrum estimation WP 07 , Test nr. 2111
Repititon 6−10
x 10^−4
Test 6
Test 7
Test 8
Test 9
Test 10
S(ω) [m^2*s]
Angular frequency [rad/s]
0
1
2
3
4
5
6
0
5
10
15
20
25

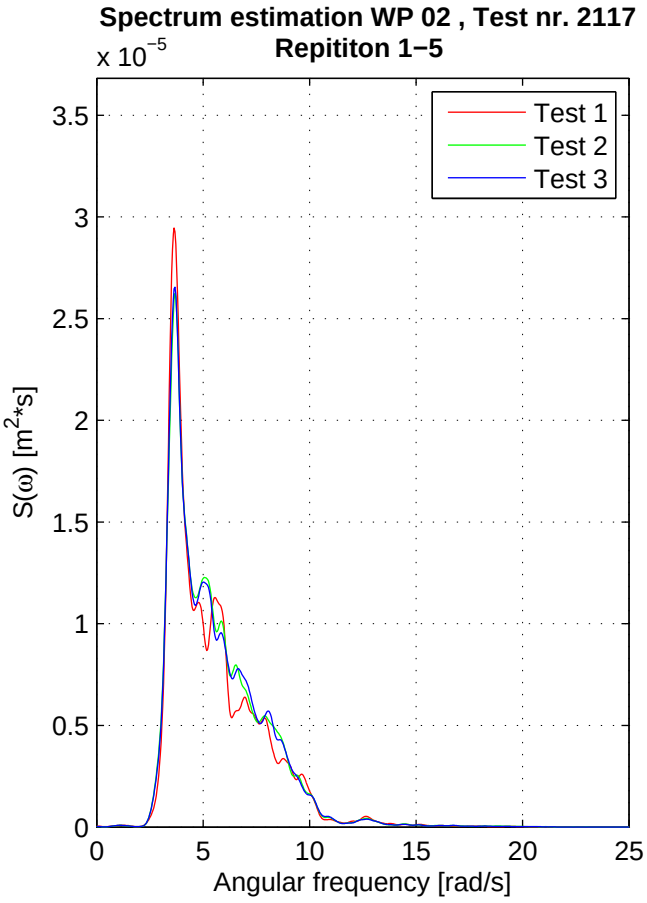
Spectrum estimation WP 02 , Test nr. 2117
Repititon 1−5
x 10^−5
Test 1
Test 2
Test 3
S(ω) [m^2*s]
Angular frequency [rad/s]
0
0.5
1
1.5
2
2.5
3
3.5
0
5
10
15
20
25

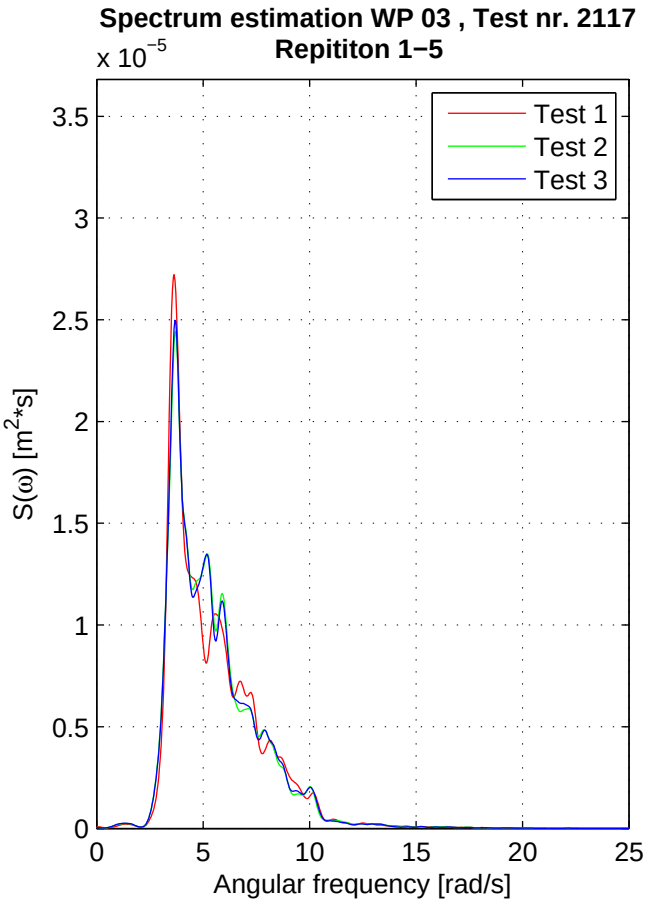
Spectrum estimation WP 03 , Test nr. 2117
Repititon 1−5
x 10^−5
Test 1
Test 2
Test 3
S(ω) [m^2*s]
Angular frequency [rad/s]
0
0.5
1
1.5
2
2.5
3
3.5
0
5
10
15
20
25

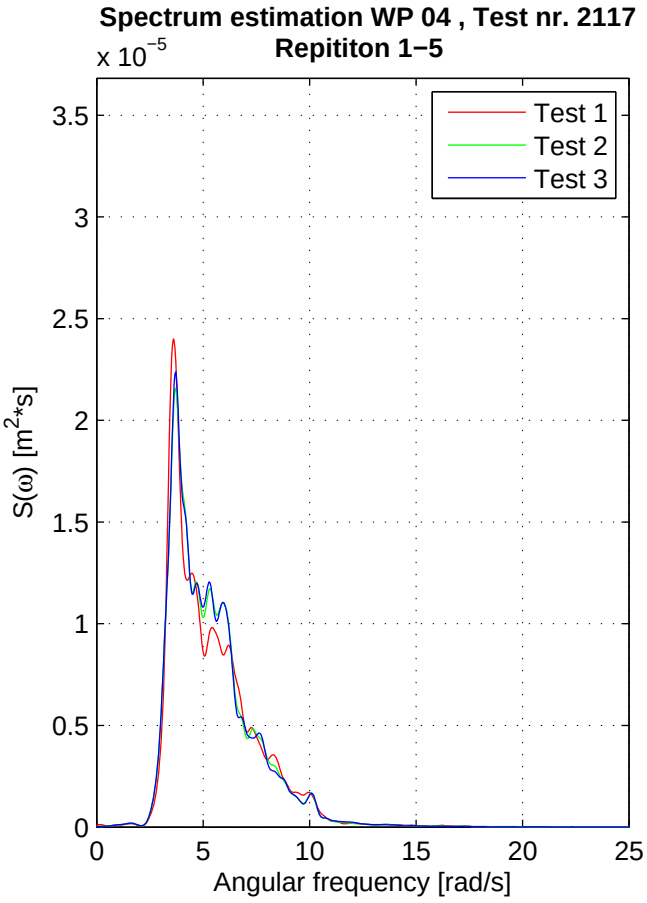
Spectrum estimation WP 04 , Test nr. 2117
Repititon 1−5
x 10^−5
Test 1
Test 2
Test 3
S(ω) [m^2*s]
Angular frequency [rad/s]
0
0.5
1
1.5
2
2.5
3
3.5
0
5
10
15
20
25

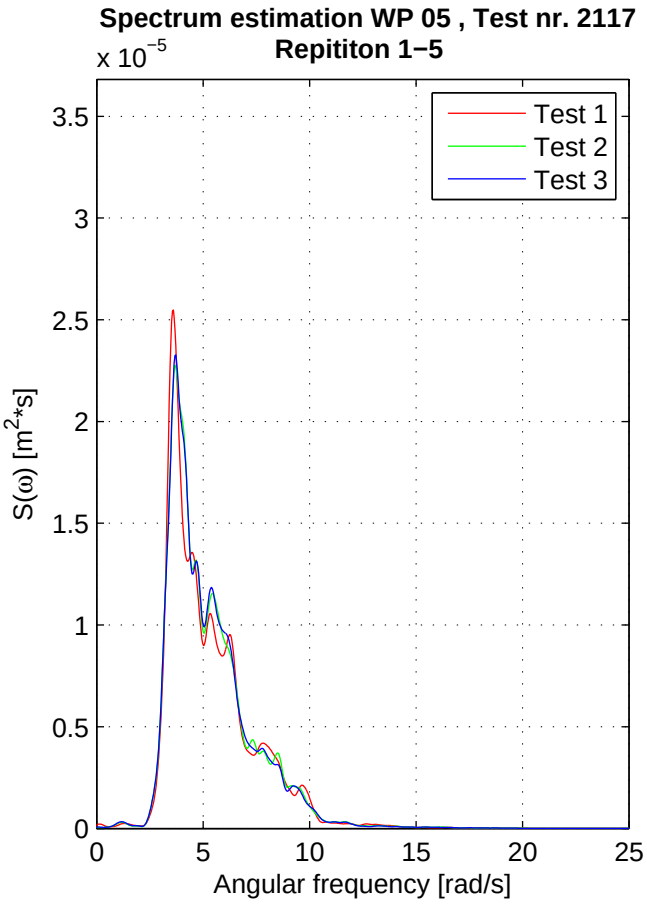
Spectrum estimation WP 05 , Test nr. 2117
Repititon 1−5
x 10^−5
Test 1
Test 2
Test 3
S(ω) [m^2*s]
Angular frequency [rad/s]
0
0.5
1
1.5
2
2.5
3
3.5
0
5
10
15
20
25

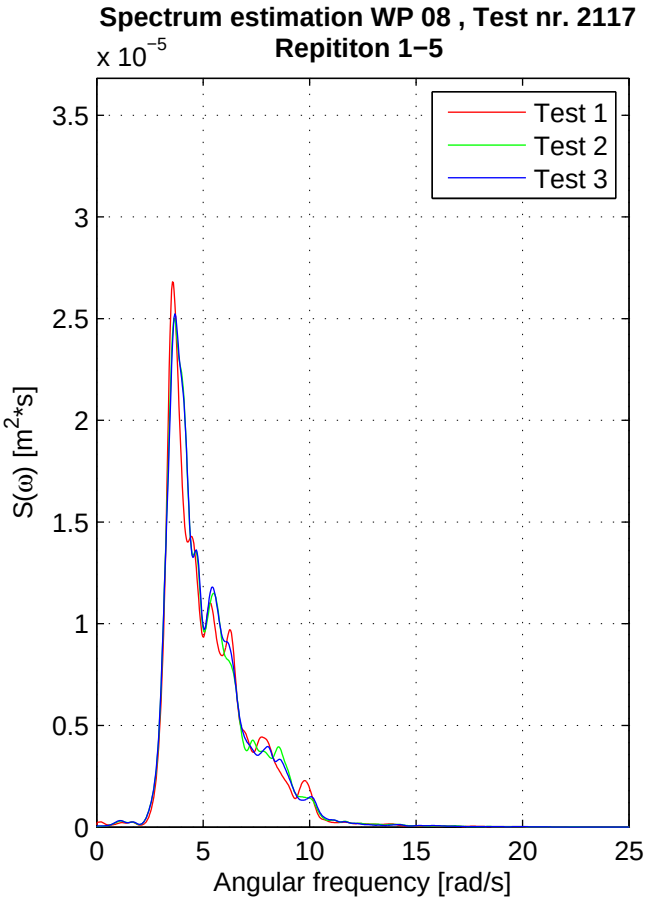
Spectrum estimation WP 08 , Test nr. 2117
Repititon 1−5
x 10^−5
Test 1
Test 2
Test 3
S(ω) [m^2*s]
Angular frequency [rad/s]
0
0.5
1
1.5
2
2.5
3
3.5
0
5
10
15
20
25

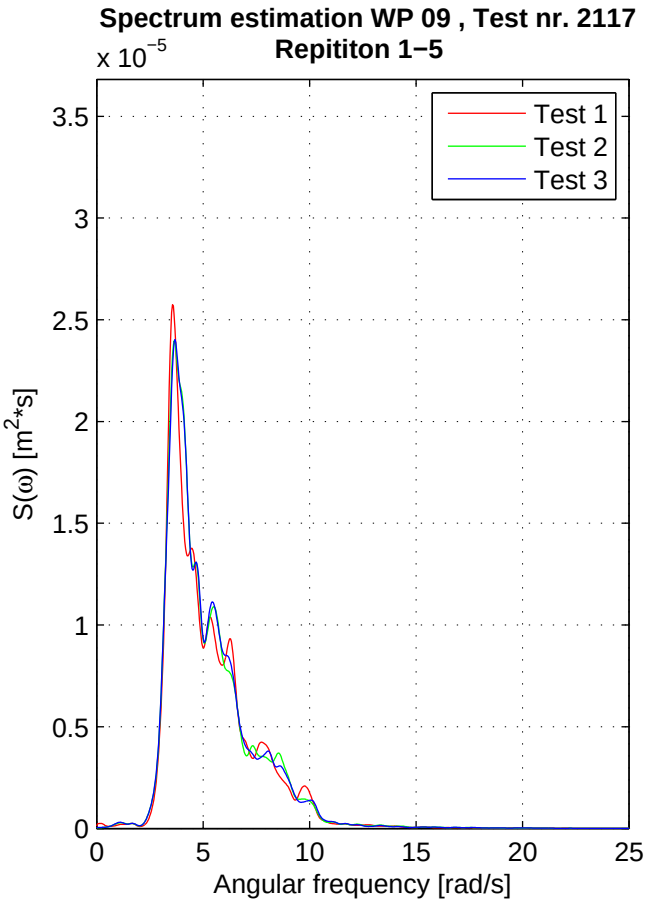
Spectrum estimation WP 09 , Test nr. 2117
Repititon 1−5
x 10^−5
Test 1
Test 2
Test 3
S(ω) [m^2*s]
Angular frequency [rad/s]
0
0.5
1
1.5
2
2.5
3
3.5
0
5
10
15
20
25

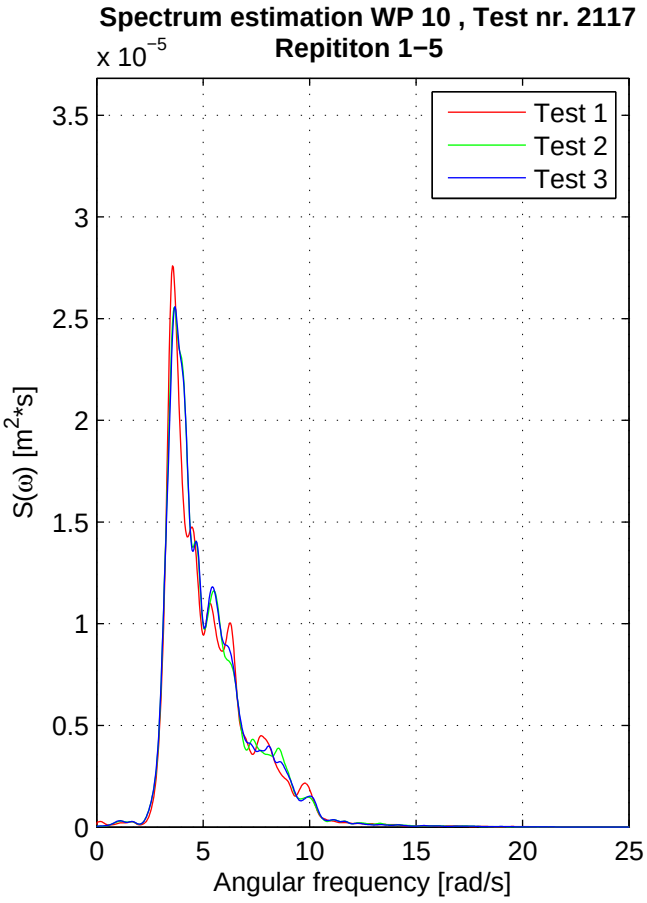
Spectrum estimation WP 10 , Test nr. 2117
Repititon 1−5
x 10^−5
Test 1
Test 2
Test 3
S(ω) [m^2*s]
Angular frequency [rad/s]
0
0.5
1
1.5
2
2.5
3
3.5
0
5
10
15
20
25

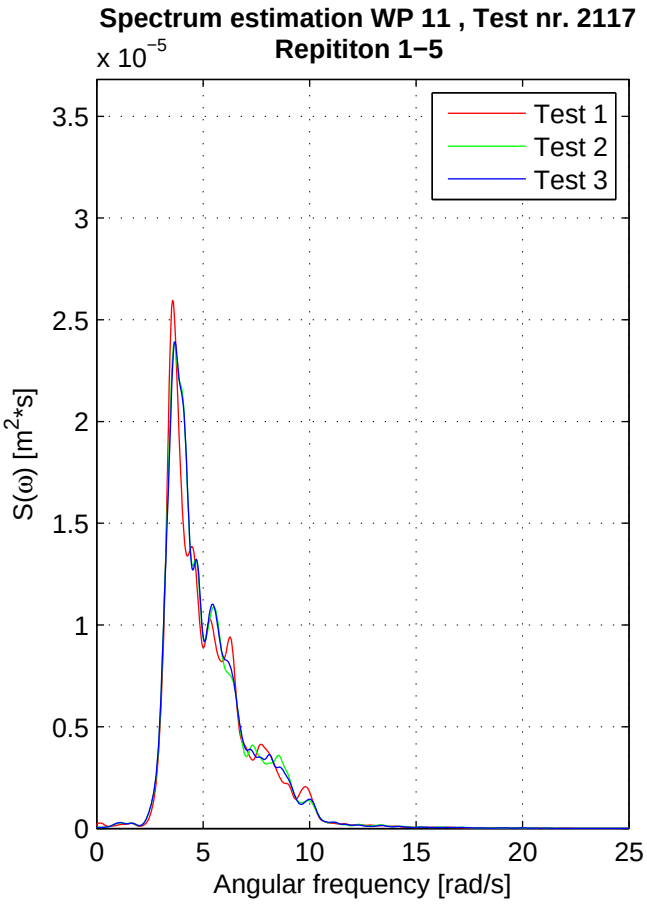
Spectrum estimation WP 11 , Test nr. 2117
Repititon 1−5
x 10^−5
Test 1
Test 2
Test 3
S(ω) [m^2*s]
Angular frequency [rad/s]
0
0.5
1
1.5
2
2.5
3
3.5
0
5
10
15
20
25

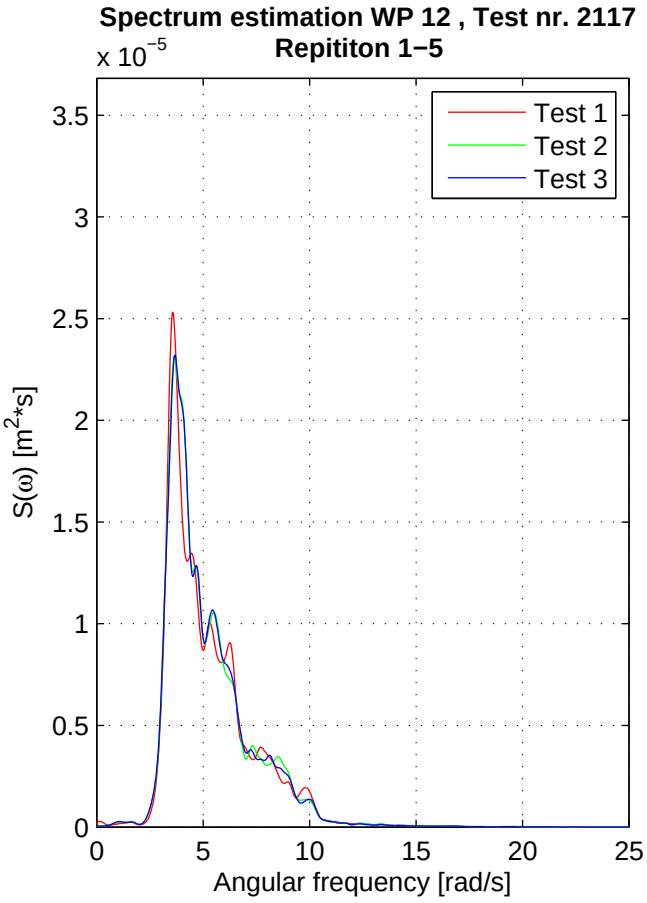
Spectrum estimation WP 12 , Test nr. 2117
Repititon 1−5
x 10^−5
Test 1
Test 2
Test 3
S(ω) [m^2*s]
Angular frequency [rad/s]
0
0.5
1
1.5
2
2.5
3
3.5
0
5
10
15
20
25

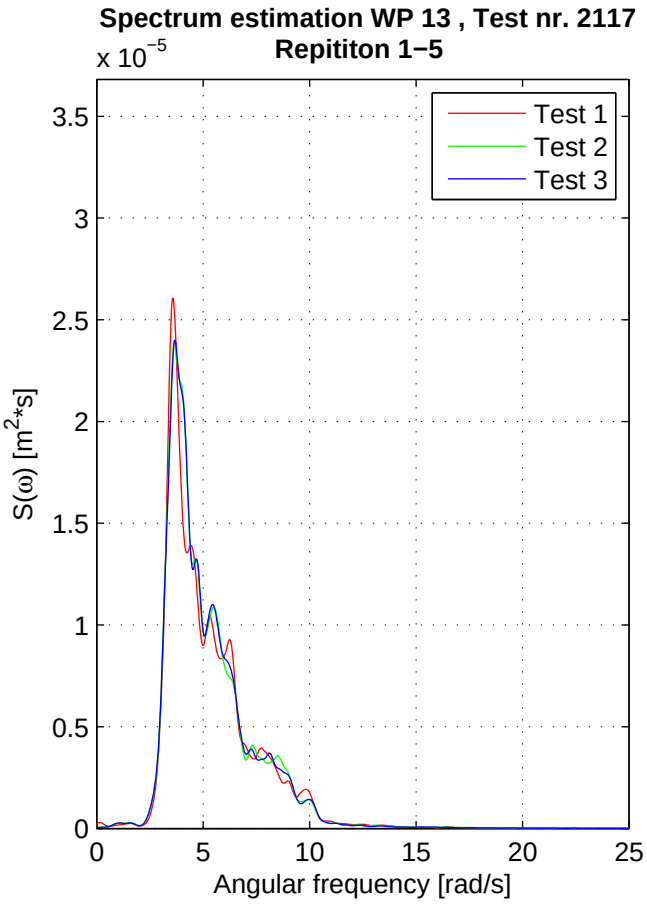
Spectrum estimation WP 13 , Test nr. 2117
Repititon 1−5
x 10^−5
Test 1
Test 2
Test 3
S(ω) [m^2*s]
Angular frequency [rad/s]
0
0.5
1
1.5
2
2.5
3
3.5
0
5
10
15
20
25

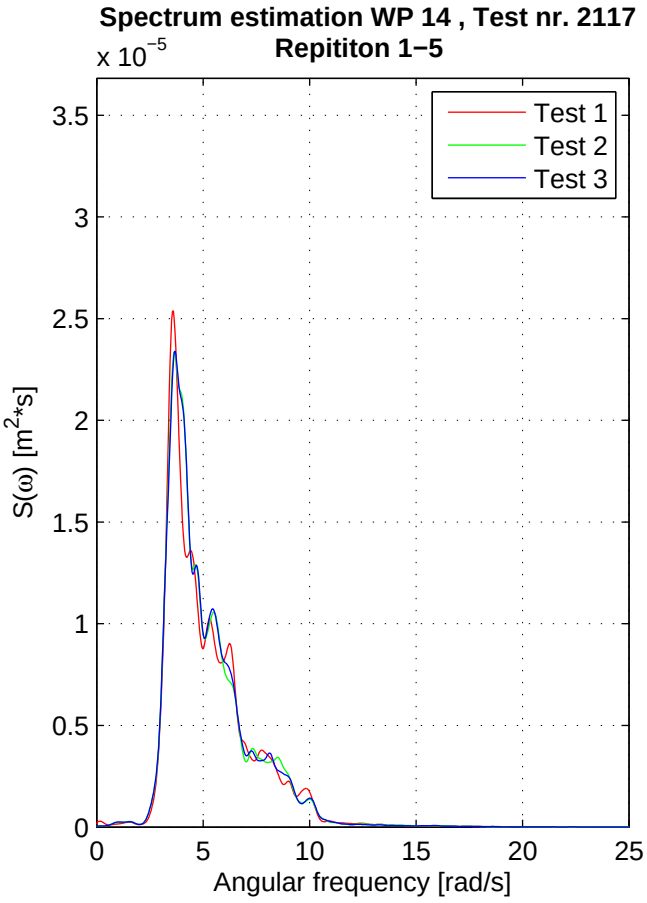
Spectrum estimation WP 14 , Test nr. 2117
Repititon 1−5
x 10^−5
Test 1
Test 2
Test 3
S(ω) [m^2*s]
Angular frequency [rad/s]
0
0.5
1
1.5
2
2.5
3
3.5
0
5
10
15
20
25

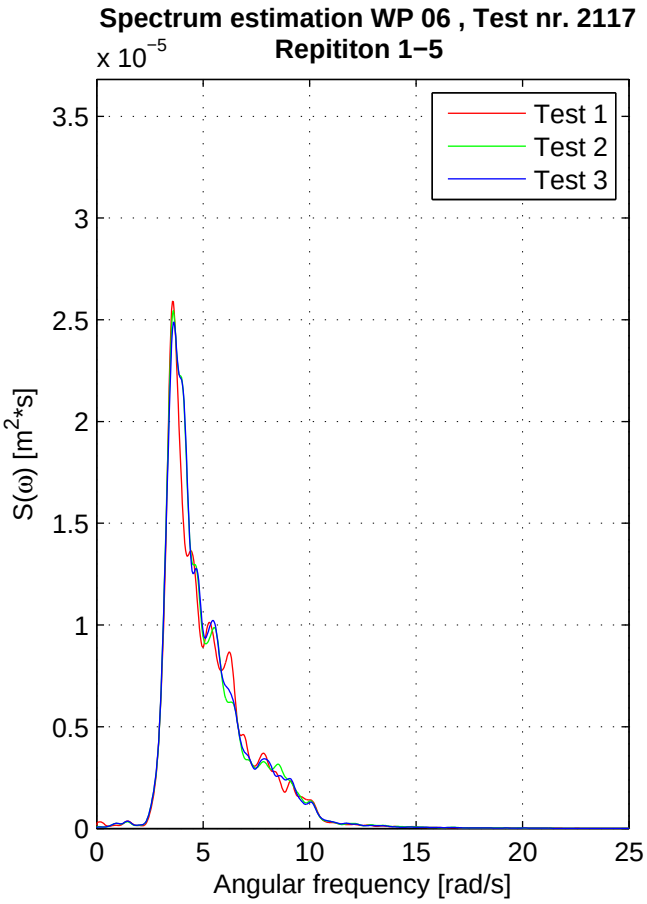
Spectrum estimation WP 06 , Test nr. 2117
Repititon 1−5
x 10^−5
Test 1
Test 2
Test 3
S(ω) [m^2*s]
Angular frequency [rad/s]
0
0.5
1
1.5
2
2.5
3
3.5
0
5
10
15
20
25

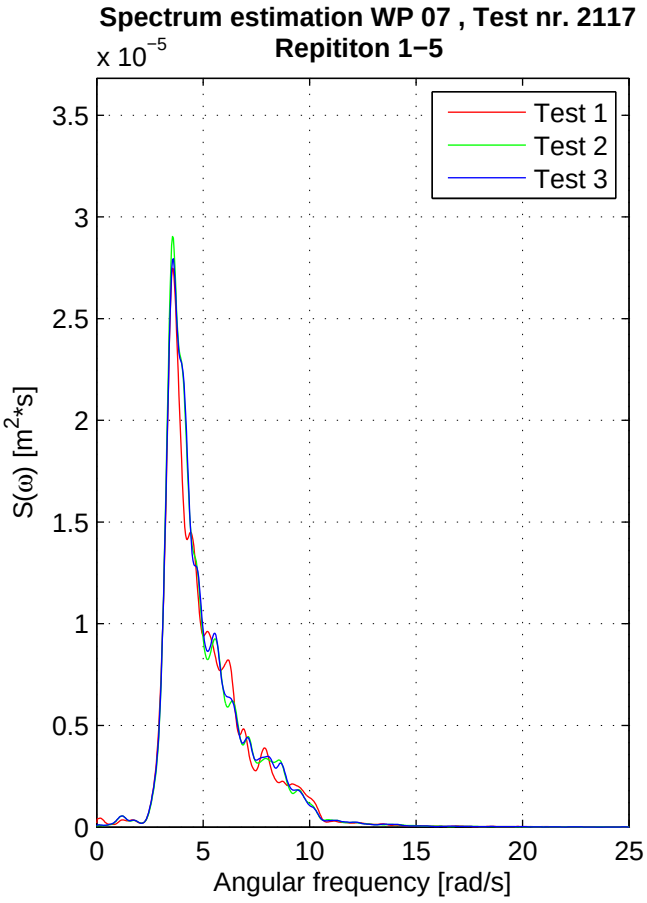
Spectrum estimation WP 07 , Test nr. 2117
Repititon 1−5
x 10^−5
Test 1
Test 2
Test 3
S(ω) [m^2*s]
Angular frequency [rad/s]
0
0.5
1
1.5
2
2.5
3
3.5
0
5
10
15
20
25

Appendix D

High frequency tail of the spectra

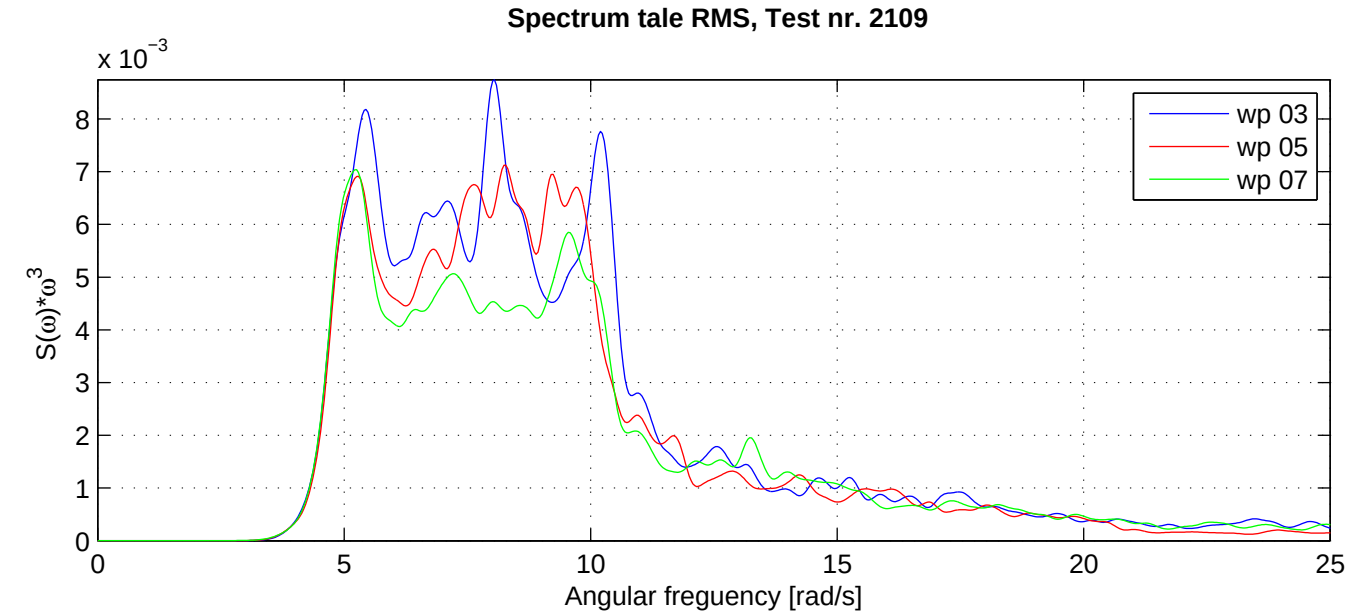
Spectrum tale RMS, Test nr. 2109
x 10^-3
S(ω)*ω^3
Angular freguency [rad/s]
wp 03
wp 05
wp 07

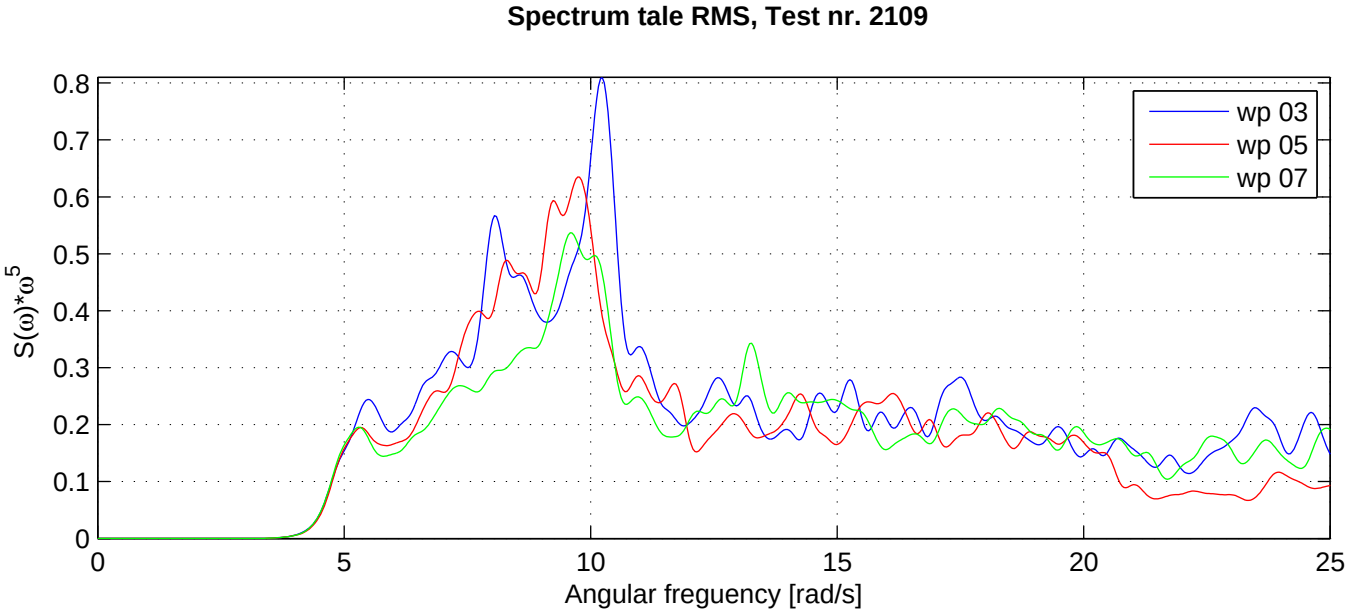
Spectrum tale RMS, Test nr. 2109
S(ω)*ω^5
Angular freguency [rad/s]
wp 03
wp 05
wp 07

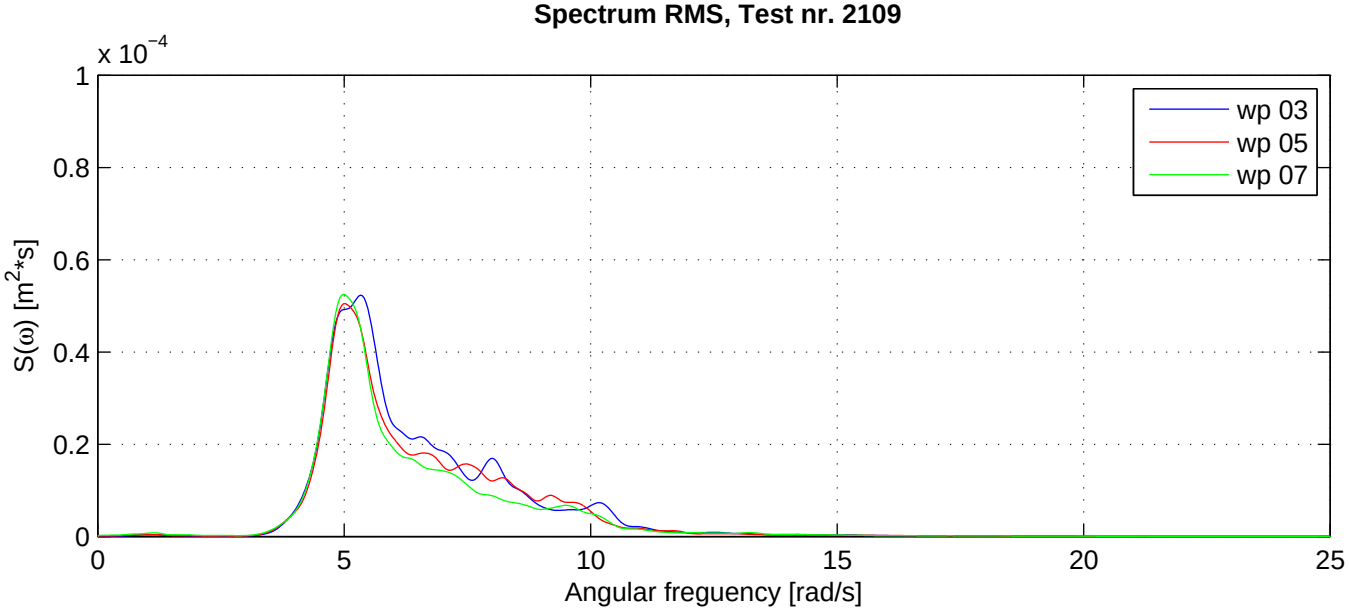
Spectrum RMS, Test nr. 2109
x 10^-4
S(ω) [m^2*s]
Angular freguency [rad/s]
wp 03
wp 05
wp 07

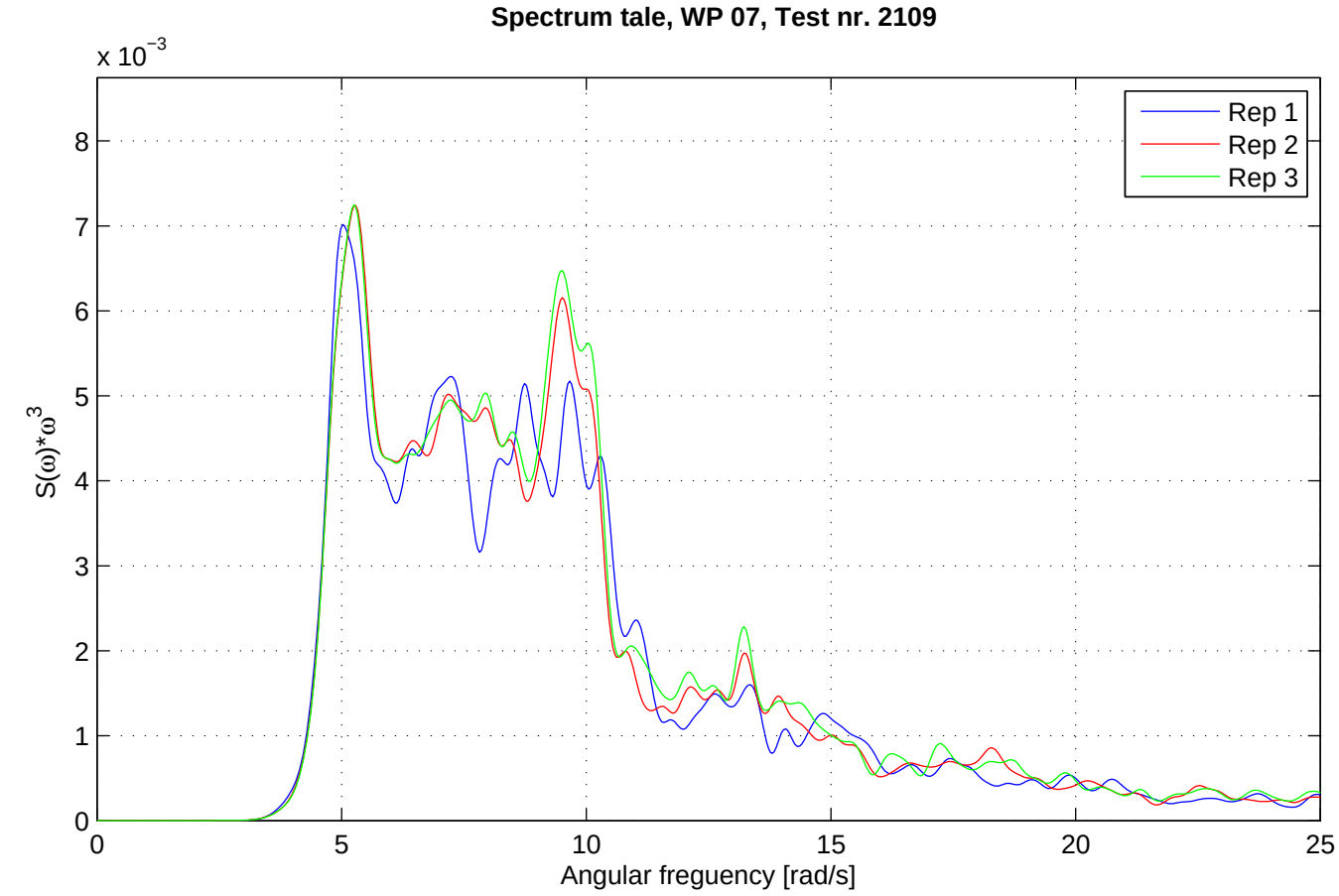
Spectrum tale, WP 07, Test nr. 2109
x 10^-3
S(ω)*ω^3
Angular freguency [rad/s]
Rep 1
Rep 2
Rep 3
0
1
2
3
4
5
6
7
8
0
5
10
15
20
25

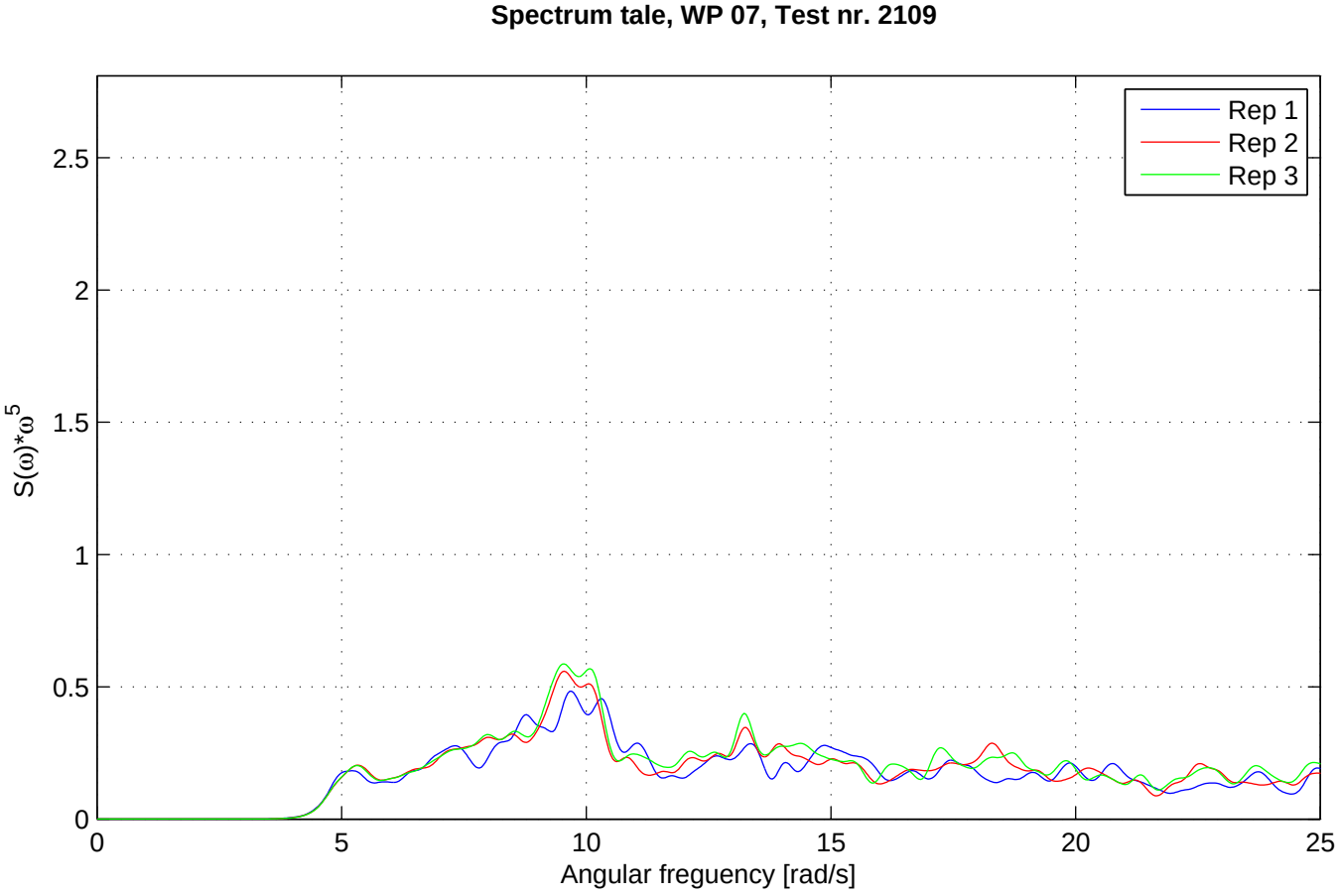
Spectrum tale, WP 07, Test nr. 2109
S(ω)*ω^5
Angular freguency [rad/s]
Rep 1
Rep 2
Rep 3
0
0.5
1
1.5
2
2.5
0
5
10
15
20
25

Spectrum tale RMS, Test nr. 2111

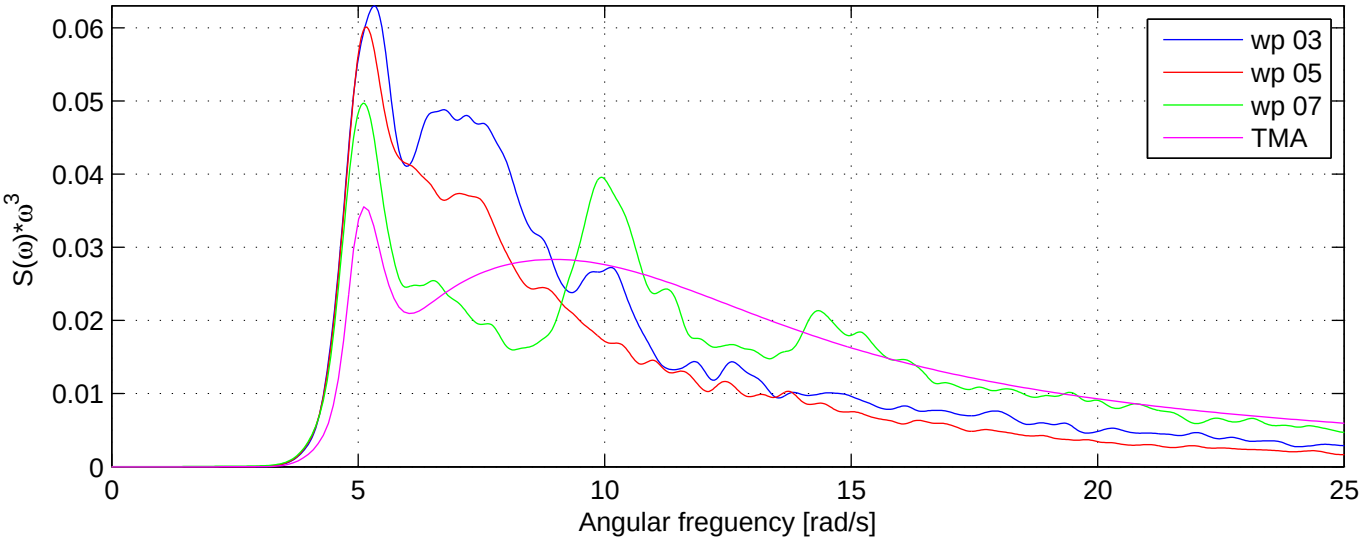

Spectrum tale RMS, Test nr. 2111

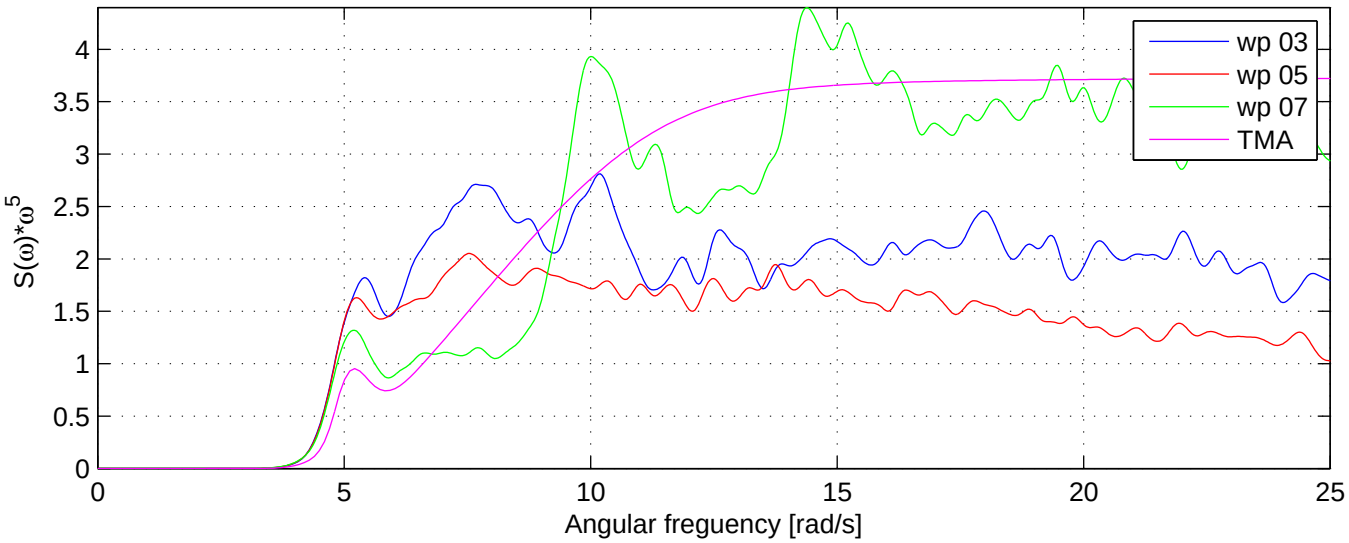

Spectrum RMS, Test nr. 2111

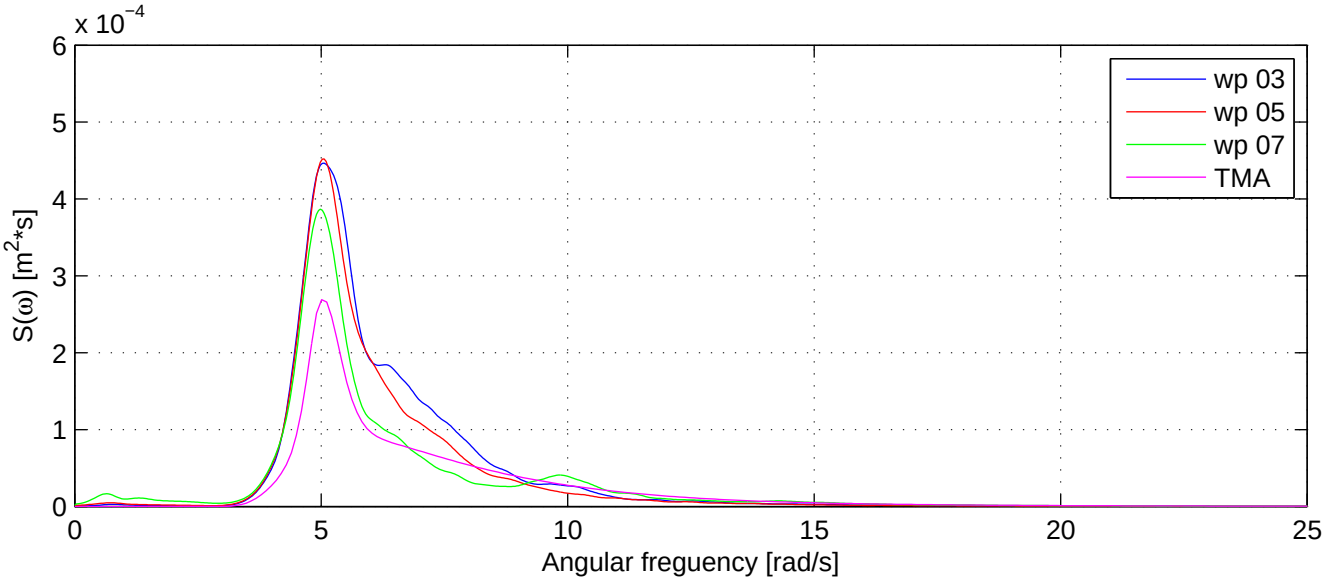

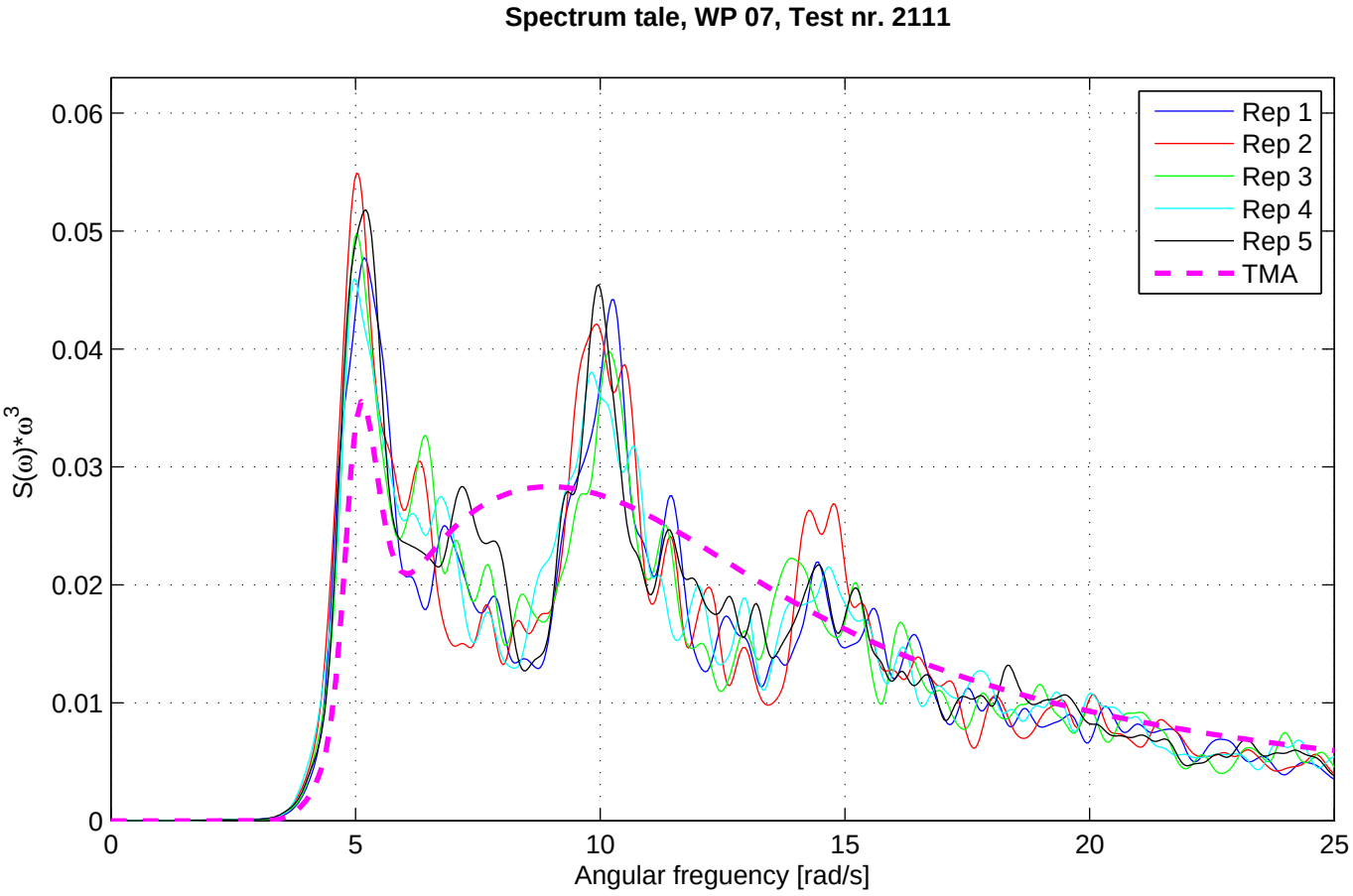
Spectrum tale, WP 07, Test nr. 2111
Rep 1
Rep 2
Rep 3
Rep 4
Rep 5
TMA
S(ω)*ω^3
Angular freguency [rad/s]
0
0.01
0.02
0.03
0.04
0.05
0.06
0
5
10
15
20
25

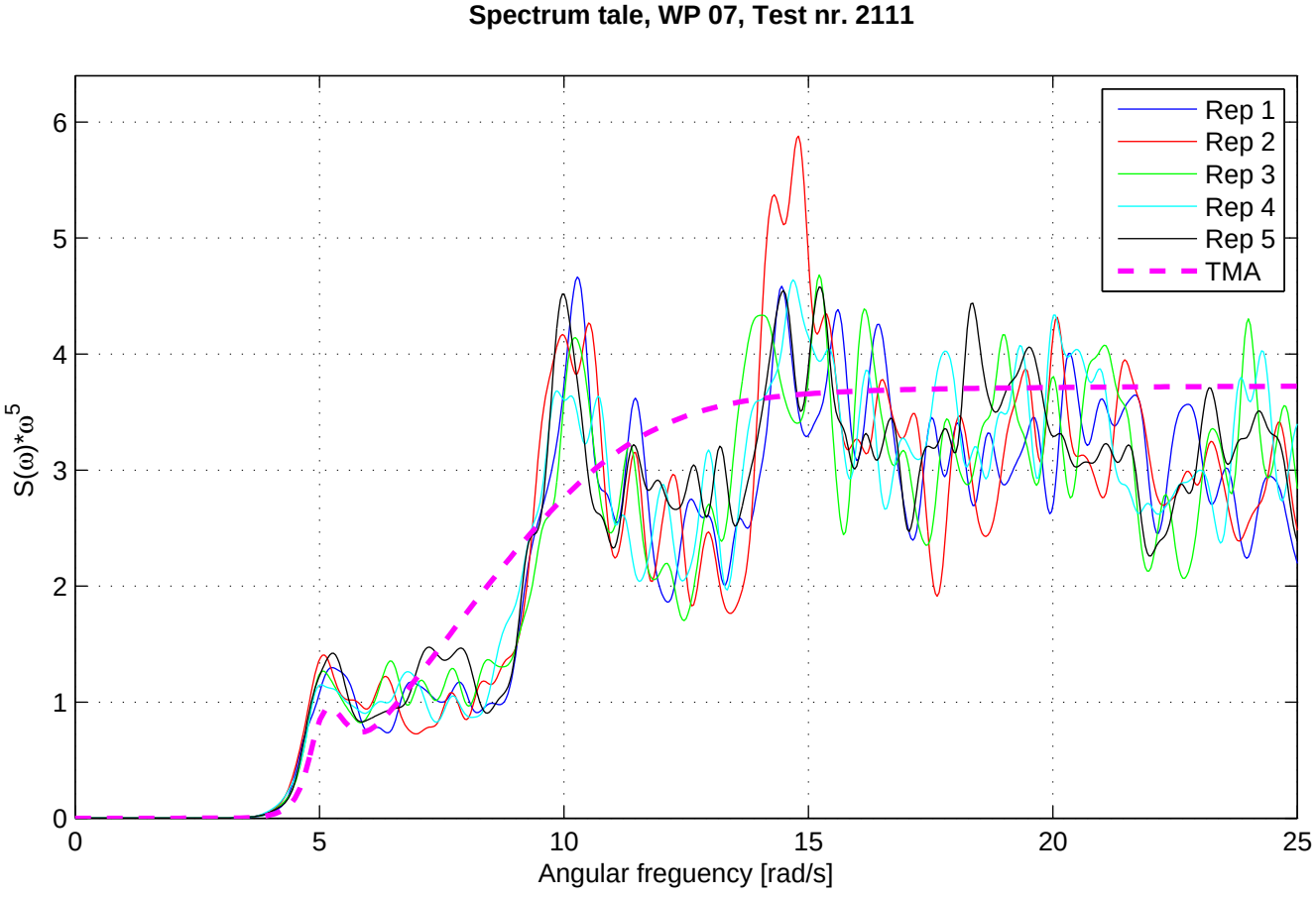
Spectrum tale, WP 07, Test nr. 2111
Rep 1
Rep 2
Rep 3
Rep 4
Rep 5
TMA
S(ω)*ω^5
Angular freguency [rad/s]
0
1
2
3
4
5
6
0
5
10
15
20
25

Spectrum tale RMS, Test nr. 2112

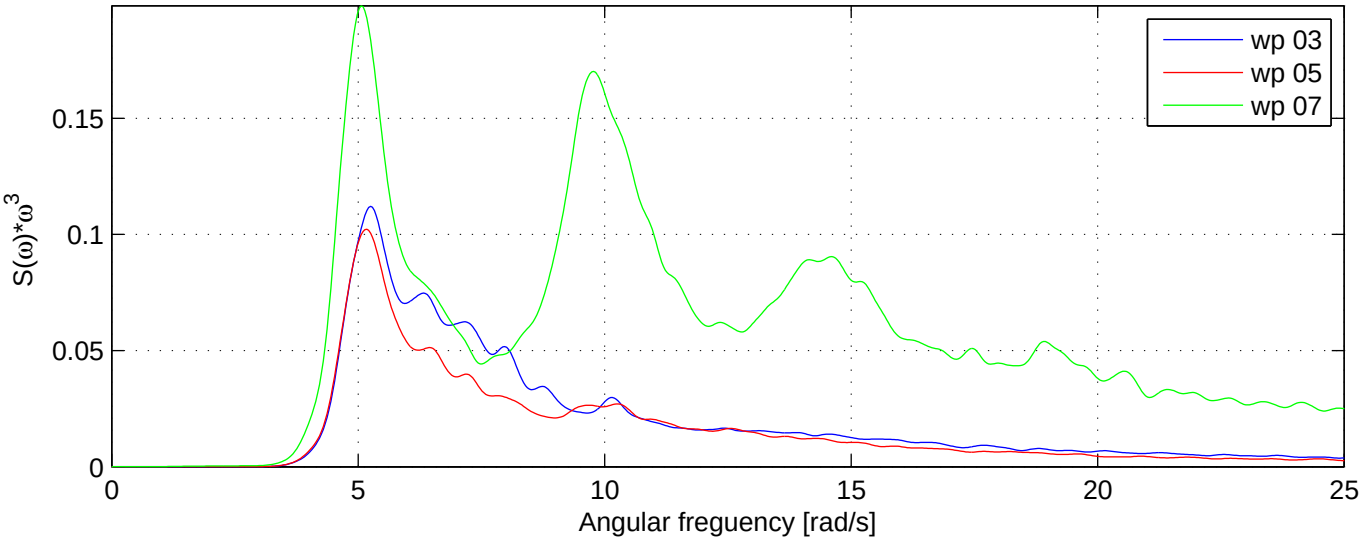

Spectrum tale RMS, Test nr. 2112

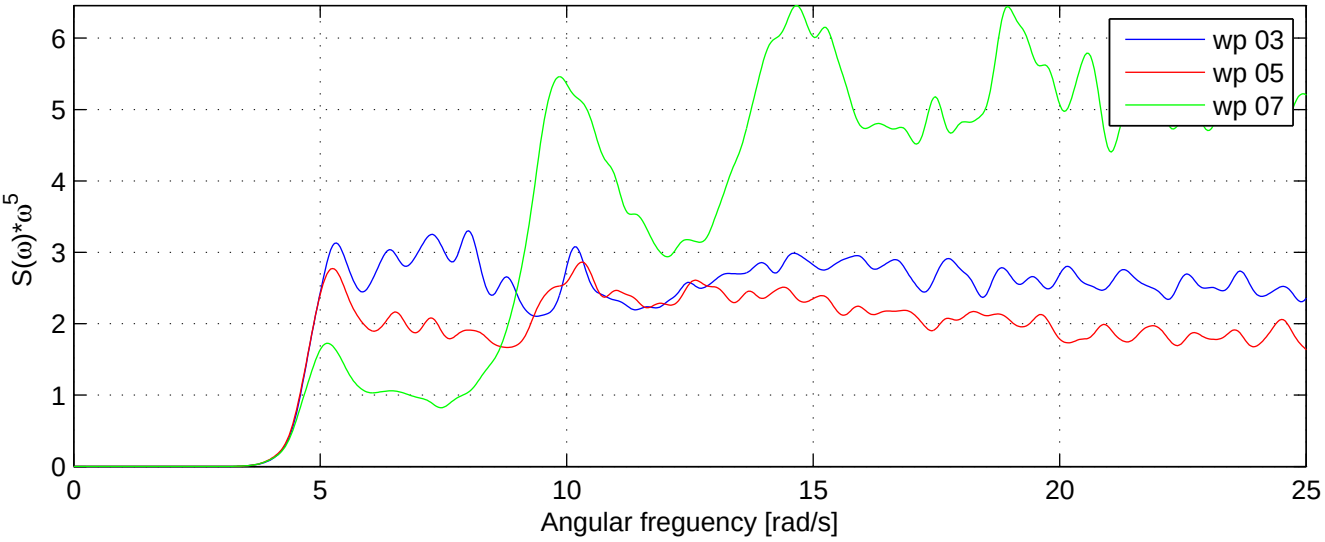

Spectrum RMS, Test nr. 2112

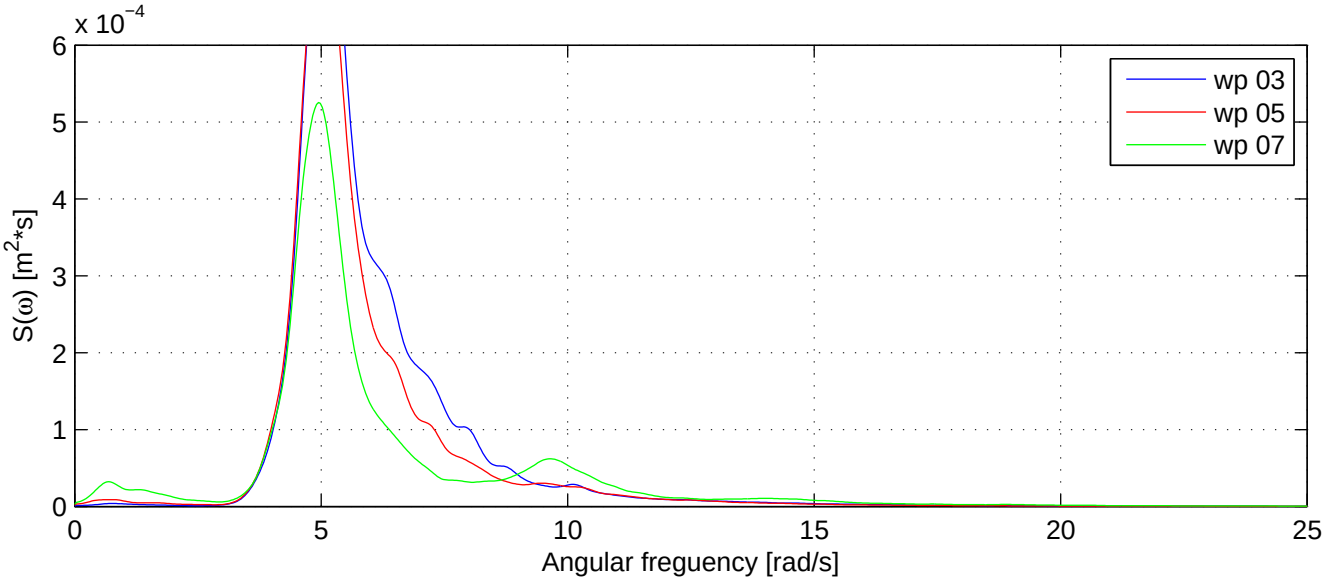

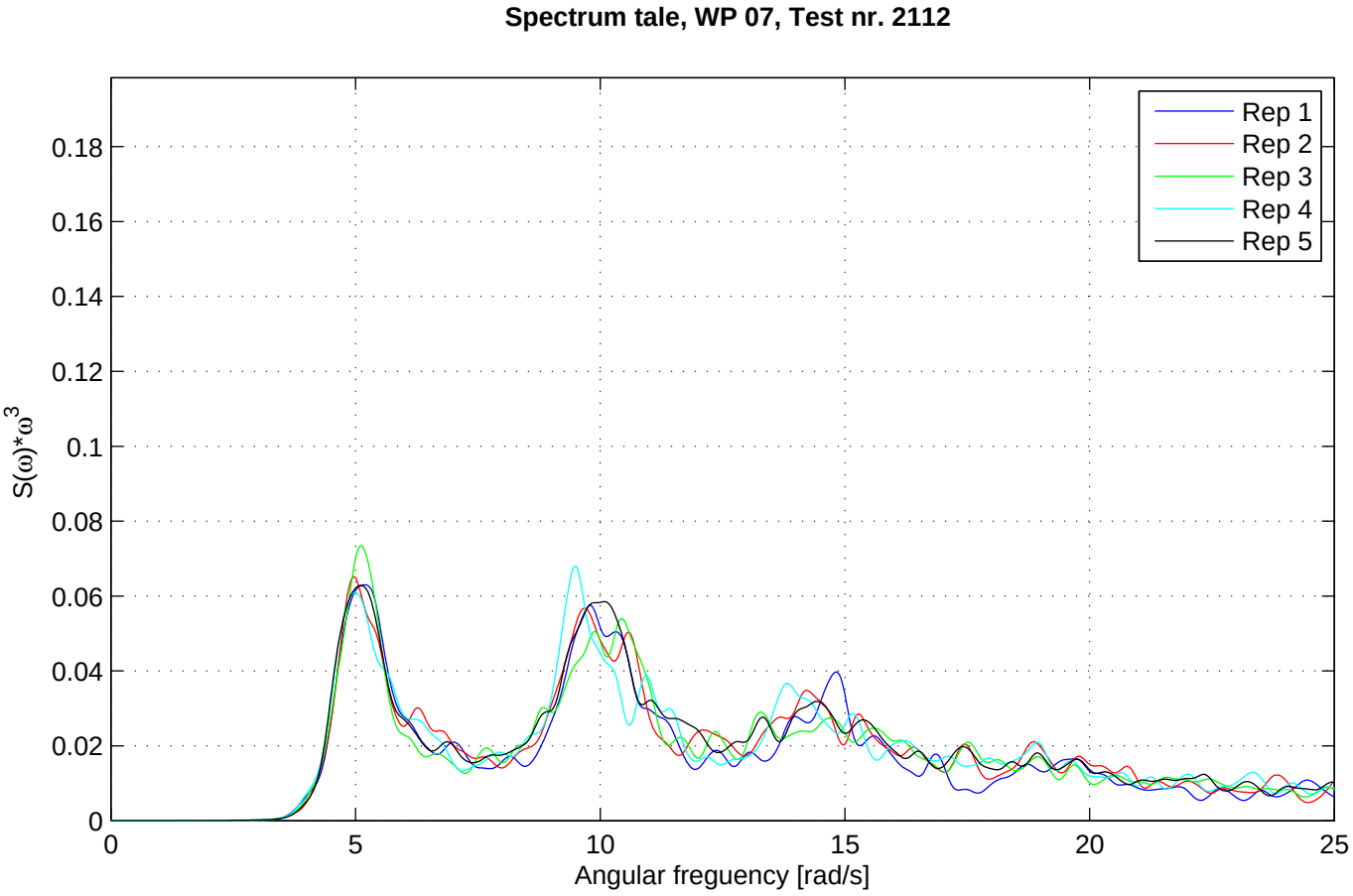
Spectrum tale, WP 07, Test nr. 2112
Rep 1
Rep 2
Rep 3
Rep 4
Rep 5
S(ω)*ω^3
0
0.02
0.04
0.06
0.08
0.1
0.12
0.14
0.16
0.18
0
5
10
15
20
25
Angular freguency [rad/s]

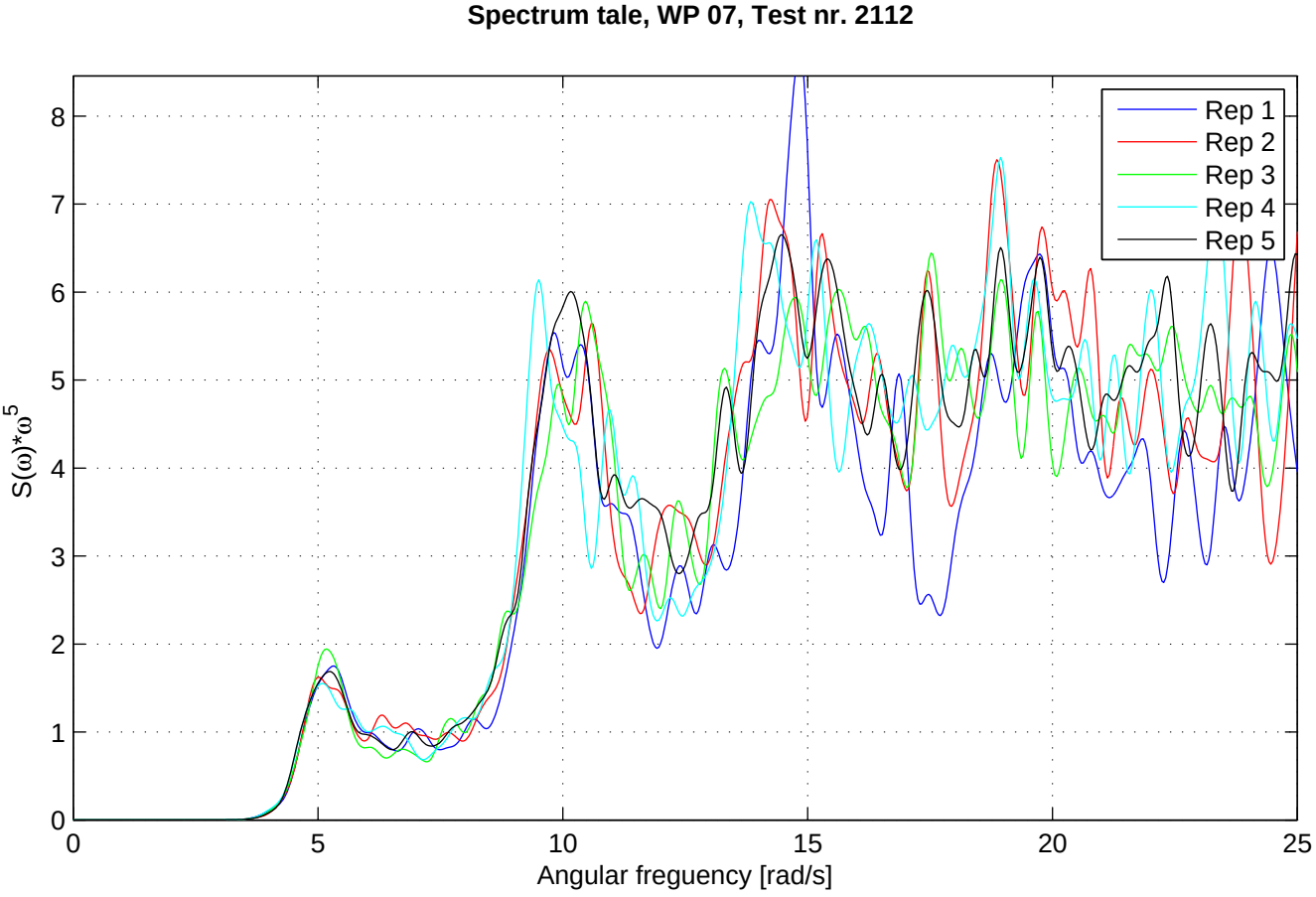
Spectrum tale, WP 07, Test nr. 2112
Rep 1
Rep 2
Rep 3
Rep 4
Rep 5
S(ω)*ω^5
0
1
2
3
4
5
6
7
8
0
5
10
15
20
25
Angular freguency [rad/s]

Spectrum tale RMS, Test nr. 2115

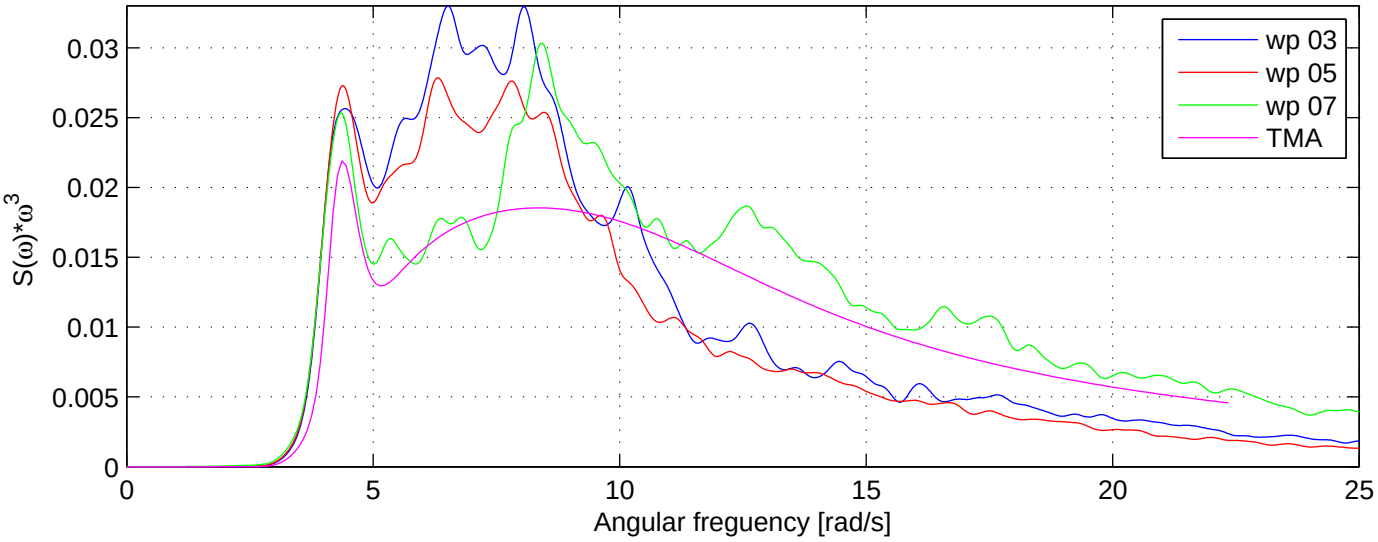

Spectrum tale RMS, Test nr. 2115

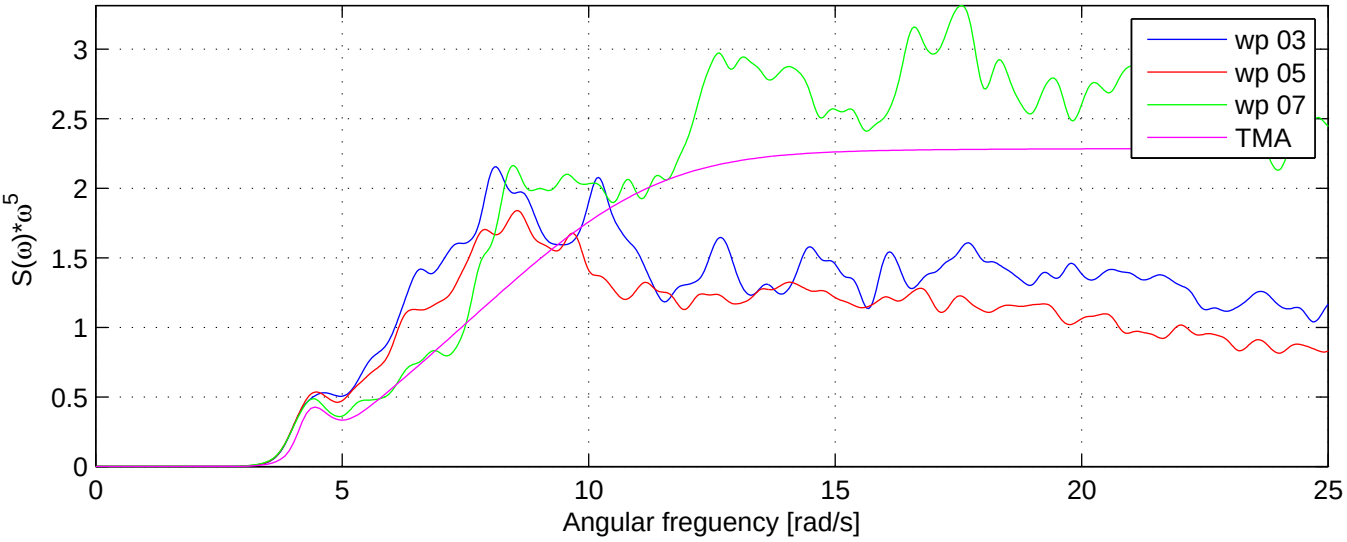

Spectrum RMS, Test nr. 2115

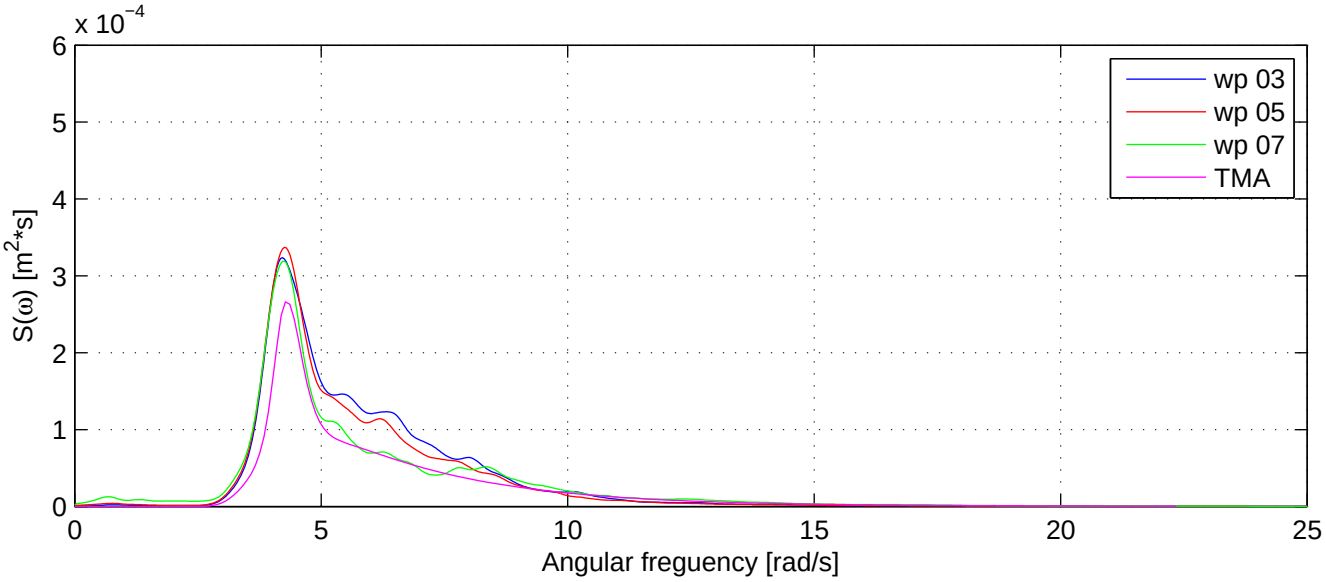

Spectrum tale RMS, WP 07, Test nr. 2115

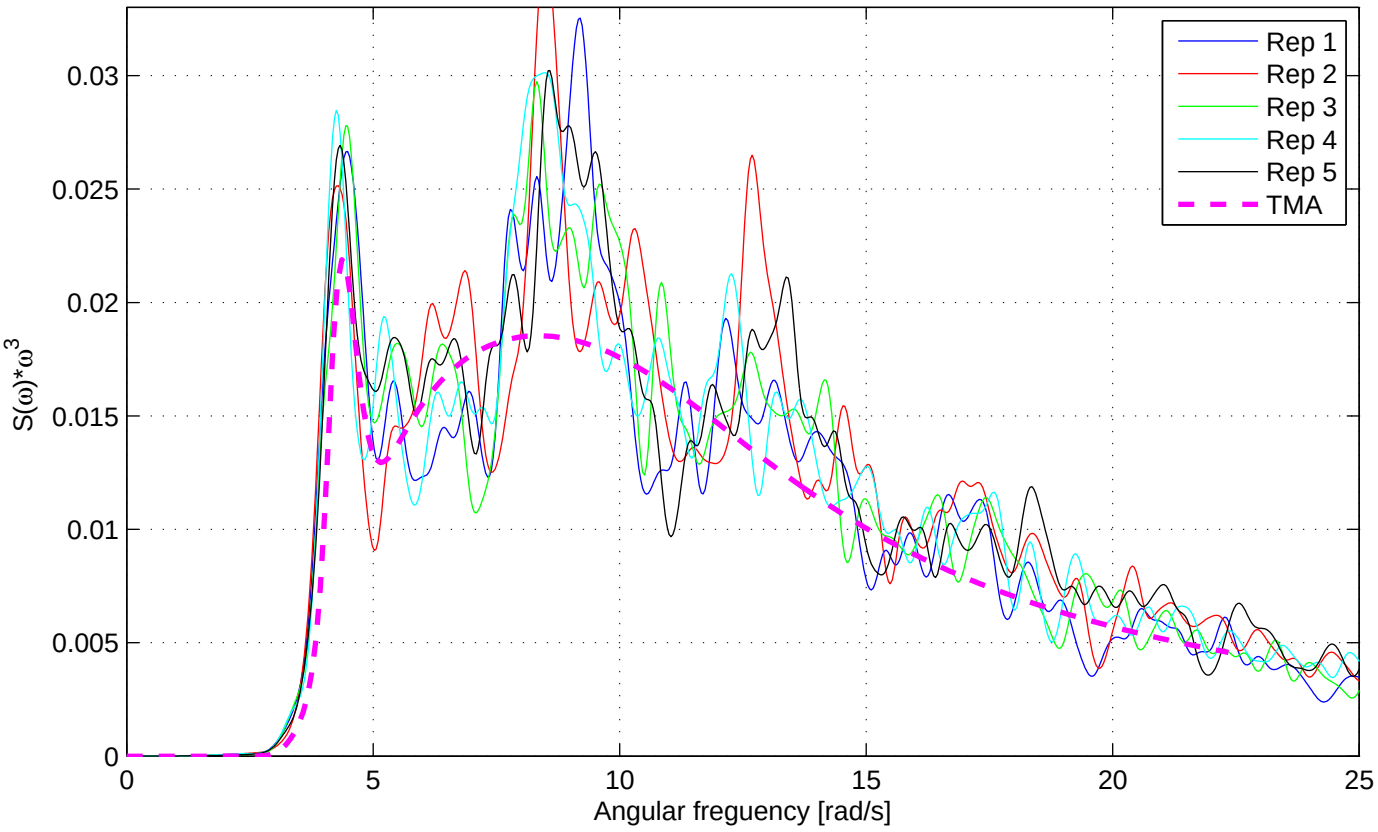

Spectrum tale RMS, WP 07, Test nr. 2115

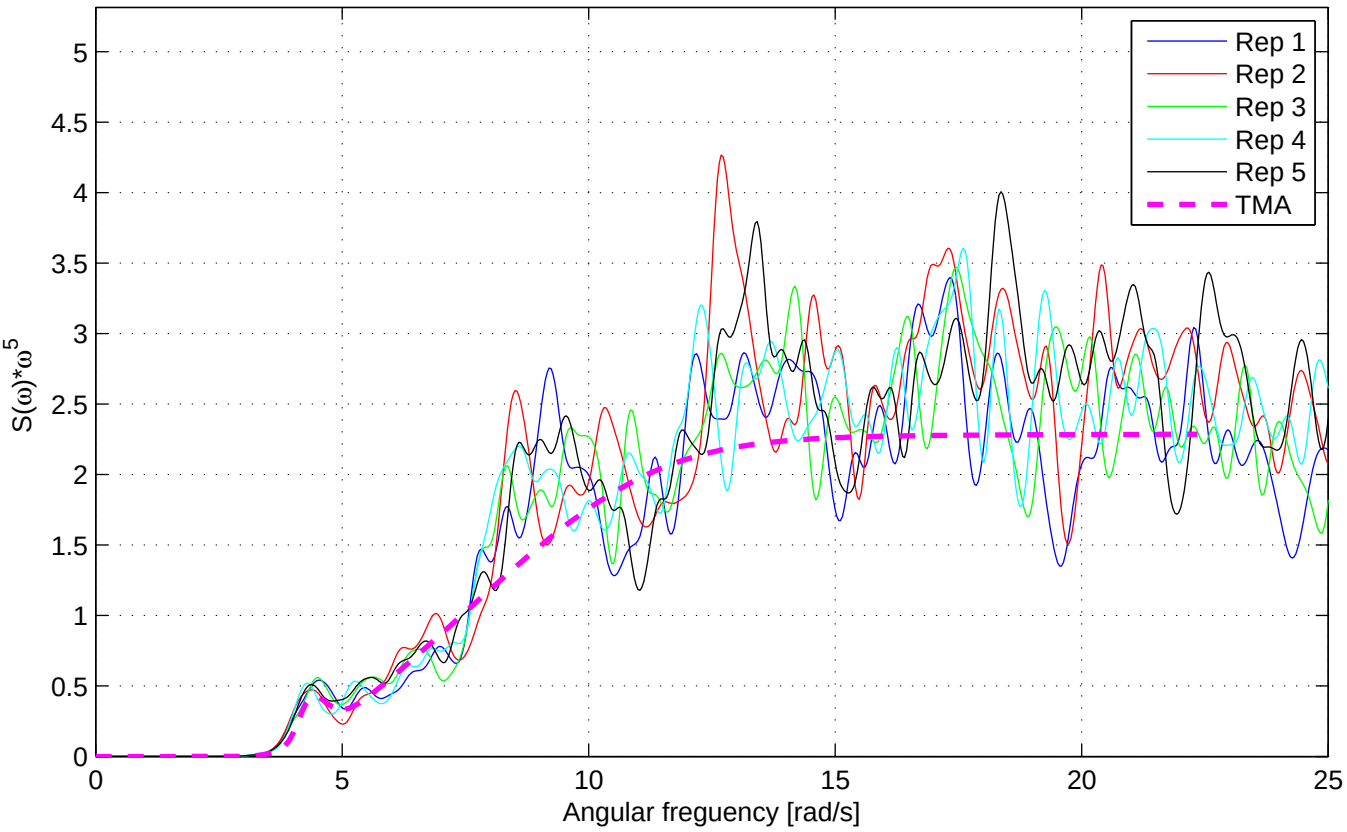

Spectrum tale RMS, Test nr. 2116

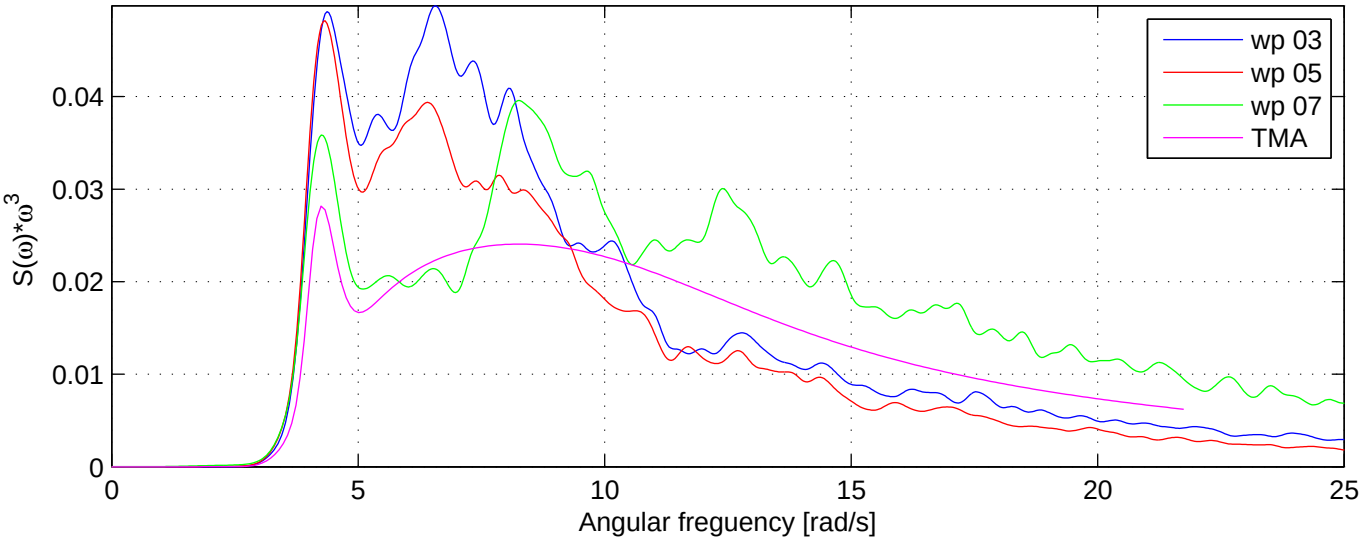

Spectrum tale RMS, Test nr. 2116

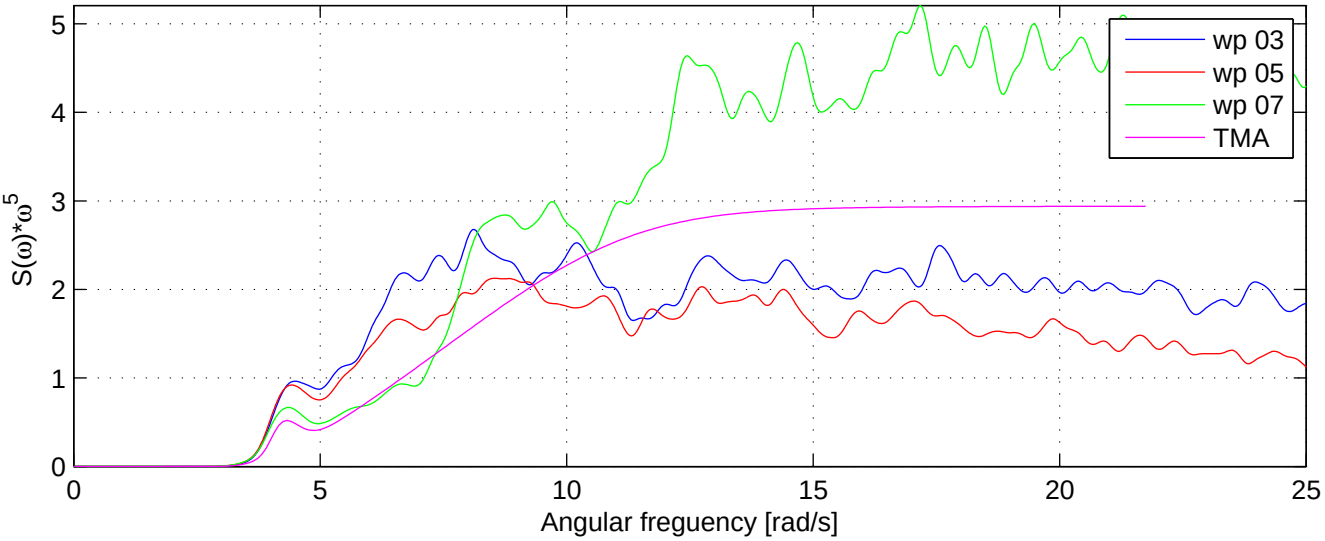

Spectrum RMS, Test nr. 2116

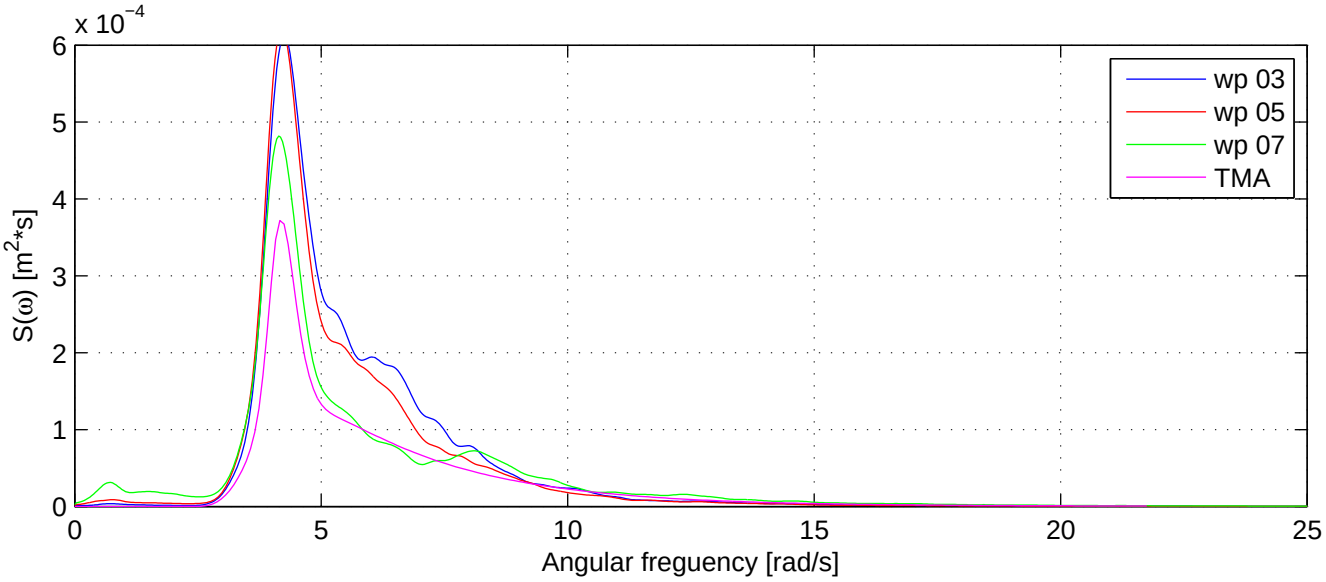

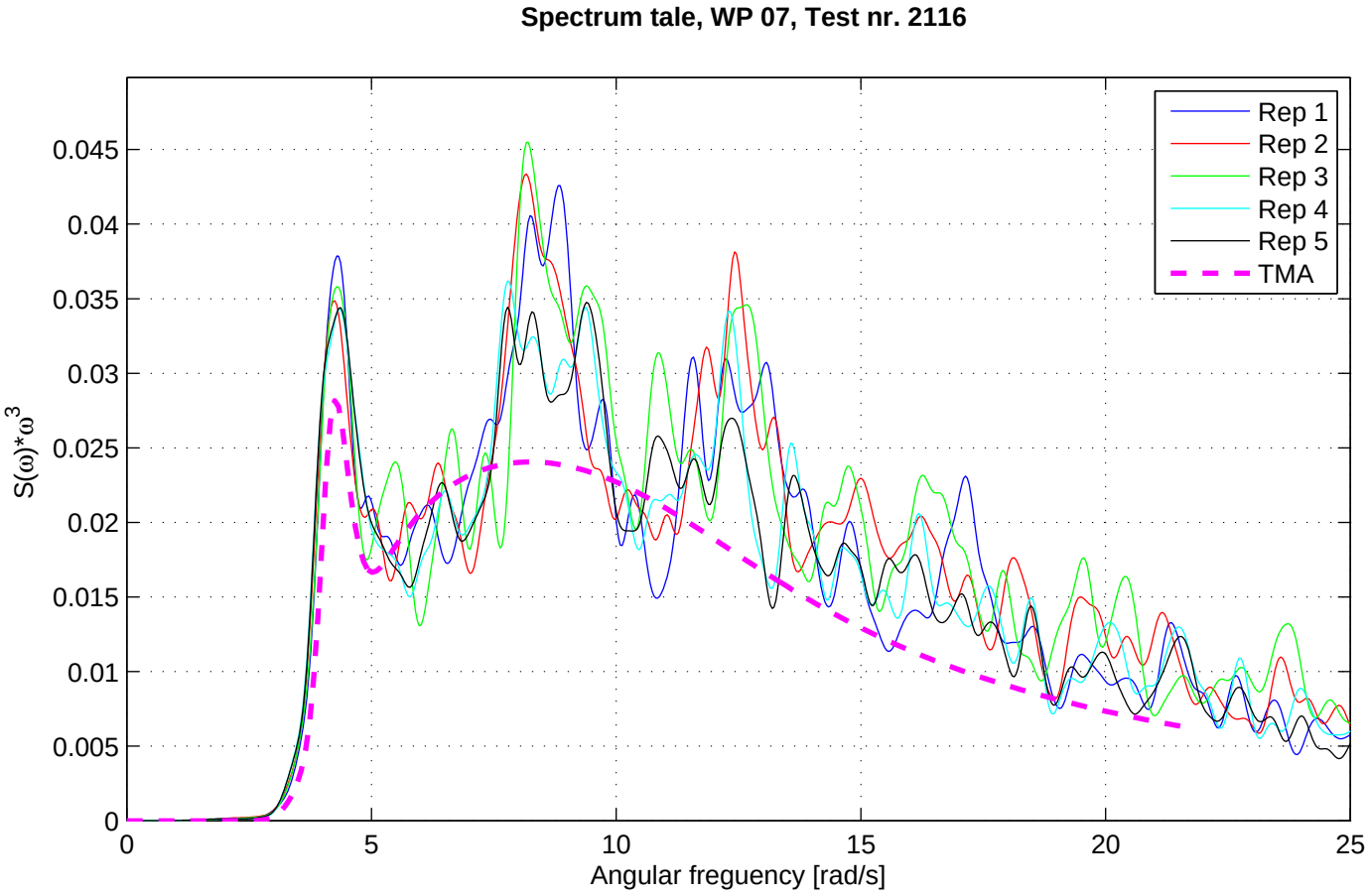
Spectrum tale, WP 07, Test nr. 2116
Rep 1
Rep 2
Rep 3
Rep 4
Rep 5
TMA
S(ω)*ω^3
Angular freguency [rad/s]
0
0.005
0.01
0.015
0.02
0.025
0.03
0.035
0.04
0.045
0
5
10
15
20
25

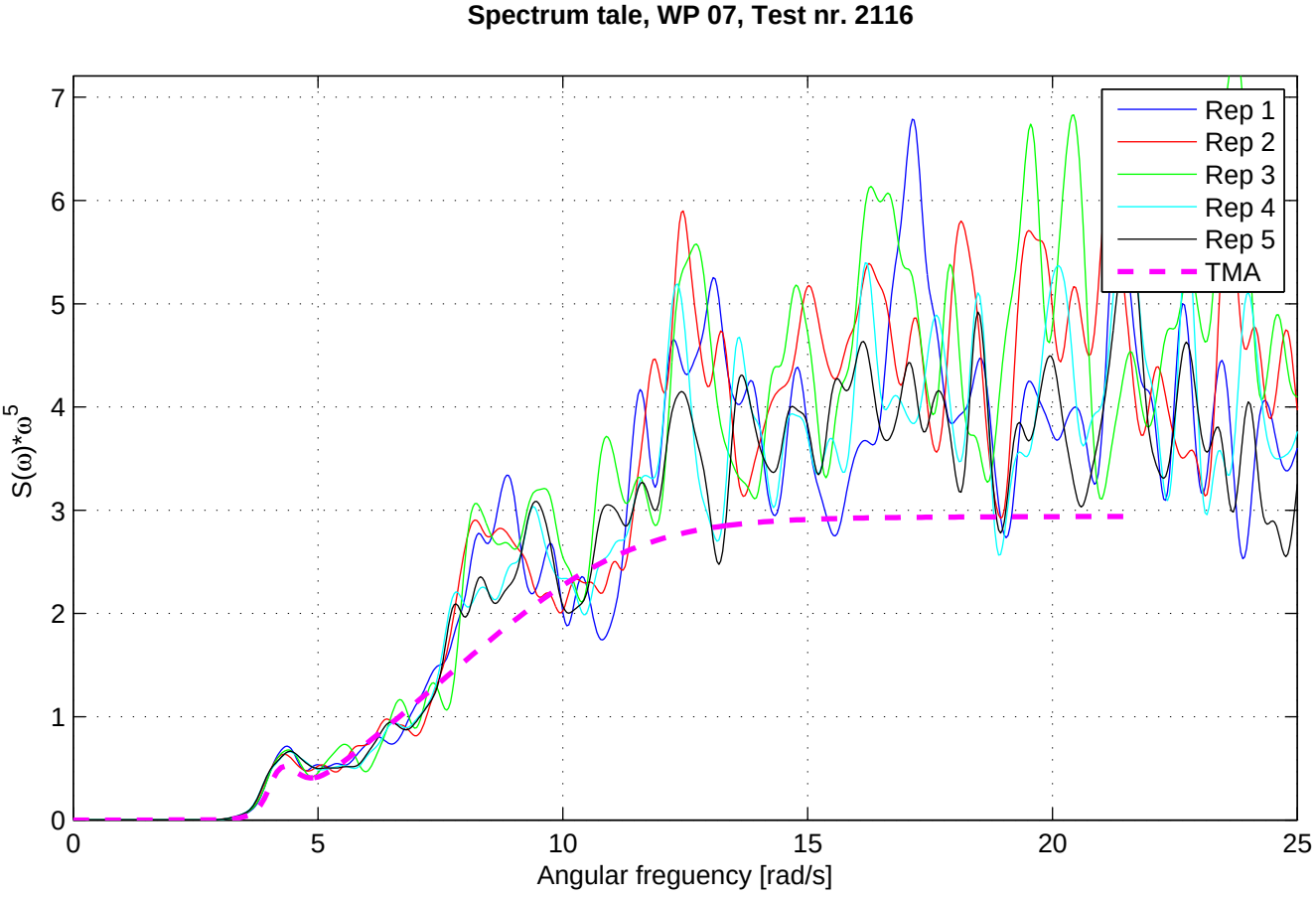
Spectrum tale, WP 07, Test nr. 2116
Rep 1
Rep 2
Rep 3
Rep 4
Rep 5
TMA
S(ω)*ω^5
Angular freguency [rad/s]
0
1
2
3
4
5
6
7
0
5
10
15
20
25

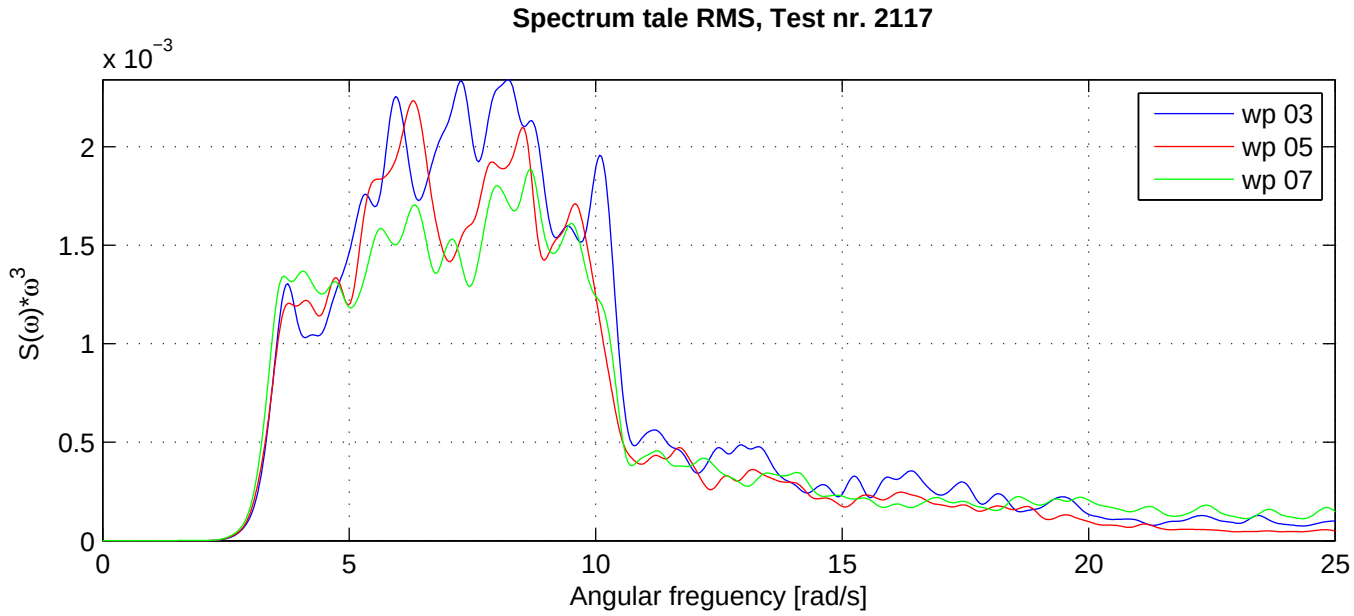
Spectrum tale RMS, Test nr. 2117
x 10^-3
S(ω)*ω^3
wp 03
wp 05
wp 07
Angular freguency [rad/s]

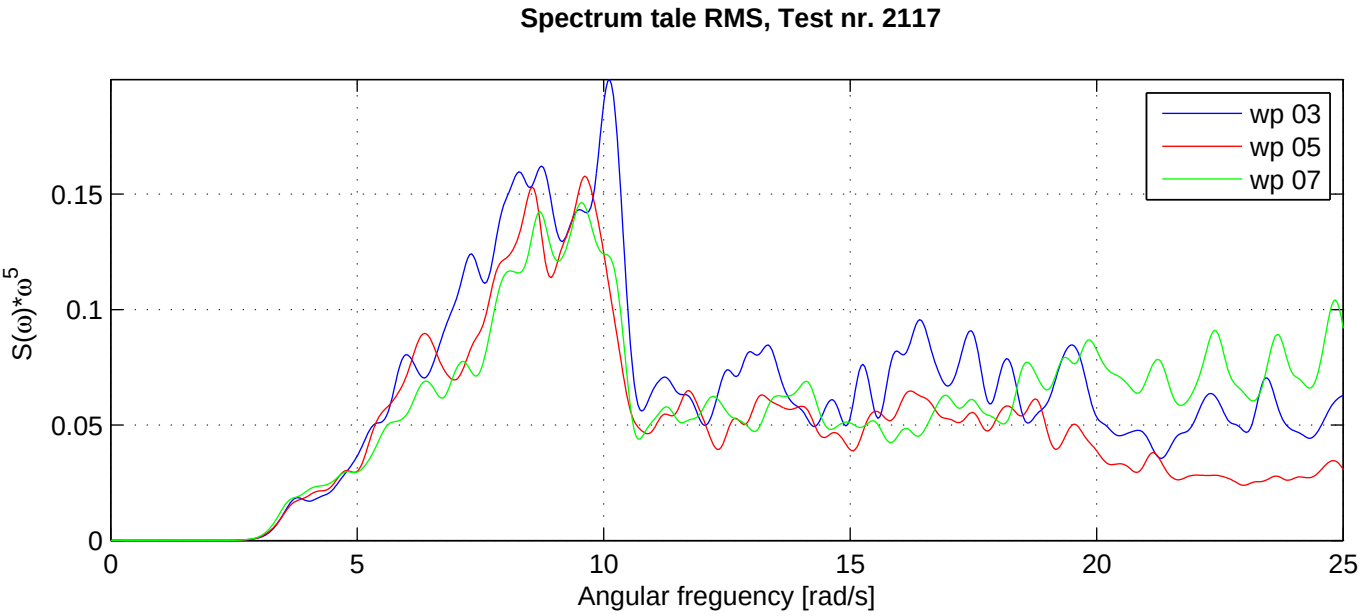
Spectrum tale RMS, Test nr. 2117
S(ω)*ω^5
wp 03
wp 05
wp 07
Angular freguency [rad/s]

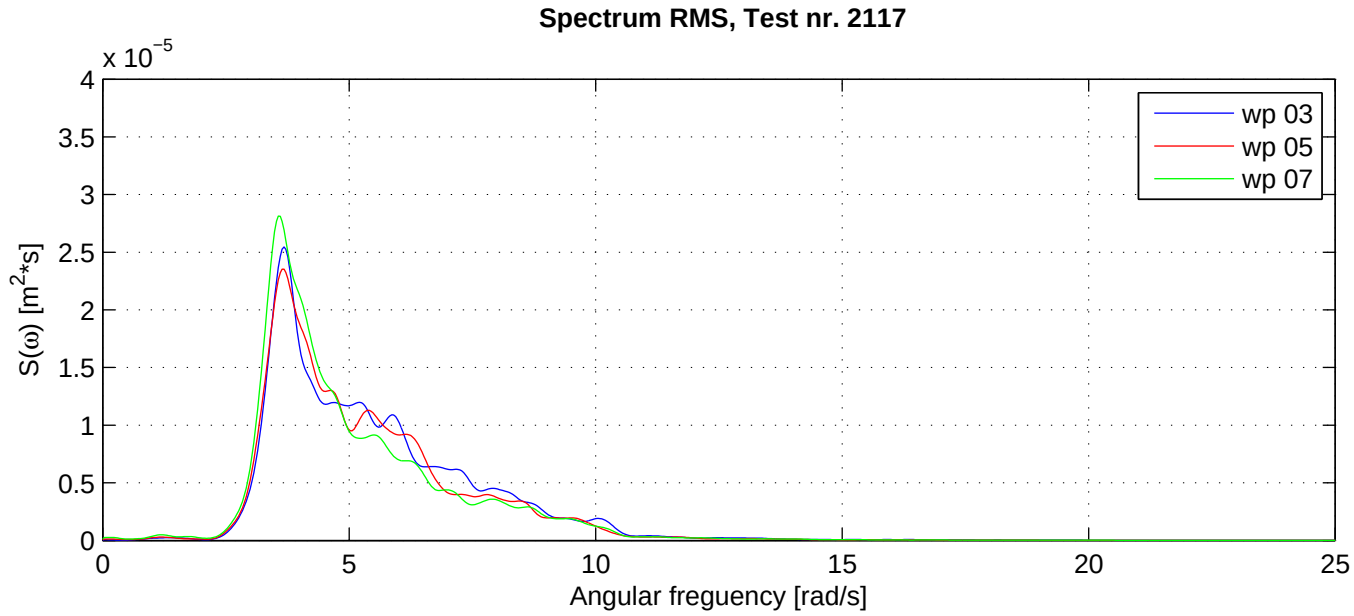
Spectrum RMS, Test nr. 2117
x 10^-5
S(ω) [m^2*s]
wp 03
wp 05
wp 07
Angular freguency [rad/s]

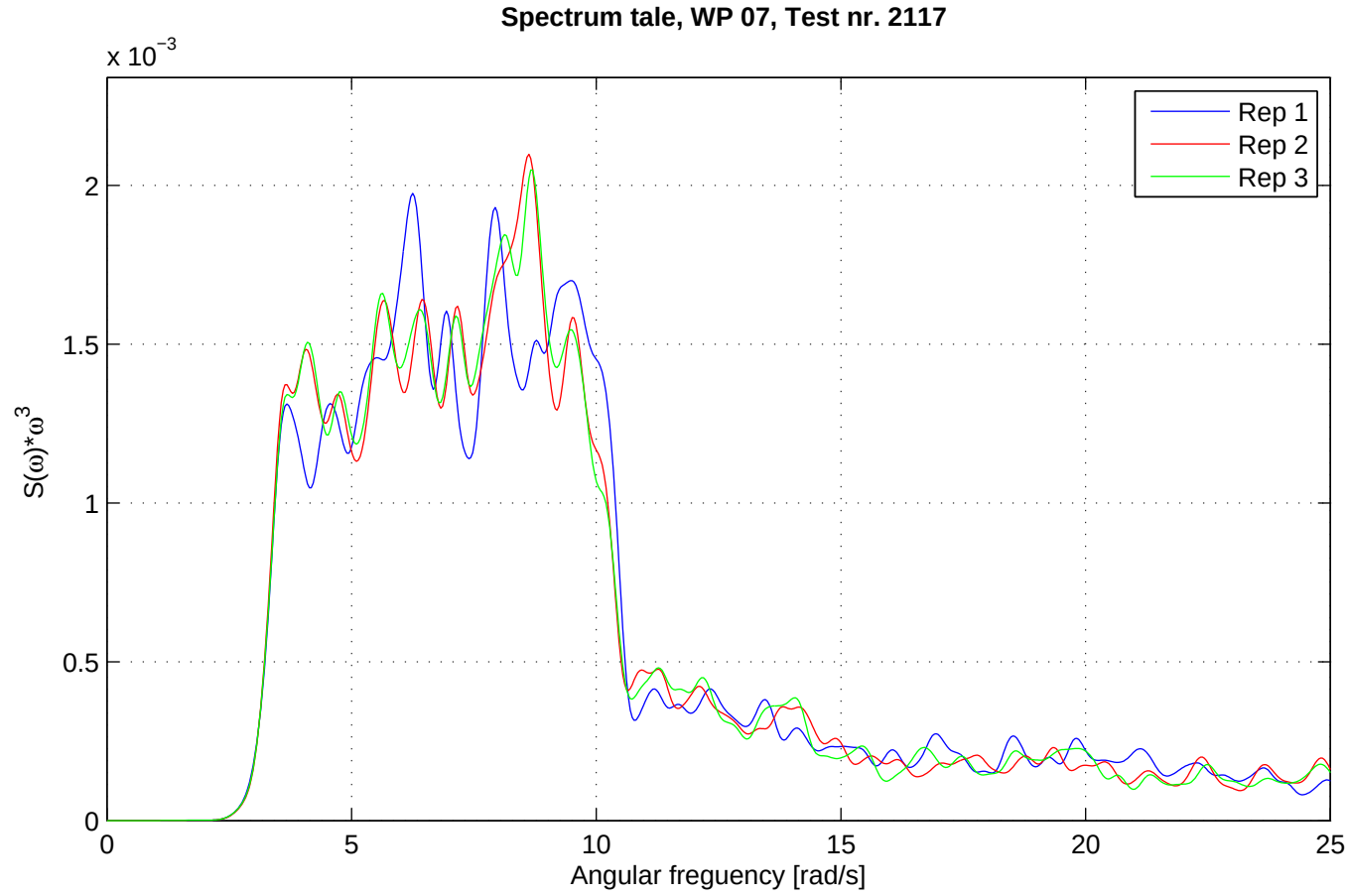
Spectrum tale, WP 07, Test nr. 2117
x 10^-3
S(ω)*ω^3
Angular freguency [rad/s]
Rep 1
Rep 2
Rep 3
0
0.5
1
1.5
2
0
5
10
15
20
25

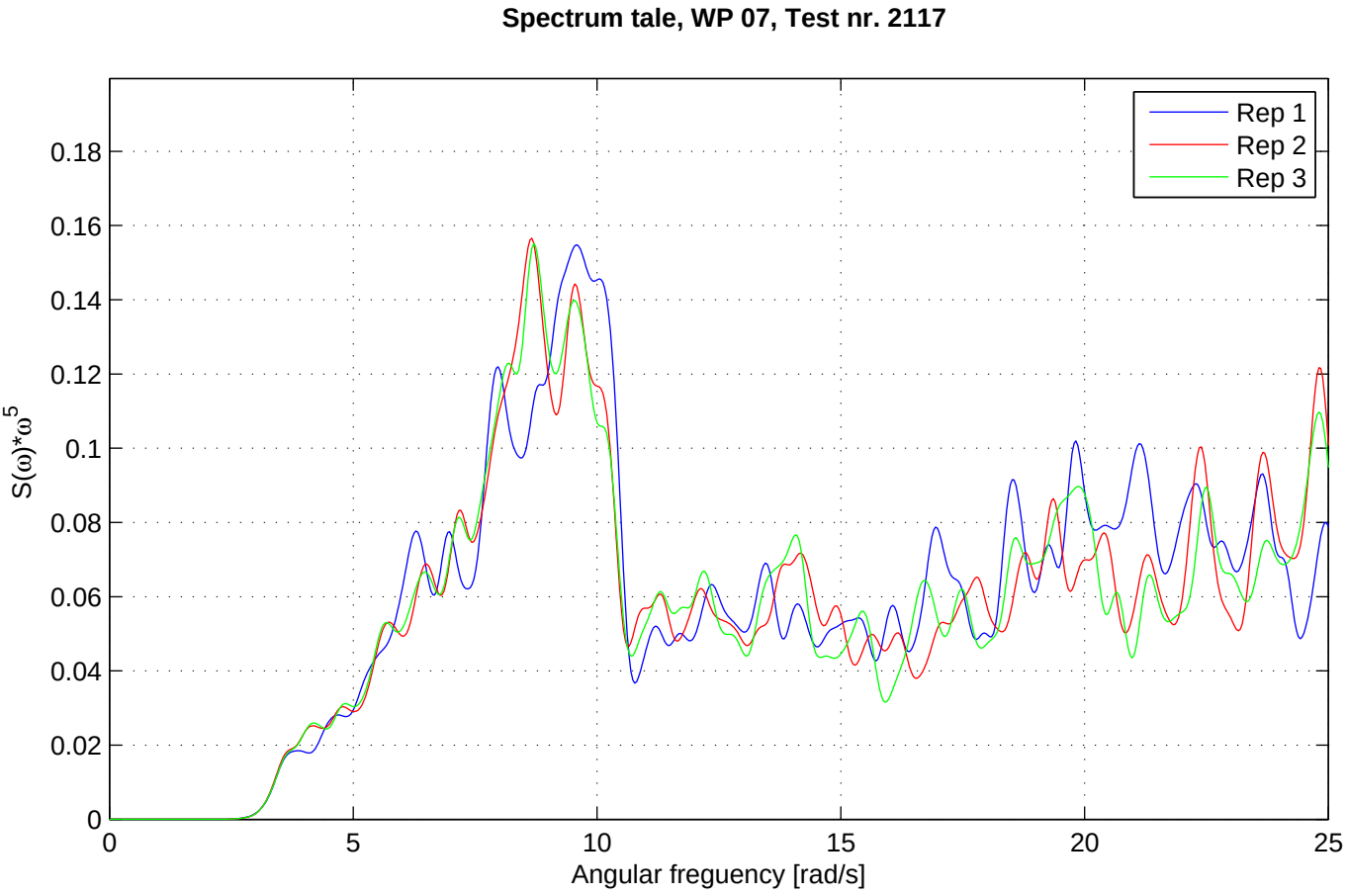
Spectrum tale, WP 07, Test nr. 2117
S(ω)*ω^5
Angular freguency [rad/s]
Rep 1
Rep 2
Rep 3
0
0.02
0.04
0.06
0.08
0.1
0.12
0.14
0.16
0.18
0
5
10
15
20
25

Spectrum tale RMS, Test nr. 2118

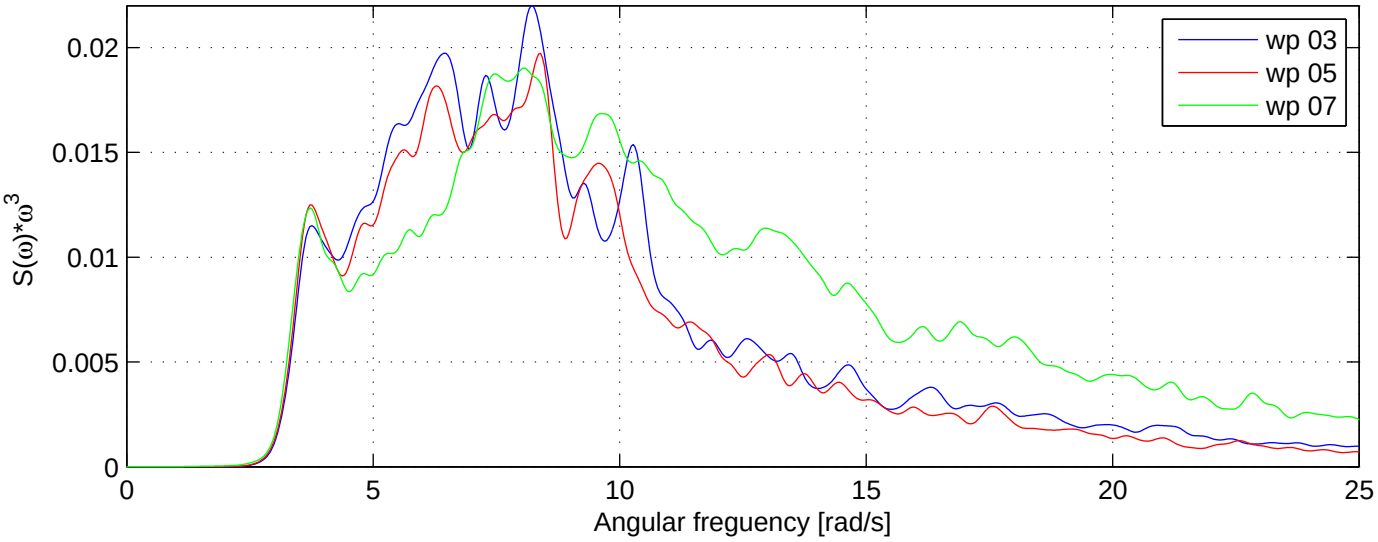

Spectrum tale RMS, Test nr. 2118

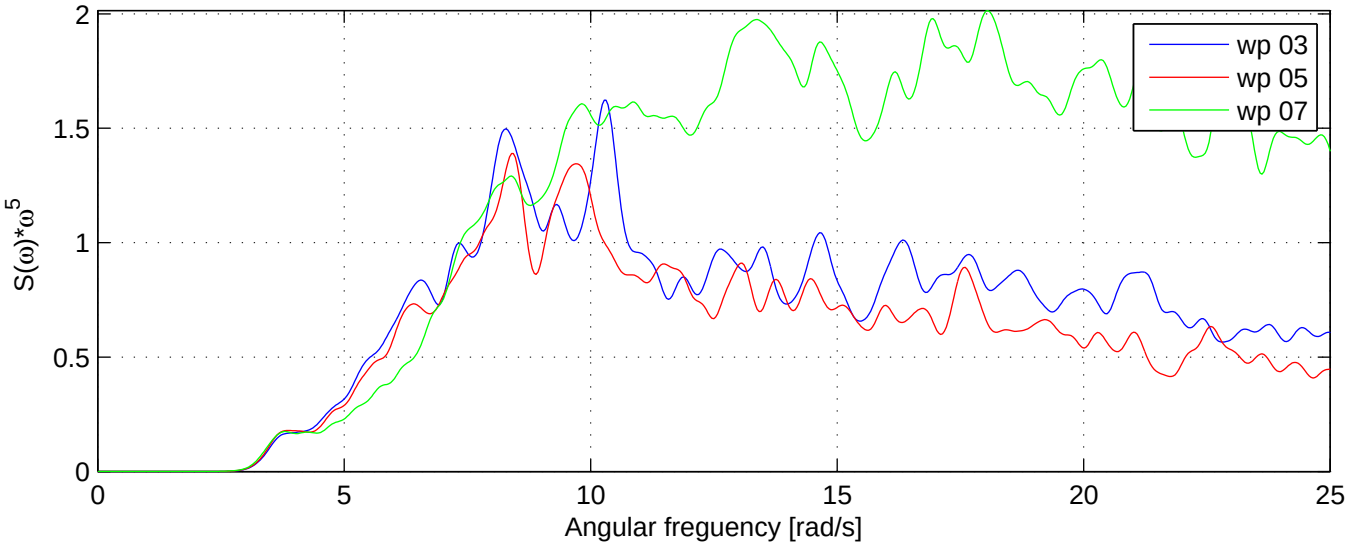

Spectrum RMS, Test nr. 2118

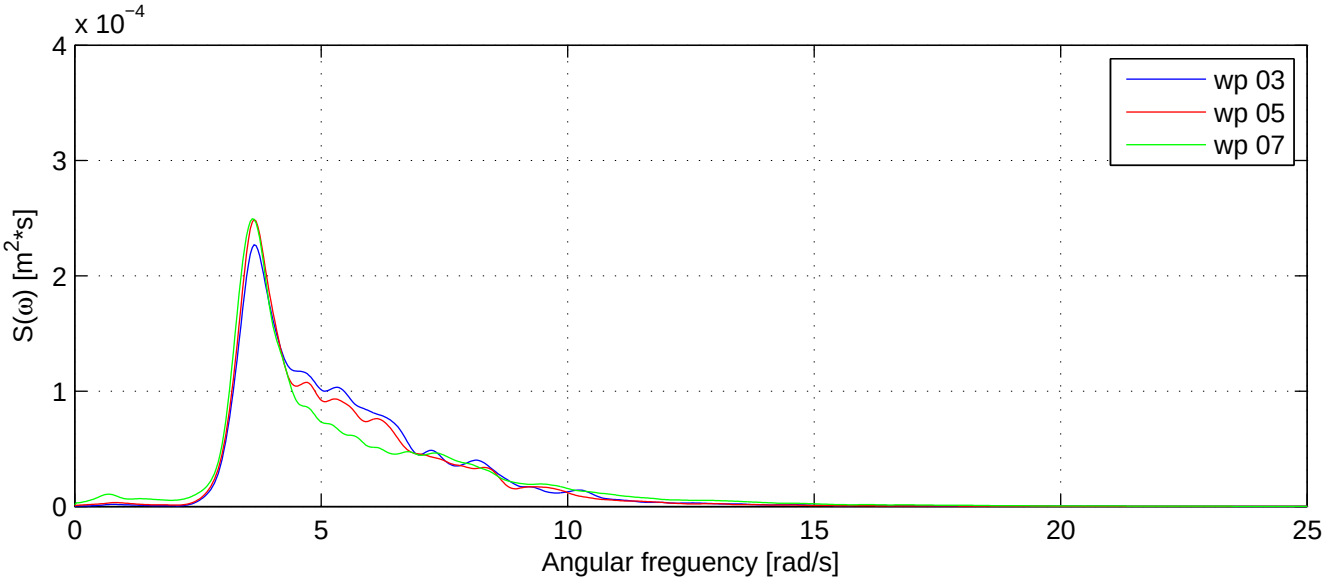


Spectrum tale, WP 07, Test nr. 2118
Rep 1
Rep 2
Rep 3
S(ω)*ω^3
0
0.002
0.004
0.006
0.008
0.01
0.012
0.014
0.016
0.018
0.02
0
5
10
15
20
25
Angular freguency [rad/s]

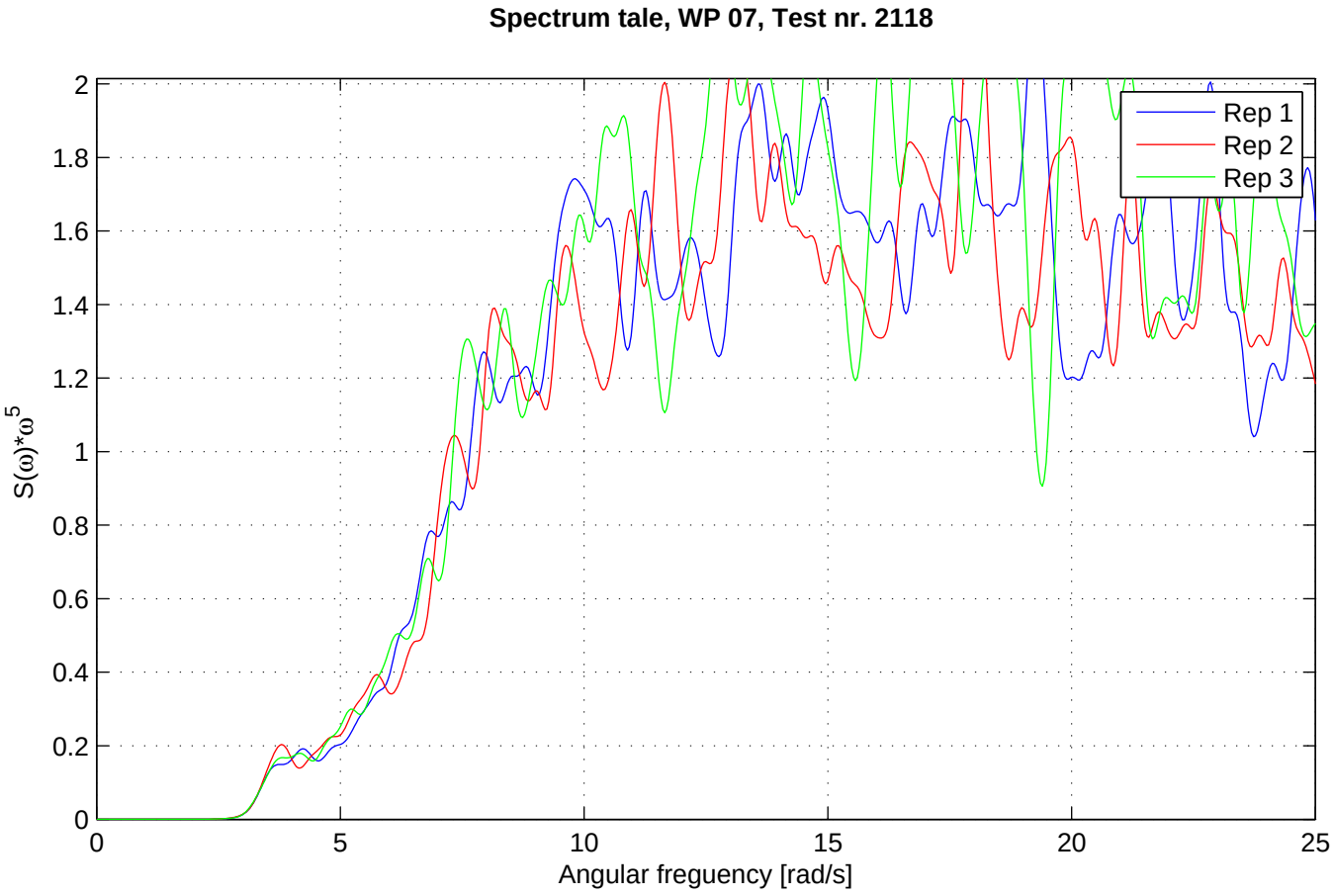
Spectrum tale, WP 07, Test nr. 2118
Rep 1
Rep 2
Rep 3
S(ω)*ω^5
0
0.2
0.4
0.6
0.8
1
1.2
1.4
1.6
1.8
2
0
5
10
15
20
25
Angular freguency [rad/s]

Spectrum tale RMS, Test nr. 2119

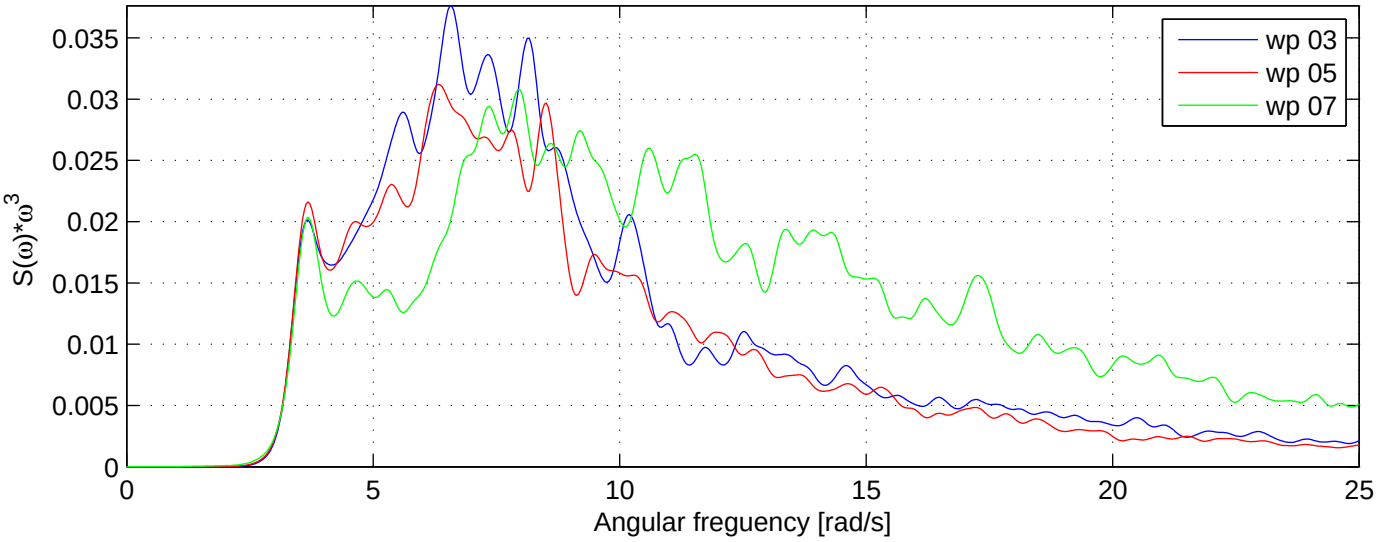

Spectrum tale RMS, Test nr. 2119

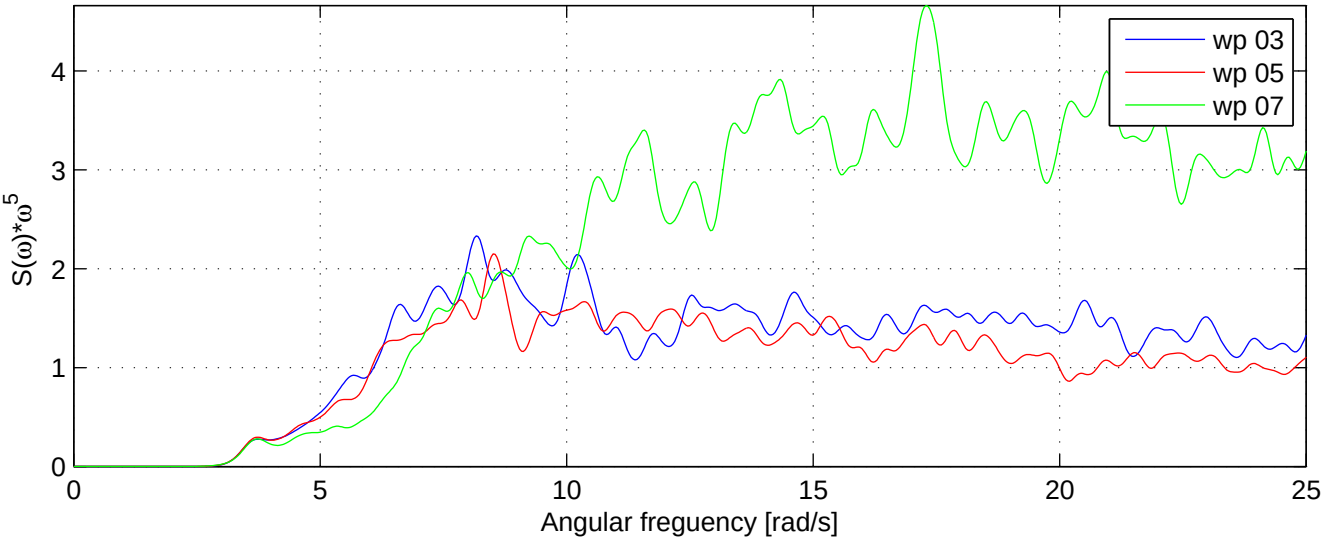

Spectrum RMS, Test nr. 2119

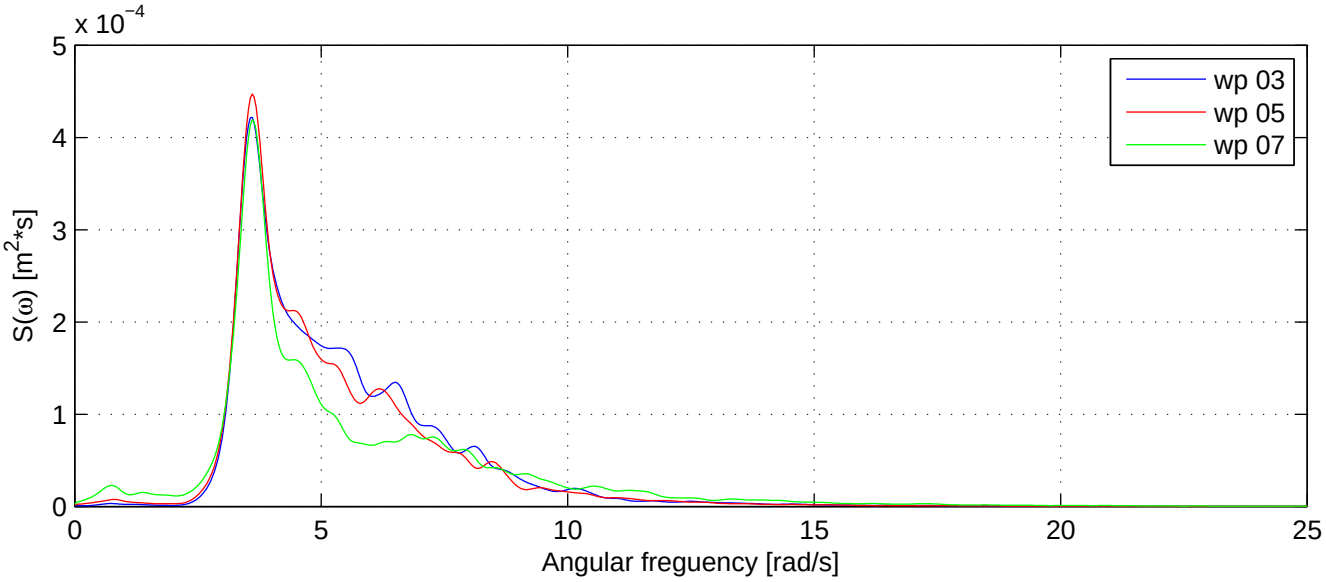

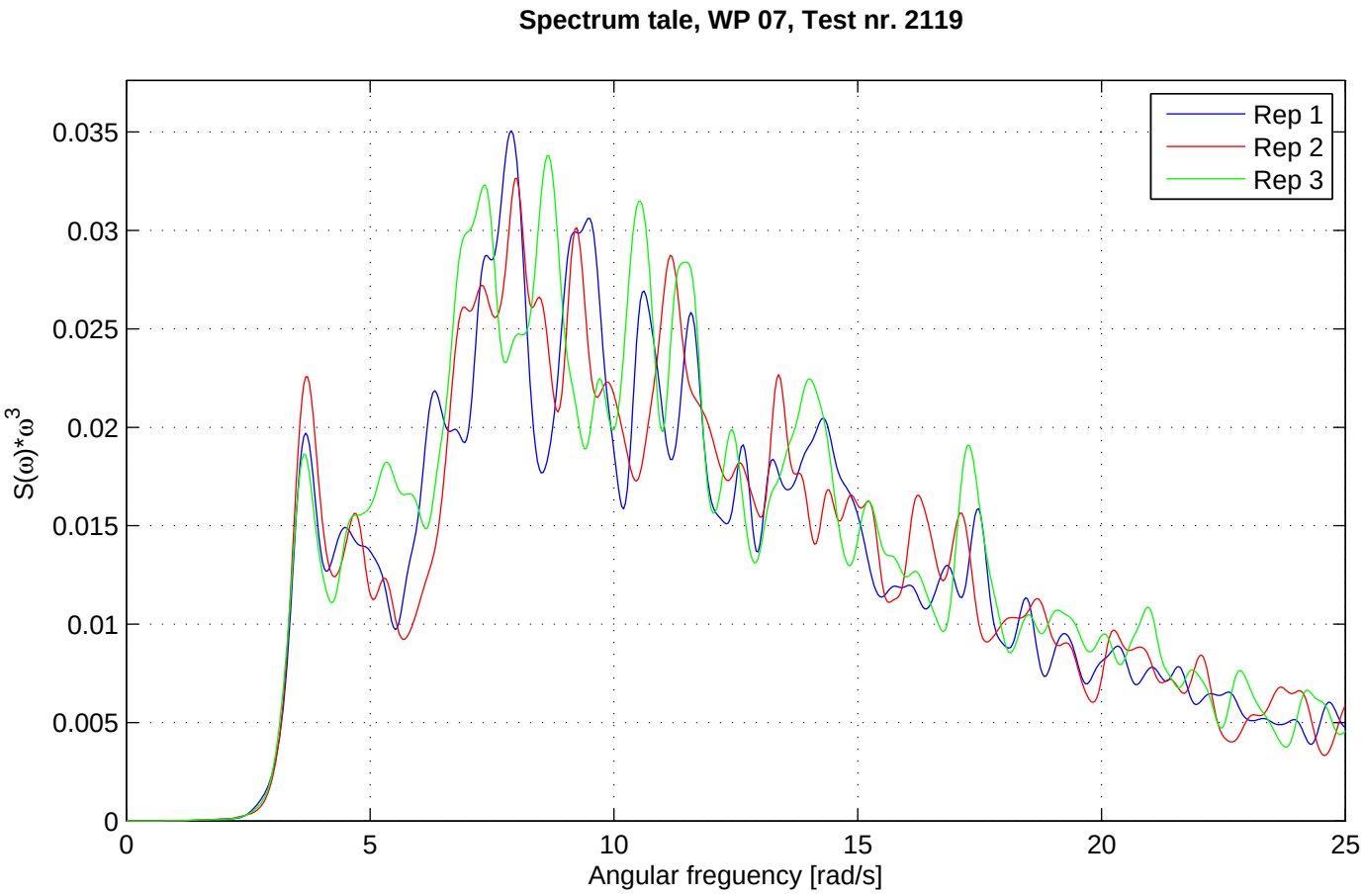
Spectrum tale, WP 07, Test nr. 2119
Rep 1
Rep 2
Rep 3
S(ω)*ω^3
0.035
0.03
0.025
0.02
0.015
0.01
0.005
0
0
5
10
15
20
25
Angular freguency [rad/s]

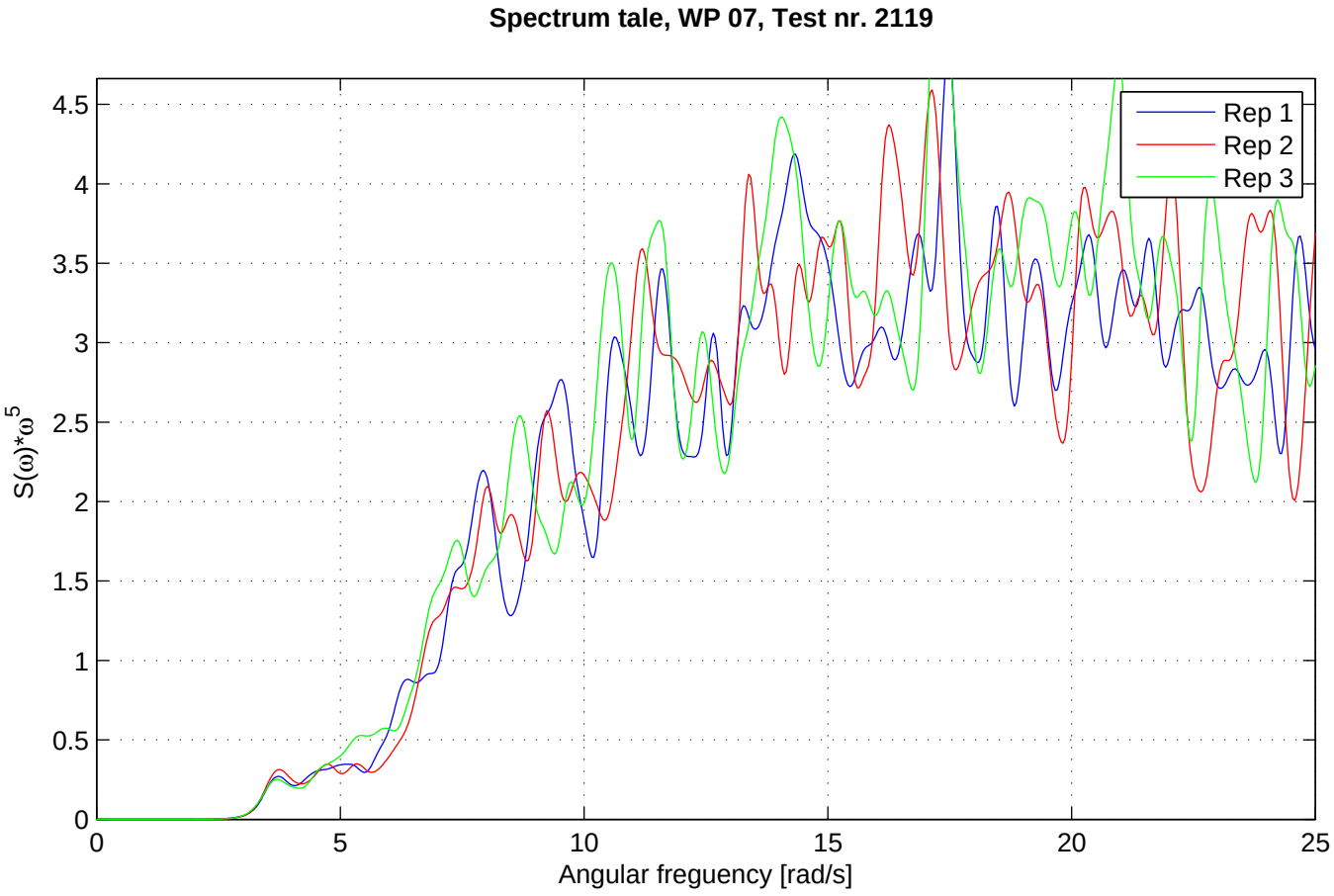
Spectrum tale, WP 07, Test nr. 2119
Rep 1
Rep 2
Rep 3
S(ω)*ω^5
4.5
4
3.5
3
2.5
2
1.5
1
0.5
0
0
5
10
15
20
25
Angular freguency [rad/s]

Appendix E

TMA spectrum

Spectrum estimation skp, Test nr. 2116, Rep 1

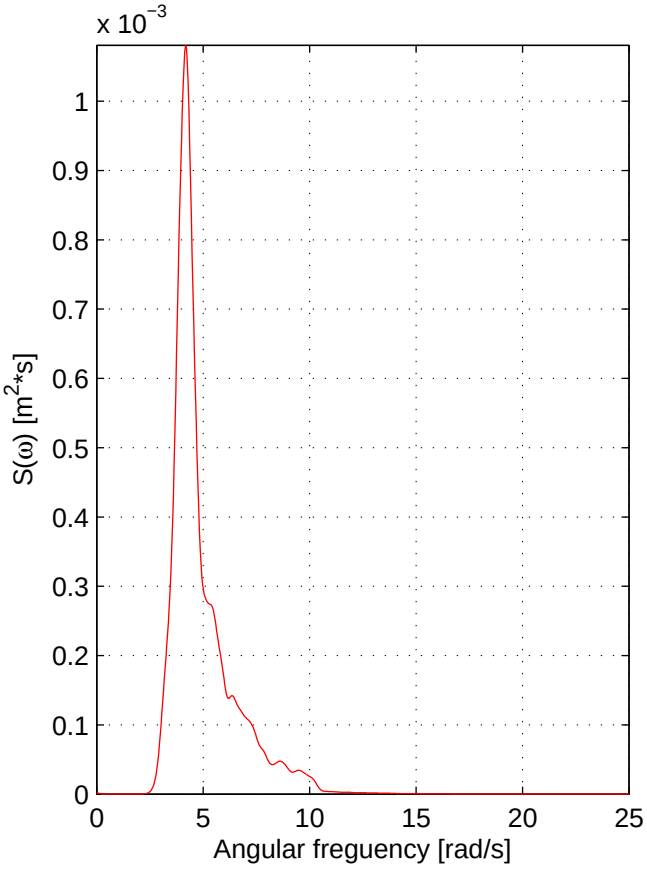

Spectrum estimation WP 16, Test nr. 2116, Rep 1

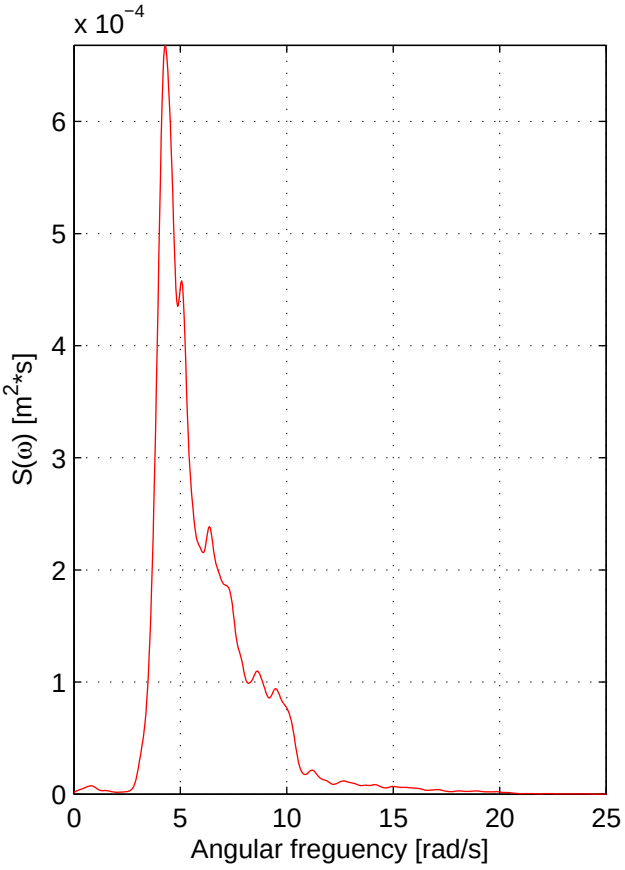

Spectrum estimation WP 02, Test nr. 2116, Rep 1

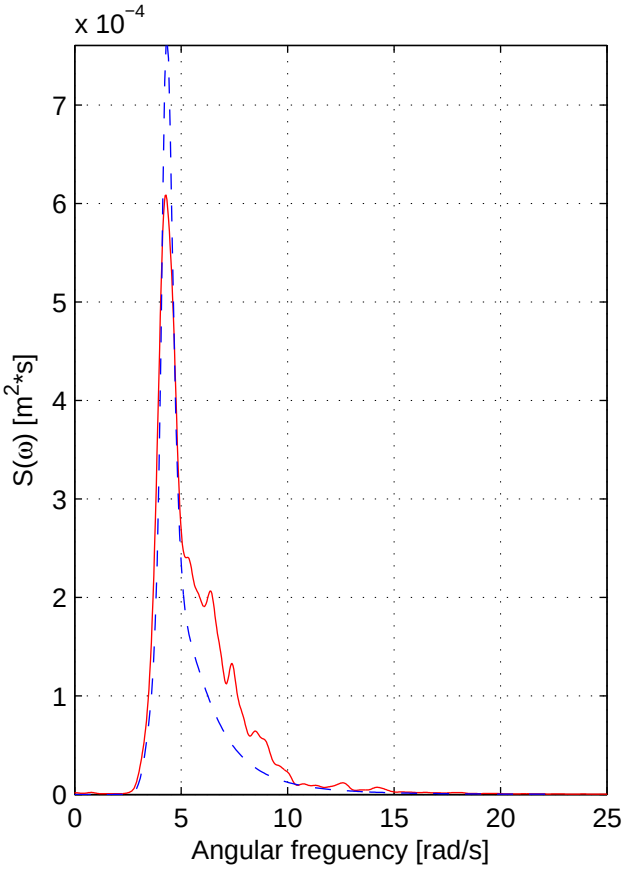

Spectrum estimation WP 03, Test nr. 2116, Rep 1

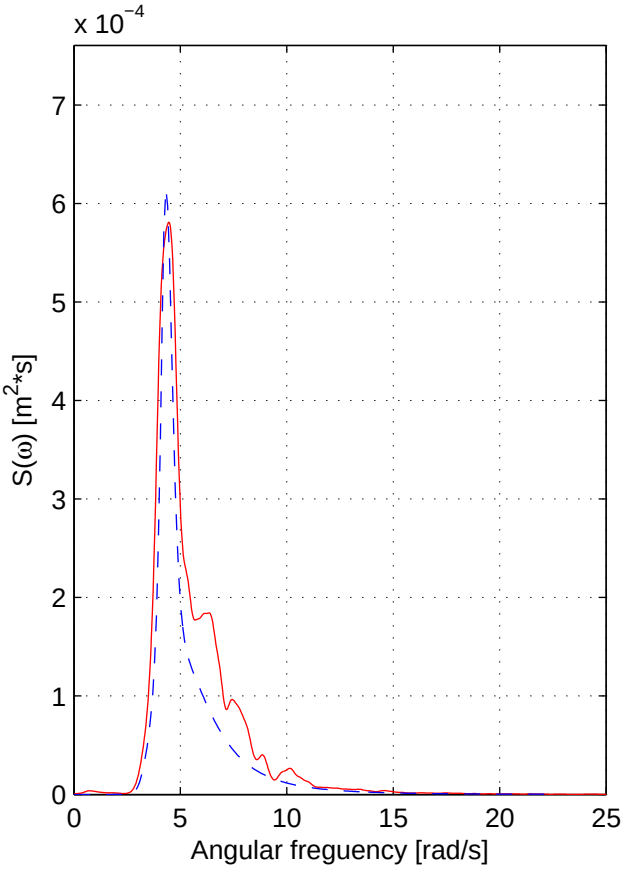

Spectrum estimation WP 04, Test nr. 2116, Rep 1

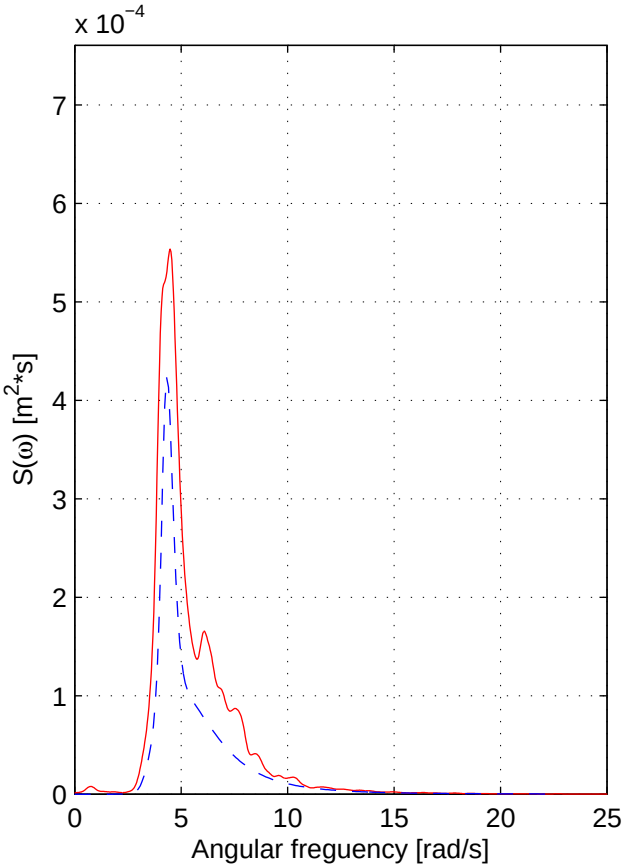

Spectrum estimation WP 05, Test nr. 2116, Rep 1

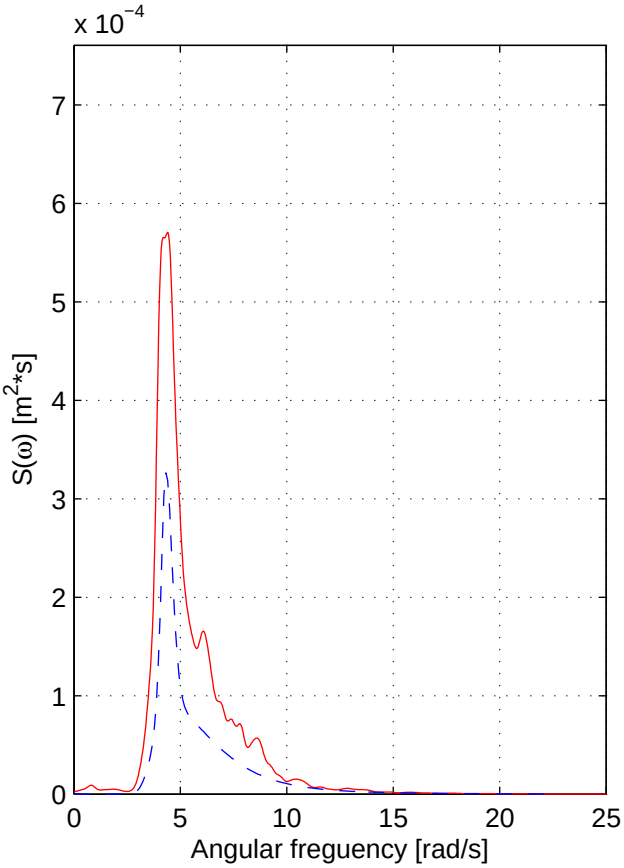

Spectrum estimation WP 08, Test nr. 2116, Rep 1

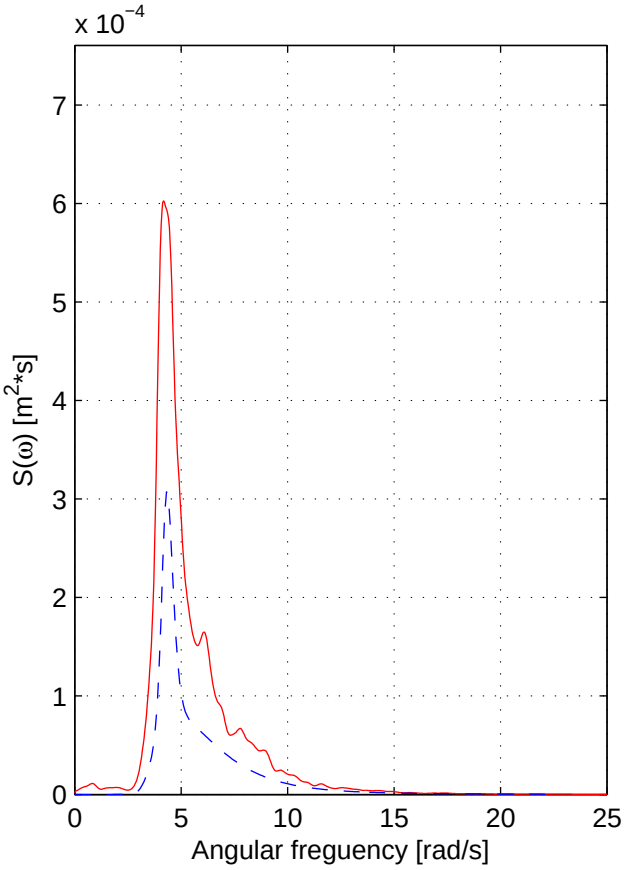

Spectrum estimation WP 09, Test nr. 2116, Rep 1

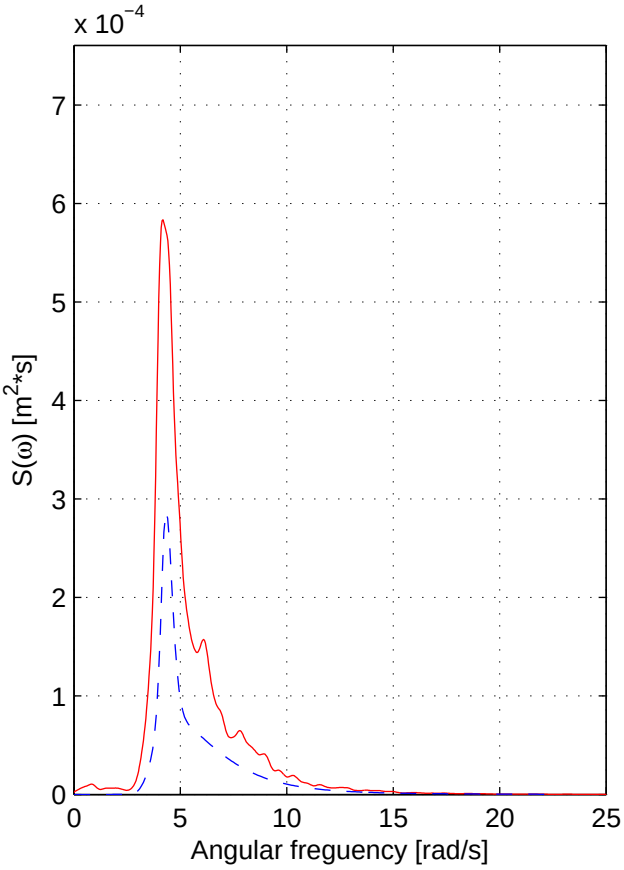

Spectrum estimation WP 10, Test nr. 2116, Rep 1

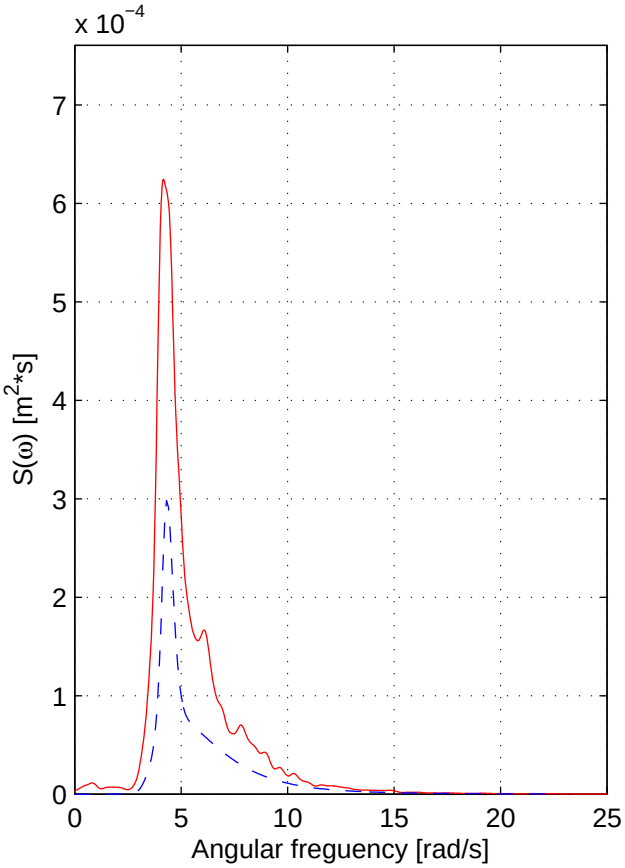

Spectrum estimation WP 11, Test nr. 2116, Rep 1

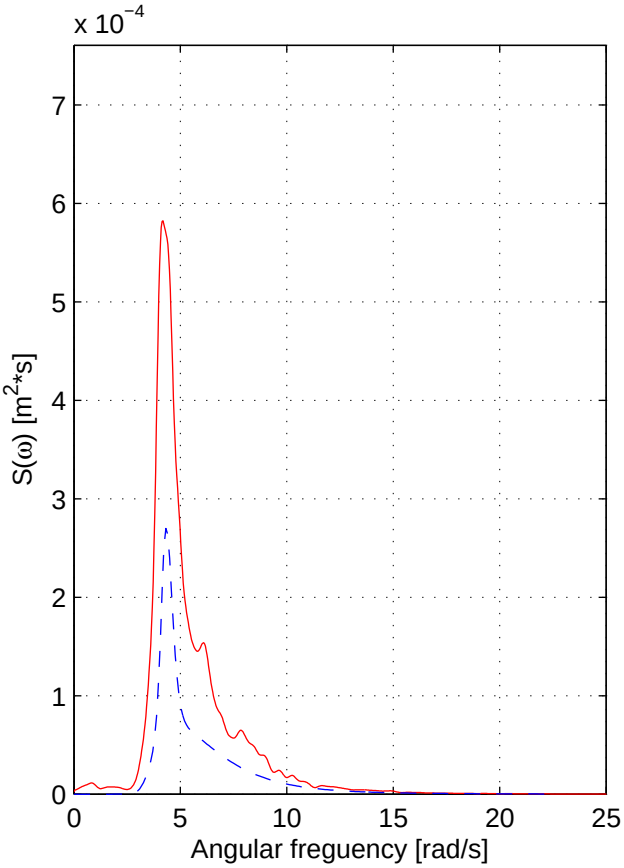

Spectrum estimation WP 12, Test nr. 2116, Rep 1

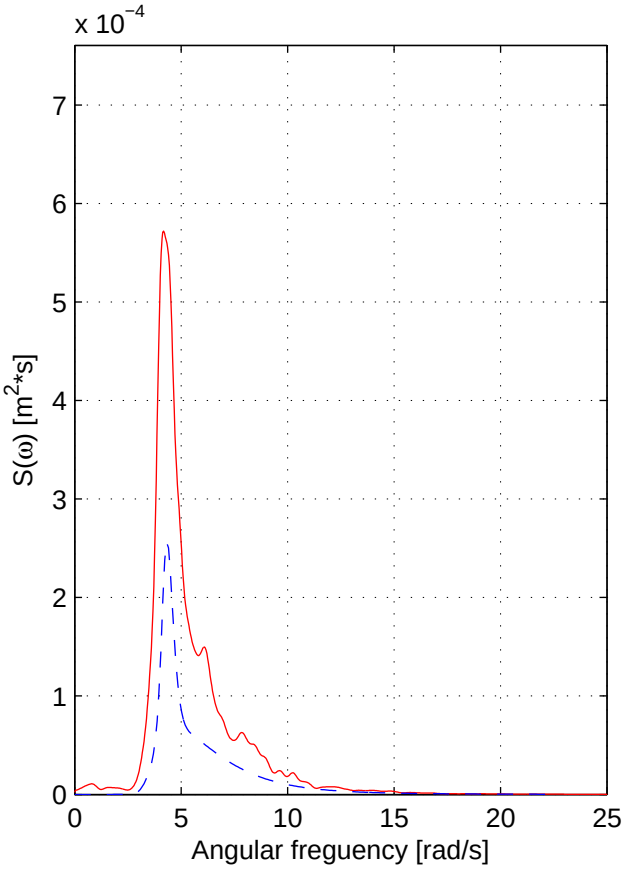

Spectrum estimation WP 13, Test nr. 2116, Rep 1

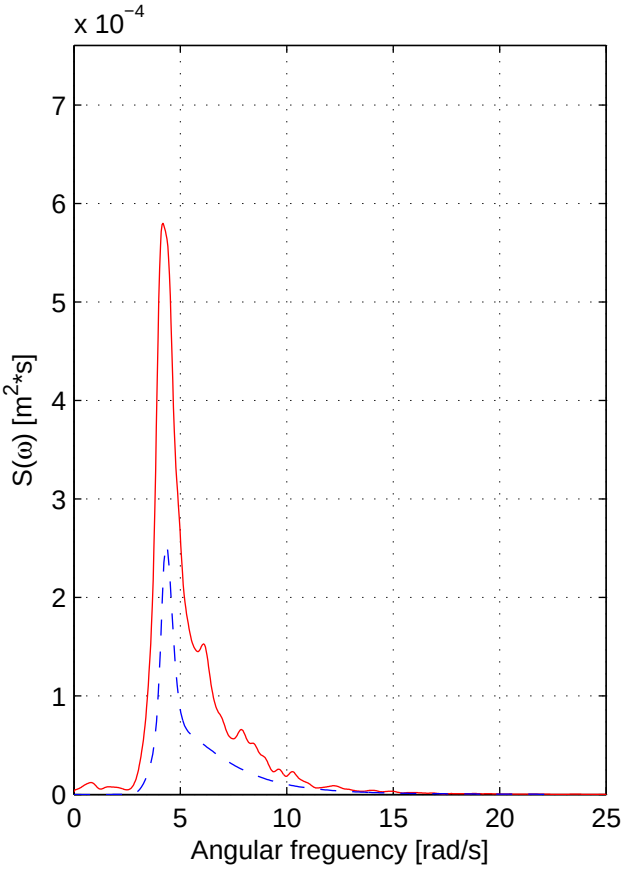

Spectrum estimation WP 14, Test nr. 2116, Rep 1

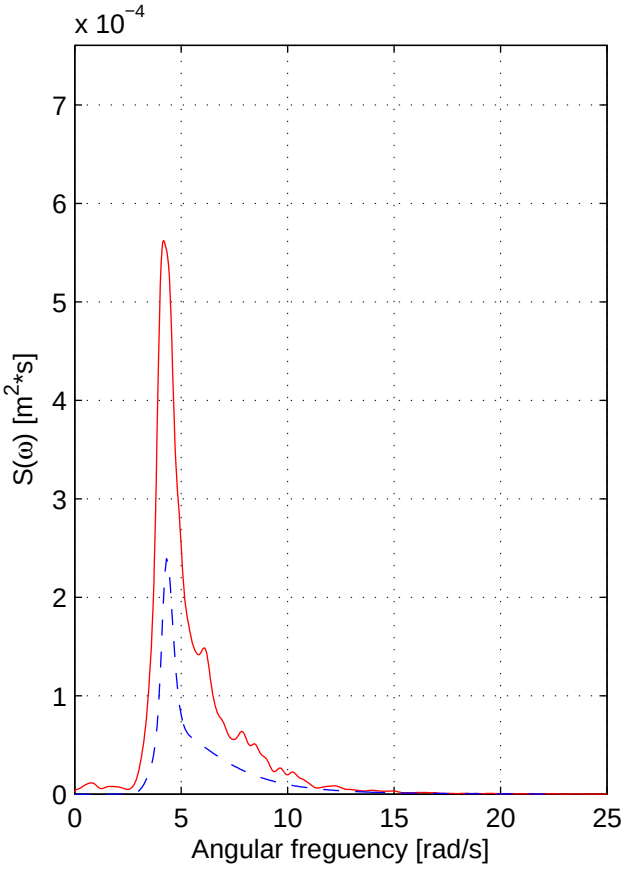

Spectrum estimation WP 06, Test nr. 2116, Rep 1

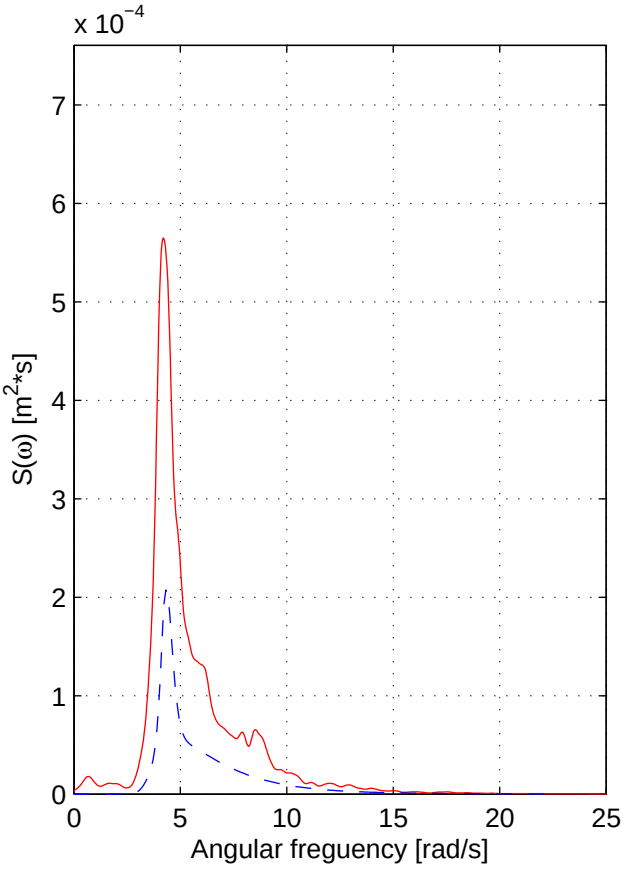

Spectrum estimation WP 07, Test nr. 2116, Rep 1

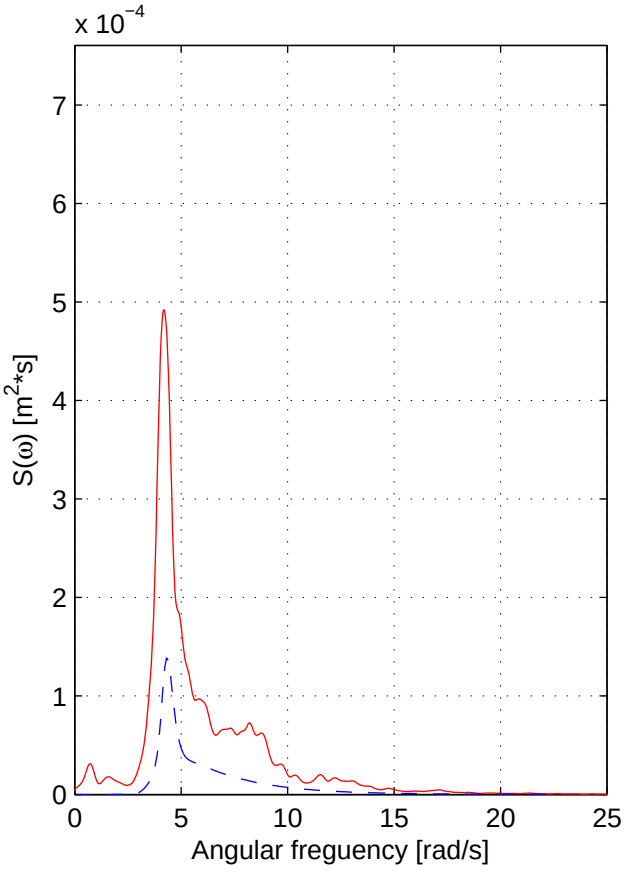

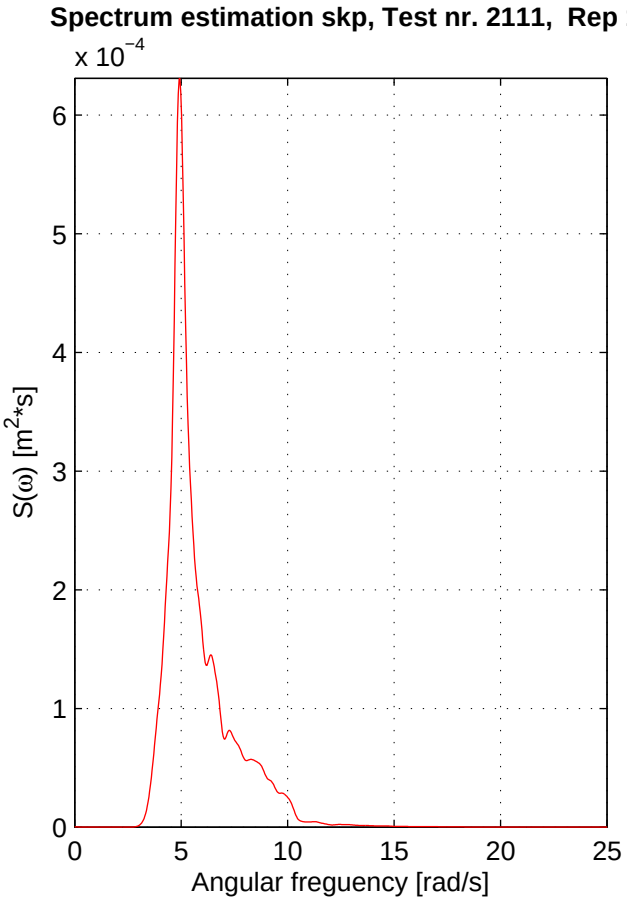
Spectrum estimation skp, Test nr. 2111, Rep 1
x 10^-4
S(ω) [m^2*s]
Angular freguency [rad/s]

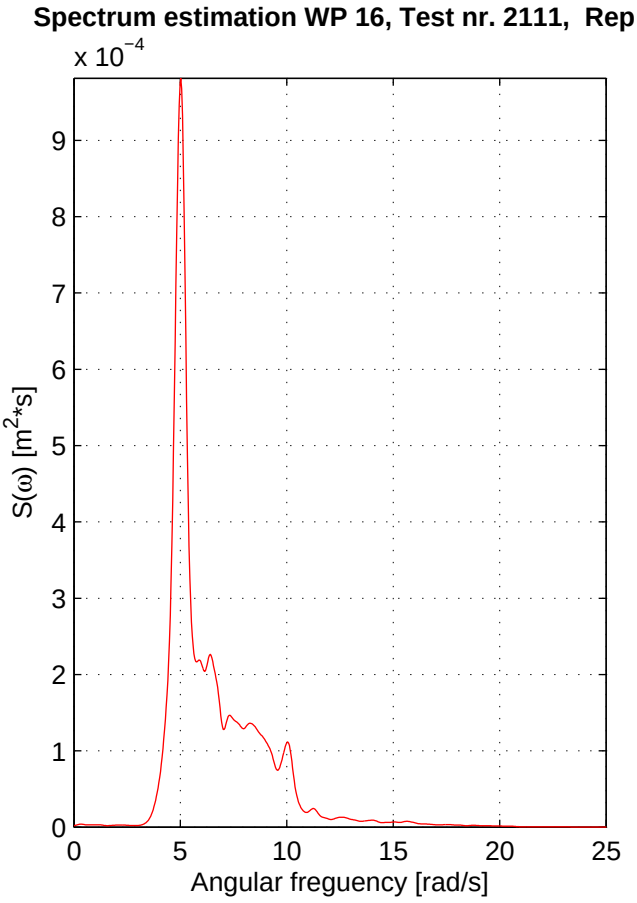
Spectrum estimation WP 16, Test nr. 2111, Rep 1
x 10^-4
S(ω) [m^2*s]
Angular freguency [rad/s]

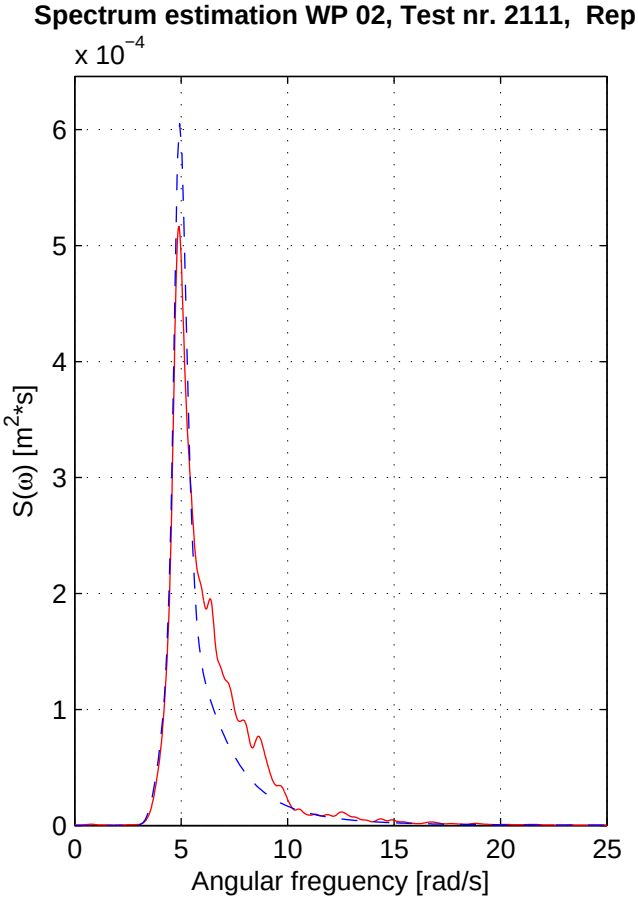
Spectrum estimation WP 02, Test nr. 2111, Rep 1
x 10^-4
S(ω) [m^2*s]
Angular freguency [rad/s]

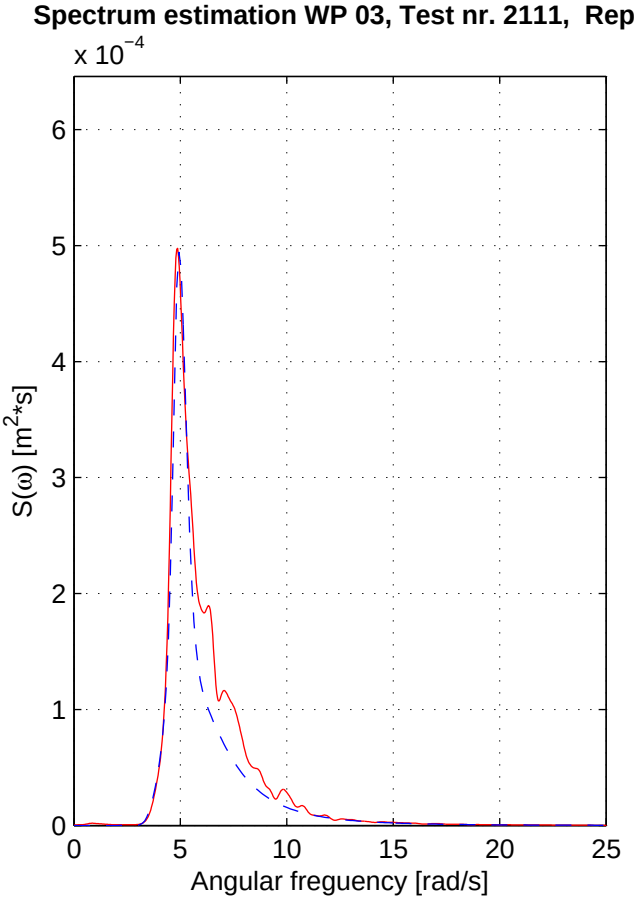
Spectrum estimation WP 03, Test nr. 2111, Rep 1
x 10^-4
S(ω) [m^2*s]
Angular freguency [rad/s]

Spectrum estimation WP 04, Test nr. 2111, Rep 1

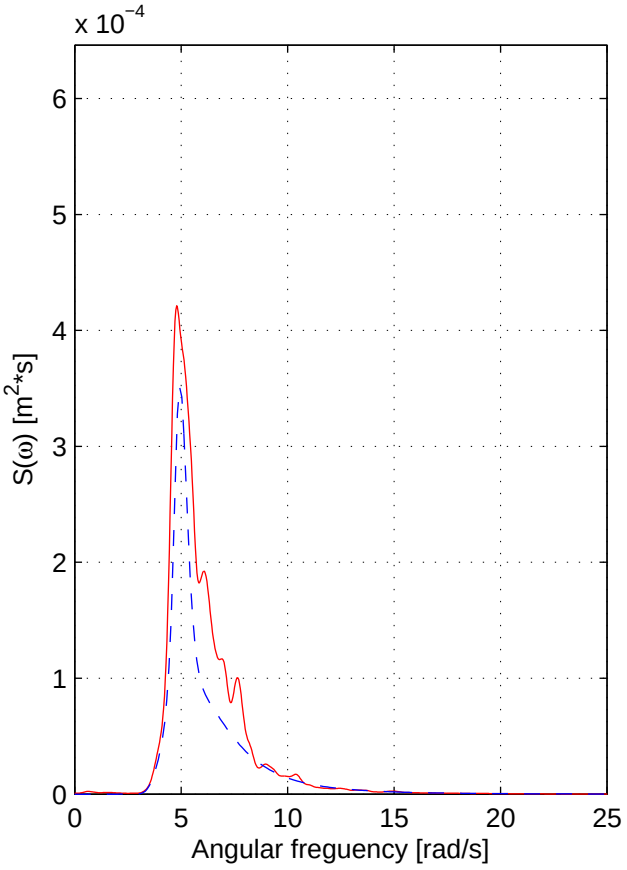

Spectrum estimation WP 05, Test nr. 2111, Rep 1

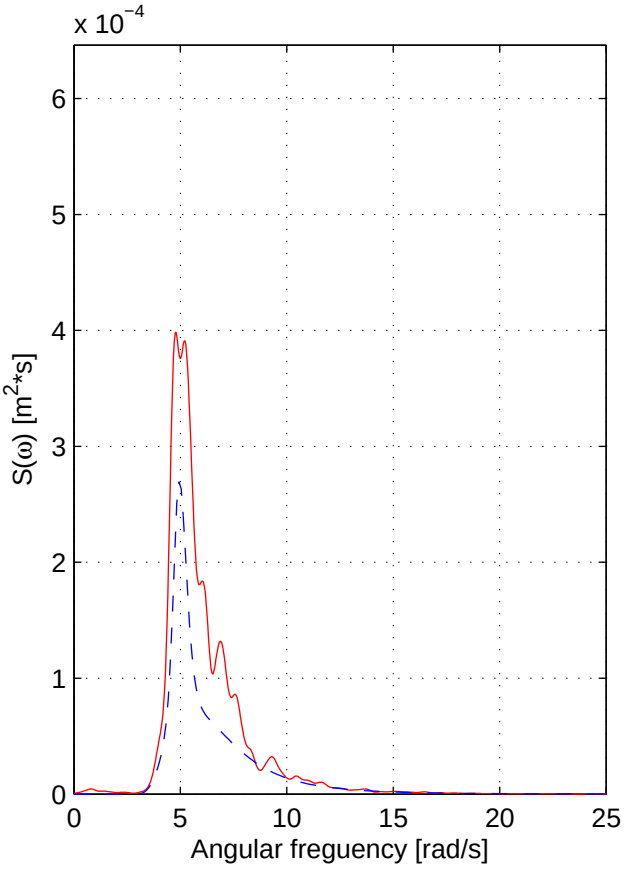

Spectrum estimation WP 08, Test nr. 2111, Rep 1

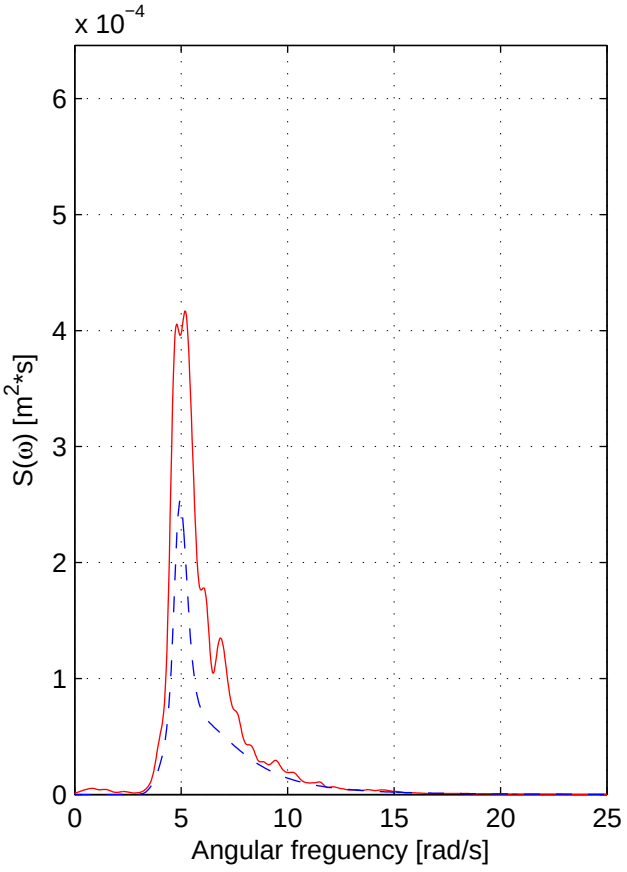

Spectrum estimation WP 09, Test nr. 2111, Rep 1

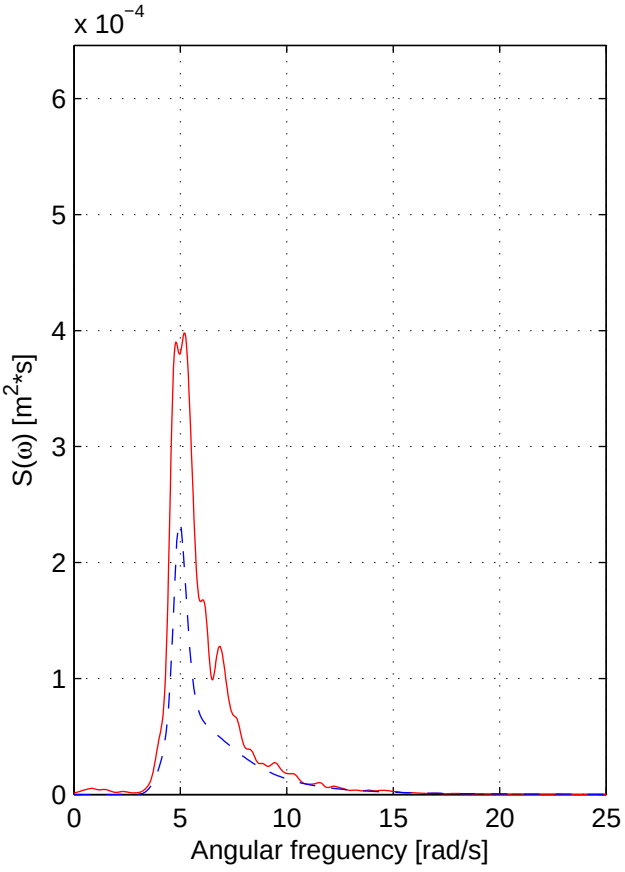

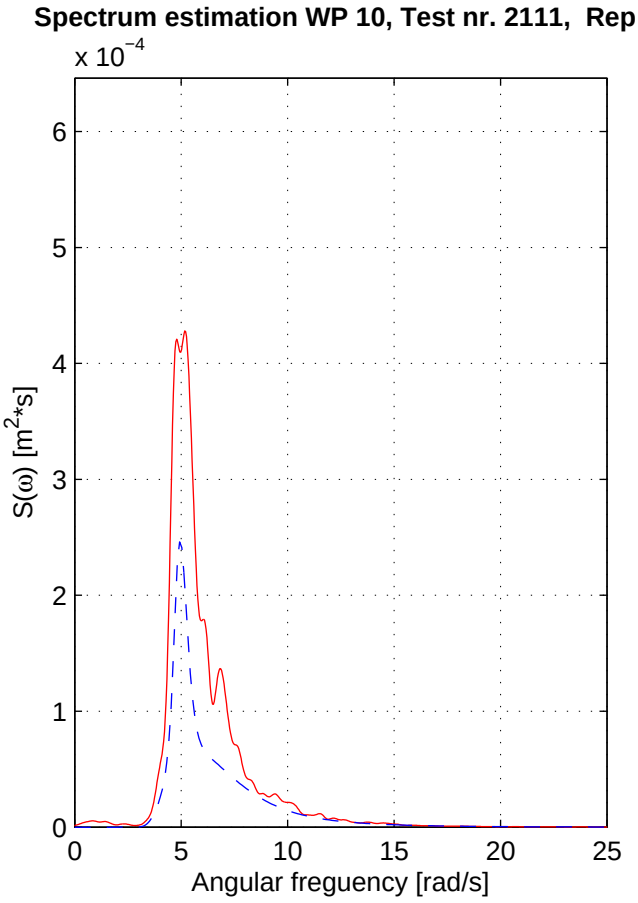
Spectrum estimation WP 10, Test nr. 2111, Rep 1
x 10^-4
S(ω) [m^2*s]
Angular freguency [rad/s]
0
1
2
3
4
5
6
0
5
10
15
20
25

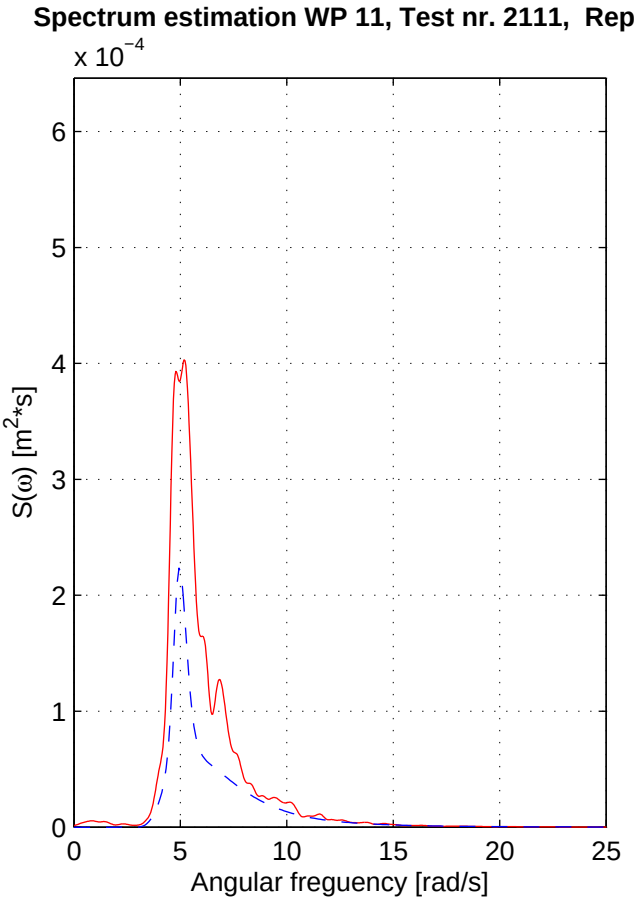
Spectrum estimation WP 11, Test nr. 2111, Rep 1
x 10^-4
S(ω) [m^2*s]
Angular freguency [rad/s]
0
1
2
3
4
5
6
0
5
10
15
20
25

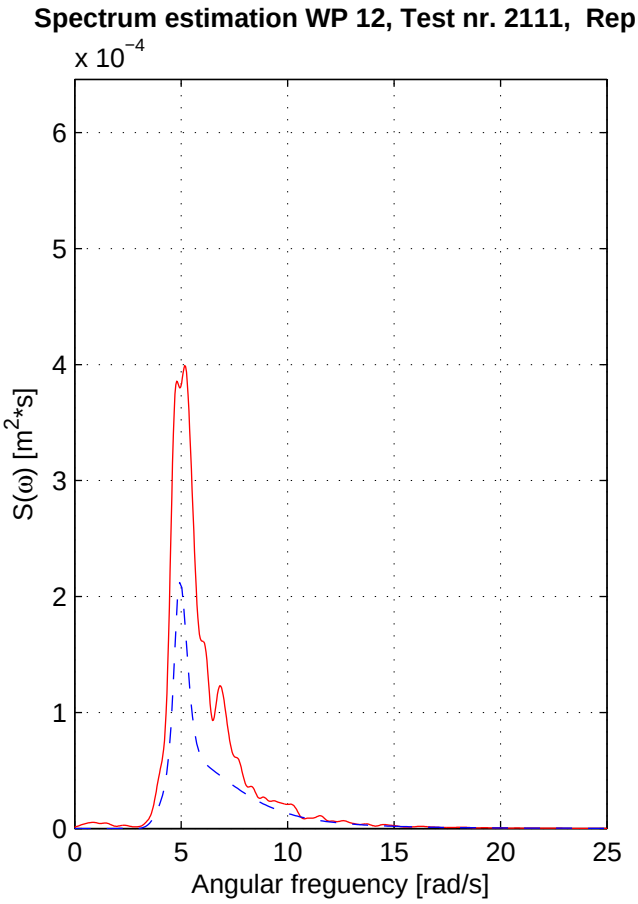
Spectrum estimation WP 12, Test nr. 2111, Rep 1
x 10^-4
S(ω) [m^2*s]
Angular freguency [rad/s]
0
1
2
3
4
5
6
0
5
10
15
20
25

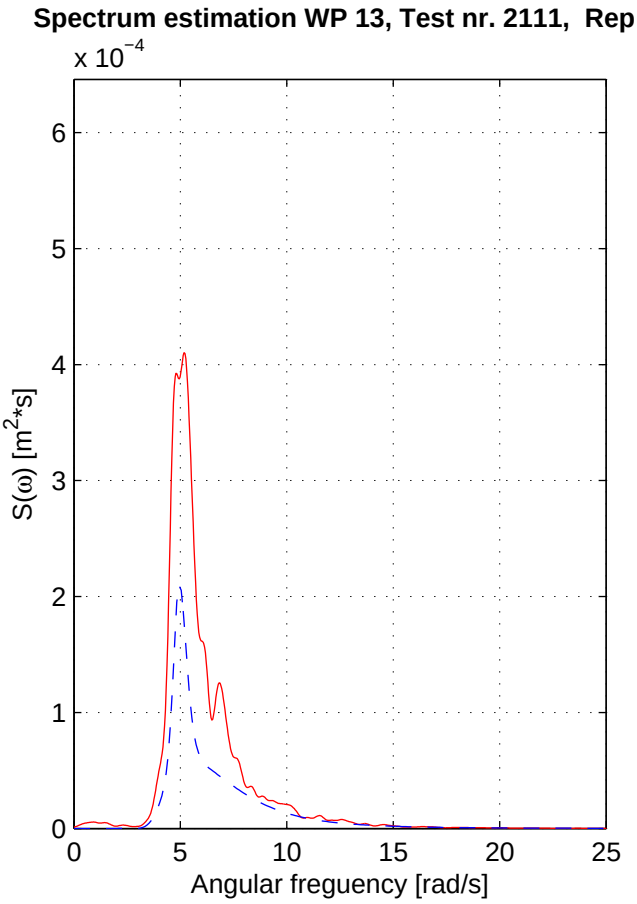
Spectrum estimation WP 13, Test nr. 2111, Rep 1
x 10^-4
S(ω) [m^2*s]
Angular freguency [rad/s]
0
1
2
3
4
5
6
0
5
10
15
20
25

Spectrum estimation WP 14, Test nr. 2111, Rep 1

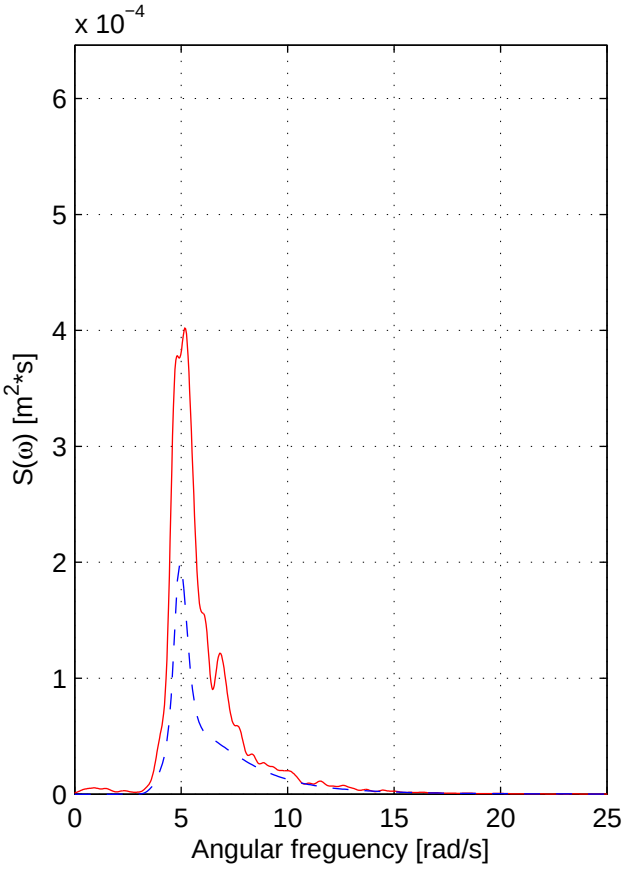

Spectrum estimation WP 06, Test nr. 2111, Rep 1

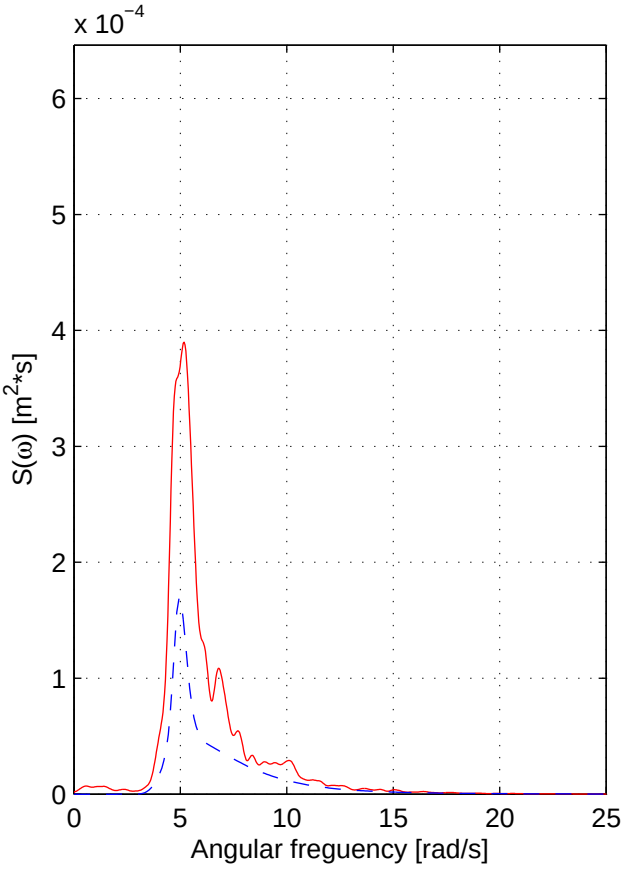

Spectrum estimation WP 07, Test nr. 2111, Rep 1

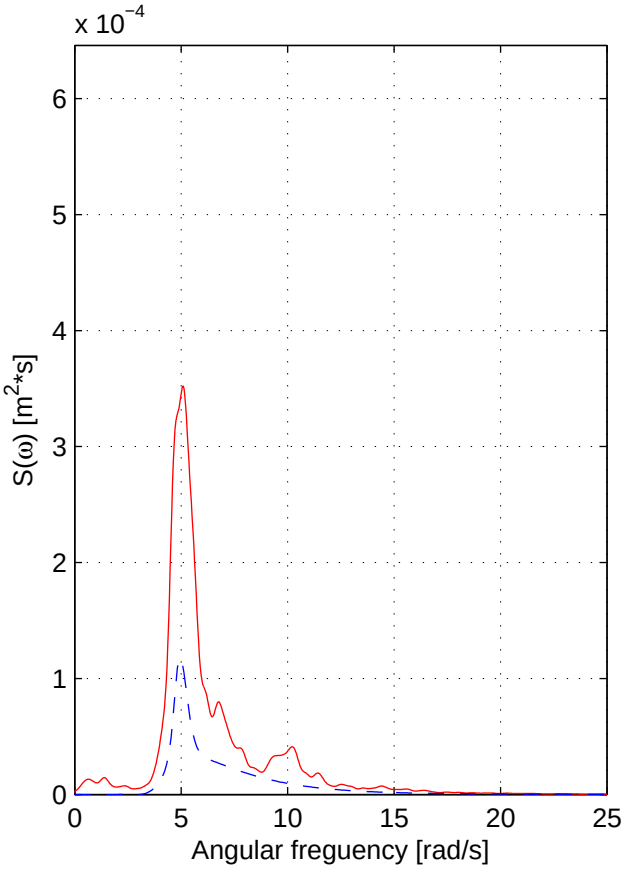

Spectrum estimation skp, Test nr. 2117, Rep 1

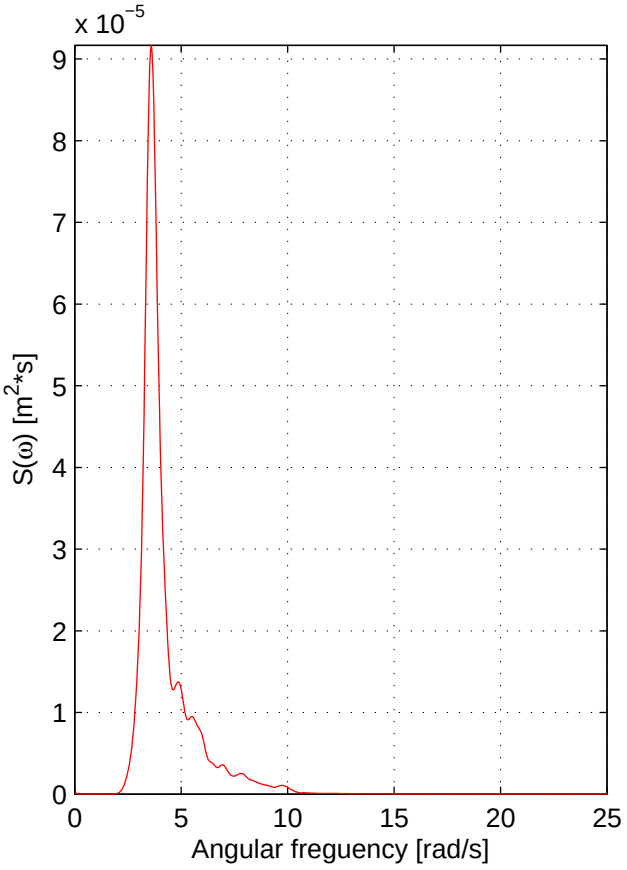

Spectrum estimation WP 16, Test nr. 2117, Rep 1

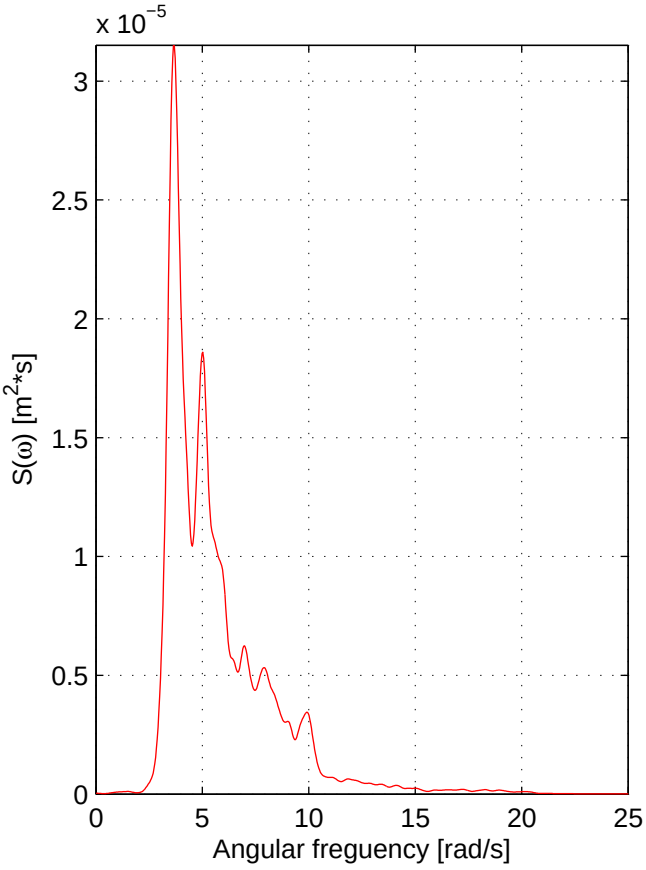

Spectrum estimation WP 02, Test nr. 2117, Rep 1

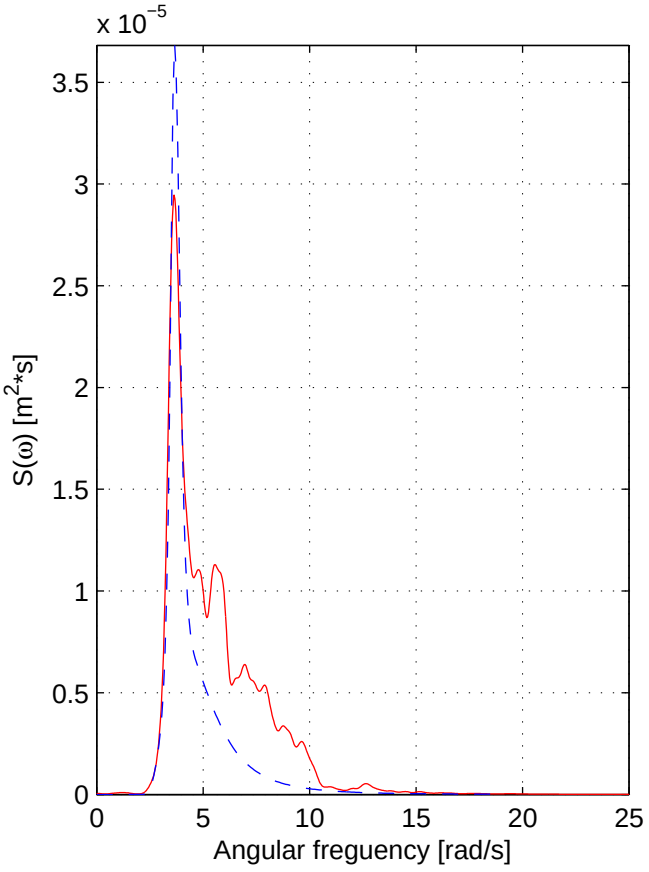

Spectrum estimation WP 03, Test nr. 2117, Rep 1

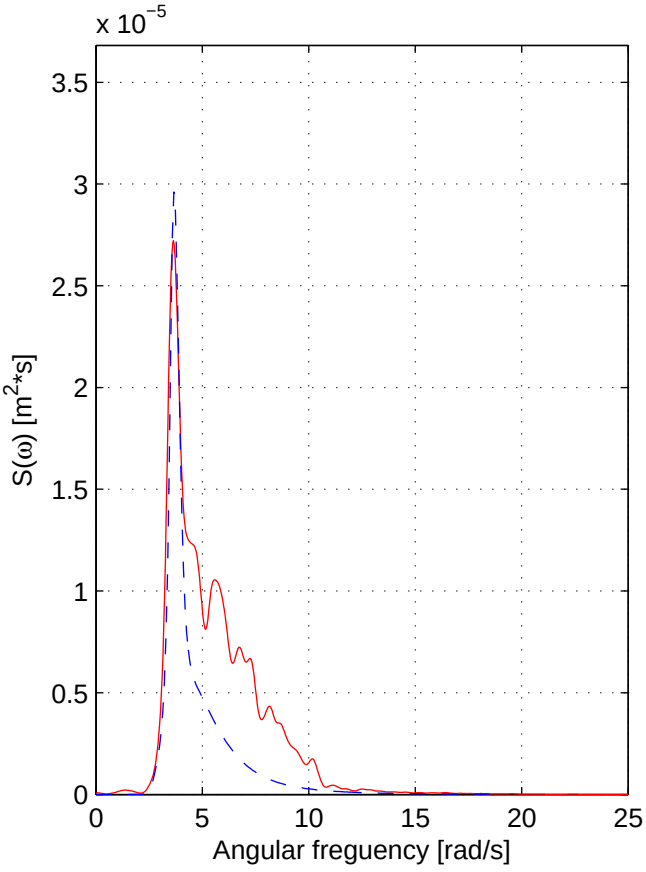

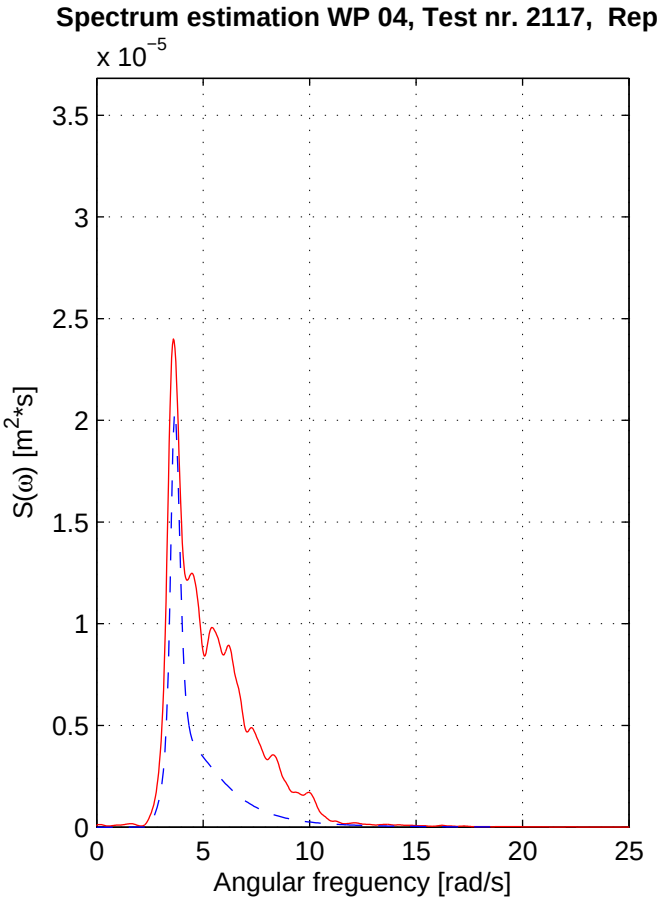
Spectrum estimation WP 04, Test nr. 2117, Rep 1
x 10^-5
S(ω) [m^2*s]
Angular freguency [rad/s]

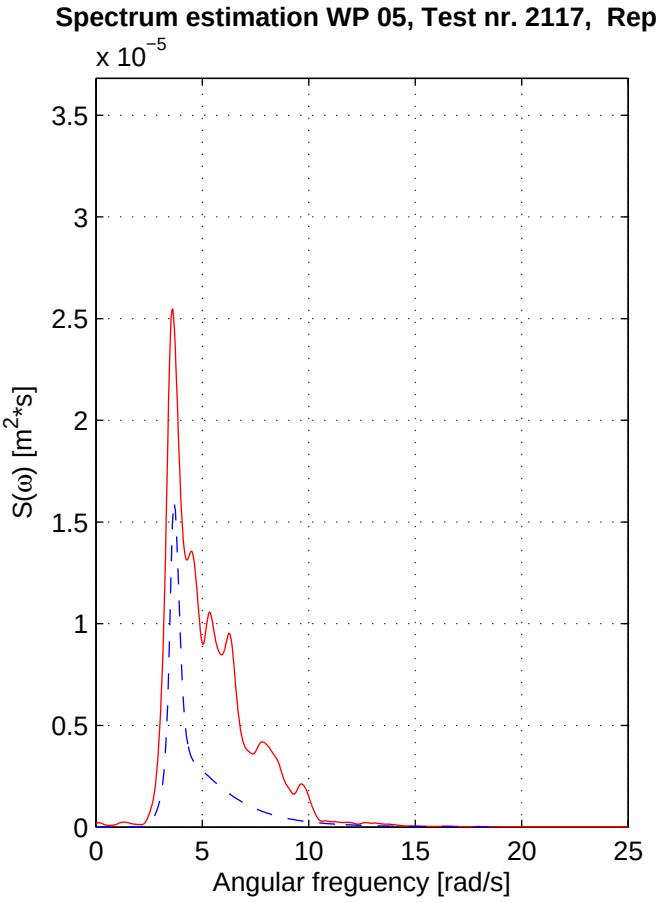
Spectrum estimation WP 05, Test nr. 2117, Rep 1
x 10^-5
S(ω) [m^2*s]
Angular freguency [rad/s]

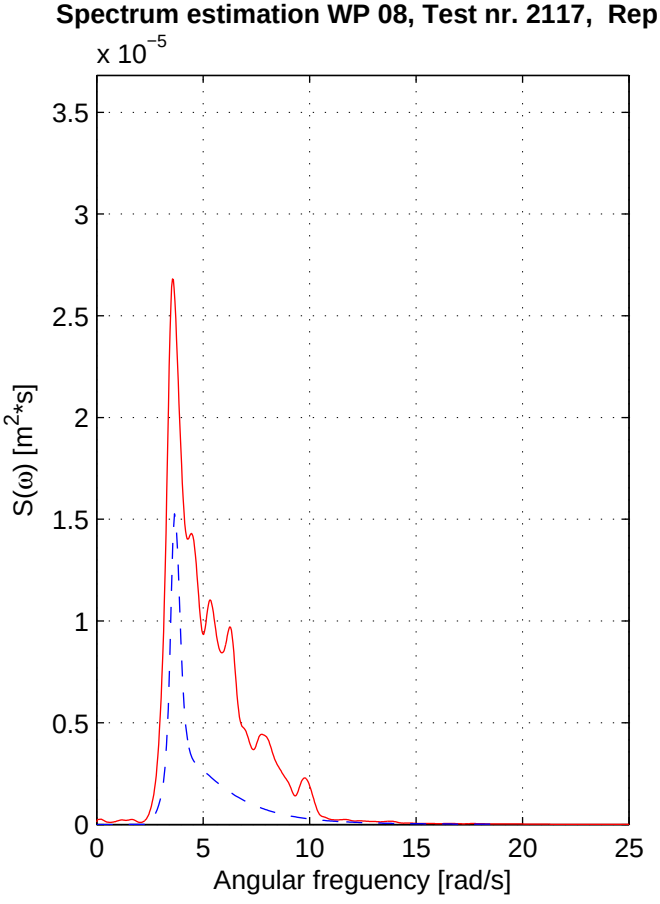
Spectrum estimation WP 08, Test nr. 2117, Rep 1
x 10^-5
S(ω) [m^2*s]
Angular freguency [rad/s]

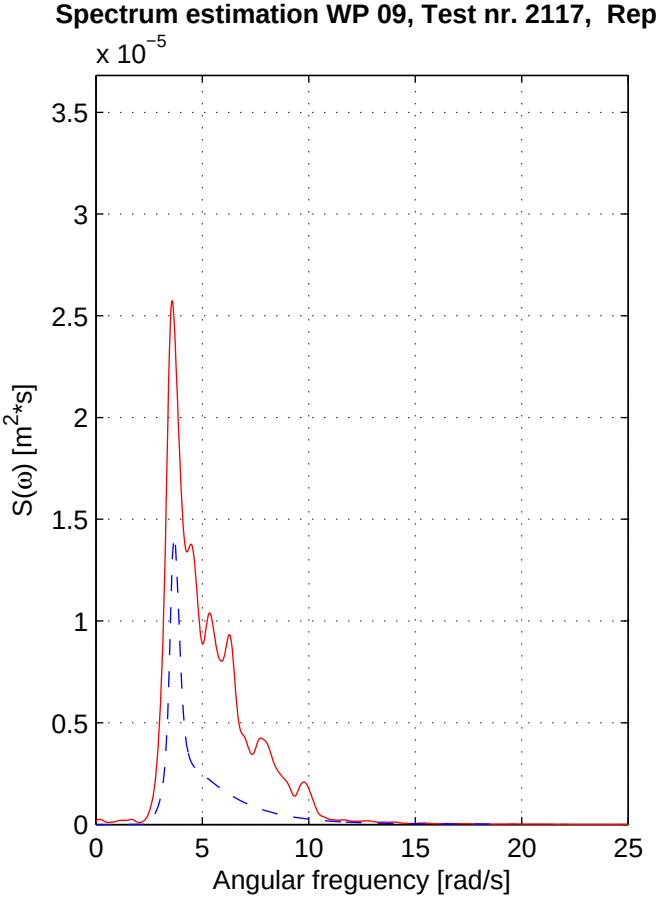
Spectrum estimation WP 09, Test nr. 2117, Rep 1
x 10^-5
S(ω) [m^2*s]
Angular freguency [rad/s]

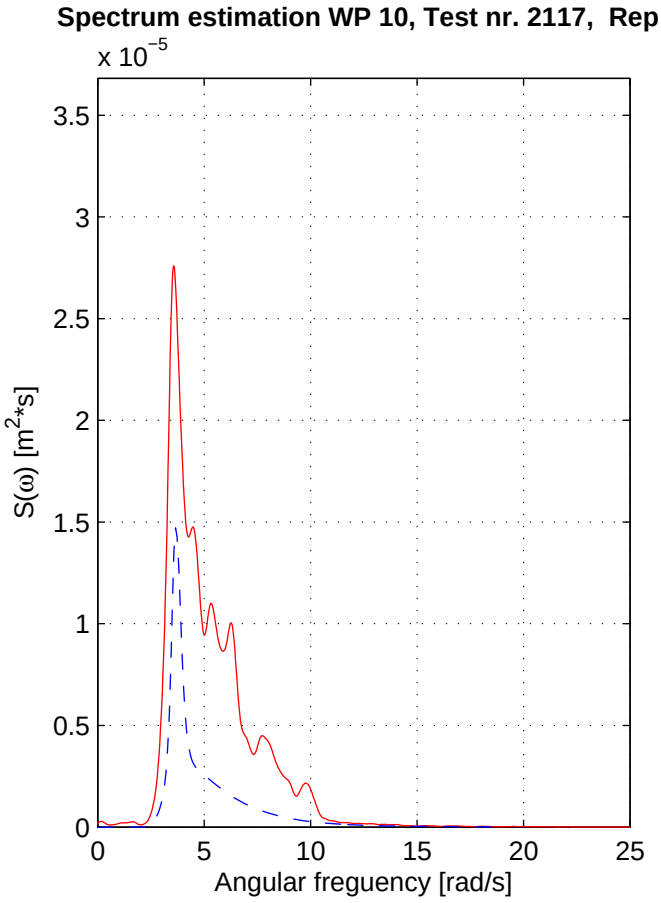
Spectrum estimation WP 10, Test nr. 2117, Rep 1
x 10^-5
S(ω) [m^2*s]
Angular freguency [rad/s]

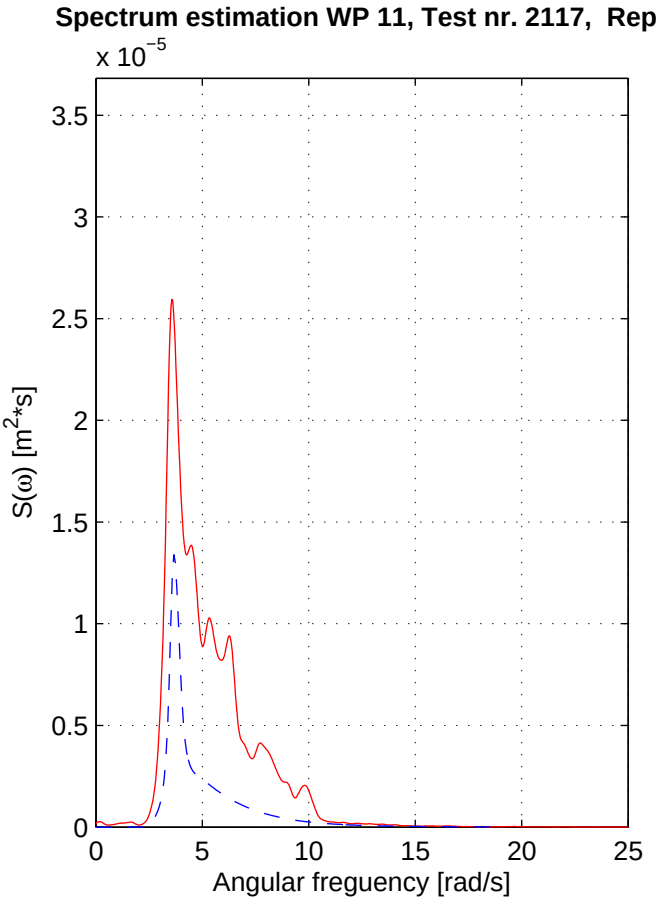
Spectrum estimation WP 11, Test nr. 2117, Rep 1
x 10^-5
S(ω) [m^2*s]
Angular freguency [rad/s]

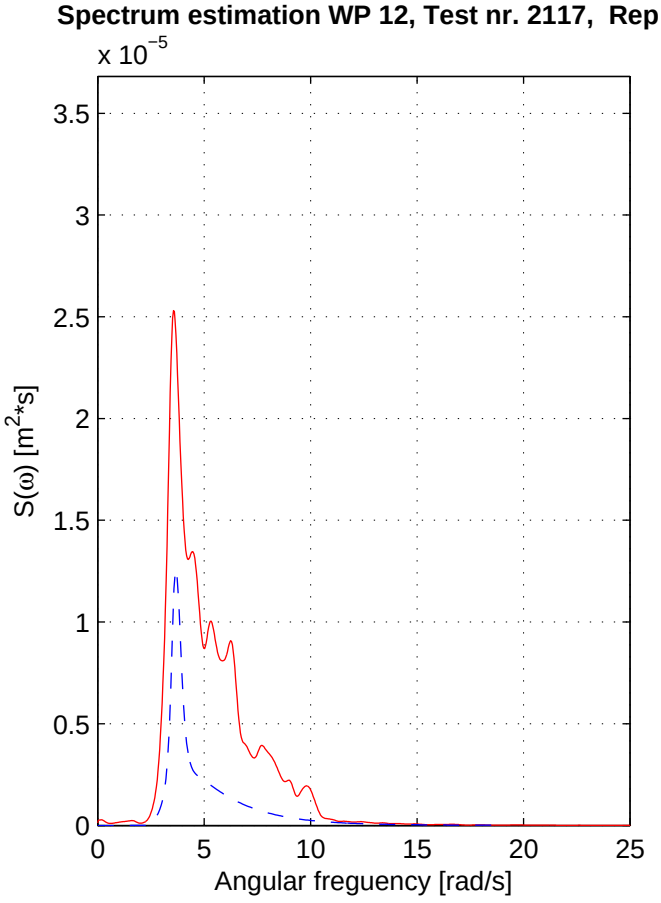
Spectrum estimation WP 12, Test nr. 2117, Rep 1
x 10^-5
S(ω) [m^2*s]
Angular freguency [rad/s]

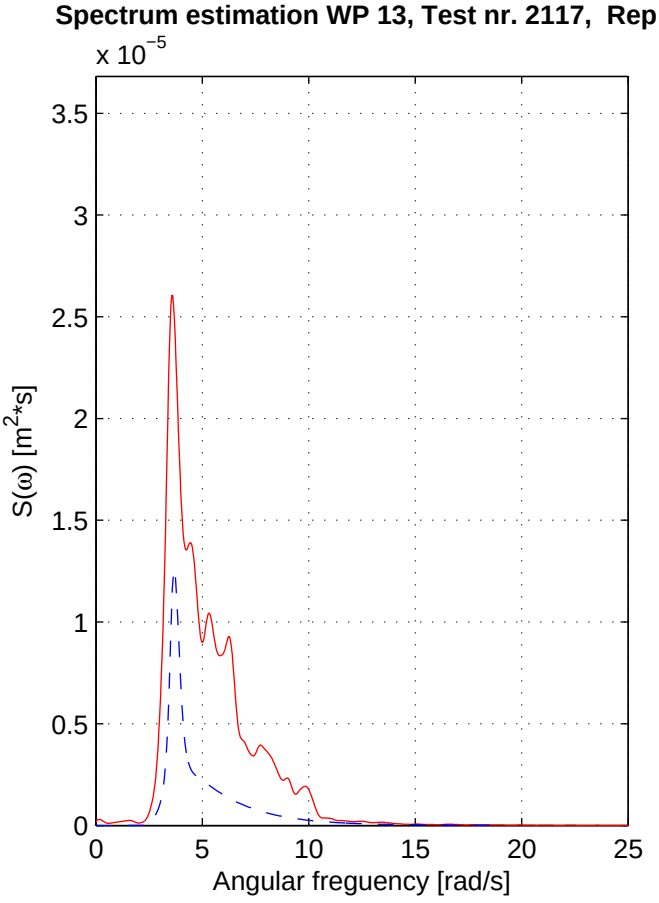
Spectrum estimation WP 13, Test nr. 2117, Rep 1
x 10^-5
S(ω) [m^2*s]
Angular freguency [rad/s]

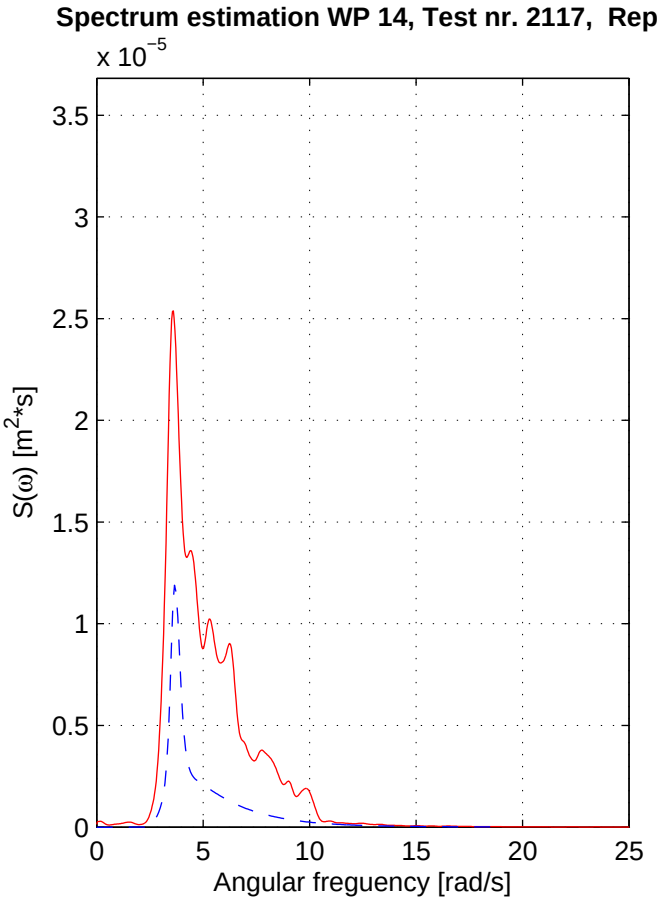
Spectrum estimation WP 14, Test nr. 2117, Rep 1
x 10^-5
S(ω) [m^2*s]
Angular freguency [rad/s]
0
0.5
1
1.5
2
2.5
3
3.5
0
5
10
15
20
25

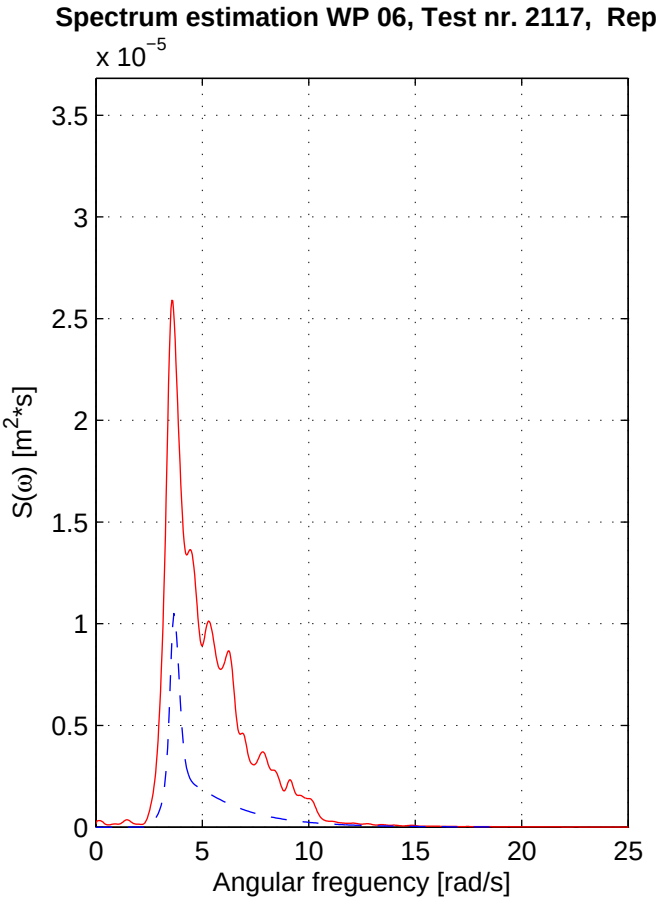
Spectrum estimation WP 06, Test nr. 2117, Rep 1
x 10^-5
S(ω) [m^2*s]
Angular freguency [rad/s]
0
0.5
1
1.5
2
2.5
3
3.5
0
5
10
15
20
25

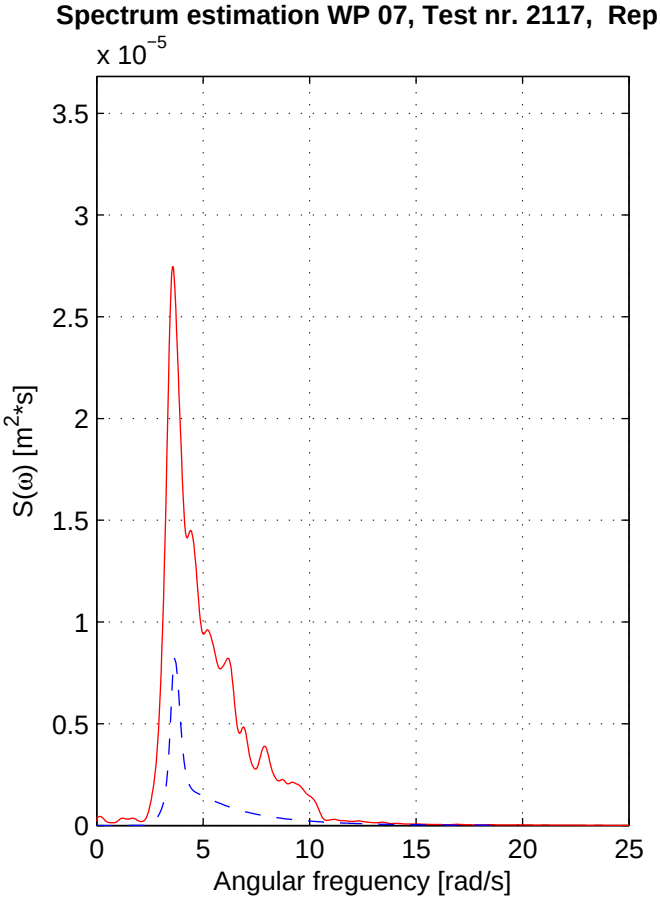
Spectrum estimation WP 07, Test nr. 2117, Rep 1
x 10^-5
S(ω) [m^2*s]
Angular freguency [rad/s]
0
0.5
1
1.5
2
2.5
3
3.5
0
5
10
15
20
25

Appendix F

Wave height distributions

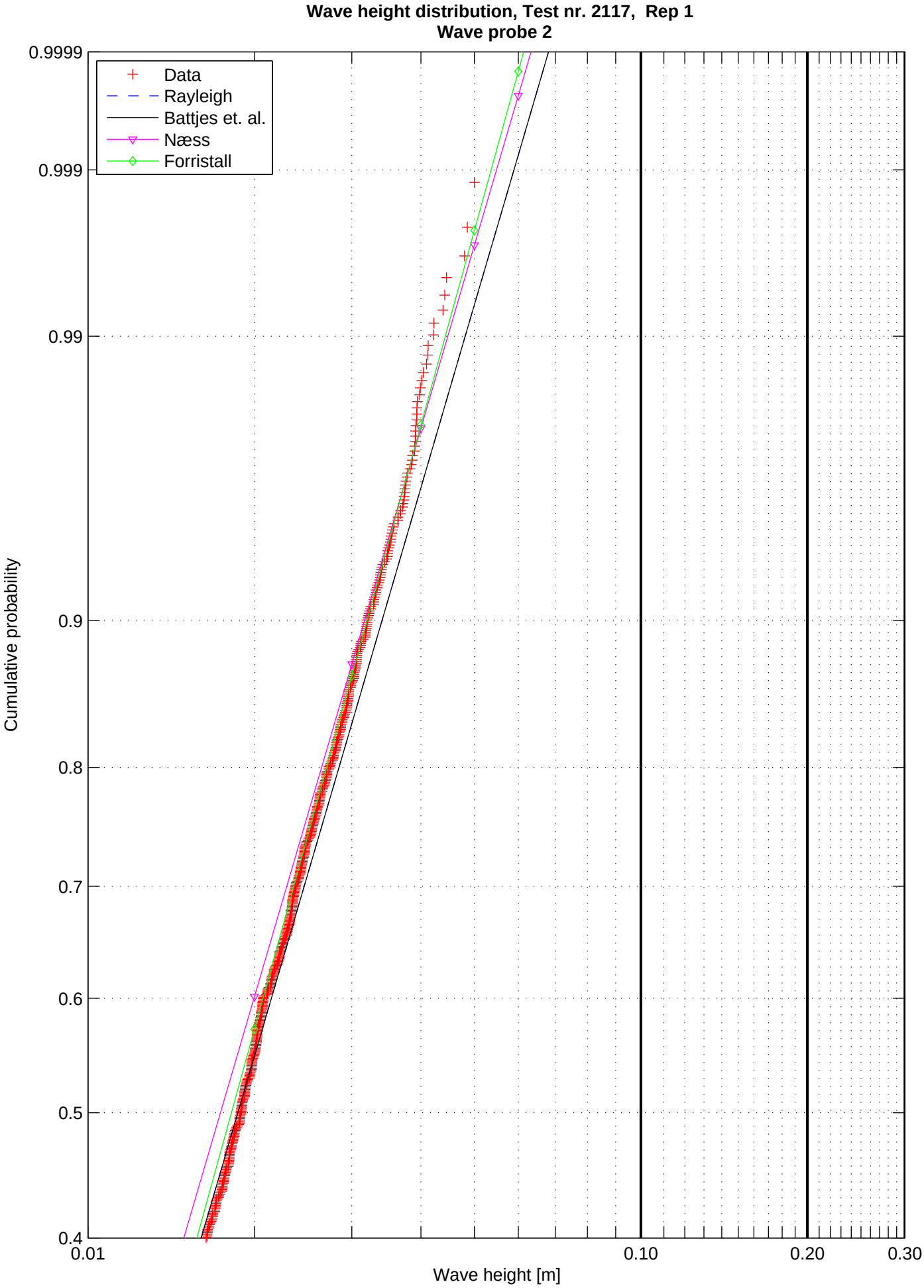
Wave height distribution, Test nr. 2117, Rep 1
Wave probe 2
Data
Rayleigh
Battjes et. al.
Næss
Forristall
Cumulative probability
0.9999
0.999
0.99
0.9
0.8
0.7
0.6
0.5
0.4
0.01
0.10
0.20
0.30
Wave height [m]

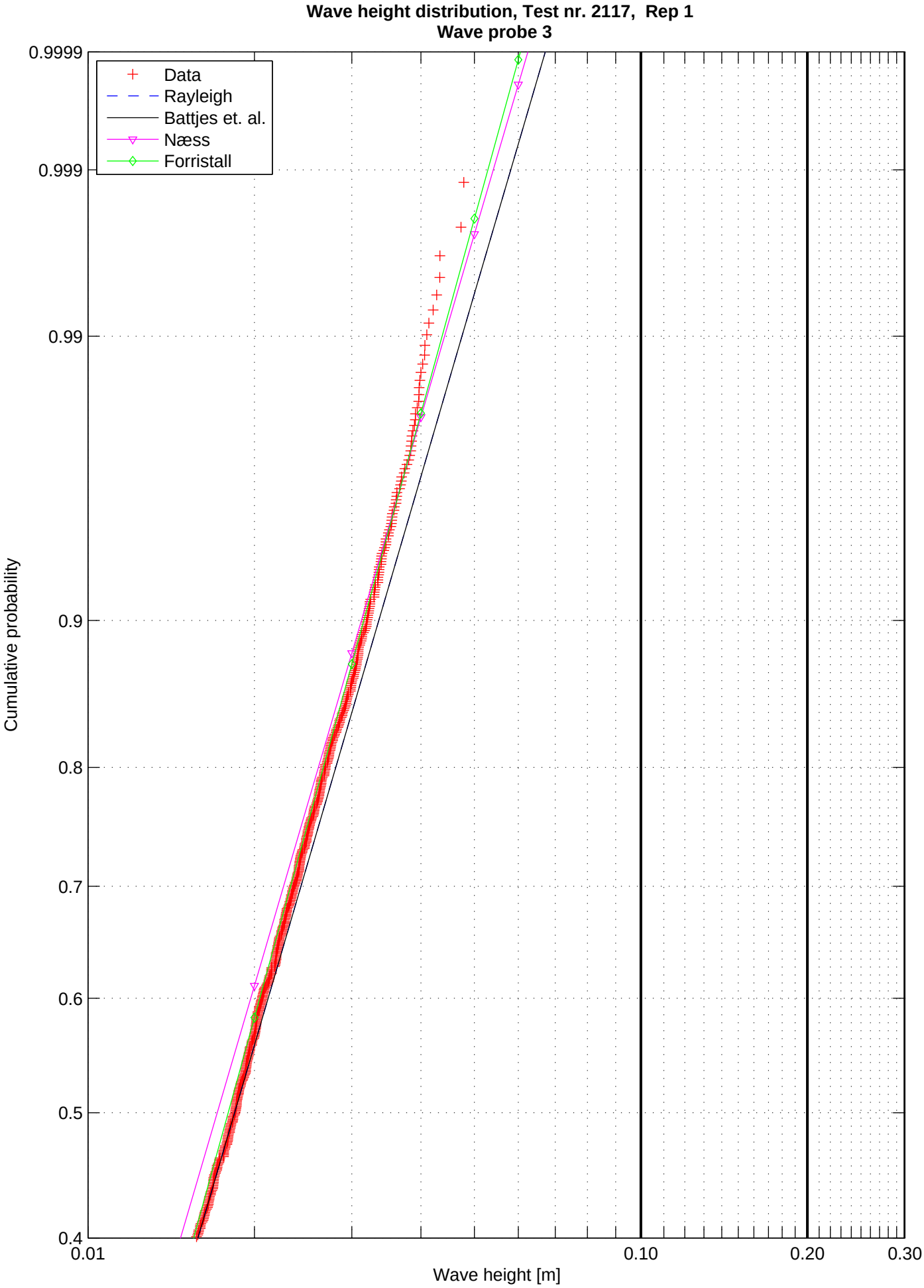
Wave height distribution, Test nr. 2117, Rep 1
Wave probe 3
Data
Rayleigh
Battjes et. al.
Næss
Forristall
0.9999
0.999
0.99
0.9
0.8
0.7
0.6
0.5
0.4
Cumulative probability
0.01
0.10
0.20
0.30
Wave height [m]

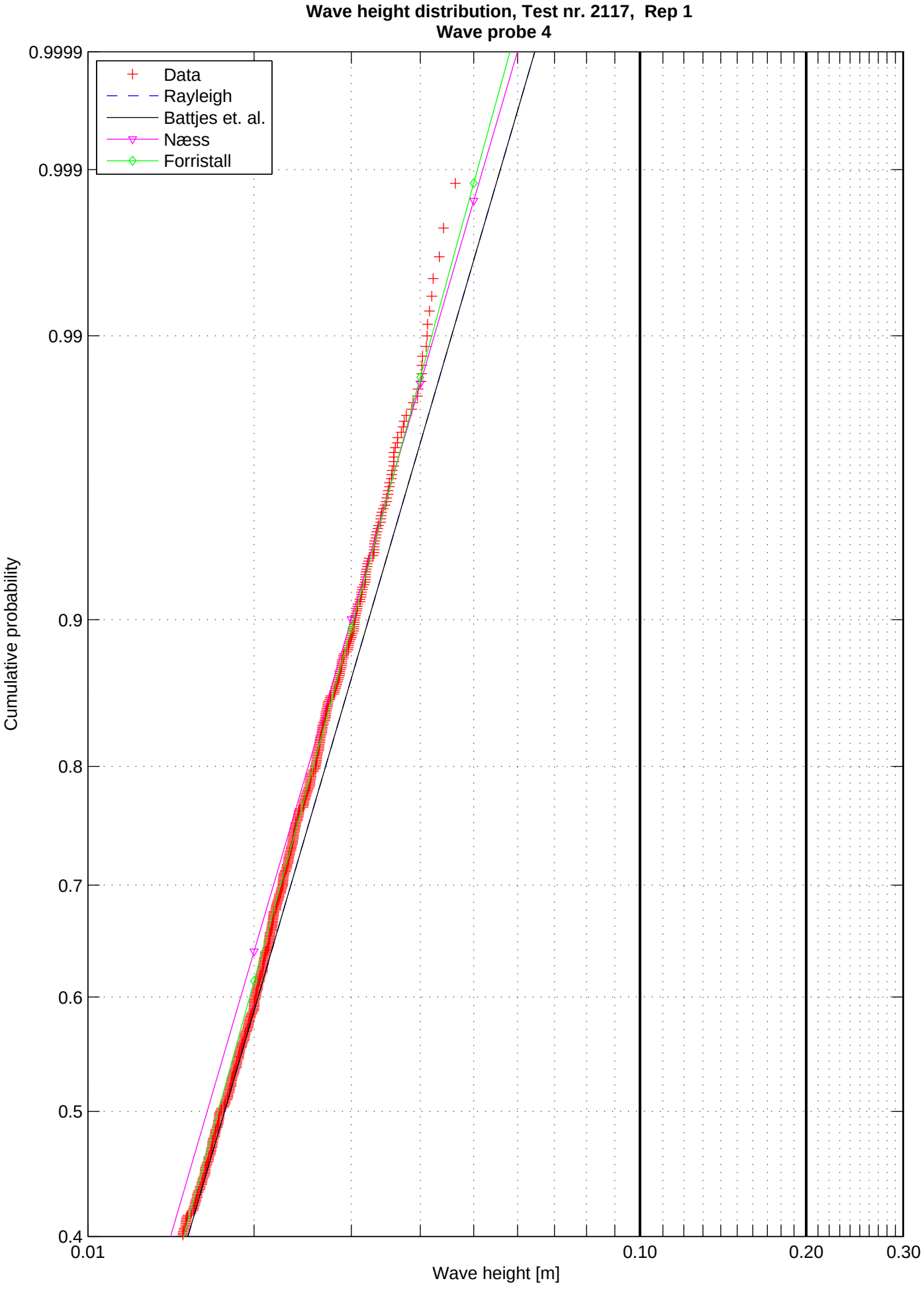
Wave height distribution, Test nr. 2117, Rep 1
Wave probe 4
Data
Rayleigh
Battjes et. al.
Næss
Forristall
Cumulative probability
0.9999
0.999
0.99
0.9
0.8
0.7
0.6
0.5
0.4
0.01
0.10
0.20
0.30
Wave height [m]

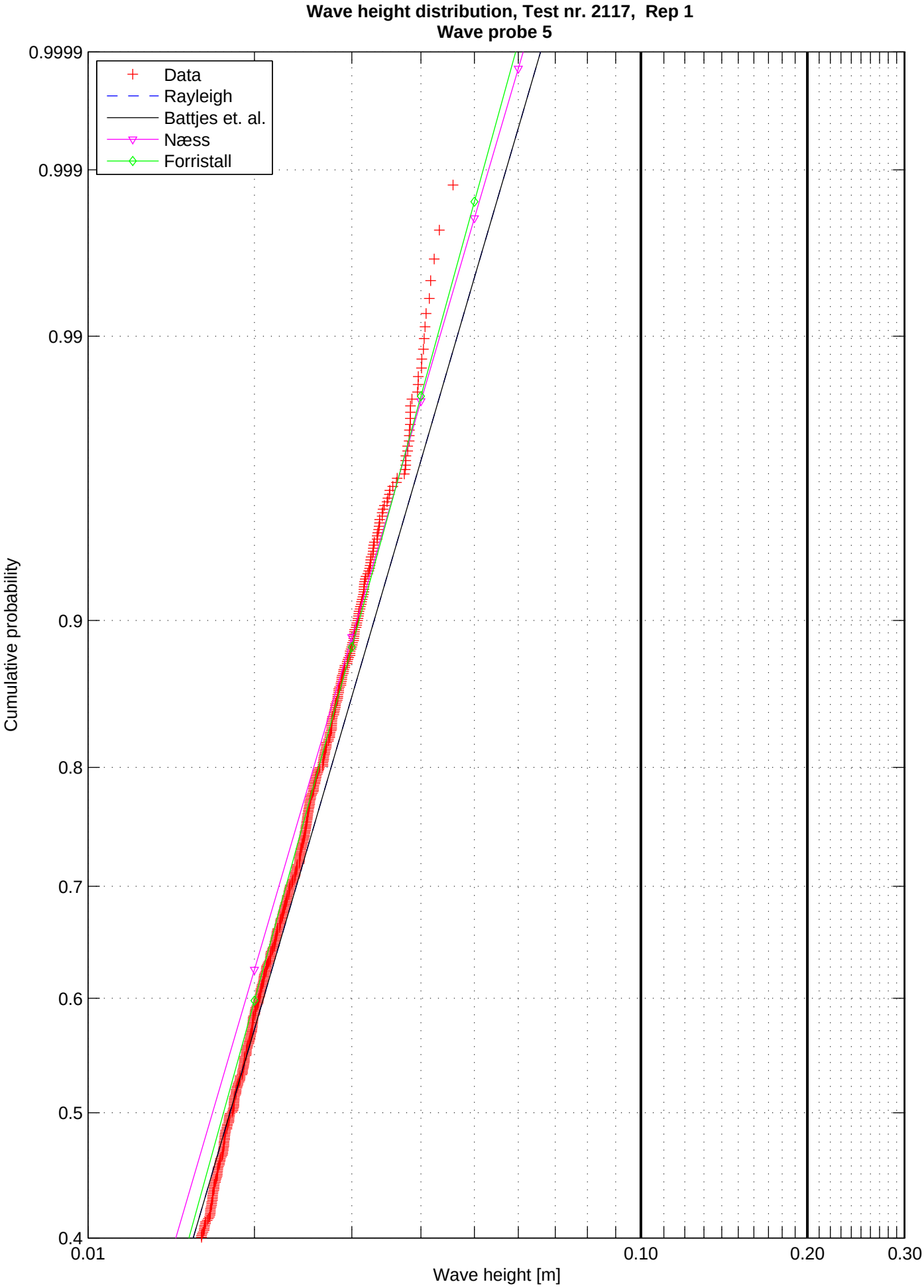
Wave height distribution, Test nr. 2117, Rep 1
Wave probe 5
Data
Rayleigh
Battjes et. al.
Næss
Forristall
Cumulative probability
0.9999
0.999
0.99
0.9
0.8
0.7
0.6
0.5
0.4
0.01
0.10
0.20
0.30
Wave height [m]

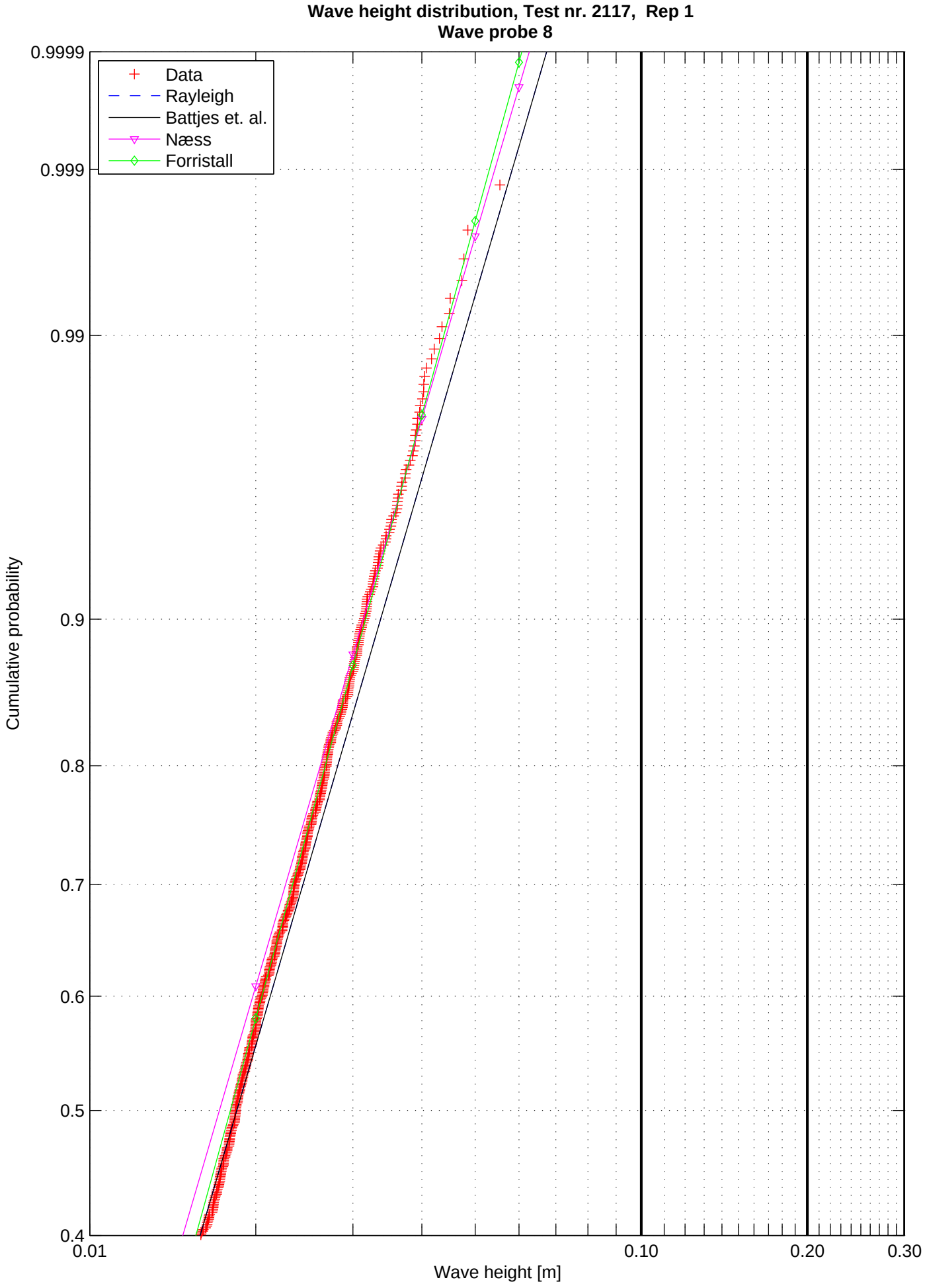
Wave height distribution, Test nr. 2117, Rep 1
Wave probe 8
Data
Rayleigh
Battjes et. al.
Næss
Forristall
Cumulative probability
0.9999
0.999
0.99
0.9
0.8
0.7
0.6
0.5
0.4
0.01
0.10
0.20
0.30
Wave height [m]

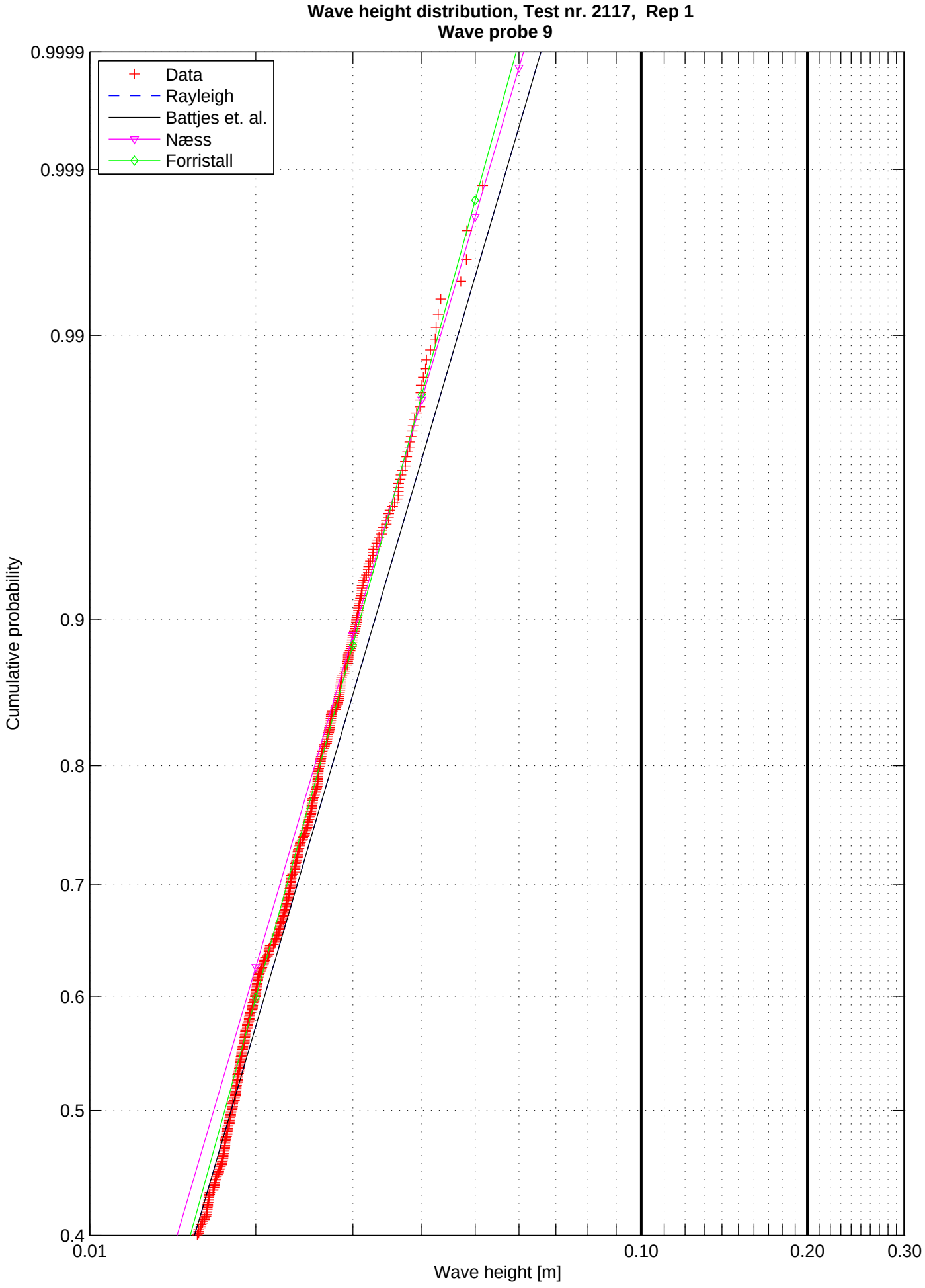
Wave height distribution, Test nr. 2117, Rep 1
Wave probe 9
Data
Rayleigh
Battjes et. al.
Næss
Forristall
Cumulative probability
0.9999
0.999
0.99
0.9
0.8
0.7
0.6
0.5
0.4
0.01
0.10
0.20
0.30
Wave height [m]

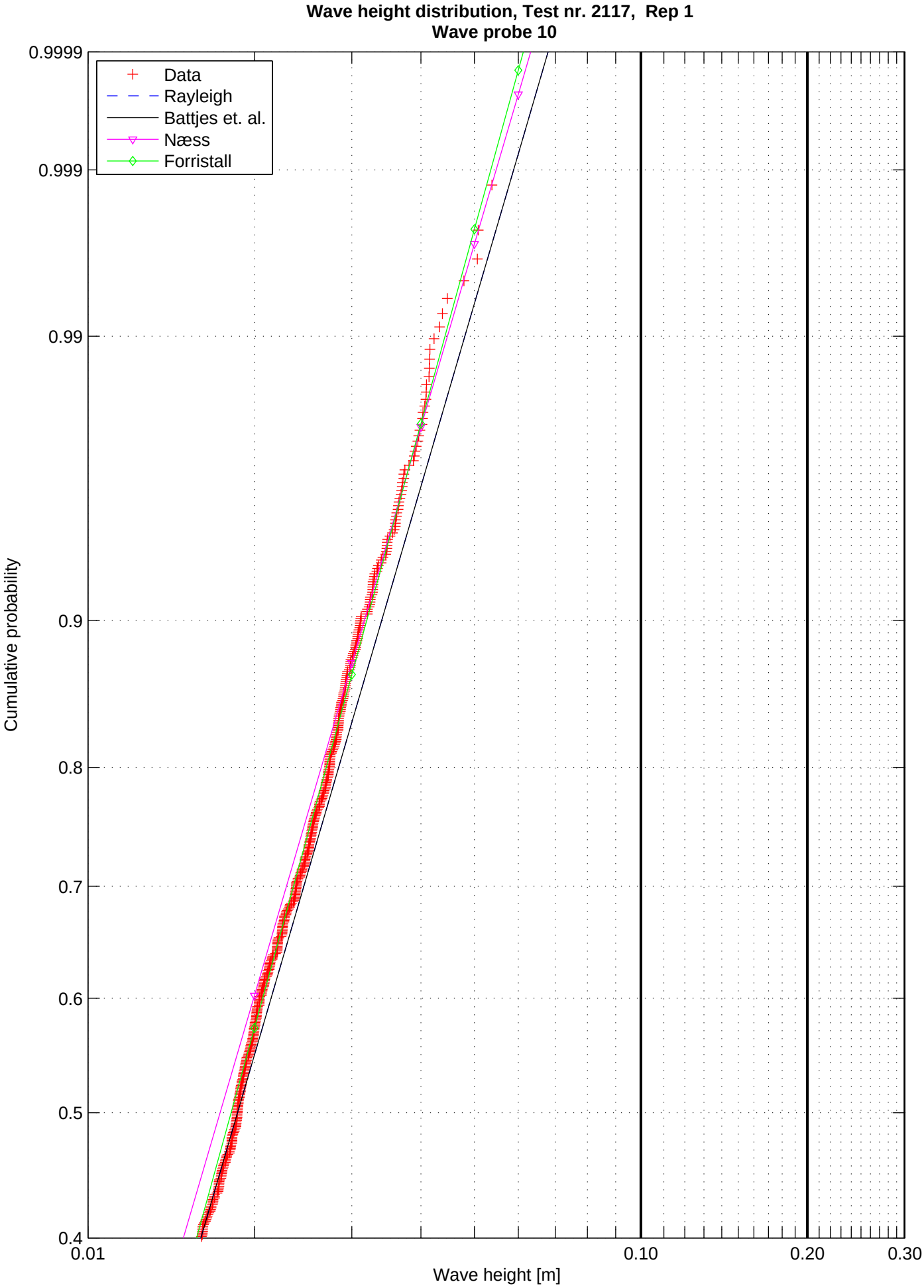
Wave height distribution, Test nr. 2117, Rep 1
Wave probe 10
Data
Rayleigh
Battjes et. al.
Næss
Forristall
0.9999
0.999
0.99
0.9
0.8
0.7
0.6
0.5
0.4
Cumulative probability
0.01
0.10
0.20
0.30
Wave height [m]

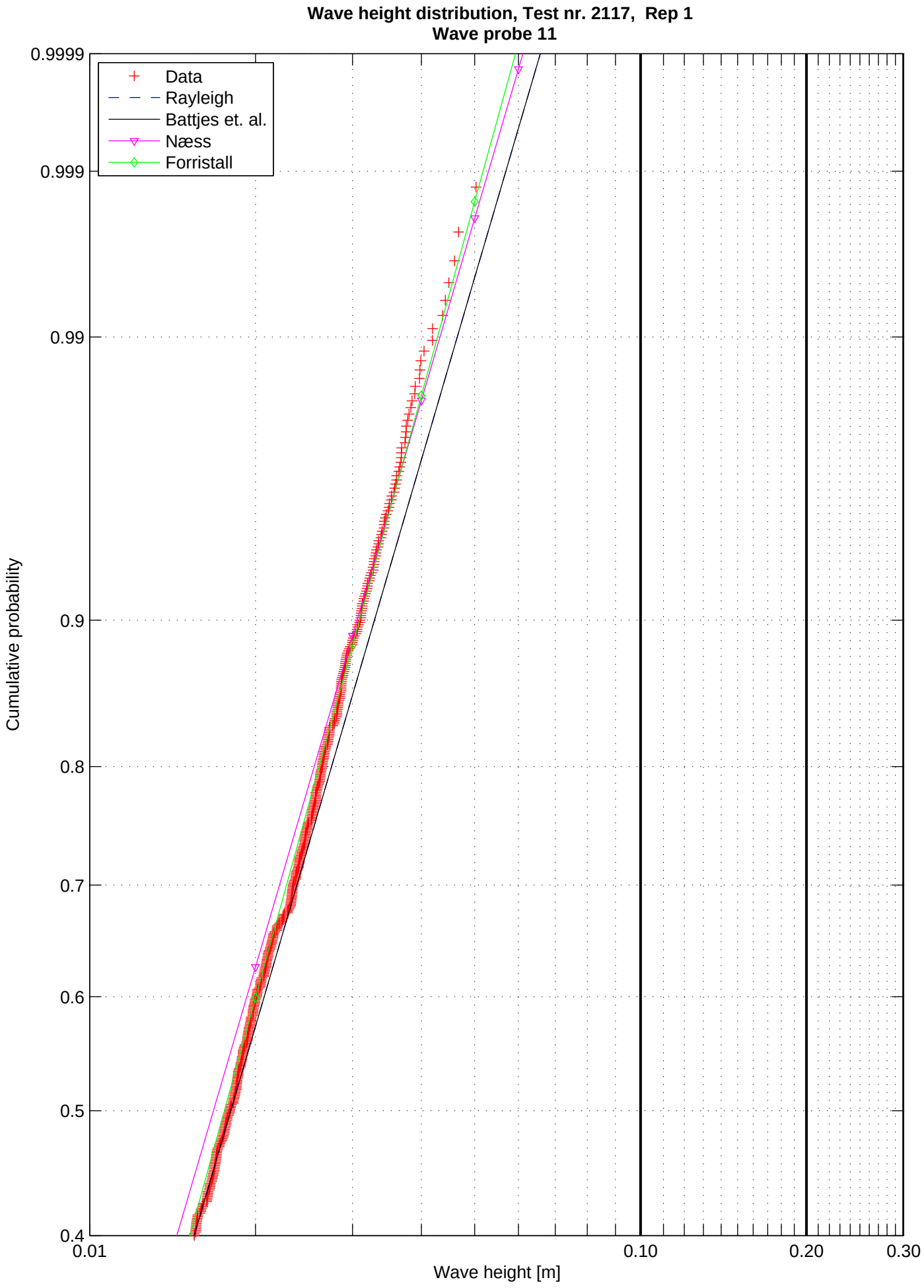
Wave height distribution, Test nr. 2117, Rep 1
Wave probe 11
Data
Rayleigh
Battjes et. al.
Næss
Forristall
Cumulative probability
0.9999
0.999
0.99
0.9
0.8
0.7
0.6
0.5
0.4
0.01
0.10
0.20
0.30
Wave height [m]

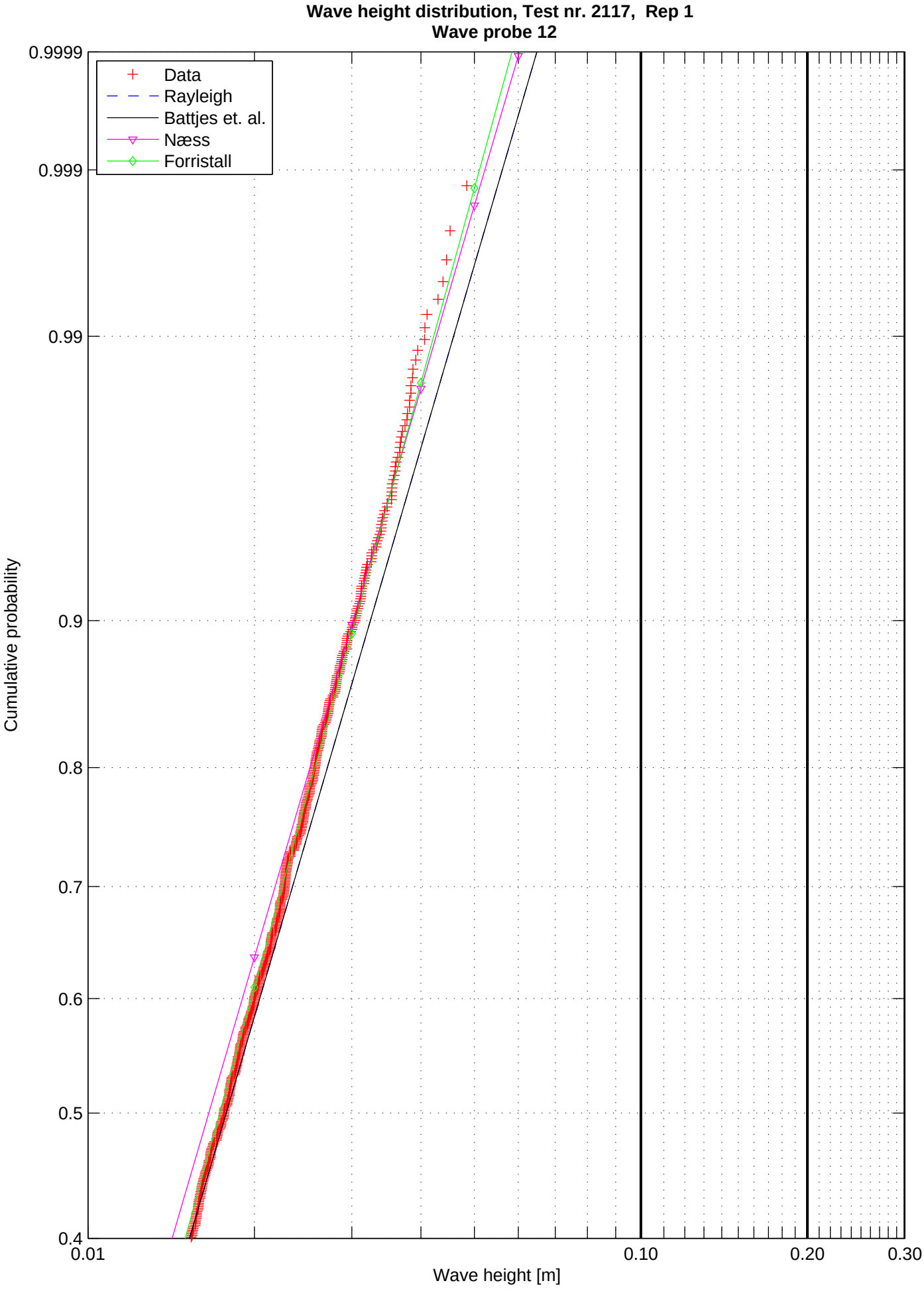
Wave height distribution, Test nr. 2117, Rep 1
Wave probe 12
Data
Rayleigh
Battjes et. al.
Næss
Forristall
Cumulative probability
0.9999
0.999
0.99
0.9
0.8
0.7
0.6
0.5
0.4
0.01
0.10
0.20
0.30
Wave height [m]

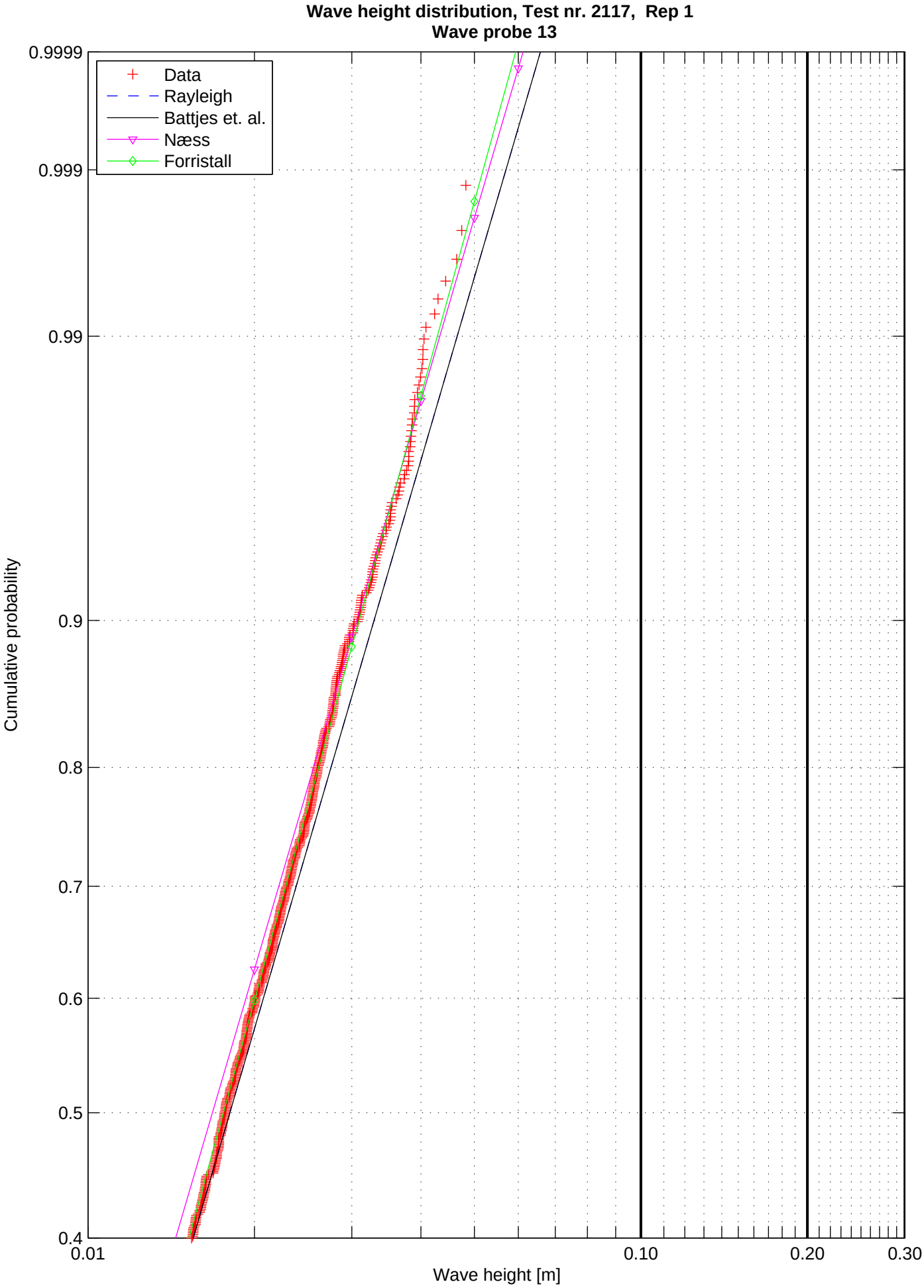
Wave height distribution, Test nr. 2117, Rep 1
Wave probe 13
Data
Rayleigh
Battjes et. al.
Næss
Forristall
Cumulative probability
0.9999
0.999
0.99
0.9
0.8
0.7
0.6
0.5
0.4
0.01
0.10
0.20
0.30
Wave height [m]

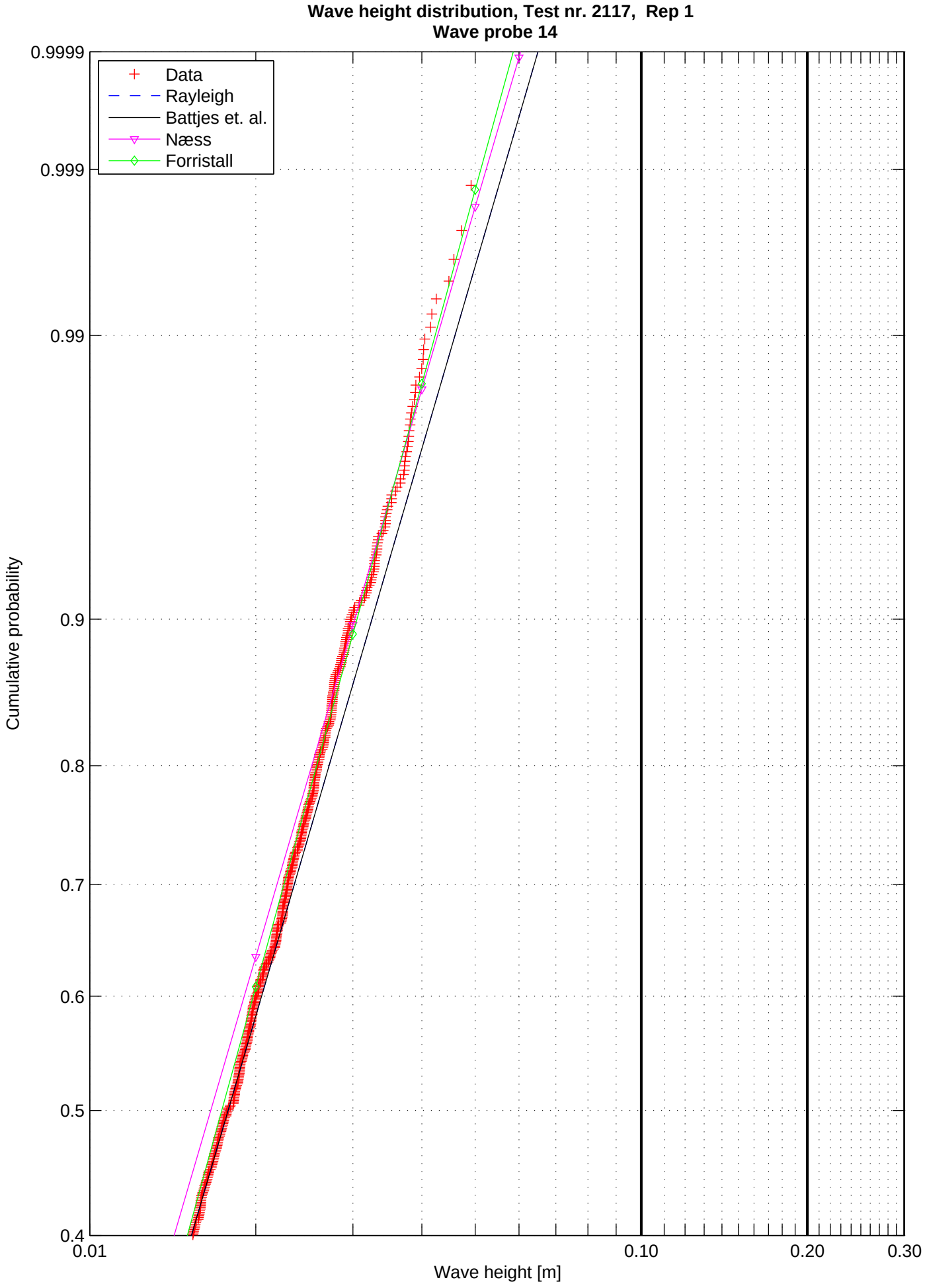
Wave height distribution, Test nr. 2117, Rep 1
Wave probe 14
Data
Rayleigh
Battjes et. al.
Næss
Forristall
0.9999
0.999
0.99
0.9
0.8
0.7
0.6
0.5
0.4
Cumulative probability
0.01
0.10
0.20
0.30
Wave height [m]

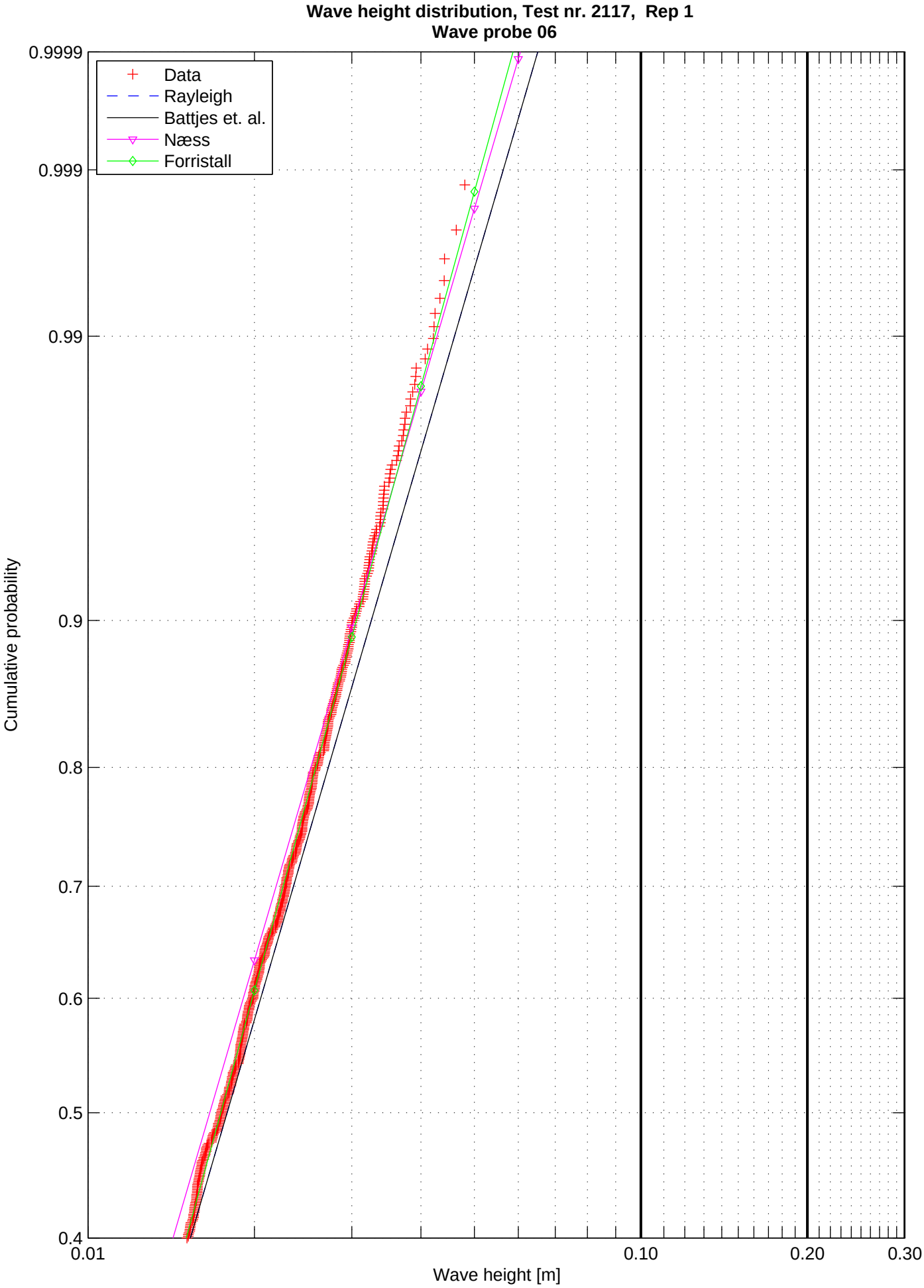
Wave height distribution, Test nr. 2117, Rep 1
Wave probe 06
Data
Rayleigh
Battjes et. al.
Næss
Forristall
Cumulative probability
0.9999
0.999
0.99
0.9
0.8
0.7
0.6
0.5
0.4
0.01
0.10
0.20
0.30
Wave height [m]

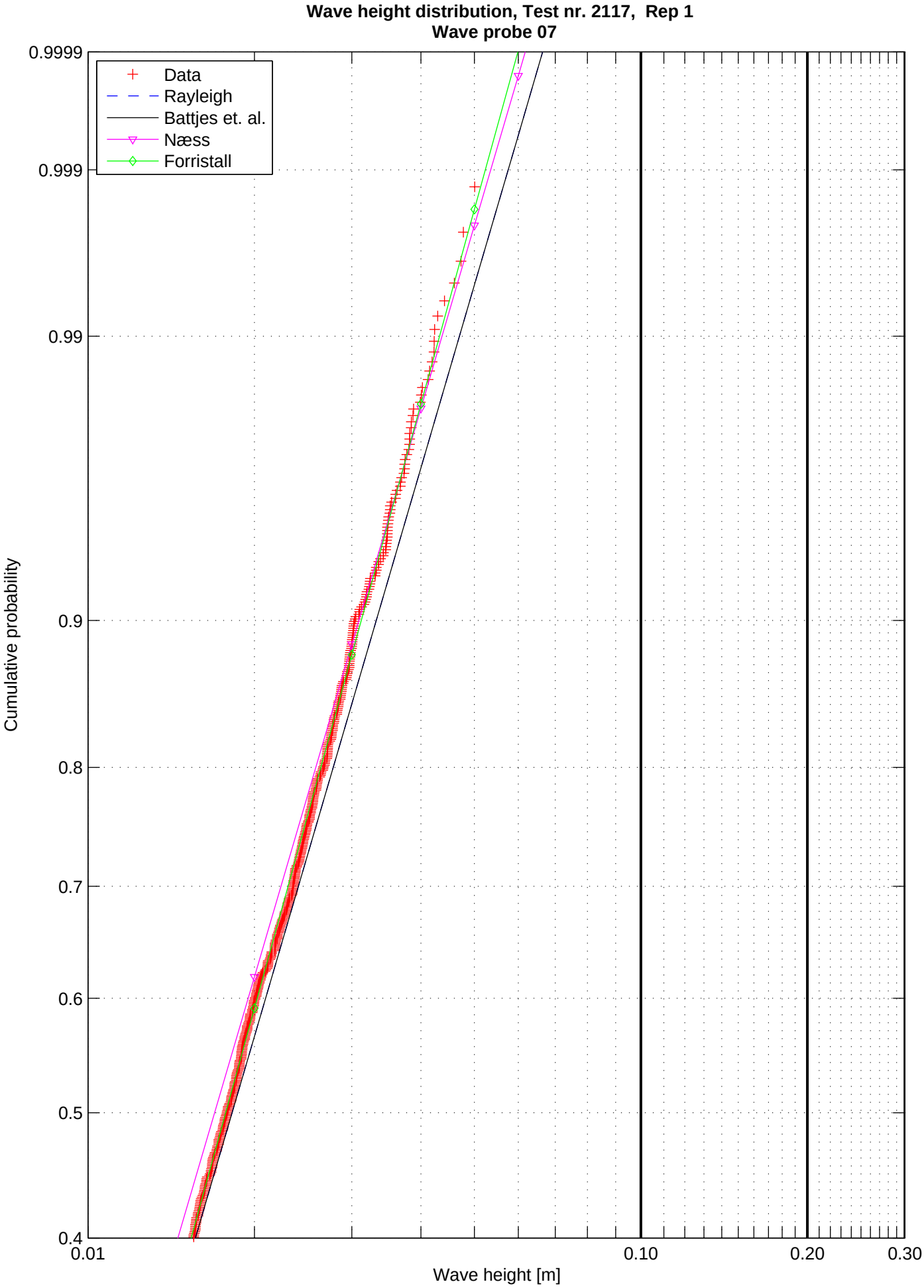
Wave height distribution, Test nr. 2117, Rep 1
Wave probe 07
Data
Rayleigh
Battjes et. al.
Næss
Forristall
Cumulative probability
0.9999
0.999
0.99
0.9
0.8
0.7
0.6
0.5
0.4
0.01
0.10
0.20
0.30
Wave height [m]

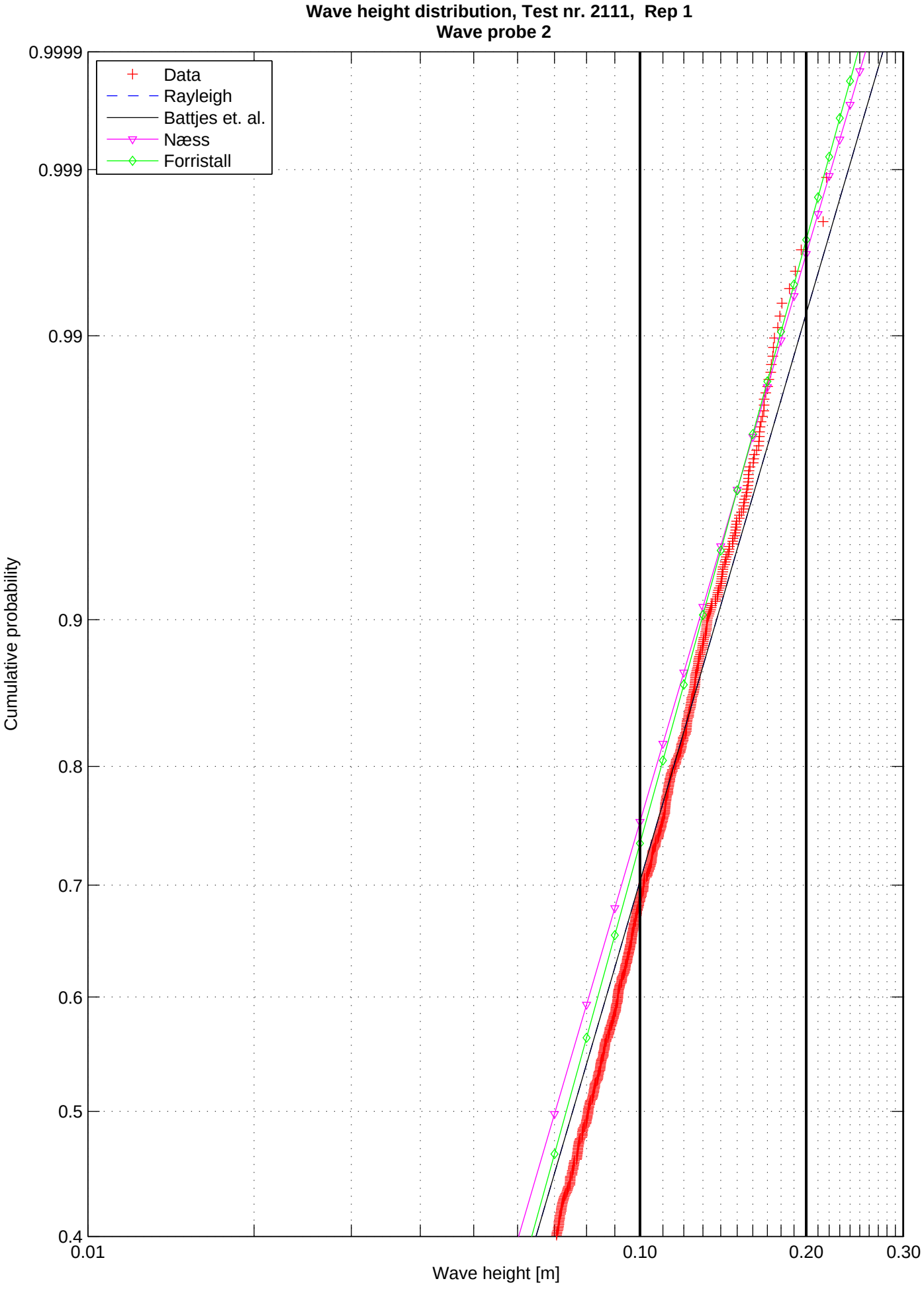
Wave height distribution, Test nr. 2111, Rep 1
Wave probe 2
Data
Rayleigh
Battjes et. al.
Næss
Forristall
Cumulative probability
0.9999
0.999
0.99
0.9
0.8
0.7
0.6
0.5
0.4
0.01
0.10
0.20
0.30
Wave height [m]

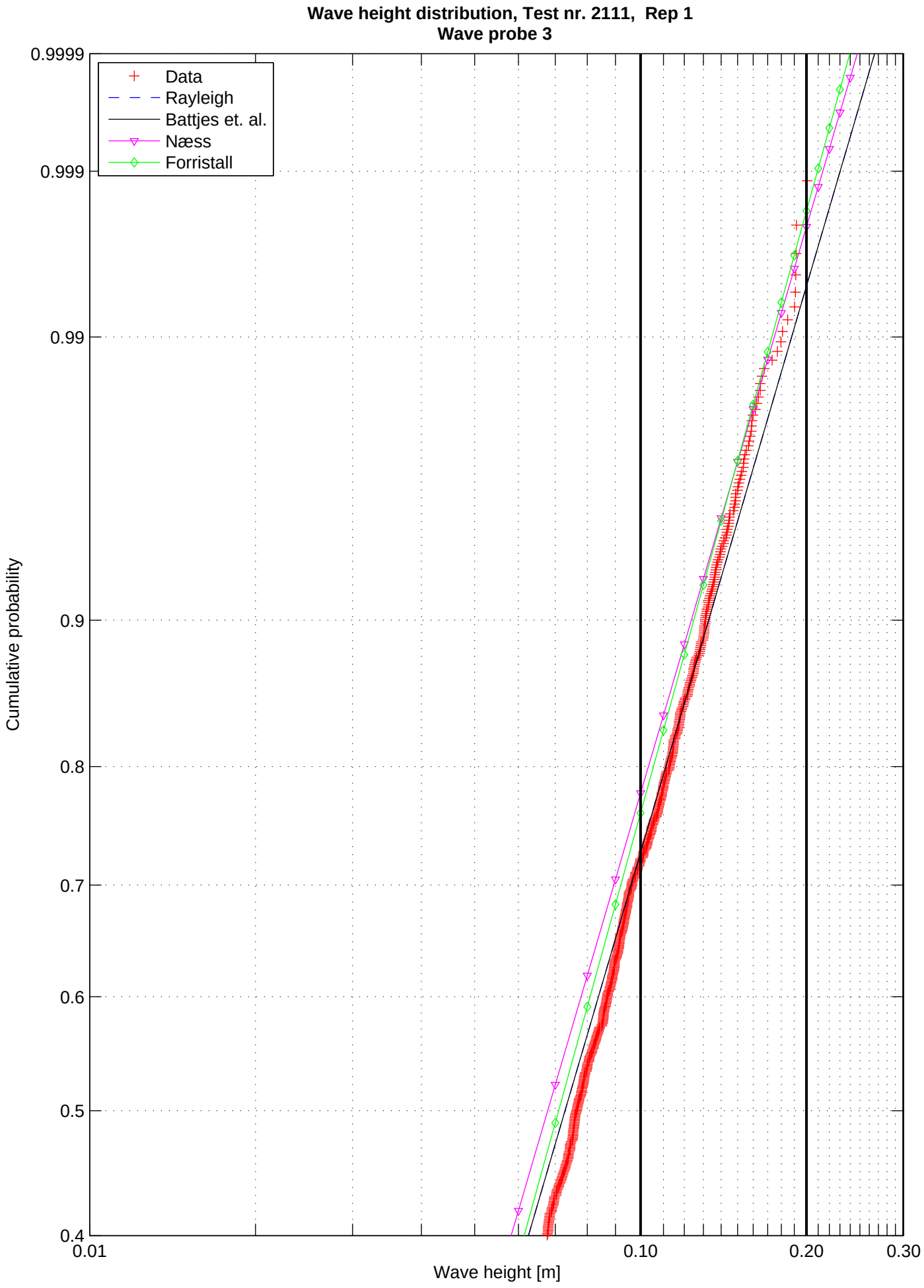
Wave height distribution, Test nr. 2111, Rep 1
Wave probe 3
Data
Rayleigh
Battjes et. al.
Næss
Forristall
Cumulative probability
0.9999
0.999
0.99
0.9
0.8
0.7
0.6
0.5
0.4
0.01
0.10
0.20
0.30
Wave height [m]

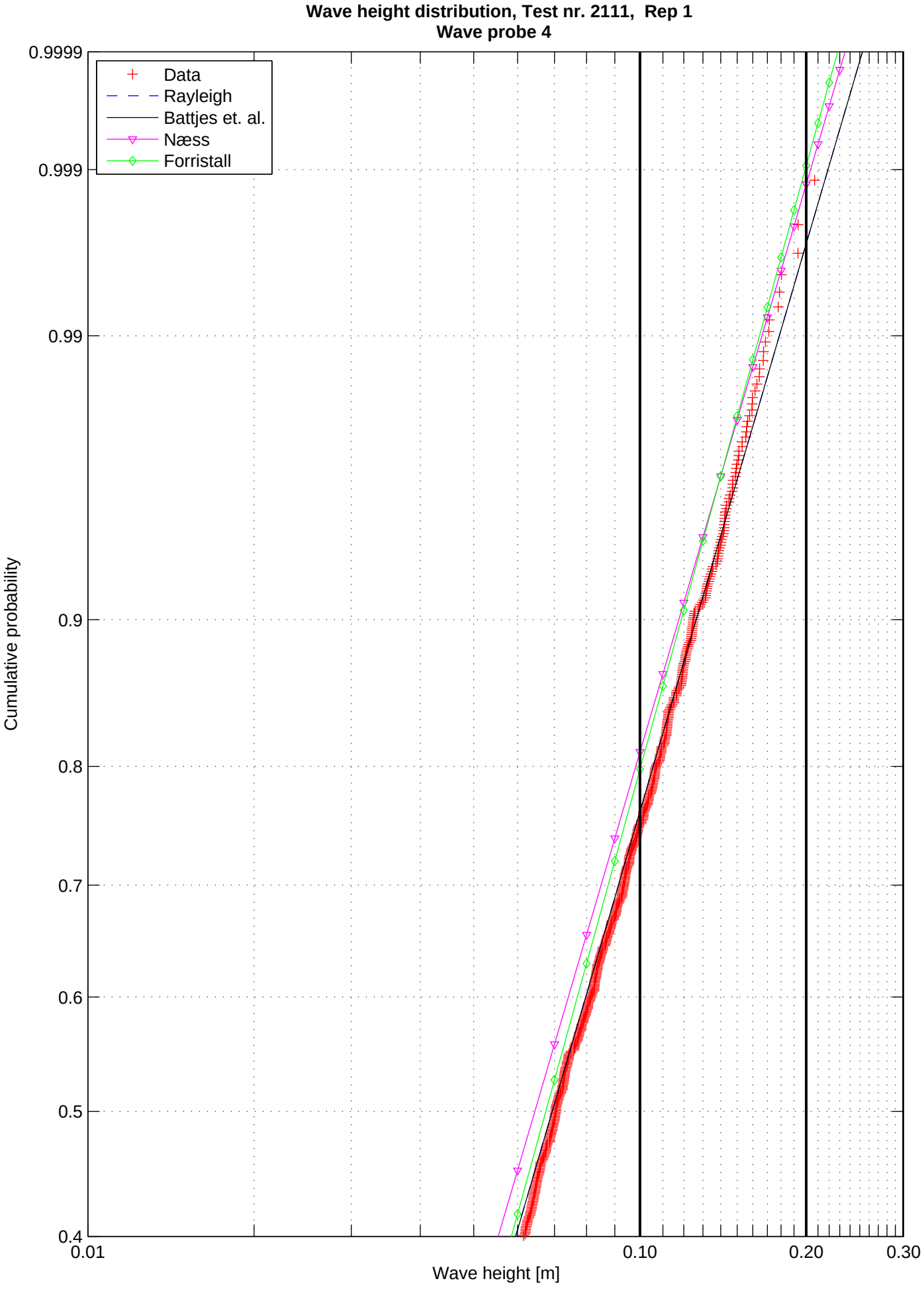
Wave height distribution, Test nr. 2111, Rep 1
Wave probe 4
Data
Rayleigh
Battjes et. al.
Næss
Forristall
0.9999
0.999
0.99
0.9
0.8
0.7
0.6
0.5
0.4
Cumulative probability
0.01
0.10
0.20
0.30
Wave height [m]

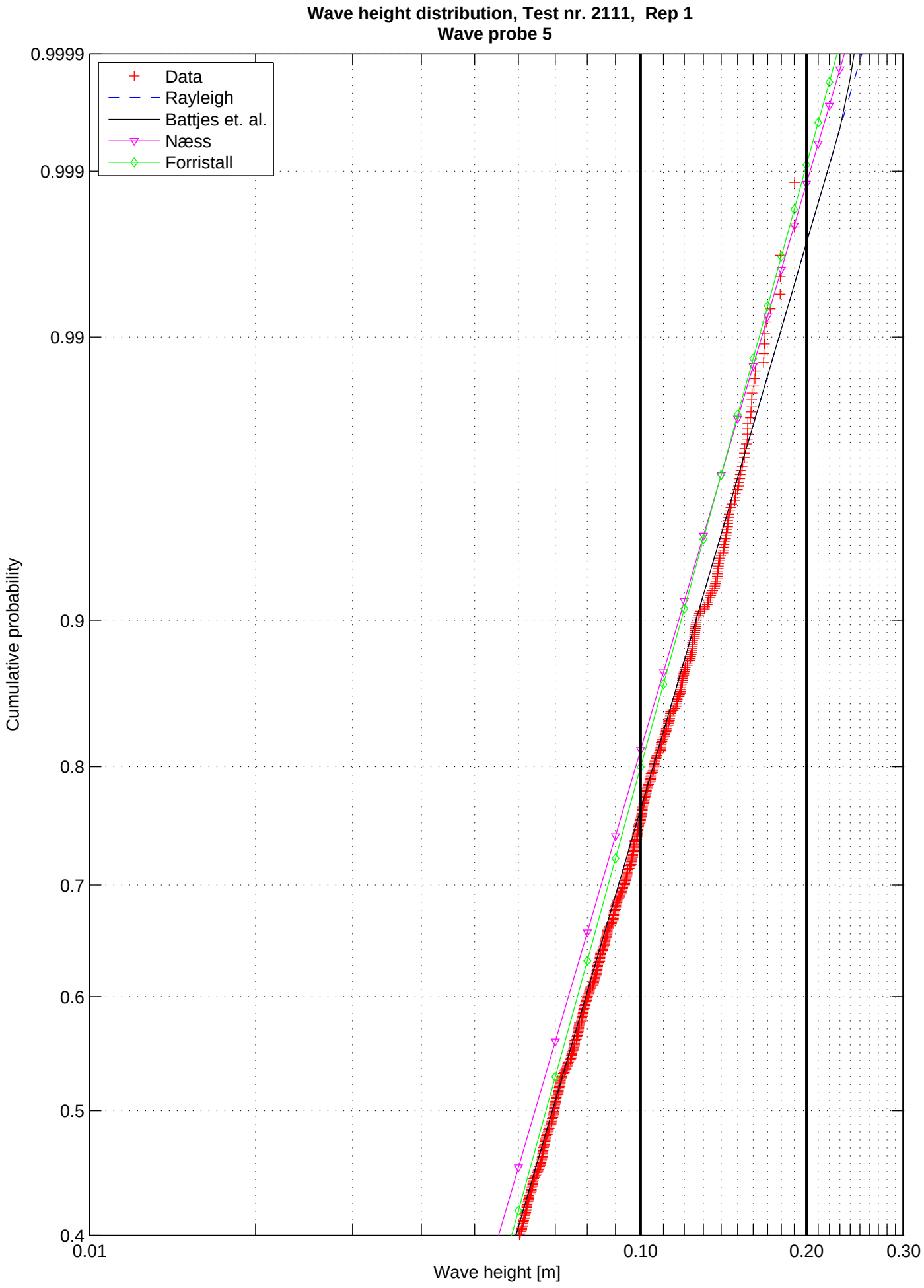
Wave height distribution, Test nr. 2111, Rep 1
Wave probe 5
Data
Rayleigh
Battjes et. al.
Næss
Forristall
Cumulative probability
0.9999
0.999
0.99
0.9
0.8
0.7
0.6
0.5
0.4
0.01
0.10
0.20
0.30
Wave height [m]

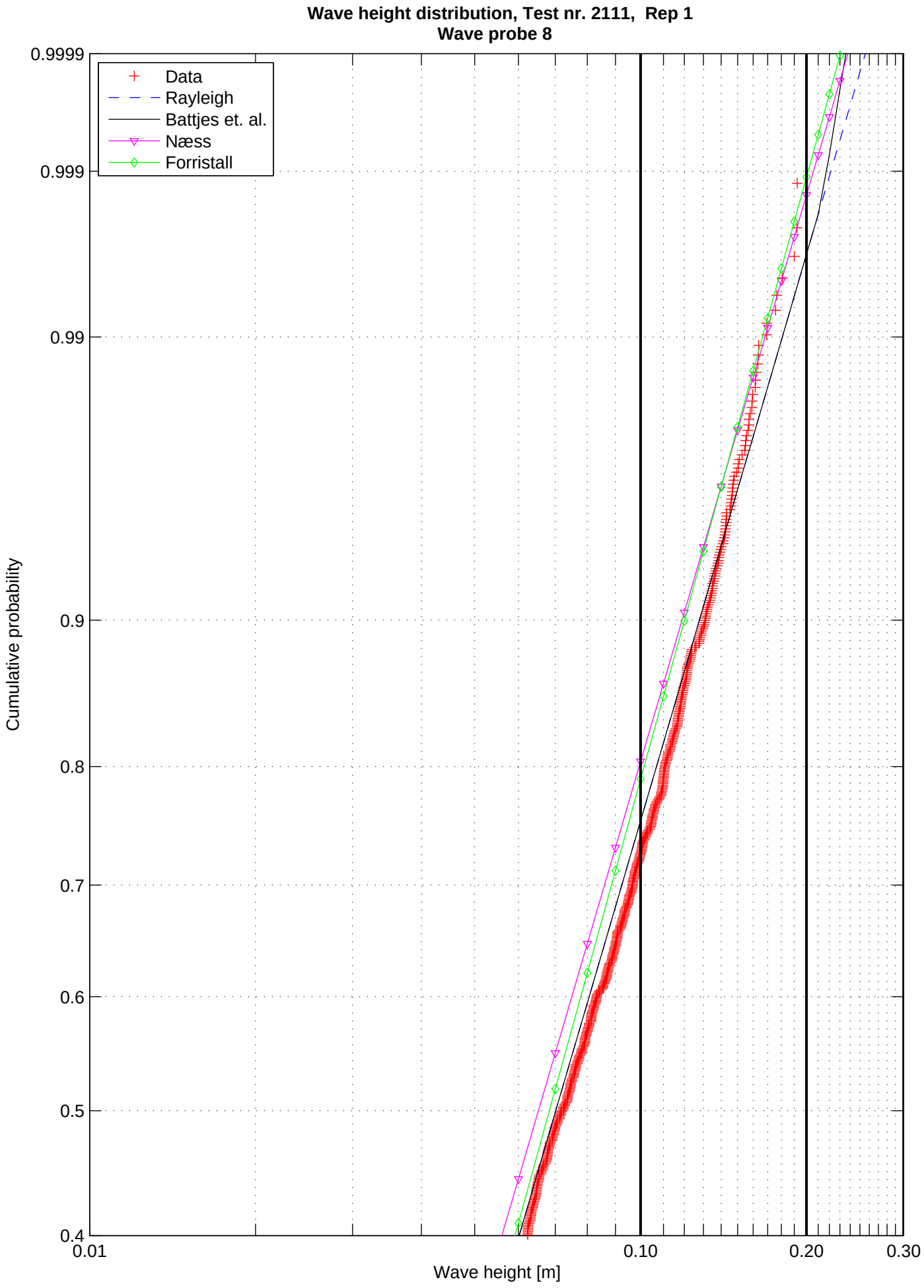
Wave height distribution, Test nr. 2111, Rep 1
Wave probe 8
Data
Rayleigh
Battjes et. al.
Næss
Forristall
Cumulative probability
0.9999
0.999
0.99
0.9
0.8
0.7
0.6
0.5
0.4
0.01
0.10
0.20
0.30
Wave height [m]

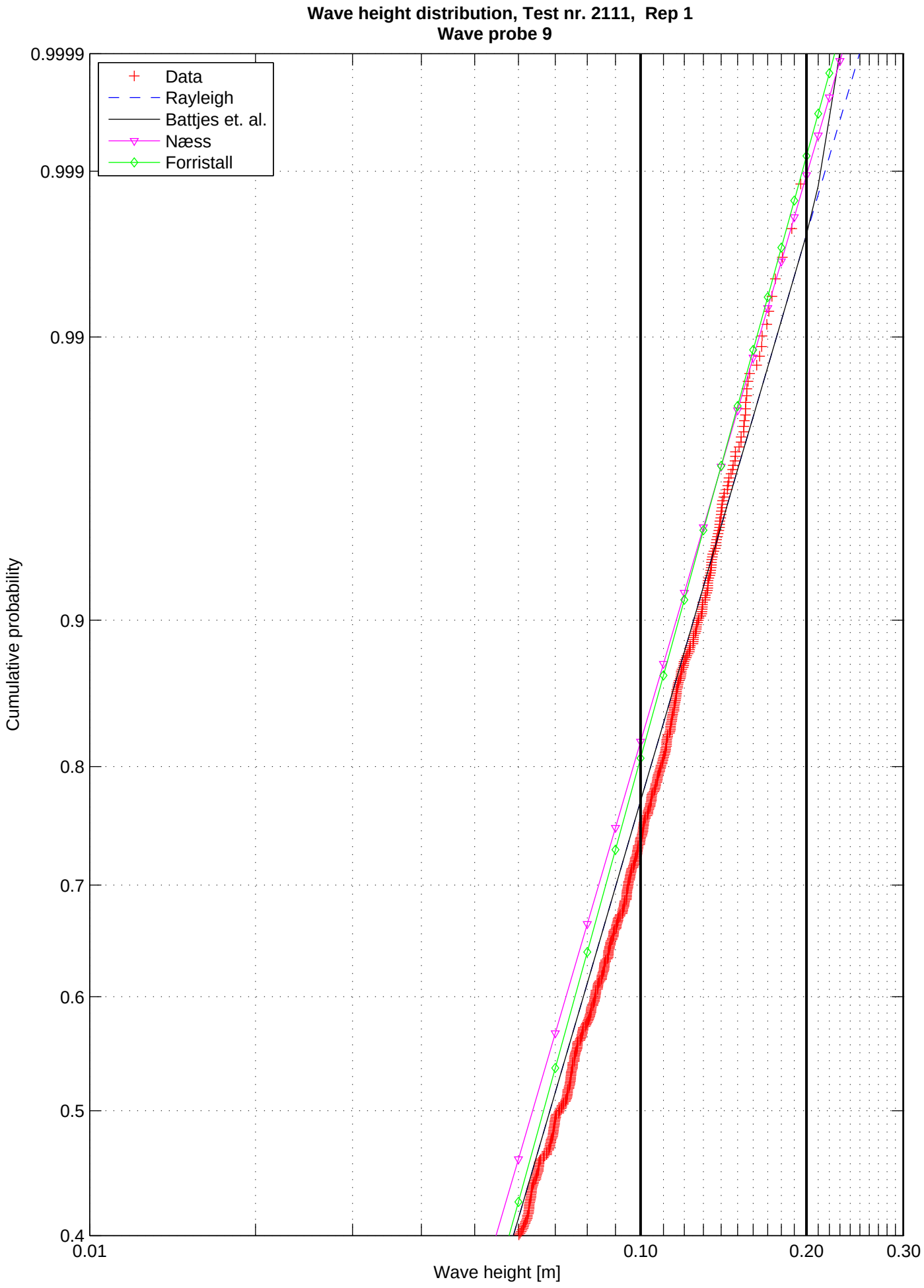
Wave height distribution, Test nr. 2111, Rep 1
Wave probe 9
Data
Rayleigh
Battjes et. al.
Næss
Forristall
Cumulative probability
0.9999
0.999
0.99
0.9
0.8
0.7
0.6
0.5
0.4
0.01
0.10
0.20
0.30
Wave height [m]

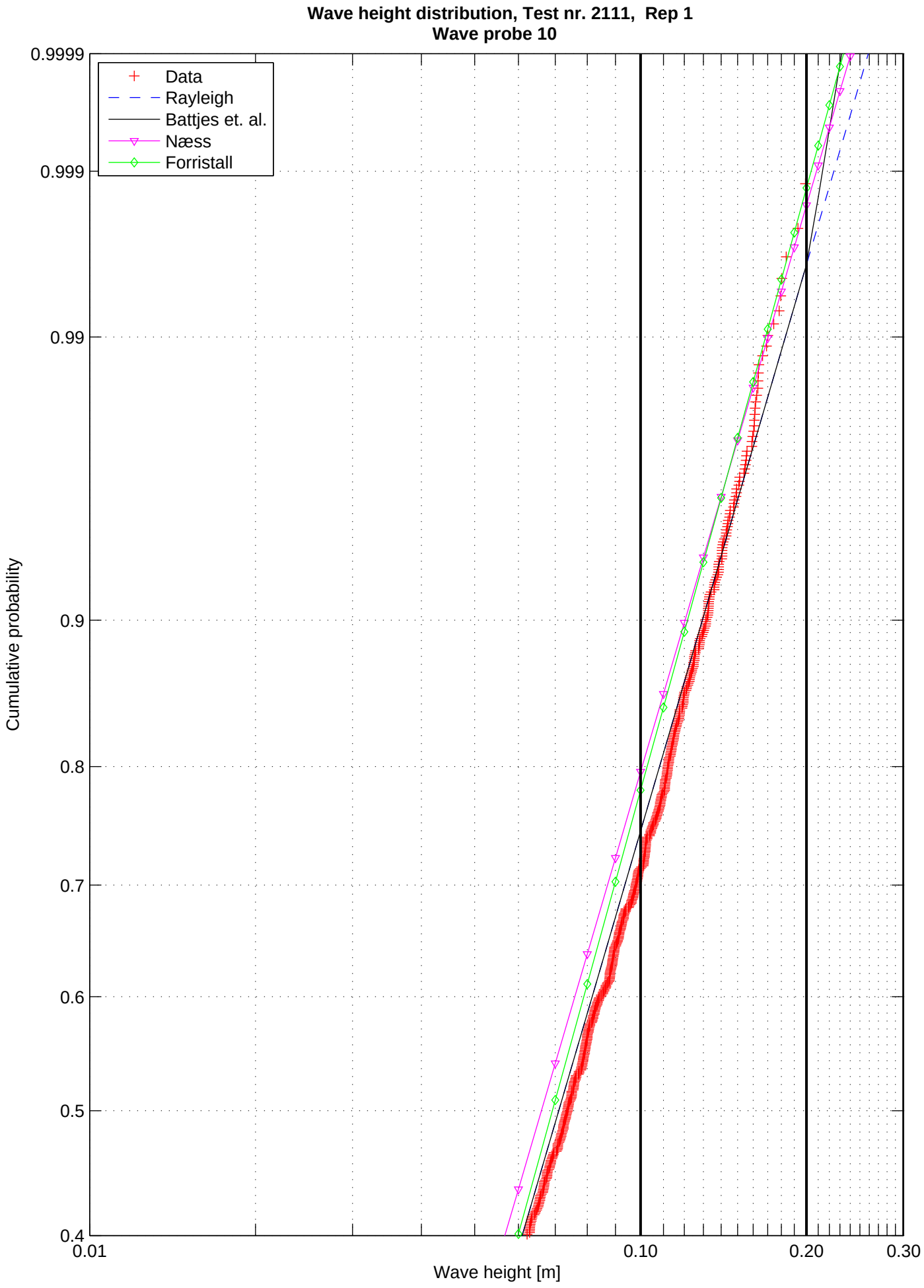
Wave height distribution, Test nr. 2111, Rep 1
Wave probe 10
Data
Rayleigh
Battjes et. al.
Næss
Forristall
Cumulative probability
0.9999
0.999
0.99
0.9
0.8
0.7
0.6
0.5
0.4
0.01
0.10
0.20
0.30
Wave height [m]

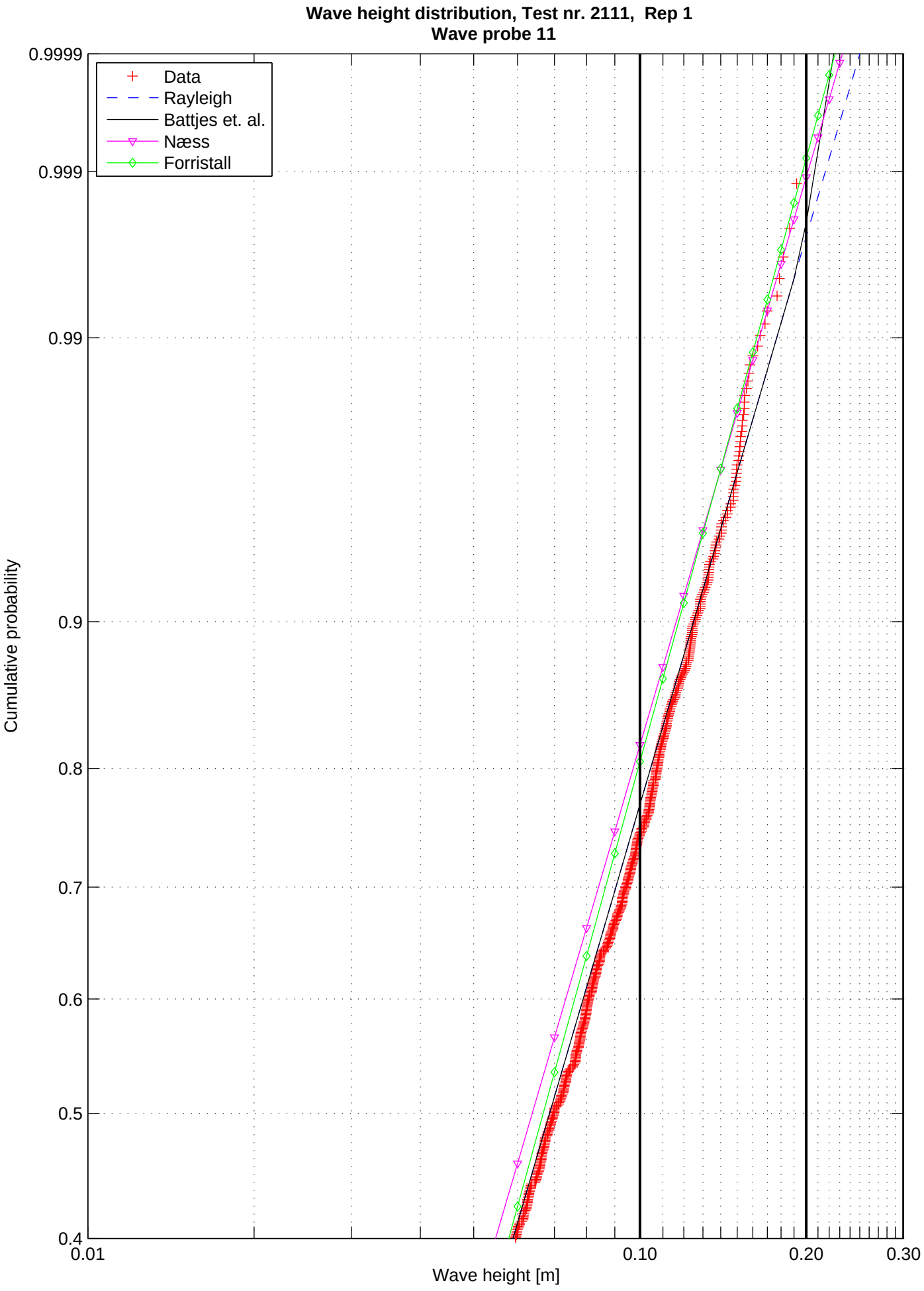
Wave height distribution, Test nr. 2111, Rep 1
Wave probe 11
Data
Rayleigh
Battjes et. al.
Næss
Forristall
0.9999
0.999
0.99
0.9
0.8
0.7
0.6
0.5
0.4
Cumulative probability
0.01
0.10
0.20
0.30
Wave height [m]

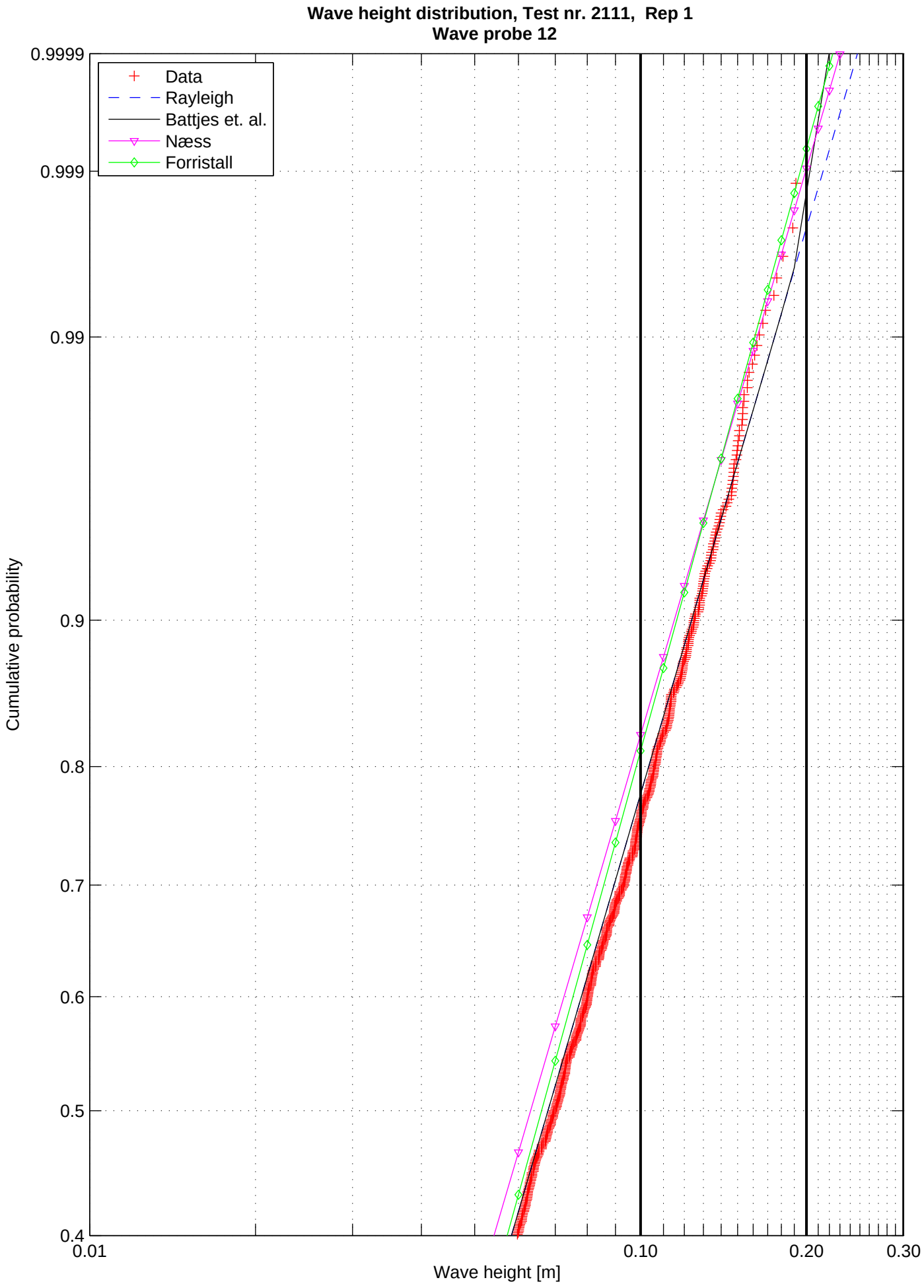
Wave height distribution, Test nr. 2111, Rep 1
Wave probe 12
Data
Rayleigh
Battjes et. al.
Næss
Forristall
0.9999
0.999
0.99
0.9
0.8
0.7
0.6
0.5
0.4
Cumulative probability
0.01
0.10
0.20
0.30
Wave height [m]

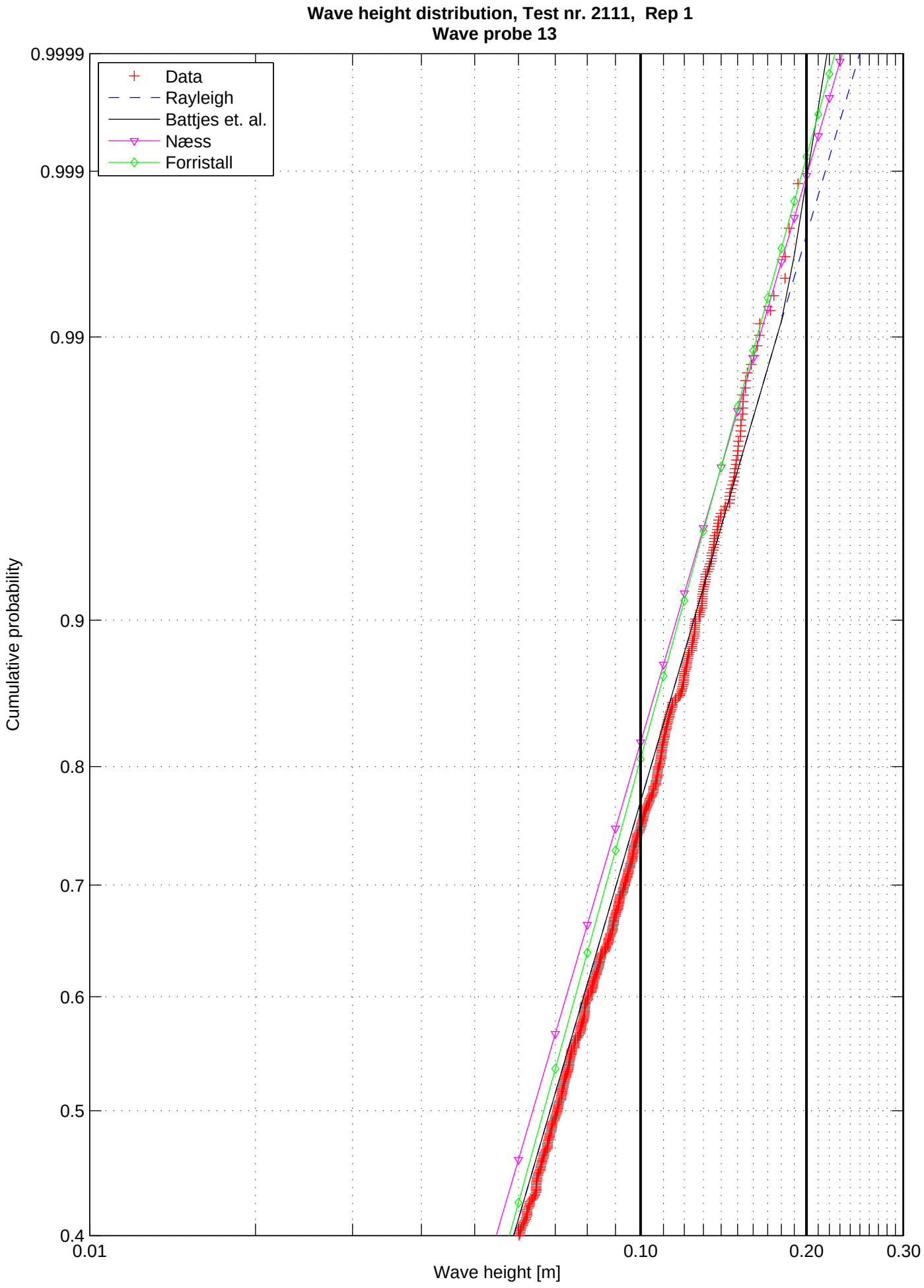
Wave height distribution, Test nr. 2111, Rep 1
Wave probe 13
Data
Rayleigh
Battjes et. al.
Næss
Forristall
0.9999
0.999
0.99
0.9
0.8
0.7
0.6
0.5
0.4
Cumulative probability
0.01
0.10
0.20
0.30
Wave height [m]

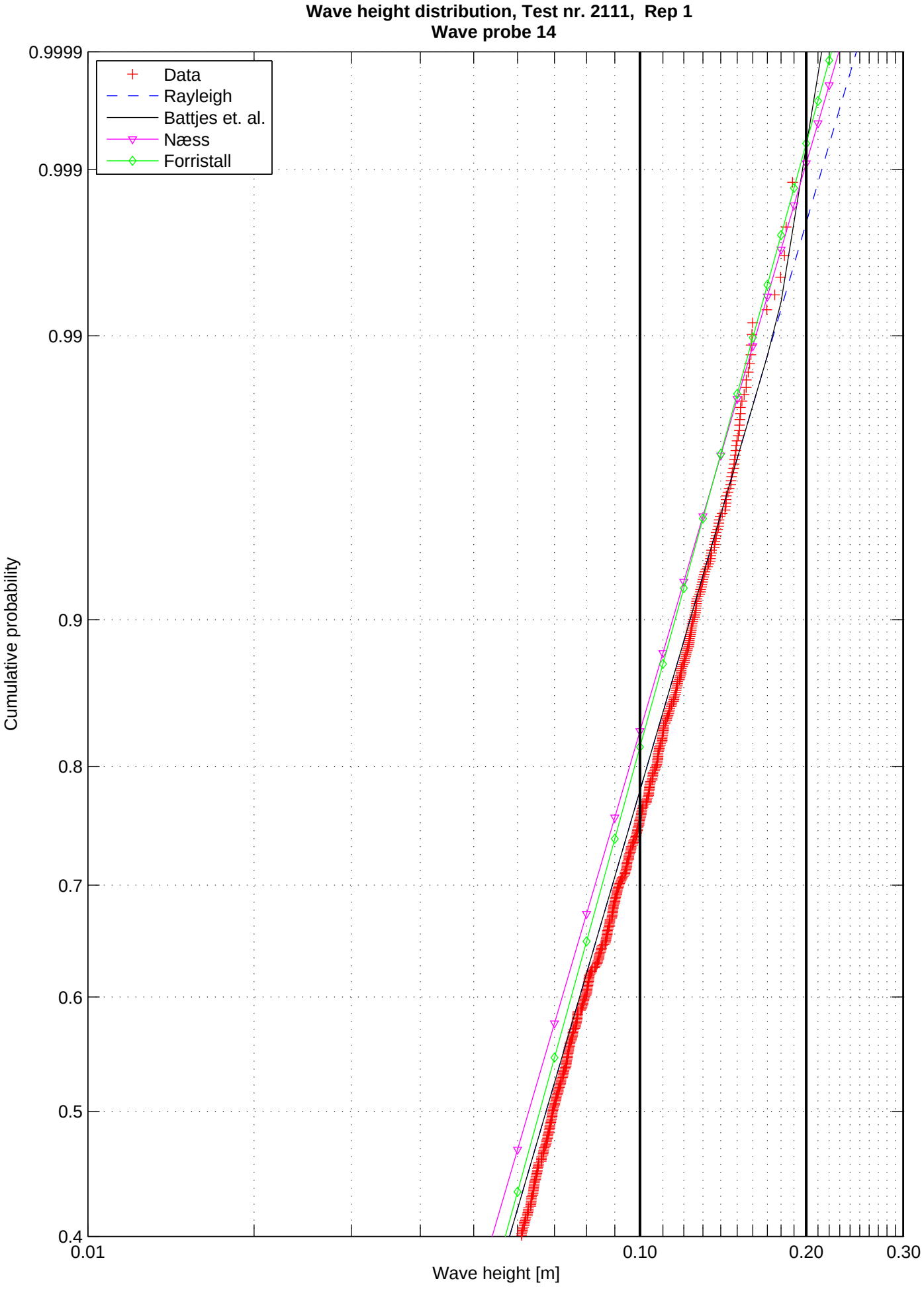
Wave height distribution, Test nr. 2111, Rep 1
Wave probe 14
Data
Rayleigh
Battjes et. al.
Næss
Forristall
Cumulative probability
0.9999
0.999
0.99
0.9
0.8
0.7
0.6
0.5
0.4
0.01
0.10
0.20
0.30
Wave height [m]

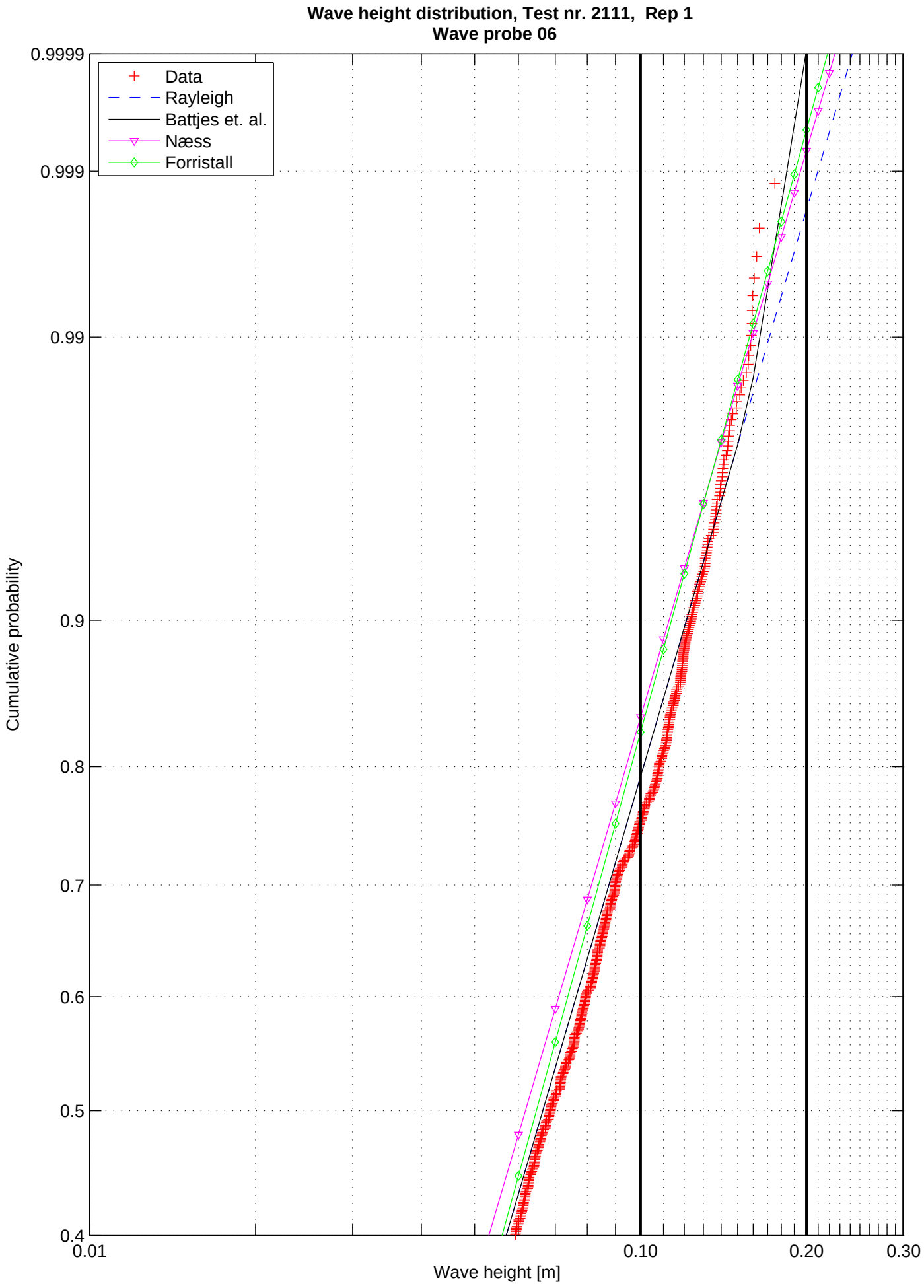
Wave height distribution, Test nr. 2111, Rep 1
Wave probe 06
Data
Rayleigh
Battjes et. al.
Næss
Forristall
0.9999
0.999
0.99
0.9
0.8
0.7
0.6
0.5
0.4
Cumulative probability
0.01
0.10
0.20
0.30
Wave height [m]

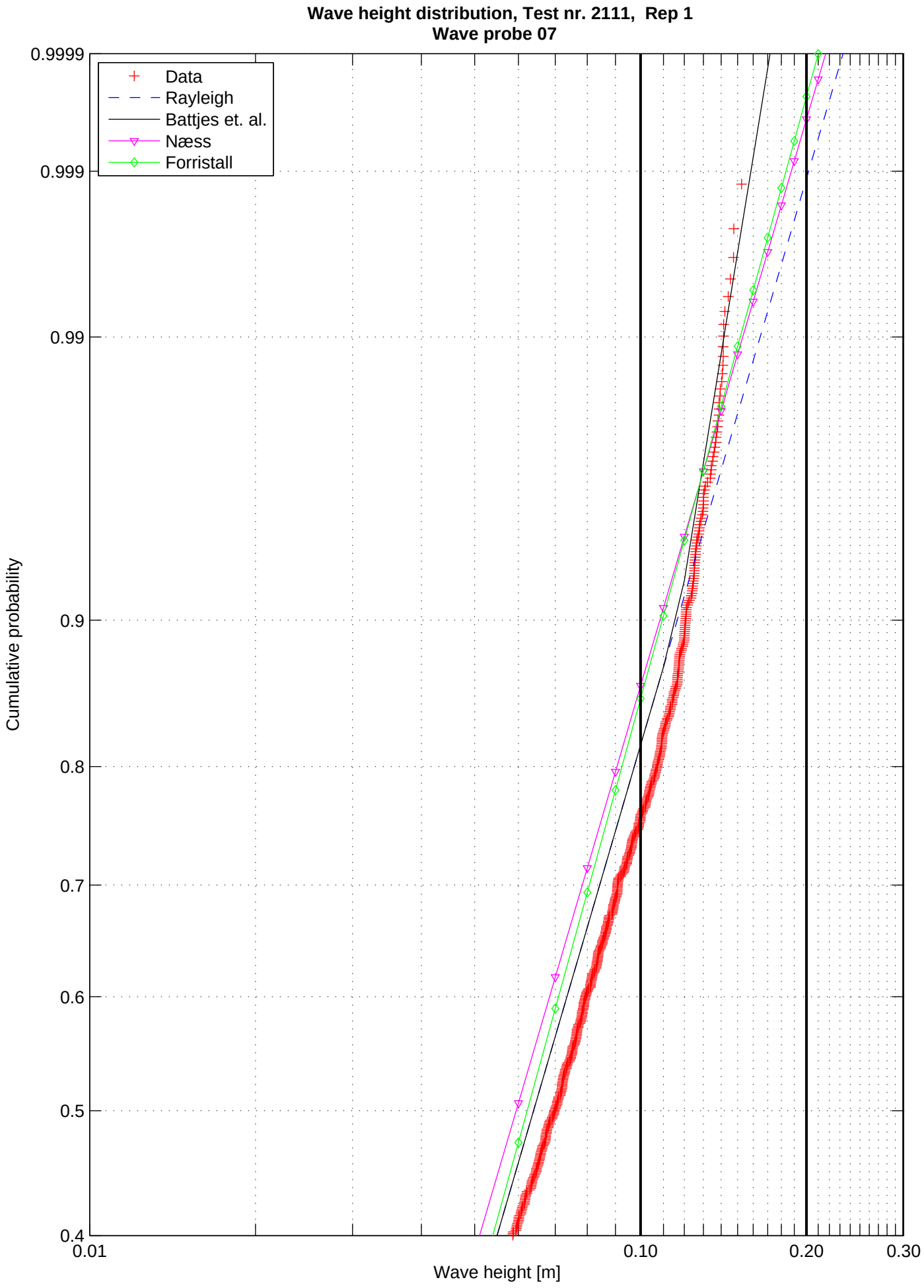
Wave height distribution, Test nr. 2111, Rep 1
Wave probe 07
Data
Rayleigh
Battjes et. al.
Næss
Forristall
0.9999
0.999
0.99
0.9
0.8
0.7
0.6
0.5
0.4
Cumulative probability
0.01
0.10
0.20
0.30
Wave height [m]

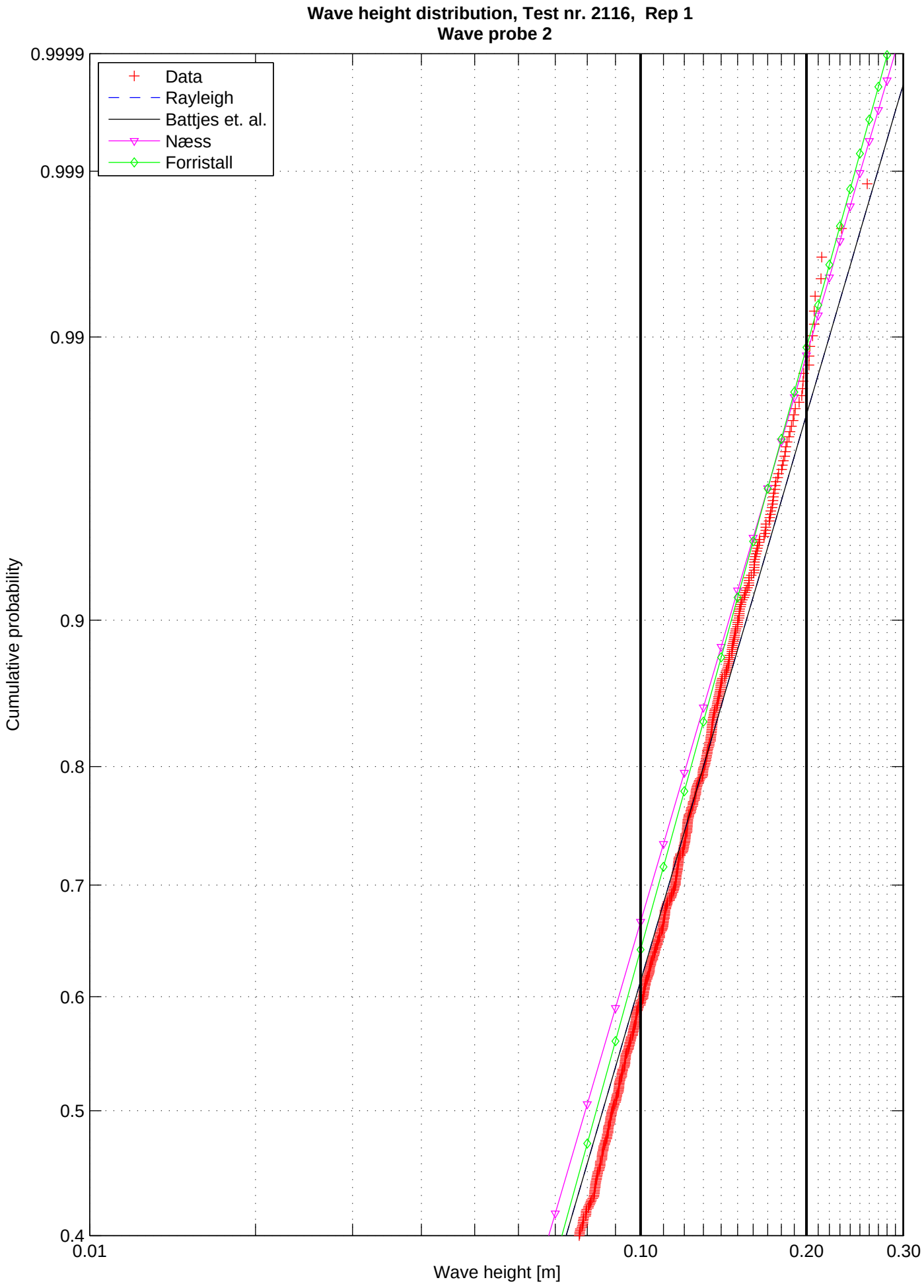
Wave height distribution, Test nr. 2116, Rep 1
Wave probe 2
Data
Rayleigh
Battjes et. al.
Næss
Forristall
Cumulative probability
0.9999
0.999
0.99
0.9
0.8
0.7
0.6
0.5
0.4
0.01
0.10
0.20
0.30
Wave height [m]

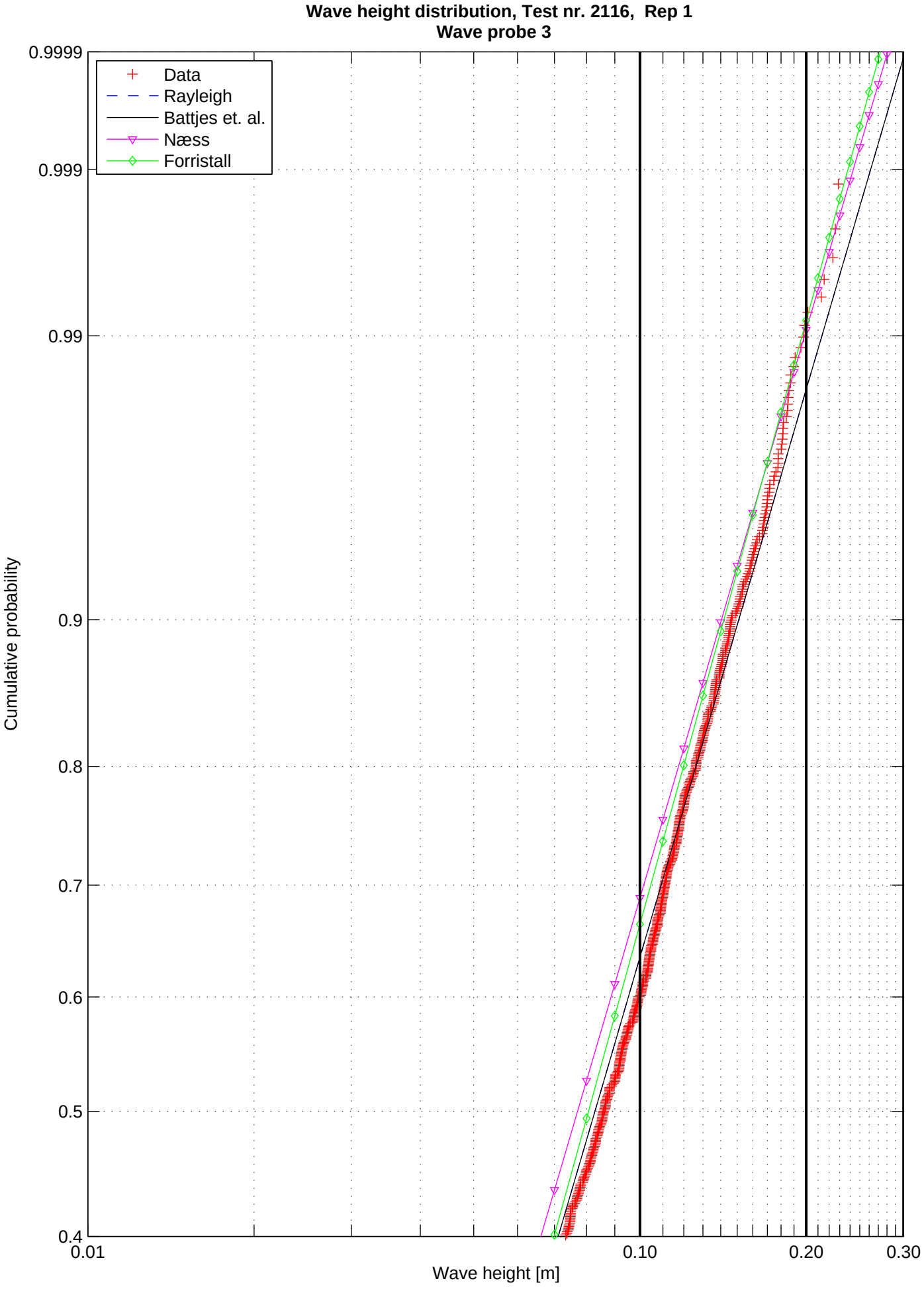
Wave height distribution, Test nr. 2116, Rep 1
Wave probe 3
Data
Rayleigh
Battjes et. al.
Næss
Forristall
Cumulative probability
0.9999
0.999
0.99
0.9
0.8
0.7
0.6
0.5
0.4
0.01
0.10
0.20
0.30
Wave height [m]

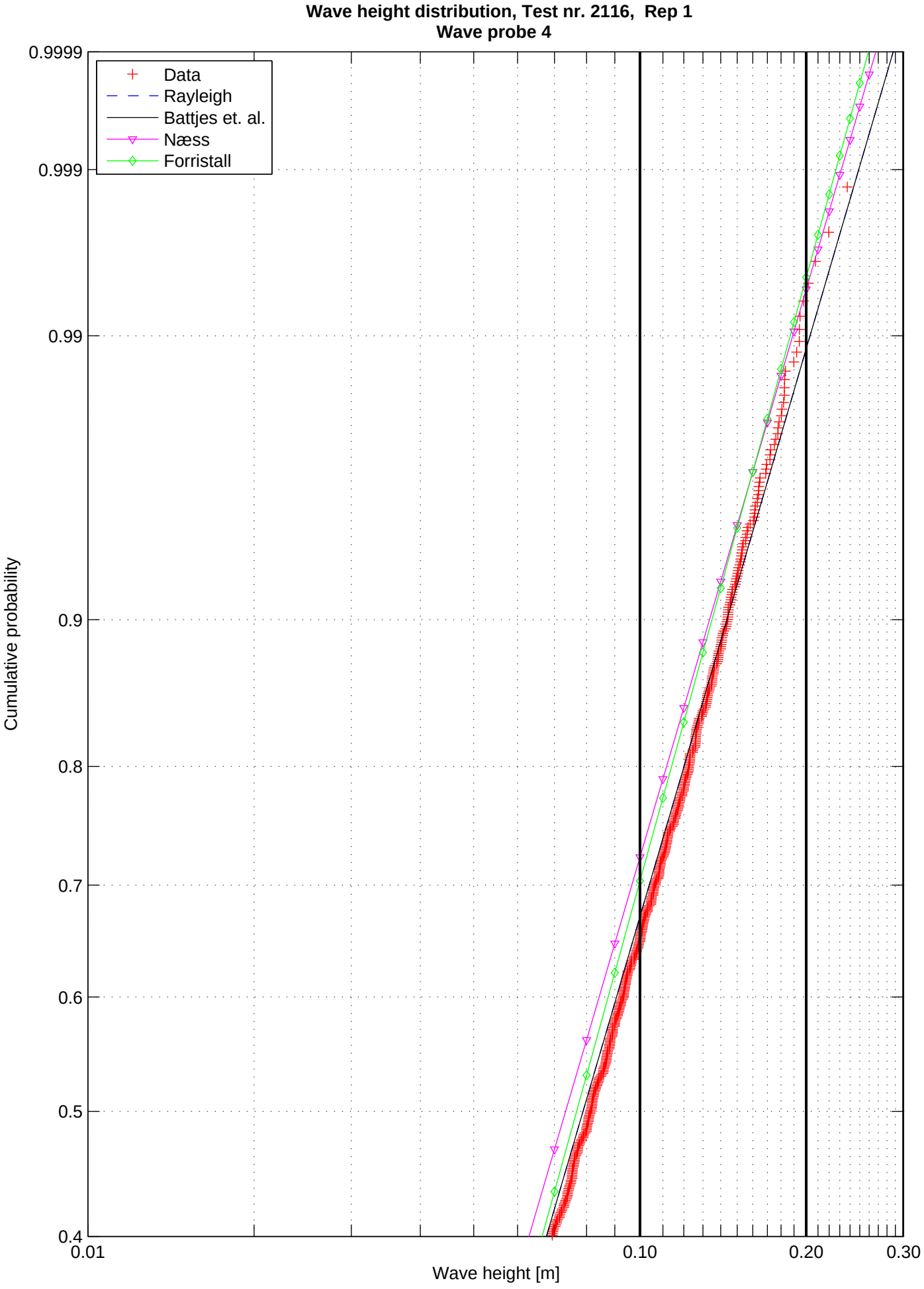
Wave height distribution, Test nr. 2116, Rep 1
Wave probe 4
Data
Rayleigh
Battjes et. al.
Næss
Forristall
Cumulative probability
0.9999
0.999
0.99
0.9
0.8
0.7
0.6
0.5
0.4
0.01
0.10
0.20
0.30
Wave height [m]

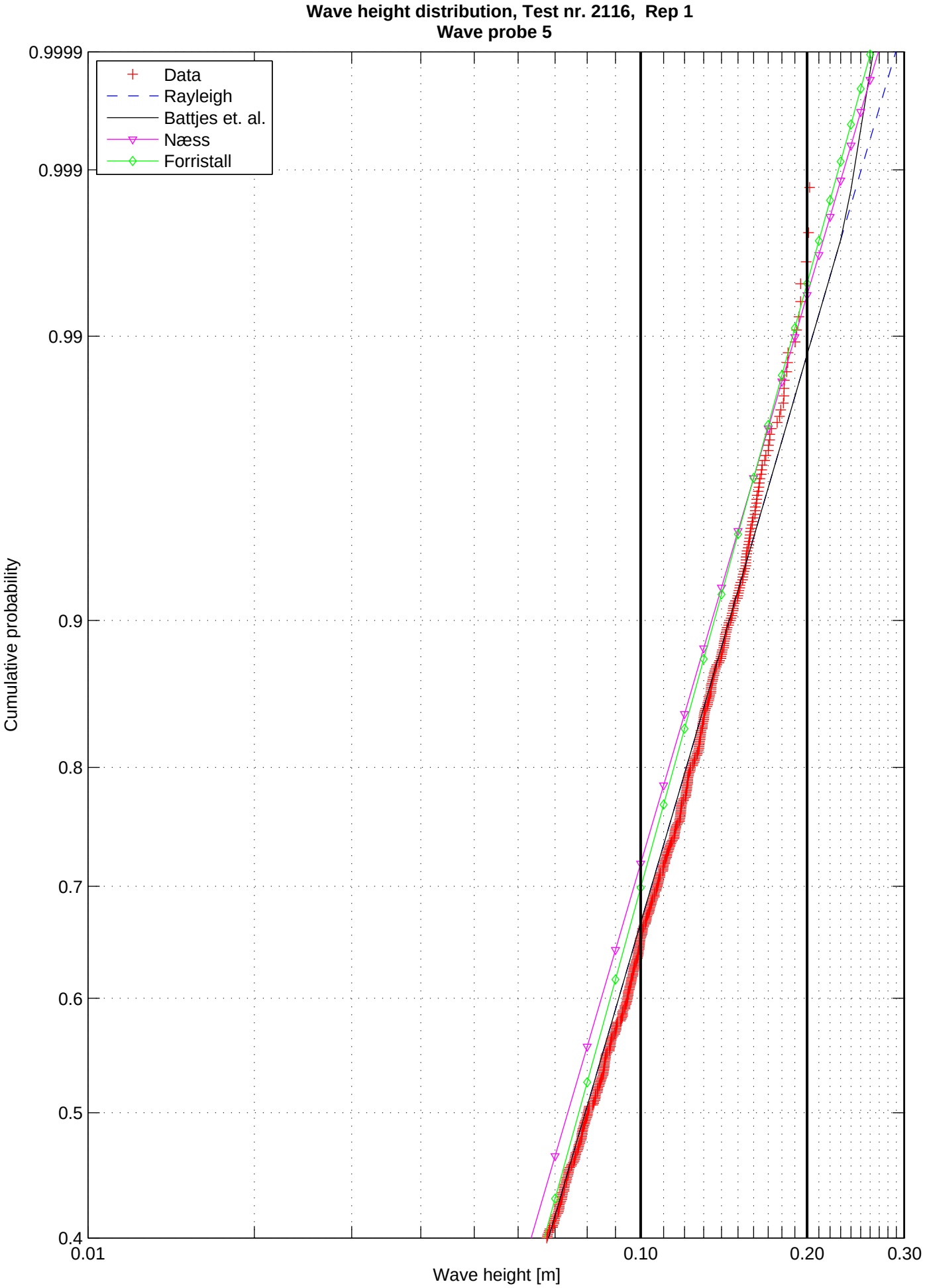
Wave height distribution, Test nr. 2116, Rep 1
Wave probe 5
Data
Rayleigh
Battjes et. al.
Næss
Forristall
Cumulative probability
0.9999
0.999
0.99
0.9
0.8
0.7
0.6
0.5
0.4
0.01
0.10
0.20
0.30
Wave height [m]

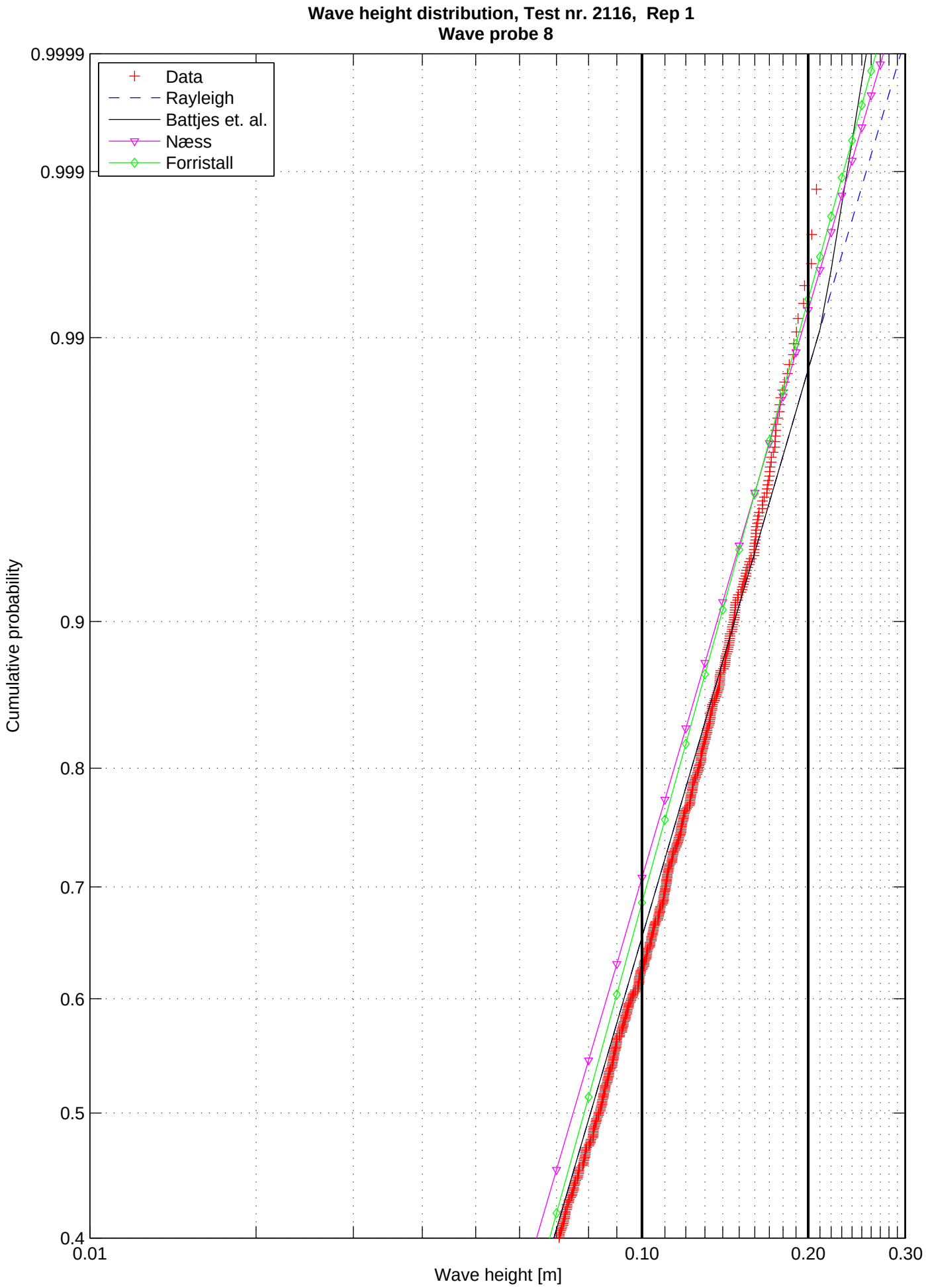
Wave height distribution, Test nr. 2116, Rep 1
Wave probe 8
Data
Rayleigh
Battjes et. al.
Næss
Forristall
Cumulative probability
0.9999
0.999
0.99
0.9
0.8
0.7
0.6
0.5
0.4
0.01
0.10
0.20
0.30
Wave height [m]

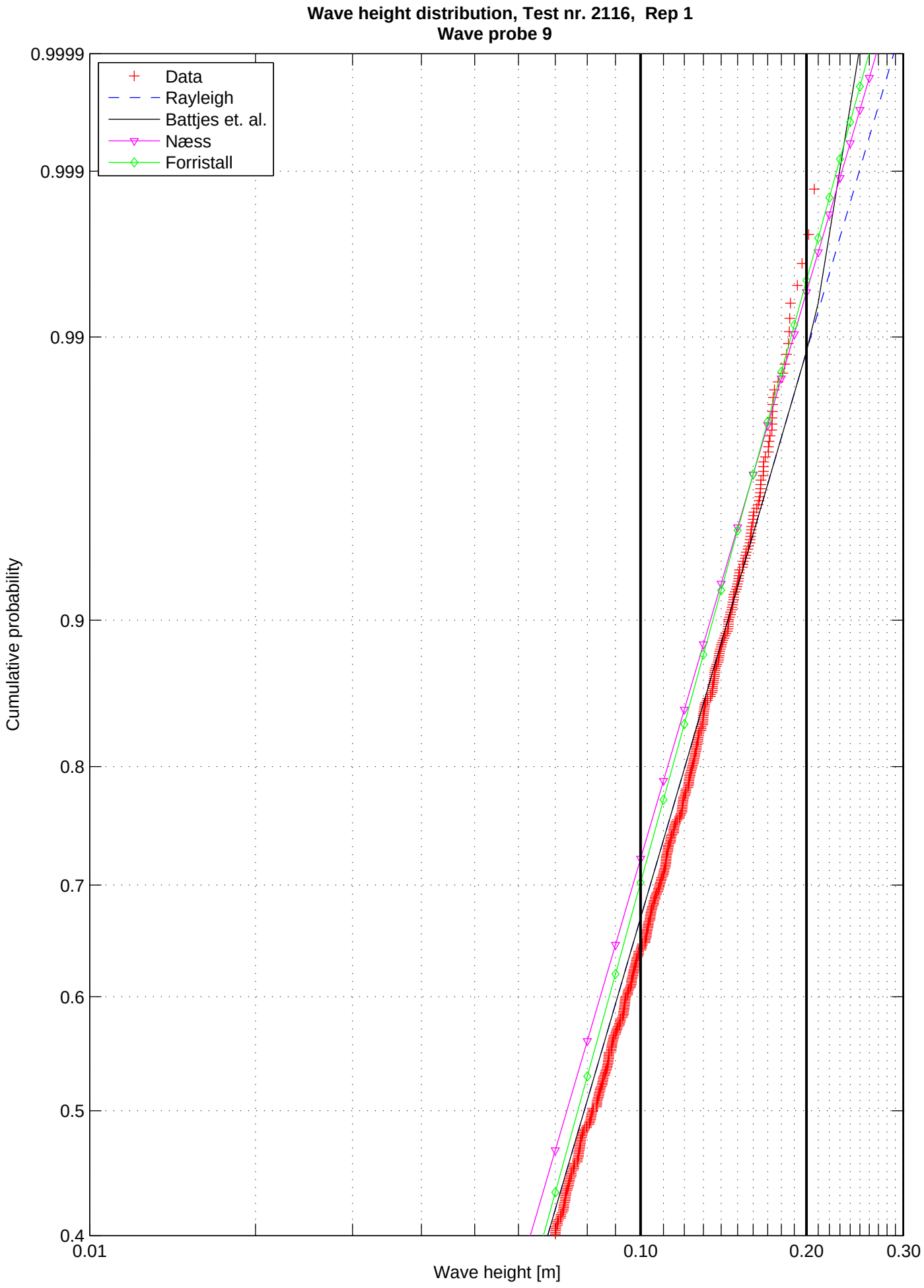
Wave height distribution, Test nr. 2116, Rep 1
Wave probe 9
Data
Rayleigh
Battjes et. al.
Næss
Forristall
Cumulative probability
0.9999
0.999
0.99
0.9
0.8
0.7
0.6
0.5
0.4
0.01
0.10
0.20
0.30
Wave height [m]

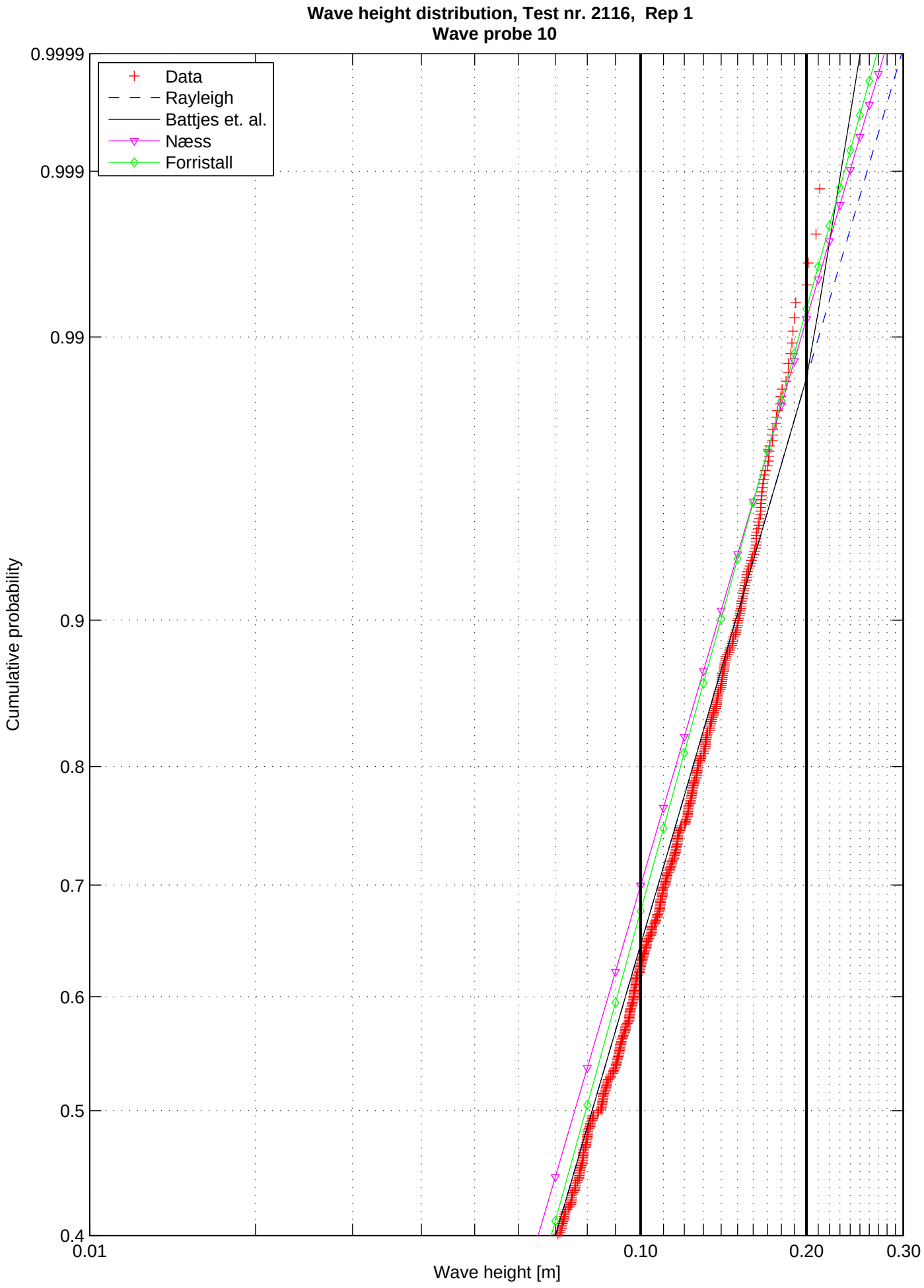
Wave height distribution, Test nr. 2116, Rep 1
Wave probe 10
Data
Rayleigh
Battjes et. al.
Næss
Forristall
0.9999
0.999
0.99
0.9
0.8
0.7
0.6
0.5
0.4
Cumulative probability
0.01
0.10
0.20
0.30
Wave height [m]

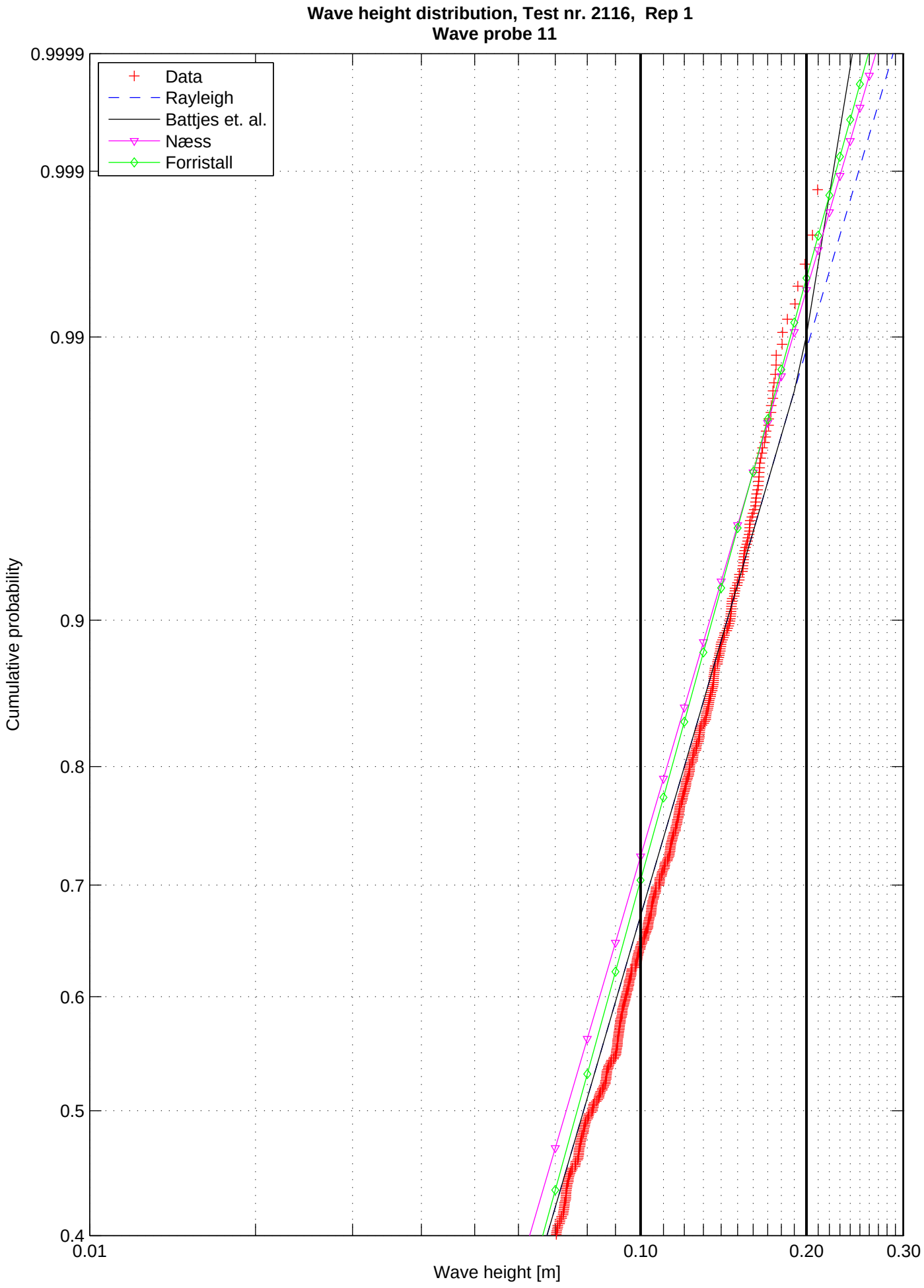
Wave height distribution, Test nr. 2116, Rep 1
Wave probe 11
Data
Rayleigh
Battjes et. al.
Næss
Forristall
Cumulative probability
0.9999
0.999
0.99
0.9
0.8
0.7
0.6
0.5
0.4
0.01
0.10
0.20
0.30
Wave height [m]

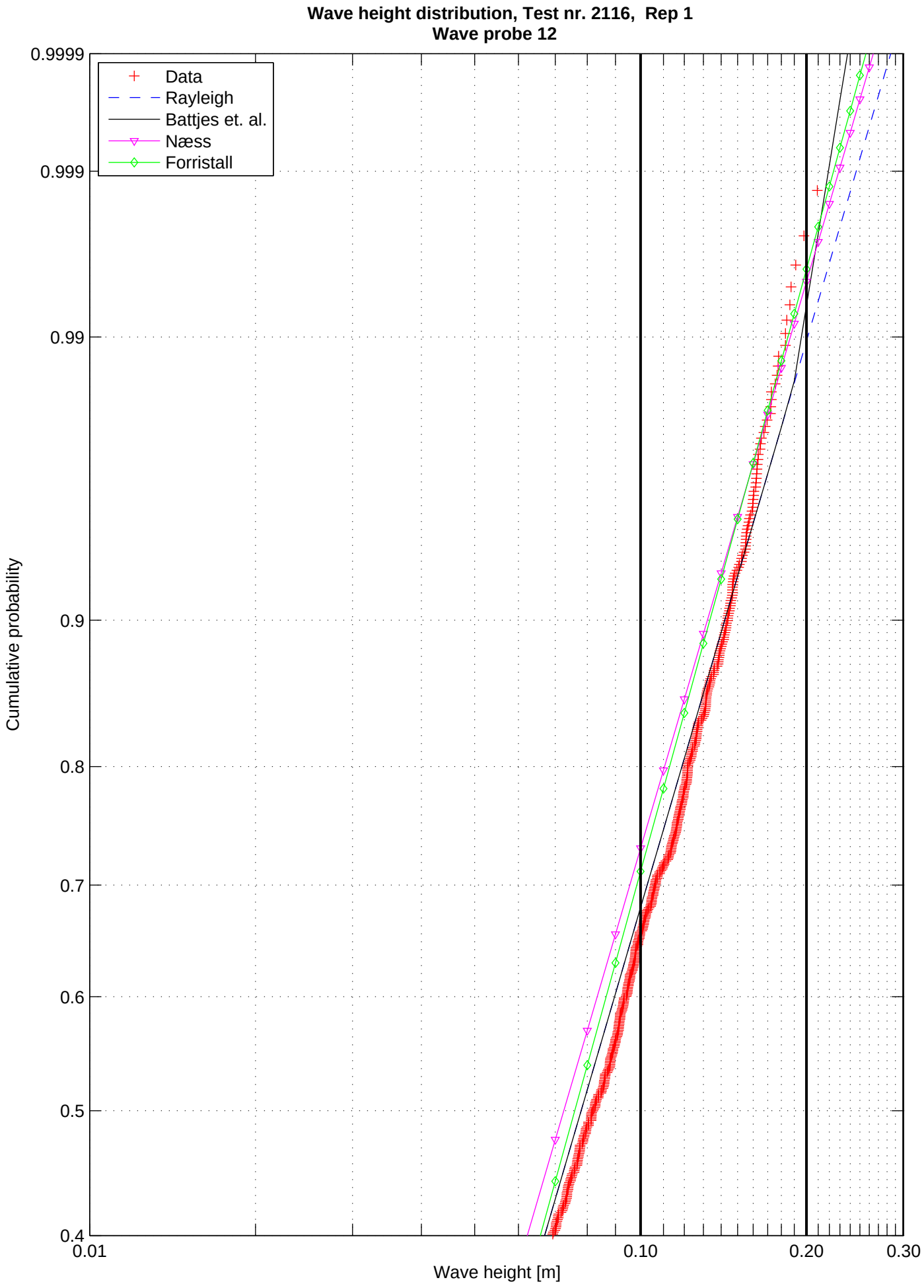
Wave height distribution, Test nr. 2116, Rep 1
Wave probe 12
Data
Rayleigh
Battjes et. al.
Næss
Forristall
0.9999
0.999
0.99
0.9
0.8
0.7
0.6
0.5
0.4
Cumulative probability
0.01
0.10
0.20
0.30
Wave height [m]

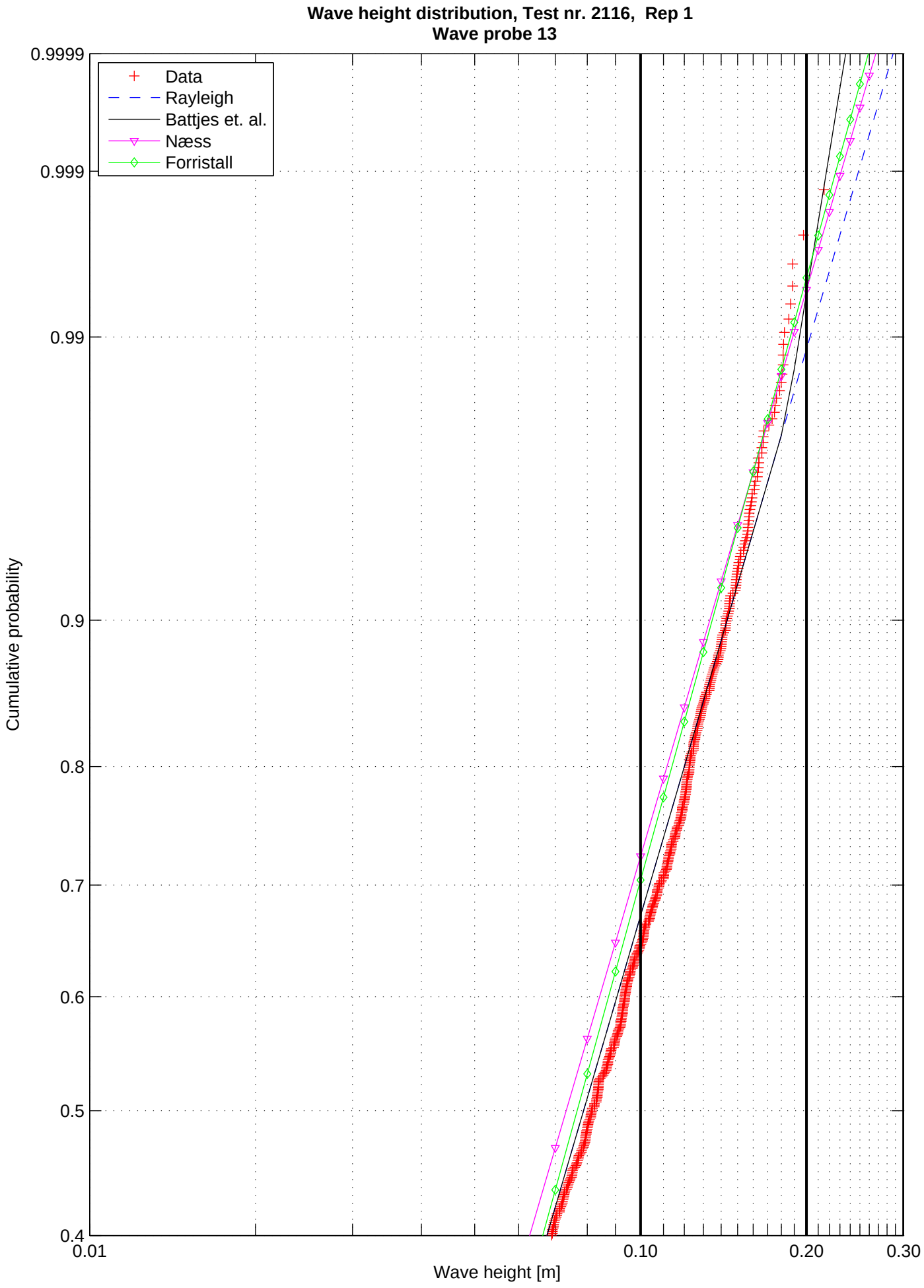
Wave height distribution, Test nr. 2116, Rep 1
Wave probe 13
Data
Rayleigh
Battjes et. al.
Næss
Forristall
Cumulative probability
0.9999
0.999
0.99
0.9
0.8
0.7
0.6
0.5
0.4
0.01
0.10
0.20
0.30
Wave height [m]

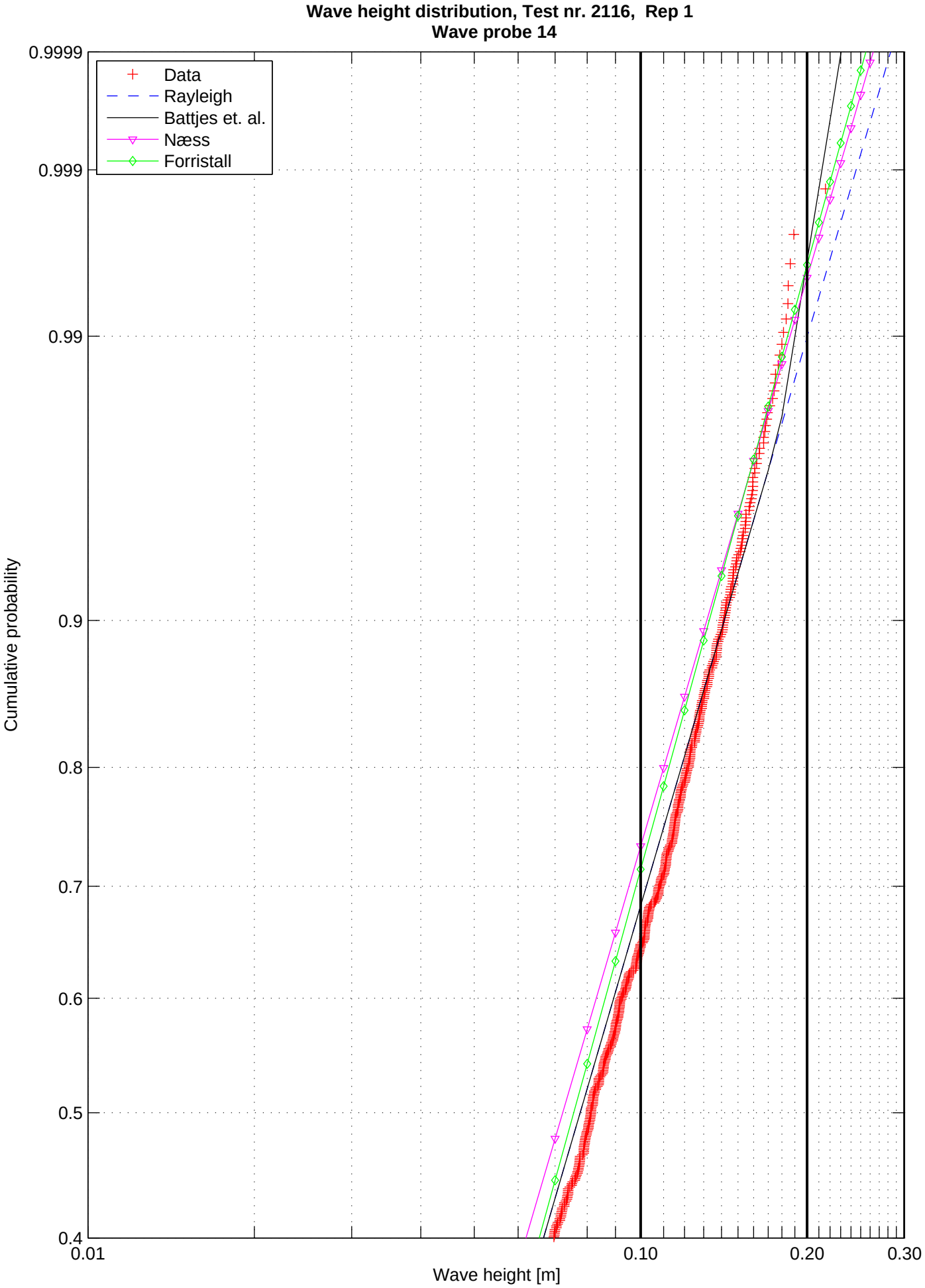
Wave height distribution, Test nr. 2116, Rep 1
Wave probe 14
Data
Rayleigh
Battjes et. al.
Næss
Forristall
Cumulative probability
0.9999
0.999
0.99
0.9
0.8
0.7
0.6
0.5
0.4
0.01
0.10
0.20
0.30
Wave height [m]

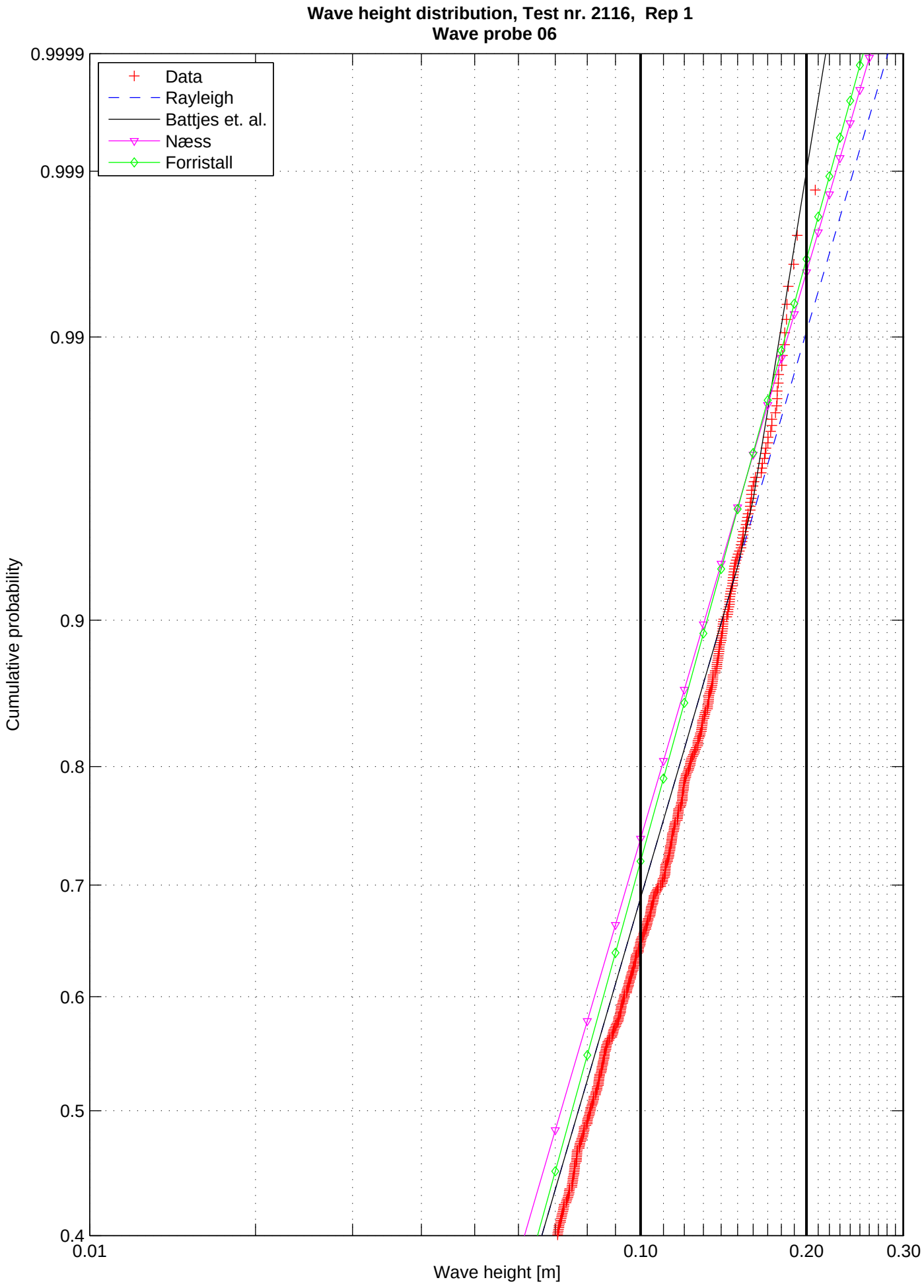
Wave height distribution, Test nr. 2116, Rep 1
Wave probe 06
Data
Rayleigh
Battjes et. al.
Næss
Forristall
Cumulative probability
0.9999
0.999
0.99
0.9
0.8
0.7
0.6
0.5
0.4
0.01
0.10
0.20
0.30
Wave height [m]

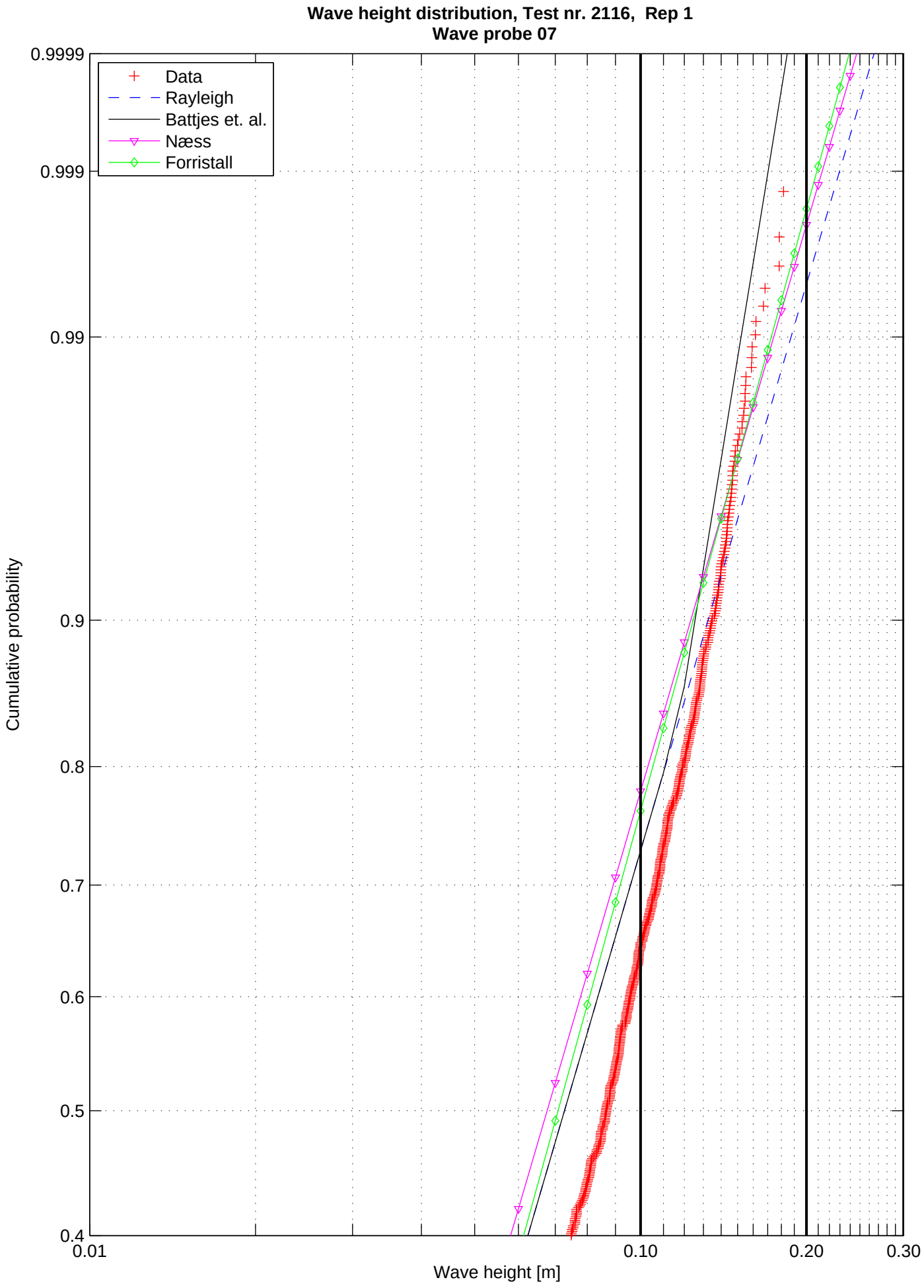
Wave height distribution, Test nr. 2116, Rep 1
Wave probe 07
Data
Rayleigh
Battjes et. al.
Næss
Forristall
Cumulative probability
0.9999
0.999
0.99
0.9
0.8
0.7
0.6
0.5
0.4
0.01
0.10
0.20
0.30
Wave height [m]

Appendix G

Crest height distributions

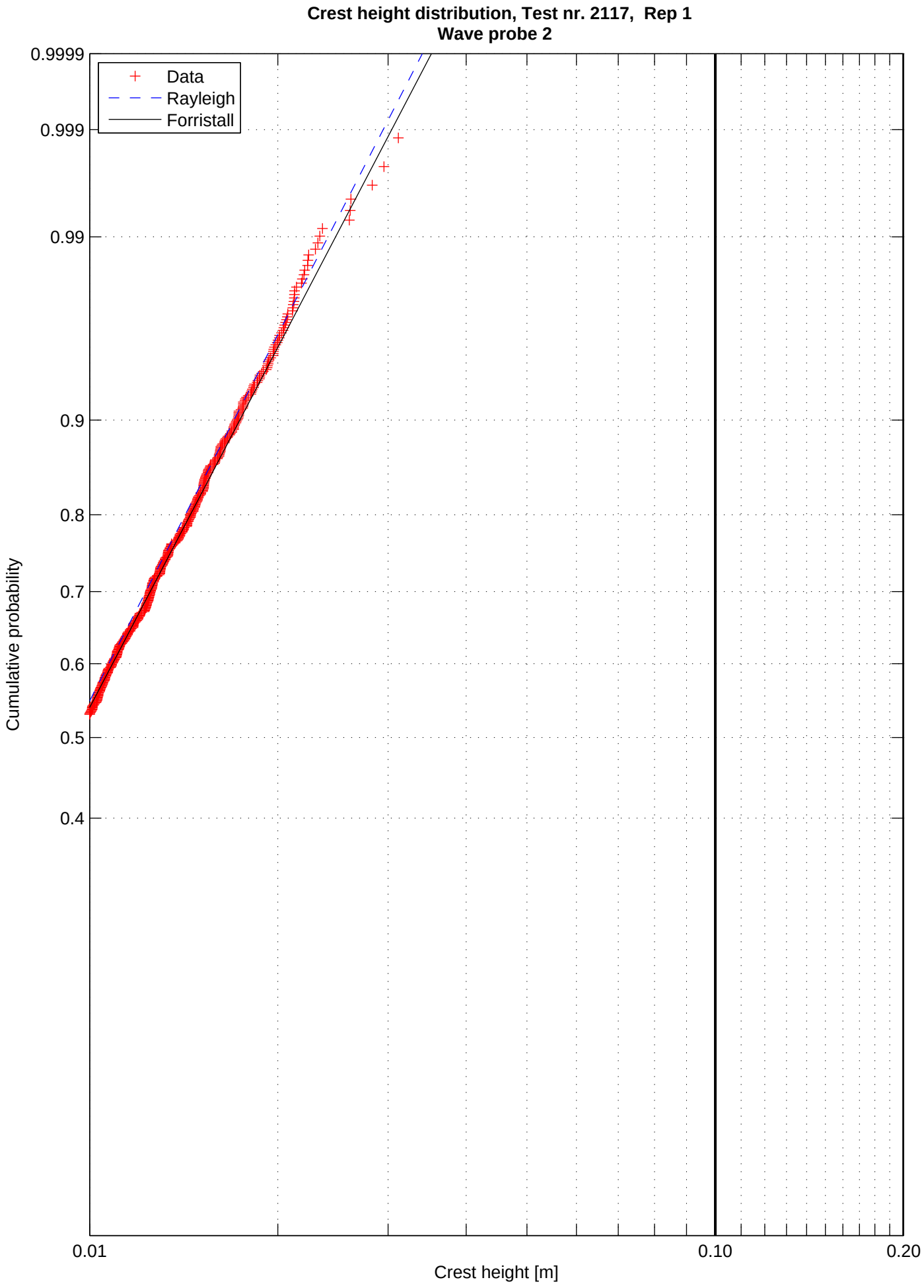
Crest height distribution, Test nr. 2117, Rep 1
Wave probe 2
Data
Rayleigh
Forristall
0.9999
0.999
0.99
0.9
0.8
0.7
0.6
0.5
0.4
Cumulative probability
0.01
0.10
0.20
Crest height [m]

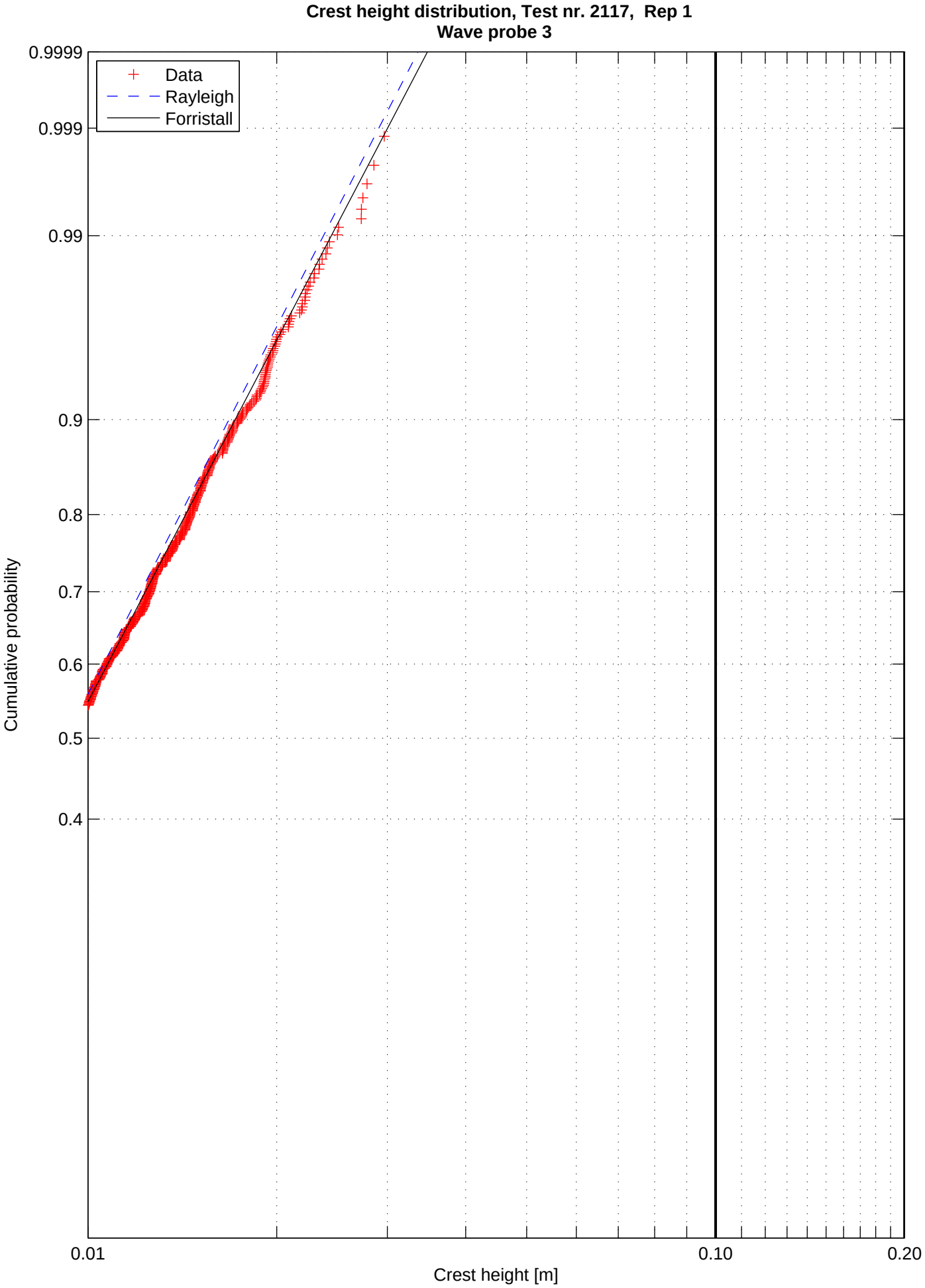
Crest height distribution, Test nr. 2117, Rep 1
Wave probe 3
Data
Rayleigh
Forristall
0.9999
0.999
0.99
0.9
0.8
0.7
0.6
0.5
0.4
Cumulative probability
0.01
0.10
0.20
Crest height [m]

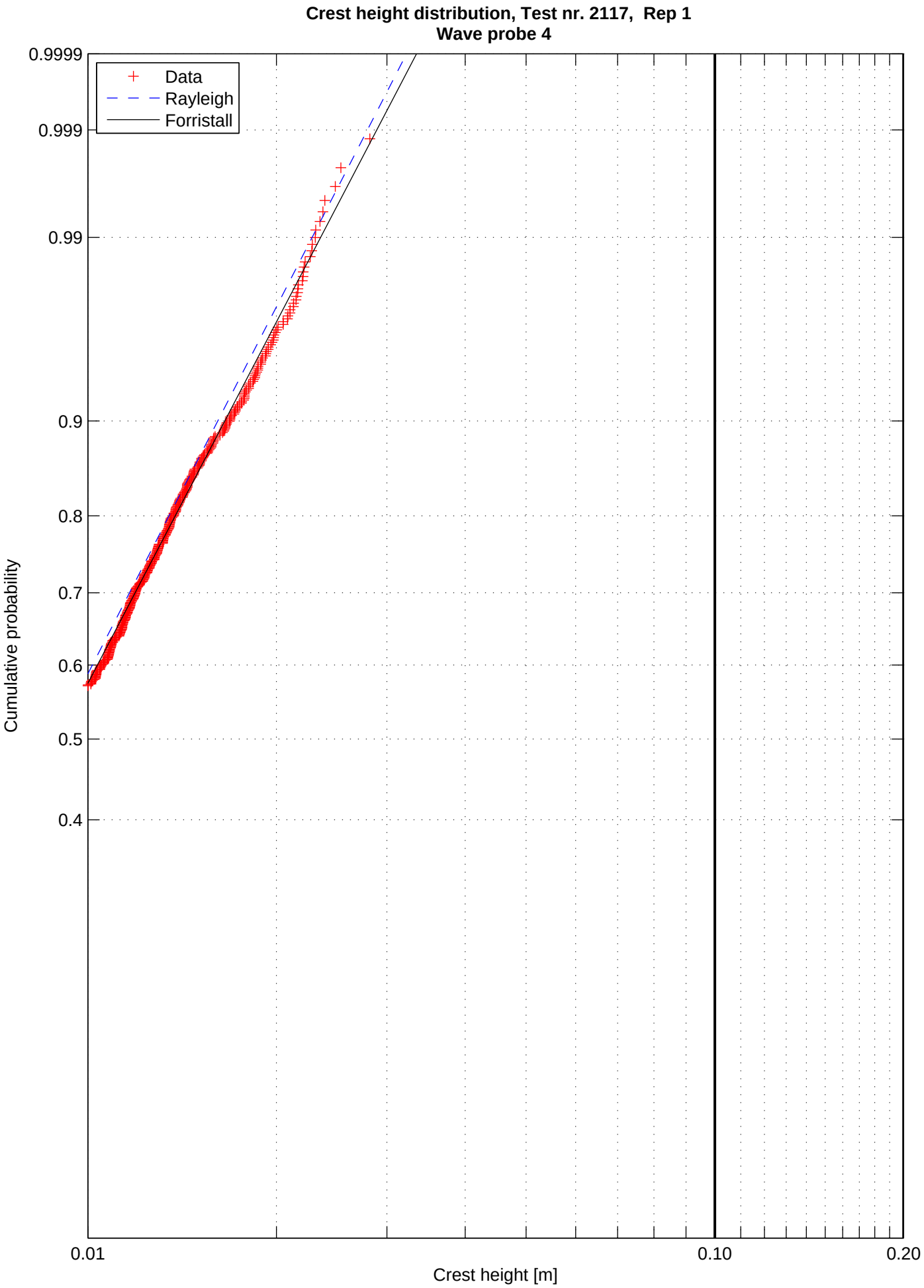
Crest height distribution, Test nr. 2117, Rep 1
Wave probe 4
Data
Rayleigh
Forristall
0.9999
0.999
0.99
0.9
0.8
0.7
0.6
0.5
0.4
Cumulative probability
0.01
0.10
0.20
Crest height [m]

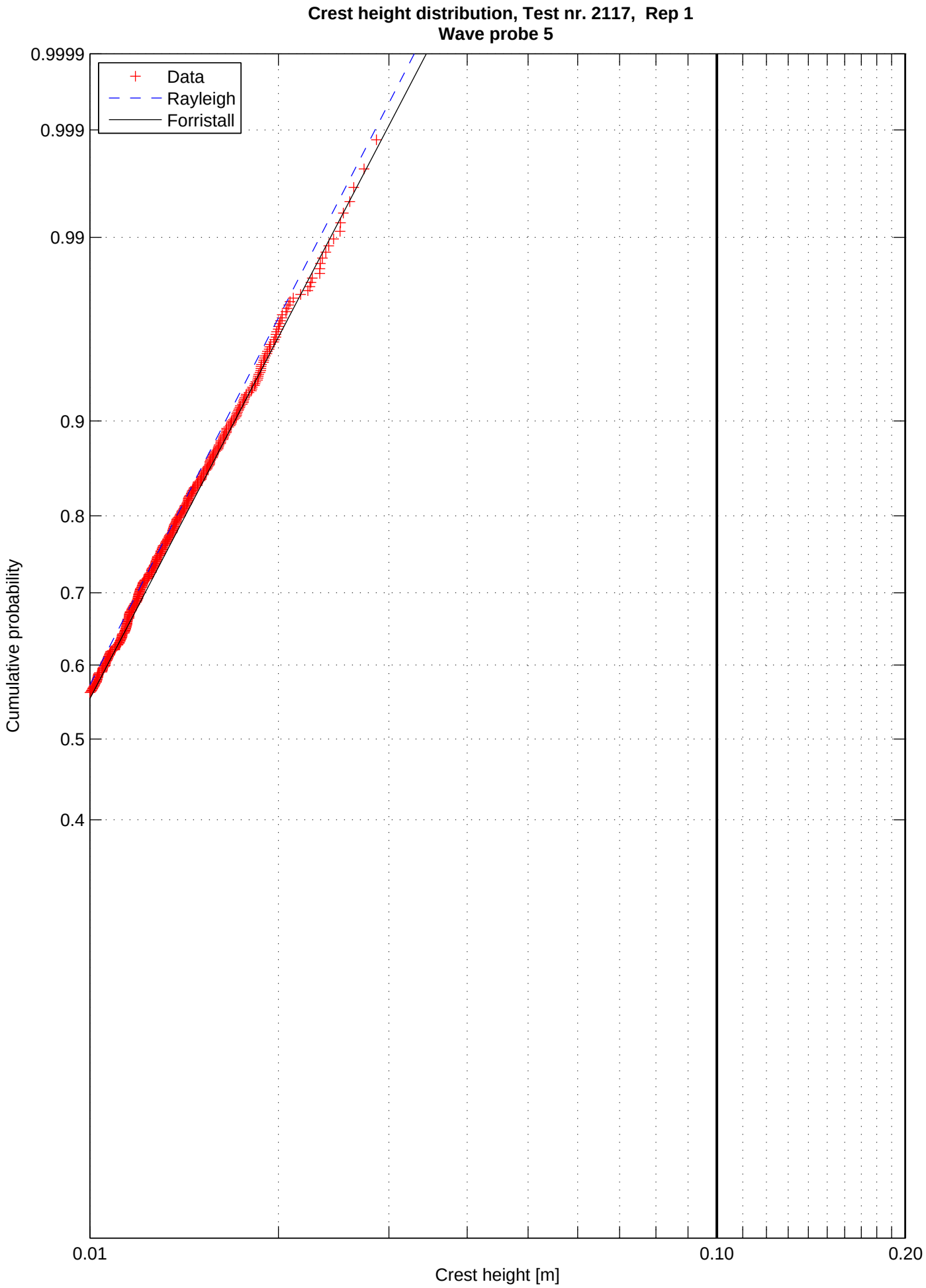
Crest height distribution, Test nr. 2117, Rep 1
Wave probe 5
Data
Rayleigh
Forristall
0.9999
0.999
0.99
0.9
0.8
0.7
0.6
0.5
0.4
Cumulative probability
0.01
0.10
0.20
Crest height [m]

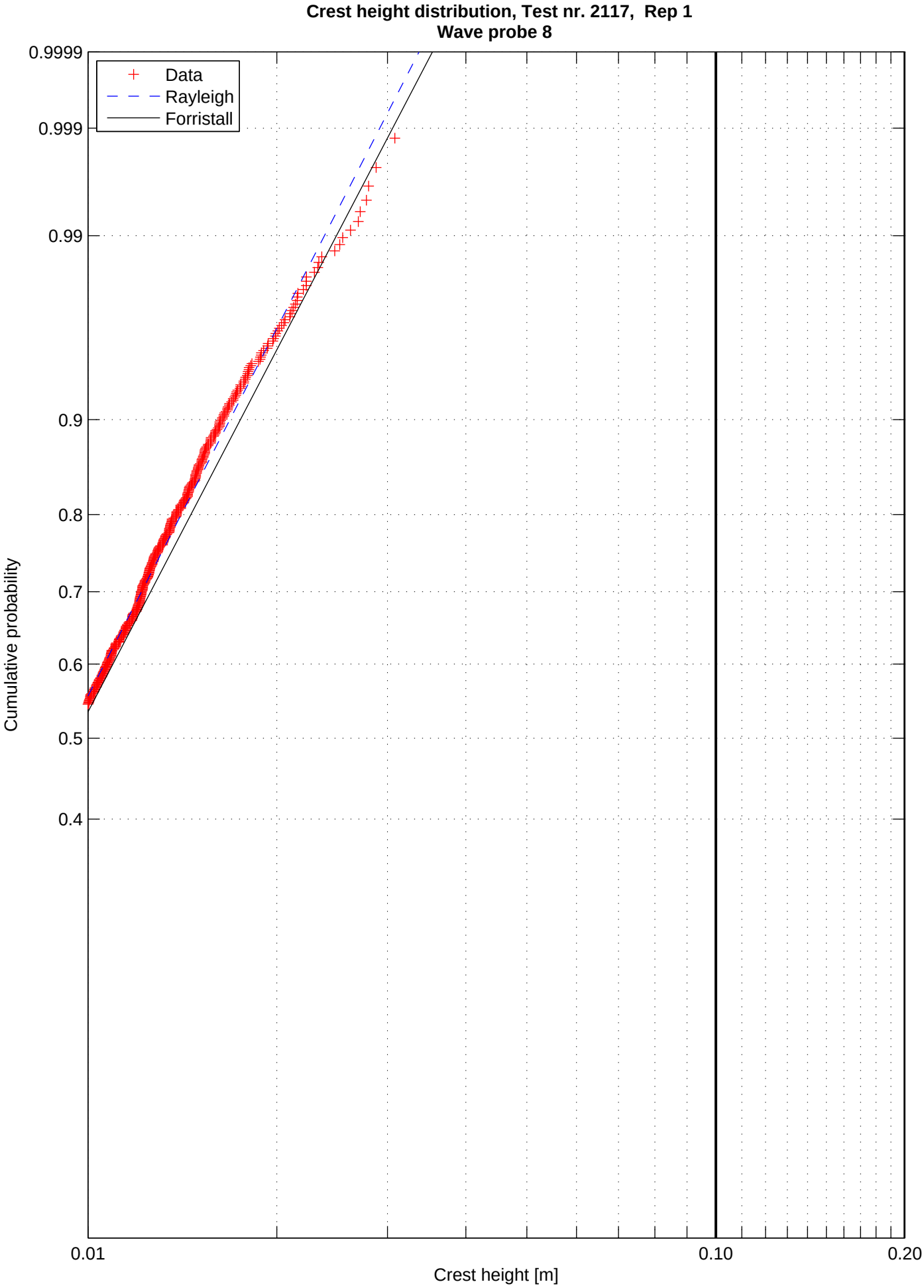
Crest height distribution, Test nr. 2117, Rep 1
Wave probe 8
Data
Rayleigh
Forristall
0.9999
0.999
0.99
0.9
0.8
0.7
0.6
0.5
0.4
Cumulative probability
0.01
0.10
0.20
Crest height [m]

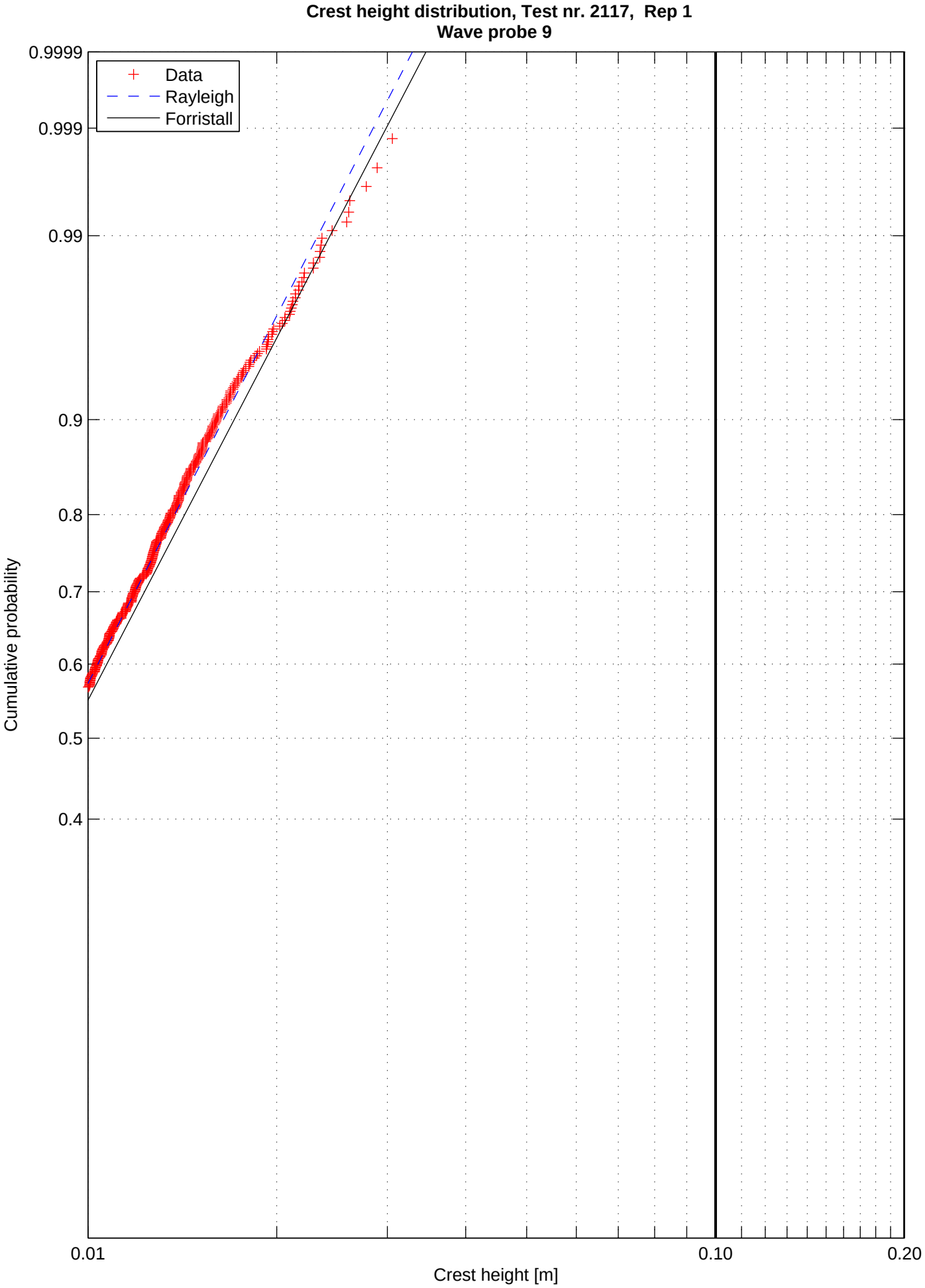
Crest height distribution, Test nr. 2117, Rep 1
Wave probe 9
Data
Rayleigh
Forristall
0.9999
0.999
0.99
0.9
0.8
0.7
0.6
0.5
0.4
Cumulative probability
0.01
0.10
0.20
Crest height [m]

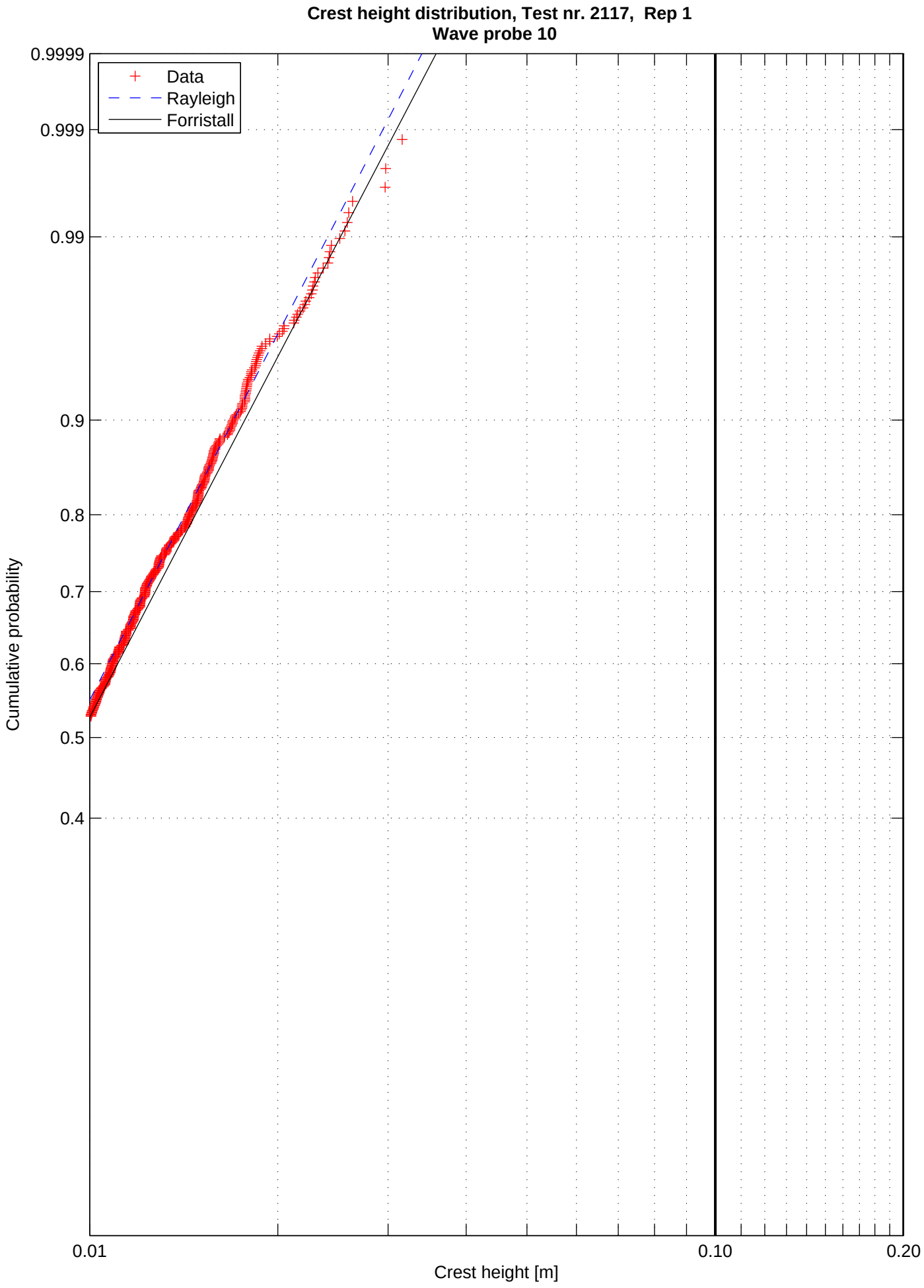
Crest height distribution, Test nr. 2117, Rep 1
Wave probe 10
Data
Rayleigh
Forristall
0.9999
0.999
0.99
0.9
0.8
0.7
0.6
0.5
0.4
Cumulative probability
0.01
0.10
0.20
Crest height [m]

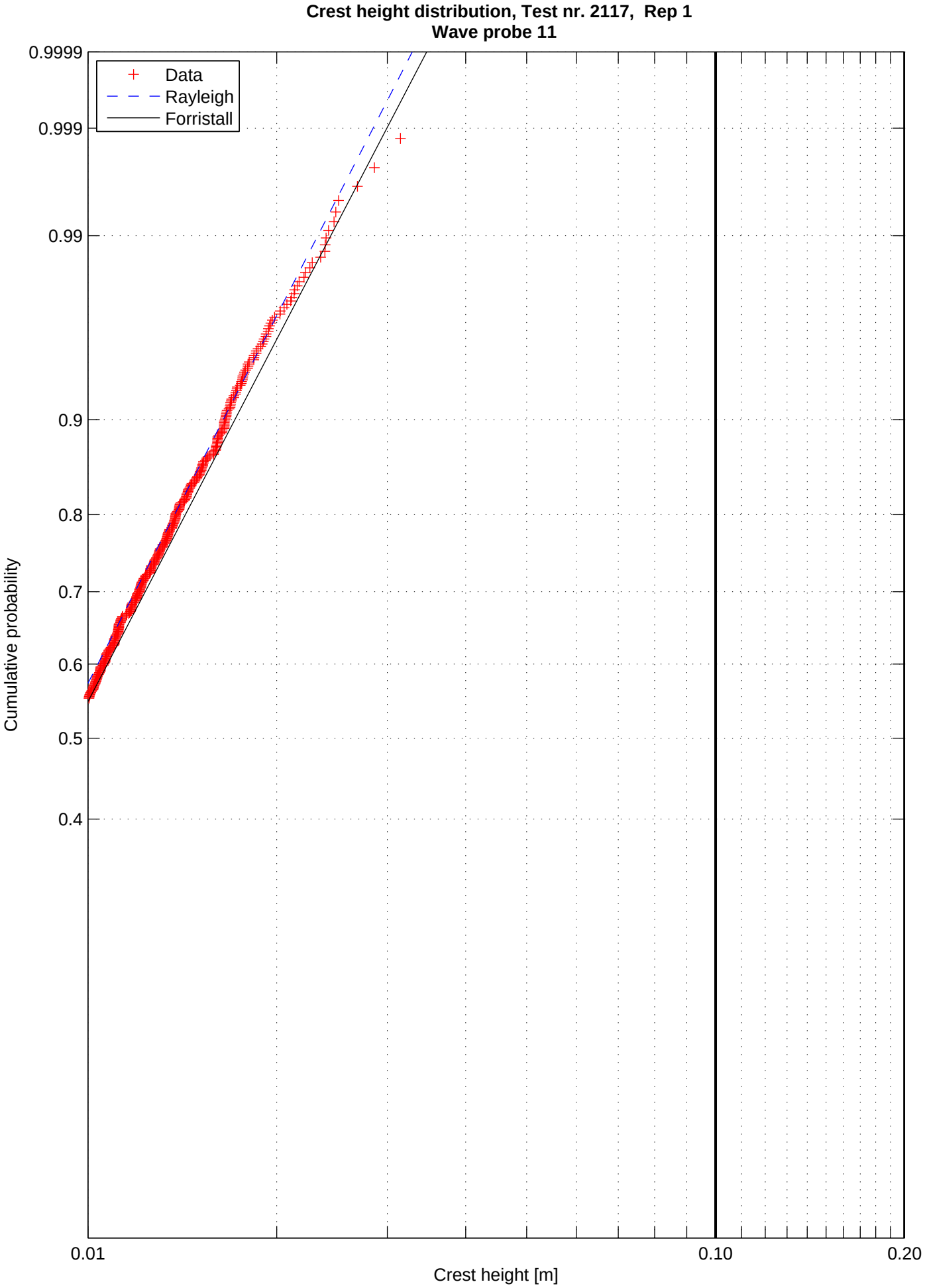
Crest height distribution, Test nr. 2117, Rep 1
Wave probe 11
Data
Rayleigh
Forristall
0.9999
0.999
0.99
0.9
0.8
0.7
0.6
0.5
0.4
Cumulative probability
0.01
0.10
0.20
Crest height [m]

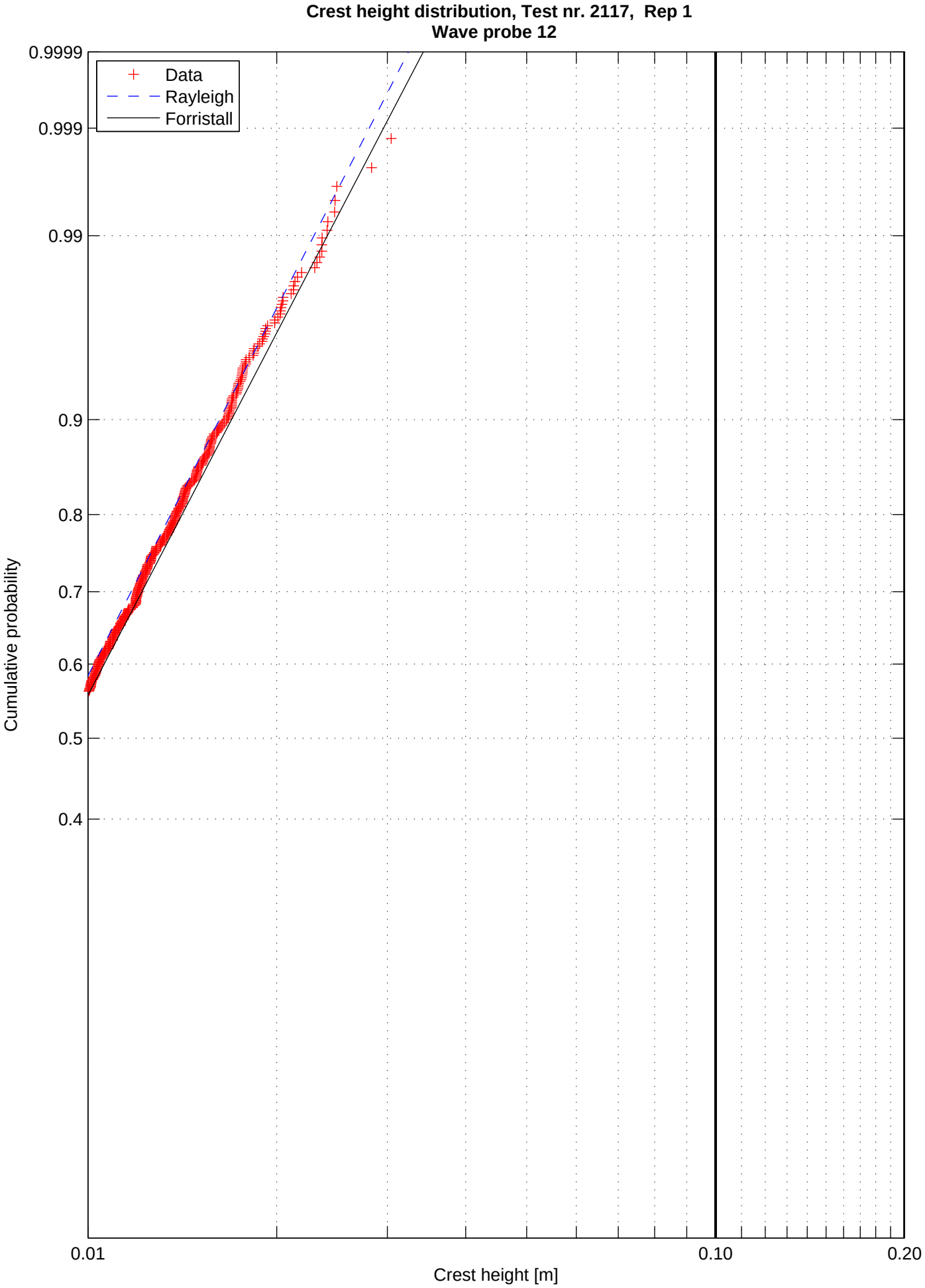
Crest height distribution, Test nr. 2117, Rep 1
Wave probe 12
Data
Rayleigh
Forristall
0.9999
0.999
0.99
0.9
0.8
0.7
0.6
0.5
0.4
Cumulative probability
0.01
0.10
0.20
Crest height [m]

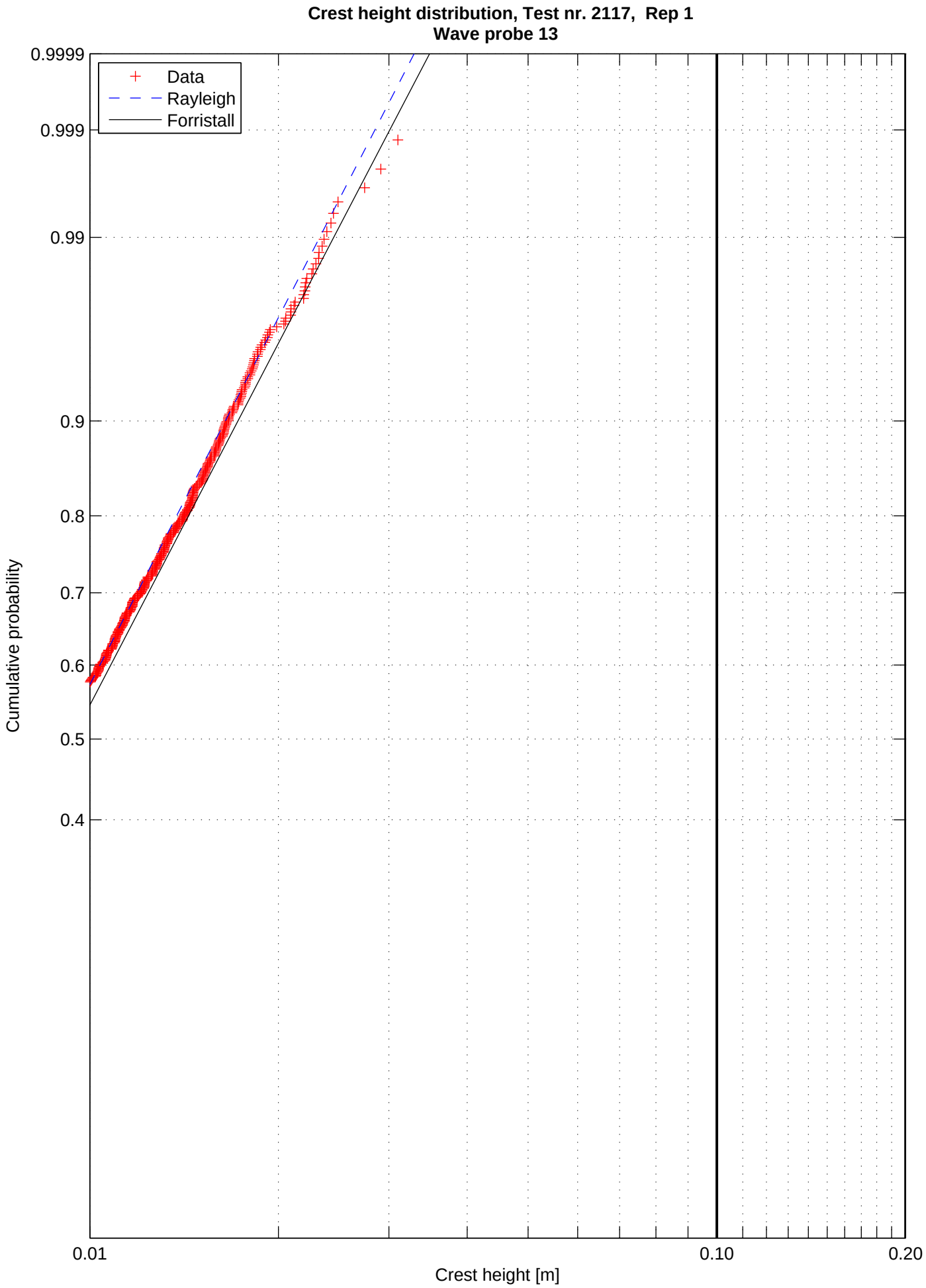
Crest height distribution, Test nr. 2117, Rep 1
Wave probe 13
Data
Rayleigh
Forristall
0.9999
0.999
0.99
0.9
0.8
0.7
0.6
0.5
0.4
Cumulative probability
0.01
0.10
0.20
Crest height [m]

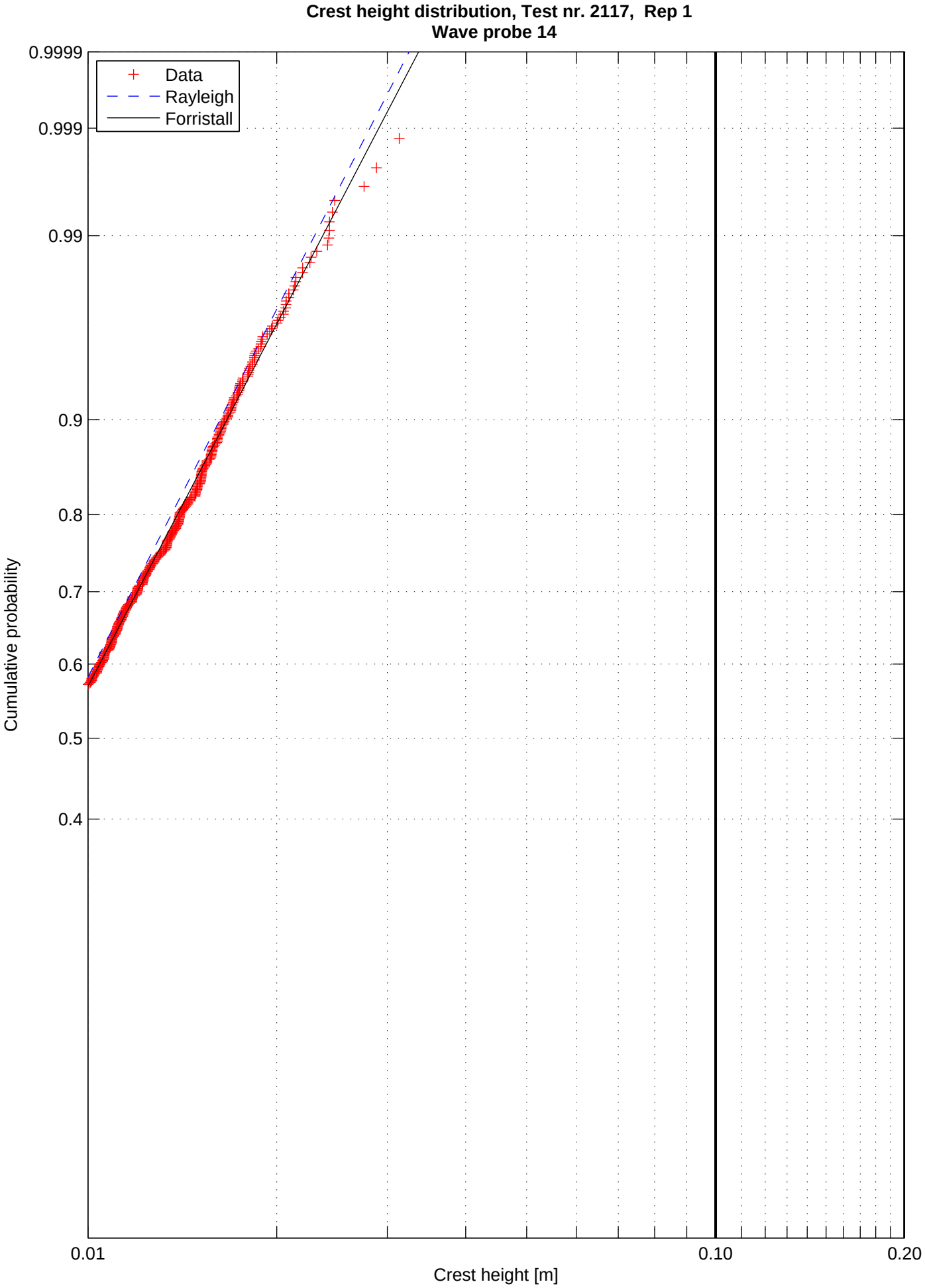
Crest height distribution, Test nr. 2117, Rep 1
Wave probe 14
Data
Rayleigh
Forristall
0.9999
0.999
0.99
0.9
0.8
0.7
0.6
0.5
0.4
Cumulative probability
0.01
0.10
0.20
Crest height [m]

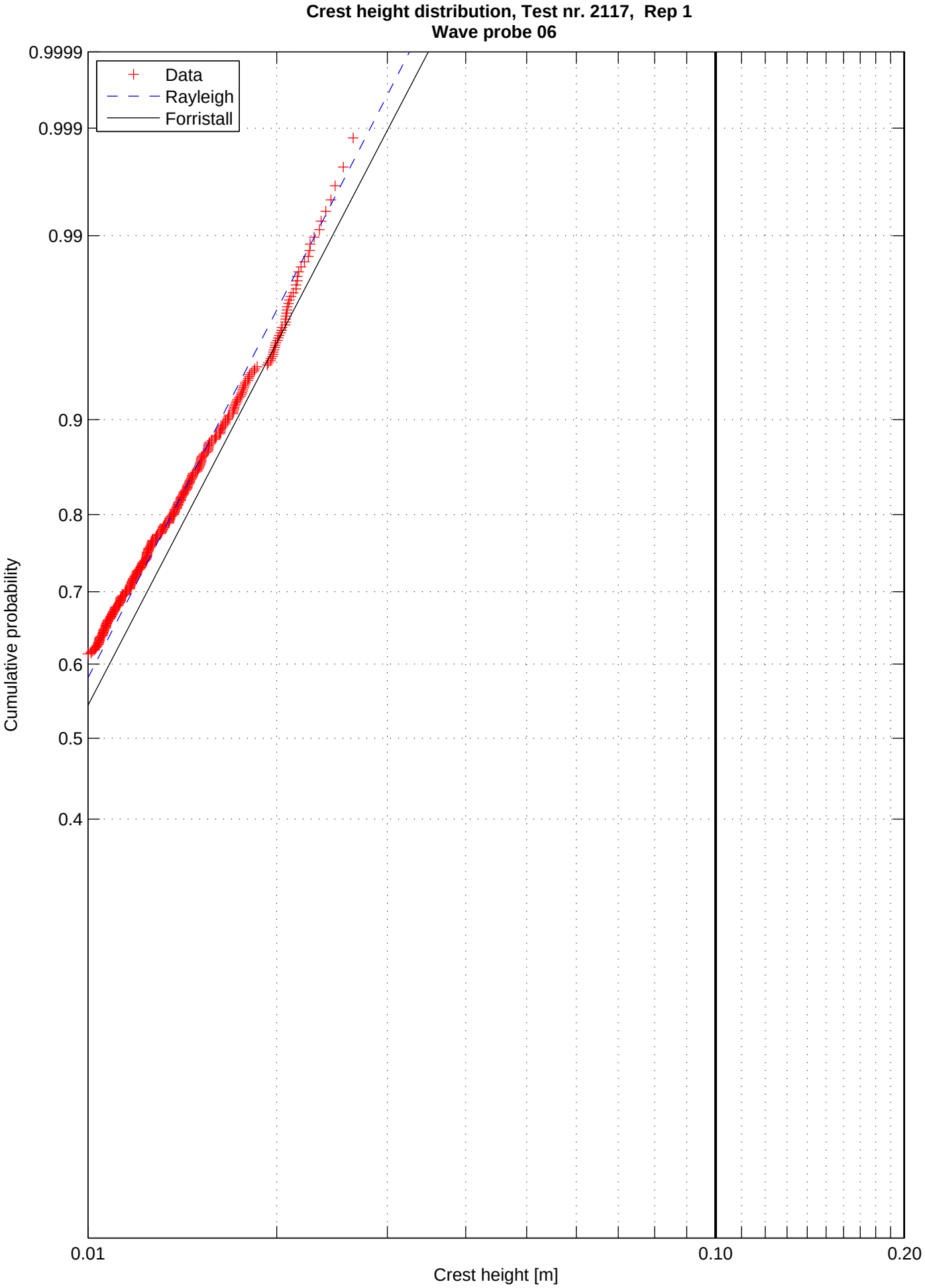
Crest height distribution, Test nr. 2117, Rep 1
Wave probe 06
Data
Rayleigh
Forristall
0.9999
0.999
0.99
0.9
0.8
0.7
0.6
0.5
0.4
Cumulative probability
0.01
0.10
0.20
Crest height [m]

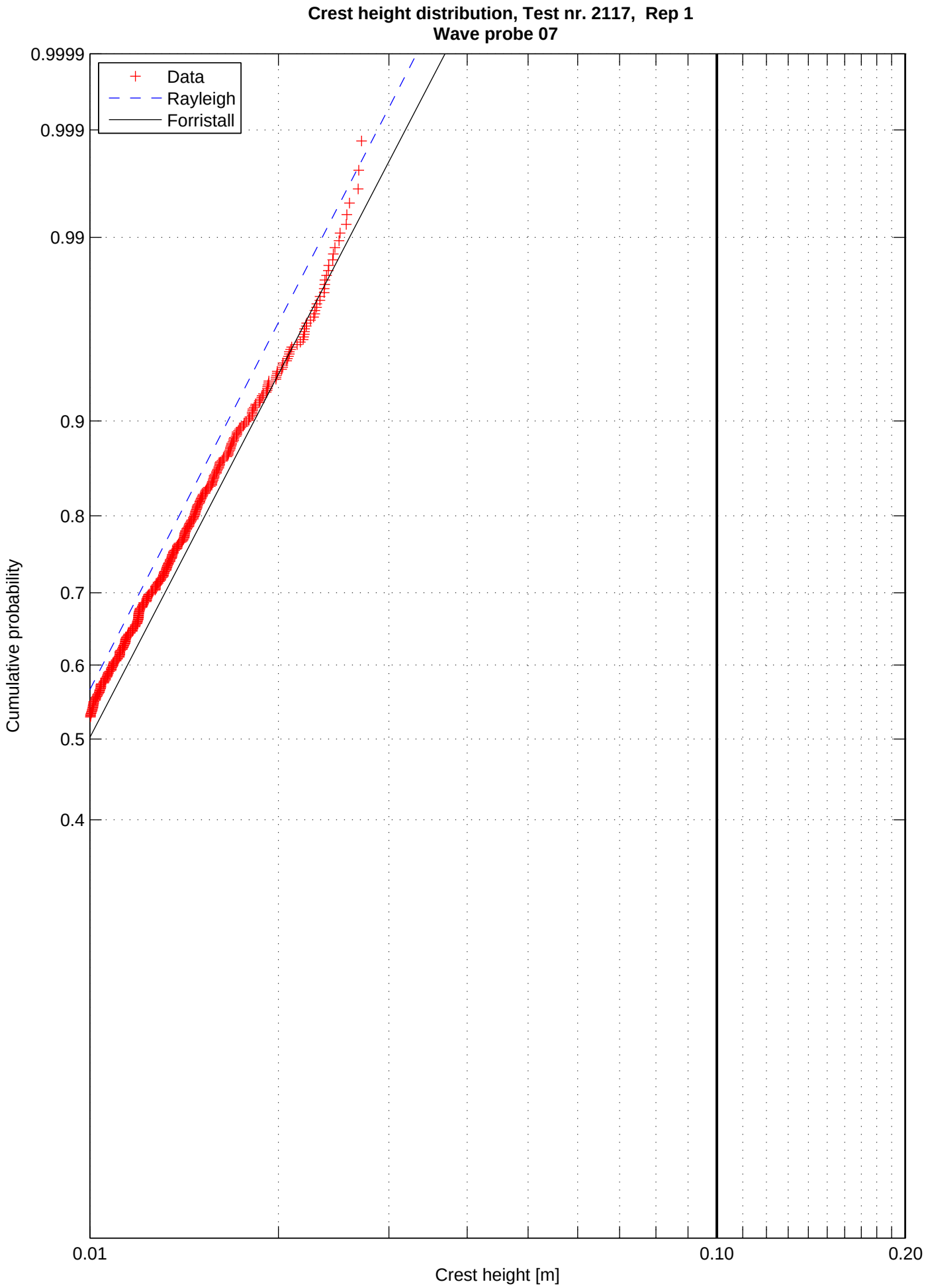
Crest height distribution, Test nr. 2117, Rep 1
Wave probe 07
Data
Rayleigh
Forristall
0.9999
0.999
0.99
0.9
0.8
0.7
0.6
0.5
0.4
Cumulative probability
0.01
0.10
0.20
Crest height [m]

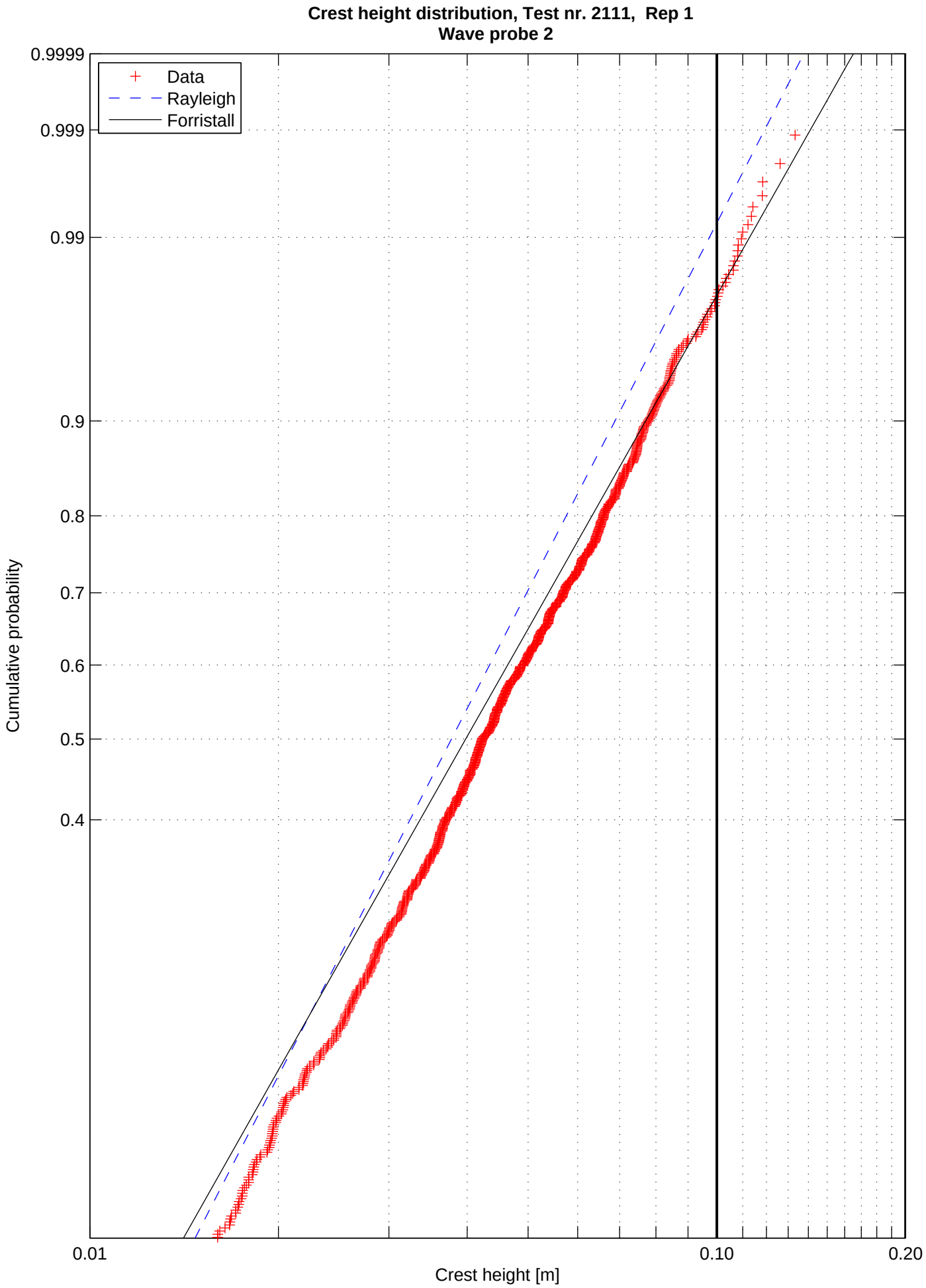
Crest height distribution, Test nr. 2111, Rep 1
Wave probe 2
Data
Rayleigh
Forristall
0.9999
0.999
0.99
0.9
0.8
0.7
0.6
0.5
0.4
Cumulative probability
0.01
0.10
0.20
Crest height [m]

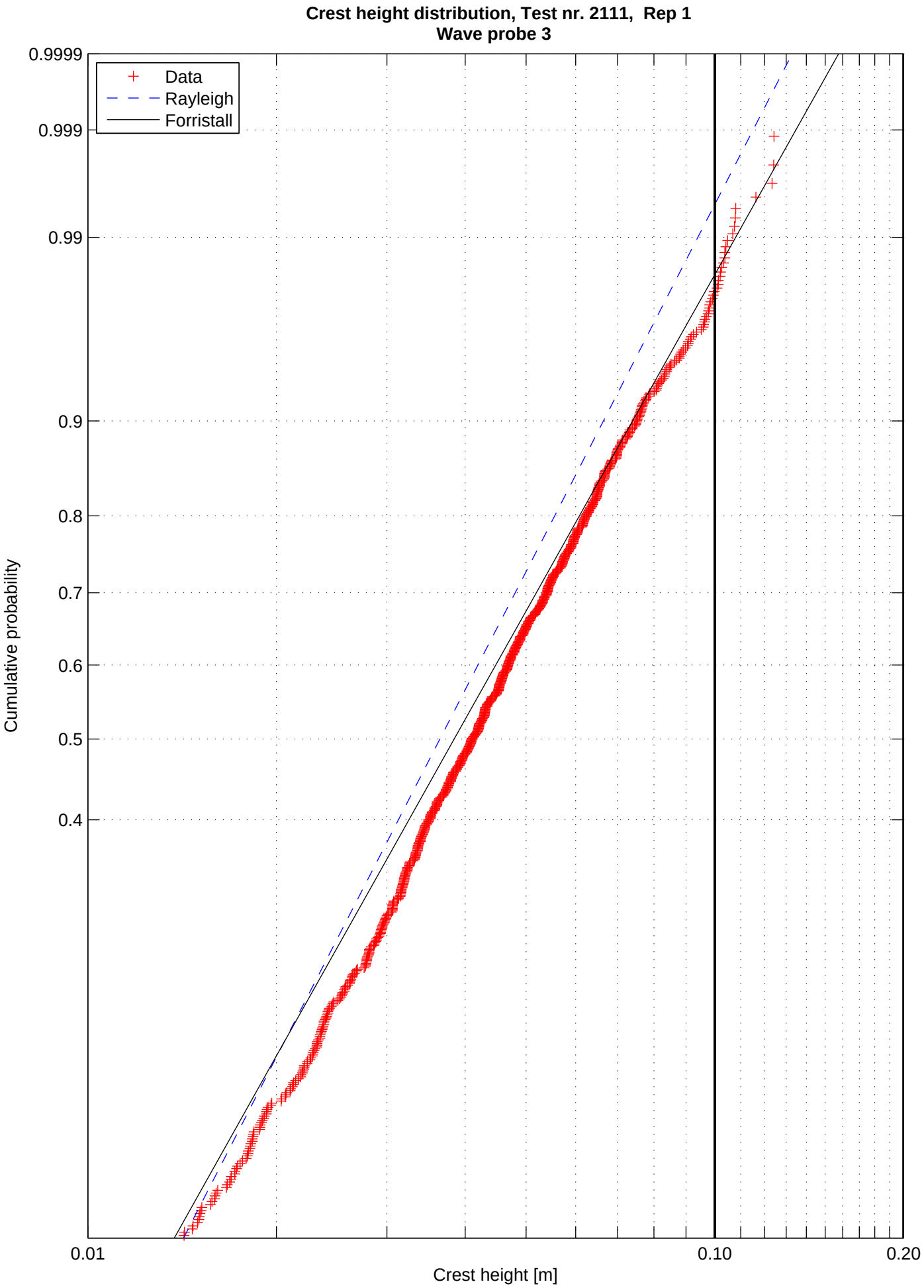
Crest height distribution, Test nr. 2111, Rep 1
Wave probe 3
Data
Rayleigh
Forristall
0.9999
0.999
0.99
0.9
0.8
0.7
0.6
0.5
0.4
Cumulative probability
0.01
0.10
0.20
Crest height [m]

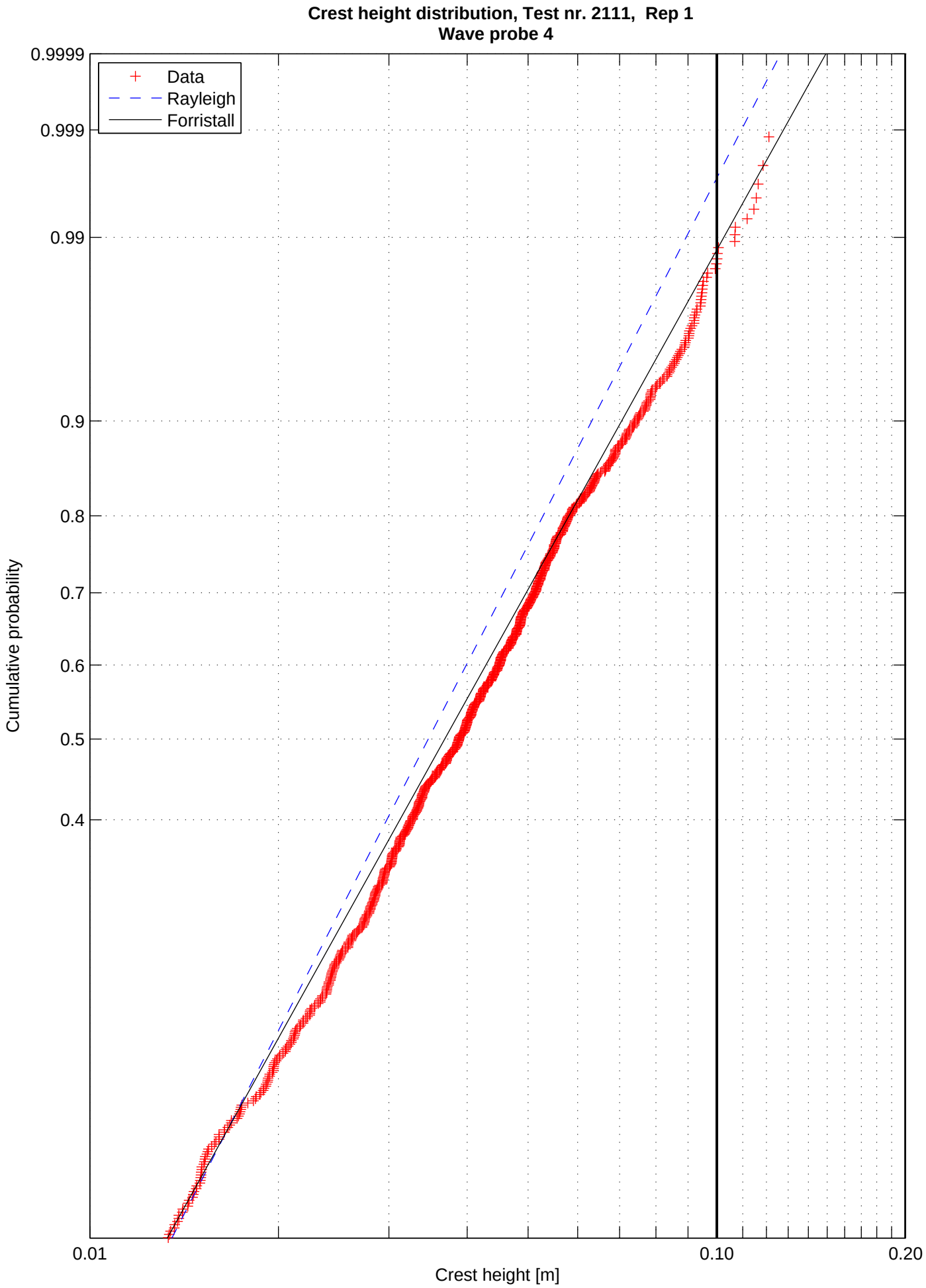
Crest height distribution, Test nr. 2111, Rep 1
Wave probe 4
Data
Rayleigh
Forristall
0.9999
0.999
0.99
0.9
0.8
0.7
0.6
0.5
0.4
Cumulative probability
0.01
0.10
0.20
Crest height [m]

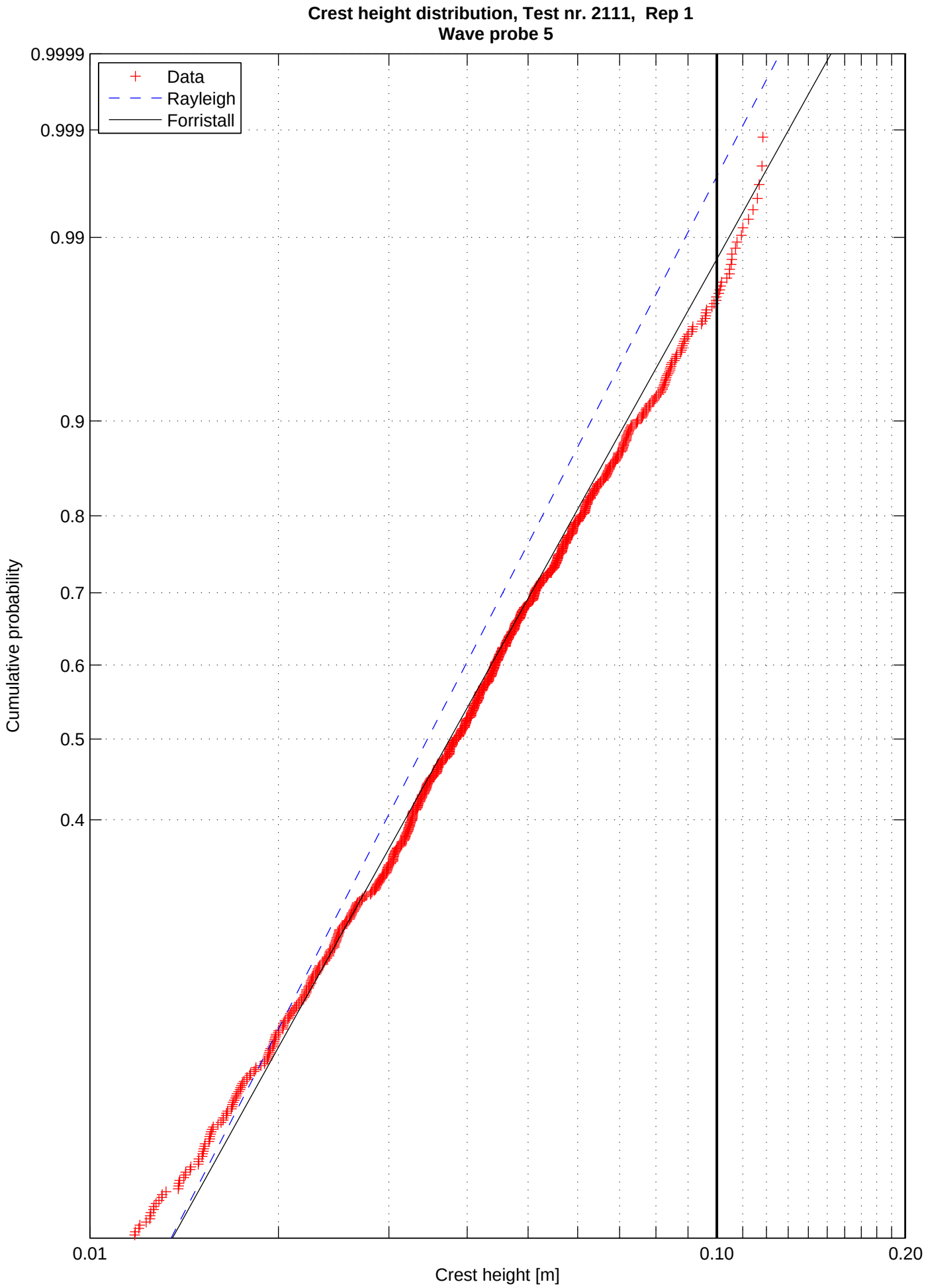
Crest height distribution, Test nr. 2111, Rep 1
Wave probe 5
Data
Rayleigh
Forristall
0.9999
0.999
0.99
0.9
0.8
0.7
0.6
0.5
0.4
Cumulative probability
0.01
0.10
0.20
Crest height [m]

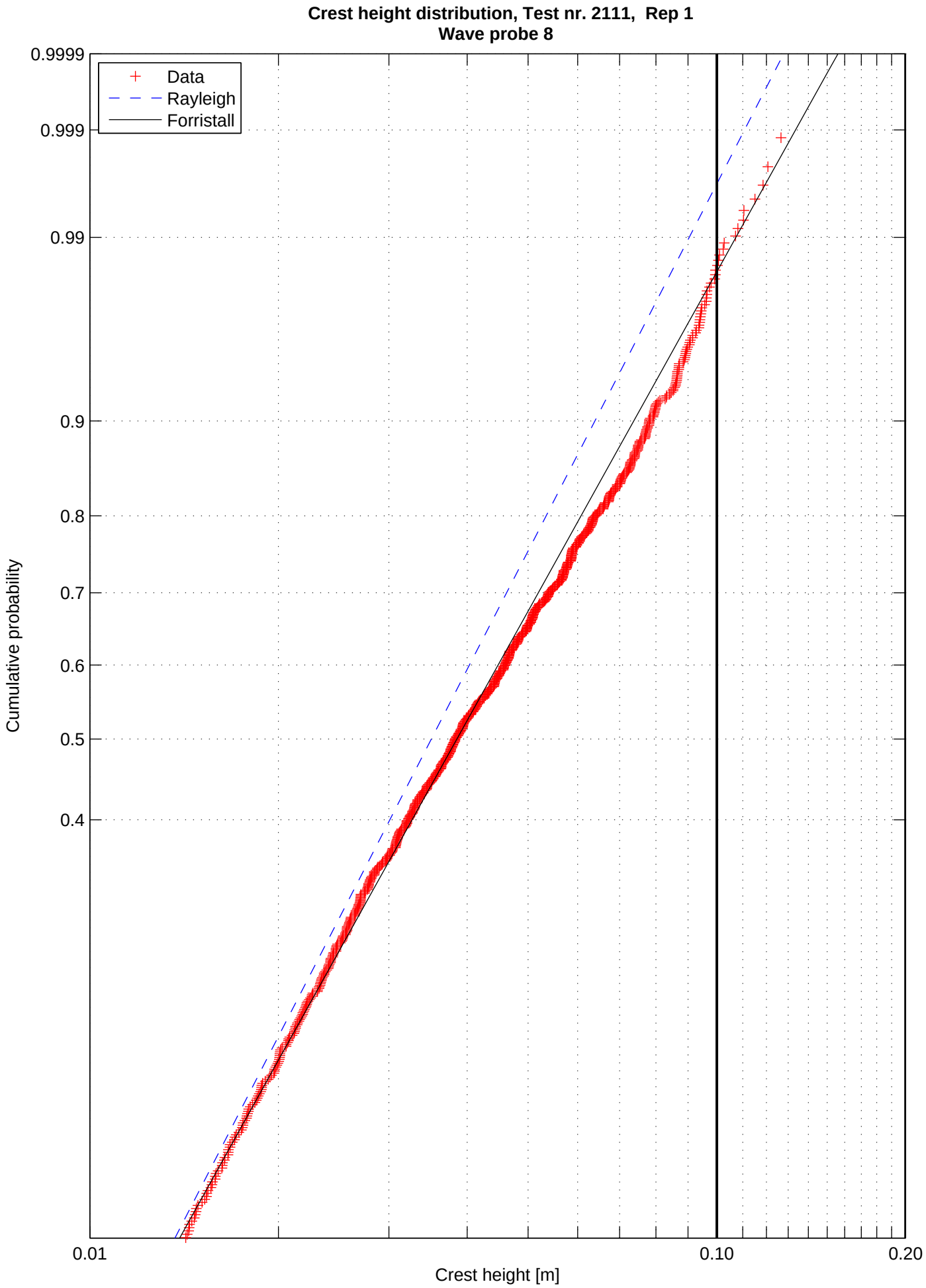
Crest height distribution, Test nr. 2111, Rep 1
Wave probe 8
Data
Rayleigh
Forristall
0.9999
0.999
0.99
0.9
0.8
0.7
0.6
0.5
0.4
Cumulative probability
0.01
0.10
0.20
Crest height [m]

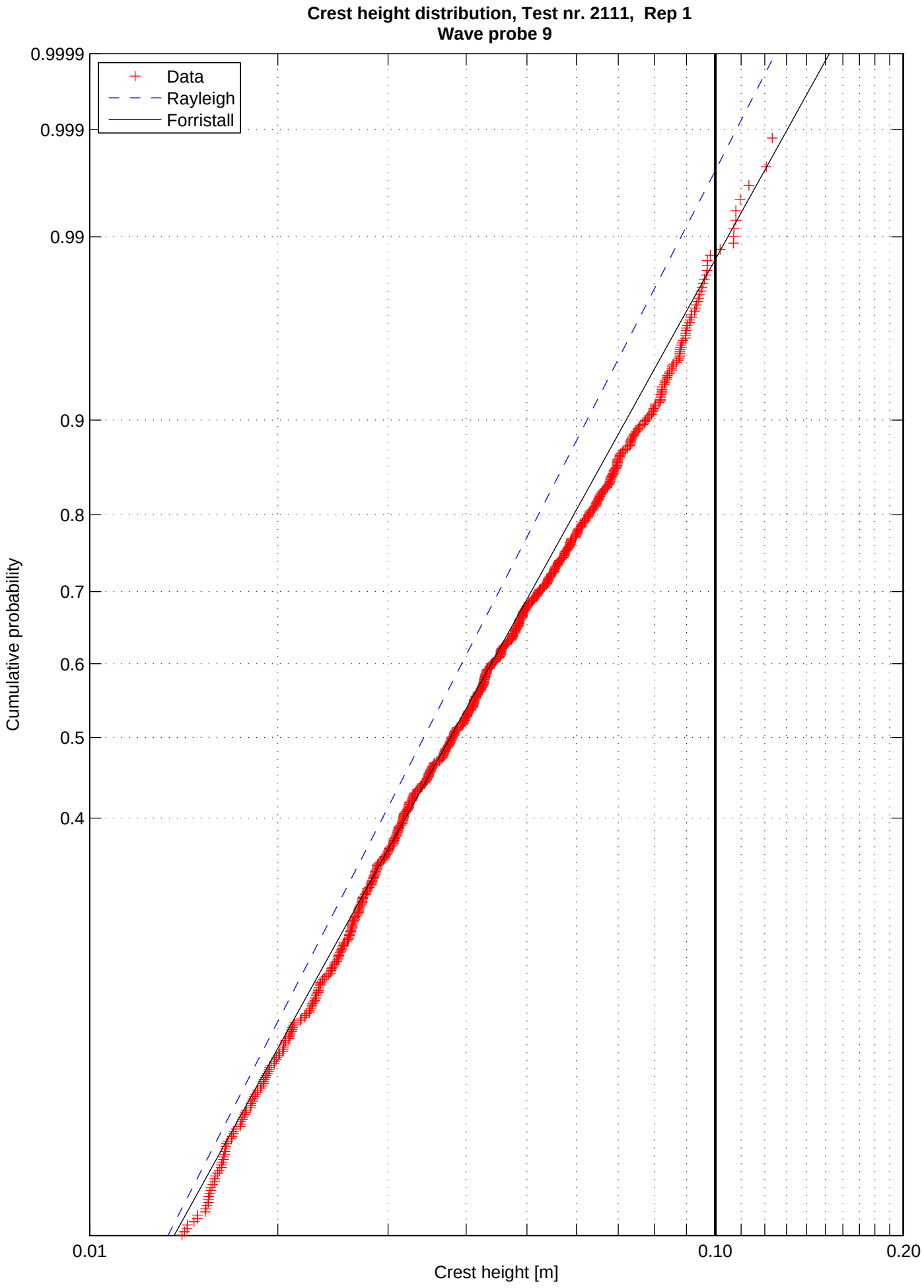
Crest height distribution, Test nr. 2111, Rep 1
Wave probe 9
Data
Rayleigh
Forristall
0.9999
0.999
0.99
0.9
0.8
0.7
0.6
0.5
0.4
Cumulative probability
0.01
0.10
0.20
Crest height [m]

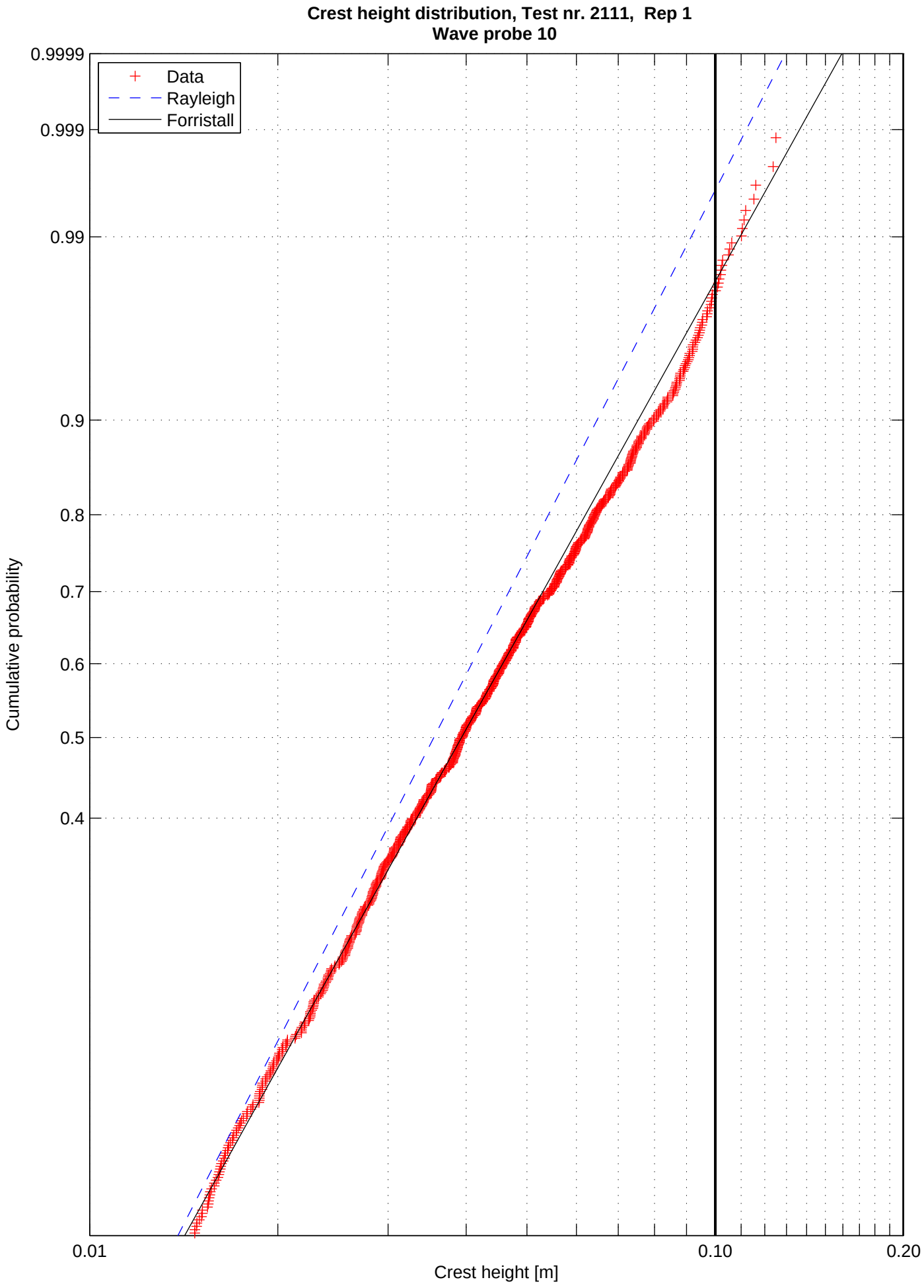
Crest height distribution, Test nr. 2111, Rep 1
Wave probe 10
Data
Rayleigh
Forristall
0.9999
0.999
0.99
0.9
0.8
0.7
0.6
0.5
0.4
Cumulative probability
0.01
0.10
0.20
Crest height [m]

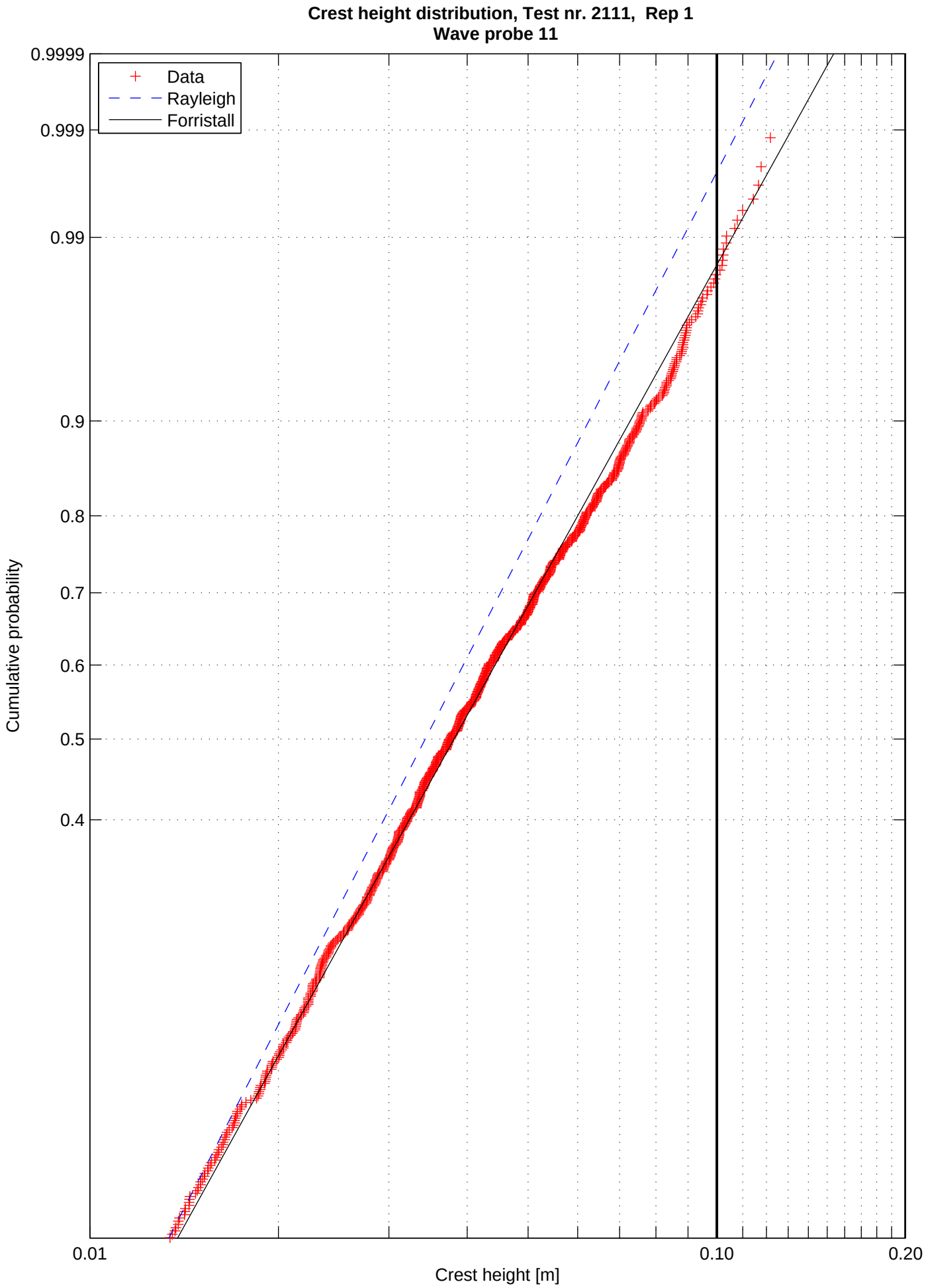
Crest height distribution, Test nr. 2111, Rep 1
Wave probe 11
Data
Rayleigh
Forristall
0.9999
0.999
0.99
0.9
0.8
0.7
0.6
0.5
0.4
Cumulative probability
0.01
0.10
0.20
Crest height [m]

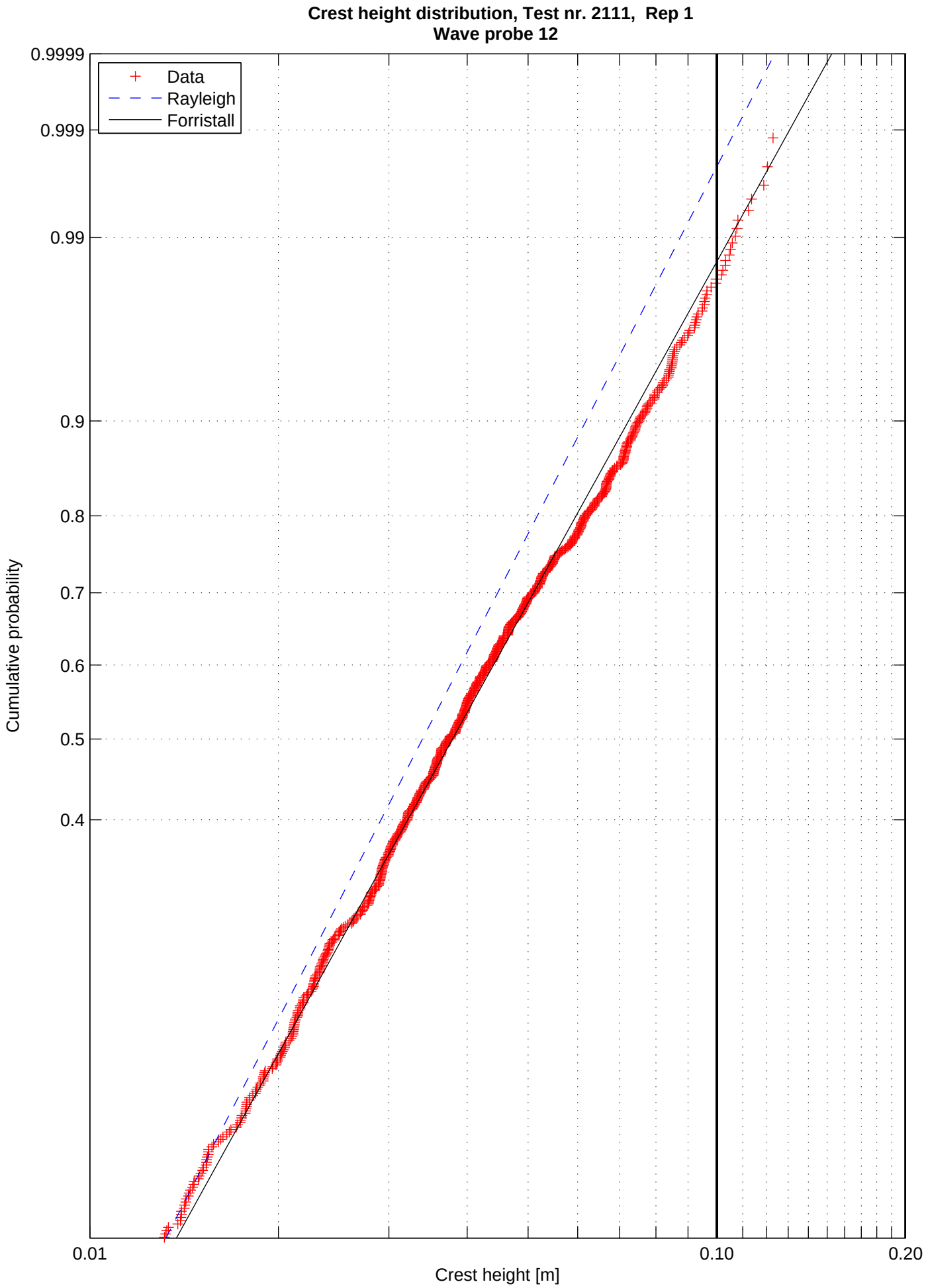
Crest height distribution, Test nr. 2111, Rep 1
Wave probe 12
Data
Rayleigh
Forristall
0.9999
0.999
0.99
0.9
0.8
0.7
0.6
0.5
0.4
Cumulative probability
0.01
0.10
0.20
Crest height [m]

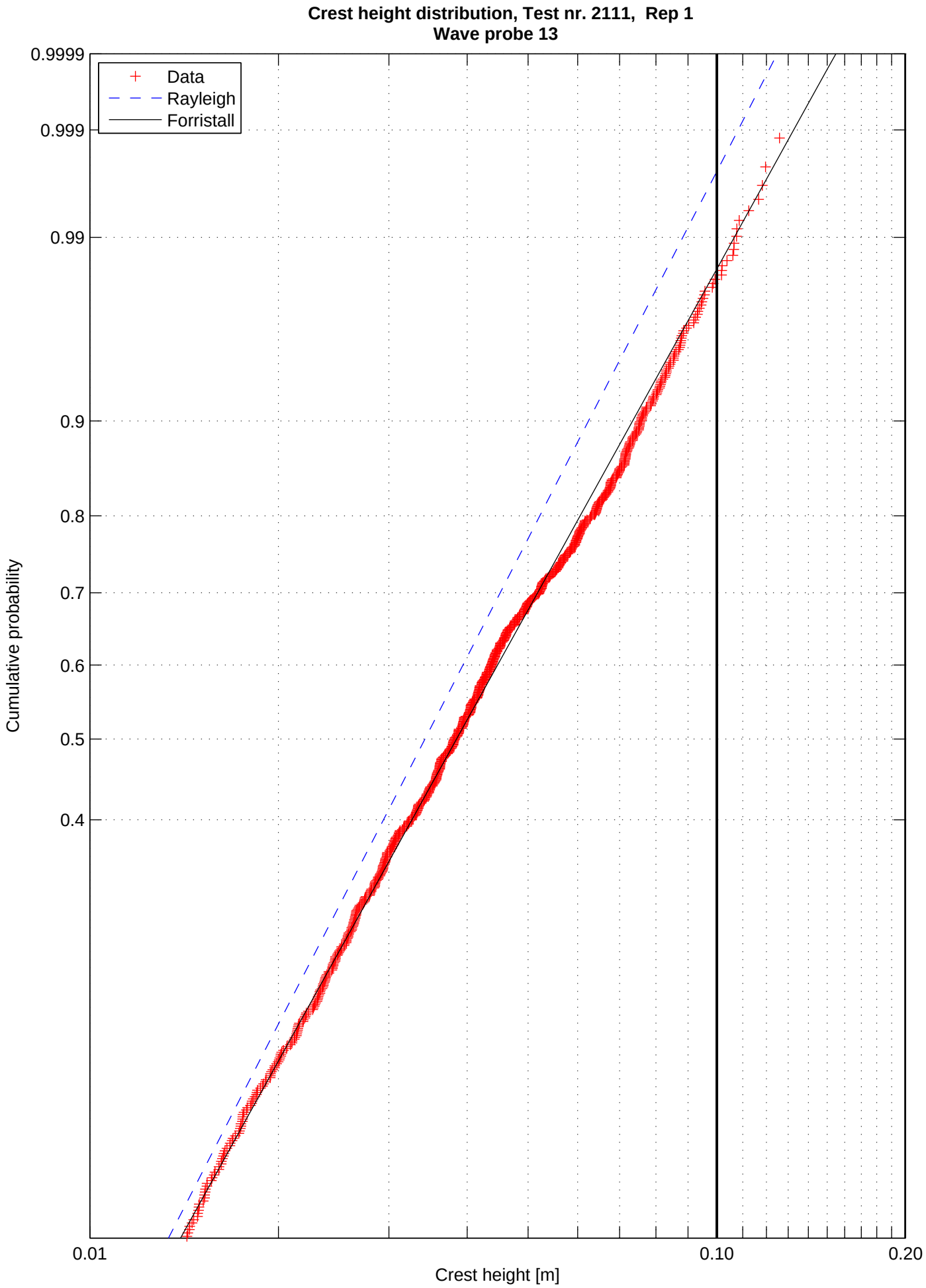
Crest height distribution, Test nr. 2111, Rep 1
Wave probe 13
Data
Rayleigh
Forristall
0.9999
0.999
0.99
0.9
0.8
0.7
0.6
0.5
0.4
Cumulative probability
0.01
0.10
0.20
Crest height [m]

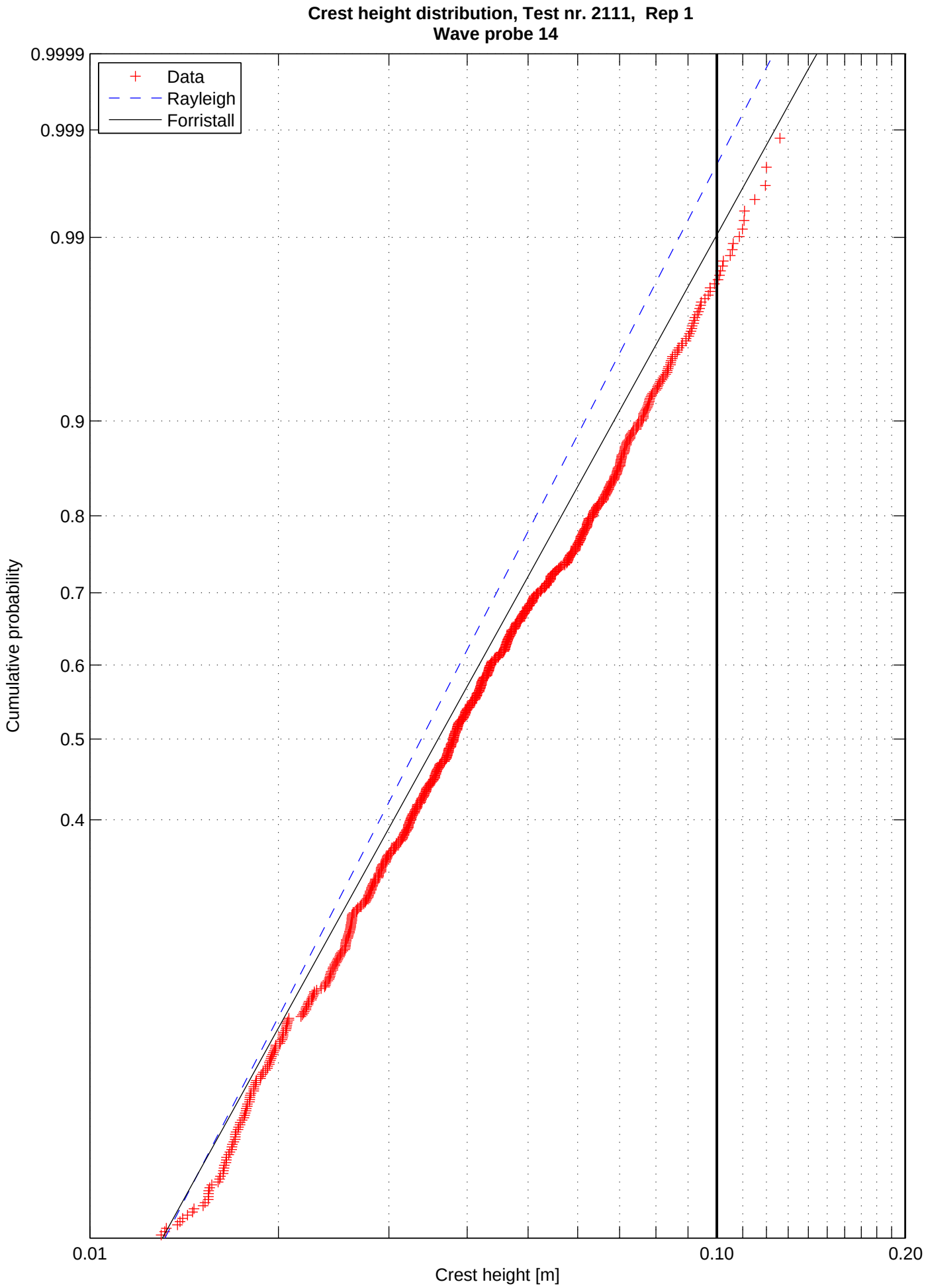
Crest height distribution, Test nr. 2111, Rep 1
Wave probe 14
Data
Rayleigh
Forristall
0.9999
0.999
0.99
0.9
0.8
0.7
0.6
0.5
0.4
Cumulative probability
0.01
0.10
0.20
Crest height [m]

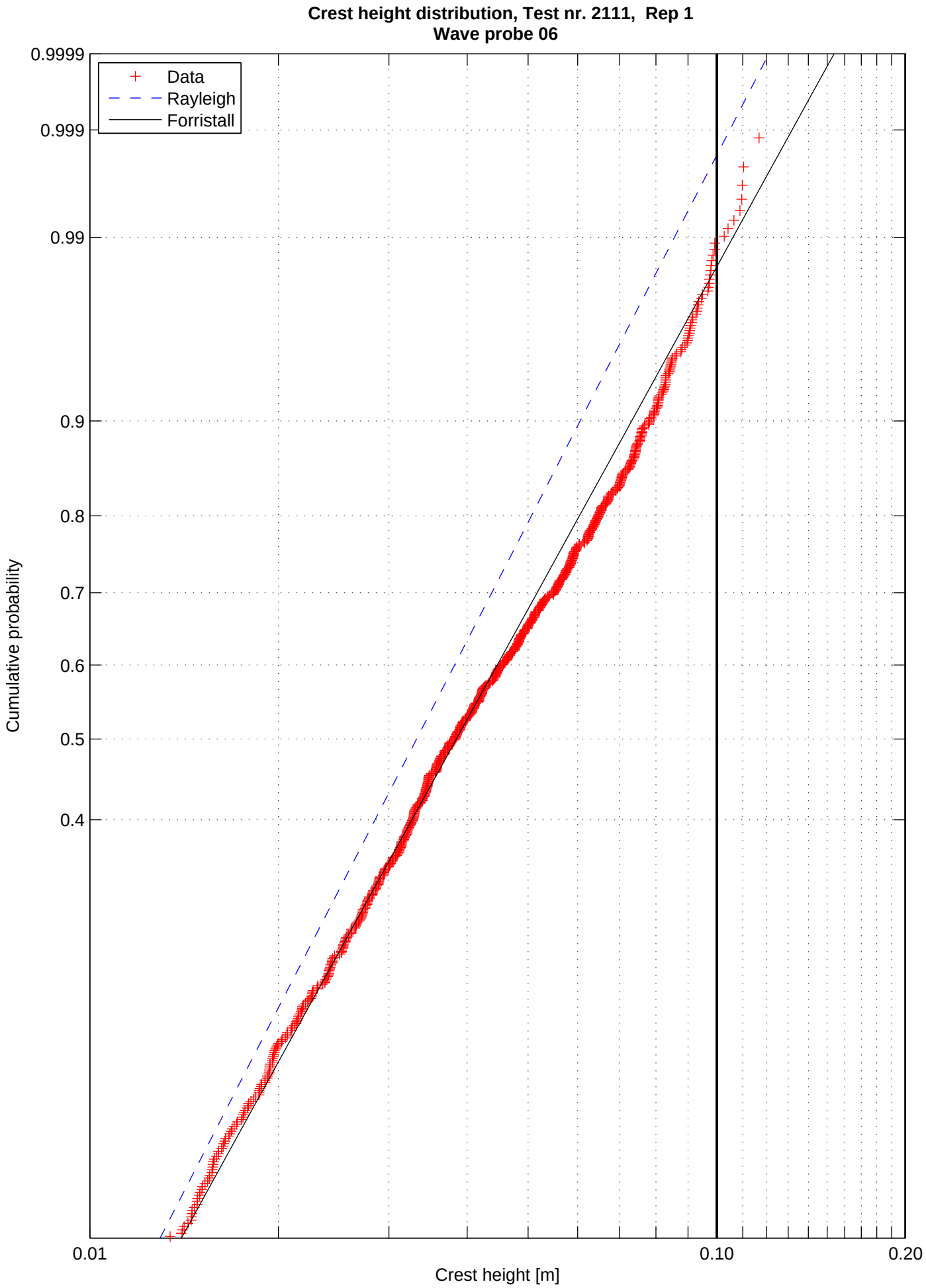
Crest height distribution, Test nr. 2111, Rep 1
Wave probe 06
Data
Rayleigh
Forristall
0.9999
0.999
0.99
0.9
0.8
0.7
0.6
0.5
0.4
Cumulative probability
0.01
0.10
0.20
Crest height [m]

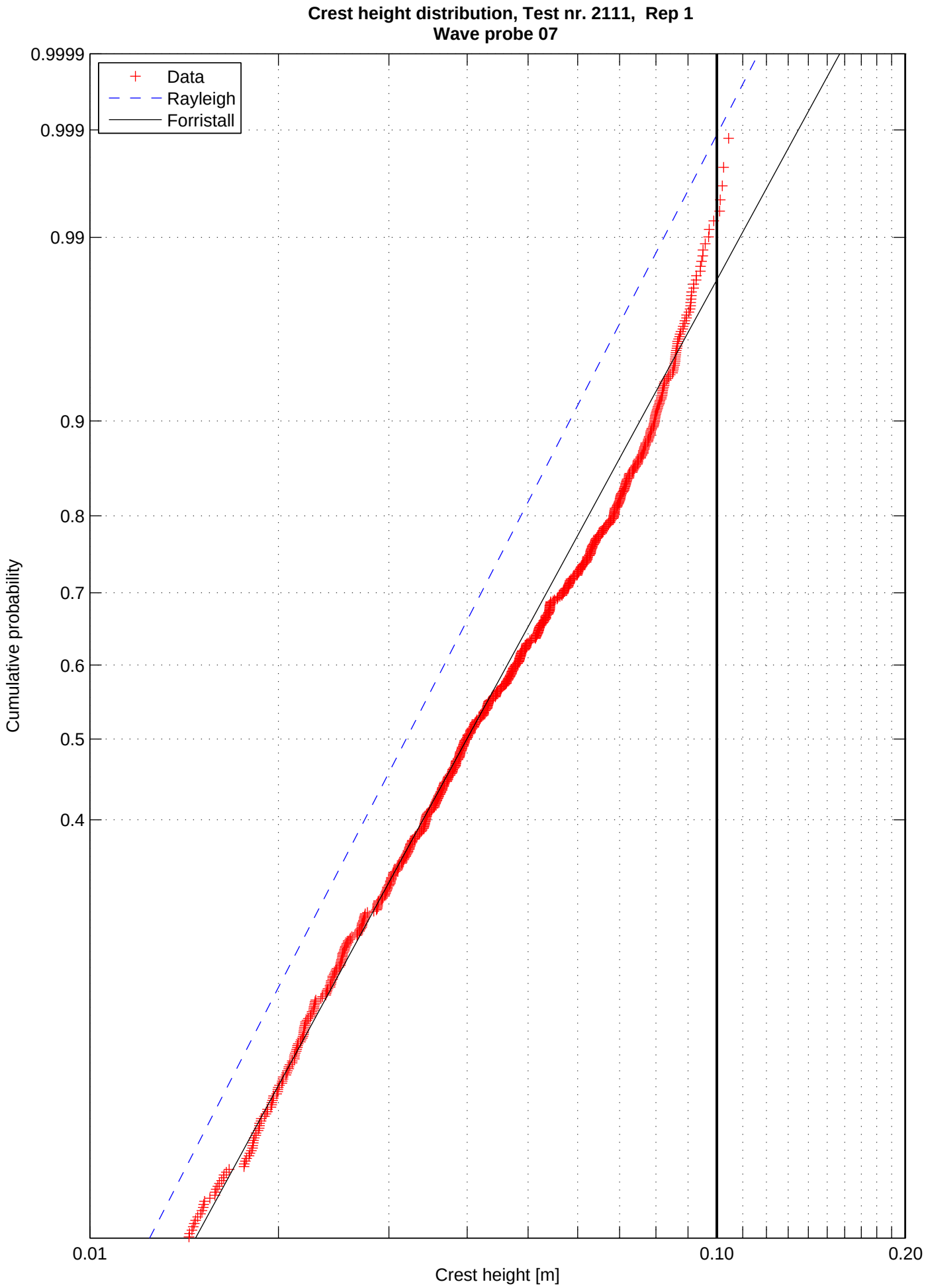
Crest height distribution, Test nr. 2111, Rep 1
Wave probe 07
Data
Rayleigh
Forristall
0.9999
0.999
0.99
0.9
0.8
0.7
0.6
0.5
0.4
Cumulative probability
0.01
0.10
0.20
Crest height [m]

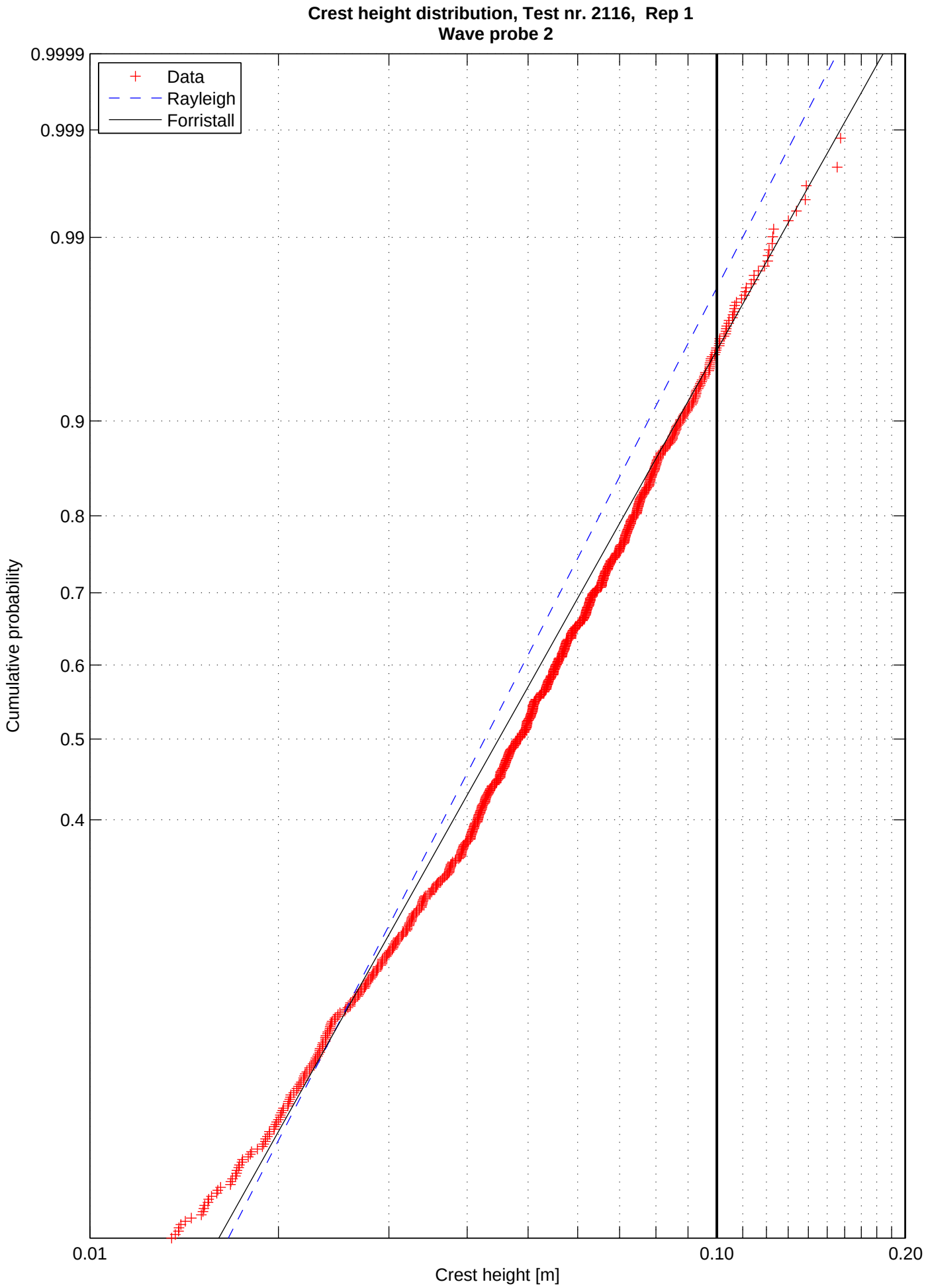
Crest height distribution, Test nr. 2116, Rep 1
Wave probe 2
Data
Rayleigh
Forristall
0.9999
0.999
0.99
0.9
0.8
0.7
0.6
0.5
0.4
Cumulative probability
0.01
0.10
0.20
Crest height [m]

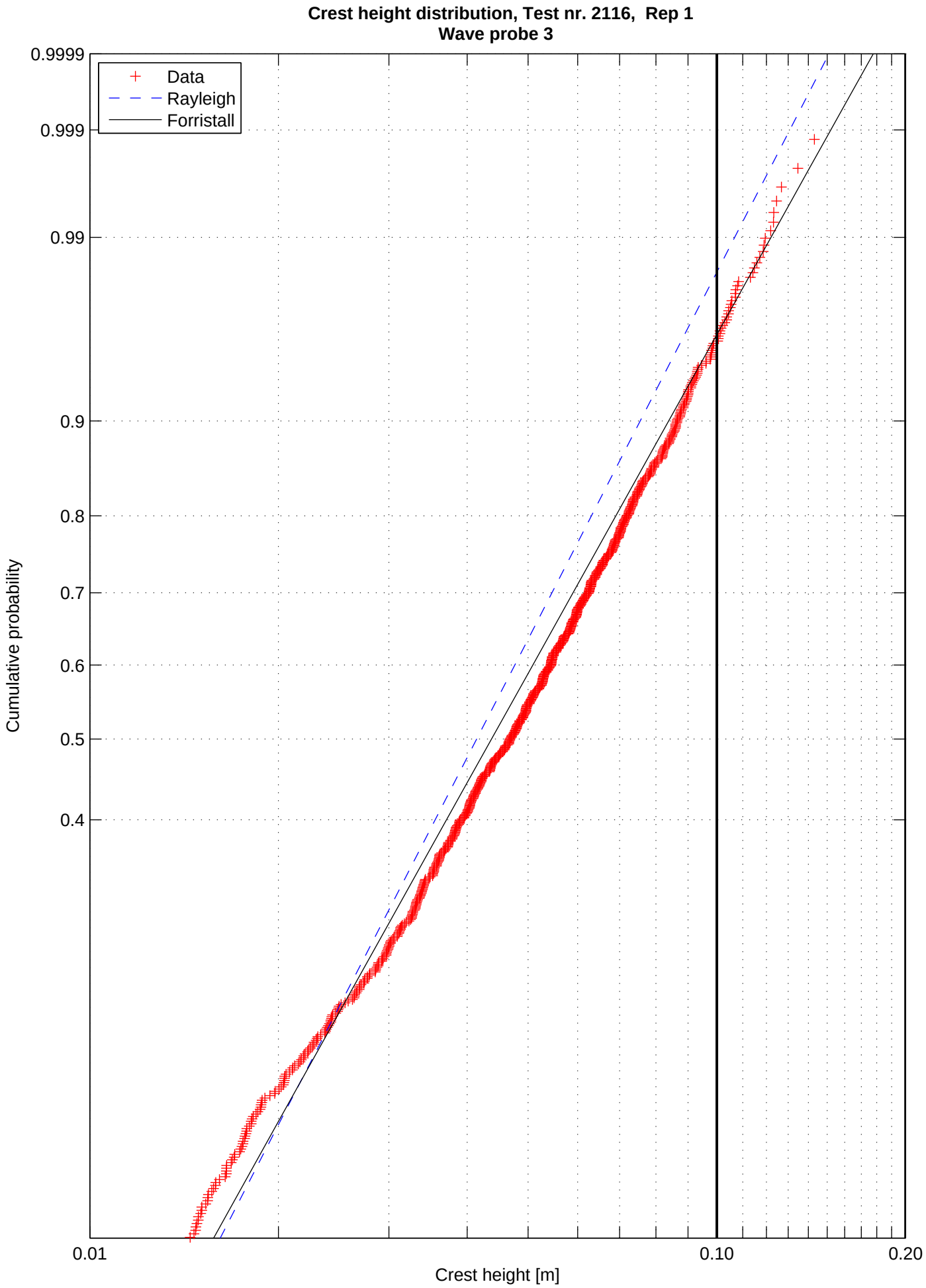
Crest height distribution, Test nr. 2116, Rep 1
Wave probe 3
Data
Rayleigh
Forristall
0.9999
0.999
0.99
0.9
0.8
0.7
0.6
0.5
0.4
Cumulative probability
0.01
0.10
0.20
Crest height [m]

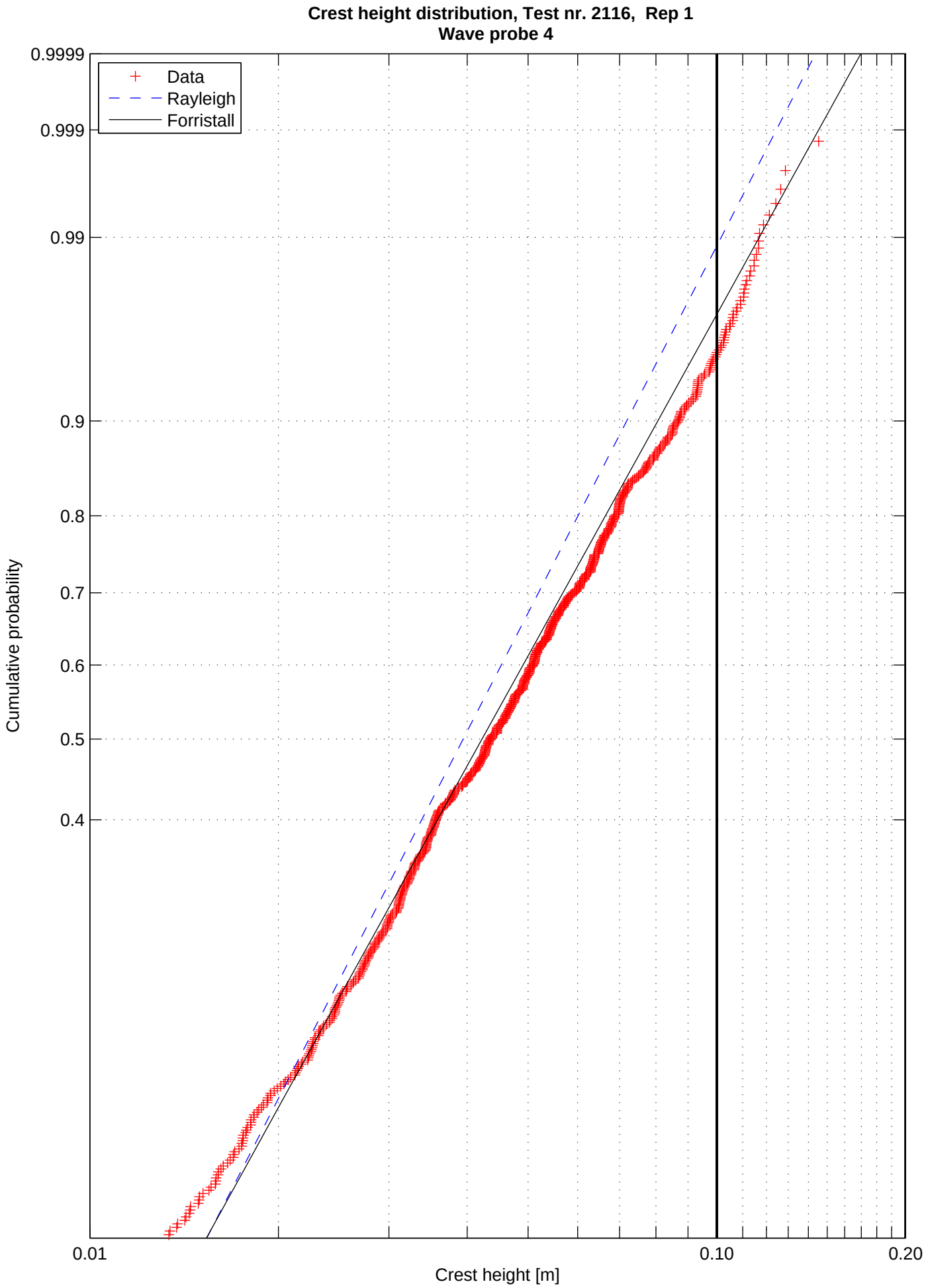
Crest height distribution, Test nr. 2116, Rep 1
Wave probe 4
Data
Rayleigh
Forristall
0.9999
0.999
0.99
0.9
0.8
0.7
0.6
0.5
0.4
Cumulative probability
0.01
0.10
0.20
Crest height [m]

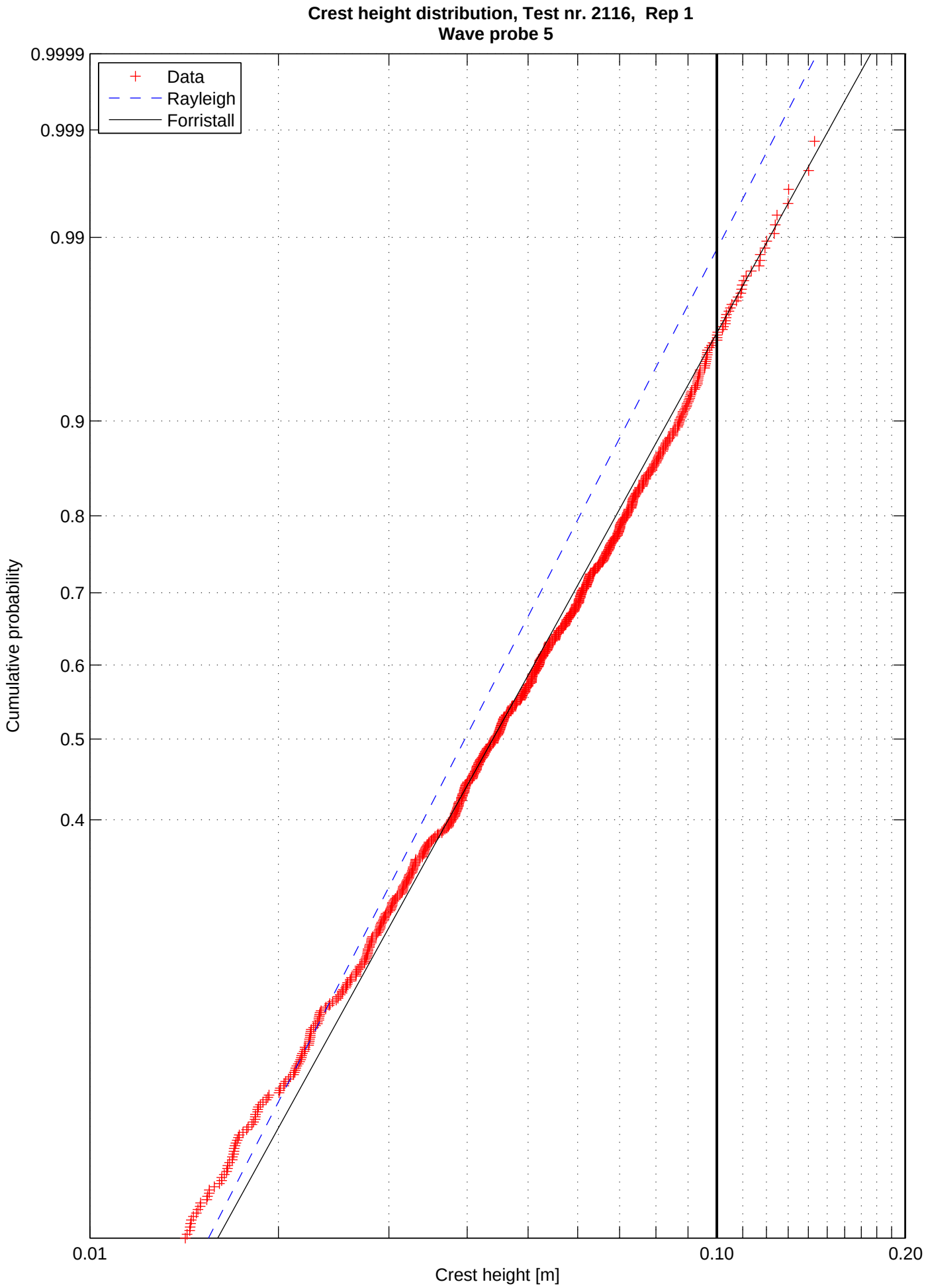
Crest height distribution, Test nr. 2116, Rep 1
Wave probe 5
Data
Rayleigh
Forristall
0.9999
0.999
0.99
0.9
0.8
0.7
0.6
0.5
0.4
Cumulative probability
0.01
0.10
0.20
Crest height [m]

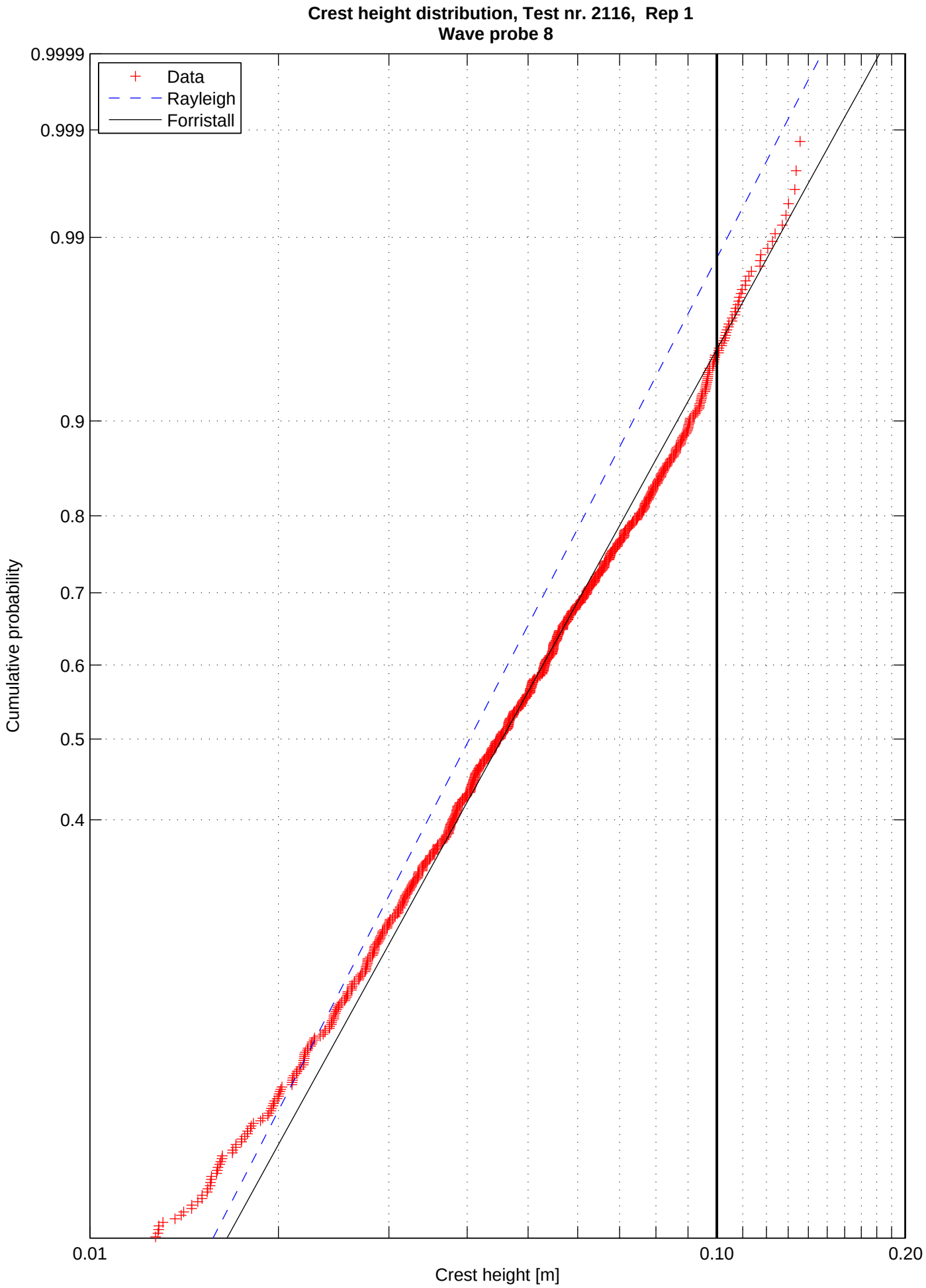
Crest height distribution, Test nr. 2116, Rep 1
Wave probe 8
Data
Rayleigh
Forristall
0.9999
0.999
0.99
0.9
0.8
0.7
0.6
0.5
0.4
Cumulative probability
0.01
0.10
0.20
Crest height [m]

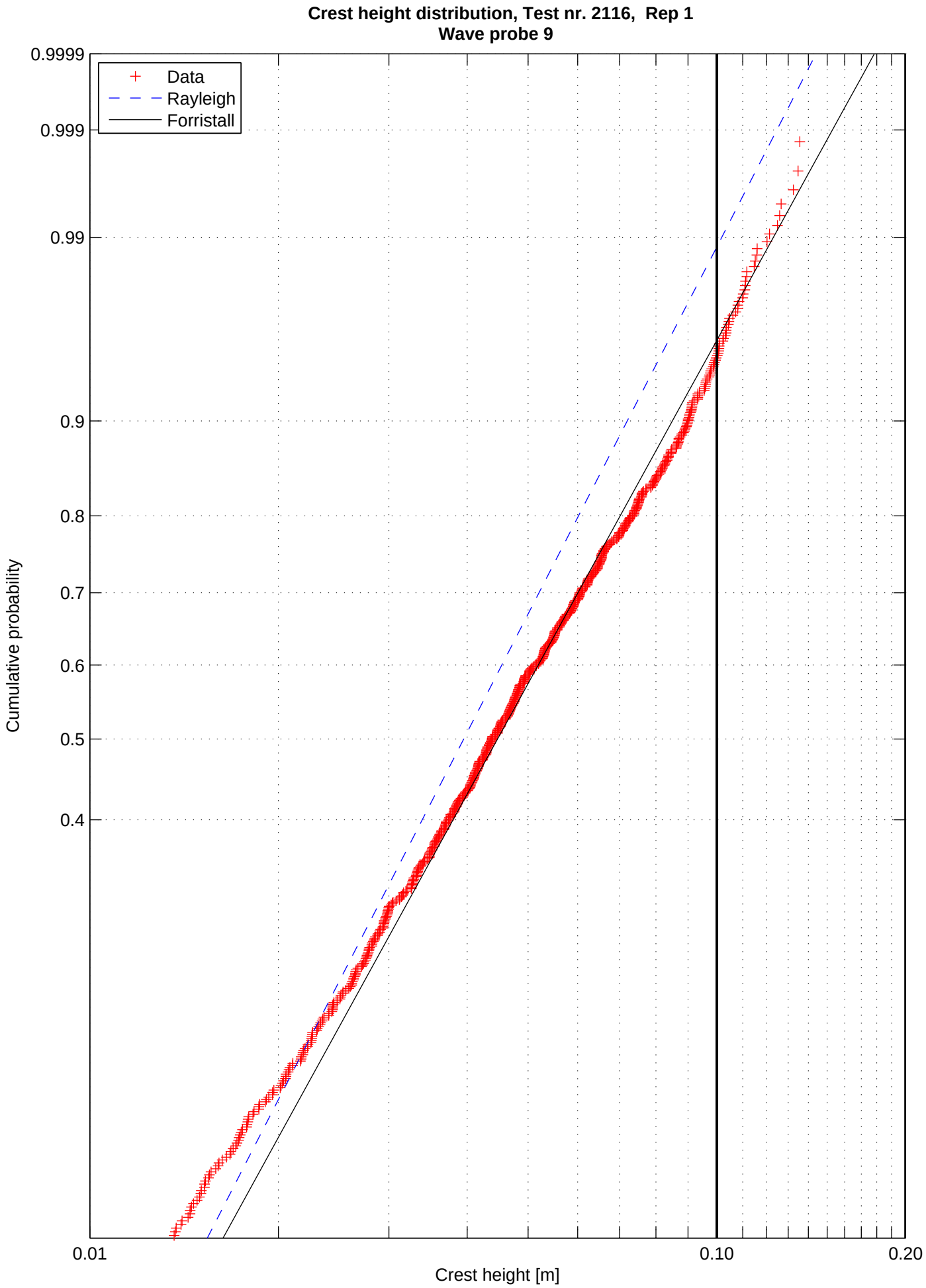
Crest height distribution, Test nr. 2116, Rep 1
Wave probe 9
Data
Rayleigh
Forristall
0.9999
0.999
0.99
0.9
0.8
0.7
0.6
0.5
0.4
Cumulative probability
0.01
0.10
0.20
Crest height [m]

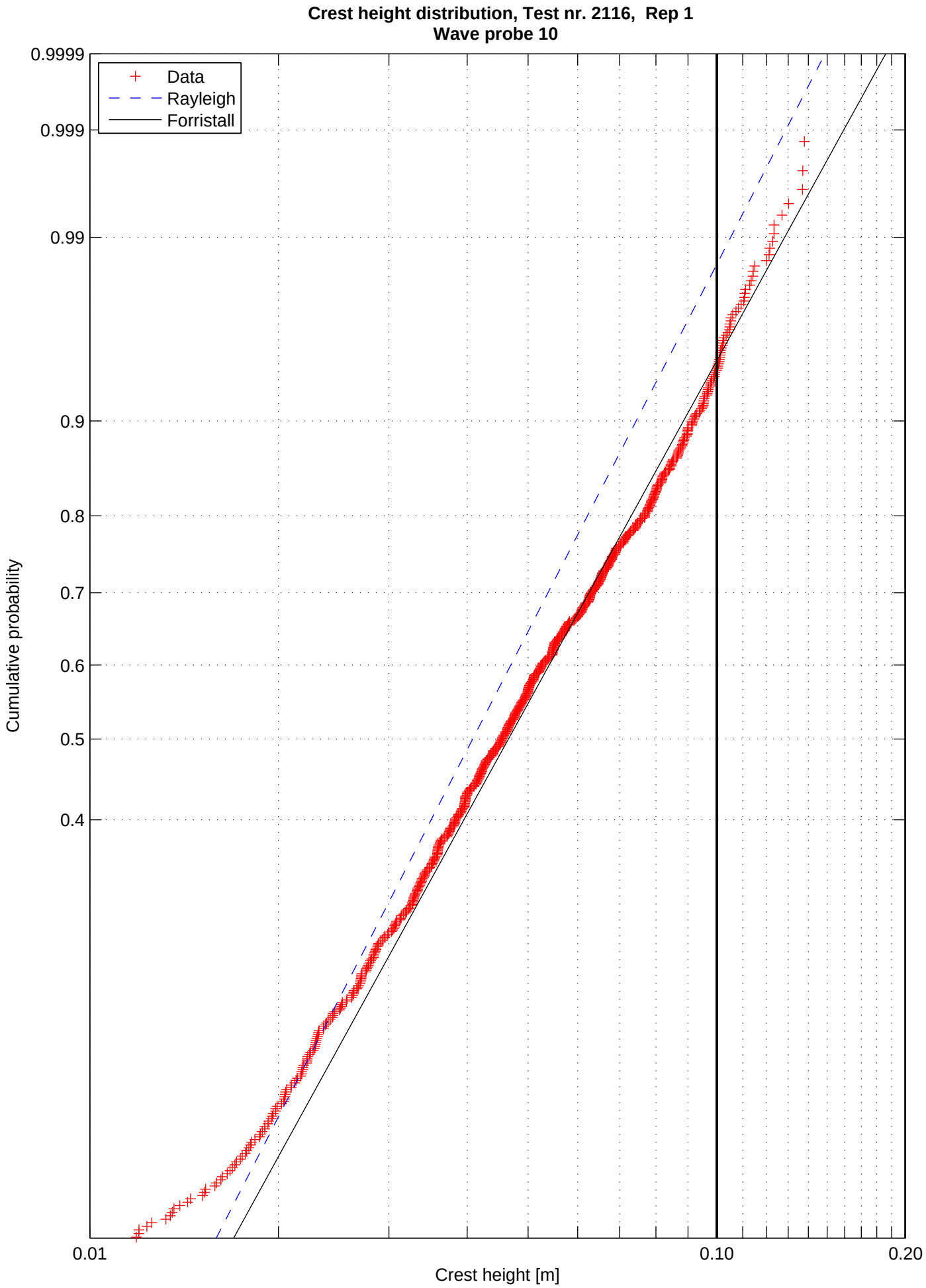
Crest height distribution, Test nr. 2116, Rep 1
Wave probe 10
Data
Rayleigh
Forristall
0.9999
0.999
0.99
0.9
0.8
0.7
0.6
0.5
0.4
Cumulative probability
0.01
0.10
0.20
Crest height [m]

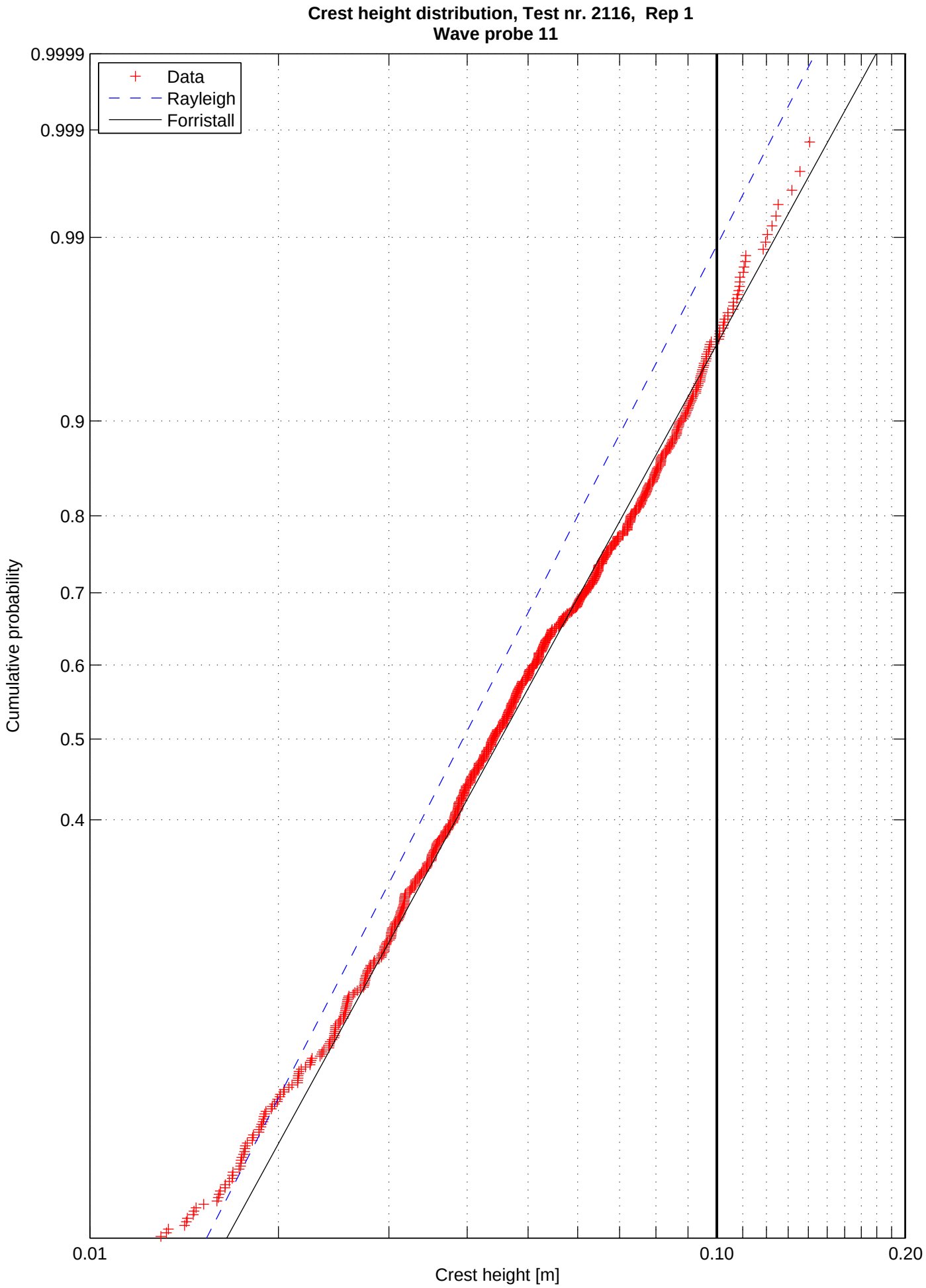
Crest height distribution, Test nr. 2116, Rep 1
Wave probe 11
Data
Rayleigh
Forristall
0.9999
0.999
0.99
0.9
0.8
0.7
0.6
0.5
0.4
Cumulative probability
0.01
0.10
0.20
Crest height [m]

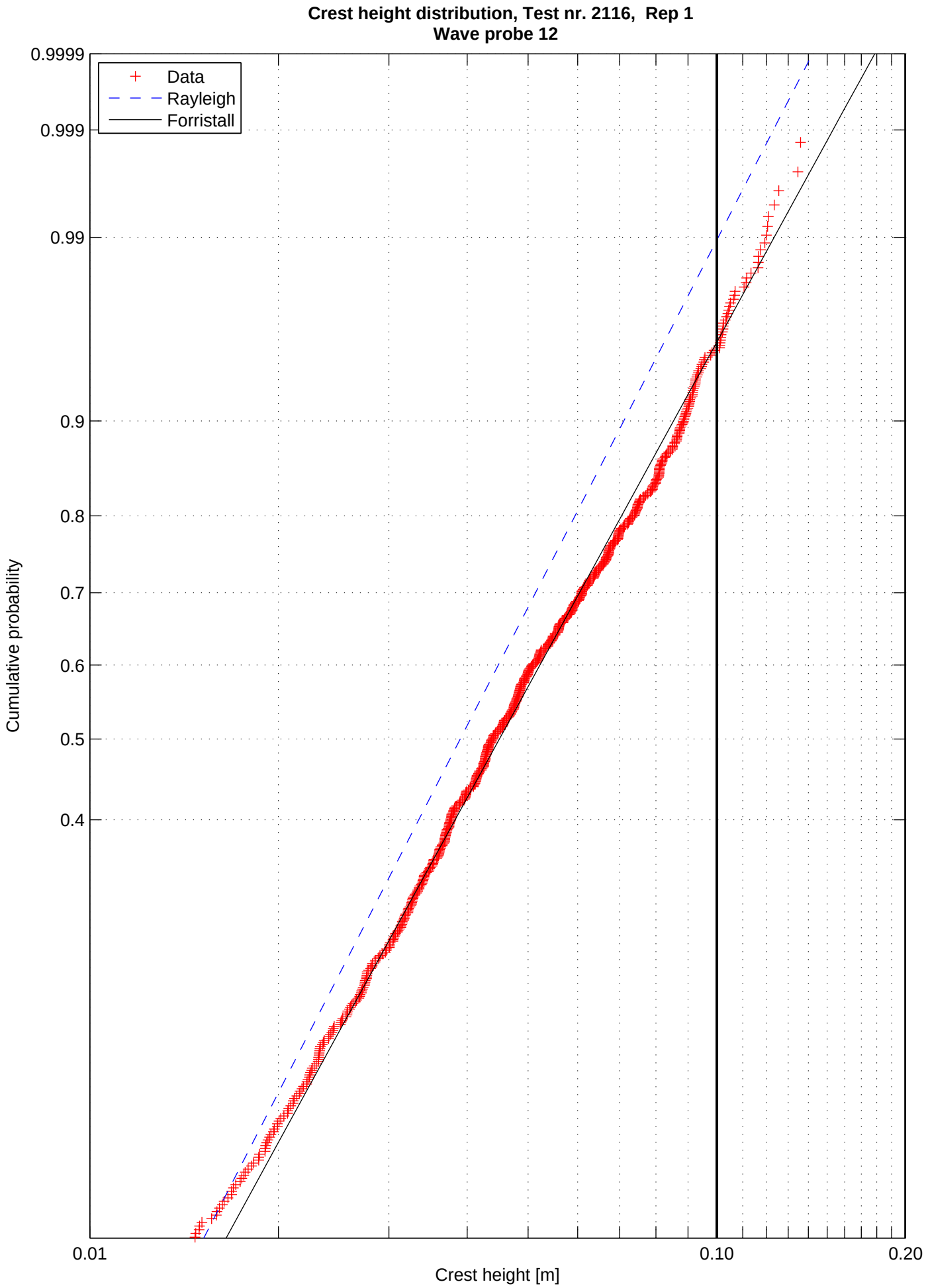
Crest height distribution, Test nr. 2116, Rep 1
Wave probe 12
Data
Rayleigh
Forristall
0.9999
0.999
0.99
0.9
0.8
0.7
0.6
0.5
0.4
Cumulative probability
0.01
0.10
0.20
Crest height [m]

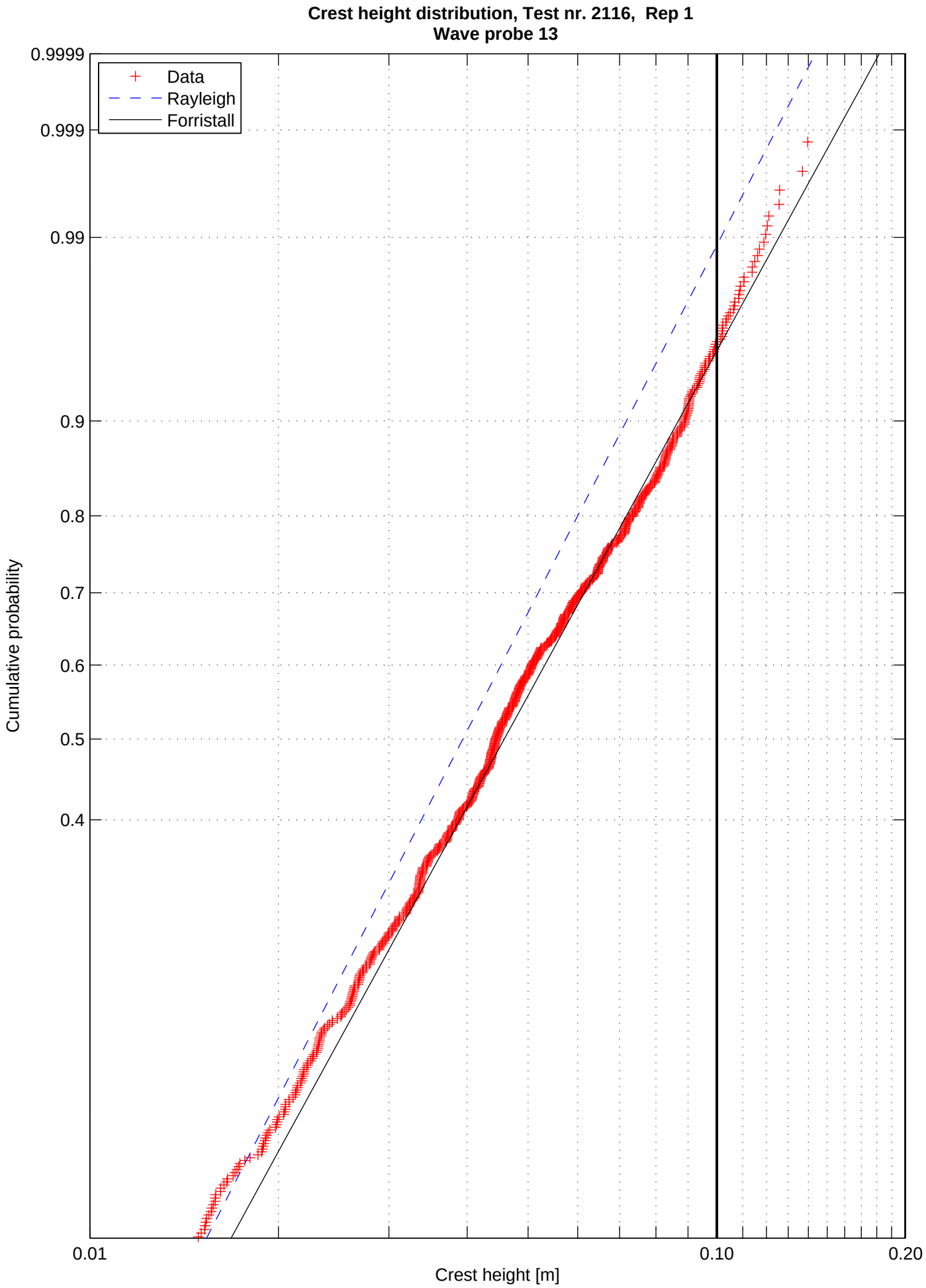
Crest height distribution, Test nr. 2116, Rep 1
Wave probe 13
Data
Rayleigh
Forristall
0.9999
0.999
0.99
0.9
0.8
0.7
0.6
0.5
0.4
Cumulative probability
0.01
0.10
0.20
Crest height [m]

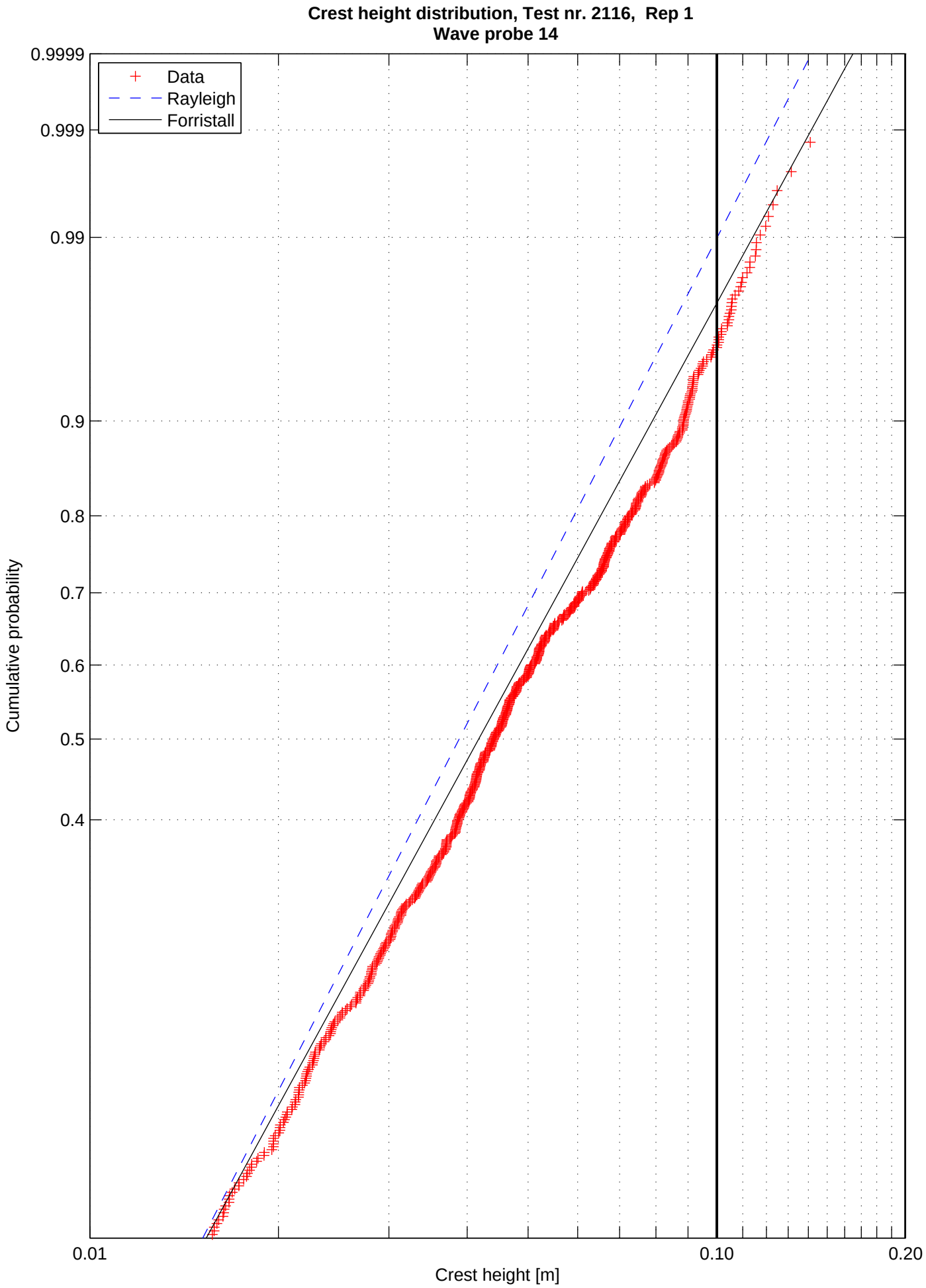
Crest height distribution, Test nr. 2116, Rep 1
Wave probe 14
Data
Rayleigh
Forristall
0.9999
0.999
0.99
0.9
0.8
0.7
0.6
0.5
0.4
Cumulative probability
0.01
0.10
0.20
Crest height [m]

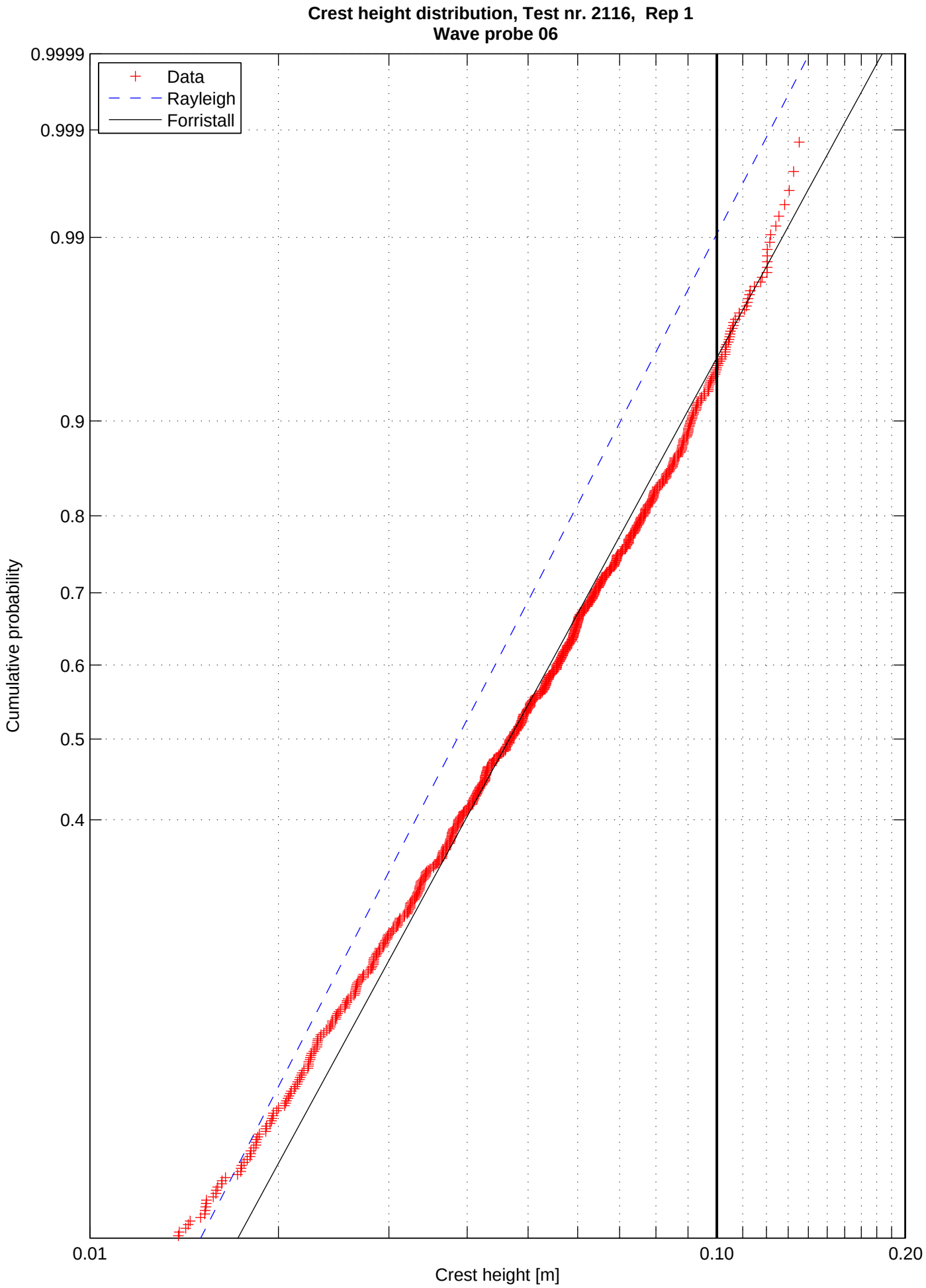
Crest height distribution, Test nr. 2116, Rep 1
Wave probe 06
Data
Rayleigh
Forristall
0.9999
0.999
0.99
0.9
0.8
0.7
0.6
0.5
0.4
Cumulative probability
0.01
0.10
0.20
Crest height [m]

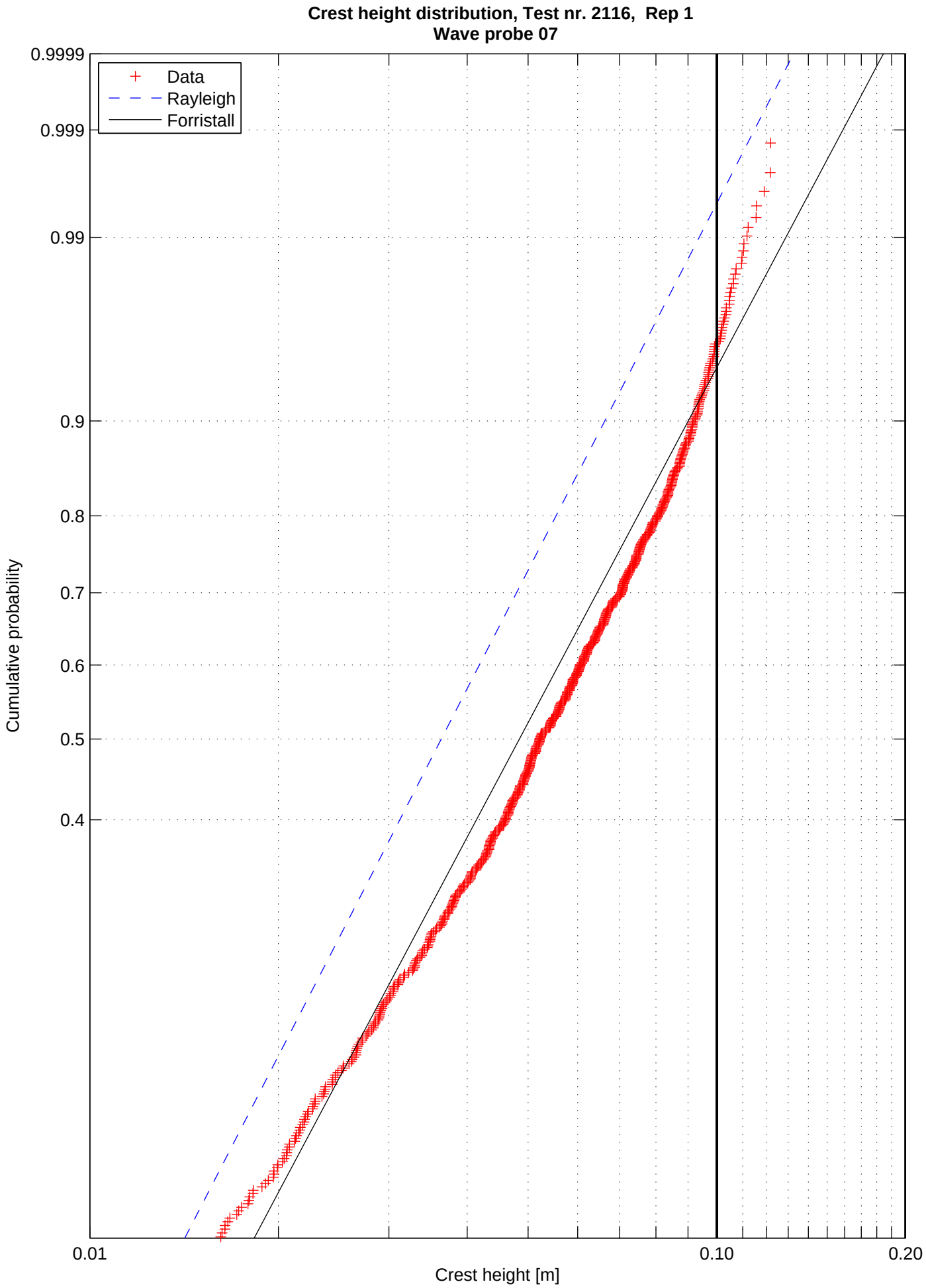
Crest height distribution, Test nr. 2116, Rep 1
Wave probe 07
Data
Rayleigh
Forristall
0.9999
0.999
0.99
0.9
0.8
0.7
0.6
0.5
0.4
Cumulative probability
0.01
0.10
0.20
Crest height [m]

Appendix H

Individual events

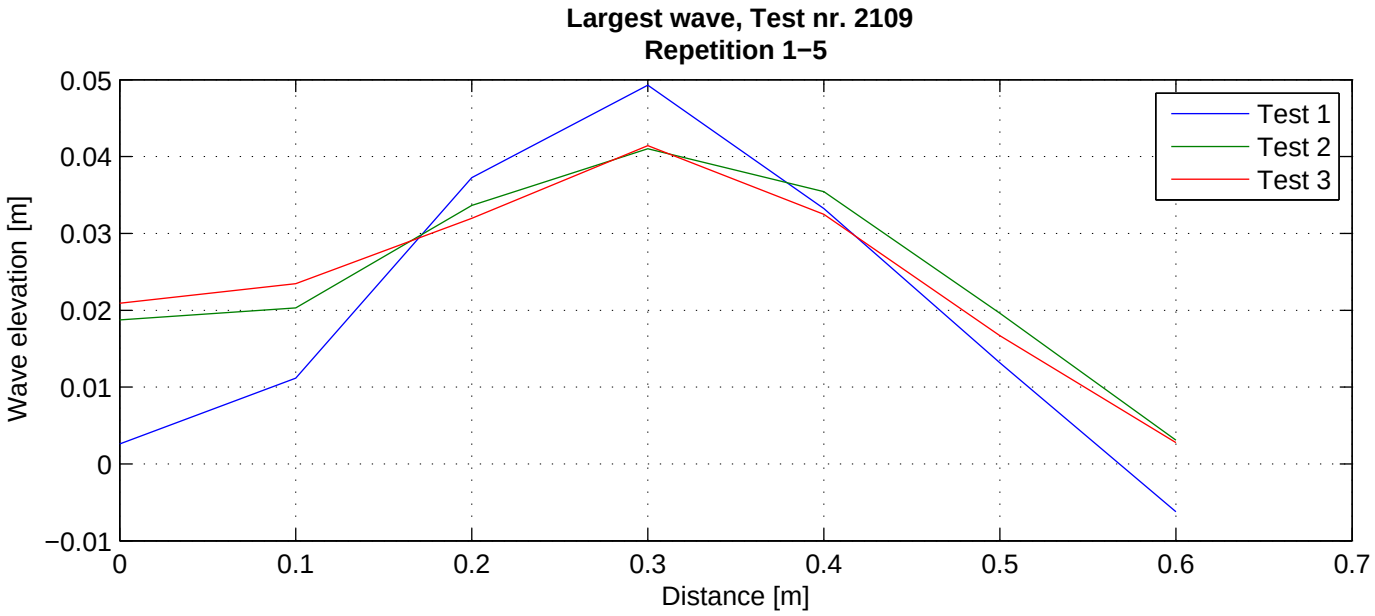
Largest wave, Test nr. 2109
Repetition 1−5
Test 1
Test 2
Test 3
Wave elevation [m]
Distance [m]
0.05
0.04
0.03
0.02
0.01
0
−0.01
0
0.1
0.2
0.3
0.4
0.5
0.6
0.7

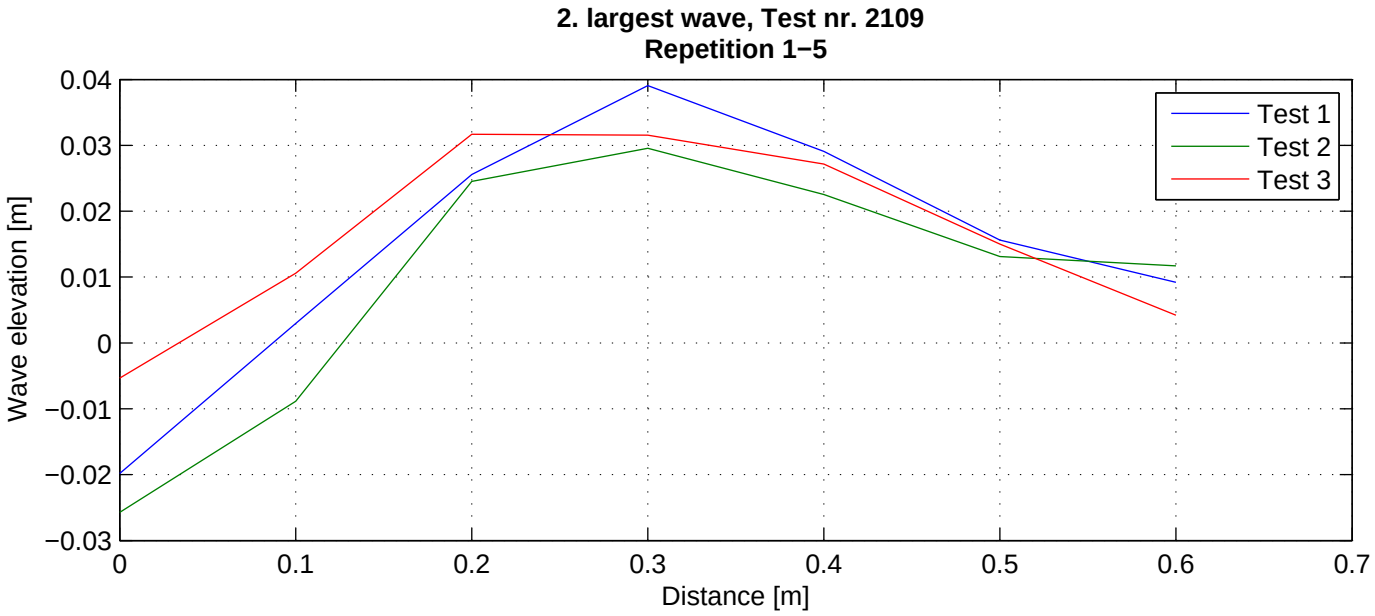
2. largest wave, Test nr. 2109
Repetition 1−5
Test 1
Test 2
Test 3
Wave elevation [m]
Distance [m]
0.04
0.03
0.02
0.01
0
−0.01
−0.02
−0.03
0
0.1
0.2
0.3
0.4
0.5
0.6
0.7

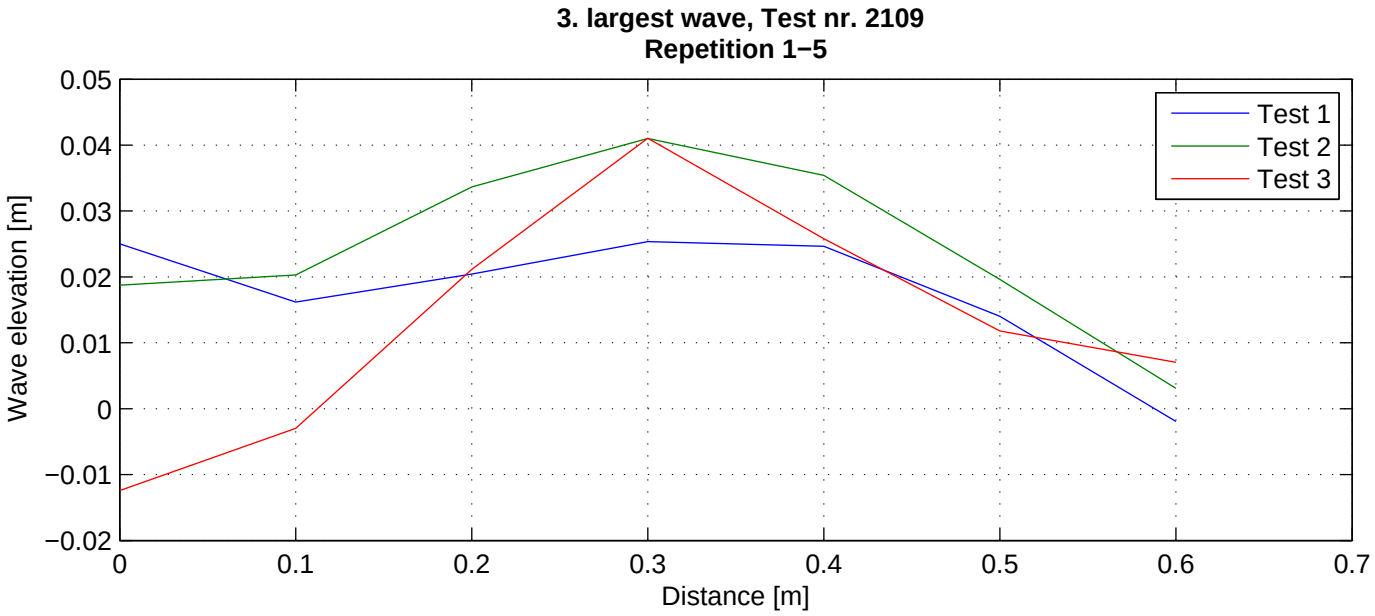
3. largest wave, Test nr. 2109
Repetition 1−5
Test 1
Test 2
Test 3
Wave elevation [m]
Distance [m]
0.05
0.04
0.03
0.02
0.01
0
−0.01
−0.02
0
0.1
0.2
0.3
0.4
0.5
0.6
0.7

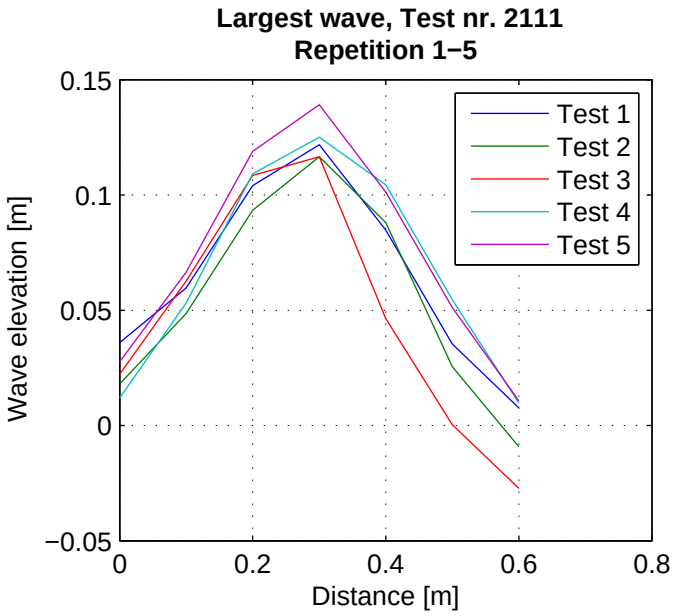
Largest wave, Test nr. 2111
Repetition 1−5
Wave elevation [m]
Distance [m]
Test 1
Test 2
Test 3
Test 4
Test 5

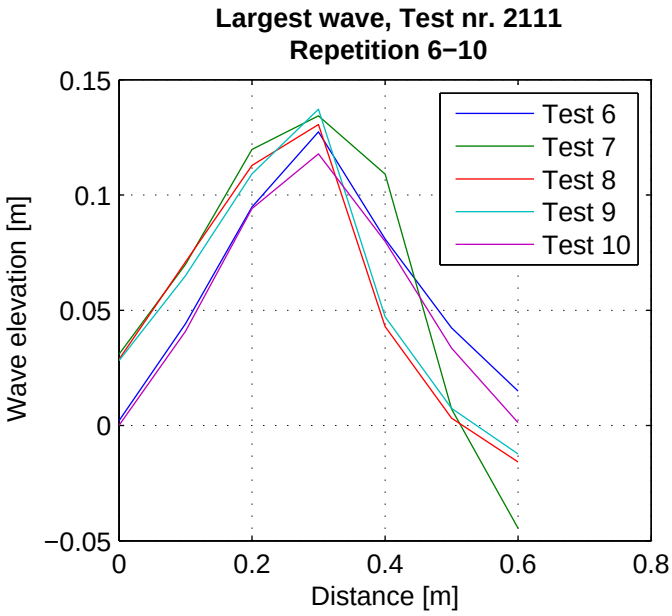
Largest wave, Test nr. 2111
Repetition 6−10
Wave elevation [m]
Distance [m]
Test 6
Test 7
Test 8
Test 9
Test 10

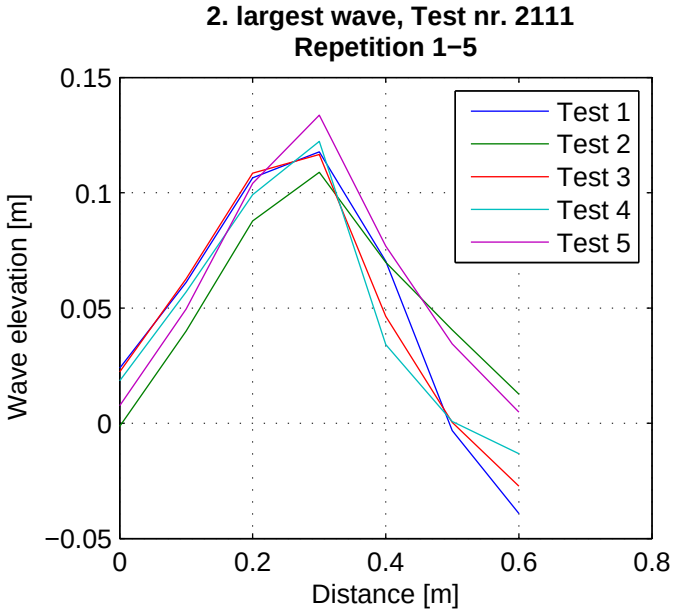
2. largest wave, Test nr. 2111
Repetition 1−5
Wave elevation [m]
Distance [m]
Test 1
Test 2
Test 3
Test 4
Test 5

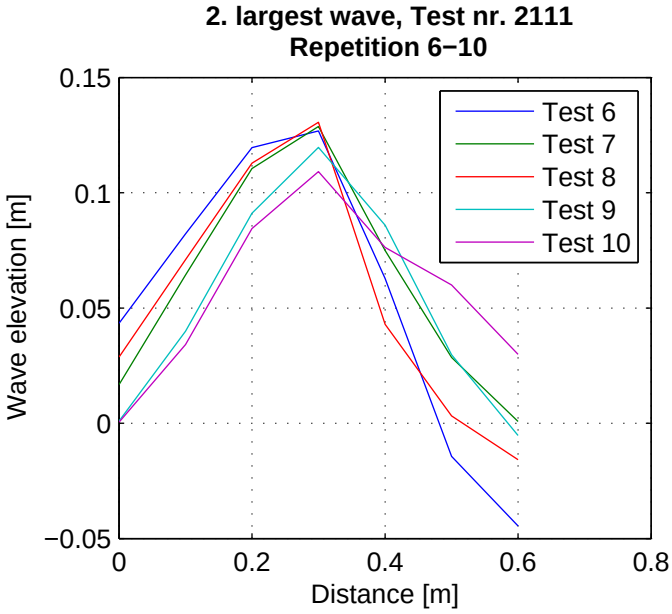
2. largest wave, Test nr. 2111
Repetition 6−10
Wave elevation [m]
Distance [m]
Test 6
Test 7
Test 8
Test 9
Test 10

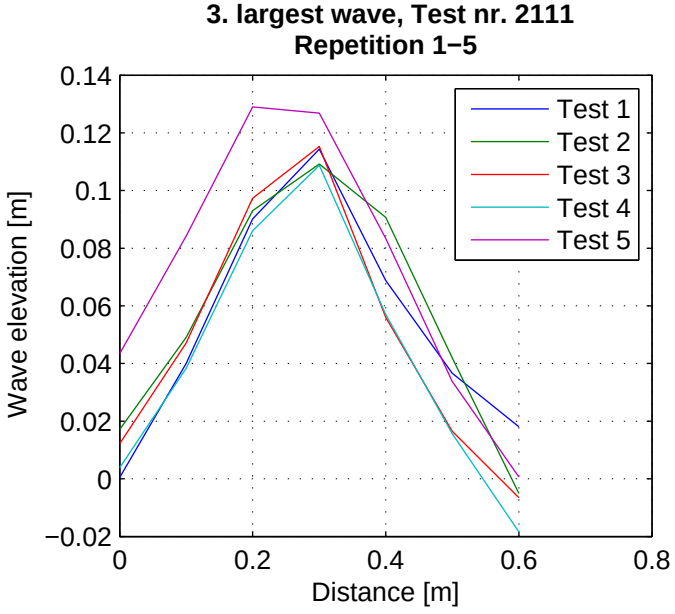
3. largest wave, Test nr. 2111
Repetition 1−5
Wave elevation [m]
Distance [m]
Test 1
Test 2
Test 3
Test 4
Test 5

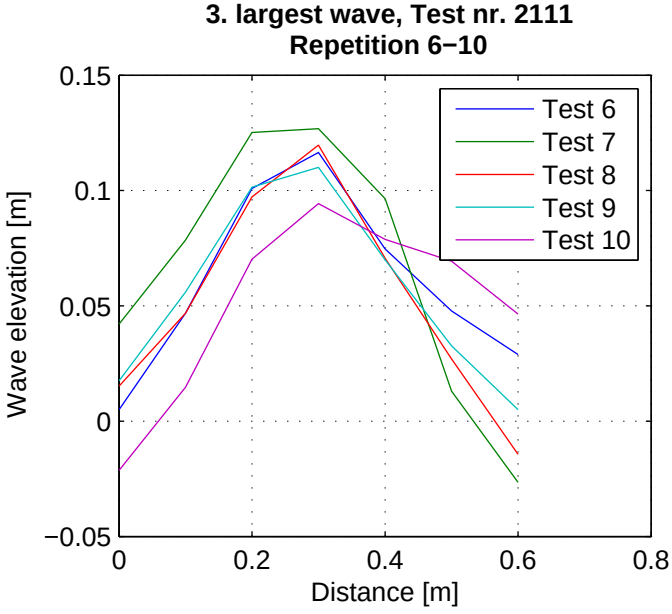
3. largest wave, Test nr. 2111
Repetition 6−10
Wave elevation [m]
Distance [m]
Test 6
Test 7
Test 8
Test 9
Test 10

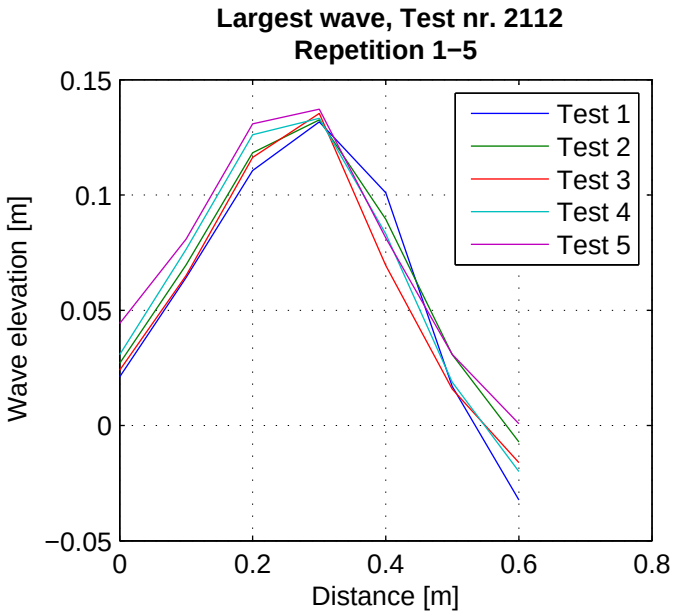
Largest wave, Test nr. 2112
Repetition 1−5
Wave elevation [m]
Distance [m]
Test 1
Test 2
Test 3
Test 4
Test 5

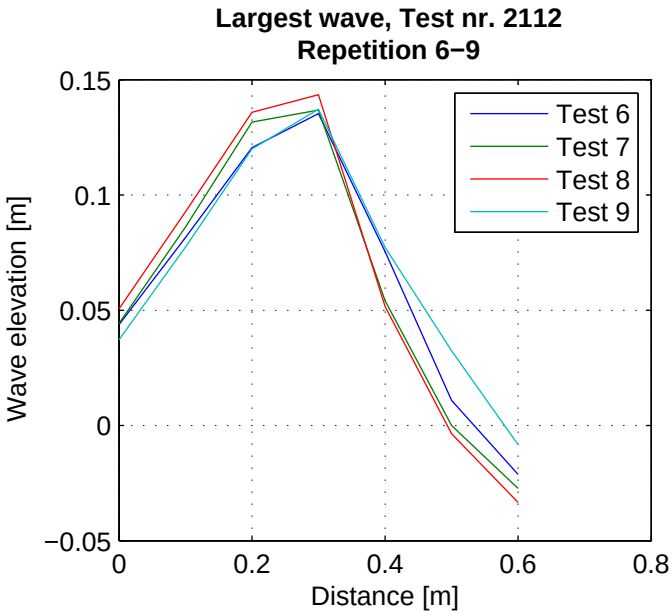
Largest wave, Test nr. 2112
Repetition 6−9
Wave elevation [m]
Distance [m]
Test 6
Test 7
Test 8
Test 9

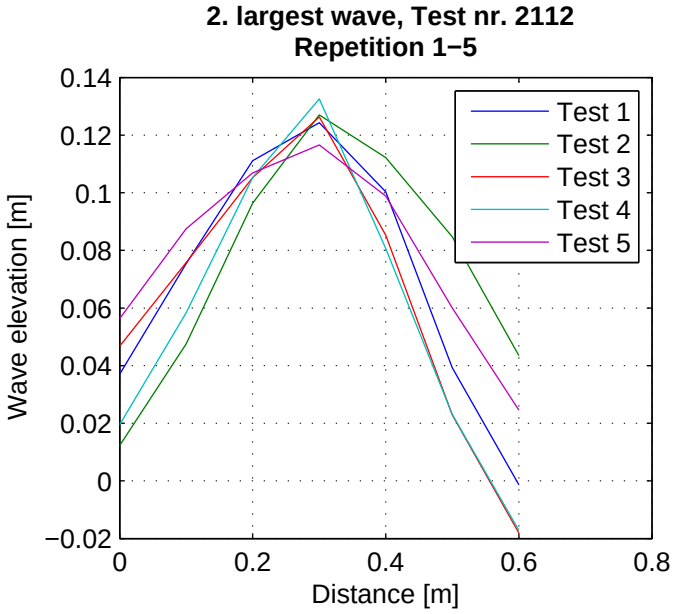
2. largest wave, Test nr. 2112
Repetition 1−5
Wave elevation [m]
Distance [m]
Test 1
Test 2
Test 3
Test 4
Test 5

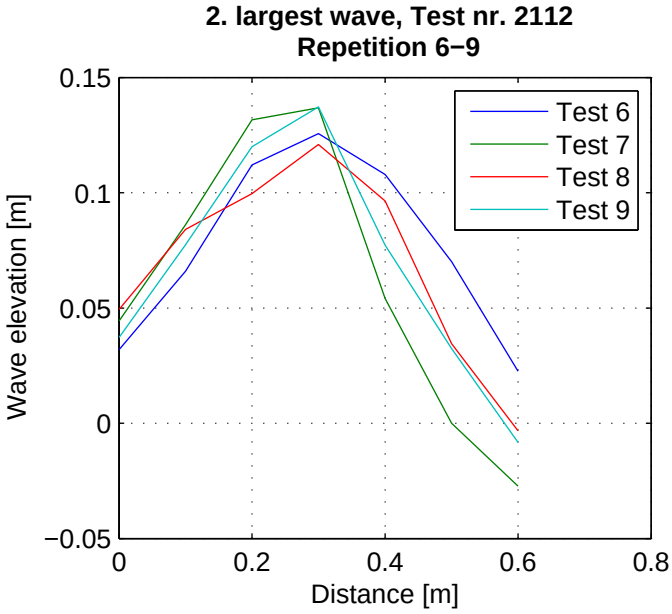
2. largest wave, Test nr. 2112
Repetition 6−9
Wave elevation [m]
Distance [m]
Test 6
Test 7
Test 8
Test 9

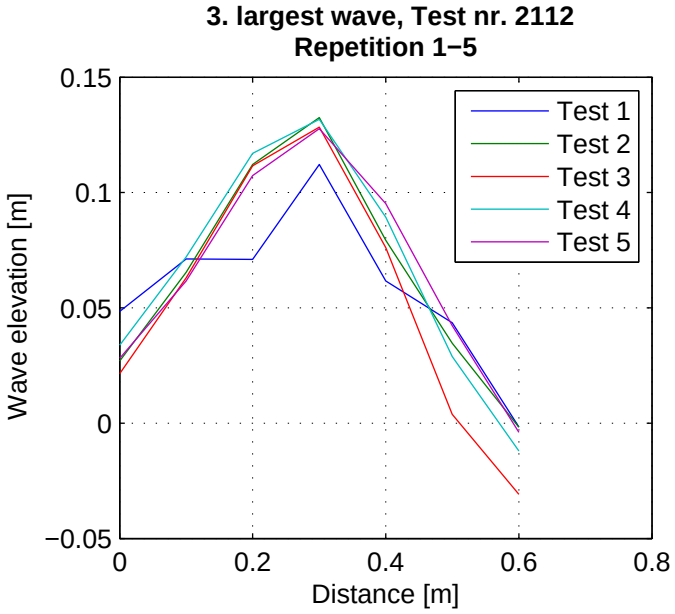
3. largest wave, Test nr. 2112
Repetition 1−5
Wave elevation [m]
Distance [m]
Test 1
Test 2
Test 3
Test 4
Test 5

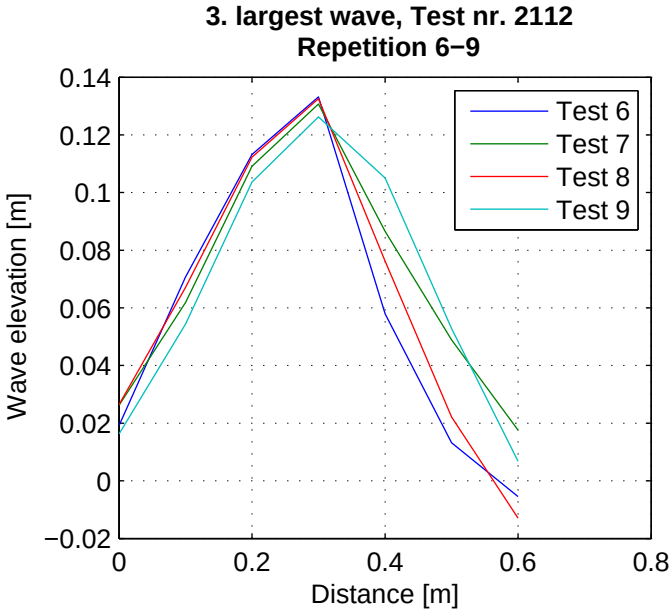
3. largest wave, Test nr. 2112
Repetition 6−9
Wave elevation [m]
Distance [m]
Test 6
Test 7
Test 8
Test 9

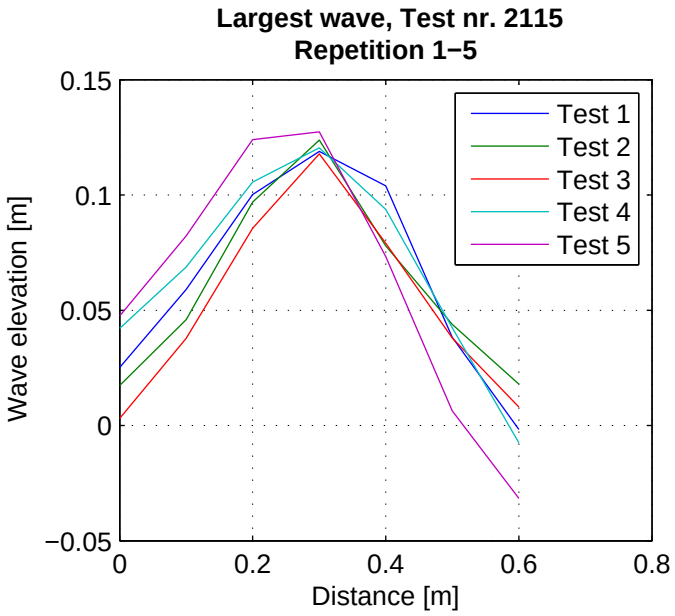
Largest wave, Test nr. 2115
Repetition 1−5
Wave elevation [m]
Distance [m]
Test 1
Test 2
Test 3
Test 4
Test 5

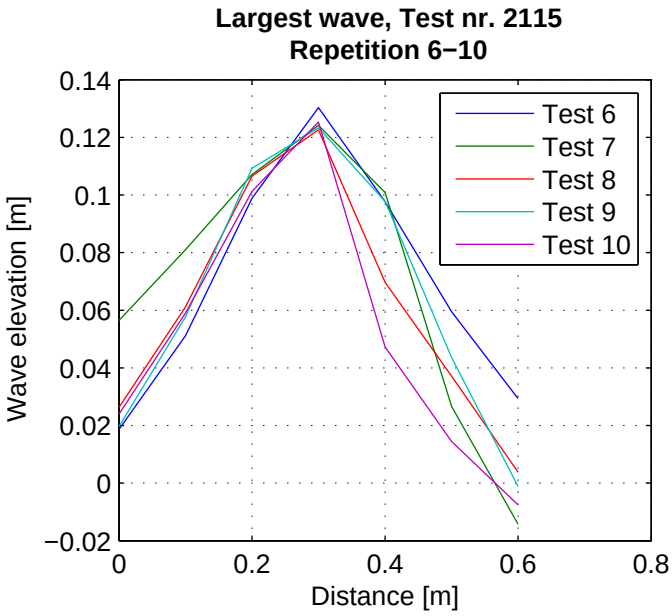
Largest wave, Test nr. 2115
Repetition 6−10
Wave elevation [m]
Distance [m]
Test 6
Test 7
Test 8
Test 9
Test 10

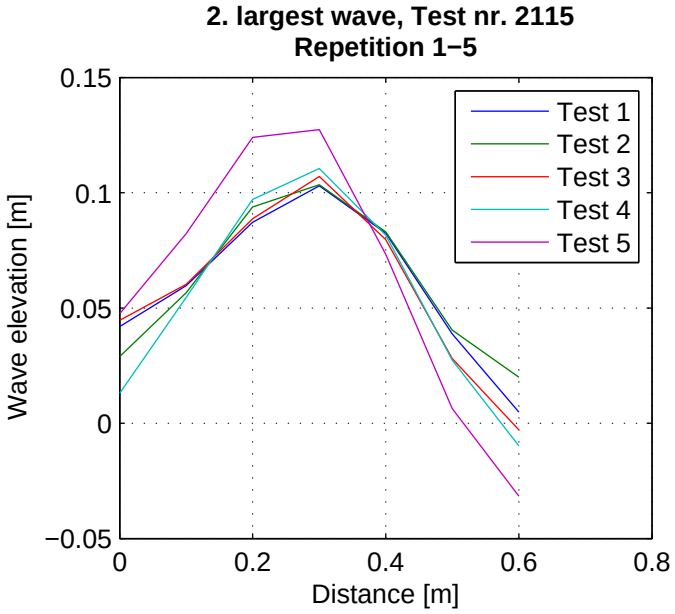
2. largest wave, Test nr. 2115
Repetition 1−5
Wave elevation [m]
Distance [m]
Test 1
Test 2
Test 3
Test 4
Test 5

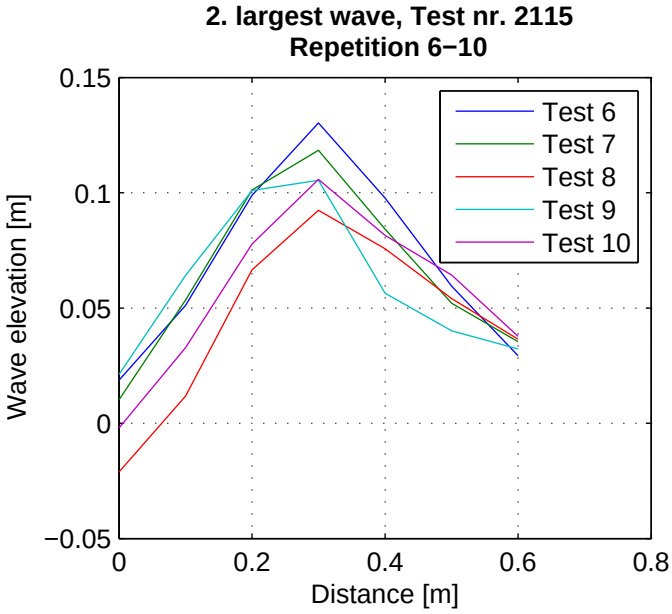
2. largest wave, Test nr. 2115
Repetition 6−10
Wave elevation [m]
Distance [m]
Test 6
Test 7
Test 8
Test 9
Test 10

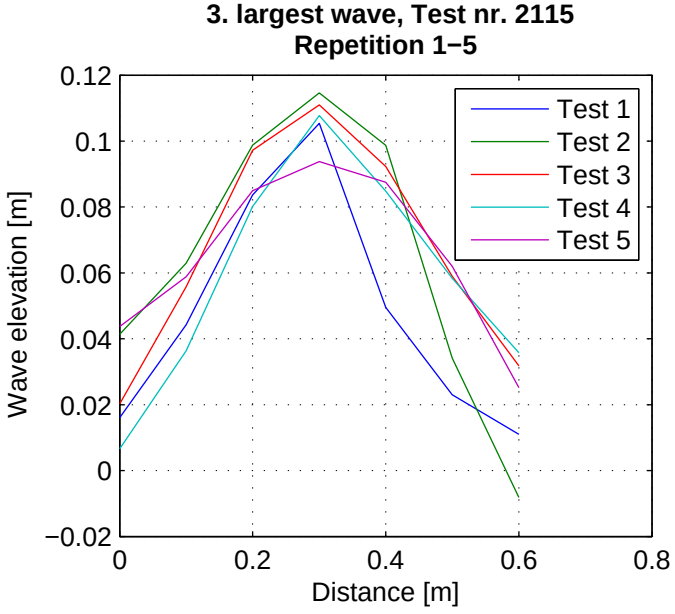
3. largest wave, Test nr. 2115
Repetition 1−5
Wave elevation [m]
Distance [m]
Test 1
Test 2
Test 3
Test 4
Test 5

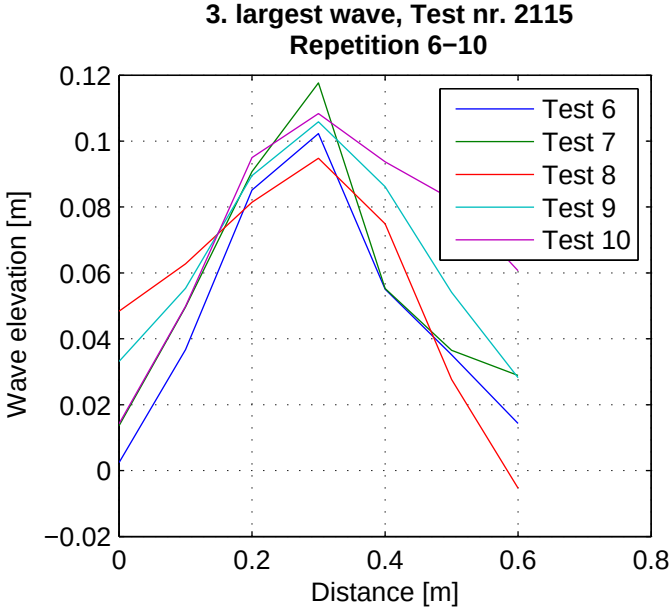
3. largest wave, Test nr. 2115
Repetition 6−10
Wave elevation [m]
Distance [m]
Test 6
Test 7
Test 8
Test 9
Test 10

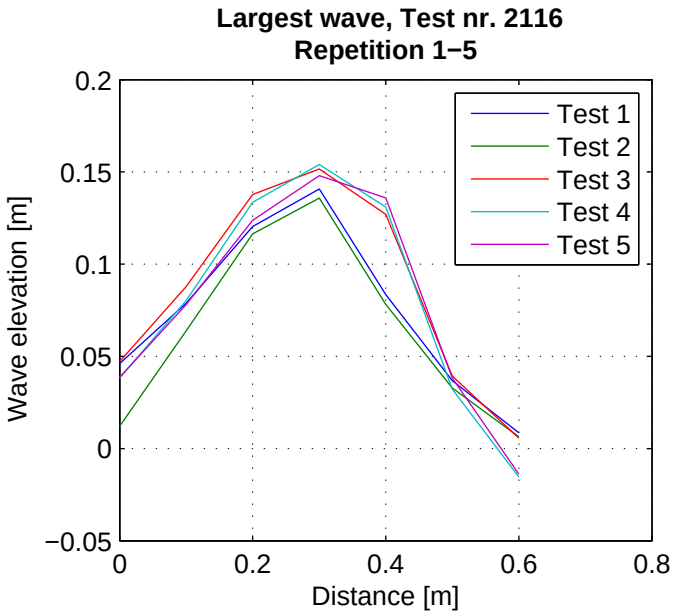
Largest wave, Test nr. 2116
Repetition 1−5
Wave elevation [m]
Distance [m]
Test 1
Test 2
Test 3
Test 4
Test 5

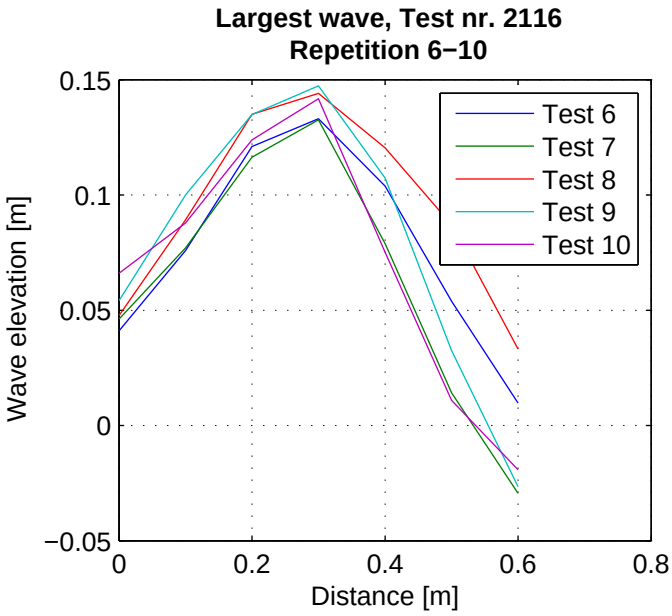
Largest wave, Test nr. 2116
Repetition 6−10
Wave elevation [m]
Distance [m]
Test 6
Test 7
Test 8
Test 9
Test 10

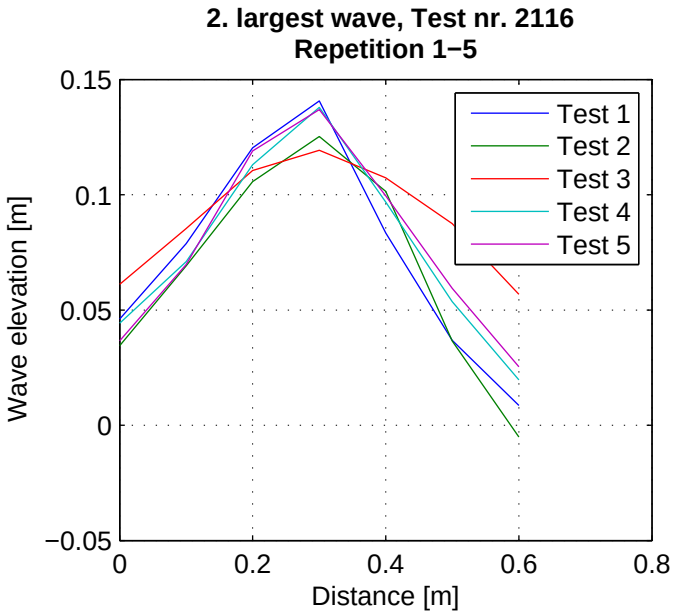
2. largest wave, Test nr. 2116
Repetition 1−5
Wave elevation [m]
Distance [m]
Test 1
Test 2
Test 3
Test 4
Test 5

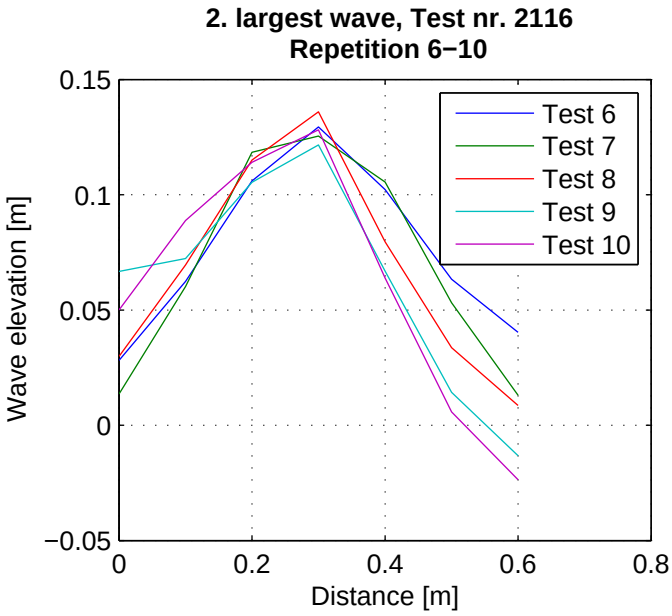
2. largest wave, Test nr. 2116
Repetition 6−10
Wave elevation [m]
Distance [m]
Test 6
Test 7
Test 8
Test 9
Test 10

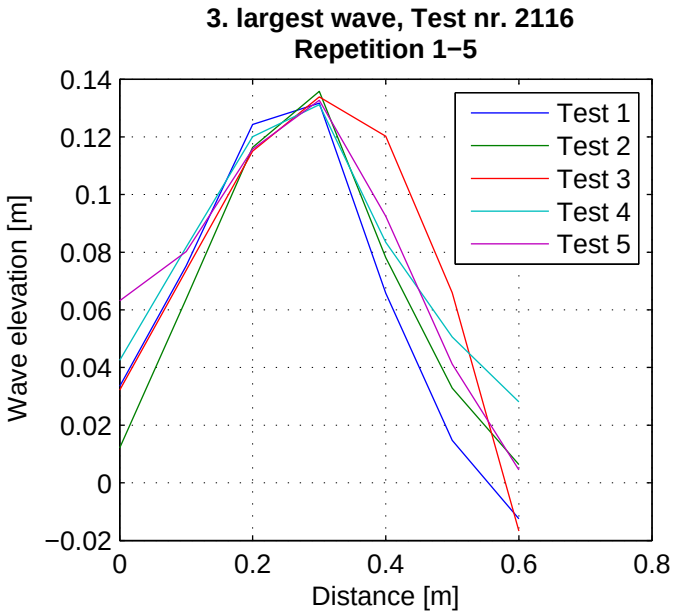
3. largest wave, Test nr. 2116
Repetition 1−5
Wave elevation [m]
Distance [m]
Test 1
Test 2
Test 3
Test 4
Test 5

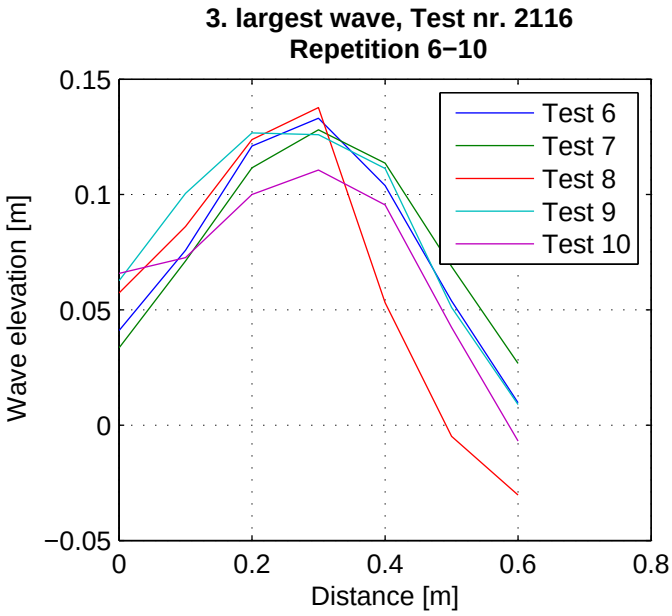
3. largest wave, Test nr. 2116
Repetition 6−10
Wave elevation [m]
Distance [m]
Test 6
Test 7
Test 8
Test 9
Test 10

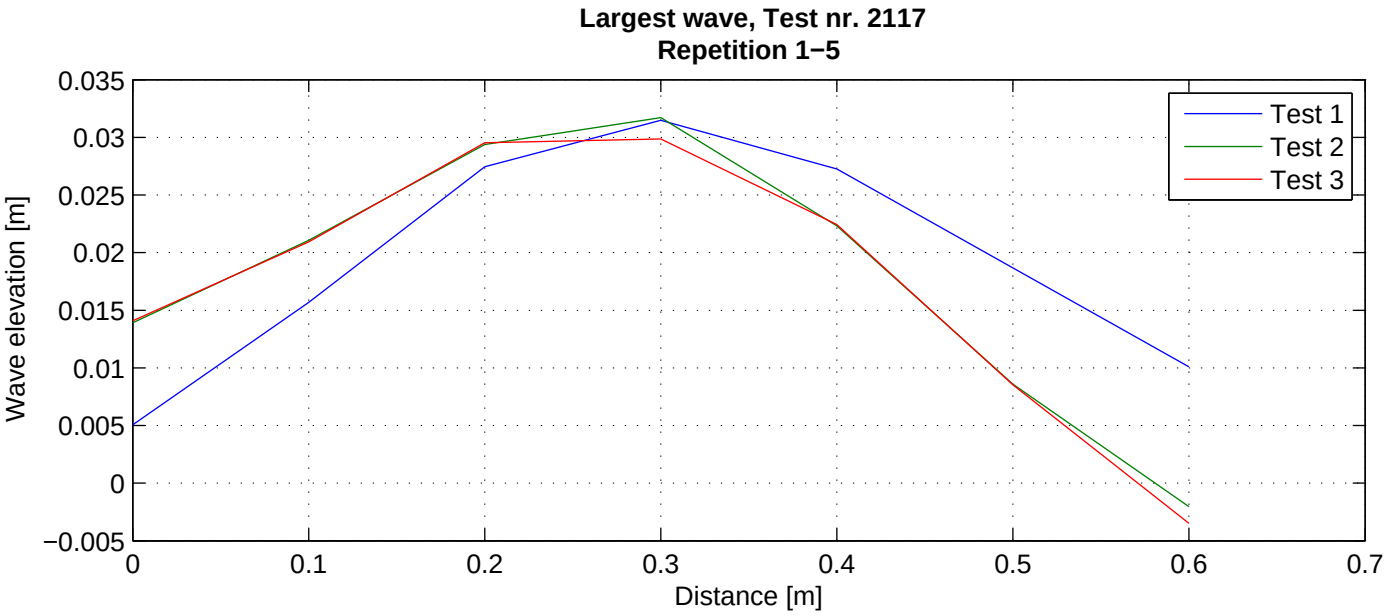
Largest wave, Test nr. 2117
Repetition 1−5
Wave elevation [m]
Distance [m]
Test 1
Test 2
Test 3
0.035
0.03
0.025
0.02
0.015
0.01
0.005
0
−0.005
0
0.1
0.2
0.3
0.4
0.5
0.6
0.7

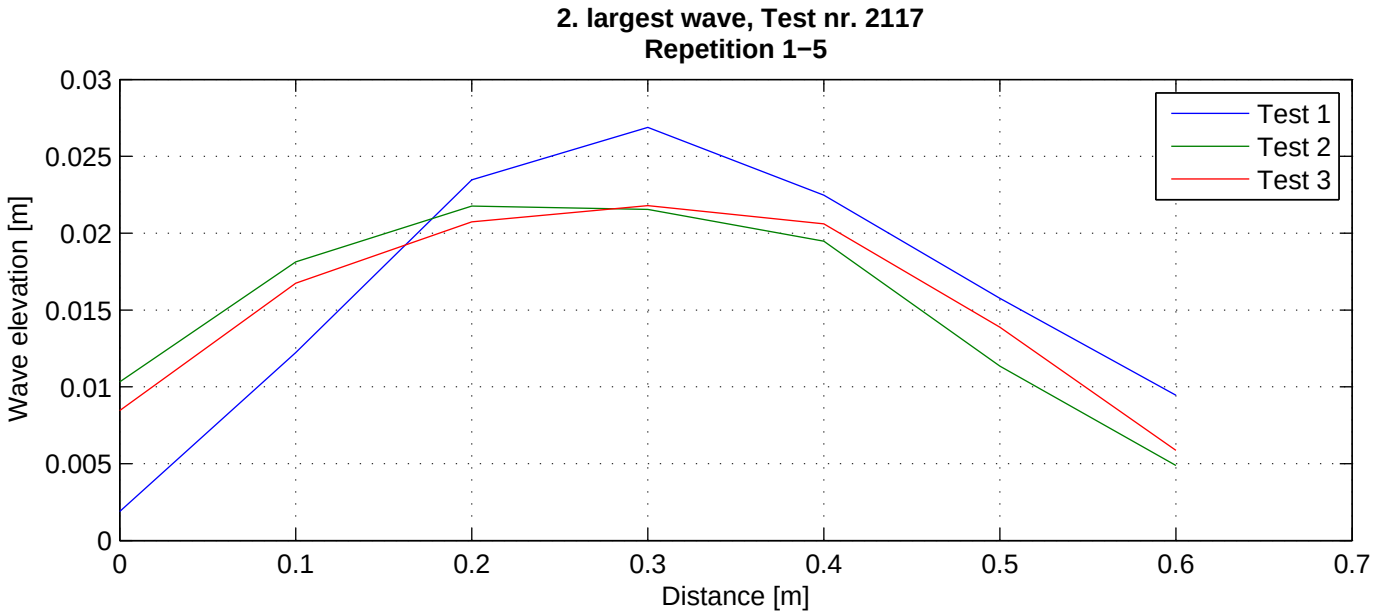
2. largest wave, Test nr. 2117
Repetition 1−5
Wave elevation [m]
Distance [m]
Test 1
Test 2
Test 3
0.03
0.025
0.02
0.015
0.01
0.005
0
0
0.1
0.2
0.3
0.4
0.5
0.6
0.7

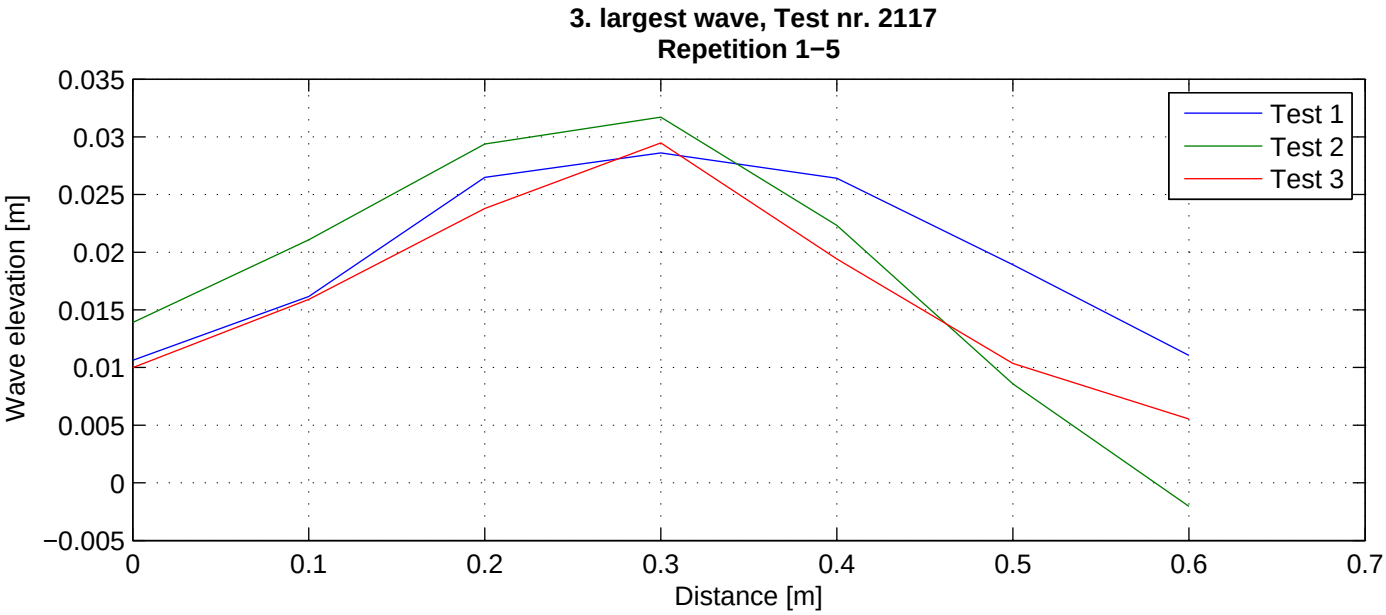
3. largest wave, Test nr. 2117
Repetition 1−5
Wave elevation [m]
Distance [m]
Test 1
Test 2
Test 3
0.035
0.03
0.025
0.02
0.015
0.01
0.005
0
−0.005
0
0.1
0.2
0.3
0.4
0.5
0.6
0.7

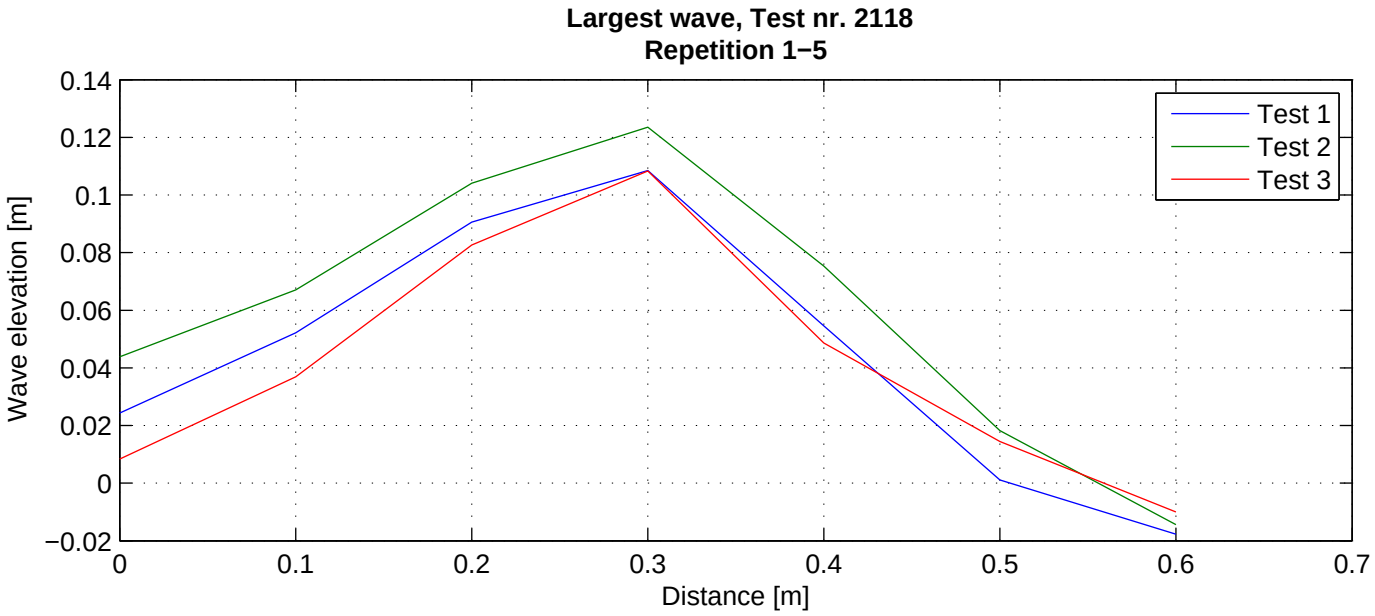
Largest wave, Test nr. 2118
Repetition 1−5
Test 1
Test 2
Test 3
Wave elevation [m]
Distance [m]
0.14
0.12
0.1
0.08
0.06
0.04
0.02
0
−0.02
0
0.1
0.2
0.3
0.4
0.5
0.6
0.7

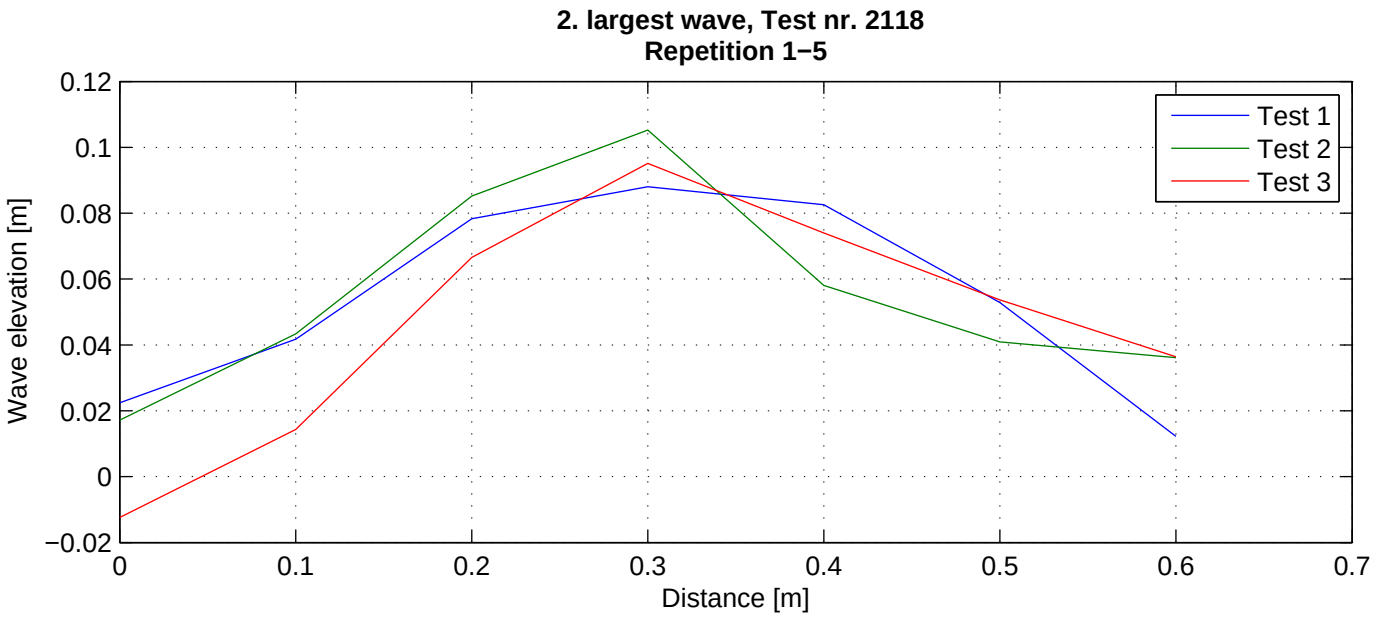
2. largest wave, Test nr. 2118
Repetition 1−5
Test 1
Test 2
Test 3
Wave elevation [m]
Distance [m]
0.12
0.1
0.08
0.06
0.04
0.02
0
−0.02
0
0.1
0.2
0.3
0.4
0.5
0.6
0.7

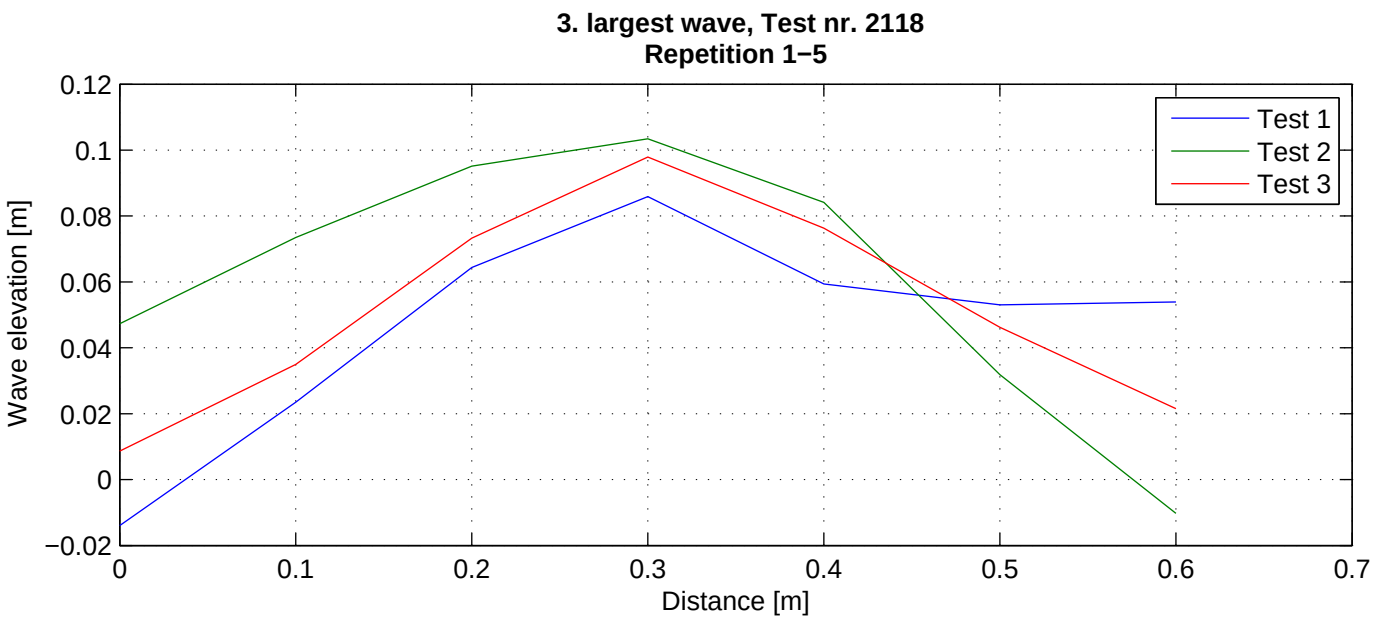
3. largest wave, Test nr. 2118
Repetition 1−5
Test 1
Test 2
Test 3
Wave elevation [m]
Distance [m]
0.12
0.1
0.08
0.06
0.04
0.02
0
−0.02
0
0.1
0.2
0.3
0.4
0.5
0.6
0.7

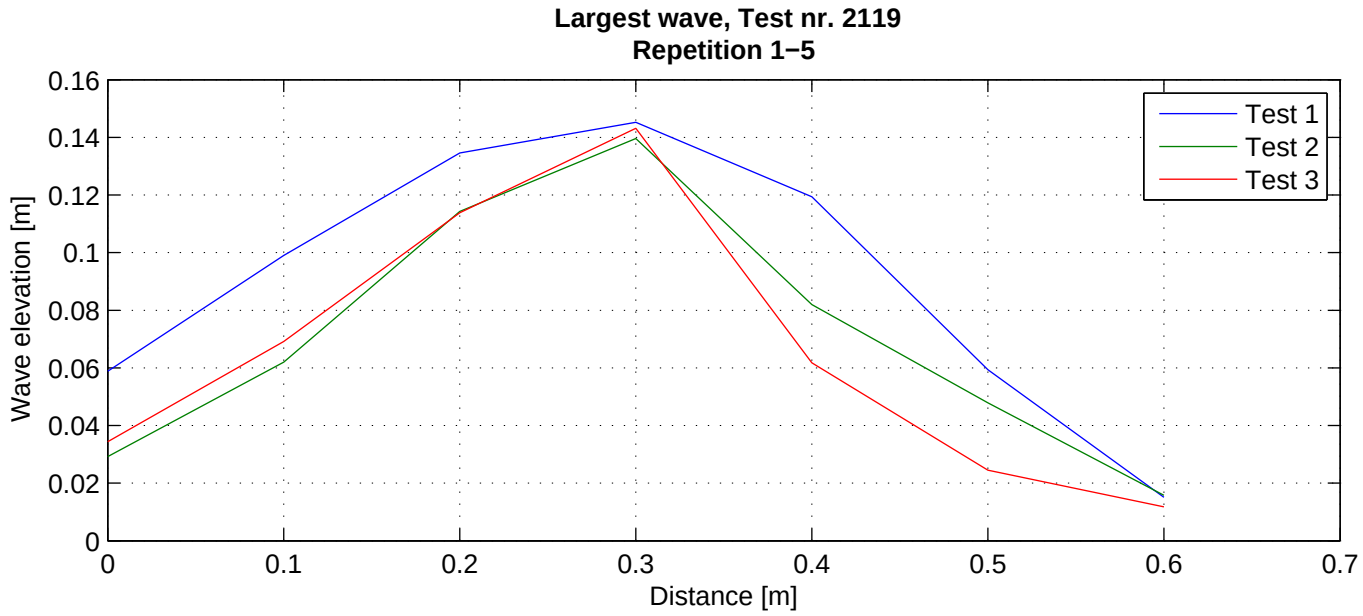
Largest wave, Test nr. 2119
Repetition 1−5
Wave elevation [m]
Distance [m]
Test 1
Test 2
Test 3

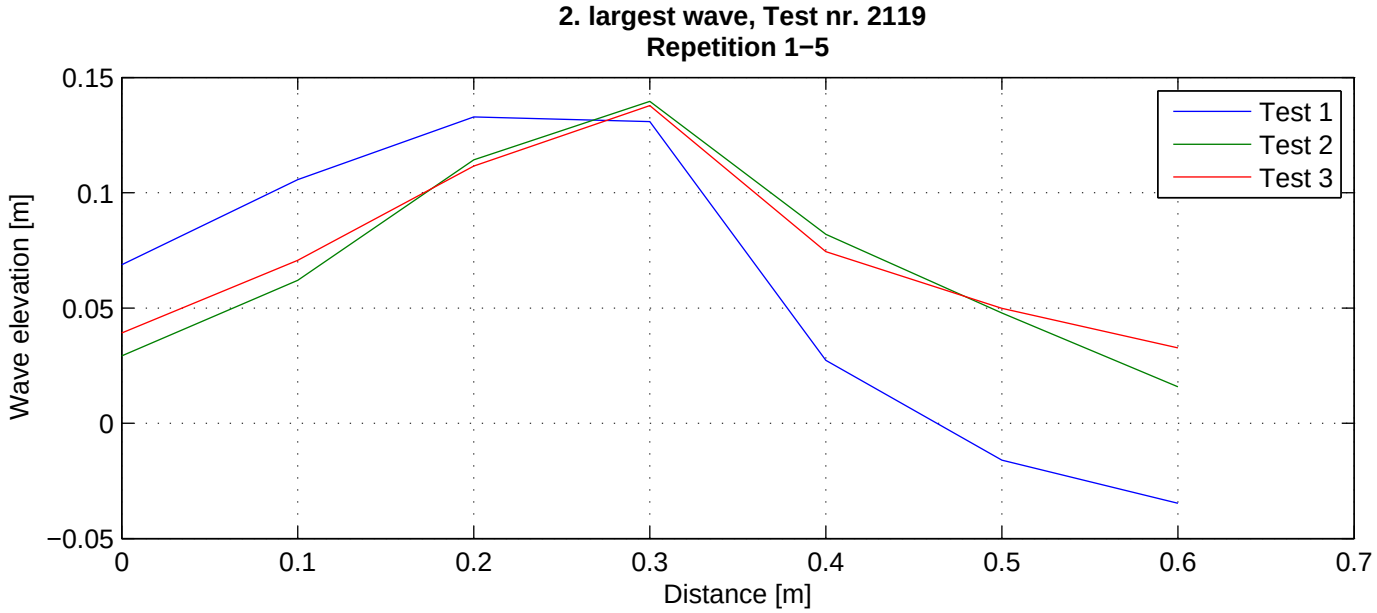
2. largest wave, Test nr. 2119
Repetition 1−5
Wave elevation [m]
Distance [m]
Test 1
Test 2
Test 3

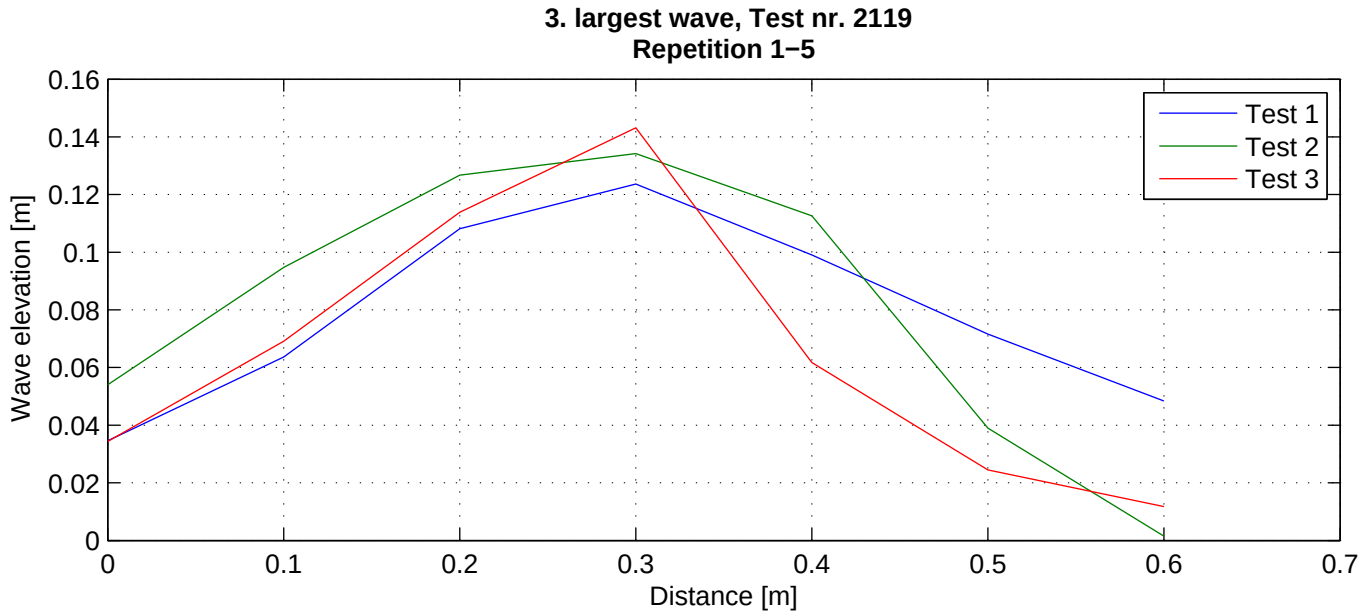
3. largest wave, Test nr. 2119
Repetition 1−5
Wave elevation [m]
Distance [m]
Test 1
Test 2
Test 3

Test nr.2109

Largest wave in time series

Rep nr	H/L	kA	Ursell
Rep.1	0.0502	0.1578	7.6172
Rep.2	0.0479	0.1504	5.1061
Rep.3	0.0413	0.1297	6.9711

Second largest wave in time series

Rep nr	H/L	kA	Ursell
Rep.1	0.0648	0.2035	4.3768
Rep.2	0.0393	0.1236	6.8808
Rep.3	0.0465	0.1462	4.9636

Third largest wave in time series

Rep nr	H/L	kA	Ursell
Rep.1	0.0343	0.1076	9.6172
Rep.2	0.0336	0.1055	8.6316
Rep.3	0.0615	0.1932	2.5495

Test nr.2111

Largest wave in time series

Rep nr	H/L	kA	Ursell
Rep.1	0.1087	0.3414	20.3509
Rep.2	0.0997	0.3131	18.6644
Rep.3	0.1159	0.3641	16.3209
Rep.4	0.1012	0.3181	21.6240
Rep.5	0.0989	0.3107	30.2369
Rep.6	0.1158	0.3639	19.5591
Rep.7	0.1044	0.3281	25.2803
Rep.8	0.1044	0.3279	20.8953
Rep.9	0.1188	0.3733	20.7774
Rep.10	0.1076	0.3381	17.5462

Second largest wave in time series

Rep nr	H/L	kA	Ursell
Rep.1	0.1161	0.3649	16.3538
Rep.2	0.1107	0.3478	15.0103
Rep.3	0.1081	0.3395	17.6174
Rep.4	0.1222	0.3838	14.1465
Rep.5	0.1116	0.3506	22.3393
Rep.6	0.1115	0.3502	20.8770
Rep.7	0.1108	0.3479	22.1697
Rep.8	0.1115	0.3501	18.1670
Rep.9	0.1142	0.3587	16.6882
Rep.10	0.1021	0.3208	17.8594

Third largest wave in time series

Rep nr	H/L	kA	Ursell
Rep.1	0.1145	0.3596	15.5154
Rep.2	0.0884	0.2778	21.4048
Rep.3	0.1075	0.3377	16.3021
Rep.4	0.1204	0.3781	13.3776
Rep.5	0.0966	0.3036	27.9207
Rep.6	0.0977	0.3070	24.3798
Rep.7	0.1030	0.3235	24.1746
Rep.8	0.1192	0.3743	14.9485
Rep.9	0.1028	0.3231	19.9149
Rep.10	0.0953	0.2994	20.3519

Test nr.2112

Largest wave in time series

Rep nr	H/L	kA	Ursell
Rep.1	0.1113	0.3496	23.7726
Rep.2	0.1074	0.3375	27.6244
Rep.3	0.0994	0.3122	31.2361
Rep.4	0.1132	0.3557	24.1796
Rep.5	0.1107	0.3477	31.0720
Rep.6	0.1069	0.3358	25.8748
Rep.7	0.1092	0.3429	26.4199
Rep.8	0.1177	0.3697	25.1371
Rep.9	0.1165	0.3659	24.0885

Second largest wave in time series

Rep nr	H/L	kA	Ursell
Rep.1	0.1067	0.3354	22.7976
Rep.2	0.1007	0.3164	29.1065
Rep.3	0.1023	0.3214	26.3000
Rep.4	0.1228	0.3857	18.6190
Rep.5	0.1006	0.3161	28.2439
Rep.6	0.0967	0.3039	30.4093
Rep.7	0.1182	0.3714	22.1395
Rep.8	0.0983	0.3089	31.7700
Rep.9	0.1062	0.3337	24.9326

Third largest wave in time series

Rep nr	H/L	kA	Ursell
Rep.1	0.0916	0.2877	29.5890
Rep.2	0.1004	0.3153	28.1812
Rep.3	0.1218	0.3826	18.4721
Rep.4	0.0956	0.3003	30.0433
Rep.5	0.1013	0.3182	26.0413
Rep.6	0.1214	0.3813	19.0909
Rep.7	0.1100	0.3455	24.2487
Rep.8	0.1053	0.3308	25.4930
Rep.9	0.1030	0.3235	25.6922

Test nr.2115

Largest wave in time series

Rep nr	H/L	kA	Ursell
Rep.1	0.0969	0.3043	24.9060
Rep.2	0.0765	0.2403	31.2685
Rep.3	0.0950	0.2984	22.2979
Rep.4	0.0769	0.2415	30.6355
Rep.5	0.0927	0.2911	29.9361
Rep.6	0.0907	0.2850	29.3099
Rep.7	0.0990	0.3109	27.7867
Rep.8	0.0838	0.2632	28.5748
Rep.9	0.0809	0.2540	31.4269
Rep.10	0.1030	0.3235	19.2850

Second largest wave in time series

Rep nr	H/L	kA	Ursell
Rep.1	0.0961	0.3020	19.8827
Rep.2	0.0782	0.2458	28.8867
Rep.3	0.0813	0.2555	30.0249
Rep.4	0.0994	0.3121	17.9841
Rep.5	0.0909	0.2856	27.0238
Rep.6	0.0931	0.2926	26.9129
Rep.7	0.0861	0.2706	32.6223
Rep.8	0.0856	0.2691	24.7491
Rep.9	0.0814	0.2559	27.0419
Rep.10	0.0866	0.2721	22.2736

Third largest wave in time series

Rep nr	H/L	kA	Ursell
Rep.1	0.0921	0.2893	20.9563
Rep.2	0.0739	0.2322	29.4666
Rep.3	0.0739	0.2322	31.7379
Rep.4	0.0825	0.2593	23.1751
Rep.5	0.0714	0.2244	31.4382
Rep.6	0.0948	0.2977	22.2392
Rep.7	0.0916	0.2878	27.2304
Rep.8	0.1003	0.3150	15.7723
Rep.9	0.0735	0.2308	33.1175
Rep.10	0.0769	0.2416	27.6626

Test nr.2116

Largest wave in time series

Rep nr	H/L	kA	Ursell
Rep.1	0.0884	0.2778	39.8664
Rep.2	0.0916	0.2877	37.4298
Rep.3	0.0957	0.3007	38.1601
Rep.4	0.0989	0.3106	41.4334
Rep.5	0.1010	0.3172	39.2342
Rep.6	0.0947	0.2974	36.7894
Rep.7	0.0897	0.2819	34.8674
Rep.8	0.0937	0.2945	43.2915
Rep.9	0.0958	0.3010	38.1913
Rep.10	0.0962	0.3021	31.9266

Second largest wave in time series

Rep nr	H/L	kA	Ursell
Rep.1	0.0838	0.2634	41.5529
Rep.2	0.1010	0.3172	29.1766
Rep.3	0.0834	0.2620	47.3510
Rep.4	0.0894	0.2809	44.3128
Rep.5	0.0855	0.2685	43.3499
Rep.6	0.0858	0.2696	41.5442
Rep.7	0.1004	0.3153	27.3747
Rep.8	0.1036	0.3254	26.6325
Rep.9	0.0985	0.3093	31.8145
Rep.10	0.1065	0.3346	24.2377

Third largest wave in time series

Rep nr	H/L	kA	Ursell
Rep.1	0.1042	0.3275	24.4643
Rep.2	0.1073	0.3372	23.6717
Rep.3	0.0959	0.3011	31.8266
Rep.4	0.0863	0.2712	37.9854
Rep.5	0.0790	0.2481	44.8352
Rep.6	0.0860	0.2702	32.5839
Rep.7	0.0853	0.2678	34.8484
Rep.8	0.1013	0.3182	27.6230
Rep.9	0.0841	0.2641	41.6620
Rep.10	0.0962	0.3024	29.4276

Test nr.2117

Largest wave in time series

Rep nr	H/L	kA	Ursell
Rep.1	0.0241	0.0758	7.3810
Rep.2	0.0215	0.0677	8.1624
Rep.3	0.0216	0.0678	8.3824

Second largest wave in time series

Rep nr	H/L	kA	Ursell
Rep.1	0.0280	0.0880	4.4051
Rep.2	0.0258	0.0809	4.8234
Rep.3	0.0262	0.0822	4.7374

Third largest wave in time series

Rep nr	H/L	kA	Ursell
Rep.1	0.0197	0.0619	8.4663
Rep.2	0.0197	0.0618	8.0463
Rep.3	0.0200	0.0628	7.1889

Test nr.2118

Largest wave in time series

Rep nr	H/L	kA	Ursell
Rep.1	0.0590	0.1853	39.7248
Rep.2	0.0738	0.2319	30.9315
Rep.3	0.1017	0.3194	15.9933

Second largest wave in time series

Rep nr	H/L	kA	Ursell
Rep.1	0.0682	0.2144	25.1878
Rep.2	0.0560	0.1761	41.7863
Rep.3	0.0667	0.2096	25.9303

Third largest wave in time series

Rep nr	H/L	kA	Ursell
Rep.1	0.0704	0.2213	22.7560
Rep.2	0.0660	0.2072	28.3312
Rep.3	0.0809	0.2543	16.7388

Test nr.2119

Largest wave in time series

Rep nr	H/L	kA	Ursell
Rep.1	0.0793	0.2491	50.1590
Rep.2	0.0742	0.2332	48.9664
Rep.3	0.0748	0.2348	54.6306

Second largest wave in time series

Rep nr	H/L	kA	Ursell
Rep.1	0.1036	0.3256	22.8508
Rep.2	0.0889	0.2792	30.3111
Rep.3	0.0818	0.2570	42.4460

Third largest wave in time series

Rep nr	H/L	kA	Ursell
Rep.1	0.0705	0.2214	47.4793
Rep.2	0.0753	0.2364	41.7857
Rep.3	0.0787	0.2474	39.0294